RobertsonNickerson CONSULTING ENGINEERS & MANAGEMENT CONSULTANTS
Limited
75 ALBERT STREET, SUITE 610, OTTAWA, ONTARIO K1P 5E7 CANADA (613) 238-4625

REQ. NO. 3-9070

CONTRACT REPORT NO. OGS 83-00307

STUDY TO DETERMINE THE CANADIAN MARKET FOR A PORTABLE X-RAY STRESS DIFFRACTOMETER AND TO IDENTIFY A SOURCE OF POSITION-SENSITIVE DETECTORS FOR THE UNIT

VOLUME 1

MARCH, 1984

79pp

OCT 23 1985
MICROMEDIA

This Document is the property of Robertson Nickerson Limited and their client, and may not be used or reproduced without permission.

RobertsonNickerson CONSULTING ENGINEERS & MANAGEMENT CONSULTANTS
Limited
75 ALBERT STREET, SUITE 610, OTTAWA, ONTARIO K1P 5E7 CANADA (613) 238-4625

April 10, 1984

Dr. Dennis White
Energy, Mines, and Resources
CANMET, Physical Metallurgy Research
Laboratories
555 Booth Street
OTTAWA, Ontario
K1A 0G1

Dear Dr. White:

Re: D.S.S. Contract 05GS.23440-3-9070

We are pleased to enclose our final report entitled "Study to Determine The Canadian Market For A Portable X-ray Stress Diffractometer And To Identify A Source Of Position-Sensitive Detectors For The Unit".

X-ray sensitive silicon photodiode arrays exist as modifications of the more popular visible light detectors. Major suppliers to the North American market are EG&G Reticon, Fairchild CCD, and Texas Instruments. No domestic sources of these detectors were identified, however, six Canadian companies who have similar products or capabilities were located.

The CANMET portable stress diffractometer is perceived by industry as a potentially useful tool. Due to cost of the unit and the relatively low level of awareness about residual stress measurements, the market is limited. Buyer education will be the key to developing the market.

Thank you for the opportunity to conduct this interesting study on your behalf. If we can be of further assistance, please do not hesitate to contact us.

Yours truly,

George M Robertson

G. M. Robertson, P.Eng.

TABLE OF CONTENTS

1.0 EXECUTIVE SUMMARY 1

- 1.1 Report Highlights From Part I 1
- 1.2 Report Highlights From Part II 4

2.0 PART I - A Marketing Survey For A Source Of Position-Sensitive Detectors For X-Ray Measurement 6

3.0 PART II - A Study Of The Canadian Market For A Portable X-Ray Stress Diffractometer 31

PART I

TABLE OF CONTENTS

2.1 Objective 7
2.2 Background 8
2.3 The Product - Silicon Photodiode Array 9

2.4 Sources of Supply

2.4.1 EG&G Reticon 13
2.4.2 Fairchild CCD 13
2.4.3 Texas Instruments 21
2.4.4 Other Available Products 21

2.5 Canadian Sources

2.5.1 Silonex Inc. 23
2.5.2 Northern Telecom 24
2.5.3 Opto-Electronics 25
2.5.4 Photovac Inc. 26
2.5.5 Proto Manufacturing Ltd......... 27
2.5.6 Aptec Engineering Limited 27

2.6 Market Information

2.6.1 Size of Market 28
2.6.2 Applications 28
2.6.3 Price 29
2.6.4 Patents 29

PART II

TABLE OF CONTENTS

3.1 Objective 32

3.2 Scope of the Report 35

3.3 CANMET Portable Stress Diffractometer 35

3.4 Market Analysis 37

- 3.4.1 Market Forecast 37
- 3.4.2 Canadian Buyer Profile 44
- 3.4.3 Purchasing Decision 48
- 3.4.4 Functional Characteristics 49
- 3.4.5 Marketing Strategy............. 52

3.5 Competition

- 3.5.1 Rigaku "Strainflex" 53
- 3.5.2 Technology For Energy (TEC) 1600 Systems 56
- 3.5.3 Denver X-Ray Instruments 59
- 3.5.4 American Analytical "Fastress" . 60
- 3.5.5 Siemens-Allis 60
- 3.5.6 Competitive Technology 62

3.6 Selected Bibliography 66

LIST OF TABLES

TABLE I Advantages and Disadvantages of Silicon Photodiode Arrays as Compared to Position-Sensitive Proportional Counters 12

TABLE II Summary of Reticon Image Sensors 16

TABLE III Summary of Fairchild CCD Line Scan Sensors 20

TABLE IV Summary of Texas Instrument CCD Image Sensors 22

TABLE V Typical Prices of Silicon Photodiode Arrays 30

TABLE VI List of Contacts 40

TABLE VII Market Forecast 42

TABLE VIII Contact Summary of Interested Respondents 45

TABLE IX Specifications of Rigaku's "Strainflex" 55

TABLE X Comparison of X-Ray Diffraction Residual Stress Systems 63

TABLE XI Selection of Residual Stress Measurement Methods 65

LIST OF FIGURES

Figure 1 Linear Photodiode Array 10
Figure 2 Geometry of Reticon's Linear Arrays 14
Figure 3 CANMET's Portable Stress Diffractometer.......... 36
Figure 4 Distribution of Responses........................ 38
Figure 5 Response by Industry............................. 39
Figure 6 Distribution of Responses by Industry Sector..... 47
Figure 7 Distribution of Canadian Responses by Number of Employees................................ 47
Figure 8 Rigaku "Strainflex".............................. 54
Figure 9 TEC Diffractometer............................... 57
Figure 10 American Analytical "Fastress".................. 61

LIST OF APPENDICES

APPENDIX A - EG&G Reticon
  1. Product Summary - Solid State Image Sensors
  2. Application of Reticon Photodiode Arrays as Electron and X-ray Detectors
  3. Preliminary Data Sheet SFX-Series X-ray Sensitive Solid State Line Scanners

APPENDIX B - Fairchild CCD
  1. CCD Fundamentals
  2. Charge-Coupled Device
  3. CCD151 3456-Element Line Scan Image Sensor
  4. Technical Note on X-ray Imaging with Fairchild CCD Image Sensors
  5. Advanced Charge-Coupled Device (CCD) Line Imaging Devices
  6. CCD 111
  7. CCD 122/142
  8. CCD 133/143
  9. CCD Imaging Products Price Schedule

APPENDIX C - Texas Instruments
  1. Virtual Phase CCD Technology
  2. Type TC102 Linear Image Sensor
  3. Type TC101
  4. Type TC103
  5. Type TC104

APPENDIX D - Other Available Products
  1. Threshold Detection of Visible and Infrared Radiation with PIN Photodiodes
  2. Xarray Linear Position Sensitive X-ray Detector

APPENDIX E - Silonex Inc.
  1. PIN Photodiode
  2. Blue Sensitive Photodiodes
  3. Silicon Planar Photodetectors

APPENDIX F - Northern Telecom
  1. Charge-Coupled Device (CCD): Imaging Systems at the University of British Columbia

APPENDIX G - Opto-Electronics
  1. High Speed Component Photodetectors
  2. Germanium Photodiodes
  3. High Speed Amplified Photodetectors

APPENDIX H - Canadian Patents
  1. Photodiode Detector with Selective Frequency Response
  2. Buried-Channel Charge-Coupled Linear Device
  3. Document Scanning Head
  4. Photoconductor Device for Imaging a Linear Object

APPENDIX I - Interview Guideline

APPENDIX J - CANMET Portable Diffractometer

APPENDIX K - Rigaku "Strainflex"

APPENDIX L - TEC 1600 Stress Analysis Systems

APPENDIX M - American Analytical Corporation
  1. "Fastress" Automatice Stress Analyzer
  2. "Fastress" User List
  3. Retained Austenite in Steels

APPENDIX N - Siemens-Allis
    1. X-ray Measurement of Residual Stress on a Welded Stainless Steel Pipe Joint Connection
    2. X-ray Analysis of a Pipeline

APPENDIX O - Selected Articles
    1. "PARS" - A Portable X-ray Analyzer for Residual Stresses
    2. X-ray Analysis and Advances in Portable Field Instrumentation
    3. Position-sensitive Detector Improves X-ray Powder Diffraction
    4. X-ray Residual Stress Measurement Systems for Army Material Problems
    5. Problems With Residual Stress in the Railroad Industry

RobertsonNickerson CONSULTING ENGINEERS & MANAGEMENT CONSULTANTS
Limited
75 ALBERT STREET, SUITE 610, OTTAWA, ONTARIO K1P 5E7 CANADA (613) 238-4625

STUDY TO DETERMINE THE CANADIAN MARKET FOR A PORTABLE X-RAY STRESS DIFFRACTOMETER AND TO IDENTIFY A SOURCE OF POSITION-SENSITIVE DETECTORS FOR THE UNIT

1.0 EXECUTIVE SUMMARY

1.1 Report HIghlights From Part I

- Silicon photodiode arrays are primarily designed to detect light in the 200 to 1,100 nanometer range.
- Light sensitive photodiode arrays can be modified to detect x-rays by:
    - i) converting the x-ray image into visible light by means of an image converter tube and then detecting the visible light with the array;
    - ii) depositing an x-ray phosphor directly onto the array or fibre optic face plate; or
    - iii) letting the x-ray excite the sensor directly.

- The major sources of supply of silicon photodiode arrays are: EG&G Reticon, Sunnyvale, CA
  Fairchild CCD, Palo Alto, CA
  Texas Instruments, Dallas TX

- EG&G Reticon has a 30% to 40% market share. They offer arrays with 64 to 4,096 elements with various spacings and aperture widths. Series C and S arrays are most suited to x-ray applications.

- Fairchild CCD also has a 30% to 40% market share. Their product range includes arrays with 256 to 3,456 elements. The most common element size is 13 x 13 microns.

- Texas Instruments is a relatively new entrant into the photodiode array market. They offer four models with 128, 1,728, 2,048, and 3,456 elements. Element size is 12.7 x 12.7 microns.

- No Canadian sources were identified who could supply a product to meet CANMET's requirements.

- The following Canadian companies have similar product lines and the capability to develop a silicon photodiode array:

  Silonex, Montreal, PQ
  Northern Telecom, Nepean, On
  Opto-Electronics, Oakville, ON
  Photovac Inc., Thornhill, ON
  Proto Manufacturing, Old Castle, ON
  Aptec Engineering, Ottawa, ON

- The North American market for all linear silicon photodiode arrays is estimated to be $2 to $5 million (U.S.). The market for x-ray sensitive detectors is estimated to be 2% to 5% of the total market.

- The price of silicon photodiode arrays ranges from $75 (U.S.) to $5,000 (U.S.).

- Major applications for light sensitive detectors are facsimile, optical character recognition, and document scanning. The largest area of growth is expected to be in surveillance systems, inspection, and robot vision.

- Prominent applications for x-ray detectors include scientific research and medical instrumentation.

1.2 Report Highlights From Part II

- A portable diffractometer is perceived by industry as a useful tool. An interest and need for this capability was demonstrated.

- A limited demand for a portable diffractometer was shown within the private sector. Of the 57 Canadian firms contacted, 5 had a "Yes" response and 12 had a "Maybe" response.

- Extrapolated to a total population, this represents a five-year market forecast of 12 to 17 units in Canada.

- These estimates are consistent with the competition's experience, i.e., a limited number over a period of time.

- Competitive units are offered by Rigaku, TEC, Denver X-ray Instruments, American Analytical, and Siemens Allis.

- The potential buyer population is a spectrum of buyers with varying needs, ranging from the automotive sector to utilities to consulting engineers.

- Industry requires more education about residual stress and its measurement techniques in order to increase their level of awareness.

- The major applications are research and development, inspection of critical welds, and failure analysis.

- The high price of a portable diffractometer limits its saleability. Several contacts suggested they would be interested if it was priced at $30,000. Further development to simplify the unit and thereby reduce its cost, would open the potential market.

- Because of the unit's high cost, some contacts stated that they would use a service rather than buy a unit. The service is perceived as a complete service offering equipment and personnel to examine individual situations, set up and operate the equipment, and report and interpret the results. It is not equipment rental.

- The U. S. market appears to be similar to the Canadian market in terms of industry sectors, applications, users, level of awareness, etc.

- The success of the CANMET portable stress diffractometer depends on a strong marketing campaign directed at:

    - education of buyers about residual stress and its measurement techniques;

    - position titles rather than industry sectors;

    - why the unit is different from its competition.

PART I

A MARKETING SURVEY FOR A SOURCE OF POSITION SENSITIVE DETECTORS FOR X-RAY MEASUREMENT

2.1 Objective

To determine the potential for a reliable domestic source to supply economically significant X-Ray responsive Silicon Photodiode Array detectors, for the CANMET Portable X-Ray Diffractometer currently under development. In particular:

a) To identify Canadian suppliers and/or manufacturers of X-Ray responsive, position sensitive SPDAs.

b) If domestic sources for SPDAs cannot be identified, the survey will confirm the availability of UV responsive detectors and will identify domestic or potential suppliers of the detectors.

c) The operating characteristics of SPDA detectors will be estimated, taking into account accuracy, response time, ruggedness, reliability, convenience (operating services), weight, service life, and servicing requirements, etc.

d) To determine the patent situation for existing UV responsive SPDA detectors, and estimate the scope for developing X-Ray responsive SPDA detectors unfettered by patents for UV units, together with the opportunities for patentable Canadian technology (this will be a preliminary investigation only).

e) To estimate the probablility of success in adapting UV detectors for X-Ray application and developing associated electronics, in terms of market size and outlays of risk capital. The scope of the market for X-Ray responsive SPDA detectors will include applications other than stress diffractometers.

2.2 Background

The CANMET Portable X-ray Stress Diffractometer is a unit for the non-destructive measurement of surface stresses in solid materials. It is of the single exposure kind, using two x-ray position sensitive detectors. These detectors are gas-filled proportional counters. As an x-ray photon enters the chamber of the detector it produces a few hundred primary electron-ion pairs in the gas. An electron avalanche at the anode wire occurs as electrons are attracted to the wire. Positive ions left behind move away rapidly creating a pulse in the anode. The number of pulses (or ion pairs produced) is proportional to the energy in the photon.

CANMET's Physical Metallurgy Research Laboratories are presently evaluating the operating characteristics of the diffractometer. The use of the proportional counter type detectors presents some problems:

i) there is no Canadian source of these detectors;

ii) the current supplier makes a competitive portable x-ray stress diffractometer;

iii) the detectors and their associated electronics account for approximately half of the projected price of the diffractometer.

An alternative position sensitive detector, a charge coupled device known as a silicon photo diode array is being considered. This type of detector is expected to have higher spatial resolution, high absolute position stability, negligible spatial distortion. It will be smaller in physical size, requiring less associated electronics, and be considerably less expensive.

This report will discuss silicon photodiode arrays in general, describe existing products with respect to their applications and characteristics, and present a list of Canadian companies who have the capability to produce the detector.

2.3 The Product - Silicon Photodiode Array

Silicon photodiode arrays were designed primarily for the detection of visible and near infrared light. Detection of x-rays and electrons is also possible with some modifications. Arrays are available in linear or matrix format. For the purposes of this report, the discussion is limited to linear arrays.

Arrays consist of a row of image sensing elements (photodiodes) and shift register on a single silicon chip enclosed in an integrated circuit type package. The signal from a silicon photodiode array is produced by electron-hole production. Light energy falling on the photosites produces electron-hole pairs which diffuse through the crystal and reduce the potential across the diode. These charge packets are then transferred to the shift register. The operating cycle for each photodiode is: reset, collect light, and read the resultant potential. This cycle distinguishes the photodiode array from a photon counter. The output signal is a representation of spatial distribution of light intensity across the array. Photon beam location is easily determined since a large number of very small diodes are used. This gives the array its position-sensitive characterisitic.

Figure 1 illustrates a diode and an array.

Visible light sensitive detectors can be modified for x-ray applications.

FIGURE 1

LINEAR PHOTODIODE ARRAY

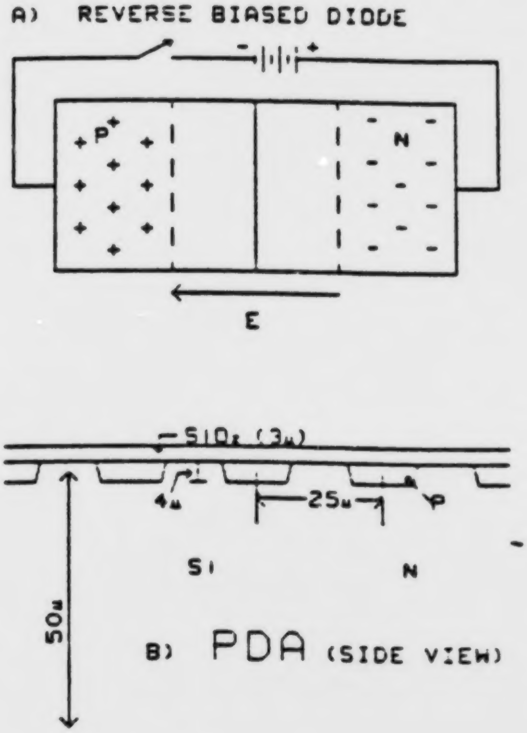
A) REVERSE BIASED DIODE
P
N
E
SiO₂ (3µ)
4µ
25µ
P
Si
N
50µ
B) PDA (SIDE VIEW)

Figure 1 a) - Reverse biased diode. Signs indicate charge carriers. In the carrier-depleted region there is an electric field as shown. Electrons or holes diffusing into this region replenish the carriers and reduce the field. b) Schematic view of the photodiode array drawn to scale. If photons are absorbed within 50 microns of the P-N boundaries they can be detected.

Source: X-Ray Detection With A Linear Photodiode Array
F. Zutavern, T. Aton, C. Franck, S. Schnatterly

Three methods are used:

1) Convert the x-ray image into visible light by means of an image converter tube and view the visible light with the array.

2) Deposit an x-ray phosphor directly onto the array or a fibre-optics face plate.

3) Let the x-ray excite the sensor directly.

The first two methods are the most popular since direct x-ray exposure can degrade the array.

2.3.1 CANMET's Desired Operating Characteristics

CANMET has defined their requirements for a silicon photodiode array as follows:

The detector should:

- Detect X-Rays at 2Å (5 KeV)
- Be self-scanning
- Be Position sensitive
- Be able to be cooled by Thermoelectric coolers
- Count at 100 to 1000 counts/sec-channel
- Have spatial resolution of 100 µm with 25 µm being ideal
- Have a maximum of 5% loss in the SiO_2 layer
- Enclosure as close to chip ends as possible
- Active area 3.5 to 5 cm long
- The array and associated electronics be lightweight, reliable, rugged, fast, and easily serviced.

The advantages and disadvantages of a silicon photodiode array compared to a position-sensitive proportional counter are outlined in Table I.

TABLE I

ADVANTAGES AND DISADVANTAGES OF SILICON PHOTODIODE ARRAYS AS COMPARED TO POSITION-SENSITIVE PROPORTIONAL COUNTERS

ADVANTAGES	DISADVANTAGES
Higher Spatial Resolution	More Prone to X-ray Damage
High Absolute Position Stability	Require Cooling
Negligible Spatial Distortion and Lag	Limit X-ray Range
Direct Photon Counting	Relatively New Technology
Small Physical Size	
Reduced Cost	

2.4 Sources of Supply

The major sources of supply for silicon photodiode arrays in North America are:

EG&G Reticon
Fairchild CCD
Texas Instruments

Their products are discussed below.

2.4.1 EG&G Reticon, Sunnyvale, CA

EG&G Reticon offers a complete line of self-scanning photodiode arrays in linear, matrix or circular format. Linear arrays were designed to detect light in the 250 to 1100 nanometer range. Applications include pattern recognition, OCR, facsimile, size and position monitoring, and inspection and surveillance. These devices have the advantages of high scan rates, small size, low voltage, low power, solid state ruggedness and reliability.

The range of Reticon's linear arrays results from various geometries, i.e., number of elements (or photodiodes), centre-to-centre spacing of the diodes, and aperture width, see Figure 2. Certain configurations are better suited to high resolution requirements and others are better suited to high sensitivity applications. The following highlights some of Reticon's arrays.

A-Series - available with 64 elements on 2 mil centres with an aperture width of 2 mils.

C-Series - available with 256, 512, or 1024 elements on 1 mil centres with two options in aperture width: 1 mil for high resultion applications and 17 mils for high sensitivity applications.

EC-Series - identical to C-Series except only alternate diodes are sampled

G-Series - available with 128, 256, 512, or 1024 elements on 25 µm centres with an aperture width of

FIGURE 2

GEOMETRY OF RETICONS

LINEAR ARRAYS

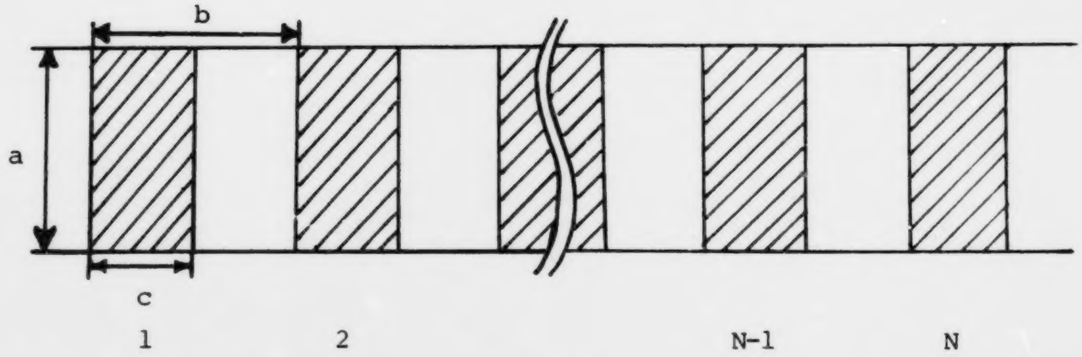

a) Aperture Width

b) Centre-to-centre

c) Width of Diode

▨ Photo Diodes

22 μm. These units are considered by Reticon to be industry standards combining ease of use, high performance and low cost.

H-Series - available with 1024, 1728, or 2048 elements on 15 μm centres with an aperture width of 16 μm to provide the high resultion required for full page width facsimile applications.

S-Series - available with 128, 512, or 1024 elements on 25 μm centres with an aperture of 2.5 mm. This series was specifically designed and optimized for applications in spectroscopy.

W-Series - available with 64 elements on 25 μm centres with an aperture width of 10 mm. This wide aperture can be applied in spectroscopy where sensitivity is important and a limited number of lines are to be monitored.

RL4096 - available with 4096 elements on 15 μm centres with an aperture of either 16 μm or 508 μm. This array was designed for document scanning applications.

CCPD - is a charge coupled photodiode available with 512 or 1024 elements on 18 μm centres with an aperture of 18 μm for applications requiring high speed operations.

Table II presents a summary of the characteristics of Reticon's image sensors. Appendix A provides additional information.

Table II — Summary of Reticon Image Sensors

Series	Number of Elements	Spacing	Aperture Width	Max Sample Rate	Recharge Output	Integrated Sample-and-Hold Output	Comments
Linear							
A	64	2 mil	2 mil	10 MHz	RC200/201		2 Phase Clocks
C	256, 512, 1024	1 mil	1 or 17 mils	10 MHz	RC400A/403, 404, 406	RC100B/101, 102, 103	4 Phase Clocks
CCPD 128 × 4, 8	512, 1024	18 μm	18 μm	8 MHz (per output tap)		RC716A-4, 8	8 μs line time, CCD readout. Tapped structure (2 outputs each 128 element block)
EC	128, 256, 512	2 mil	1 or 17 mils	5 MHz	RC200/203, 204, 206	RC100B/101, 102, 103	2 Phase Clocks
EL	64	5 mil	3 mil	10 MHz	RC200/202		2 Phase Clocks
G	128, 256, 512, 1024	25 μm	26 μm	1 MHz	RC301, 301, 302, 303	RC100B/104, 104, 105, 106	Single Phase TTL Clock Differential Output
H	1024, 1728, 2048	15 μm	16 or 300 μm	3 MHz	RC1024H, 1728H, 1728H	RC100B/107, 108, 108 RC1728H/LN (RL1728H only)	6 Phase Clocks Differential Output
L	128	2.5 mil	3 mil	10 MHz	RC400A/402		4 Phase Clocks
S	128, 512, 1024	25 μm	2.5 mm	5 MHz		RC1024S (300 KHz max)	4 Phase Clocks Differential Output Optional Fiber Optic Window
W	64	25 μm	10 mm	2 MHz	RC64W		Wide aperture, high sensitivity
RL4096	4096	15μm	16 or 508μm	10MHz	RC4096		6 Phase Clocks

Although designed to detect light, Reticon arrays can also be useful in detecting x-rays. The C and S series arrays are most suited to detect soft x-rays in the range of 1 to 10A wavelength (1.2 to 12 KeV). On these models the quartz window must be omitted. Since the protective silicon dioxide layer, 3 microns thick, will partially absorb the incident x-ray beam, it is desirable to reduce the thickness of the oxide layer to improve sensitivity in these applications.

The SFX Series array can be used to detect x-rays in the 10 to 75 KeV energy range. This unit is a modification of the S-Series detector with the fibre optic face plate option. The modification consists of adding an x-ray phosphor to the input side of the fibre optic face plate to provide spectral sensitivity in the 10 to 100 KeV range. The fibre optic face plate acts as an interface between the phosphor and the diode array, as well as protection of the array from x-ray damage. For more details see Appendix A.

2.4.2 Fairchild CCD
Palo Alto, CA

Fairchild CCD has been a leader in charge-coupled device (CCD) technology since 1970. (Appendix B discusses CCD technology.) Their emphasis has been on the development of CCD cameras for scientific and industrial applications. Line scan cameras are useful for acquisition of optical data for objects in motion such as microfiche and microfilm scanning. Area cameras are suited to industrial environments, e.g., to provide standard output signals for display of high resolution images on low-cost monitors or to provide image data output for automatic inspection, recognition, and robot guidance.

Other products offered include signal processing devices for the delay and temporary storage of analog video signals as well as the line scan and area image sensing components used in the CCD cameras.

Key advantages of Fairchild's line scan sensors, due to Fairchild's isoplanar buried structure, include high data rates, high charge transfer efficiencies, low noise, and relatively small die sizes. Linear image devices are used where the subject is a line pattern such as bar code reading or facsimile (text, maps, fingerprints, photographs). Fairchild's range of line scan image sensors is discussed below.

CCD111 - available with 256 elements on 13 µm centres. The device is designed for optical character recognition and other imaging applications that require high sensitivity and high speed.

CCD122/142 - available with 1728 and 2048 elements respectively on 13 µm centres. The devices are designed for page scanning applications which require high resolution and high sensitivity. The CCD122 provides a 200-line per inch resolution across an 8-1/2" page adopted as an international facsimile standard.

CCD133/143 - available with 1024 and 2048 elements respectively on 13 µm centres. These devices are designed for page scanning applications which require high resolution, high sensitivity and high data rates. The CCD133 provides a 120-line per inch resolution across an 8-1/2" page. These units are second generation devices having an overall improved performance compared with the first generation devices including higher sensitivity, an enhanced blue response, and a lower dark signal.

CCD151 - Available with 3456 elements on 7 µm centres. This device was designed for facsimile, copier, optical character recognition and other imaging applications requiring very high resolution, high sensitivity and high data rates.

Table III summarizes the characteristics of Fairchild CCD's line scan sensors. Appendix B provides additional information.

As with Reticon devices, Fairchild's line scan sensors are designed to detect light in the 350 to 1200 nanometer range. Solid state image sensors can be used for x-ray imaging. Approaches include:

1) to use an x-ray phosphor that is deposited directly on a fibre optics faceplate on the sensor.

TABLE III

SUMMARY OF FAIRCHILD CCD LINE SCAN SENSORS

ORDERING CODE	NUMBER OF ELEMENTS	ELEMENT SIZE - MICRONS	MAXIMUM DATA RATE	DYNAMIC RANGE (TYPICAL)	RESPONSIVITY (TYPICAL)
CCD111DC	256x1	13x17	10MHz	2500:1	0.5V per $\mu j/cm^2$
CCD133DC	1023x1	13x13	20MHz	2500:1	3.0V per uj/cm^2
CCD122DC	1728x1	13x13	2MHz	2500:1	3.5V per $\mu j/cm^2$
CCD142DC	2048x1	13x13	2MHz	2500:1	3.5V per $\mu j/cm^2$
CCD143DC	2048x1	13x13	20MHz	2500:1	3.0V per $\mu j/cm^2$
CCD151DC	3456x1	7x7	5MHz	2500:1	4.0V per $\mu j/cm^2$

2) to let the x-rays excite the sensor directly.

The second method is not recommended since it can lead to degradation of the device causing increased dark signal, decreased charge transfer efficiency, and drift in optimum drive voltages. See Appendix B for more details.

2.4.3 Texas Instruments
Dallas, TX

Texas Instruments is a leader in integrated circuit production. After several years of development, Texas Instruments introduced their first commercial CCD image sensors in 1982. These devices utilize virtual phase CCD technology. (See Appendix C for further details.) Applications include document reading, facsimile and optical character recognition. Table IV presents a summary of the characteristics of Texas Instruments' CCD image sensors. Appendix C provides more information.

2.4.4 Other Available Products

Hewlett-Packard is a high volume supplier of LED displays, LED lamps, light bars, bar graph arrays, optocouplers, fibre optics, shaft encoders, and bar code products. They offer specific end products or individual photodiodes (see Appendix D). They do not offer photodiode arrays.

Scientific Development Technologies in Napierville, IL, offers a packaged detector system for x-ray detection using a Reticon S-series photo diode array and including a liquid nitrogen cooling mechanism. Appendix D has more details. At the time of writing, the availability of this item is not known.

TABLE IV

SUMMARY OF TEXAS INSTRUMENTS' CCD IMAGE SENSORS

CODE	NUMBER OF ELEMENTS	ELEMENT SIZE μm^2	MAXIMUM DATA RATE	DYNAMIC RANGE TYPICAL	RESPONSIVITY TYPICAL	SPACING CENTRE TO CENTRE μm
TC101	1728	12.7 x 12.7	10 MHz	1000:1	3.5V/μJ/cm2	12.7
TC102	128	12.7 x 12.7	10 MHz	1000:1	3.5	12.7
TC103	2048	12.7 x 12.7	10 MHz	1000:1	3.5	12.7
TC104	3456	10.7 x 10.7	8 MHz	1000:1	2	10.7

Contacts with General Electric and RCA indicated that their involvement in this area was primarily area arrays for internal use in such products as CCD cameras.

2.5 Canadian Sources

No Canadian sources were discovered who could offer a product that meets CANMET's desired operating characteristics. However, several companies were identified who had similar products or capabilities to produce the array. These companies are briefly highlighted in the following sections.

2.5.1 Silonex Inc.

Montreal, P.Q.

Formerly known as National Semiconductors Ltd., Silonex has been making silicon photodiodes for almost 20 years. They are in the process of expanding their photodiode facility in order to produce planar and PIN type photodiodes which are increasingly substituted for the older Mesa types. Silonex has not made integrated circuits using photodiodes or phototransistors with a monolithic composition. It is anticipated that their new facility will be capable of producing planar PIN arrays of miniature microsizes but making integrated circuitry around them has not been contemplated. Applications for planar photodiodes include luggage x-rays, CT scanners, inspection, and human body scanners.

Among Silonex's optoelectronics products are:

- CdS and CdSe photocells
- CdS and Si photodetector lamp assemblies
- PIN photodiodes
- Si photodiodes
- Si phototransistors and photo darlingtons
- UV/Blue sensitive LDRs.

The product range of Si photodiodes includes:

PIN - designed for high speed switching applications such as optical data transmission, laser and low light level detection, and light demodulation.

Blue sensitive - designed for photographic and photometer applications such as illumination and exposure meters, and colorimeters. These devices are well suited for operation with reverse bias.

Planar photodetectors - designed for photovoltaic and photoconductive applications. Its high sensitivity and low dark currents make the device ideal for low light detection. Its low capacitance and high speed are suited to fast rise time applications.

Appendix E contains further information.

2.5.2 Northern Telecom
Nepean, ON

Northern Telecom manufactures a unique sensing array primarily for optical scanning in military surveillance. They have also been doing work under contract to an American company on CCDs for x-ray applications in the Advanced X-ray Astronomy Facility's satellite.

The device is an area array, one inch in length with pixel size of 13 μm x 13 μm. There are no photodiodes -- sensing is accomplished with metal oxide semi-conductor CCDs.

The area arrays can be modified to be linear. Also, two arrays can be physically butted together to make a two inch array. While this has been successfully accomplished in optical work it has not been proven in x-ray work. The photosilicon layer on the device would have to be reduced in thickness to allow penetration of soft x-ray. Again, this has not been attempted.

Current cost estimates of the unit are approximately $3,500.

Appendix F discusses the use of a Bell-Northern Research CCD used in an imaging photometer.

2.5.3 Opto-Electronics Ltd.
Oakville, ON

Opto-Electronics Ltd. conducts research in electro-optics for industrial electro-optic controllers, optical communication systems, and electro-optical instruments. A leader in very fast photodiodes, their products include:

- signal enhancers
- optical fibre splitter
- ultra high speed pulsed diode lasers
- ultra high speed general purpose photodetectors
- ultra high speed visible spectrum photodetectors
- ultra high speed near infrared photodetectors
- ultra high speed high sensitivity near infrared photodetectors

Opto-Electronics' Series CD10/20 are high speed component photodetectors. They are large area, non-avalanche photodiodes used to detect high frequency CW optical signals or short optical pulses. Two photodiodes are available: 1) silicon which is sensitive in the 300 to 1,100 nanometer range, and 2) germanium which can be used up to 1,800 nanometers.

Series GD are high quality germanium diodes with photosensitive areas ranging from 70 µm x 90µm to 1,000 µm x 1,000 µm. They have the lowest dark current and highest sensitivity available with current fabrication technology. Applications include fibre optic power measurements, optical communications, IR/thermal instruments, and semi-conductor laser monitors. Appendix G gives more details.

Opto-Electronics has not considered UV or x-ray applications for their detectors.

2.5.4 Photovac Inc.
Thornhill, ON

Photvac has manufactured a selenium-iodine on platinum UV detector on special order for the French government. At the time, they did not foresee a demand for the detector. Therefore they are not produced commercially. However they are always interested in proposals. Operations involve vacuum capabilities and a small in-house R&D staff. Other products offered by Photovac include portable gas chromatographs, oxygen partial pressure sensors, and microcomputer systems.

2.5.5 Proto Manufacturing Ltd.

Old Castle, ON

Proto Manufacturing Ltd. is specialized in producing custom non-destructive testing (NDT) equipment for the automotive and aircraft industries. They are under contract to design and fabricate the engineering model of the CANMET diffractometer. Proto does not have in-house chip facilities. They are considering purchasing the silicon photodiode array from an outside supplier and assembling the required electronics to go with it.

2.5.6 Aptec Engineering Limited

Ottawa, ON

Aptec's Toronto plant manufactures high purity germanium detectors for nuclear applications. They have no experience in working with silicon.

Aptec represents United Detector Technology of Hawthorne, CA, whose product range includes:

- UV/Blue Si photodiodes
- large area Si photdetectors
- planar diffused Si PIN photodiodes
- fibre optic PIN photodiodes
- Schottky barrier photodiodes
- position sensing photo detectors

2.6 Market Information

2.6.1 Size of Market

The North American market for silicon photodiode arrays is dominated by two companies -- Fairchild CCD and EG&G Reticon -- each having 30% to 40% of the market. Texas Instruments is the third major supplier.

Fairchild and Reticon estimate the North American linear imaging array market to be $2 to $3 million (U.S.). Only 2% to 5% of this market are for x-ray applications.

2.6.2 Applications

As previously mentioned, most silicon photodiode arrays are designed to detect light in the 200 to 1,100 nanometer range. The major applications according to the three industry leaders are:

facsimile
optical character recognition
document scanning
pattern recognition
size and position monitoring
inspection and surveillance
spectroscopy

Contacts foresee the largest areas of growth as being surveillance systems, inspection, and robot vision.

Light sensitive silicon photodiode arrays can be modified to detect x-rays. Two prominent applications are scientific research and medical instrumentation. Others areas include x-ray diffraction, astronomy, small angle x-ray scattering, and synchrotrons. Because x-ray sensitive silicon photodiodes are relatively new technology and because existing methods of detecting x-rays are satisfactory, the growth potential is considered to be limited.

2.6.3 Price

The price of silicon photodiode arrays varies from manufacturer to manufacturer. It is dependent on the number of elements, the type or model, and any special requirements. Prices range from $75 (U.S.) for a 128-element Texas Instrument device to $5,000 (U.S.) for a 1,024-element Reticon device. Table V presents typical prices for silicon photodiode arrays from the three leading suppliers. Associated electronics are estimated to cost $100 (U.S.) to $2,500 (U.S.).

2.6.4 Patents

A search of Canadian patents in the subject area revealed the following items.

1) "Photodiode Detector with Selective Frequency Response" granted to Bell Canada and Northern Electric Company Limited on January 18, 1977.

2) "Buried-Channel Charge-Coupled Linear Device" granted to Fairchild Camera and Instrument Corporation on November 8, 1977.

3) "Document Scanning Head" granted to Northern Telecom Limited on May 12, 1981.

4) "Photoconductor Device for Imaging a Linear Object" granted to Northern Telecom Limited on May 27, 1981.

This search was not intended to be a rigorous one. The patents have been included in Appendix H for CANMET's perusal.

TABLE V
TYPICAL PRICES FOR SILICON PHOTODIODE ARRAYS

COMPANY	No. of Elements	Price
Fairchild	256	$80-150 (U.S.)
	1,024	633-750
	1,728	730-950
	2,048	1,300-1,500
	3,456	1,500
Texas Instruments	128	75
	1,728	600
	2,048	800
	3,456	1,500
EG&G Reticon	Series C - 256	750
	512	1,600
	1,024	3,000
	Series S - 128	495
	512	1,950
	1,024	3,800
	Series SFX - 128	1,445
	512	3,000
	1,024	5,000

PART II

STUDY TO DETERMINE THE CANADIAN MARKET FOR A PORTABLE X-RAY STRESS DIFFRACTOMETER

3.1 Objective

To conduct a market study for portable x-ray stress diffractometers in Canada. In particular:

- determine the most likely Canadian buyers of the diffractometer;
- delineate the potential buyers according to their needs;
- discuss the desired functional characteristics of the diffractometer with the buyer and ascertain their price sensitivity; and
- estimate the number of units each buyer will likely purchase over a specified period.

3.2 Scope of the Report

The report covers the Canadian market for a portable x-ray stress diffractometer. Over 60 interviews were conducted throughout Canada in various industry sectors. Budget limitations did not permit an exhaustive study of all industry sectors. The industry sectors covered were:

- research organizations and academic institutions
- petroleum (oil and gas pipelines and petrochemicals)
- railway
- automotive
- aircraft
- testing and inspection
- utilities
- steel mills

Two companies were considered known prospects and therefore were not contacted -- Ontario Hydro due to their involvement in the CANMET diffractometer study, and AECL due to previous knowledge of their requirements.

Twelve personal interviews were conducted in Ontario and Quebec because of the concentration of manufacturing activities in those provinces. We were accompanied by a CANMET technical authority on the diffractometer during these interviews. This technique proved to be very useful. Technical questions could be answered in the required detail and it allowed the client to get first-hand impressions of industry's reaction to the diffractometer.

Information gathered during the personal interviews was augmented by telephone contacts. This meant broader geographical and industry coverage. Interviews were also conducted with industry associations, companies offering competitive products, and other industry observers. Appendix I contains the interview guideline.

A few contacts were made in the United States in order to get a brief insight to the market for a portable x-ray stress diffractometer.

3.3 CANMET Portable Stress Diffractometer

The CANMET diffractometer is designed to measure elastic stress non-destructively in structures on site and in the field. Two position-sensitive detectors measure lattice strains simultaneously in two directions in a specimen, providing a measure of the relative strain difference and giving the stress directly. The diffractometer can rotate through 360 degrees on an axis normal to the specimen surface, permitting the surface stress to be measured for any orientation, and enabling the principal stresses to be detrmined. The diffractometer is connected by a 20 ft. umbilical cord to a high tension supply and to the dual detector electronic circuits. A microcomputer, remotely located, controls and operates the diffractometer, collects and analyzes the x-ray diffraction data, providing stress measurement in real time. The system is modular in design consisting of:

1. Diffractometer head with dual position-sensitive detectors, x-ray tube, and rotation mount.
2. Translation drives, X and Y parallel, and Z normal to the specimen surface, controlled by a stepping motor.
3. Detector electronics/power supply with 20 ft umbilical cord connector to the diffractometer.
4. Computer/video terminal/disk storage.
5. Mount is according to application.[1]

Figure 3 is a photograph of an early version of the diffractometer. Appendix I is the most recent brochure on the diffractometer detailing its specifications and features.

---

[1] The foregoing information was obtained from the brochure "CANMET Portable Stress Diffractometer", January, 1984.

FIGURE 3

CANMET PORTABLE STRESS DIFFRACTOMETER

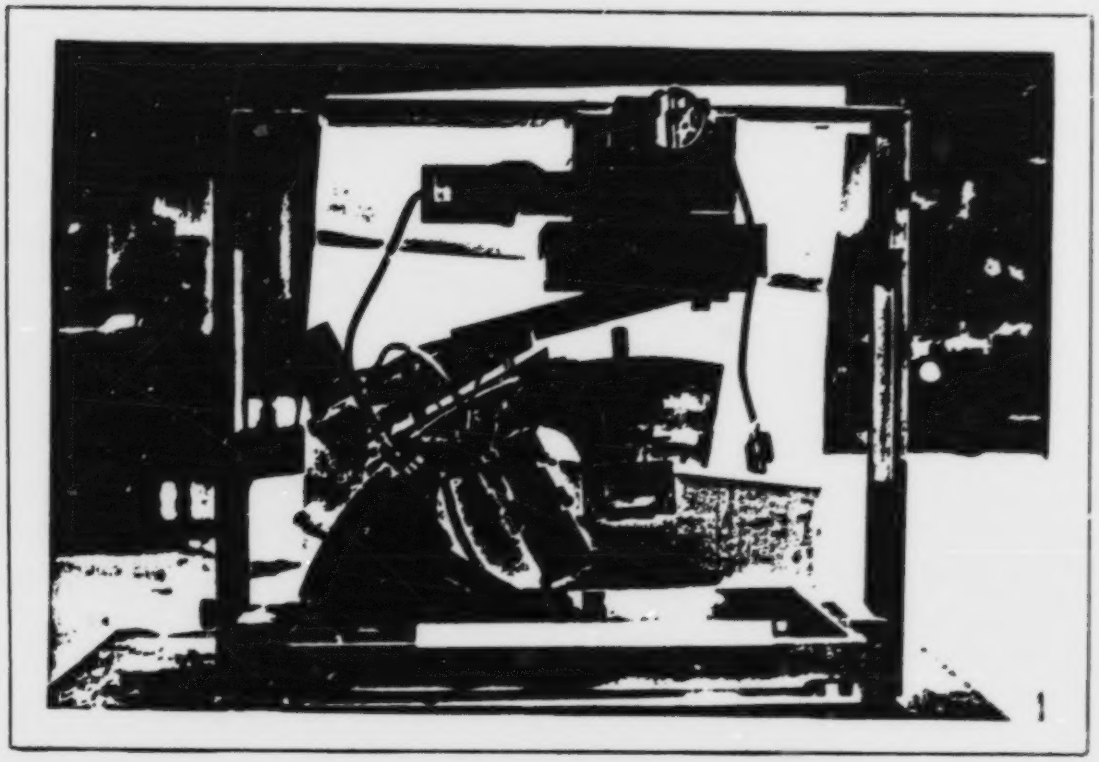

3.4 MARKET ANALYSIS

3.4.1 Market Forecast

Our survey indicates there is a limited demand for a portable x-ray stress diffractometer. Of the 57 Canadian firms contacted, five are interested in a unit. The results are illustrated in Figures 4 and 5. Table VI is a list of contacts.

Results have been extrapolated to a total population. The following assumptions are made:

1) Industry sectors are those covered in the survey.

2) Potential customers are those establishments with more than 500 employees. (In the case of research and testing firms and consulting engineers, the cut-off point was 50 employees.) These figures are based on these sources:

    i) Statistics Canada Catalogue 31-203, 1980 for the specified manufacturing sectors
    ii) Dun and Bradstreet's Canadian Key Business Directory 1984 for the specified non-manufacturing sectors
    iii) Association of Consulting Engineers in Canada directory.

   This represents a maximum number.

3) The diffractometer is largely considered to be a research and development tool. Therefore, those firms who are subsidiaries of foreign firms and rely on the parent firm's R&D work should be eliminated. Also, even for these relatively large firms, research and development may be conducted outside the firm. For these reasons, the maximum number

FIGURE 4

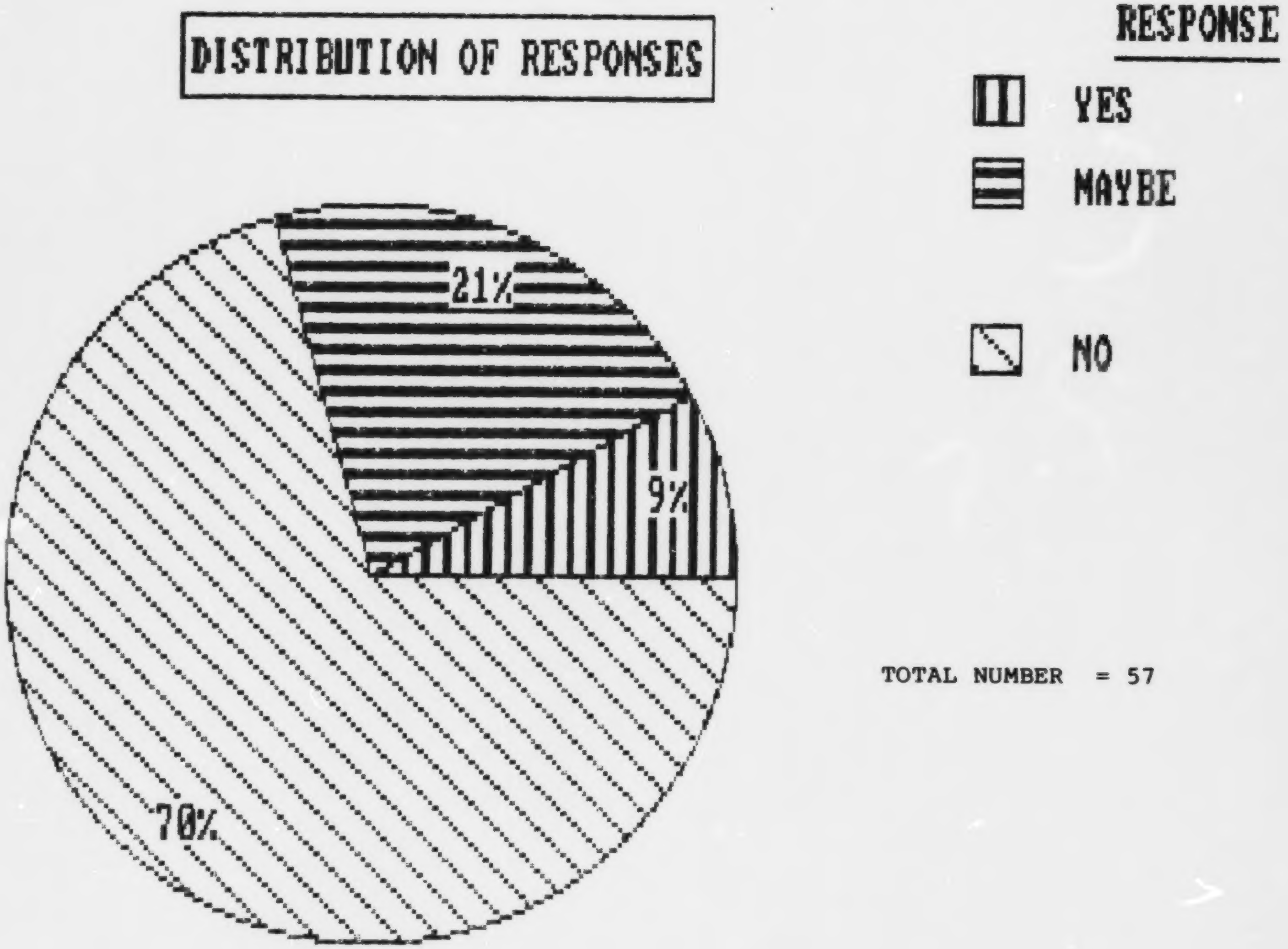
DISTRIBUTION OF RESPONSES
RESPONSE
YES
MAYBE
NO
21%
9%
70%
TOTAL NUMBER = 57

FIGURE 5

RESPONSE BY INDUSTRY

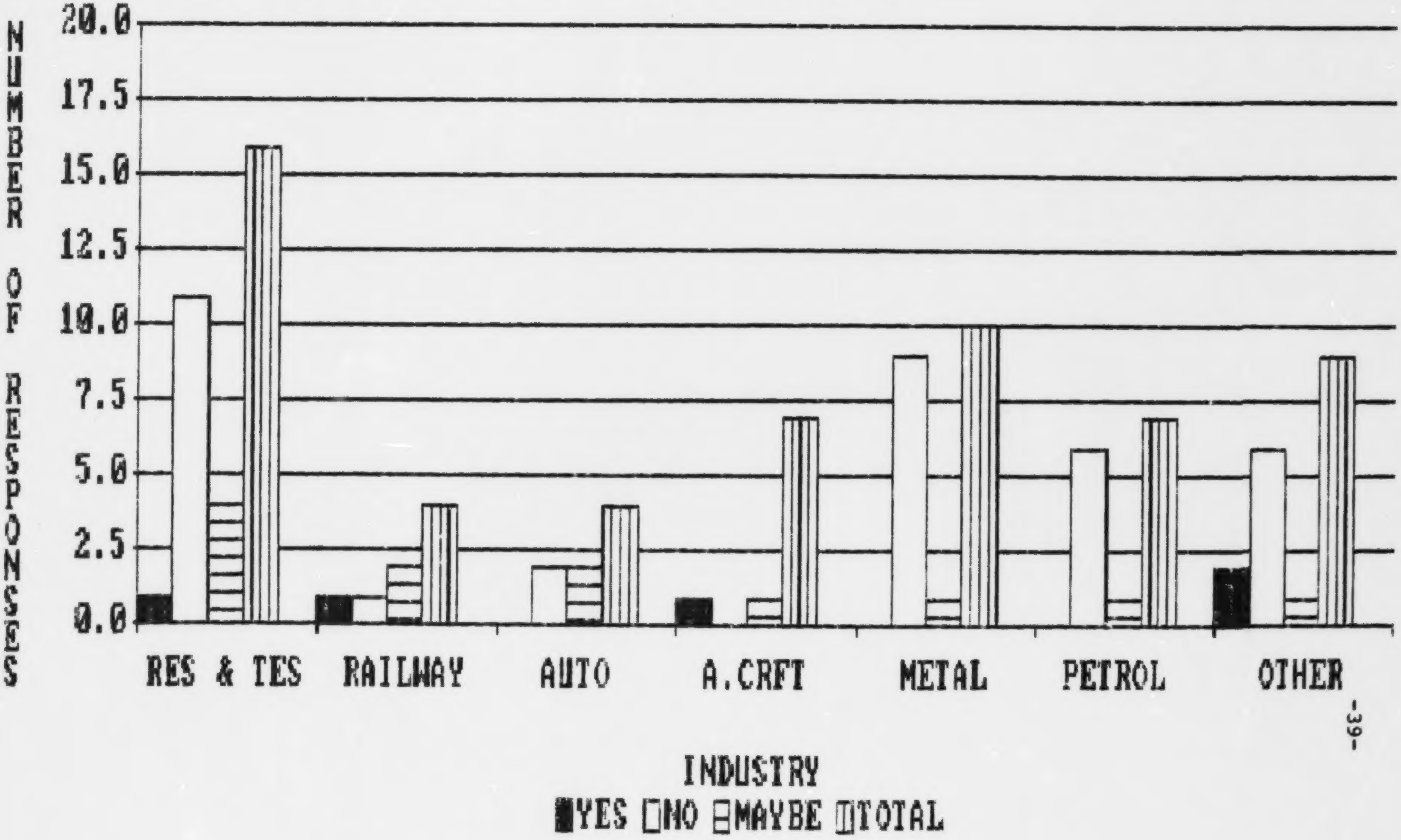

TABLE VI

LIST OF CONTACTS

COMPANY	BUSINESS	PURCHASE
MAGNAFLUX	TESTING	NO
ALTAS TESTING	TESTING	NO
AEROCON	TESTING	NO
WELD PROCESS	TESTING	NO
QUANTUM	TESTING	NO
NDT TECH.	TESTING	NO
HYDRO QUEBEC	UTILITY	MAYBE
NOVA	PIPELINE	MAYBE
WEST COAST	PIPELINE	NO
TRANSCANADA	PIPELINE	NO
CONSUMERS GAS	GAS LINES	NO
DOW CHEMICAL	CHEMICALS	NO
C.I.L.	CHEMICALS	NO
GULF RESEARCH	PETROLEUM	NO
METAL IMPROVE	SHOT PEEN	MAYBE
DOFASCO	STEEL	NO
VERSATILE VICKER	METAL FAB	NO
DOMINION BRIDGE	METAL FAB	NO
FOSTER WHEELER	METAL FAB	NO
HEPBURN	METAL FAB	NO
WELMET	METAL FAB	NO
CBI HORTON	METAL FAB	NO
AECL	NUCLEAR	NO
ELDORADO	URANIUM	NO
F.A.G. BEARINGS	BEARINGS	NO
CHROMALOX	ELECTRIC	NO
WOTHERSPOON	FOUNDRY	NO
DOFASCO	STEEL	NO
SANDVIK	TUBING	NO

COMPANY	BUSINESS	PURCHASE
SHIP REPAIR	NAVY	FREE UNIT
SYNCRUDE	MINING	YES
CN RAIL	RAILWAY	YES
CP RAIL	RAILWAY	MAYBE
PROCOR	RAIL CARS	MAYBE
HAWKER-SIDDELEY	WHEELS	NO
RAILWAY LAB	RESEARCH	MAYBE
PULP & PAPER	RESEARCH	MAYBE
ORF	RESEARCH	MAYBE
NB RESEARCH	RESEARCH	NO
U of T	RESEARCH	NO
WELDING INST.	RESEARCH	NO
NORANDA RESEARCH	RESEARCH	NO
MASSEY-FERGUSON	TRACTORS	MAYBE
FORD USA	AUTOS	MAYBE
FORD CANADA	AUTOS	NO
CHRYSLER USA	AUTOS	MAYBE
GM CANADA	AUTOS	MAYBE
AMC CANADA	AUTOS	NO
MCDONNEL DOUG	AIRCRAFT	MAYBE
DeHAVILLAND	AIRCRAFT	NO
NORTHROP USA	AIRCRAFT	MAYBE
CANADAIR	AIRCRAFT	NO
PRATT&WHITTNEY	A/C ENGINES	YES
HAWKER SIDDELEY	A/C ENGINES	NO
AIR CANADA	AIRLINE	NO
BRISTOL AERO	ROCKETS	NO
CDN GE	TURBINES	NO
WARNOCK HERSEY	TESTING	YES
HANSON MATERIAL	TESTING	MAYBE
GLENCOR	TESTING	NO

in each sector was reduced by 25% to represent a more realistic population.

4) The percentage of "Yes" respondents on the survey can be applied to the total population.

5) The percentage of "Maybe" respondents can also be applied. Only one in ten will buy a unit given its high cost.

Table VII presents the Canadian market forecast. Because the diffractometer is costly, justification and budgetting will take time. Therefore it is forecasted that these purchases will be over a five year period. A typical distribution may be:

Year 1	1 - 2 Units
Year 2	2 - 3
Year 3	3 - 4
Year 4	3 - 4
Year 5	3 - 4
Total	12 - 17

as the level of awareness and marketing increase.

These market estimates are consistent with competitive firms' experiences. Rigaku has sold only one unit in Canada and about five to ten units in the United States. American Analytical has averaged about three units per year over the last fourteen years. (See Section 3.5 Competition.)

Although an investigation of the U.S. market was not within the terms of reference for this study, a general impression of that market was obtained from interviews with relevant associations, industry observers, companies currently using x-ray diffraction for residual stress measurements, parent companies of Canadian firms, and competition. The U.S. market demonstrates characteristics

TABLE VII

MARKET FORECAST

INDUSTRY SECTOR	POPULATION (No. of Establishments)
Automotive & Machinery (Agricultural Implement Industry, Misc. Machinery & Equipment Mfr., Motor Vehicle Mfr., Motor Vehicle Pts. & Acc. Mfr.)	40 - 53
Metal Industry (Iron & Steel Mills, Steel Pipe & Tube Mills, Fabricated Structural Metal Industry)	20 - 26
Railway Industry (Railroad rolling stock, Railroad - line haul operators)	10 - 14
Aircraft Industry (Aircraft & Aircraft Parts Mfr., Certified Air Carriers)	17 - 22
Petroleum Industry (Petroleum Refining, Oil & Gas Pipelines)	13 - 17
Research & Testing (Research & Development Labs, Testing Facilities, Consulting Engineers)	21 - 28
TOTAL POPULATION	121 - 160

Based on "Yes" Response $\left(\frac{5}{57}\right)$ = 10 - 14

Based on "Maybe" Response $\left(\frac{12}{57} \times \frac{1}{10}\right)$ = 2 - 3

CANADIAN 5-YEAR MARKET FORECAST 12 - 17 UNITS similar to the Canadian market, i.e., industry sectors with applications, size of company, level of awareness, etc. The market for diffractometers in the United States may be relatively larger than the Canadian market due to a higher level of R&D effort, greater military applications, number of electric utilities, etc. Automotive and related industries represent over half the U. S. applications.

3.4.1.1 Stress Measurement Service

An examination of the market for a service providing stress measurements was not within the present study's terms of reference. However, due to the high cost of the unit, many contacts stated that such a purchase would be difficult to justify in terms of their present activities, or they had higher priorities for capital expenditures. Many of these contacts expressed interest in utilizing a service if it existed. This service should not just be rental of equipment. Rather, it should involve qualified personnel examining individual applications, setting up and operating the unit, and reporting and interpreting the results. Respondents indicated that the frequency of use of this service would be sporadic -- once a year, or once every two years.

3.4.2 Canadian Buyer Profile

The typical end users of an x-ray diffractometer are in these positions -- metallurgist, stress analyst, NDT/NDE specialists. It is these individuals who are most directly involved in the justification and specification stage of purchasing a diffractometer. Senior management such as head of engineering, is responsible for allocating funds for such a unit due to its high cost.

The typical end use of an x-ray diffractometer is in support functions such as problem solving or design. These areas are not generally considered a profit generating group, making justification of such capital expenditures more important and difficult.

The best sales prospects are aware of residual stress and familiar with measurement techniques. In our survey half the respondents had used some type of stress measurement. Many of the negative responses were unaware of stress measurement techniques, particularly x-ray diffraction. Sales to this population will initially require a buyer education program.

Table VIII is a contact summary of interested respondents. Note that "interested" includes:

i) those who said they are interested in buying a unit;
ii) those who expressed interest in the unit but were hesitant because of price; and
iii) those who were not interested in buying a unit but expressed interest in using a service.

The buyer population is a spectrum of buyers with varying requirements as evidenced in Table VIII with respect

TABLE VIII

CONTACT SUMMARY OF INTERESTED RESPONDENTS*

COMPANY	BUSINESS	STRESS TECH.	APPLICATION	LOCATION	MATERIALS	PORTABILITY	KSI	CABLE	OPERATOR	CONTROL	OUTPUT	PURCHASE	PRICE
SHIP REPAIR	NAVY	HOLE DRILLING	SUBMARINE HULLS			HIGH						FREE UNIT	
SYNCRUDE	MINING	STRAIN GAUGE	EQUIPMENT	FIELD	VARIES	HIGH	→1	100m	ENGINEER	LOW	LOW	YES	100,000
CN RAIL	RAILWAY	DRF-XRD	FAILURE ANAL	LAB/PLANT	S.IRON	MEDIUM		10m	TECH.			YES	
CP RAIL	RAILWAY								TECH.			MAYBE	
PROCOR	RAIL CARS	NO	WELD R&D	LAB	STEEL	LOW	→2					MAYBE	
RAILWAY LAB	RESEARCH	NO	R&D	FIELD		HIGH	→0.1			HIGH	HIGH	MAYBE	
PULP & PAPER	RESEARCH	NONE	WELD PLATES	LAB/FIELD	STEEL	HIGH			ENGINEER	HIGH	HIGH	MAYBE	50,000
ORF	RESEARCH	GE-XRD	SERVICE	LAB		LOW			ENGINEER	HIGH		MAYBE	
NB RESEARCH	RESEARCH	NO	FAILURE ANAL	LAB		LOW	→2		TECH.			SERVICE	
MASSEY-FERGUSON	TRACTORS	DRF-XRD	FAILURE ANAL	LAB	ALLOY S	LOW			ENGINEER	HIGH	HIGH	MAYBE	
FORD USA	AUTOS	FASTRESS	FAILURE,R&D	LAB	STEEL	MEDIUM			ENGINEER	HIGH	HIGH	MAYBE	
CHRYSLER USA	AUTOS	FASTRESS	FAILURE,R&D	LAB	STEEL	LOW	→5		ENGINEER	HIGH	HIGH	MAYBE	60^80,000
GM CANADA	AUTOS	FASTRESS	R&D	LAB		LOW						MAYBE	
MCDONNEL DOUG	AIRCRAFT	NO	SALVAGE	LAB/PLANT	AL,TI,SS	MEDIUM			TECH.	HIGH	HIGH	MAYBE	
NORTHROP USA	AIRCRAFT	FAST/RIGAKU	R&D	LAB	AL,TI,S	MEDIUM			ENGINEER			MAYBE	
PRATT&WHITTNEY	A/C ENGINES	GE-XRD	R&D	LAB	TI,S,NI,AL	LOW			ENGINEER	HIGH	HIGH	YES	
HAWKER SIDDELEY	A/C ENGINES	HOLE DRILLING	R&D	LAB		LOW						SERVICE	
CDN GE	TURBINES	HOLE DRILLING	INSPECTION	PLANT/FIELD	STEEL	HIGH	→2		TECH.	LOW	LOW	SERVICE	TOO HIGH
WARNOCK HERSEY	TESTING	NO	INSPECTION	FIELD	S,BRONZE	HIGH	→2		ENGINEER	HIGH	LOW	YES	50,000
HANSON MATERIAL	TESTING	NO	INSPECTION	FIELD		HIGH	→0.5		ENGINEER			MAYBE	<50,000
GLENCOR	TESTING	NO	WELD INSPECT	FIELD		HIGH	→2	20m+	ENGINEER	HIGH	HIGH	SERVICE	
HYDRO QUEBEC	UTILITY	BARKHAUSEN	INSPECTION	PLANT	STEELS	HIGH	→2	25m	ENGINEER	HIGH	HIGH	MAYBE	
NOVA	PIPELINE	SPLIT RING	WELDS	FIELD	STEEL	HIGH	→2	10m	TECH.	LOW	LOW	MAYBE	
WEST COAST	PIPELINE	NO	WELD INSPEC	FIELD		HIGH	→2	10m				SERVICE	
CONSUMERS GAS	GAS LINES	NO	INSPECTION	FIELD		HIGH						SERVICE	
GULF RESEARCH	PETROLEUM	NO	R&D/INSPEC	LAB/FIELD	S,BRASS	HIGH	→1	20^200	ENGINEER	HIGH	HIGH	SERVICE	TOO HIGH
METAL IMPROVE	SHOT PEEN	NO	PRODUCTION	PLANT	S,TI,AL	MEDIUM	→5	10m	TECH.			MAYBE	<50,000
DOFASCO	STEEL	HOLE DRILLING	R&D	PLANT		MEDIUM						SERVICE	

*This includes companies who were positive, undecided, or interested in the service.

to industry and application. This trend was also apparent in a previous study on the x-ray diffractometer, see Figure 6. Desired functional characteristics are discussed later in Section 3.4.4.

Prospective buyers have similar company characteristics. They tend to be large companies, i.e., over 500 employees. (This also was the case in the earlier study, see Figure 7 .) The exception is research and service firms although, here too, it is the larger firms, i.e., over 50 employees. The companies generally have research and design capabilities or metallurgical facilities. The products being tested are those with low design safety factors, e.g., aircraft and automotive industries, or those with welds under pressure or corrosive environments, such as pipelines and process plants.

Our survey identified these companies as good prospects for purchasing the CANMET portable stress diffractometer:

1) Syncrude, Edmonton, Alberta
2) CN Rail, Montreal, Quebec
3) Pratt & Whitney, Montreal, Quebec
4) Warnock Hersey, Mississauga, Ontario
5) Ship Repair Unit Atlantic, CFB Halifax, Nova Scotia

FIGURE 6

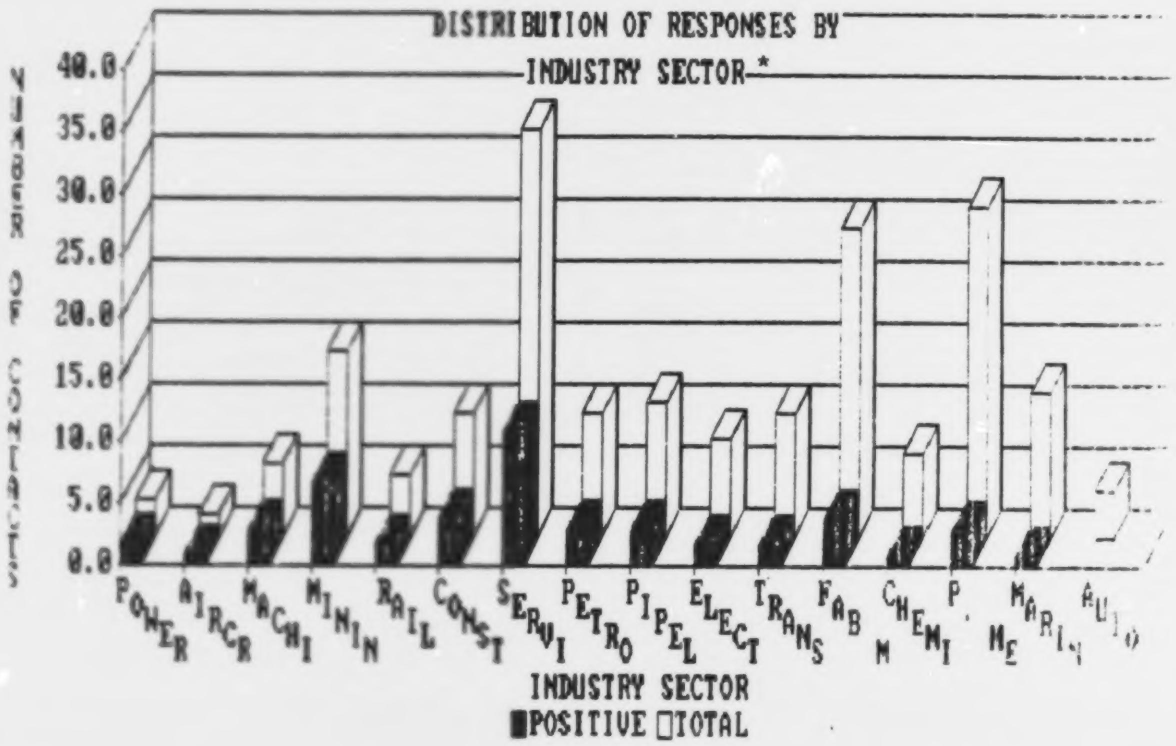

FIGURE 7

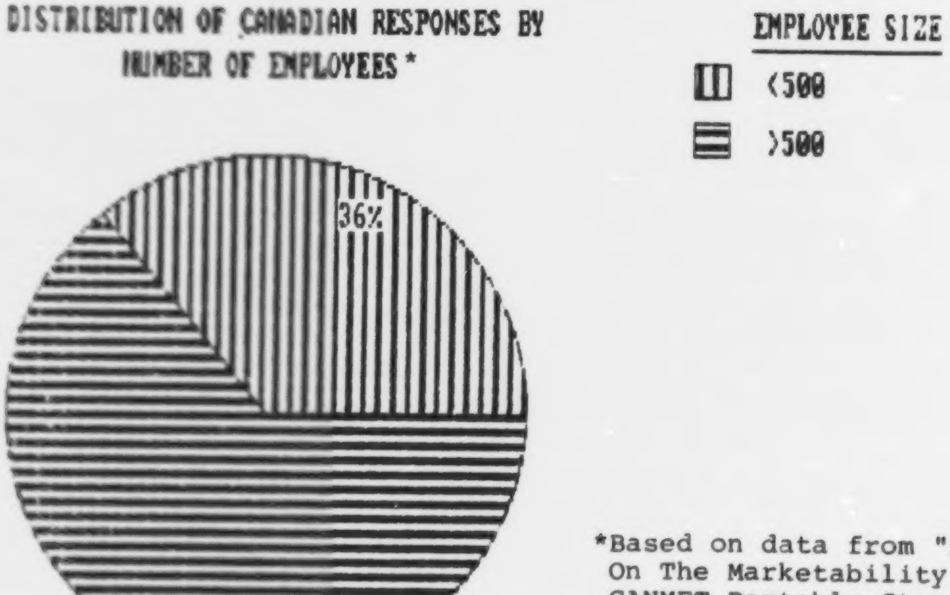

*Based on data from "Report On The Marketability of the CANMET Portable Stress Diffractometer", Hitech Canada Ltd.

3.4.3 Purchasing Decision

Creation and the realization of the need for the unit is the first step in the purchasing decision. Contacts exhibited a low level of awareness of the technique and available technology along with an attitude of ignoring surface stresses. (Previous attitudes towards residual stress have been: 1) to replace component when failure occurs; 2) to overdesign the component; and 3) to assume stress relieving techniques have worked.) Therefore, educating potential buyers will be a major activity. Two levels of education need to be achieved. The first level is to inform people of the problems surface stresses cause and why they should measure them. The second level is to inform people of the existing technology and its advantages.

Once a need is established, a potential buyer must justify to himself and to his superior the expense of the unit. In larger companies often more than one department has potential applications for the unit. If these groups are brought together initially to discuss their requirements, justification may be easier. Thus, it is important to inform other potential users within the organization of the possible purchase. It is likely that a purchase of this magnitude will require advance budgeting and must be supported with adequate arguments in its favour.

The specifications for the unit will be determined to meet the operational characteristics as laid out in the justification step and meet the budget limits. The end user will proceed to investigate all the potential units available. With the small number of systems on the market this is easy to achieve. Most contacts said they would want to visit an operating system and perhaps hire a service firm with such a unit to do some measurements for them on site.

After careful analysis the final purchase decision is made. Once the unit has been purchased, support must be provided to ensure customer satisfaction. Future sales depend on a good track record. The lack of support or service is a common complaint of the two manufacturers (Rigaku and American Analytical) who have supplied the market to date.

3.4.4 Functional Characteristics

Applications:

Most applications were in the following areas: Research & Development, Inspection of critical welds, and Failure analysis. Only two contacts foresee use in a production setting. Over half of the respondents stated the unit would be used in a laboratory setting. Welding and repair inspection are applications that would occur in the field or plant. Plant applications were generally considered to be an extension of laboratory or field applications.

Portability:

Fifty percent of the respondents want a high level of portability. The ability to mount the instrument vertically or in other orientations is a definite advantage in field and plant applications. Some laboratory groups see portability as an advantage in increasing the potenial use of the unit and therefore improving justification. Low or no portability is desired by 30% of the respondents, most of whom are involved in strictly lab applications.

Accuracy:

The present accuracy of ± 2 ksi is accepted by most respondents. A few wanted accuracies of ± 1 ksi or ± 0.5 ksi.

Cable Length:

The 10m cable length is generally sufficient. It is suggested that extensions could be supplied to those requiring greater lengths.

Operator:

Due to the cost of the equipment and the knowledge of x-ray diffraction required to ensure meaningful results, most respondents stated that operating personnel were likely to be engineers, scientists, or senior technologists.

Environment:

Since many contacts regard the diffractometer as a laboratory tool, environment does not pose a problem. However field applications are subject to temperature extremes of -30 to 40 degrees C. Plant applications could be exposed to steam, dust, or corrosive/explosive atmospheres.

Materials:

Steel is the most common material to be tested ranging from plain carbon steels to low and high alloy steels to stainless steels. Aluminum and titanium are common in the aerospace industry. Brass and bronze are found in the process industries.

Control and Output:

Most respondents want a high level of control and data presentation without being swamped with data. Companies that anticipated field work expressed interest in a simple strip chart or raw data storage on a floppy to reduce the bulk of the system.

After Sales:

This has been a complaint of competitive units. Respondents generally are interested in an extended service plan that would provide a loaner unit during repairs. Companies involved in field or production applications require very fast service.

Price Sensitivity:

Two price groups exist. One group is willing to spend $100,000 once the unit has been justified. The other group is only interested in a unit if the price is $30,000. This group may be interested in using a service company.

3.4.5 Marketing Strategy

A major obstacle to the marketing of x-ray diffractometers is the level of awareness of potential buyers. Residual stresses are often ignored, assumed not to pose any problems due to overdesign, or relieved by methods assumed to perform the task. Therefore, successful marketing of an x-ray diffractometer requires educating the buyer population in two areas -- 1) residual stress and, 2) x-ray diffraction methods of measuring residual stress. This can be accomplished through seminars, technical papers, application notes, generic brochures, etc. Education at the levels indicated can be a costly exercise for a commercial company. It should only be undertaken for a limited number of potential buyers.

Due to the spectrum of potential industry sectors, this education process should be targetted at position titles such as stress analyst, metallurgist, NDT/NDE supervisor, etc.

The best marketing tool is prior experience. In the case of stress diffractometers, the techique must be proven in diverse applications before it will be widely accepted.

Competitive units often have similar features -- modular design to allow for relatively easy customization of the unit, portability, high speed, and flexibility. Therefore, it is important to delineate your unit from the competition. The question -- "What makes it different?" -- was asked many times during our interviews.

In conclusion, the success of the CANMET portable stress diffractometer will depend on a strong marketing campaign with a significant educational component, in at least the initial stages.

3.5 Competition

Competition for CANMET's portable stress diffractometer will come from two sources: 1) other portable units on the market, and 2) existing stationary units for laboratory applications. The following sections describe competitive products.

3.5.1 Rigaku "Strainflex"

Rigaku is a Japanese x-ray and thermal analysis equipment manufacturer.

They manufacture two models: the wheeled stand mounted MSF-2M and the potable PSF-2M. The two models consist of the same modular components (Goniometer, x-ray generator, control data processing unit, and heat exchanger) with different mounting configurations. See Figure 8 . The unit uses the Sine-Square-Psi multi-exposure technique with an oscillation feature for large grain measurement. The system has a built-in software package to produce a strip print-out of data. An output capability to computers (user supplied) is available. Table IX details the unit's specifications.

Options include: strip chart recorder, retained austenite measuring attachment, back reflection camera, electrolytic polisher, and custom stands.

FIGURE 8

RIGAKU "STRAINFLEX

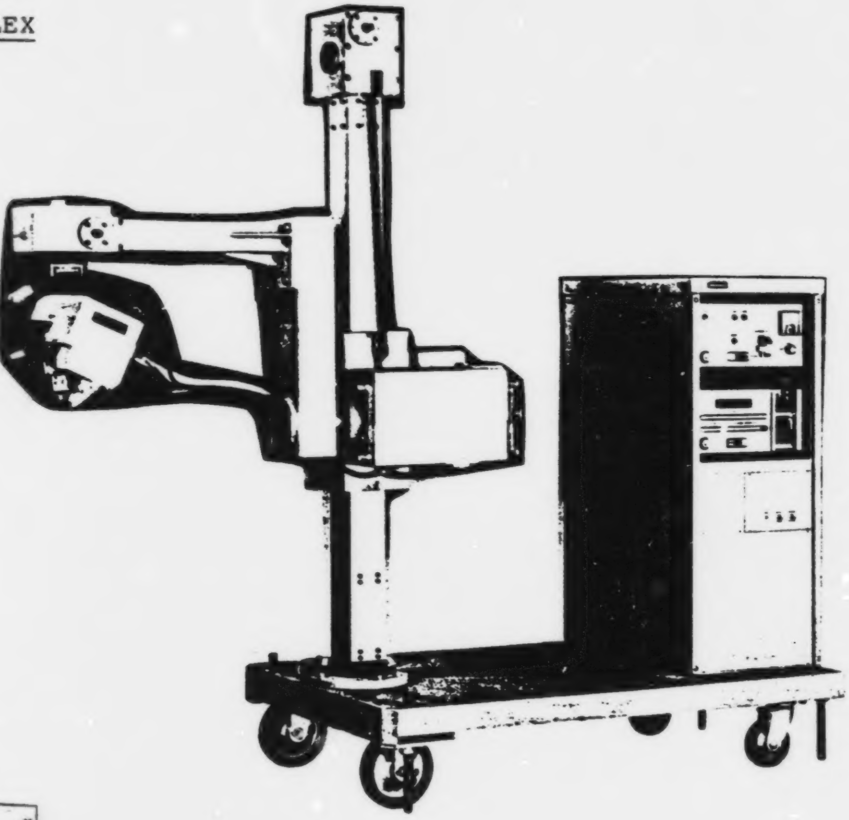

MODEL MSF-2M

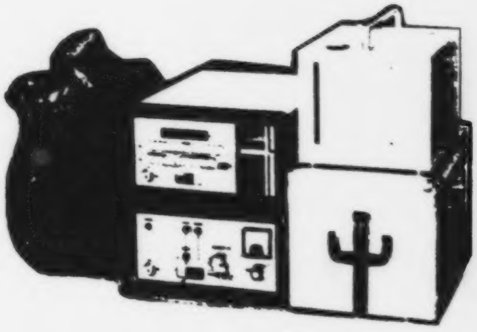

-in storage

MODEL PSF-2M

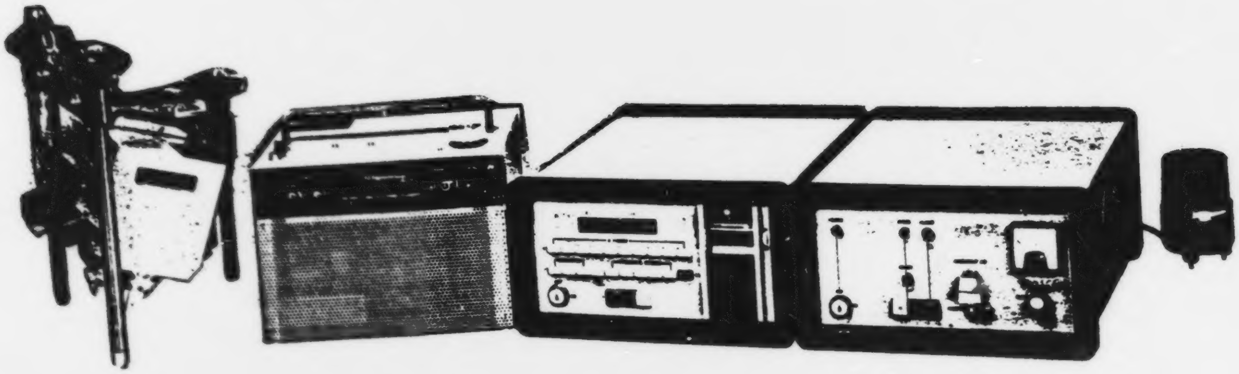

TABLE IX

SPECIFICATIONS OF RIGAKU'S "STRAINFLEX"

	MSF-2M	PSF-2M
Goniometer 2905G1	The iso-inclination method, side-inclination method, oscillation method, and $\theta - 2\theta$ method are available. (Utility Model No.1016485, U.S.Pat.No.3634686) $2\theta = 140° \sim 170°$ ($120° \sim 150°$: option)	
X-ray generator 4005A1	30 kV (constant potential), 2 ~ 10 mA continuously variable, solid-state negative feedback control	
Control/data processing unit 5072S2	Once the goniometer is set up, the microprocessor will select optimum measuring conditions and execute measurement for printout of the final data. Incident angle selection: 0°, 5°, 10°, . . . 40°, 45°; 10 steps Sample selection: Fe, SUS, Aℓ, Cu, other Oscillation: OFF, ± 3°, ± 5°, ± 7° Operation: Peak search, output of the stress value, quantitation of retained austenite	
Detector 5721S1	Scintillation counter probe	
X-ray tube 9432	One out of Cr, Co, and Cu. Cr unless specified. Max. load: 30 kV, 10 mA	
High voltage cable 4262S1	10 m, 1 pc	
MSF Stand for Medium Structure 2905S1 **PSF Stand for Field Operation 2912S2**	Patent pending (U.S.Pat.No. 3868506, U.K. Pat.No.1390710) Allows measurement in X-Y directions, and the iso-inclination method and side-inclination method. A measuring device for two-dimensional stress distribution is newly added.	Suitable for field operation as well as for use as a desktop stand. (Pat.No.991292)
Heat exchanger 4810A1	Compact type self-containing a radiator equipped with forced air cooling fan.	

The unit as sold by Radonics Scientific in Canada costs $72,000 to $100,000 (Cdn). In Canada only one unit has been sold. It is owned by the Defence Research Establishment Pacific. The United States market is also small with only 5 units accounted for by contacts. The United States model is limited in its capabilities apparently by pantent restrictions. In Europe and Japan the unit is very popular and has sold well.

Contacts who use Rigaku units were pleased that custom-made units were available with many features but found the unit under-engineered and after sales service poor. Read-out time is slow, taking 10 to 40 minutes. The Rigaku unit also suffers from the inability to update software unless the user supplies a computer and writes his own software.

The Rigaku unit will represent competition in lab applications where low cost is an important factor. It is too slow for much production work and its poor construction limits its field use -- but again, low cost will attract some users.

Appendix K gives additional details on the unit.

3.5.2 Technology for Energy Corporation (TEC) "1600 Systems"

TEC is the exclusive licencee for the "PARS" technology as developed by Dr. Jerry Cohen of Northwestern University. The PARS technology is sold in 1,600 systems.

Three configurations exist: Model 1600 Stationary System, Model 1610 Mobile (Wheeled) System, and Model 1620 Portable System. Like the Rigaku, each system consists of common components packaged to the appropriate application. See Figure 9. Common components are: Manual Diffractometer, collimater and shutter, x-ray source, power supply and recirculating heat exchanger, position-sensitive proportional

FIGURE 9

TEC DIFFRACTOMETER

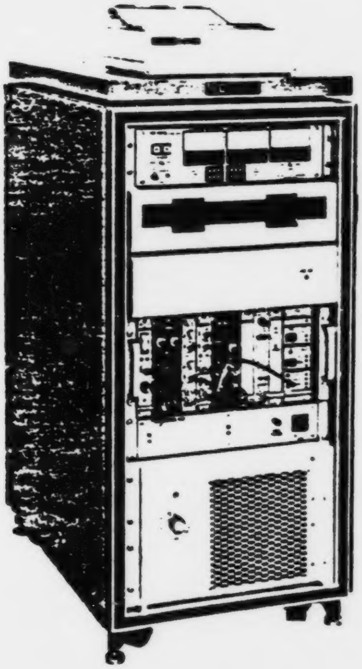

Model 1600 Stationary System

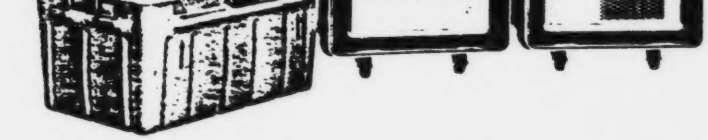

Model 1620 Portable System

counter with electronics, PDP 11/03 computer with dual floppy disks, printer-plotter, graphics display screen, x-ray safety system, and the TEC Stress Analysis Monitor software system.

The Sine-Square-Psi multi-exposure technique is used. The system can read in 10 to 120 seconds.

TEC offers a wide range of options which are: Diffractometer Motor Drive (allows for Psi oscillation), Psi-angle encoder, Computer-controlled Robot Arm, 115/230 volt Power Distribution systems, watertight instrument enclosure, alignment telescope and alignment jigs, retained austenite accessory, training courses, extended service contract, software update, and user's groups.

TEC never disclosed their price but other contacts have stated it is $150,000 to $200,000 (U.S.). It is rumoured that TEC has sold two units at $90,000 (U.S.) each but that may have been at a reduced price.

TEC has been offering a stress measuring service with their equipment since August, 1983. This has proven popular with utilities.

So far TEC has sold very few units. Caterpillar Tractor has apparently had limited success with the production inspection units which TEC helped them to build. TEC has also sold a unit to the Redstone Arsenal. They have been havng problems selling to high technology industries such as aerospace.

To overcome problems in some industries they have aimed their marketing at NDT/E users through organizations such as ASTM and ASM, and by advertising in magazines such as Materials Evaluation.

The TEC unit represents the greatest competition to the CANMET unit. TEC has a 3-year jump in development and marketing of their system along with access to the United States civilian and military market.

Appendix L has more information on the TEC units.

3.5.3 Denver X-Ray Instruments (DXI)

DXI is marketing the unit developed by Dr. Clayton Ruud of Pennsylvania State University. Presently no brochures are available describing its commercial configuration. Once units are sold they will put together a brochure. They claim to have orders for 2 systems and it will take 6 months to fill each order.

The unit uses the single exposure technique with two fibre optic x-ray sensors that send the signal to an electronic detector. The detector head is claimed to fit inside a 4" diameter pipe. System accuracy ranges from ± 1½ ksi to ± 5ksi. The system uses the PDP 11/23 computer. Reading time can be as fast as 1 second, but typical times are 10 to 20 seconds. The present prototype has 6 degrees of freedom but it is likely the commercial unit will only have 2 degress of freedom.

The unit will sell from $120,000 to $130,000 (U.S.) for a basic system. They foresee selling 5 in the next year, 5 to 10 per year for the next 2 to 3 years and then 50 in the following 2 years.

DXI could represent serious competition with what seems to be a fine instrument. While the instrument has been in use at Penn State for 3½ years it has been actively marketed. This puts it in a time frame of 1 to 2 years ahead of the CANMET unit.

3.5.4 American Analytical "Fastress"

This unit while not technically portable, does represent comptition in laboratory and some plant applications. It is light enough that it can be transported within a plant.

The unit was originally developed by General Motors in 1967 and is manufactured under licence by American Analytical. (See Figure 10) It uses 2 x-ray tubes and 2 detectors to rapidly obtain the data. Readings take 10 to 120 seconds. In a go-no-go mode it can perform production line tests. Two models are available; the Model 1200 Residual Stress Measurement Analyzer costing $63,500 (U.S.) and the Model 1300 Residual Stress Measurement and Retained Austenite Analyzer costing $84,040.

In the past 12 years over 40 units have been sold, half of them to the automotive industry. (See Appendix M.)

The unit is noted to be old technology and service is a problem. It is still relatively fast though and its low price as well as years of refinement have given it a niche in the laboratory market and some plant applications. It still can represent competition in those applications.

Appendix M gives further details.

3.5.5 Siemens-Allis

Siemens-Allis are known as manufacturers of laboratory diffractometers. They have added a portable goniometer to their product line. No brochure seems to be available and most people in the industry think Siemens is not a force in the x-ray diffractometer market place. Their D500 diffractometer

FIGURE 10

AMERICAN ANALYTICAL'S

"FASTRESS"

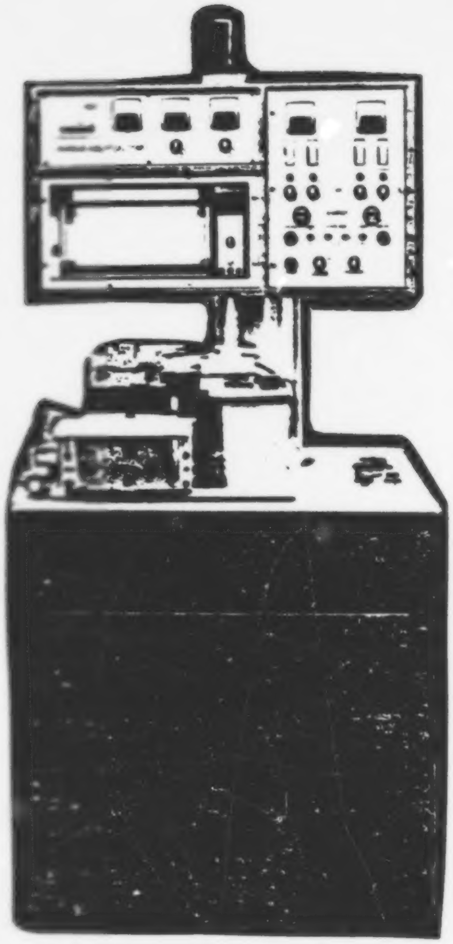

is not portable and only suited for laboratory applications where the unit would be used for more than just residual stress measurement.

Appendix N provides information from Siemens on x-ray measurement of residual stress on pipelines and pipe joints.

Table X is a comparison of existing units by Charles Gazzara of the U.S. Army. The table was published in 1983 but assembled in 1981. The Denver Research Institute unit and Penn State unit are similar. The TEC unit is a successor to the "PARS" unit. Uvlt stands for the Watervliet Arsenal where a custom-made automated x-ray diffractometer is used.

3.5.6 Competitive Technology

The use of X-ray diffractometers for residual stress measurement faces competition from other methods. Four competitive technologies were encountered during the study: neutron diffraction, hole drilling, ultrasonics, and Baukhausen. Each method is briefly discussed below based on comments from contacts.

Neutron diffraction is similar to x-ray diffraction except high energy neutrons are used. As such, neutrons are only available at reactors. The technique is not portable. It is non-destructive and can measure beneath the surface (3cm in steel, 20 cm in aluminum). At least 4 facilities in North America are starting to supply the service: Chalk River, Washington, D.C., Missouri, and Argonne Lab. in Illinois. The facilities can handle quite large items.

Hole drilling involves measuring the stress with strain gauges before and after the material is stress relieved by drilling a small hole. The technique is well refined and

TABLE X

COMPARISON OF X-RAY DIFFRACTION RESIDUAL STRESS SYSTEMS

	Rigaku	Fast Stress	DRI	GE/DIANO	Siemens	"PARS" (J.B. Cohen)	Wvlt.	TEC (Hendricks)	Penn St. (Ruud)
Portability	Yes	No	?	No	No	Yes	No	Yes	Semi 1
Specimen Adaptability	Flexible	Flexible	Flexible	Not Flexible	Flexible	Flexible	Flexible	Flexible	Flexible
Line-up Adaptability	Excellent	Good	Fair	Fair	Fair	Excellent	Fair	Excellent	V. Good 2
Resolution*	<0.01°	0.01°	0.05°	<0.01°	<0.01°	~0.05°	<0.01°	>0.02	>0.02
Availability	Yes	Yes	No	?	Yes	?	Custom Made	Special Order	Special Order
2θ Range	140-170°	-	155-175°	0-165°	-	?	115-160°	Flexible	Flexible
Reading Time **	10 min.	2 min.	20 sec.	20 min. 2 hrs	10 min.	~20 sec.	15 min. 1 hr.	20 sec.	15 sec.
Setting Angles	Automatic	Automatic	Manual	Manual	Manual	Automatic	Automatic	Automatic	Single Exposure
Specimen Surface	Large 16mm	Small 7mm	v. small 1mm	v. lge. 30mm	-	-	Variable	Variable	Variable
Tube Power	300 watts	1000 watts		1000 watts	1000 watts	150 watts Air Cooled	700 watts	100 watts Air Cooled	~2000 watts H_2O Cooled 3

* Resolution dependent on distance from target to specimen [TEC and Penn State University have 60μM resolution of detector, same as DRI, PARS-i (180μM)]

** These times are given as indications of the reading time magnitude. Times vary depending upon individual specimens.

1. Changed to 'Yes'
2. Changed to 'Excellent'
3. A 120 watt unit is available

Source: The Measurement of Residual Stress With X-Ray Diffraction, by C. Gazzara relatively inexpensive. Being semi-destructive creates problems. The hole drilling can cause plastic deformation and product erroneous results. The part thickness must be at least 4 times the hole diameter. High stress gradients also can not be measured. The technique's major advantage over x-ray diffraction is price but it takes longer and the chance of error is greater.

Ultrasonics and Baukhausen are both techniques in the research stage. Ultrasonics represent the most likely potential competition in the future according to contacts. The technique, once perfected will offer bulk stress measurement in a portable package. Baukhausen is a less promising technique capable of working only on the surfact of ferro-magnetic materials. Contacts did not see much hope for this technique in the future.

Table XI is a summary of the major portable techniques.

In conclusion the effective competition consists of 4 firms each with specific advantages. Rigaku can sell on portability with low price: American Analytical with low price, shop mobility, and a track record. TEC has a modern unit with a jump on marketing. DRI has an excellent instrument with marketing beginning. All of these units also have a larger domestic market (U.S.A. or Japan) to base sales on than the CANMET (Canada) unit.

TABLE XI

Selection of residual stress measurement methods

Method	Non-destructive	Reliability	Bulk stress	Stress direction	Resolution	Cost*	Portability	Speed
Stress relief techniques (mechanical methods)	No	Good	Yes	Yes	$\sim 4\ \mathrm{mm}^3$	1 to 10	Yes	Poor
Hole drilling	Partially	Good	No	Yes	$> 30\ \mathrm{mm}^3$	1	Yes	Poor
X-ray diffraction	Surface	Good	No	Yes	$< 1\ \mathrm{mm}^3$	0.1 to 1	Yes	Poor to excellent
Ultrasonics	Yes	Poor	Yes	Yes	$> 5\ \mathrm{mm}^3$	< 0.1	Yes	excellent
Barkhausen noise	Surface	Poor	No	Yes	$> 10\ \mathrm{mm}^3$	< 0.1	Yes	excellent

* These estimated costs per reading are mainly for labour and do not include cost of equipment. They are normalized against the cost per reading of hole drilling.

Source: A Review of Nondestructive Methods for Residual Stress Measurements, C. O. Ruud. Society for Experimental Stress Analysis, 1981

3.6 Selected Bibliography

1. Noyan, I. C., and J. B. Cohen. The Nature of Residual Stress and Its Measurement, Residual Stress and Strain Relaxation. Sagamore Army Materials Research, Conference Proceedings #28, July 13-17, 1981, 1-17

2. Weiss, V., Y. Oshida, and A. Wu. A Note on Fatigue Damage Assessment by X-ray Diffraction Techniques For A 304L Stainless Steel Specimen. Journal of Nondestructive Evaluation, 1980, 207-213.

3. Doig, P., and P. E. J. Flewitt. Nondestructive Stress Measurement Using X-ray Diffraction Methods. NDT International June 1978, 127-131.

4. Mordfin, L. Measurement of Residual Stresses: Problems and Opportunities. Residual Stress For Designers and Metallurgists - ASM Materials/Metalworking Technology Series, April 9-10, 1980, 189-210.

5. Ruud, C. O. X-ray Analysis and Advances in Portable Field Instrumentation. Journal of Metals, June 1979, 10-15.

6. --- and D. J. Snaha. Displacement Errors in Application of Portable X-ray Diffraction Stress Measurement Instrumentation. Journal of Metals, February 1984, 32-38.

7. --- Position-sensitive Detector Improfes X-ray Powder Diffraction. Industrial Research and Development, January 1983, 84-87.

8. --- A Review of Nondestructive Methods For Residual Stress Measurement. Society for Experimental Stress Analysis, Spring Meeting Proceedings, 1981, 175-178.

9. ---, P. S. Di Mascio, and D. M. Melcher. Application of a Position Sensitive Scintillation Detector for Nondestructive Residual Stress Measurements Inside Stainless Steel Pipe.

10. --- A Review of Selected Nondestructive Methods For Residual Stress Measurement. NDT International, February 1982, 15-23.

11. James, M., and J. B. Cohen. "PARS" - A Portable X-ray Analyzer For Residual Stress. Journal of Testing and Evaluation, JTEVA, March 1978, 91-97.

12. Gazzara, C. P. X-Ray Residual Stress Measurement Systems For Army Material Problems. Residual Stress and Strain Relaxation, Sagamore Army Materials Research Converence Proceedings #28, July 13-17, 1981, 369-389.

13. Bazzara, C. P. The Measurement of Residual Stress With X-ray Diffraction. Arm. Materials and Mechanics Research Center, Watertown, Mass., 1983.

14. --- A General Purpose Residual Stress Analyzer. Army Materials and Mechanics Research Center, Watertown, Mass., 1983.

15. Moskel, M. D. Measurement of Residual Welding Stresses in a Continuous Digester. Corrosion Problems in the Pulp and Paper Industry, Volume 5. National Association of Corrosion Engineers, Houston, Texas, 1983, 32-36.

16. --- and G. W. Eggeman. The Effect of Residual Stresses on Corrosion Fatigue of Suction Press Rolls. Corrosion Problems in the Pulp and Paper Industry, Volume 3. National Association of Corrosion Engineers, Houston, Texas, 1977, 94-99.

17. Rinik, C., J. E. Hilliard, and J. B. Cohen. SOL-X: An On-line Nondestructive Method for Measuring Grain Size With X-rays. Journal of Nondestructive Evaluation, Volume 2, No. 2, 1981, 133-138.

18. Maeder, G., J. L. Lebrun, and J. M. Spravel. Present Possibilities For The X-ray Diffraction Method of Stress Measurement. NDT International, October 1981, 235-247.

19. Shibata, M., and K. Ona. Magnetomechanical Acoustic Emission - a New Method For Nondestructive Stress Measurment. NDT International, October 1981, 227-234.

20. Allen, A., C. Andreani, M. T. Hutchings, and C. G. Windsor. Measurement of Internal Stress Within Bulk Materials Using Neutron Diffraction. NDT International, October, 1981, 249-254.

21. Chant, M. J., R. A. Griffiths, and L. Miles. Comparison of Two Methods of Measuring Residual Stresses Arising From Surface Treatment. Journal of Mechanical Working Technology, 1983, 181-191.

22. Witt, F., F. Lee, and W. Rider. A Comparison of Residual Stress Measurements Using Blind Hole, Abrasive Jet and Trepan Ring Methods. Society For Experimental Stress Analysis, Spring Meeting Proceedings, 1981, 73-78.

23. Parlane, A. S. A., et al. Residual Stresses and Their Effect. The Welding Institute, Abington Hall, Abington, Cambridge, Mass.

24. Hauk, V., E. Schneider, P. Stuitje, W. Theiner. Comparison of Different Methods to Determine Residual Stresses Nondestructively. Proceedings of the Germany-U.S. Workshop, Saarbucken, Germany, August 30 - September 3, 1982, 561-574.

Other Literature

1. Proceedings of the Qualtest 2 Conference SME, Dallas, Texas, October 1983.

   Note: The Railway section has a paper on XRD.

2. Residual Stress Measurement by X-Ray Diffraction, SAEJ784a, SAE Inc., Warrendale, Penn. (1971).

Volume

2

3-9070

RobertsonNickerson CONSULTING ENGINEERS & MANAGEMENT CONSULTANTS
Limited
75 ALBERT STREET, SUITE 610, OTTAWA, ONTARIO K1P 5E7 CANADA (613) 238-4625

REQ. NO. 3-9070

CONTRACT REPORT NO. OGS 83-00307

STUDY TO DETERMINE THE CANADIAN MARKET FOR A PORTABLE X-RAY STRESS DIFFRACTOMETER AND TO IDENTIFY A SOURCE OF POSITION-SENSITIVE DETECTORS FOR THE UNIT

APPENDICES

DRAFT

MARCH, 1984

211 PP

OCT 23 1985
MICROMEDIA

This Document is the property of Robertson Nickerson Limited and their client, and may not be used or reproduced without permission.

APPENDIX A

EG&G RETICON

1. Product Summary - Solid State Image Sensors
2. Application of Reticon Photodiode Arrays as Electron and X-ray Detectors
3. Preliminary Data Sheet SFX-Series X-ray Sensitive Solid State Line Scanners

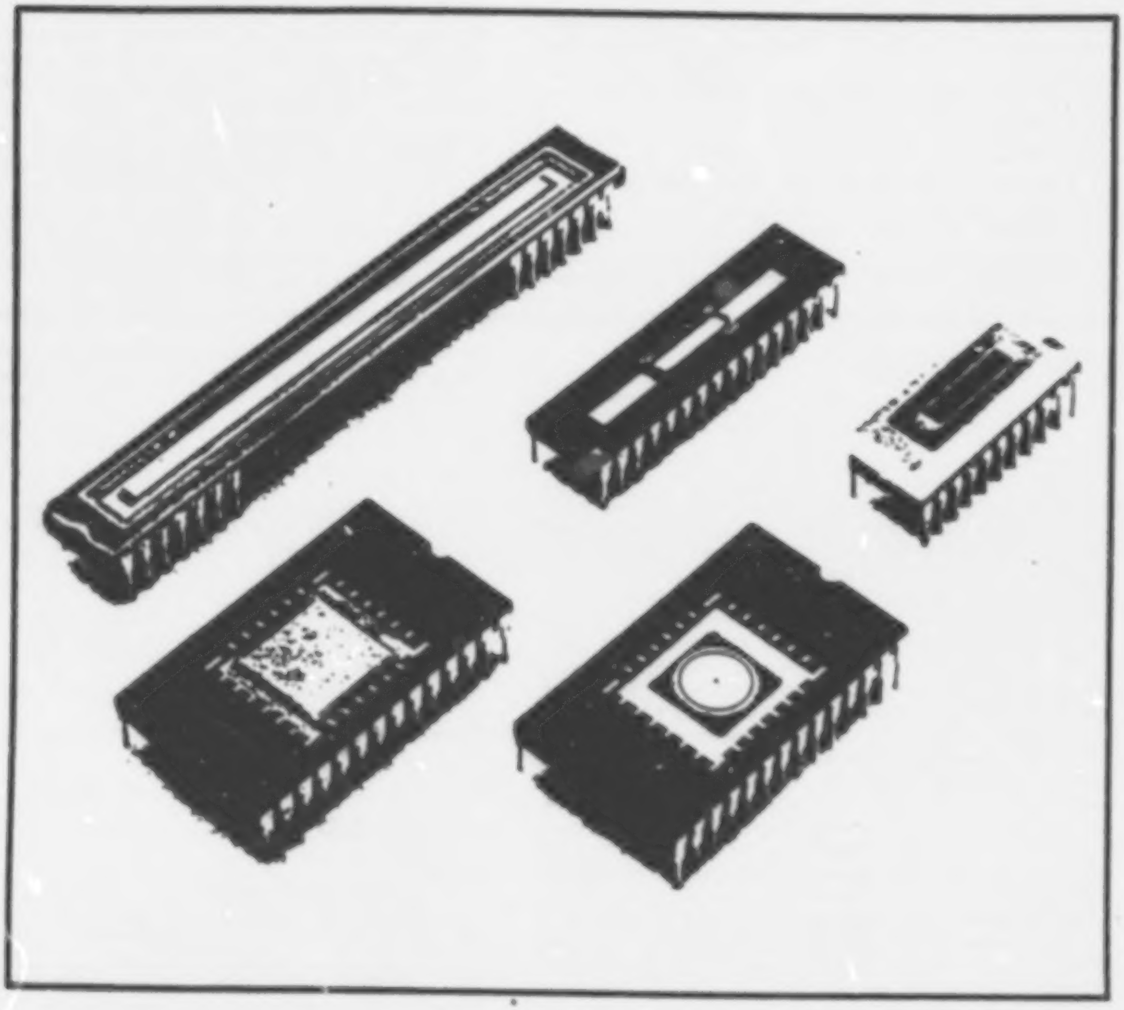

Product Summary
SOLID STATE IMAGE SENSORS

EG&G RETICON

345 Potrero Avenue, Sunnyvale, California 94086
(408) 738-4266, TWX: 910-339-9343

C Series

These devices are available with 256, 512 or 1024 elements on one mil (25.4 µm) centers. There are two options in aperture width: one mil for high resolution applications such as facsimile, and 17 mils for high sensitivity in applications such as spectroscopy and non-contact measurement. The device part number indicates the number of elements and the aperture width option; i.e., RL512C and RL512C/17 indicates 512 element arrays with one and 17 mil apertures, respectively.

External four-phase clocking allows sample rates up to 10 MHz. Either recharge or integrate, sample-and-hold amplifiers may be used.

Evaluation circuits with both types of amplifiers are available. The RC100B circuits with scan, integrate, sample-and-hold amplifiers give highest performance at scan rates up to 2 MHz. The RC400A circuits with recharge amplifiers operate at scan rates up to 5 MHz.

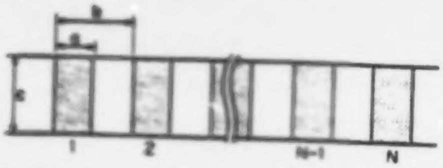

Figure 5. Typical sensor geometry of Reticon line scanner. Center-to-center spacing of diodes is b. Aperture width is a.

EC Series

These devices are identical in design to the C series with the exception that only alternate diodes are sampled. Thus they are available with 128, 256, or 512 elements on two mil (50.8 µm) centers. As with the C series, one and 17 mil aperture width options are standard.

External two-phase clocking allows sample rates up to 5 MHz. Two families of evaluation circuits are available. TheRC300 series operates to 5 MHz with recharge amplifiers. The RC100B series operates to 2 MHz with integrate, sample-and-hold amplifiers.

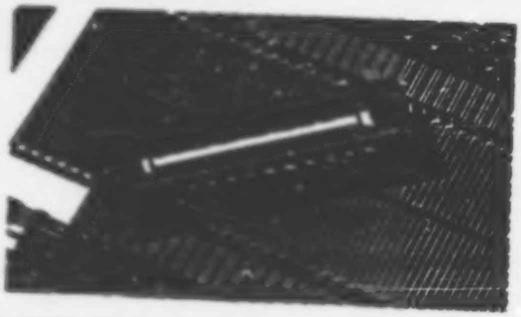

Figure 6. Photograph of 1024 element linear array with enlarged view of silicon chip in background. One mil wide sensing aperture runs down center of chip.

G Series

These devices have become industry standards combining ease of use, high performance, and low cost. They are available with 128, 256, 512, and 1024 elements on 25µm (0.984 mil) centers. Aperture width is 26 µm.

Because of an integrated drive circuit, the G series devices require only a single-phase, TTL-level clock for operation at any scan rate up to 1 MHz. A differential output configuration reduces clock noise and gives wide dynamic range with a simple, low cost recharge amplifier.

On-chip integrated buffer amplifiers and reset switches facilitate use of an integrate, sample-and-hold amplifier for applications requiring even higher dynamic range.

G series devices may be easily cascaded to provide higher resolution because the end-of-scan output is properly timed to be used as the start pulse for the next array.

Two families of evaluation circuits are available for G series devices–the RC300 series with recharge amplifiers–and the RC100B series with integrate, sample-and-hold amplifier.

H Series

These devices have a 15 µm (0.59 mil) center-to-center spacing and a 16 µm aperture to provide the high resolution required for full page width facsimile applications. They are available with 1024, 2048, or 1728 elements, the latter being a facsimile industry standard. Wide aperture versions, 300 µm (11.8 mil), are available in the 1024 and 2048 element arrays. The H-series devices use six easily generated clock phases, and operate at scan rates up to 3 MHz. The differential output configuration reduces clock noise and provides wide dynamic range with a very simple amplifier circuit.

Evaluation circuits are the RC1728H and RC1024H with recharge output, and the RC100B series with sampled-and-held output.

The RC1728H/LN low noise circuit board is now available for the 1728H array. This low cost circuit is simple to operate and provides a sampled-and-held video output with a typical P-P dynamic range of 375:1.

L and EL Series

The RL128L linear photodiode array has diodes on 2.5 mil centers with a 3 mil aperture. The RL64EL is similar to the 128L except that only one of the two shift registers and its associated video lines is connected. Thus it is a 64 element array with diodes on 5 mil centers and the same 3 mil aperture. Both the RL128L and 64EL operate to sampling rates of 10 MHz.

S Series

The S series (scientific) linear arrays have been specifically designed and optimized for applications in spectroscopy. A version is also available that is sensitive to x-rays in the 10 to 75 KeV range. Devices are available with 128, 512, and 1024 photodiodes on 25 µm centers. There is a choice of quartz window, fiber optic face plate (see front cover) and fiber optic face plate with an x-ray phosphor. Aperture width is 2.5 mm giving each sensor element a 100:1 aspect ratio suitable for coupling to monochromators or spectrographs.

The devices feature differential outputs to cancel clock switching transients and fixed patterns, and low output capacitance for low and wide dynamic range.

The model RC1024S low noise circuit with sampled-and-held video output is available for all S series devices. It operates at clock rates up to 300 KHz and provides a typical rms dynamic range of 10,000:1.

W Series

The Reticon RL64W is a wide aperture linear photodiode array with 64 interdigitated elements 10 mm wide and 25µm center-to-center spacing. The W-series has been

Solid State Image Sensors

A-2

RETICON has combined optoelectronics with the most advanced integrated circuit technology to produce a complete line of self-scanning photodiode arrays. These arrays are available both in linear and area configurations, and contain from 64 to 65,536 individual photodiodes which are internally scanned to provide serial output on a single video line.

Applications include pattern recognition, OCR, facsimile, size and position monitoring, inspection and surveillance. In many areas, these devices are functionally equivalent to flying spot scanners or vidicon camera tubes—but with the advantages of higher scan rates, small size, low voltage, low power and all solid state ruggedness and reliability.

To assist the user in evaluating and applying self-scanning photodiode arrays, Reticon also offers circuit cards which contain all of the required peripheral drive and video amplifier circuits.

In addition to supplying photodiode arrays in component form, Reticon manufactures complete electronic camera systems including a photodiode array, drive and signal processing circuitry, and optics. These systems which are described in a separate product summary, are finding application in a wide variety of non-contact measurement, inspection and control functions.

Linear Arrays

The Reticon family of linear photodiode arrays (line scanners) includes devices having from 64 to 4096 elements. These devices are enclosed in an integrated circuit type package with a ground and polished window. On a single silicon chip they contain the row of photodiodes each with an associated capacitance and an MOS multiplex switch. Also contained on-chip is either a digital shift register or an analog CCD shift register for serial readout. In addition, some devices also contain internal drive and/or amplifier circuits. The characteristics of the various Reticon line scanners are compared and summarized in Table 1, and simplified schematics showing the two types of readout circuits are shown in Figures 1 and 2. In both cases the sensing elements are diffused p-n junction photodiodes for high quantum efficiency and full silicon spectral response. Light incident on these diodes is converted to electric charge which is integrated and stored on the diode capacitance until readout. In devices with an RL part number (Figure 1), readout is controlled by a digital shift register which sequentially activates the multiplex switches and empties the charge on each diode in turn into a common output line. In the CCPD series devices (Figure 2), readout is initiated by a transfer pulse which simultaneously empties all the diodes into corresponding stages of a CCD analog shift register. The charges are then clocked through the CCD register to appear sequentially at an output node. In either case the output signal is a discrete time analog representation of the spatial distribution of light intensity across the array. Reticon devices operate over a wide range of scan rates and speed can be traded directly for sensitivity because the lower the scan rate the longer the diodes can integrate charge.

Reticon linear arrays are available in several basic designs or series and within each series there is a choice of several array lengths. The most popular of these are described in the following paragraphs. The CCPD Series utilizes the readout circuit of Figure 2. All others utilize the circuit of Figure 1. All have a linear output up to a saturation point as illustrated in Figure 3, and all have the typical spectral response illustrated in Figure 4. Sensor geometry is defined by the center-to-center diode spacing and the aperture width as shown in Figure 5.

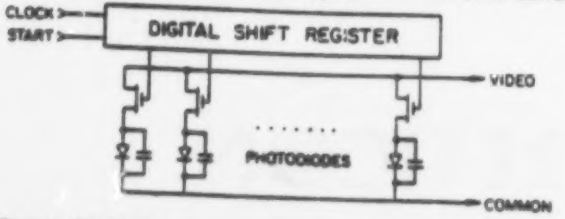

Figure 1. Simplified schematic diagram of typical Reticon line scanner.

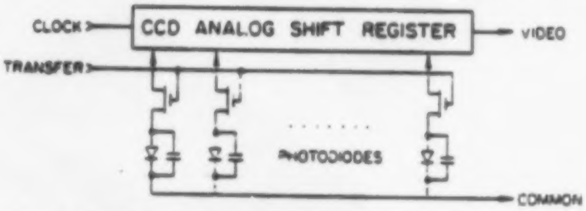

Figure 2. Simplified schematic diagram of Reticon CCPD line scanner.

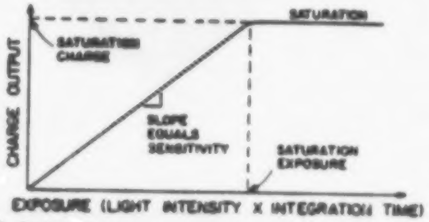

Figure 3. Output charge versus exposure characteristic.

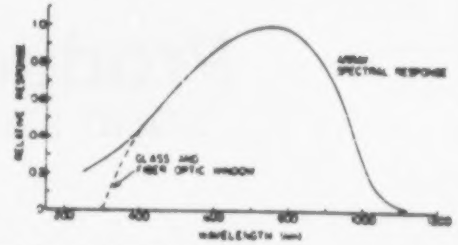

Figure 4. Typical spectral response.

A Series

These devices are available with 64 elements on two mil centers. Aperture width is also two mils. The RL64A is driven by two phase external clocks and operates at scan rates up to 10 MHz.

The RC200/201 circuit with recharge output is available for the RL64A.

Peripheral Circuits

To aid the user in evaluating self-scanned photodiode arrays Reticon offers complete driver/amplifier circuit boards for each device (see Table 1). These circuits operate over a wide range of scan rates and require only 5 to 15 volt power supplies to produce a high level video output. These circuits can be divided into two general classes, those giving an output which is a train of recharge pulses (Figure 11), and those which give a sampled-and-held boxcar output waveform (Figure 10).

Recharge Circuits

The RC200 and RC400A series circuits, which are available for all A, C, EC and L series linear arrays, operate at scan rates up to 5 MHz. They consist of a motherboard (e.g., RC200) which contains only those components which must be located near the array. The array board may be plugged directly into the motherboard or remotely located and connected by the optional RX30/16 ribbon extension cable. Recharge amplifier circuits are also available for the G (RC300 series), H (RC1024H and RC1728H) and 4096 devices. Because of the noise cancelling differential output of these devices, the recharge circuit give excellent dynamic range with low clock noise. They are completely self-contained on a single small circuit board. The RC064 circuit board is available for the RO64 circular array.

Integrate, Sample-and-Hold Circuits

The RC100-series circuits which operate at scan rates up to 2 MHz are available for all C, EC, G and H series linear arrays as well as the RA50 × 50A and RA32 × 32A matrix. They provide a sampled-and-held boxcar output waveform with much improved dynamic range. All these circuits consist of a motherboard (e.g., RC100B) which contains most of the circuitry, and a small array board (e.g. RC101, 102, etc.) which contains only those components which must be located near the array. Other sample-and-hold circuits are available as follows: The model RC1728H/LN (RL1728H only), model RC1024SA (S-series), RC84W (W-series), RC716 (Tapped CCPD 128 × (N), RCO720B (RO720B circular array), RC501 (RA14 × 41 matrix) and the model RC502A (RA100 × 100A matrix).

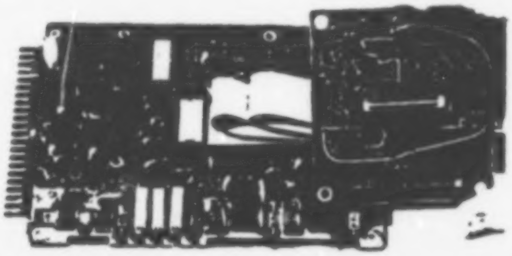

Figure 8. RC100/103 circuit board set with RL1024C photodiode array and optional RX30/16 extension cable.

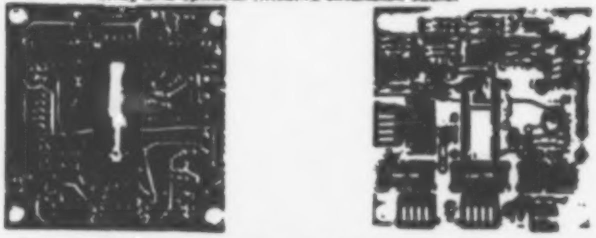

Figure 9. RC303 circuit board with RL1024G photodiode array.

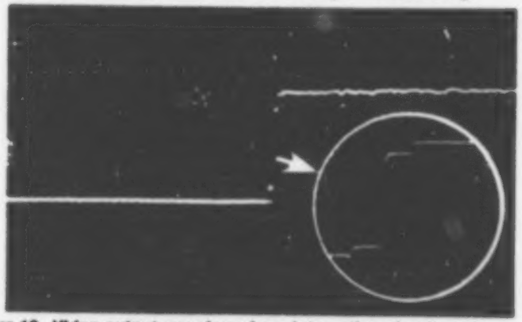

Figure 10. Video output waveform from integrating circuit such as that shown in Figure 8.

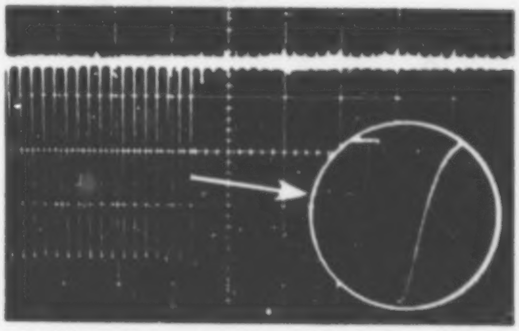

Figure 11. Video output waveform from recharge circuit such as shown in Figure 10.

DIRECT SALES

Western Region
(Corporate Hdqrs)
345 Potrero Avenue
Sunnyvale, CA 94086
(408) 738-4266
TWX: 910-339-9343

North Central
2260 Landmeier Rd. Suite J
Elk Grove Village, IL 60007
(312) 640-7713

Eastern
35 Congress Street
Salem, MA 01970
(617) 745-7400

Mid-Atlantic
416 Hungerford Drive, Suite 307
Rockville, MD 20850
(301) 251-0088

Southern California
12833 Monarch Street
Garden Grove, CA 92641
(714) 895-3367

Contact the nearest direct sales office for the name of the sales representative or distributor in your area.

DIRECT EUROPEAN OFFICES

United Kingdom
EG & G Reticon
c/o EG&G Instruments Ltd.
Seymour House
The Courtyard, Denmark Street
Wokingham, Berks RG11 2DR
England
Tel: (0734) 790772
Telex: 847510 EGGUK G

Europe/West Germany
EG&G Reticon
c/o EG&G Instruments GmbH
Hohenlindenerstr. 12
D-8000 Munich 80
West Germany
Tel: (49)089-918080
Telex: 528357 EGGI D

EG&G RETICON

APPLICATION NOTES

Nº 101

APPLICATION OF RETICON PHOTODIODE ARRAYS AS ELECTRON AND X-RAY DETECTORS

EG&G RETICON • 345 Potrero Avenue • Sunnyvale, California 94086
Phone: (408) 738-4266 • TWX: 910-339-9343

570F

Reticon self-scanning photodiode arrays were designed primarily for detection of visible and near infrared light; however, these devices make excellent detectors of more energetic radiation as well. They are particularly usefully for detecting soft X-rays in the 1 to 10A wavelength (1.2 to 12 KeV photon energy) range and electrons in the 10 to 100 KeV range. These ranges can be extended by relatively minor changes in the device structure.

Although, in principle any Reticon photodiode array can be used to detect electrons or X-rays, the most suitable standard devices are the "C" and "B" series with the wide aperture option.[1] [2] The "C" series devices have a 17 mil wide sensing area with 128, 256, 384 or 512 individual sensors on 2 mil centers or 256, 512, 768 or 1024 sensors on one mil centers. The "B" series devices have a 24 mil wide sensing area and either 512 or 1024 elements on 1 mil centers.

The user should provide an external shield to protect the areas of the silicon chip outside the sensing aperture. These areas contain multiplex switches and shift register scanning circuits which can be damaged by exposure to ionizing radiation. The actual sensing area should then be defined by an aperture in the shield which is aligned inside the 17 or 24 mil aperture on the silicon chip. The proper alignment is illustrated in Figure 1.

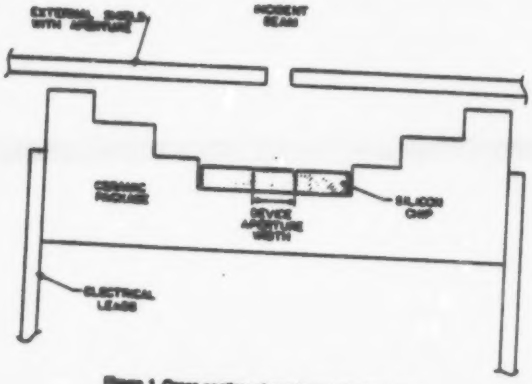

Figure 1 Cross section of packaged Reticon array showing required alignment of external shield to device aperture.

Reticon arrays are normally assembled in a ceramic dual-in-line package and sealed with a quartz window 20 mils thick. For X-ray or electron sensing applications this window must of course be omitted. In addition the sensing area of a standard array is covered by a protective silicon dioxide layer nominally 3 microns thick. This layer is completely transparent to light but will partially absorb an incident electron or X-ray beam. For this reason, it is sometimes desirable to reduce the thickness of the oxide layer. With a relatively minor process change devices can be produced which have the silicon dioxide layer thickness reduced to 1 micron. With more substantial process changes, the oxide layer can be eliminated completely in the area over the diodes. An oxide layer should reamain between the diodes for reliability reasons.

ELECTRON DETECTION

An incident high energy electron dissipates its energy over some path length by the creation of secondary electron-hole pairs. In silicon, one electron-hole pair is created for each 3.66 eV of energy dissipated. All of the secondary holes generated in the silicon within a diffusion length of the surface (approximately 50 microns) will be collected and stored on the nearest photodiode. This charge will be read-out as signal charge when the array is scanned. Holes generated within the oxide or deeper than one diffusion length within the silicon will not be collected and will not contribute to the signal charge.

Low energy electrons will lose all or most of their energy in the oxide layer covering the silicon surface and may therefore not be detected. The calculated range of electrons in SiO_2 is shown in Figure 2 as a function of energy.[3] It can be seen from the figure that electrons with energy less than about 25 KeV will be stopped in a 3 micron thick oxide layer and electrons with energy less than about 12 KeV will be stopped in a 1 micron oxide layer. Energies in excess of these minimum values but less than about 100 KeV will be deposited in the silicon within one diffusion length of the surface and will generate a signal of 1 electronic charge per 3.66 eV of energy. Electrons with energy greater than 100 KeV will penetrate deeper than a diffusion length and only a fraction of the generated secondaries will be collected.

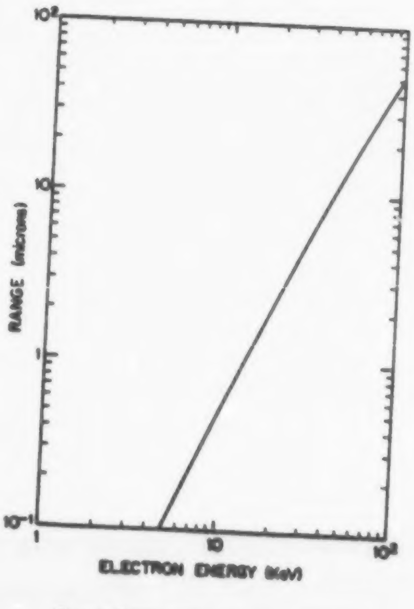

Figure 2 Range-energy relationship for electrons in SiO_2 (See Reference 3)

An experimental curve of charge gain as a function of incident electron energy is shown in Figure 3 for a device with a 1 micron oxide layer.[4] The offset of about 11 KeV agrees reasonably well with the theoretical range-energy curve of Figure 2. Note that a single incident 30 KeV electron will produce a detectable signal of 5000 electronic charges. Studies on standard Reticon devices with a 3 micron oxide layer [5] show similar results except that the offset voltage is increased to approximately 25 KeV as expected from Figure 2.

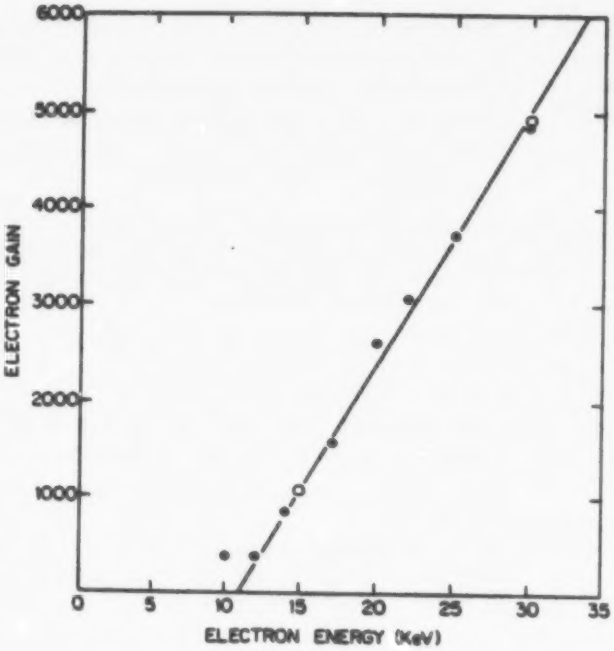

Figure 3 Charge gain versus electron energy for RL-1024S with 1 micron oxide layer (See Reference 4)

One application in which Reticon arrays are used as electron detectors is in the self-scanned digicon tubes manufactured by Electronic Vision Corporation, 11661 Sorrento Valley Road, San Diego, California 92121.

These devices consist of a semitransparent photocathode, a magnetically focused electron imaging section and a Reticon photodiode array target. An optical image on the photocathode generates photoelectrons which are accelerated through approximately 20 KeV and focused onto the Reticon array where one incident photoelectron generates several thousand secondary electron-hole pairs to produce a corresponding charge gain. The read-out noise is sufficiently low that single electron events can be detected.[4] [5] A discussion of the self-scanned digicon for applications in low light level astronomical spectroscopy is presented in Reference 4.

In addition to low light level imaging tubes such as the Digicon, Reticon arrays may be used in electron spectroscopy and a variety of other electron detecting applications.

X-RAY DETECTION

When an X-ray beam is incident on a material such as silicon, it is attenuated exponentially i.e., its intensity decreases with distance according to the relation $I = I_o \exp(-x/\alpha)$ where I is the incident intensity and I is the intensity at any distance x from the surface. The parameter α (the absorption coefficient) is the probability per unit path length of an X-ray photon being absorbed. On the average a photon will travel a distance of $1/\alpha$ before being absorbed.

When a photon is absorbed its energy is transferred to an electron which then gives up the energy by generating secondary electron-hole pairs. From here on the problem is the same as for direct detection of electrons. One secondary is produced for each 3.66 eV of absorbed energy and all the secondary holes produced in the silicon within a diffusion length of the surface will be collected and contribute to the signal charge.

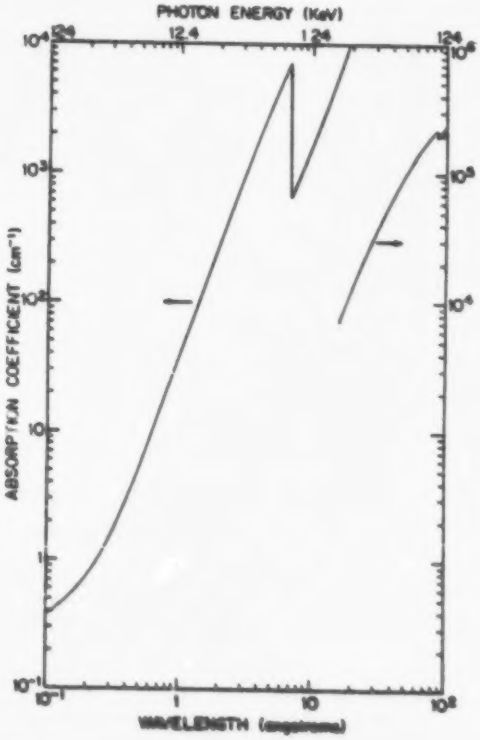

Figure 4 X-ray absorption coefficient of silicon as a function of wavelength and Photon energy.

The absorption coefficient of silicon is shown as a function of wave-length (or photon energy) in Figure 4. The absorption coefficient of SiO_2 is slightly different but has a similar wavelength dependence. Note that short wavelength (high energy) X-rays have a very low absorption coefficient and a beam would penetrate all the way through a silicon device with very little energy being absorbed. Long wavelength (low energy) X-rays, on the other hand, have a very large absorption coefficient and most of the beam energy will be absorbed in the oxide without reaching the silicon. Calculated response curves considering both effects are shown in Figure 5. The calculations were carried out for three oxide thicknesses: 0,1 and 3 microns. A diffusion length of 50 microns was assumed in each case. The notch in the response curves is due to an absorption edge associated with silicon atoms in the SiO_2 layer.

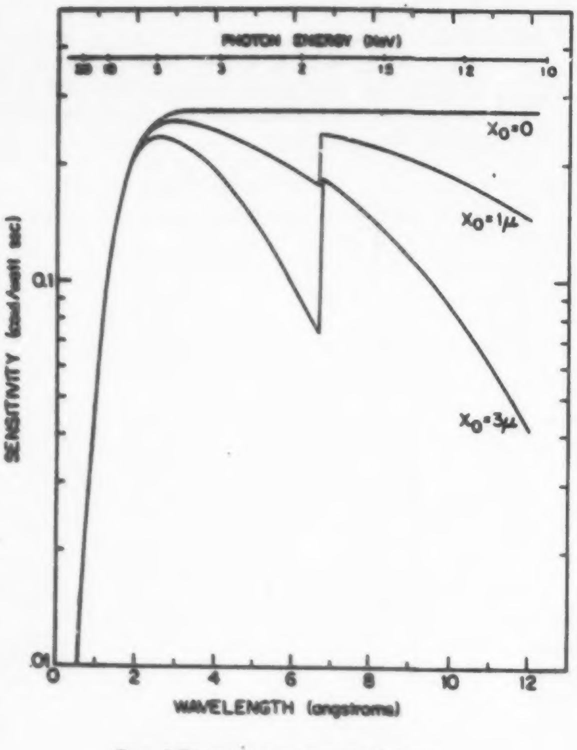

Figure 5 Theoretical X-ray response of Reticon photodiode arrays for 0, 1 and 3 micron oxide thickness and 50 micron diffusion length.

It can be seen from Figure 5 that the peak sensitivity is at about 5 angstroms wavelength and that standard devices make quite good detectors over a range from about 1 to 12 angstroms. At long wavelengths the sensitivity can be significantly improved by reducing or eliminating the oxide layer. For wavelengths longer than 15 or 20 angstroms, the sensitivity is expected to decrease even for zero oxide thickness. This is because most of the energy is absorbed so close to the silicon surface that some of the secondary electron-hole pairs will be lost by surface recombination.

For wavelengths between very soft X-rays (about 20 A) and the ultraviolet (about 2500 A) no experimental work has been reported and calculations are difficult. It is possible, however, that Reticon devices could be useful over a portion of this range.

For wavelengths shorter than 1 A the sensitivity falls off rapidly, but the devices may still be useful for high intensity beams. In this range the sensitivity in coul/watt sec is approximately given by 1.4 x 10^{-3} times α in cm^{-1}.

The method of calculating the signal charge which will be read-out of each cell when the array is scanned is illustrated by the following example:

Consider a standard "C/17" series array masked externally to expose a 10 mil wide sensing area. Each cell then has a sensing area of 1 mil x 10 mil = 10 mil ^{2} = 6.5×10^{-5} cm ^{2}. Suppose an X-ray beam with an intensity of 10 μ watt/cm ^{2} and a wavelength of 4 A is to be detected and the array is scanned at 100 lines/sec. The energy incident on each cell per line is then:

$$10^{-5}\,\frac{\text{watts}}{\text{cm}^2}\times 6.5\times10^{-5}\ \text{cm}^2\times .01\ \text{sec} =$$

$$6.5\times10^{-12}\ \text{watt sec}$$

From Figure 5 the sensitivity at 4 A is 0.2 coul/watt sec. Therefore, the signal charge is:

$$0.2\ \frac{\text{coul}}{\text{watt sec}}\times 6.5\times10^{-12}\ \text{watt sec} = 1.3\ \text{pcoul.}$$

Since the saturation charge of a "C/17" device (see data sheet) is 3.2 pcoul, the above exposure results in a signal equal to 40% of saturation.

RADIATION DAMAGE

While many Reticon devices are being used in electron and X-ray applications with no serious problems, the user should be aware that continued exposure to high energy radiation can cause radiation damage effects. [6] [7] These effects are cumulative and permanent.

The most serious effect, which can fortunately be eliminated by shielding, is a shift in the threshold voltage of the MOS transistors used in the multiplex switches and scanning circuits of the array. If these are not shielded, the scanning circuit will cease to function after a radiation dose of about 10^5 rads. The absorbed dose varies with the oxide thickness and the electron or X-ray energy. For 20 KeV electrons incident on a silicon surface covered by 1 micron of oxide it is about 3×10^{-7} rads per incident electron/cm ^{2}. Working through the numbers, this means that the device would fail after an exposure sufficient to cause saturation about 2000 times.

With proper shielding the failure mechanism described above can be completely eliminated. However, there is a second radiation effect which relates to the sensor elements themselves and therefore cannot be eliminated by shielding. This effect is an increase in the dark leakage current which has a typical initial value of about 1 pA per cell and increases by about a factor of 10 after a dose of 10^7 rads. The effect is not catastrophic and saturates after the above dose. A dark current of 10 pA is not objectionable for most applications. If it is a problem it can be reduced by cooling the device. Dark current changes by about a factor of 2 every 7°C.

ORDERING AND HANDLING INFORMATION

Reticon photodiode arrays for use as radiation detectors must be specially ordered WITHOUT SEALED WINDOW. Devices so ordered will be shipped with a window taped in place to provide mechanical protection during shipping and handling. The devices can be functionally tested as light detectors while this temporary window is in place. After removal of the window, care should be taken to avoid touching the silicon surface or the delicate 1 mil diameter wire bonds. Unsealed devices should be stored and handled in a clean, dry environment.

Any standard Reticon array with a 3 micron oxide layer may be ordered unsealed at the regular price. Any "C/17" or "B/24" series devices may also be ordered with a 1 micron oxide layer. However, a 10% premium is charged for special processing and handling. Tooling is now available to fabricate "B/24" devices with zero oxide thickness over the diodes and one micron oxide between diodes. These are also available at a 10% premium over standard prices.

For applications not covered by standard "B/24" or "C/17" series devices, Reticon has a complete custom design capability. Custom devices can be built in a wide variety of geometric configurations.

DISCLAIMER

While the information contained in this article is believed to be accurate, Reticon sensor arrays are designed and tested only as optical detectors and no specific performance guarantees can be made for devices used to detect X-ray or electrons.

REFERENCES

1. Reticon data sheet, *C-Series Solid State Line Scanners*
2. Reticon data sheet, *Solid State Line Scanners: RL-1024B and RL-512B*
3. L. Katz and A.S. Penfold, Rev. Mod. Phys. 24. 1952
4. R.G. Tull, J.P. Choisser and E.H. Snow, "The Self-Scanned Digicon: a Digital Image Tube for Astronomical Spectroscopy", Applied Optics 14, May 1975
5. S.B. Mende and E.G. Shelley, "Single Electron Recording by Self-Scanned Diode Arrays", Applied Optics 14, March 1975
6. E.H. Snow, A.S. Grove and D.J. Fitzgerald, "Effects of Ionizing Radiation on Oxidized Silicon Surfaces and Planar Devices", Proc. IEEE 55, July 1967
7. J.P. Mitchell and D.K. Wilson, "Surface Effects of Radiation on Semiconductor Devices", Bell System Technical Journal 46, January 1967

Copyright RETICON Corporation 1975. Contents may not be reproduced in whole or in part without the written consent of RETICON Corporation. Specifications are subject to change without notice. Printed in U.S.A.

Information furnished herein is believed to be accurate and reliable. However, no responsibility is assumed by RETICON Corporation for its use; nor for any infringement of patents or other rights of third parties which may result from its use. No license is granted by implication or otherwise under any patent or patent rights of RETICON Corporation.

EG&G RETICON SFX-SERIES X-RAY SENSITIVE SOLID STATE
LINE SCANNERS: 128, 512, 1024 ELEMENTS
CUSTOM PRODUCT NO. CP1025-01, -02, -03

GENERAL DESCRIPTION

Part Number CP1025 is a custom modification of the S-series solid state line scanner with the fiber optic face plate option. A dash number is placed after the part number to indicate 128, 512 or 1024 elements; -01, -02, -03 respectively. The modification consists of adding an X-ray phosphor to the input side of the fiber optic face plate. This provides spectral sensitivity to X-rays in the range of 10 to 100 KeV. The fiber optic face plate acts as an interface between the phosphor and the diode array as well as protects the array from X-ray damage. For detection of soft X-rays (1.2 to 12 KeV) see reference No. 2.

Optical alignment of the SFX device is possible because the X-ray phosphor has approximately 50% transmission to visible light. During operation, X-rays striking the phosphor are converted to green light. The green light is transmitted through the fiber optic face plate to the silicon photodiodes where the light is converted to an electronic charge. The resulting charge is integrated on each photodiode so that after a period of time each photosite has collected a charge proportional to the local flux of the X-ray beam. When the array circuitry scans the diodes, the charge packets are sequentially converted to a voltage level which, when displayed on an oscilloscope, reproduces a spatially resolved one dimensional X-ray image. Integration times of .026 to 500 msec are possible at room temperature. Cooling the array can extend integration time to minutes or hours by reducing dark current.

The SFX-series has all the advantages of the S-series arrays. Refer to the S-series data sheet for detailed information on the internal scanning circuitry, the package and pin configuration, electrical characteristics, dark signal and noise characteristics, amplifier requirements and evaluation circuit.

ELECTRO-RADIOLOGICAL CHARACTERISTICS (25°C)

PARAMETER	TYPICAL	UNITS	NOTES
Center-to-Center Spacing	25	μm	
Aperture Width	2.5	mm	
Responsivity	24	pcoul/mR	1
Non-Uniformity of Response	10	±%	
Saturation Exposure	0.6	mR	1
Saturation Charge	14	pcoul	
Average Dark Current	5	pamp	
Spectral Response Range	10-100	KeV	
Resolution	8	lp/mm	

NOTES:
1. Tungsten target X-ray tube, 40KVP, 20ma, 0.04" aperture, 10.5" from aperture to device.

7/3/80

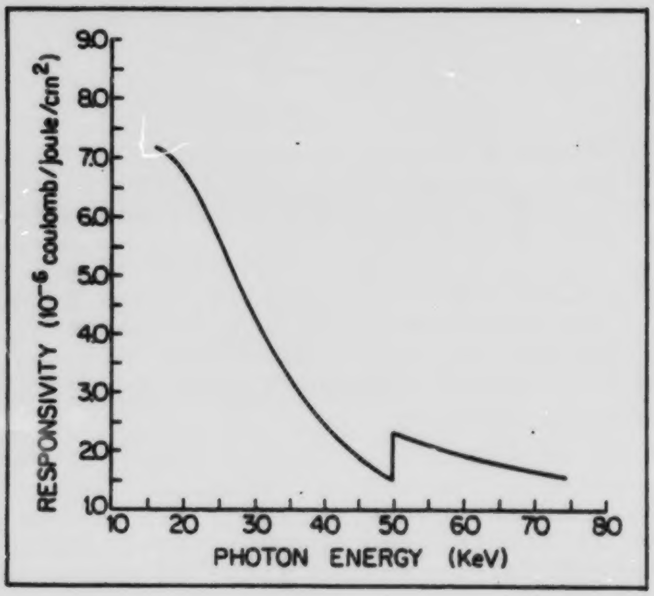

Figure 1. Typical Spectral Response.

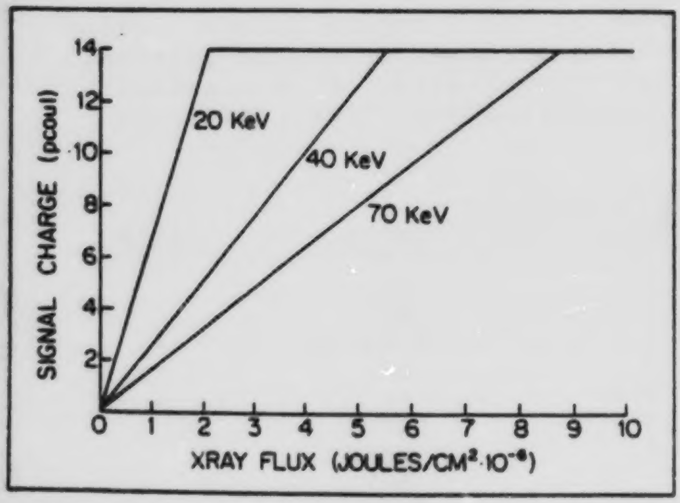

Figure 2. Signal Charge vs X-Ray Flux for 20KeV, 40KeV, and 70KeV Monochromatic Sources.

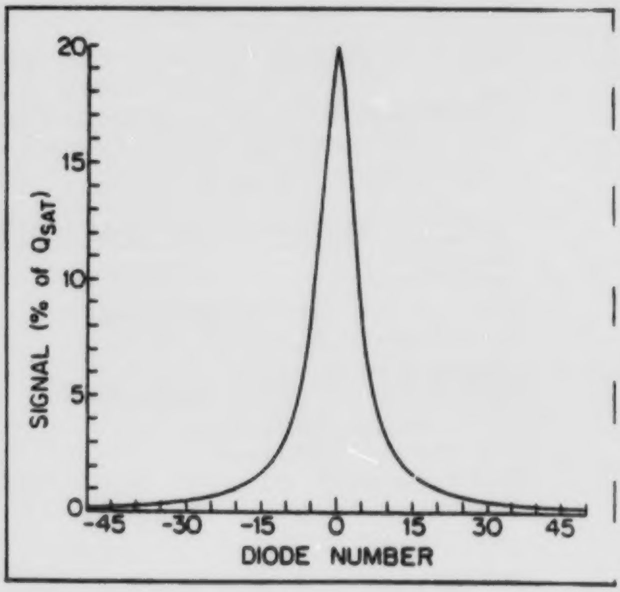

Figure 3. Typical Resolution, 0.05mm Lead Slit.

RETICON Corporation is a subsidiary of EG&G, Inc., Wellesley, Massachusetts.

Copyright RETICON Corporation 1978. Contents may not be reproduced in whole or in part without the written consent of RETICON Corporation. Specifications are subject to change without notice. Printed in U.S.A.

Information furnished herein is believed to be accurate and reliable. However, no responsibility is assumed by RETICON Corporation for its use, nor for any infringement of patents or other rights of third parties which may result from its use. No license is granted by implication or otherwise under any patent or patent rights of RETICON Corporation.

ORDERING INFORMATION

Array Type	No. Of Elements	Custom Product No.	*Evaluation Circuit
RL128SFX	128	CP1025-01	RC1024S-01
RL512SFX	512	CP1025-02	RC1024S-02
RL1024SFX	1024	CP1025-03	RC1024S-03

* Evaluation circuits must be shielded from X-ray exposure.

References

1. John McGinnis, "An X-Ray Sensitive Photodiode Array".
2. Reticon Application Note 101, "Application of Reticon Photodiode Arrays as Electron and X-Ray Detectors".
3. Louis N. Koppel, "An Active-Recording X-Ray Crystal Spectrometer For Laser-Induced Plasmas", Review of Scientific Instruments, 47, 9(Sept. 1976).
4. R.D. Bleach & D.J. Nagel, "X-Ray Applications of Self-Scanning Silicon Diode Arrays", Applied Optics, Vol. 16, March 1977.

APPENDIX B

FAIRCHILD CCD

1. CCD Fundamentals
2. Charge-Coupled Devices
3. CCD 151 3456 - Element Line Scan Image Sensor
4. Technical Note on X-ray Imaging with Fairchild CCD Image Sensors
5. Advanced Charge-Coupled Device (CCD) Line Imaging Devices
6. CCD 111
7. CCD 122/142
8. CCD 133/143
9. CCD Imaging Products Price Schedule

17 B-1

CCD FUNDAMENTALS

No math—just a straightforward explanation of how CCD memory units and video devices operate and what they can do for you!

By Frank H. Bower
Fairchild Camera and Instrument Corp.
Mountain View, California

Charge-coupled devices (CCDs) are a new family of silicon semiconductor components capable of performing the general functions of image sensing, analog signal processing, and digital or analog memory. To realize the CCD concept's full capability, improved LSI techniques have been developed and basic NMOS processes substantially refined. Recognizing the technical advantages of using CCDs in defense systems, military and other government agencies started funding a number of research and development programs in the early seventies to accelerate the development of practical devices.

Today, there is a small but growing number of manufacturers offering high-performance CCD image sensing devices, analog signal processing devices, and large capacity digital memory integrated circuits. Several laboratories are also developing and building small numbers of special devices with government contractual support.

CCD Linear Imaging Devices (LIDs) have made possible the new generation of fast facsimile machines now reaching the market. They are also used in high speed mail sorting, rapid non-contact inspection and quality control measurement, and "smart" computer-controlled material handling systems. Real-time aerial mapping, reconnaissance, and surveillance systems have been improved by the application of high resolution LIDs as optical sensors.

CCD Area Imaging Devices (AIDs) are used in small, rugged, low power TV cameras capable of operation in very low light levels such as one-quarter moonlight. They have been applied in robots and automatic production systems as well as in miniature TV cameras for military systems (Figure 1).

The Charged-Coupled Device

The CCD operating principle is called "charge-coupling." Finite amounts of electrical charge called "packets" are created in specific locations in the silicon semiconductor material. Each specific location, called a

Figure 1: Cockpit TV camera system.

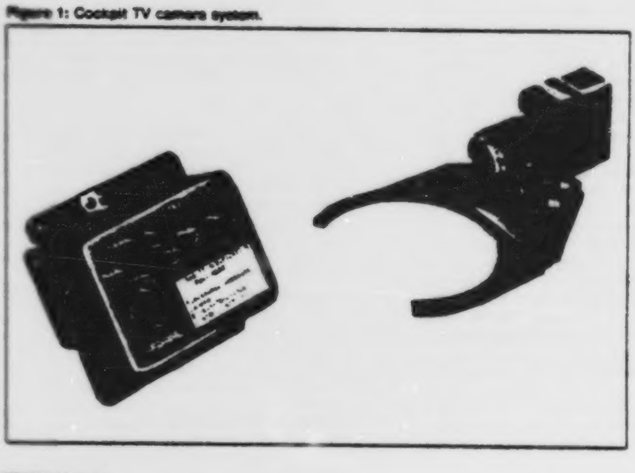

"storage element," is created by the field of a pair of gate electrodes very close to the surface of the silicon at that location. By placing the storage elements adjacent to each other, in a line for instance, voltages on the adjacent gate electrodes can be alternately raised and lowered and cause the individual charge packets beneath them to be passed from one storage element to the next (Figure 2). Since each charge packet may be of different size, the line of elements becomes a very simple analog shift register. All CCDs are basically shift registers, and because the transfer of charge from each storage element to the next adjacent element is very efficient, the amount of charge in each packet stays substantially the same, even after it has been passed from one element to as many as a thousand sequentially adjacent elements. Since the amount of charge in each packet is unique, the string of charge packets can represent analog information. The device is, in a sense, storing that information until it is delivered as an electrical signal from the charge detector built into the device at the end of the charge-coupled register.

This shift register performance is the basic characteristic of CCDs used in analog signal processing and memory devices. Figure 3 shows a diode-gate structure by which information is put into and taken out of the CCD register to allow operation in an electronic system operating with currents and voltages rather than with the charge-packets manipulated in the CCD itself.

Performing the image sensing function utilizes another basic characteristic of silicon semiconductor devices. This is the photoelectric effect by which free electrons are created in a region of silicon illuminated by photons in the approximate spectral range of 400 (blue) to 1100 (near infrared) nanometers wavelength. Response peaks at about 800 nanometers. Absorption of such incident radiation in the silicon generates a linearly proportional number of free electrons in the specific area illuminated. If a silicon device structure having a repetitive pattern of small but finite photo-sensing sites is created, the number of free electrons generated in each site (charge-packet) will be directly proportional to the incident radiation on that specific site. If the pattern of incident radiation intensity is a focused light image from an optical system viewing a scene, the charge-packets created in the finite photo-sites array will be a faithful reproduction of the scene projected on its surface.

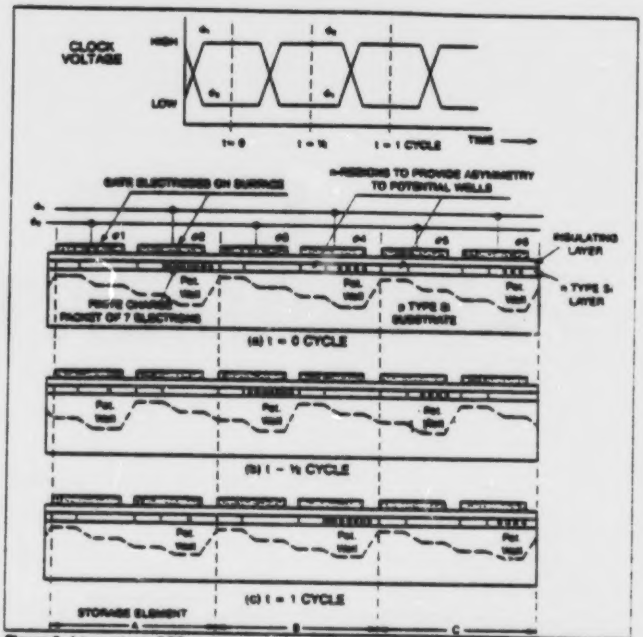

Figure 2: A two-phase CCD shift register. The two complementary clock voltage waveforms ϕ_1 and ϕ_2 are connected to alternate closely-spaced gate electrodes on the surface of the thin insulating layer on the silicon. A deep potential well which attracts electrons is created under the electrode clock voltage HIGH and disappears under the electrodes at clock voltage LOW. At t = 0, ϕ_1 voltage is HIGH and the finite charge packet of seven electrons is in the potential well under gate electrode #2 in storage element "A". At t = ½ cycle later, the potential well under gate #2 has collapsed due to ϕ_1 having gone LOW and, since at the same time the adjacent electrode #3 connected to ϕ_2 has gone HIGH, the seven electron charge packet has been attracted to the new potential well under electrode #3. Another half cycle later, at t = 1 cycle, the potential well under electrode #3 has collapsed with ϕ_2 going LOW and the electron packet moves to the new well under electrode #4 which has gone HIGH with clock voltage ϕ_1.

After an appropriate exposure time, during which the incident light on each site is generating its time and intensity proportional electron charge-packet, the charge-packets are simultaneously transferred by charge-coupling under an adjacent single long gate-electrode, to a parallel CCD analog transport shift register. The single long gate is called the transfer-gate (Figure 4).

Each charge-packet corresponds to a picture element (pixel) and when transferred to the adjacent CCD transport shift register, continues to faithfully represent the total sensed radiant energy which was absorbed in the specific photo site. The transfer gate is immediately returned to the non-transfer clock level (LOW) so photo-sites can begin integrating the next line of incident image information. At the same time, the CCD analog transport register, now loaded with a parallel-transferred line of picture information in the form of charge-packets from a line of sensor sites, is rapidly clocked to deliver the picture information, in serial format, to the device output circuitry.

The output circuitry consists of an output gate-diode structure and appropriate reset and buffering signal

19
B-3

amplifiers. The output terminal delivers a sequence of electrical pulses, the amplitude of each being directly proportional to the charge-packet size generated in the photo-site where the charge-packet originated. Sample-and-hold circuitry, either on-chip or in the video processing support circuitry ivers a line of video information.

Linear imaging devices (LIDs) sense and deliver information a line at a time: they are electronically scanned in one dimension and are often called line-scan devices.

Area imaging devices (AIDs) have an X-Y array of sense elements and sense an area image. They are built with both vertical and horizontal transfer gates and transport registers, and deliver an entire field of video information from each integration (exposure) period in the form of a series of lines of video signal.

CCD Characteristics

- Temperature: the CCD works best at low temperatures. It has no problem at −55°C and can perform at full capability to −70°C. Above 70°C, storage-related parameters degrade rapidly due to physical properties of semiconductor materials. All semiconductor materials continuously generate hole-electron pairs due to thermal energy, even at room temperature. If there is a finite packet of electrons representing information in a storage element, and thermally generated electrons add to that packet over a period of time, the packet will become larger and eventually will no longer accurately represent the original information.

In image sensors, which are very high dynamic range analog devices, it is often desirable to provide cooling for low light level applications to reduce thermal electron generation. Since image sensor devices are used as single units or as a matrix of two to six devices, and dissipate on the order of 150 mW or less, cooling is relatively simple. In CCD memory, long registers could be a problem, so the devices are designed with "refresh" cells at frequent intervals in the register. These sense-and-restore cells detect the "1" or "0" at the output end of a shift register section before enough thermal electrons can be added to cause misinterpretation of the data. Practical economic considerations, however, limit the temperature range for CCD memory to about −70°C. Because of the very low power dissipated in CCD memory, it is practical to consider providing cooling to achieve economical military electronic systems.

- Speed: the speed limitation of CCD devices is theoretically that of electron mobility in silicon and experimental devices operating in the gigahertz range has been reported. Since surface-state trapping in the silicon slows the net mobility of carriers near the surface, "buried channel" devices are faster than "surface channel" devices. The practical limitation to operating speed is caused by the edge-dependent charging current associated with delivering the clock voltages to the capacitances of the shift-register gate electrodes (C dv/dt current). The clock-driver circuitry also dissipates increased power with increasing frequency of operation. Desired operating speed is, therefore, a very strong design consideration in determining how much of the clock driving function should be put on-chip, thus increasing chip temperature, or left for the system designer to provide on the board.

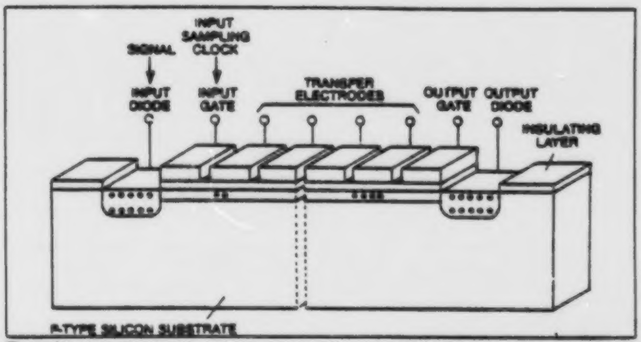

Figure 3: Input and output diode/gate structures for electrical input and output to a CCD shift register.

Figure 4: Simplified block layout of a linear image sensor.

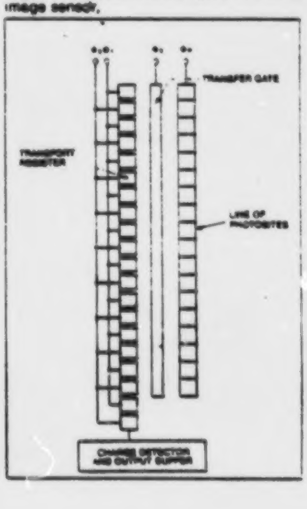

- Reliability. Since materials used and the fabrication and packaging technology for CCDs are essentially those of NMOS LSI products, CCD device reliability equals that of NMOS. CCDs are inherently lower power devices and, therefore, the occurrence of thermally-induced failure mechanisms should be lower than that of NMOS. Manufacture of CCDs utilizes state-of-the-art NMOS production technology for its N channel, silicon gate, ion-implanted, surface passivated structure. Packaging can be in any of the commercial or high-reliability packages already proven in industry.
- Noise. The basic CCD register, heart of all CCD devices, is practically noiseless because it does not have PN junctions as do MOS and bipolar devices. Associated on-chip charge detectors and buffer amplifiers do have PN junctions and introduce some noise. Dynamic ranges of 10,000:1 have been achieved with cooling; 200:1 to 500:1 is common at room temperature.
- Radiation Hardness. CCDs are not basically "hard." They are fabricated on very lightly doped, high-resistivity silicon which has characteristics more easily altered by radiation than the more heavily doped silicon in bipolar and conventional MNOS devices. Buried channel CCDs have been reported to be more radiation tolerant than surface channel devices. Government sponsored development programs are under way at several laboratories to investigate methods for radiation hardening CCD devices.

2°

84

FAIRCHILD
A Schlumberger Company

CCD

• Packing Density. CCDs have a three to five times packing density advantage over the next most dense MOS large-scale-integrated circuits. This is primarily because the basic CCD storage element requires no electrical contacts. The storage and transport of the information in the CCD register are performed by the pattern of conductive gate electrodes on the surface of the thin oxide layer over the silicon. The gates require much less area per storage element than the combination of gates and ohmic contacts required for an MOS storage element. The 64 kilobit CCD memory device presently produced by Fairchild is a chip of silicon .175" × .230" in size.' With foreseeable improvements in LSI manufacturing technology and careful selection of the memory chip organization and on-chip peripheral circuits, devices with 256 kilobits capacity will be available within the next year or two.

CCD Applications in Military Electronics

Image Sensors. A CCD image sensor device can be configured as a line-scan device or as an X-Y TV type device. It can also be configured as a combination of the two basic structures for special applications. The line-scan device has a single line of sense elements and scans itself electronically in one axis—along the sense elements' centerline. It is often referred to as a Linear Imaging Device (LID). The X-Y device is an area matrix of sense elements capable of being electronically scanned in both X and Y axes to produce an area TV picture. It is often referred to as an Area Imaging Device (AID).

Most CCD image sensors have wide spectral range, and are nominally useful over the spectral range 450 to 1000 nanometers; i.e., visible through the middle of the near infrared regions. Standard commercial CCD image sensors will operate well up to a wavelength of about 800 to 900 nanometers; beyond that wavelength, they lose resolution rapidly. Resolution loss is due to the IR image photons generating electrons much deeper in the silicon and, therefore, beyond the attractive effect of the field created by the gate electrodes at the silicon surface. The generated electrons diffuse in the bulk of the silicon until they are either lost by recombination or move nearer to the surface where they are captured in the field of one of the sense elements. However, because of the time delay, they may arrive too late or in a sense element other than the one through which their exciting photon entered the silicon. The practical result is a loss of resolution or smearing of the image sensed. In some laboratories, work is being done to develop special CCDs for long wavelength IR image sensing.

All CCD image sensors consume low power and operate on low voltages. They do not exhibit lag or memory and are not damaged by intense light. Present devices will over-saturate and "bloom" under intense illumination but are not permanently damaged. Anti-blooming structures are under development.

Linear Imaging Devices(LIDs)

LIDs are configured as a single line of sensor elements on a long narrow chip. These devices are commercially available with 256, 1024, and 1728 elements with longer devices in development. LIDs are used in facsimile machines or spectrometers where the subject is a line pattern. When relative motion of the scene with respect to the sensor is provided by other means, the array can present a high-resolution TV-type picture. A continuous real-time picture can be obtained from a LID sensor in an aircraft or satellite passing over the surface of the earth at a constant altitude and velocity. Using a scanning mirror in the optical system can accomplish a similar result. LIDs applications include:

- High speed, high resolution facsimile (text, maps, fingerprints, photographs)
- Aerial mapping with high measuring accuracy
- Real-time reconnaissance and surveillance
- Bar-code reading
- Sorting parts, mail, currency, food
- Conveyorized product non-contact inspection
- Automatic warehouse routing and palletizing control

Special configurations of LID in which the array is eight to 64 elements wide (rather than one element wide) can be used for Moving Image Integration (MII) applications and are particularly effective in very low light level applications. Combined with analog delay lines, a LID can be used as the sensor for Moving Target Indication (MTI).

Area Imaging Devices (AIDs)

AIDs produce a TV picture. They are built in an array capable of being self-scanned in both the X and Y direction. These devices are available in 100 × 100 element and 244 × 190 element arrays; they have also been built in smaller sized arrays and in arrays of 400 × 400 and 488 × 380 elements. As an example of a commercially available device, the Fairchild CCD211 is a 244 × 190 element array with a sense area format equivalent to a Super 8 movie frame, and in a 3 × 4 aspect ratio for TV presentation. The device dissipates 100 mW when operated at a 7 MHz data rate, and operates at voltages of 12V to 15V. Its dynamic range is typically 300:1 at room temperature. Chip size is

Figure 5: Artillery launched TV system concept.

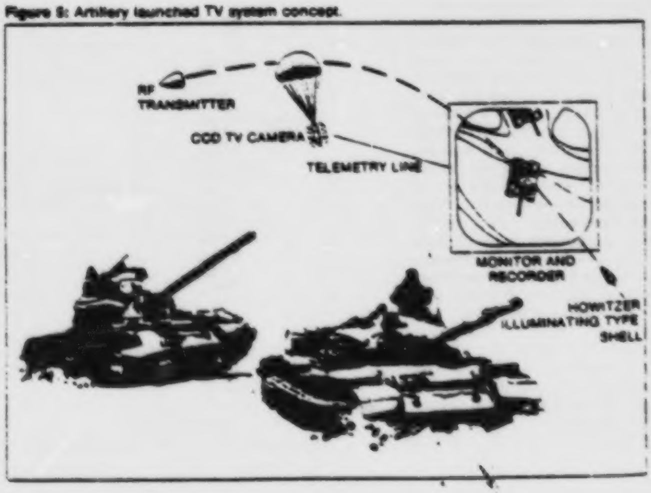

21 G-5

.245" × .245". AIDs applications include:

- Low light level search and surveillance
- Missile and RPV guidance
- Star tracking
- Remote or projectile TV reconnaissance (Figure 5)
- Cockpit or gunsight camera
- Space telescope

Large area AIDs are difficult to produce "blemish free" at low cost. Industry is aggressively addressing reduction and elimination of random defects to achieve practical, low-cost volume-producible AIDs with chip diagonal dimensions in the order of 0.500".

Analog Signal Processors

The CCD has been shown to be a nearly ideal analog shift register. The simplest analog signal processor is a variable analog delay line where the delay obtained is a direct function of the clocking frequency and the number of storage elements in the register. Differential phase and differential gain of 1% or less is available in commercial devices. Tapped CCD delay lines are excellent sampled analog filters and can be externally programmed to change filter characteristics, scan a frequency spectrum, or provide correlation of weak signals in a strong noise background. CCD Analog Signal Processor applications include:

- Video and audio variable delay lines
- Moving target indicator filter
- Signal correlation and convolution
- Sonic imaging
- Voice compression and scrambling
- Video frame-grabber
- Communications and secure communications filter
- Scan rate converter
- Spread spectrum filter

Digital Memory

All CCD memories are basically serial because of the fundamental shift register nature of charge-coupling. They are dynamic memories which require periodic refreshing and, like other semiconductor memories, they are volatile. While their latency is greater than bipolar and MOS memory, they are as much as fifty times faster than magnetic disc and drum memories. Because of the shift-register nature of CCD, the CCD memory devices are block-access oriented rather than random bit accessed. The high bit-count per package allows use of distributed memory and changes in computer architecture. CCD memory applications include:

- Cache memory
- Bulk storage
- Signal analysis for sonar, radar
- Synthetic aperture radar memory
- Digital delay
- Drum and disc replacement

As manufacturing technology continues to improve, all semiconductor memory will enjoy an increase in bit-density and a reduction in device and system costs due to the reduction in package count. CCD memory specifically will continue to remain more dense than bipolar and MOS memory for reasons previously stated. It is probable that CCD memory, because of its lower power dissipation, will be able to shift to packaging capable of being mounted more densely on P.C. boards. It is also probable that power dissipation can be reduced further by designing for operation at lower voltages. Peripheral circuitry such as on-chip drivers will be added to new CCD memory devices to the extent that added power dissipaiton can be tolerated and the additional silicon area required is economical from an overall systems cost standpoint.

Conclusion

Charge-coupled devices are now a family in production, bringing new capability to the military electronics systems designer. The high-volume, low cost production of area image sensors for TV sensing will require a combination of elimination of the causes of random defects from each step in the manufacturing process and improvement in the photo-lithographic techniques for patterning large area arrays so their area can be reduced without reducing responsivity.

Volume production of high performance analog signal processing devices such as filters requires definition of a volume market sufficient to warrant the development costs and application of resources. Increased control of manufacturing processes, particularly accuracy of the photo-lithographic process or its electron-beam successor, will allow the dimensional control necessary to produce devices which are linear over a large dynamic range and have the high rejection characteristics desired.

CCD memory will move ahead in the next few years to 256K bits per package from the present 64K level. Further, reduced power dissipation per bit and more compact packaging are probable. ∎

8-6

FAIRCHILD
A Schlumberger Company

CCD

CHARGE-COUPLED DEVICES

The products of a new concept in semiconductor electronics, they hold considerable promise in applications as diverse as image sensors and information-storage elements for computer memories

by Gilbert F. Amelio

For the past four years there has been a growing excitement among solid-state physicists about a new concept in semiconductor electronics that may someday have an impact on our lives as dramatic as that of the transistor. The new concept is charge-coupling and its practical manifestation is the charge-coupled device.

Like the transistor, the charge-coupled device is a concept of semiconductor electronics; as such it is subject to the same physical laws that govern the transistor's dynamics and fabrication. That, however, is where the similarity ends. Although the charge-coupled device shares much the same technological base with its distinguished predecessor, it is a functional concept that focuses on the manipulation of information rather than an active concept that focuses on the modulation of electric currents. Transistor technology has made possible computer-memory components with thousands of memory elements on a single chip of silicon: charge-coupling is making possible comparably sized memory components with tens of thousands or even hundreds of thousands of memory cells per silicon chip at approximately the same cost.

What is charge-coupling? It is the collective transfer of all the mobile electric charge stored within a semiconductor storage element to a similar, adjacent storage element by the external manipulation of voltages. The quantity of the stored charge in this mobile "packet" can vary widely, depending on the applied voltages and on the capacitance of the storage element. The amount of electric charge in each packet can represent information.

Perhaps the easiest way to visualize the operation of a charge-coupled device is through the use of a mechanical analogy. Imagine a machine consisting of a series of three reciprocating pistons with a crankshaft and connecting rods to drive them [*see top illustration on next two pages*]. On top of one or more of the pistons is a fluid. Note that rotating the crankshaft in a clockwise manner causes the fluid to move to the right, whereas rotating the crankshaft in a counterclockwise manner would cause the fluid to move to the left. Since it takes three pistons to repeat the pattern, this arrangement is called a three-phase system. If it is desired to move the fluid in one direction only, a two-phase system can be devised by imposing an asymmetry on the piston design [*see bottom illustration on next two pages*]. Regardless of the direction of rotation, the fluid now advances to the right.

Analogous charge-coupled devices can be fabricated of silicon [*see illustrations on page 28*]. The devices consist of a "*p* type" silicon substrate (in which electrons are normally the signal carriers) with a silicon dioxide insulating layer on its surface. An array of conducting electrodes is deposited in turn on the surface of the insulator. The electrodes can be interconnected to establish either two-phase or three-phase operation. Underlying the insulator and within the bulk of the semiconductor the electrical conductivity of the silicon can be selectively altered to form "*n* type" material (in which not electrons but electron "holes" are normally the signal carriers). The correspondence with the machine in the mechanical analogy is realized by supposing that the fluid represents an accumulation of electrons, that the pistons represent the potential energy associated with the voltages applied to the electrodes and that the crankshaft and connecting rods represent the driving voltages and their relative timing.

When a periodic wave form called a "clock" voltage is applied to the electrodes, some of the electrons in the vicinity of each electrode will form a discrete packet of charge and move one charge-coupled element, or unit cell, to the right for each full clock cycle. The packets of electron charge therefore move to the right as a result of the continuous lateral displacement of the local "potential well" in which they find themselves. They are thus—or so it seems—always falling.

The creation of the necessary potential well in the semiconductor substrate deserves some elaboration because of its central importance to the charge-coupling concept. In this context a potential well is a localized volume in the silicon that is attractive to electrons; in other words, it is the most positive place around and hence is a desirable location from the point of view of the negative electron. Potential wells are formed in a charge-coupled storage element by the interaction of the different conductivity-

CLOSEUP VIEW of a small portion near the output of a charge-coupled photosensor array is provided by this scanning electron micrograph. Each element and its associated readout electrode measures 1.9 [illegible] mils.

2

B7

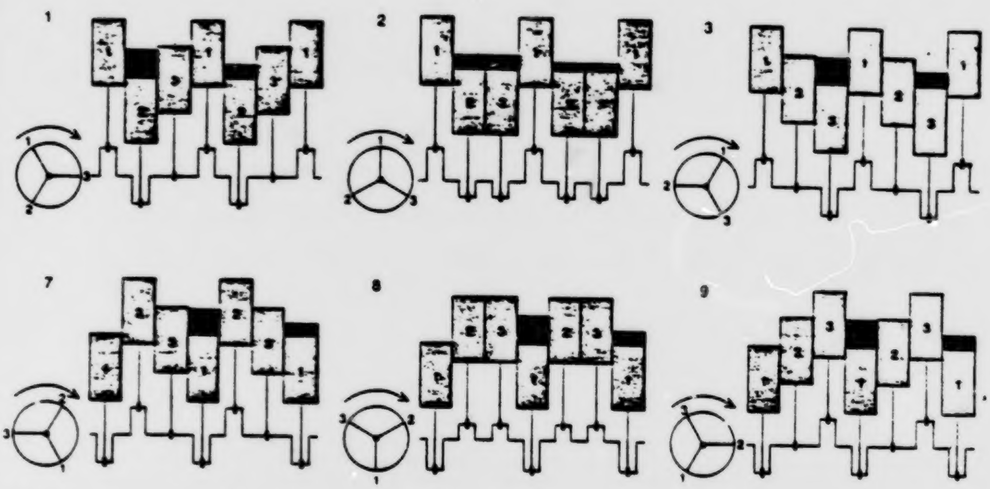

MECHANICAL ANALOGY useful in visualizing the operation of a charge-coupled device is depicted in this sequence of idealized drawings. The machine illustrated consists of a repeating series of three reciprocating pistons with a crankshaft and connecting rods to drive them. On top of one or more of the pistons is a fluid (*color*). Rotating the crankshaft in a clockwise manner, as shown

type regions of the silicon [*see illustration on page 27*]. This interaction forms a well for electrons such that the higher the clock voltage, the deeper the well. Any electrons in the well will move with the clock voltages.

Now, if two or more wells of different depths are placed close to one another, the wells will overlap and charge may be "coupled," or transferred, from one storage element to the next as the depth of the well is altered by the clock voltages. Thus the external clock voltages on the electrodes cause the electrons to move in packets through the semiconductor in a potential-energy trough known as a channel. This mode of electron transfer is the essence of charge-coupling.

The phenomenon of charge-coupling is in itself inadequate for the purpose of constructing a useful device. A practical charge-coupled device must be able to introduce the necessary electrons into the structure and also have a means at some location in the channel for detecting the amount of charge in a packet. Thus for a structure to be classified as a charge-coupled device it must possess at least three attributes: input, charge-coupling and output.

As an example of a simple yet functionally complete charge-coupled device, consider a "shift register" consisting of eight three-phase elements, an input diode and gate and an output diode and gate [*see illustration on page 28*]. This structure is in fact very similar to the first charge-coupled device ever fabricated. The signal that is to be entered into the charge-coupled device is connected to the input diode, which acts as a source of electrons. If the input gate is held at a low voltage, no signal electrons can enter the channel. In order to put a packet of electrons into the device it is necessary to wait until the first-phase electrodes are in the high-voltage condition and then "turn on" the input gate by raising its voltage. Electrons fill the potential well until the energy level for electrons in the well is the same as that for the electrons in the source. The input-gate voltage is now lowered to isolate the source, and the charge packet created is ready for transfer down the channel. In the detection of the signal

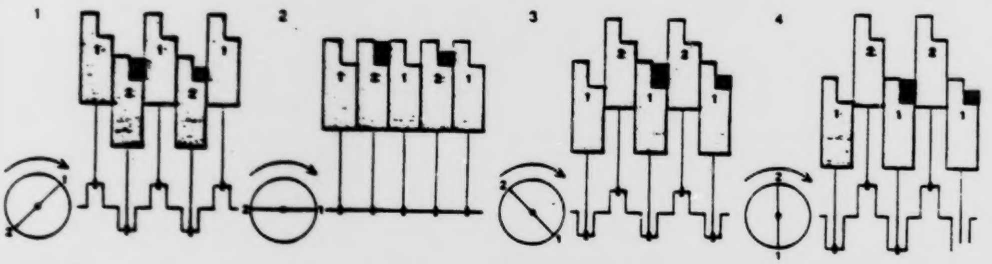

ASYMMETRICAL PISTONS are added to the mechanical analogue in order to introduce the operating principle of a two-phase system. Regardless of the direction in which the crankshaft is rotated, the fluid now advances to the right. In the correspondence

6-3

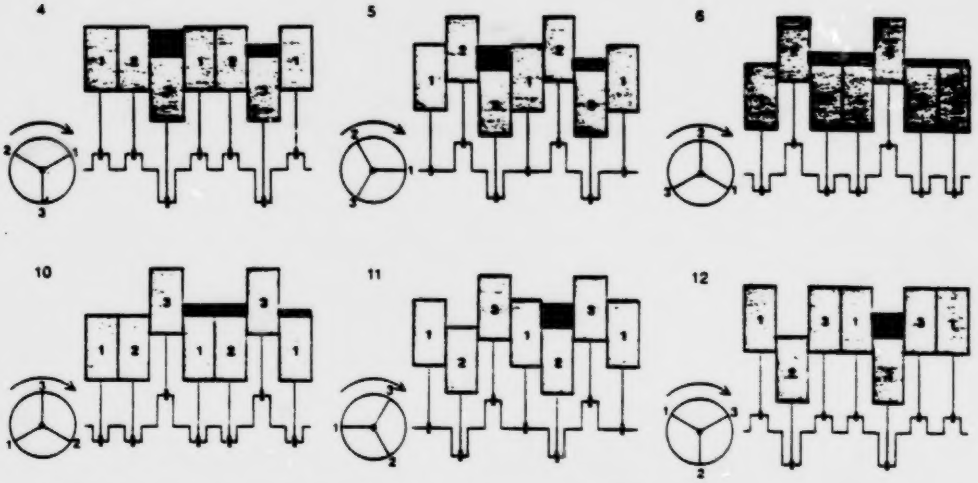

in this instance, causes the fluid to move to the right. If the crankshaft were to be rotated in a counterclockwise manner, on the other hand, the fluid would move to the left. This particular type of arrangement, which requires three pistons to repeat the pattern, is called a three-phase system. An analogous charge-coupled device can be fabricated of silicon (see top *illustration on next page*).

the charge is merely transferred to a "drain," or output diode, where it appears as a current in some external circuit. This simple charge-coupled device fulfills the function of an eight-bit shift register, a device potentially useful in computer architecture.

Devices fabricated and operated in this manner verify the predicted performance with one exception. Unfortunately not all the electrons advance with the packet on each transfer, and the residual charge appears in a trailing packet. The magnitude of such "charge-transfer inefficiency" is a function of the design of the device and the frequency of operation. Transfer inefficiency imposes a fundamental limitation on the speed and number of transfers for a practical charge-coupled device because of the resulting attenuation of the charge packet as it is moved through the device from one region to the next.

There are two reasons for charge-transfer inefficiency. First, the electrons may be inhibited from moving because of local regions of lower potential energy (corresponding to dents or ridges in the top of the piston in the mechanical analogy). Second, the frequency of operation may be so high that there is not enough time for all the electrons to follow the moving potential wells. The former problem is one that is influenced predominantly by the design details of the particular charge-coupled device. Researchers working on the development of such devices are continuing to explore this aspect of charge-coupling. Recent advances in technology have significantly reduced the seriousness of the problem. The problem of the speed of the electrons' motion, however, has more basic origins and deserves additional comment.

The electrons are induced to move to an adjacent region of lower energy (that is, a deeper potential well) by a combination of three influences: self-induced forces, field-aided forces and thermal forces. Self-induced movement results from the simple fact that a high-density packet of electrons (or any similar particles) tends to spread rapidly if the constraining force is removed, as is the case when the clock voltages change. This type of force is important during the

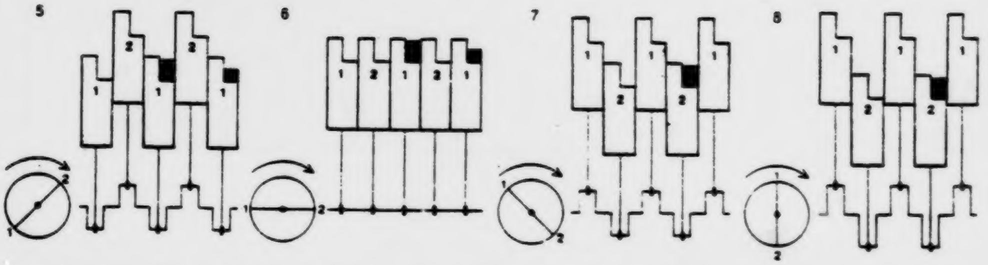

with an actual charge-coupled device the fluid represents an accumulation of electrons, the pistons represent the potential energy associated with the applied voltages and the crankshaft and the connecting rods represent the driving voltages and their timing.

39

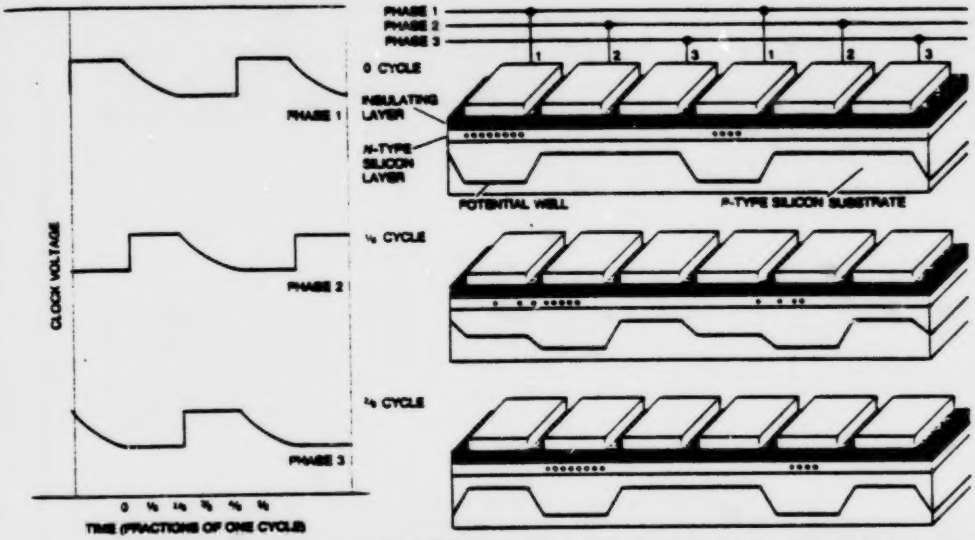
PHASE 1
PHASE 2
PHASE 3
1
2
3
1
2
3
0 CYCLE
INSULATING LAYER
N-TYPE SILICON LAYER
POTENTIAL WELL
P-TYPE SILICON SUBSTRATE
⅓ CYCLE
⅔ CYCLE
PHASE 1
PHASE 2
PHASE 3
CLOCK VOLTAGE
TIME (FRACTIONS OF ONE CYCLE)

TWO THREE-PHASE CHARGE-COUPLED ELEMENTS are shown in the cross-sectional diagram at right; the curves at left give the relative timing of the "clock voltage" wave forms for three-phase operation. The device consists of a "p type" silicon substrate (in which electrons are normally the signal carriers) with a silicon dioxide insulating layer on its surface. Conducting electrodes are deposited on the surface of the insulator. Underlying the insulator and within the bulk of the semiconductor the electrical conductivity of the silicon can be altered to form an "n type" layer (in which electron "holes" are normally the signal carriers). When the clock voltage is applied to the electrodes, some of the electrons in the vicinity of each electrode will form a discrete pocket of charge (black dots) and move one element to the right for each full clock cycle. In effect the pockets of electron charge move to the right as a result of the continuous lateral displacement of the local "potential well" in which they find themselves (white contours in substrate).

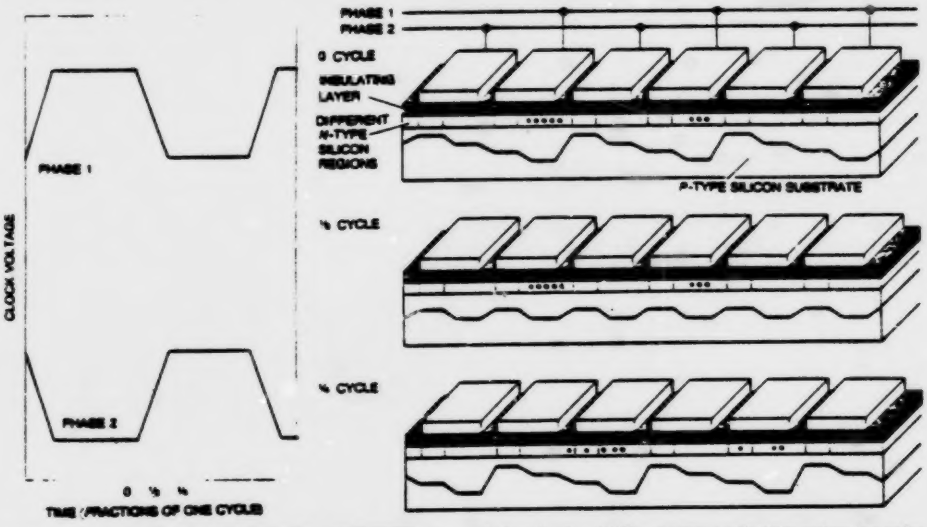
PHASE 1
PHASE 2
0 CYCLE
INSULATING LAYER
DIFFERENT N-TYPE SILICON REGIONS
P-TYPE SILICON SUBSTRATE
¼ CYCLE
½ CYCLE
PHASE 1
PHASE 2
CLOCK VOLTAGE
0
¼
½
TIME (FRACTIONS OF ONE CYCLE)

THREE TWO-PHASE CHARGE-COUPLED ELEMENTS are shown in these cross-sectional diagrams; again the curves give the relative timing of the clock voltages, this time for two-phase operation. Here the potential wells are given the required asymmetry by the introduction of different n-type conductivity regions just under the insulating layer. As in the illustration at the top, the external clock voltages on the electrodes cause the electrons to move in pockets through the n-type semiconductor layer toward the right.

B-10

early stages of charge transfer. Field-aided movement is important if the structure is designed in such a way that electric fields exist to assist the electrons' motion in the desired direction. This corresponds to adding a slope to the top of the pistons in the mechanical analogy. If such a force is present, it is important only toward the end of the charge-transfer cycle. Thermal forces arise from the fact that the electrons receive thermal energy from the silicon lattice and as a result are free to move about randomly. In their random motion they tend to move to regions of minimum electron energy. This type of force is important at the end of the transfer cycle only if field-aided forces are absent.

The self-induced force lasts for only a brief time at the beginning of the transfer cycle, but it is responsible for moving about 90 percent of a "saturation," or full, charge. If the field-aided force is present, it is responsible for moving most of the remaining charge at a rate directly proportional to the strength of the electric field and inversely proportional to the distance between the electrodes. If the field-aided force is not present, the remaining charge will move under the influence of thermal forces at a rate directly proportional to the temperature and inversely proportional to the square of the distance between the electrodes. This rate is usually lower than that resulting from the field-aided force, although at small dimensions it becomes increasingly significant because of its inverse quadratic dependence on distance.

Although these forces are responsible for moving only a comparatively small fraction of the total charge packet, they are important because very little transfer inefficiency can be tolerated in practical devices. For example, if 1 percent of the charge is left behind at each transfer, most of a charge packet will have dispersed after only 100 transfers. In general the charge-transfer inefficiency must approach one part in 10,000 to be considered acceptable for most practical applications. In spite of this requirement, devices that can be operated at frequencies of up to 100 megahertz (100 million cycles per second) are possible if the structures are made small enough. With modern microelectronic manufacturing techniques it is possible to design and build a charge-coupled unit cell with dimensions of less than a mil (a thousandth of an inch) on a side, although it is not always appropriate to do so.

Unit cells of such small dimensions are possible because of the simple nature of the charge-coupled structure, which does not require direct contact with the silicon in the array region. This arrangement is to be contrasted with conventional transistor technology, which in general requires several contacts per functional cell. Contacts consume a significant amount of valuable silicon because of the contact area and the tolerances needed to form a good electrical connection. From the manufacturing viewpoint it is this feature more than any other that makes charge-coupled devices so attractive.

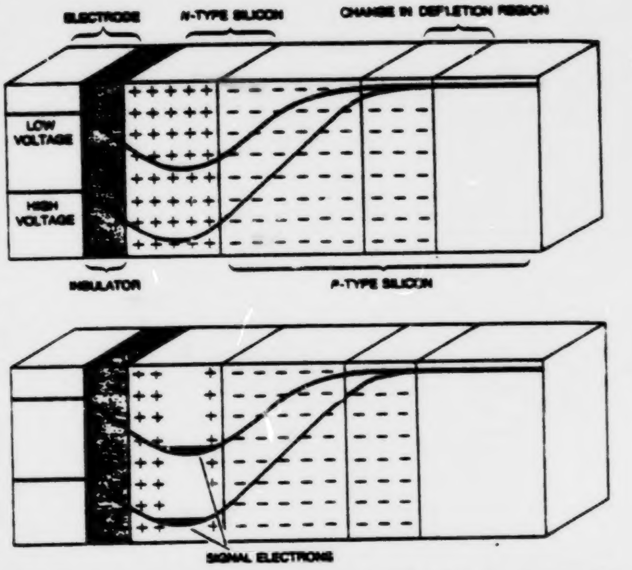

POTENTIAL-ENERGY PROFILES for a typical charge-coupled information-storage element are shown here as a function of distance into the bulk of the semiconductor at right angles to its surface. (In order to show the potential wells clearly, this diagram has been rotated by 90 degrees with respect to the preceding ones.) The charge-distribution patterns are shown for two situations: with no electrons in the well (top) and with some electrons in the well (bottom). As the curves indicate, the higher the clock voltage, the deeper the well.

The ability to generate, move about and detect many separate packets of electrons in a small piece of semiconductor material suggests that the charge-coupling principle can be applied to fulfill a number of information-processing requirements. In particular the highly ordered manipulation of charge packets characteristic of the operation of charge-coupled devices favors uses such as image sensing, computer-memory operation and sampled-signal processing. In each case the function is achieved by a proper combination of charge-coupled unit cells that operate individually exactly as described above.

Silicon, the semiconductor material of which charge-coupled devices are generally fabricated, is highly sensitive to visible and near-infrared radiation (*see illustration on page 9*). In other words, when light falls on a silicon substrate, the radiation is absorbed (by means of the Einstein photoelectric effect), which results in the generation of electrons in a quantity proportional to the amount of incident light. If there is present an array of potential wells such as the one formed by charge-coupled devices, these electrons will fill the wells to a level corresponding to the amount of light in their vicinity. This "electro-optic" creation of electrons represents an input to the charge-coupled device that is entirely different from the input method required for the shift register discussed above and makes the charge-coupling concept useful for very different kinds of application. Nonetheless, the packets of electrons generated by the light can be moved, just as in the shift register, to a point of detection and converted to an electrical signal representative of the optical image incident on the device. That signal, after some conditioning, can be displayed on a cathode ray tube. In this way a charge-coupled device can

B-11

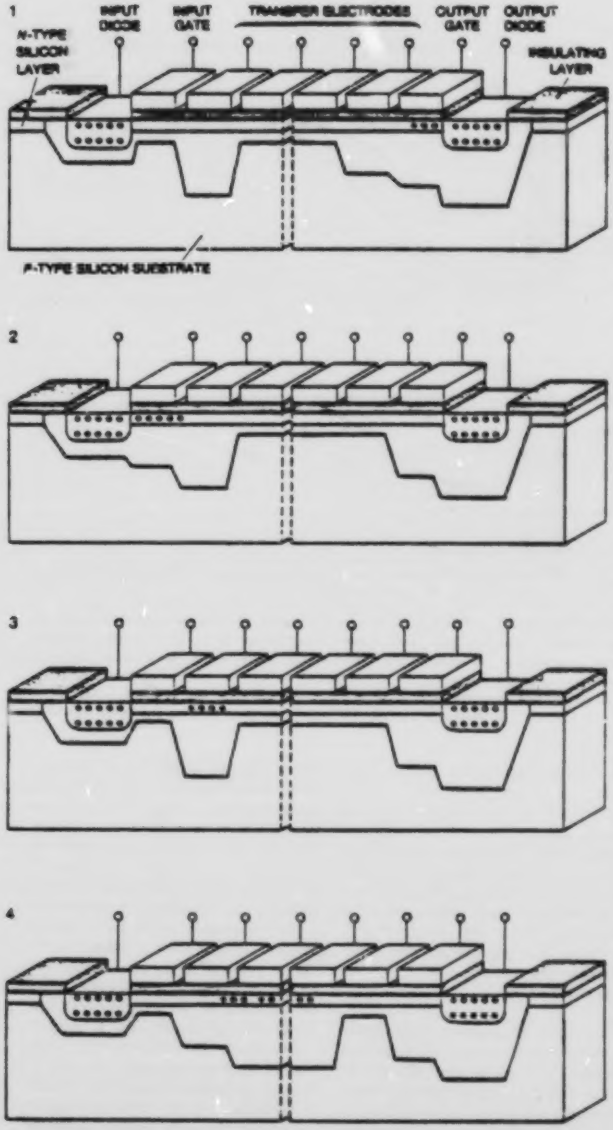

INPUT AND OUTPUT OPERATIONS of a simple eight-element, three-phase charge-coupled "shift register" are summarized in this series of diagrams. The signal enters the device by way of an input diode, which acts as a source of electrons. If the input gate is held at a low voltage, no signal electrons can enter the potential-energy "channel" (1). In order to put electrons into the device one must wait until the first-phase electrodes are in the high-voltage condition and then "turn on" the input gate by raising its voltage (2). Electrons fill the potential well until the energy level for the electrons in the well is the same as that for the electrons in the source. The input-gate voltage is now lowered to isolate the source (3), and the charge packet created is ready for transfer down the channel (4). The signal is detected by transferring the charge packet to an output diode, where it appears as a current.

become the heart of a television camera.

One of the significant advantages of charge-coupled image sensors over vacuum-tube sensors is the precise knowledge of the photosensor locations with respect to one another. In a camera tube the video image is "read" from a photosensitive material by a scanning electron beam. The position of the beam is never precisely known because of the uncertainty in the sweep circuits resulting from random electrical noise. In a charge-coupled sensor the location of the individual photosensor sites is known exactly, since it is determined during the manufacture of the component. Such "metric" accuracy is important for proper alignment in color cameras and in applications requiring data reduction of the acquired image (as in photographic missions in space and photogrammetry).

It is generally convenient for purposes of discussion to separate charge-coupled sensors into two categories: linear sensors and area sensors. A linear image sensor is a simple straight-line array of photosensors with the associated readout and sensing circuitry. An area image sensor is a two-dimensional mosaic of photosensors, again with the associated readout and sensing circuitry.

Linear image sensors are used for a host of applications, including air-to-ground and space-to-ground imaging, facsimile recording and slow-scan television. The image to be viewed is obtained by providing relative motion between the sensor and the scene with the axis of the array perpendicular to the direction of the motion. A resolution of 500 or more photosensor elements is usually required. A primitive linear imaging device can consist of nothing more than a charge-coupled shift register and an output diode. In this structure the image is acquired when one holds the potential wells stationary by stopping the voltage clocks for some period of time (the "integration time") and then rapidly reads out the information by starting the clocks. Such a simple charge-coupled device should be practical only in special applications that allow very long integration times. The reason for this limitation is the "smearing" of the image that results when the shift register is clocked at the same time that it is illuminated.

A really practical charge-coupled linear image sensor is more complex. It consists of a photosensor array for accumulating the photocharge pattern plus an associated charge-coupled shift register with one charge-coupled element for each photosensor element in order to move the resulting charge packets to an output point. The elements of the photo-

B-12

sensor array are individual charge-coupled storage elements with a common electrode called a photogate. They are electrically separated from one another by a highly concentrated *p*-type region called a channel stop. The photosensor array is separated from the charge-coupled shift register by a region over which there is an electrode called the transfer gate.

In operation the photogate voltage is held high and the charge generated by the incident radiation (the photocharge) is collected by the individual photosensor elements. At the end of the integration time the transfer-gate voltage is raised from its normally low voltage condition. The charge-coupled shift-register electrodes adjacent to the photosensor elements are also brought to a high-voltage state. The photogate voltage is then lowered and the accumulated photocharge transfers to the shift register. After that is accomplished the transfer-gate voltage is lowered and the photogate voltage is brought back to its normally high state for another integration period. Meanwhile the charge-coupled shift register is clocked for the purpose of reading out the charge pattern.

A high-density image sensor is more economically designed with one shift register on each side of the photosensor array. Since there must be one charge-coupled element for each photosensor element, the distance between photosensor elements is equal to the distance between the shift-register electrodes for a two-phase charge-coupled shift register and is equal to 1.5 times the distance between shift-register electrodes for a three-phase charge-coupled shift register. In this example the signal charge from the two three-phase shift registers is transported to a three-phase, two-element register for delivery to the on-chip preamplifier. If two-phase technology is used, however, it is possible to shift the charge directly into an output diode, which is in turn the input to the on-chip preamplifier. Note that in either case the information-output rate of the device is twice the rate of either of the long shift registers. It is clear from this example that a two-phase charge-coupled structure not only is easier to clock but also is more economical to lay out for a practical device. Even though it is somewhat more difficult to manufacture because of the required asymmetry, it is likely to dominate future designs of charge-coupled devices when fully developed.

A linear image sensor can be made to produce conventional two-dimensional images [*see illustration on next page*]. The image to be sensed is placed on a rotating drum, which provides the necessary motion of the image with respect to the device. The speed of rotation is synchronized with the vertical scan of the monitor. The charge-coupled linear image sensor provides each horizontal video line for the monitor by a complete sensing and readout operation repeated rapidly to supply all the horizontal lines for a full frame. In many applications the device is the moving element in the system, as in aerial reconnaissance, where the device is located in an airplane or a satellite.

The quality of image reproduction achievable with a linear charge-coupled sensor is excellent, reflecting the large dynamic range of the image sensor [*see illustration on page 31*]. The dynamic range is the ratio of the maximum to the minimum detectable image intensity. The quality of the reproduction demonstrates the very high transfer efficiencies and low electrical noise levels that can be achieved in existing charge-coupled devices.

Area image sensors are useful primarily for television-type camera applications. The image is obtained by conventional line-by-line scanning of the array mosaic and reproduction of the resulting video signal on a standard raster-scanned cathode-ray-tube monitor. A charge-coupled area image sensor designed for such a readout mode can be designed in a manner analogous to the linear image sensor. As in standard broadcast television, the image is read out in two separate fields by first reading all the even-numbered photosensor elements in each column and then all the odd-numbered photosensor elements in each column rather than by reading the odd and even elements in parallel, as in the case of the linear image sensor.

The area image sensor operates as follows. Light falling continuously on the photosensor sites produces electrons, which accumulate as charge packets in the potential wells created by the photogate voltage. After an interval of a thirtieth of a second the charge packets collected in the photosensors adjacent to all the phase-1 electrodes are transferred to the region under the phase-1 electrodes by raising the phase-1 voltage and lowering the photogate voltage. The charge packets in photosensor sites adjacent to the phase-2 electrodes do not transfer because the phase-2 voltage remains low. After the phase-1 transfer takes place the photogate voltage again goes to its normally high state and more electrons begin to accumulate in the depleted photosensor sites. The charge packets in the opaqued shift register are now transferred to the horizontal shift register at the top of the array. Each vertical transfer fills the horizontal register, which is then read out completely, producing a line of video information at the out-

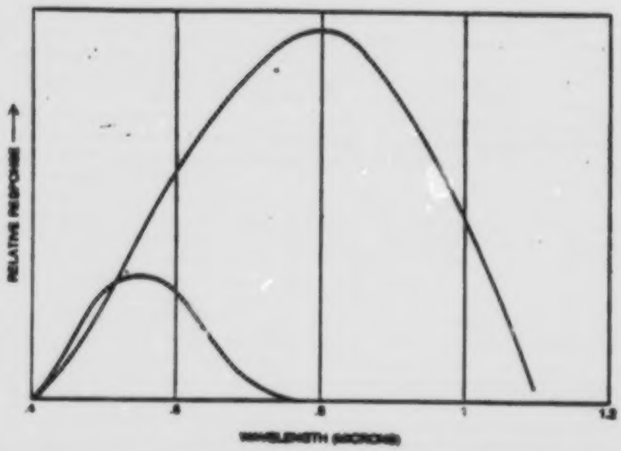

RELATIVE SPECTRAL RESPONSES of a charge-coupled silicon photosensor element (colored curve) and the human eye (black curve) are compared. The semiconductor material absorbs not only visible light (.4 to .7 micron) but also near-infrared radiation (.7 micron to 1.1 microns). The absorption of such radiation by a silicon substrate results in the generation of electrons in a quantity proportional to the amount of incident radiation. It is this "electro-optic" property that enables charge-coupled devices to be used as image sensors.

B-13

put. After all these lines are read out (a procedure that takes only a sixtieth of a second) the photosensors adjacent to all the phase-2 electrodes are read out, and in a similar manner this second field is delivered as a video signal at the output. Finally, the entire operation begins again and is completed at regular intervals of a thirtieth of a second.

A typical image sensor designed to operate in this fashion consists of a rectangular 100-by-100 photosensor grid [see illustration on page 23]. Each photosensor element and associated readout electrode occupies only 1.9 square mils. All 10,000 elements fit on a chip that measures .12 by .16 inch. An image taken with a camera system using such a device can be displayed on a television monitor.

This image-sensing device and others made by charge-coupled techniques are still somewhat primitive, but they clearly point the way toward a powerful camera technology. The combination of solid-state reliability, low-voltage operation, low power dissipation, large dynamic range, metric reproducibility and visible and near-infrared response offers to the potential user a compelling advantage over vacuum-tube image sensors and other solid-state image sensors.

The charge-coupling concept is basically one of semiconductor electronics rather than one of electro-optics. Because of the electro-optic characteristics of silicon, however, the light-sensing properties of charge-coupled arrays have tended to dominate this new technology. Nonetheless, the data-handling properties of such arrays may be of equal or even greater significance.

A charge-coupled semiconductor array is virtually ideal as a time-sampled analogue shift register. From the viewpoint of the electrical engineer this means a delay line where the delay is proportional to the readin/readout rate; if the array is long enough to contain the complete message, the readin and readout rates can be different and the maximum delay available is limited only by the thermal generation of random electrons. At low temperatures several minutes of delay are possible.

As a memory or digital-storage device, charge-coupled arrays can perform the functions of sequential access or hybrid tasks such as drum or disk storage. The use of solid-state charge-coupled arrays to eliminate all mechanical motion and parts is a strong advantage of a memory consisting of charge-coupled devices.

The intrinsic analogue nature of the charge packet in a charge-coupled device suggests broad potential for application to sampled-signal processing. In a fundamental sense the use of charge-coupled devices as image sensors is merely a special application of the device as an analogue shift register. If one restricts the definition of sampled-signal devices to those with an electrical (rather than an optical) input, then the predominant members of this class are variable delay lines and filters.

A delay line is a circuit that reproduces as accurately as possible an input signal delayed by a finite period of time. A delay line is "variable" if the time delay can be altered electrically. The charge-coupled device acts as a natural delay line since any signal placed on its input diode will appear at its output in sampled form after the interval required for the charge packets to be shifted through all the elements of the structure. The charge-coupled device can be used as a delay line in several ways. First, in the simple continuous mode the delay is equal to the number of unit cells divided by the frequency at which the device is clocked. Alternatively, whenever data appear in bursts, the charge-coupled shift register can be loaded with these data during the burst and the data retained for the desired interval and then read out. In this way the charge-coupled device is said to perform a "buffer" function.

A charge-coupled delay line offers major advantages over the more conventional glass delay line and even significant advantages over the more exotic acoustic-surface-wave devices [see "Acoustic Surface Waves," by Gordon S. Kino and John Shaw; SCIENTIFIC AMERICAN, October, 1972]. Among these are wide dynamic range (better than 60 decibels after 30 milliseconds at room temperature) and separate electronic control of propagation velocity and delay time. Delay lines with such flexibility will be of great value in communications and television applications and will simplify existing methods of producing controlled signal delays. One special application of significant interest is a "scan-rate converter" often required in video communications. Here the charge-coupled device operates in the buffer mode described above to accept and then read

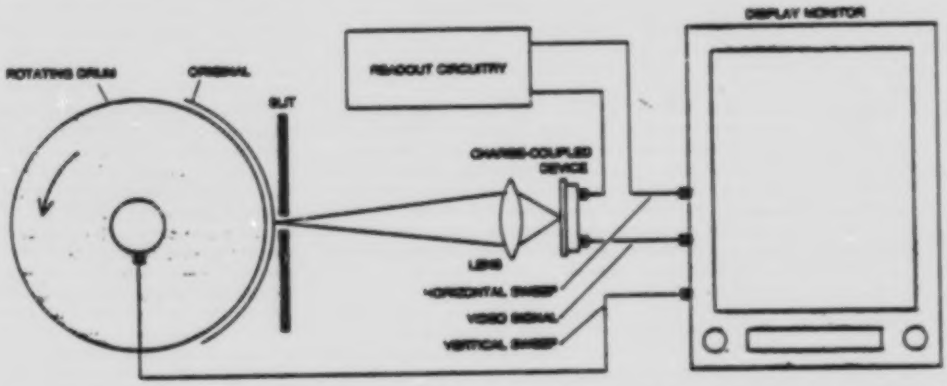

TWO-DIMENSIONAL IMAGES can be reproduced with the aid of a linear charge-coupled image sensor in a variety of ways, one of which is outlined in this schematic diagram. The image to be sensed is placed on a rotating drum (*left*) whose speed of rotation is synchronized with the vertical scan of a conventional television display monitor (*right*). The charge-coupled device and the associated readout circuitry produce horizontal video lines at a rate rapid enough to build up a full-frame image on the screen of the monitor.

6-A

FAIRCHILD
A Schlumberger Company

CCD

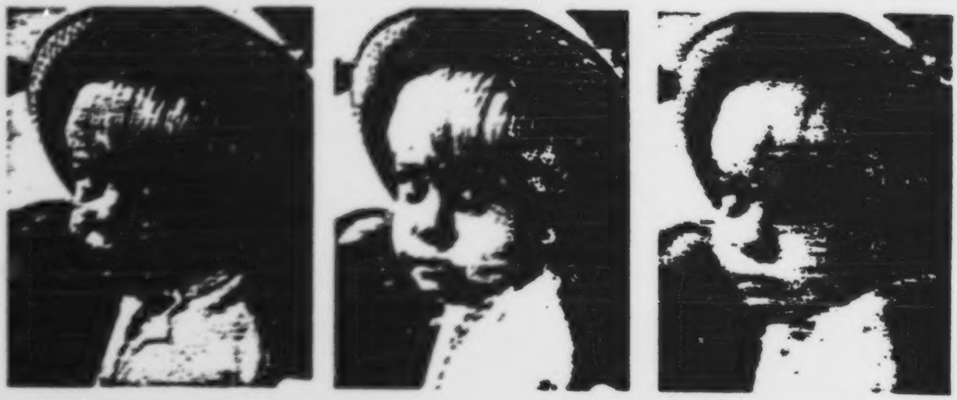

EXCELLENT REPRODUCTION obtained with a 500-element linear charge-coupled image sensor under widely varying light conditions is evident in these photographs. An apparatus similar to the one in the illustration on the opposite page was employed to scan the image. The photograph at left shows the original image to be scanned. The photograph at center shows the video display obtained from the charge-coupled system under optimum lighting conditions (30 foot-candles of illumination). The photograph at right shows the video display obtained from the same system but with the light level reduced 1,000 times; to produce this picture the charge-coupled device had to move packets of approximately 400 electrons each through a centimeter of silicon without dispersion.

out video frames at different rates so as to match practical transmission-system bandwidths with standard television-display requirements.

Extension of the simple delay-line concept leads to other sampled-signal processing devices. If a delay line is fabricated with interim taps at which the signal can be sensed and fed back to earlier stages in such a way as to affect the transmission of the data, then this structure can be used as a filter. Such a structure can be conveniently configured as a band-pass filter where the resonant frequency of the circuit is a direct function of the clock frequency. An improvement in the signal-to-noise ratio to within a decibel of the theoretical maximum has already been achieved.

Matched filters find application in wide-spectrum communications and in radar to detect weak signals in high noise backgrounds. In such applications charge-coupled devices will complement acoustic-surface-wave devices, which generally are useful only for delays of less than 100 microseconds.

As mentioned above, a charge-coupled storage element is capable of storing a packet of electrons with a varying amount of charge, depending on the design and operating conditions of the charge-coupled unit cell. Nonetheless, there is no reason one cannot conceptually quantize the charge-handling ability of the cell and view the device as a binary digital element. For example, one can arbitrarily say that if a storage element contains a charge less than half the saturation charge, it contains a "zero," whereas if it possesses a charge greater than half the saturation charge, it contains a "one." In this way the storage element becomes a memory "bit" and a charge-coupled delay line can be made to serve the function of a digital shift register or serially accessible memory. Since this function can be performed by other technologies also, one must ask what charge-coupling has to offer. The answer is cost-effectiveness. A charge-coupled memory not only has all the advantages of a conventional semiconductor component (compatibility with other electronic circuit elements, no mechanical motion, low power and voltage, variable clocking rates and other similar features) but also offers a potentially low cost-per-bit ratio approaching that of a magnetic memory. This is a result of the inherent structural simplicity of the charge-coupled device. By virtue of this simplicity, memory arrays as large as a quarter of a million bits per component on a piece of silicon less than half an inch on a side can be envisioned.

In addition, the power necessary to sustain a charge-coupled memory device is very low since the storage element is not active. The power required to move the charge stored on one charge-coupled element to an adjacent element in a microsecond is approximately a microwatt. Moreover, in a properly organized memory it is not necessary to have all bits moving simultaneously. Thus a one-megahertz, one-megabit charge-coupled memory device would require a power of somewhere between a milliwatt and a watt to sustain it, excluding logic and other functions. The volume required for such a memory is less than that of a pack of cigarettes.

Another advantage lies in the fact that the charge-coupled device is basically analogue in nature. It is thus possible to store more than one data bit in each memory cell. This can be done by storing any one of a number of discrete levels of charge in each cell, thereby greatly increasing the information-packing density. For example, a 100,000-cell device capable of handling eight levels of charge is comparable to a 300,000-bit conventional memory. Such a memory chip would be of great value in digital-to-analogue and analogue-to-digital converters and other applications where multiple levels are achieved only by the addition of vast amounts of memory.

In view of these important prospective features of charge-coupled memory devices it appears that we are at the dawn of a revolution that will ultimately bring today's powerful digital computers directly into our everyday way of life. The charge-coupling concept, in short, is a major new innovation in semiconductor electronics. By virtue of its simplicity in design and fabrication, its high performance in terms of dynamic range and low power, and its high packing density and potentially low cost, the technology of charge-coupling will create major and unique new applications for semiconductors that will have a direct impact on our lives.

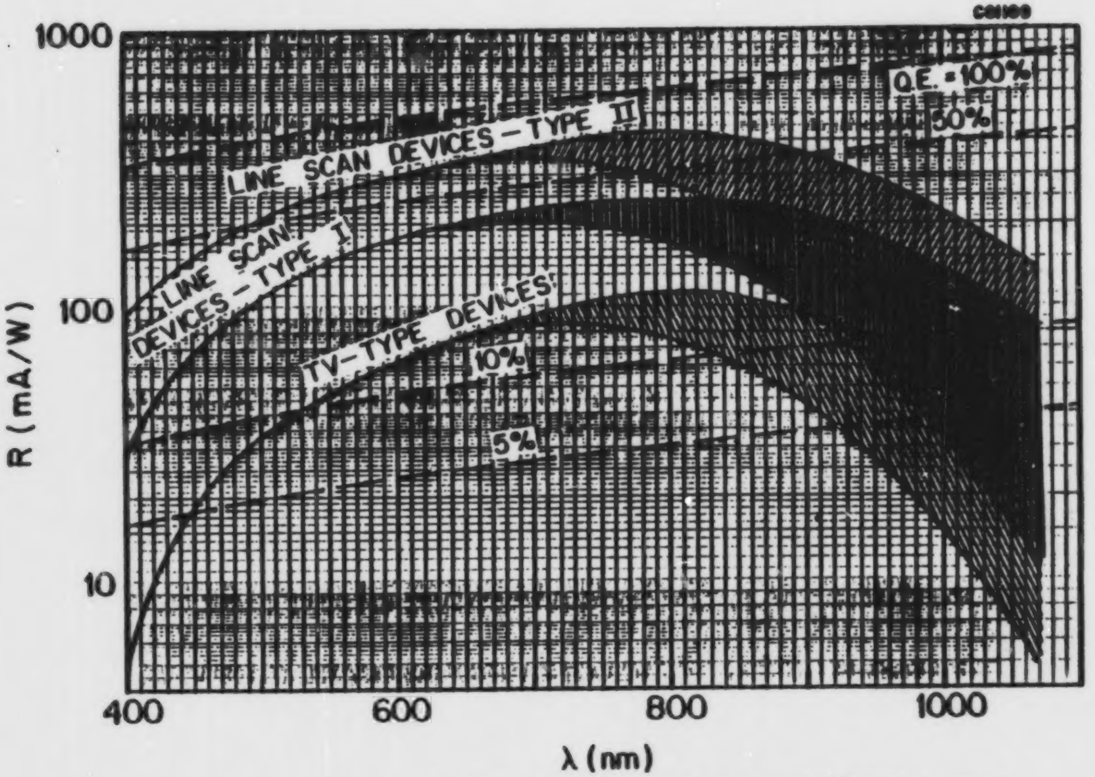

TYPICAL INTERNAL SPECTRAL RESPONSE (SMOOTHED)

B-16

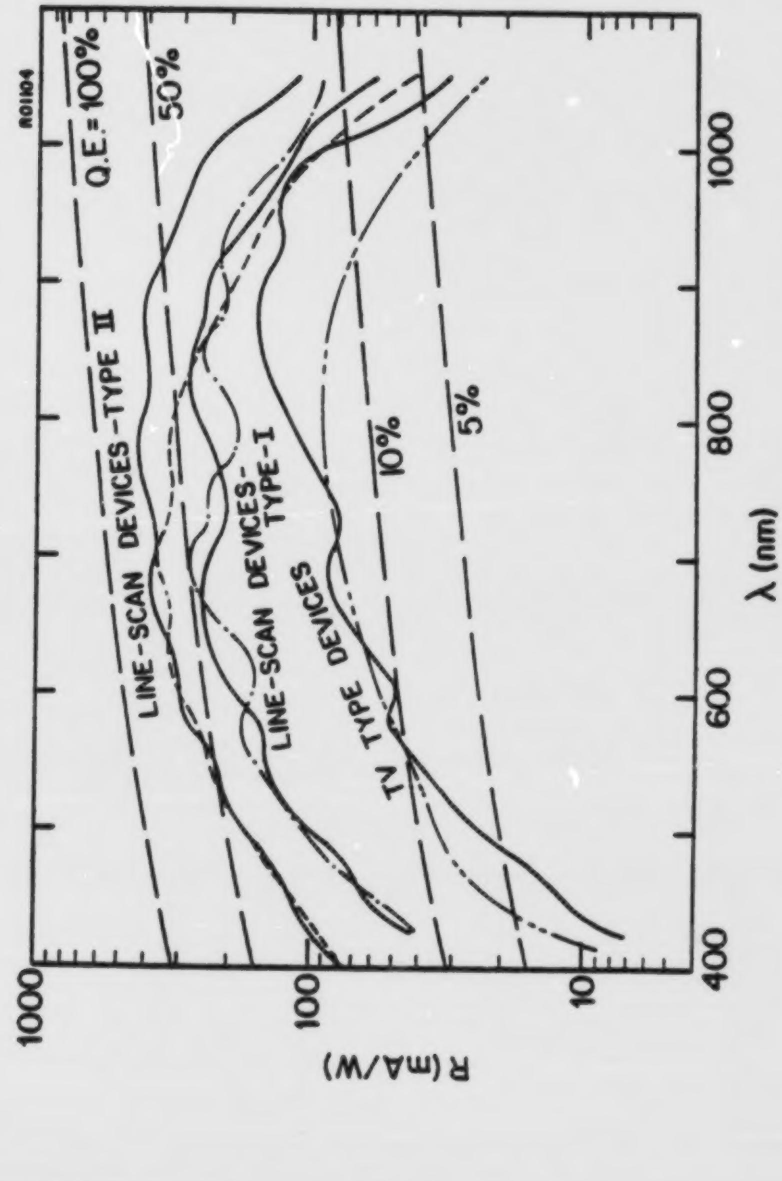

TYPICAL INTERNAL SPECTRAL RESPONSE (UNSMOOTHED)

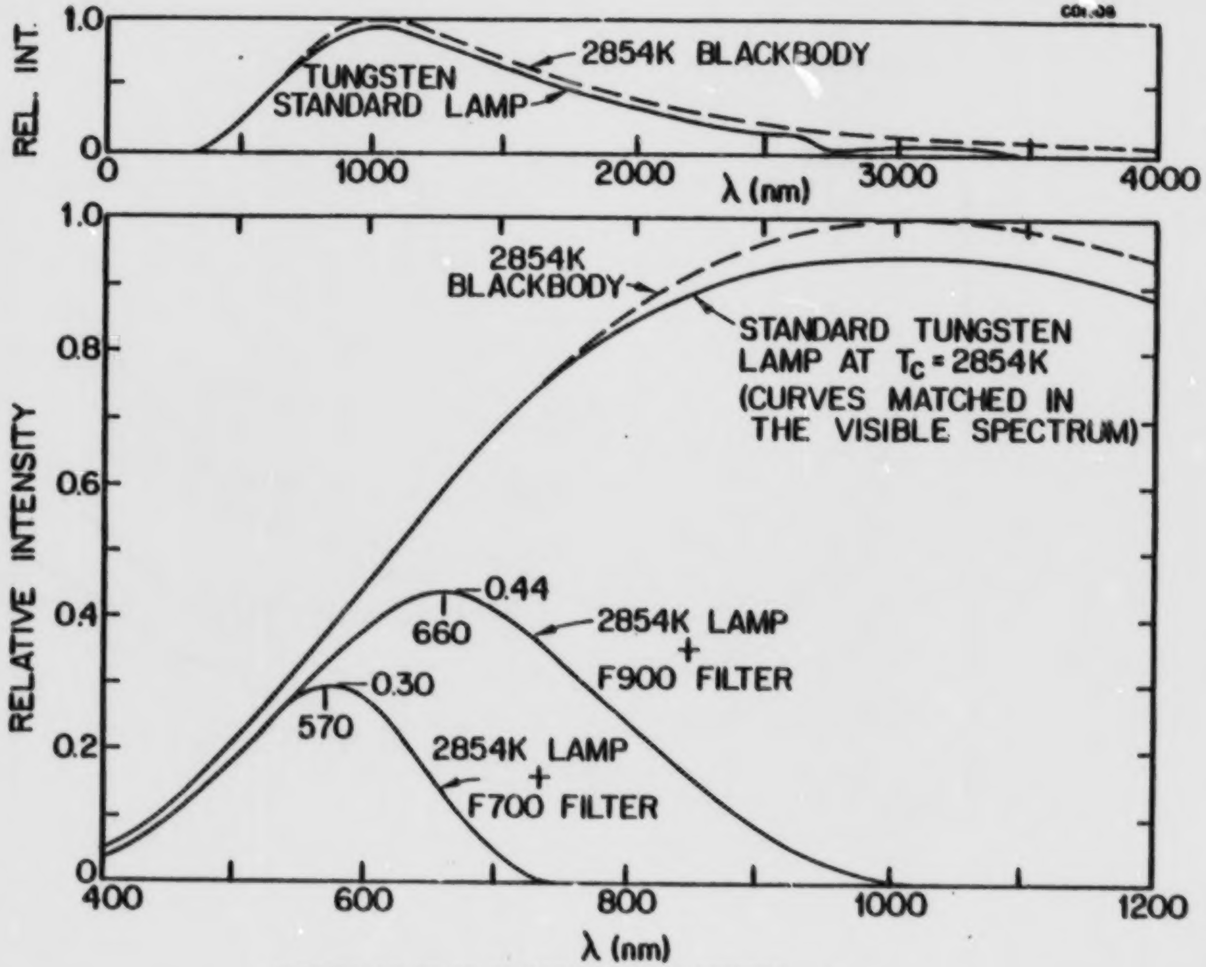

SPECTRA OF THREE BROADBAND LIGHT SOURCES

6.17

FAIRCHILD
A Schlumberger Company

CCD151
3456 – Element
Line Scan Image Sensor

CCD Imaging

DESCRIPTION

The CCD151 is a 3456-element line image sensor designed for page scanning applications including facsimile, copier, optical character recognition and other imaging applications which require very high resolution, high sensitivity and high data rates.

The 3456 sensing elements of the CCD151 provide a 400-line per inch resolution across an 8½ inch page which is double the international facsimile standard and satisfactory for many copier applications.

The photoelement size is 7μm (0.28 mils) by 7μm (0.28 mils) on 7μm (0.28 mils) centers. The device is manufactured using Fairchild advanced charge-coupled device n-channel isoplanar buried-channel technology.

FEATURES

- VERY HIGH RESOLUTION: 3456 ELEMENTS
- SMALL ELEMENT PITCH: 7μm
- LOW DARK SIGNAL
- HIGH RESPONSIVITY
- DYNAMIC RANGE TYPICAL: 2500:1
- OVER 1V PEAK-TO-PEAK OUTPUT
- DARK REFERENCE CONTAINED IN SAMPLED-AND-HELD OUTPUT

CONNECTION DIAGRAM
DIP (TOP VIEW)

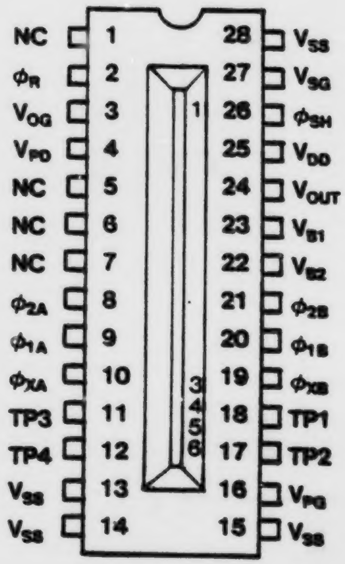

PIN NAMES

V_{PG}	Photogate
ϕ_{XA}, ϕ_{XB}	Transfer Clocks
ϕ_{1A}, ϕ_{2A} ϕ_{1B}, ϕ_{2B}	Transport Clocks
V_{OG}	Output Gate
V_{OUT}	Video Output Terminal
V_{DD}	Output Amplifier Drain
V_{B1}	Output Amplifier Bias 1
V_{B2}	Output Amplifier Bias 2
ϕ_{R}	Reset Clock
ϕ_{SH}	Sample-and-Hold-Clock
V_{SG}	Signal Ground
V_{SS}	Substrate (Ground)
NC	No Connection
TP1, TP2 TP3, TP4	Test Points
V_{PD}	Peripheral Diode

Fairchild Camera and Instrument Corporation
3440 Hillview Avenue, Palo Alto, California 94304
(415) 493-8001, TWX 910-373-2110

©1983 Fairchild Printed in U.S.A.
July 1983 Fairchild reserves the right to make changes in the circuitry or specifications at any time without notice.

BLOCK DIAGRAM

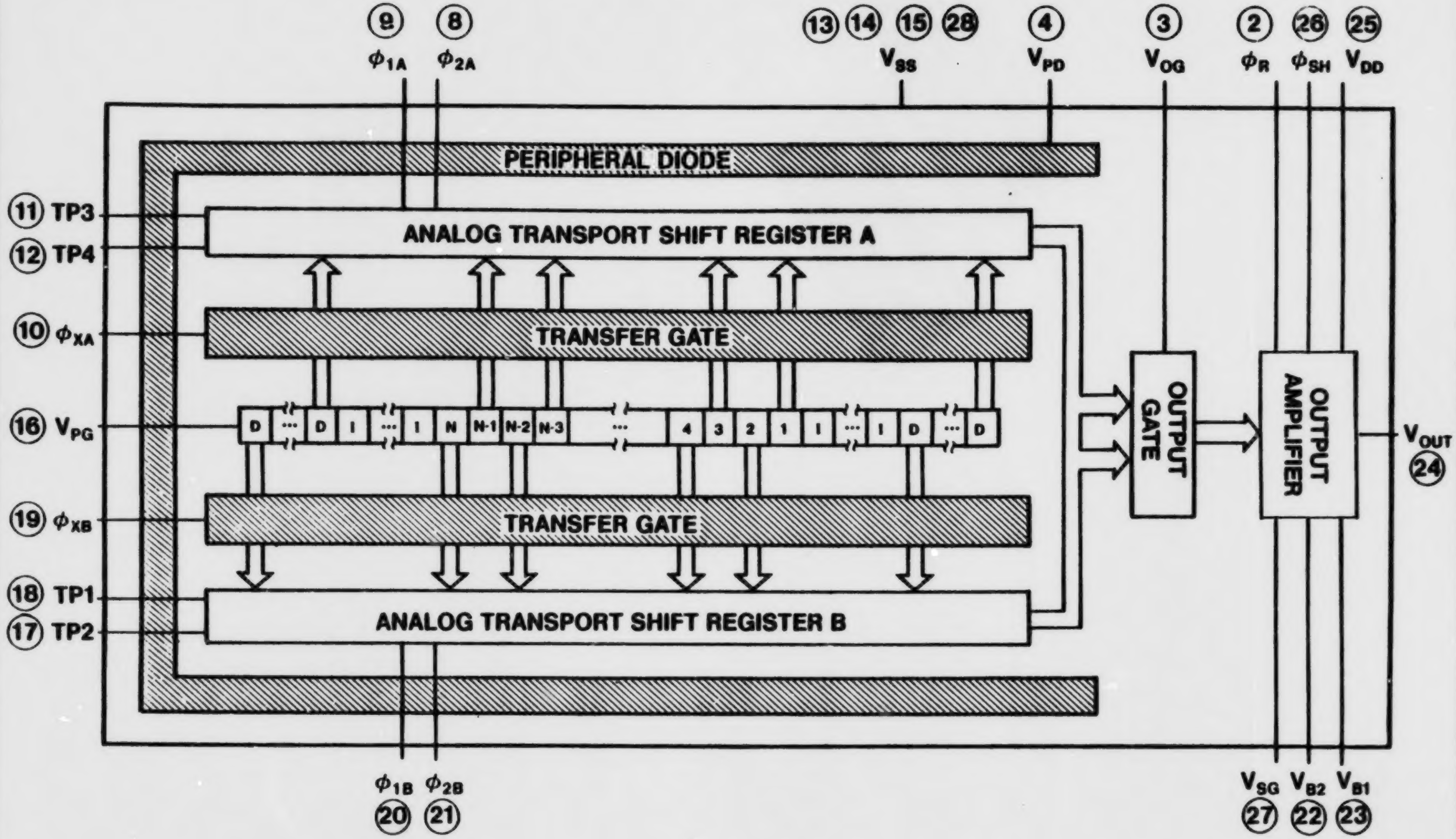
⑨ ϕ_{1A}
⑧ ϕ_{2A}
⑬ ⑭ ⑮ ㉘ V_{SS}
④ V_{PD}
③ V_{OG}
② ϕ_R
㉖ ϕ_{SH}
㉕ V_{DD}
PERIPHERAL DIODE
⑪ TP3
⑫ TP4
ANALOG TRANSPORT SHIFT REGISTER A
⑩ ϕ_{XA}
TRANSFER GATE
⑯ V_{PG}
D ... D I ... I N N-1 N-2 N-3 ... 4 3 2 1 I ... I D ... D
⑲ ϕ_{XB}
TRANSFER GATE
⑱ TP1
⑰ TP2
ANALOG TRANSPORT SHIFT REGISTER B
OUTPUT GATE
OUTPUT AMPLIFIER
V_{OUT} ㉔
ϕ_{1B} ⑳
ϕ_{2B} ㉑
V_{SG} ㉗
V_{B2} ㉒
V_{B1} ㉓

○ = CCD 151 PIN NUMBER
D = DARK REFERENCE CELL
I = ISOLATION CELL
N = 3456 FOR CCD 151

FUNCTIONAL DESCRIPTION

The CCD151 consists of the following functional elements illustrated in the Block Diagram:

Image Sensor Elements — A row of 3456 image sensor elements separated by a diffused channel stop and covered by a silicon dioxide surface passivation layer. Image photons pass through the transparent silicon dioxide layer and are absorbed in the single crystal silicon creating hole-electron pairs. The photon generated electrons are accumulated in the photosites. The amount of charge accumulated in each photosite is a linear function of the incident illumination intensity and the integration period. The output signal will vary in an analog manner from a thermally generated background level at zero illumination to a maximum at saturation under bright illumination.

Two Transfer Gates — Gate structures adjacent to the row of image sensor elements. The charge packets accumulated in the image sensor elements are transferred out via the transfer gates to the transport registers whenever the transfer gate voltages go HIGH. Alternate charge packets are transferred to the A and B transport registers.

Two Analog Transport Shift Registers — One on each side of the line of image sensor elements and are separated from it by a transfer gate. The two registers, called the transport registers, are used to move the light generated charge packets delivered by the transfer gates serially to the charge detector/amplifier. The complimentary phase relationship of the last elements of the two transport registers provides for alternate delivery of charge packets to establish the original serial sequence of the line of video in the output circuit.

A Gated Charge Detector/Amplifier — Charge packets are transported to a precharged diode whose potential changes linearly in response to the quantity of the signal charge delivered. This potential is applied to the gate of the output n-channel MOS transistor producing a signal at the output V_{OUT}. A reset transistor is driven by the reset clock (ϕ_R) and recharges the charge detector diode capacitance before the arrival of each new signal charge packet from the transport registers.

Dark Reference Circuitry — Eight additional sensing elements at both ends of the array are covered by opaque metalization. They provide a dark (no illumination) signal reference which is delivered at both ends of the line of video output representing the illuminated sensor elements (labeled "D" in the Block Diagram). These reference levels are useful as inputs to external dc restoration circuitry.

Peripheral Diode — Serves to reduce peripheral electron noise in the inner shift registers.

DEFINITION OF TERMS

Charge-Coupled Device — A charge-coupled device is a semiconductor device in which finite isolated charge packets are transported from one position in the semiconductor to an adjacent position by sequential clocking of an array of gates. The charge packets are minority carriers with respect to the semiconductor substrate.

Pixel — A picture element (photosite).

Transfer Clocks ϕ_{XA}, ϕ_{XB} — The voltage waveforms applied to the transfer gates to move the accumulated charge from the image sensor elements to the CCD transport registers.

Transport Clocks ϕ_{1A}, ϕ_{2A}, ϕ_{1B}, ϕ_{2B} — The two sets of 2-phase waveforms applied to the gates of the transport registers to move the charge packets received from the image sensor elements to the gated charge detector/amplifier.

Sample-and-Hold Clock ϕ_{SH} — The voltage waveform applied to the sample-and-hold gate in the output amplifier to create a continuous sampled video signal at the output. The sample-and-hold feature may be defeated by connecting ϕ_{SH} to V_{DD}.

Gated Charge Detector/Amplifier — The output circuit of the CCD151 that receives the charge packets from the transport registers and provides a signal voltage proportional to the size of each charge packet received. Before each new charge packet is sensed, a reset clock returns the charge detector voltage to a fixed level.

Reset Clock ϕ_R — The voltage waveform required to reset the voltage on the charge detector.

Dark Reference — Video output level generated from sensing elements covered with opaque metalization which provides a reference voltage equivalent to device operation in the dark. This permits use of external dc restoration circuitry.

Isolation Cell — This is a site on-chip producing an element in the video output that serves as a buffer between valid video data and dark reference signals. The output from an isolation cell contains no valid video information and should be ignored.

Dynamic Range — The saturation exposure divided by the rms noise equivalent exposure. (This does not take into account dark signal components.) Dynamic range is sometimes defined in terms of peak-to-peak noise. To compare the two definitions a factor of four to six is generally appropriate in that peak-to-peak noise is approximately equal to four to six times rms noise.

RMS Noise Equivalent Exposure — The exposure level that gives an output signal equal to the rms noise level at the output in the dark.

Saturation Exposure — The minimum exposure level that will provide a saturation output signal. Exposure is equal to the light intensity times the photosite integration time.

Charge Transfer Efficiency — Percentage of valid charge information that is transferred between each successive stage of the transport registers.

Spectral Response Range — The spectral band in which the response per unit of radiant power is more than 10% of the peak response.

Responsivity — The output signal voltage per unit exposure for a specified spectral type of radiation. Responsivity equals output voltage divided by exposure.

Total Photoresponse Non-uniformity — The difference of the response levels of the most and the least sensitive elements under uniform illumination. Measurement of PRNU excludes first and last elements.

Dark Signal — The output signal in the dark caused by thermally generated electrons that is a linear function of the integration time and highly sensitive to temperature.

Saturation Output Voltage — The maximum useable signal output voltage. Charge transfer efficiency decreases sharply when the saturation output voltage is exceeded.

Integration Time — The time interval between the falling edges of any two transfer pulses ϕ_{XA} or ϕ_{XB} as shown in the timing diagram. The integration time is the time between transfers of signal charge from the photosites into the transport registers.

3'

B-

TEST LOAD CONFIGURATION

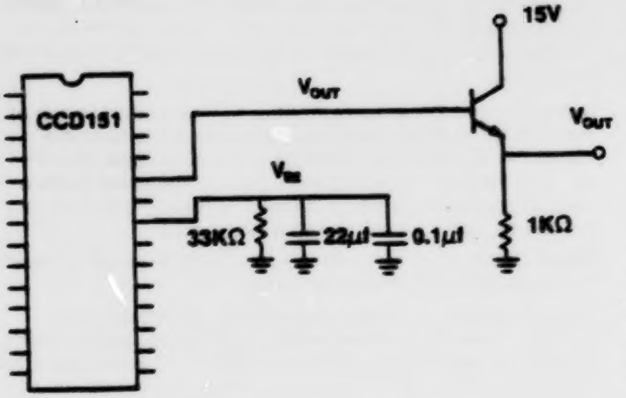

ABSOLUTE MAXIMUM RATINGS

(Above which useful life may be impaired)

Storage Temperature	−25°C to +125°C
Operating Temperature (See Curves)	−25°C to +70°C
Pins 2, 3, 4, 8, 9, 10, 11, 12, 17, 18, 19, 20, 21, 22, 23, 25, 26, 27	−0.3 V to 18V
Pin 16	−0.3 V to 16V
Pins 13, 14, 15, 28	0V
Pins 1, 5, 6, 7 (See Caution Note)	NC
Pin 24 (See Caution Note)	Video Output

CAUTION NOTE: These devices have limited built-in gate protection. It is recommended that static discharge be controlled and minimized. Care must be taken to avoid shorting V_{OUT} to V_{SS}, or V_{DD} during operation of the devices. Shorting these pins even temporarily may destroy the output amplifiers.

Do not connect anything to a pin marked NC. They may be internally connected.

DC CHARACTERISTICS: $T_p = 25°$ (Note 1)

SYMBOL	CHARACTERISTIC	RANGE			UNITS	NOTES
		MIN.	TYP.	MAX.		
V_{DD}	Output Amplifier Drain Supply Voltage	14.5	15.0	15.5	V	
I_{DD}	Output Amplifier Drain Supply Current		5.0	16.1	mA	
V_{PG}	Photogate Bias Voltage	4.0	4.5	5.0	V	
V_{PD}	Peripheral Diode Voltage	14.5	15.0	15.5	V	
V_{OG}	Output Gate Voltage	7.5	8.0	8.5	V	
V_{B1}	Output Amplifier Bias 1	4.5	5.0	5.5	V	
V_{B2}	Output Amplifier Bias 2					16
V_{SS}	Signal Ground		0.6		V	
V_{SS}	Substrate (Ground)		0.0		V	
TP1, TP3	Test Points	4.0	4.5	5.0	V	
TP2, TP4	Test Points	14.5	15.0	15.5	V	

CLOCK CHARACTERISTICS: $T_p = 25°$ (Note 1)

SYMBOL	CHARACTERISTIC	RANGE			UNITS	NOTES
		MIN.	TYP.	MAX.		
$V_{\phi 1AL}$, $V_{\phi 1BL}$ $V_{\phi 2AL}$, $V_{\phi 2BL}$	Transport Clocks LOW	0.0	0.6	1.0	V	2, 3, 4
$V_{\phi 1AH}$, $V_{\phi 1BH}$ $V_{\phi 2AH}$, $V_{\phi 2BH}$	Transport Clocks HIGH	11.5	12.0	12.5	V	3, 4
$V_{\phi XAL}$, $V_{\phi XBL}$	Transfer Clocks LOW	0.0	0.6	1.0	V	2, 5
$V_{\phi XAH}$, $V_{\phi XBH}$	Transfer Clocks HIGH	11.5	12.0	13.5	V	5
$V_{\phi RL}$	Reset Clock LOW	0.0	0.6	1.0	V	2, 6
$V_{\phi RH}$	Reset Clock HIGH	11.5	12.0	12.5	V	6
$V_{\phi SL}$	Sample Clock LOW	0.0	0.6	1.0	V	2, 7
$V_{\phi SH}$	Sample Clock HIGH	11.5	12.0	12.5	V	7
$f_{\phi R}$	Maximum Reset Clock Frequency (Output Data Rate)	2.5	5.0		MHz	8

AC CHARACTERISTICS: $T_p = 25° C$, $f_{\phi R} = 1.0MHz$, $t_{int} = 4ms$, Light Source = 2854° K + 2.0mm thick Schott BG-38 and OCLI WBHM filters.* All operating voltages nominal specified values. (Note 1)

SYMBOL	CHARACTERISTIC	RANGE			UNITS	NOTES
		MIN.	TYP.	MAX.		
DR	Dynamic Range					
	(relative to rms noise)	500:1	2500:1			9
	(relative to peak-to-peak noise)	100:1	500:1			
NEE	RMS Noise Equivalent Exposure		.0001		μJ/cm²	10
SE	Saturation Exposure		.360		μJ/cm²	10, 11
CTE	Charge Transfer Efficiency		.99999		%	12
V_O	Output DC Level	4.0	5.5	7.5	V	
P	Power Dissipation		75	250	mW	
Z	Output Impedance		1.5	3.0	kΩ	
N	Peak-to-Peak Noise		4		mV	

PERFORMANCE CHARACTERISTICS: $T_p = 25° C$, $f_{\phi R} = 1.0MHz$, $t_{int} = 4ms$, Light Source = 2854° K + 2.0mm thick Schott BG-38 and OCLI WBHM filters.* All operating voltages nominal specified values. (Note 1)

SYMBOL	CHARACTERISTICS	RANGE			UNITS	NOTES
		MIN.	TYP.	MAX.		
PRNU**	Photoresponse Non-uniformity					
	Peak-to-Peak		120	160	mV	
	Peak-to-Peak without Single-Pixel Positive and Negative Pulses		80		mV	
	Single-pixel Positive Pulses		70		mV	
	Single-pixel Negative Pulses		100		mV	
	Register Imbalance ("Odd"/"Even")		20		mV	
DS	Dark Signal					
	DC Component		.5	2	mV	13
	Low Frequency Component		.5	5	mV	13
SPDSNU	Single-pixel DS Non-uniformity		3	8	mV	14
R	Responsivity	3	4.0	9	Volts per μJ/cm²	10, 15
V_{SAT}	Saturation Output Voltage	1000	1800	3000	mV	

* OCLI WBHM = Optical Coating Laboratory, Inc. Wide Band Hot Mirror.

** All PRNU measurements are taken at an 800mV output level using an f/5.0 lens and exclude the outputs from the first and last elements of the array. The "f" number is defined as the distance from the lens to the array divided by the diameter of the lens aperture. As the "f" number increases, the resulting more highly collimated light causes the package window aberrations to dominate and increase PRNU. A lower "f" number results in less collimated light causing device photosite blemishes to dominate the PRNU.

NOTES

1. T_p is defined as the package temperature.
2. Negative transients on any clock pin going below 0.0V may cause charge injection which results in an increase of apparent DS.
3. $C_{\phi 1A,B} = 250pF$.
4. $C_{\phi 2A,B} = 250pF$.
5. $C_{\phi XA,B} = 250pF$.
6. $C_{\phi R} = 5pF$.
7. $C_{\phi SH} = 5pF$.
8. Minimum clock frequency is limited by increase in dark signal.
9. Dynamic range is defined as V_{SAT}/Peak-to-Peak (temporal) or V_{SAT}/RMS Noise
10. 1 μj/cm² = 42 lux-sec/cm² for the 2854°K source with 2.0mm Schott BG-38 and OCLI WBHM filters.
11. SE for 2854°K light without 2.0mm Schott BG-38 and OCLI WBHM filters is typically 0.42 μj/cm².
12. CTE is the measurement for a one-stage transfer.
13. Dark signal component approximately doubles for every 5–10°C increase in T_p, depending on the particular device.
14. Each SPDSNU is measured from the DS level adjacent to the base of the SPDSNU. The SPDSNU approximately doubles for every 5–15°C increase in T_p, depending on the particular device.
15. Responsivity for 2854°K source without 2.0mm Schott BG-38 and OCLI WBHM filters typically 4.3 V/μj/cm².
16. See test load configurations. V_{BB} is created internally by loading Pin 22 as shown.

B-22

TYPICAL PERFORMANCE CURVES

TYPICAL SPECTRAL RESPONSE

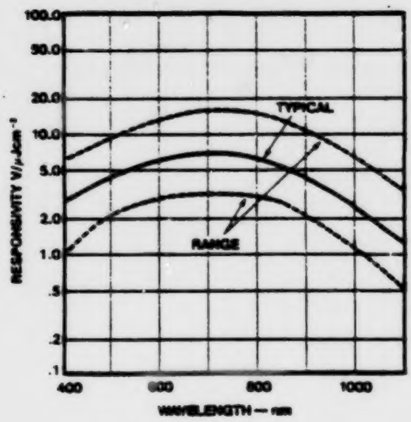

RELATIVE RADIANT FLUX VERSUS WAVELENGTH

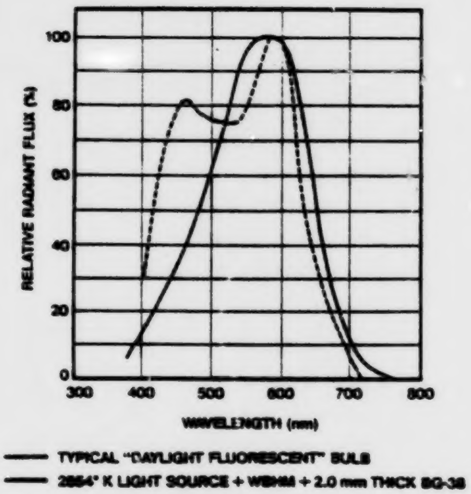

DC AND LOW-FREQUENCY DARK SIGNAL VERSUS INTEGRATION TIME

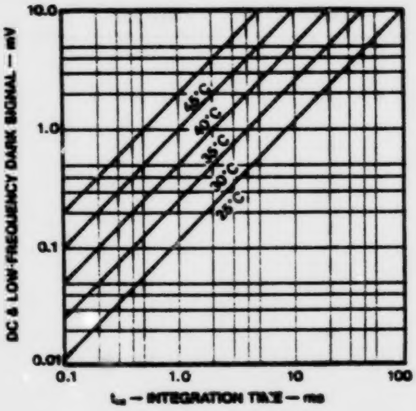

SINGLE-PIXEL DARK SIGNAL NON-UNIFORMITIES VERSUS INTEGRATION TIME

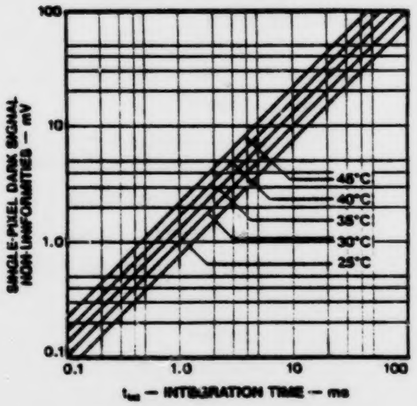

MODULATION TRANSFER FUNCTIONS FOR NARROW BAND ILLUMINATION SOURCES

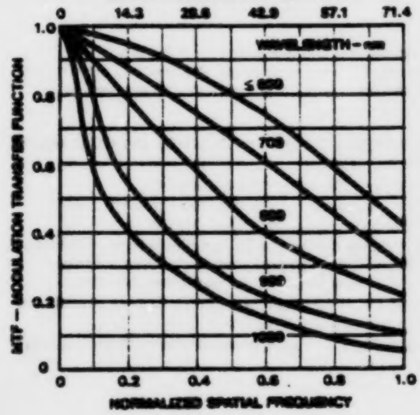

MODULATION TRANSFER FUNCTIONS FOR TWO BROADBAND ILLUMINATION SOURCES

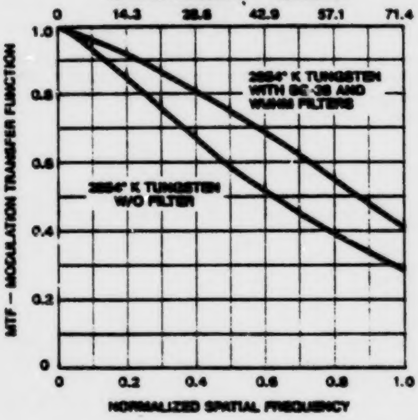

TIMING DIAGRAM

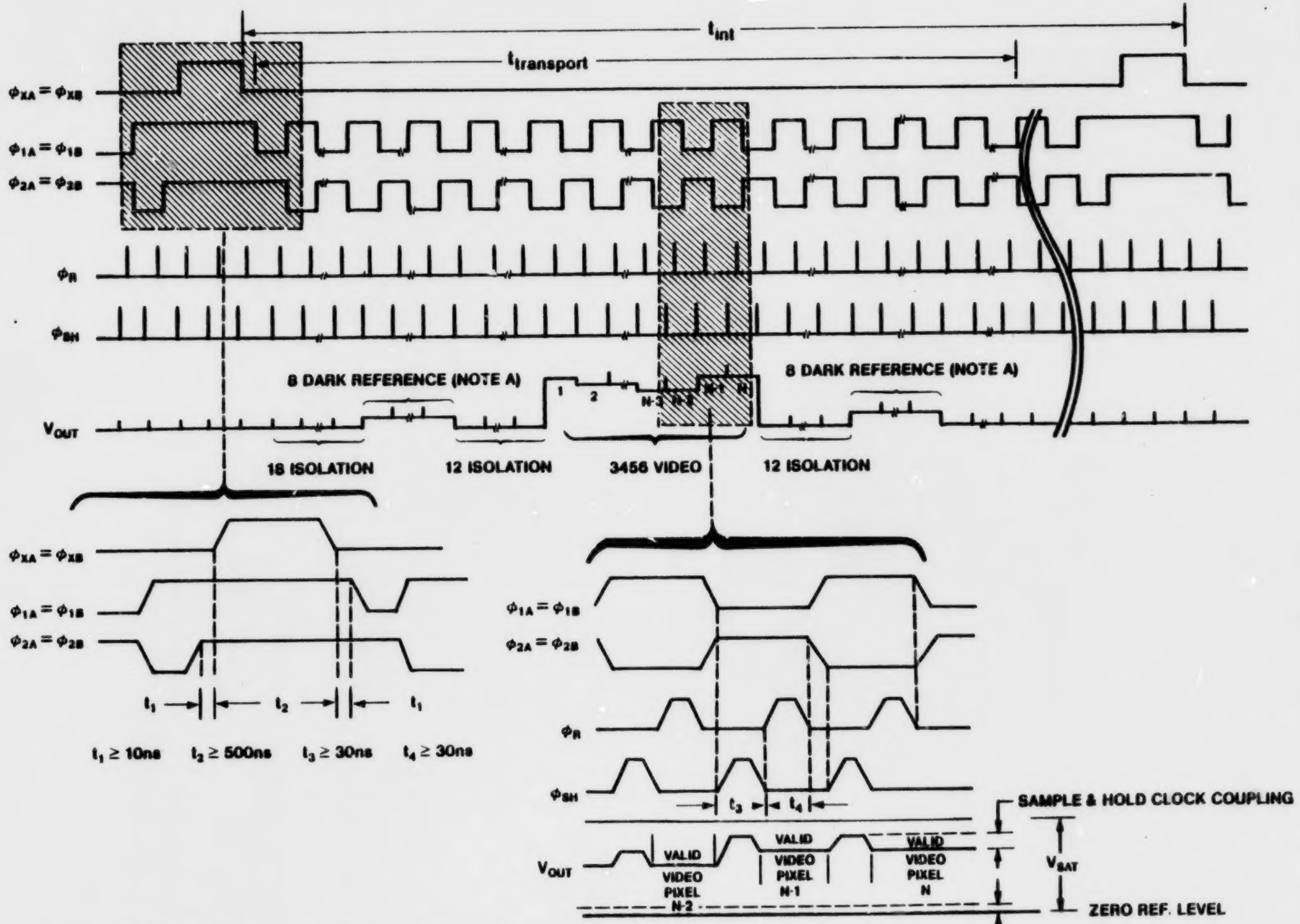
t_{int}
$t_{transport}$
$\phi_{XA} = \phi_{XB}$
$\phi_{1A} = \phi_{1B}$
$\phi_{2A} = \phi_{2B}$
ϕ_R
ϕ_{SH}
V_{OUT}
8 DARK REFERENCE (NOTE A)
1
2
N-3
N-2
N-1
N
8 DARK REFERENCE (NOTE A)
18 ISOLATION
12 ISOLATION
3456 VIDEO
12 ISOLATION
$\phi_{XA} = \phi_{XB}$
$\phi_{1A} = \phi_{1B}$
$\phi_{2A} = \phi_{2B}$
t_1
t_2
t_1
$t_1 \geq 10ns$
$t_2 \geq 500ns$
$t_3 \geq 30ns$
$t_4 \geq 30ns$
$\phi_{1A} = \phi_{1B}$
$\phi_{2A} = \phi_{2B}$
ϕ_R
ϕ_{SH}
t_3
t_4
V_{OUT}
VALID VIDEO PIXEL N-2
VALID VIDEO PIXEL N-1
VALID VIDEO PIXEL N
SAMPLE & HOLD CLOCK COUPLING
V_{SAT}
ZERO REF. LEVEL
DARK SIGNAL

NOTES

A. The first and last elements of the dark reference signal output may not contain a valid representation of that signal.
B. All rise and fall times ≥ 10ns.
C. ϕ_1 and ϕ_2 must overlap ≥ 6V.
D. ϕ_H and ϕ_{SH} must be completely underlapping.
E. ϕ_H must occur entirely within the high time of the high ϕ_1 or ϕ_2 clock. ϕ_{SH} must occur entirely within the low time of the other transport clock.

PACKAGE OUTLINE

28-Pin Dual In-line Ceramic Package

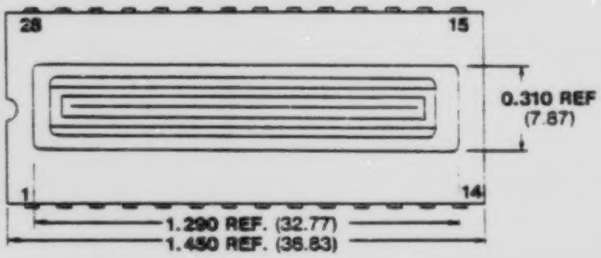
28
15
1
14
0.310 REF
(7.87)
1.290 REF. (32.77)
1.450 REF. (36.83)

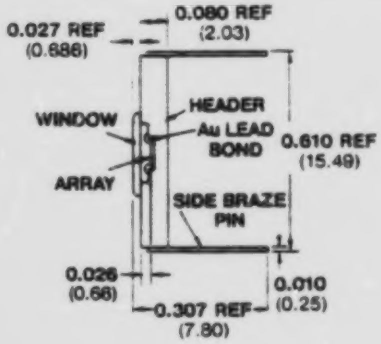
0.027 REF
(0.686)
0.080 REF
(2.03)
HEADER
WINDOW
Au LEAD BOND
0.610 REF
(15.49)
ARRAY
SIDE BRAZE PIN
0.026
(0.66)
0.010
(0.25)
0.307 REF
(7.80)

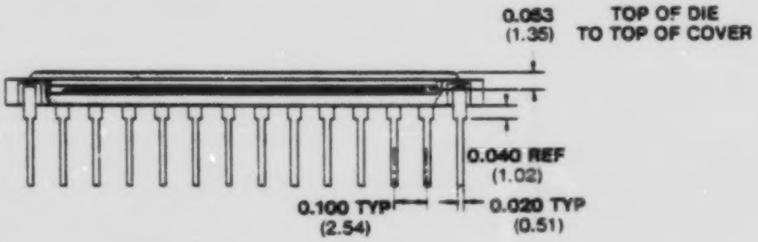
0.053
(1.35)
TOP OF DIE
TO TOP OF COVER
0.040 REF
(1.02)
0.100 TYP
(2.54)
0.020 TYP
(0.51)

NOTES

All dimensions in inches (bold) and millimeters (parentheses). Header is black ceramic (Al_2O_3). Window is glass. The amplifier of the device is located near the notched end of the package.

DEVICE CARE AND OPERATION

Glass may be cleaned by saturating a cotton swab in alcohol and lightly wiping the surface. Rinse off the alcohol with de-ionized water. Allow the glass to dry preferably by blowing with filtered dry N_2 or air.

It is important to note in design and applications considerations that the devices are very sensitive to thermal conditions. The dark signal DC and low frequency components approximately double for every 5°C temperature increase and single-pixel dark signal non-uniformities approximately double for every 12°C temperature increase. The devices may be cooled to achieve very long integration times and very low light level capability.

ORDER INFORMATION

Order CCD151 DC where "D" stands for a ceramic package and "C" for commercial temperature range.

Also available separately is a printed circuit board that includes all the necessary clocks, logic drivers and video amplifiers to operate the CCD151DC. The board is fully assembled and tested and requires only one power supply for operation (+20V). The printed circuit board order code is: CCD151DB.

Description	Device Type Order Code
CCD151 3456 × 1 Line Image Sensor	CCD151DC
Design Development Board for CCD151	CCD151DB

For further information on CCD products, call your nearest Fairchild sales office, representative or distributor. For engineering assistance call (415) 493-8001 (TWX 910-373-2110) or write Fairchild CCD Imaging, 3440 Hillview Ave., Palo Alto, CA 94304.

Fairchild cannot assume responsibility for use of any circuitry described other than circuitry embodied in a Fairchild product. No other circuit patent licenses are implied.

Manufactured under one of the following U.S. Patents: 2981877, 3015048, 3064167, 3108359, 3117260; other patents pending.

B-26

FAIRCHILD
A Schlumberger Company

CCD

TECHNICAL NOTE ON X-RAY IMAGING
WITH FAIRCHILD CCD IMAGE SENSORS

BY R. H. DYCK
JUNE, 1981

X-ray imaging is conventionally done with either photographic film, X-ray phosphor screens viewed directly, or X-ray image converter tubes coupled to a vidicon-type of television camera. Solid state image sensors can provide several advantages over the conventional approaches. For example, by simply replacing the tube-type camera by a solid state camera one achieves the advantages of:

1) a distortion-free scanning raster,
2) an ultra-stable scanning raster, and
3) full digital control of the image readout, as is desirable for interfacing to digital systems

The above example can be implemented in two ways. One way is to use relay optics to image the output of the X-ray image converter tube onto the image sensor. Because sensitivity is generally quite important, the aperture of the lens should be approximately f/1.4 or larger, i.e., a smaller f/no. The other way is to use an image sensor with a fiber optics faceplace and a converter with a fiberoptic backplate. An improvement in sensitivity of 10 to 20 times has been achieved with this approach. In terms of numerical aperture (NA), the aperture of this type of coupling can be approximately 1.0; this is approximately equivalent to f/0.5.

Other approaches to X-ray imaging with solid state image sensors are: (1) to use an X-ray phosphor that is deposited directly on a fiber optics faceplate on the sensor, and (2) to let the X-rays excite the sensor directly. This last method is not recommended, however, since the X-rays incident on an image sensor, especially when it is powered, lead to degradation of the device similar to the way devices degrade due to any other form of high energy radiation such as gamma rays and high energy electrons. The effects include (1) increased dark signal, (2) decreased charge transfer efficiency, and (3) drift in optimum drive voltages. Depending on the particular type of radiation, the dose, the device and the temperature, any one of these effects may dominate.

Where X-ray imaging directly on the sensor is considered, the following information may be of value.

1) The attenuation depth in silicon varies strongly with X-ray energy. Above approximately 6 KeV, the characteristic attenuation depth (where the incident X-ray flux is attenuated 2.72 times) is greater than 30 μm. This situation results in relatively large crosstalk between photoelements, and also in the possibility of poor uniformity of response.

2) Continued exposure to X-rays, especially while under power, causes the device to degrade. Near room temperature, this will generally be detectable at 10^3 to 10^4 rads, and may make the device unusable at 10^5 to 10^6 rads. Annealling will restore proper performance to some degree, but since the best annealling only occurs at temperatures above the maximum recommended storage temperature, low-risk annealling treatments are not expected to help very much. Annealling assisted by ultraviolet irradiation may be considerably more effective.

3) Because good imaging is only expected for relatively low X-ray energies, and because the normal glass window on the image sensor strongly attenuates these low-energy X-rays, it is important to replace the glass window by a thin beryllium cover (of course, for ultraviolet-assisted annealling a beryllium cover would need to be removable).

4) Dosimetry. A rad is defined differently in silicon device investigations relative to the conventional definition for biological and health studies. For the latter, the definition is 100 ergs/gram in carbon. For silicon devices, it is 4.2×10^{13} electron-hole pairs/cm^3 in silicon. Another useful relationship in dealing with radiation effects in silicon devices is that it takes approximately 3.5 eV of energy, on the average for high energy radiation, to create one electron-hole pair in silicon.

5) Active area. Because the aluminum that shields the CCD registers from light is transmitting for X-rays, the registers may be stopped during an exposure, and the active area may be considered to include the registers. This situation results in oddly shaped element areas for line-scan imagers unless elements are paired. For paired elements, the resulting active element area is approximately 26 X 260 μm =0.007 mm^2.

44 B-28

6) Example of an X-ray exposure and the resulting radiation dose. Assume 10 KeV radiation. Each X-ray photon will generate approximately 3000 photoelectrons. Of these, 2000 will be generated in the first 100 µm of depth. Assume all 2000 will be collected. Assume an average exposure of 50 X-ray photons per 26 x 260µm pixel. This will generate approximately 100,000 photoelectrons or approximately 10% of the saturation output voltage. This exposure expressed in radiometric units, is

$$\frac{(50\ \text{photons})(10^4\ \text{eV/photon})(1.6\text{x}10^{-19}\ \text{joule/eV})}{7\text{x}10^{-5}\ \text{cm}^2} = \underline{\underline{1.1\text{x}10^{-9}\ \text{j/cm}^2}}.$$

The radiation dose seen by the upper portion of the device can be estimated as follows: assume a characteristic absorption length of 100 µm. The absorption coefficient is then one percent per micrometer. The excitation density at the top of the device and for the average exposure used in this example is then

$$\frac{(50\ \text{photons})(3000\ \text{pairs/photon})(0.01/\mu\text{m})(10^4\ \mu\text{m/cm})}{(7\text{x}10^{-5}\ \text{cm}^2)(4.2\text{x}10^{13}\ \text{pairs/rad})} = \underline{\underline{5.1\ \text{mRad}}}$$

Therefore, if one is careful not to expose the device unnecessarily to the X-ray source, it should be possible to take as many as 200,000 exposures before the significant degradation resulting from 10^3 Rads accumulated dose will occur.

45 B-29

Advanced charge-coupled device (CCD) line imaging devices*

David D. Wen
Fairchild Camera & Instrument Corporation
4001 Miranda Avenue
Palo Alto, California 94304

Abstract

The design and operation of a new high speed family of CCD line imaging devices are presented in this paper. The devices, CCD 133 and CCD 143, contain 1024 and 2048 photosites on 13 um centers respectively. They are second generation devices having an overall improved performance compared with the first generation devices (CCD 121 and CCD 131) including higher sensitivity, enhanced blue response and lower dark signal. The devices also incorporate on-chip clock driver circuitry so that only two external clocks are required for their operation. Excellent performance has been obtained with up to 20 MHz data rate. The devices are designed for page scanning applications including high speed facsimile, optical character recognition, and other imaging systems which require high resolution, high sensitivity, and high speed.

Introduction

CCD line imaging devices manufactured by the Fairchild buried n-channel technology were first introduced commercially more than four years ago.[1] A second generation family of line imaging devices has recently been designed to replace them. The low speed second generation devices (CCD 122 and CCD 142), which operate up to 2 MHz data rate, have been described at the 1979 International Solid State Circuit Conference.[2] This paper reports the operation of the high speed second generation devices (CCD 133 and CCD 143) which are designed to operate up to 20 MHz data rate.

Device design and operation

The CCD 133/143 devices contain a line of 1024/2048 13 um x 13 um image sensor elements as shown by the block diagram in Figure 1. The photosites are separated by diffused channel stops and covered by a silicon dioxide surface passivation layer. Because there is no polysilicon gate layer over the photosites, the sensitivity is increased, particularly in the blue region of the spectrum. An N^+ region is diffused into the photosites to collect photo-generated electrons as illustrated in Figure 2. After an integration period is over, the transfer gate ϕ_X is turned HIGH to transfer the charge packets from the photosites into the two adjacent (inner) Analog Transport Shift Registers A&B. The transport registers are positioned 70 um away from the photosites so that optical crosstalk is minimized. The N^+ diffusion region, illustrated in Figure 2, also provides conductive coupling[3] between the photosite and the shift register regions. As a result, charge transfer across the 70 um distance can be accomplished in less than 30 ns.

The CCD shift registers are constructed with two polysilicon layers with self-aligned ion-implanted barriers.[1] A buried-channel ion implantation is employed so that the CCD shift registers operate in the bulk-channel mode. Excellent charge transfer efficiency can be obtained with this structure at clock frequencies in excess of 30 MHz. One-and-half phase clocking[4] is employed so that only one external clock (ϕ_T) is required for the shift register operation. A gated-charge integrator output amplifier is provided for each of the two analog transport shift registers, as illustrated in Figure 3. The gated-charge integrator contains two MOS source follower stages with a switching transistor positioned between the two stages so that sampled-and-held output waveforms are obtained. The output impedance of the gated-charge integrators is designed to be 750 ohms in order to drive an external capacitive load (approximately 10 pF) at up to 10 MHz clock rate. Since the two gated-charge integrators alternately detect charge packets transferred from the two shift registers, a combined output video data rate of 20 MHz can be obtained. On-chip MOS circuity, illustrated in Figure 4, generates all the required clock waveforms to operate the output amplifiers. The MOS clock drivers are designed with bootstrap feedback capacitors for high frequency operation. The two sample-and-hold clock waveforms (ϕ_{SHA} and ϕ_{SHB}) are each 35 ns in width to assure proper operation at 10 MHz clock rate (20 MHz data rate).

---

* Manufactured under U. S. Patent 3,931,674.
Other patents pending.

41

6-30

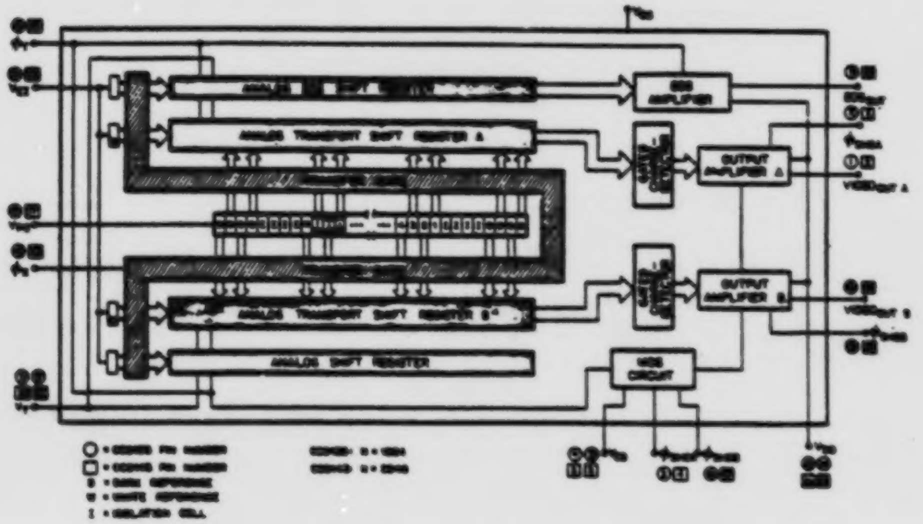
ANALOG TRANSPORT SHIFT REGISTER A
OUTPUT AMPLIFIER A
VIDEO OUT A
ANALOG TRANSPORT SHIFT REGISTER B
OUTPUT AMPLIFIER B
VIDEO OUT B
ANALOG SHIFT REGISTER
MOS CIRCUIT
DARK REFERENCE
WHITE REFERENCE
ISOLATION CELL

Figure 1. Device block diagram.

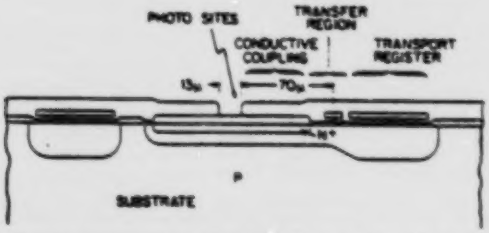
PHOTO SITES
TRANSFER REGION
CONDUCTIVE COUPLING
TRANSPORT REGISTER
13μ
70μ
N+
P
SUBSTRATE

Figure 2. Cross-section of photosites and shift register.

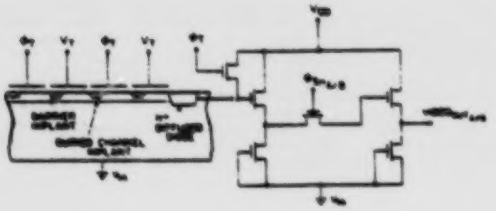
V_{DD}
BARRIER IMPLANT
BURIED CHANNEL IMPLANT
N+ DIFFUSED DIODE

Figure 3. Output amplifier schematic.

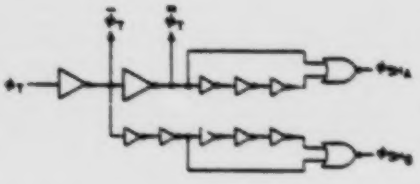

Figure 4. On-chip MOS circuit.

4 /

B-31

In addition to the regular photosites, the devices also contain four dark reference cells at each end of the array as illustrated in Figure 1. These dark reference cells are constructed the same as the regular photosites except that they are kept dark by the covering of opaque aluminum metallization. They provide an accurate dark reference level in the device output waveforms so that external signal processing such as DC restoration can be performed. Figure 1 also shows isolation cells situated between the dark reference cells and the regular photosites. These isolation cells are reverse-biased diodes which are used to eliminate optical crosstalk between the regular photosites and the dark reference cells.

An electrical injection circuit is provided at the beginning of each of the transport shift registers as indicated in Figure 1. A cross-sectional diagram of the electrical injection circuit is shown in Figure 5. It can be seen that the magnitude of the charge injected is determined by the same well and barrier potentials which determine the saturation level of the shift registers. These electrically injected signals (called white reference cells) track the device saturation level with respect to amplifier gain and temperature effects as well as process variations. These charge packets are injected at the end of the exposure period when ϕ_X is turned HIGH. They are then transported along the readout shift registers and appear at the output amplifiers after the regular photo-generated charge packets. The white and dark reference levels can be used to achieve automatic gain control in many optical system applications.

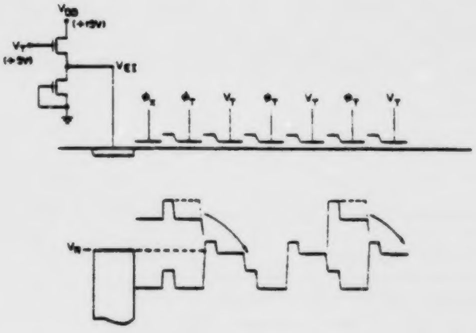

Figure 5. Electrical injection structures for the white reference level.

As illustrated in Figure 1, a total of four CCD shift registers are provided on the device. The signal charge packets from the photosites are transported along the two inner shift registers. The two outer shift registers are used to collect charge that may be generated in the field so that the signal charge packets are not affected. An electrical injection structure identical to the white reference circuit is also provided for one of the outer shift registers. The detection of this charge packet by the output amplifier indicates that the readout of a line of video data has been completed. The use of this end-of-scan (EOS) output eliminates the need for external counter chains.

The devices are designed to operate with only two external clocks (both with 12 volt amplitude). ϕ_T controls the output data rate, and ϕ_X controls the exposure time interval. Due to the fast transfer achieved with the N^+ diffusion region discussed before, ϕ_T is a continuous clock which does not need to be interrupted during the ϕ_X transfer period. Typical output waveforms of the device are shown in Figure 6. It can be seen that both outputs are sampled-and-held, and contain dark and white reference levels as discussed previously.

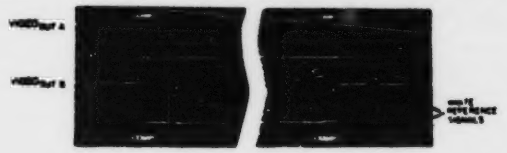

Figure 6. Device output waveforms.

48

B-32

Typical device performance characteristics are summarized in Table I. Under the standard test condition of 25°C, 5.0 MHz data rate and 1 ms integration time, the device provides 2 volt saturation output and less than 10 mV of dark signal. Temporal noise measured without illumination is typically 400 µV RMS, resulting in a 5000 : 1 dynamic range. Excellent charge transfer efficiency of better than 0.99999 per transfer is obtained. The device operates with a single 14 volt, 22mA DC power supply. Maximum output video data rate is 20 MHz. Typical spectral response and MTF (modulation transfer function) measurements are shown in Figures 7 and 8.

Table 1. CCD 133/143 Typical Performance Characteristics

Saturation output voltage	2.0 V
Responsibility	3.0 V/uJcm^{-2}
Max. dark signal*	7.0 mV
Photoresponse nonuniformity*	± 10%
Charge transfer efficiency	≥ 0.99999
Temporal noise (in dark)	400 µV RMS
Dynamic range	5000 : 1
Output impedance	750 Ω
Power dissipation	380 mW
Max. output data rate	20 MHz

* Measured at 25°C, 1 ms integration time, light source is 2854°K + BG 38 + WBHM filters (480 nm to 650 nm wavelength)

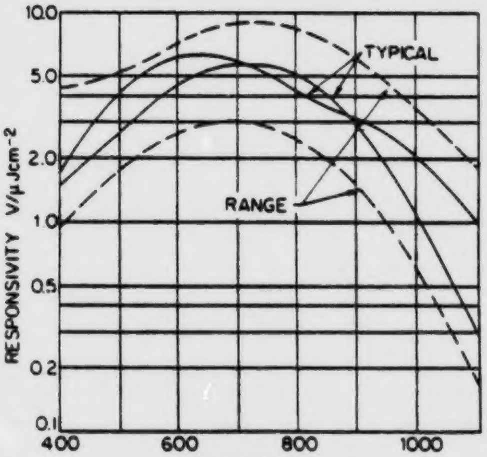

Figure 7. Spectral response measurement.

+1 6-33

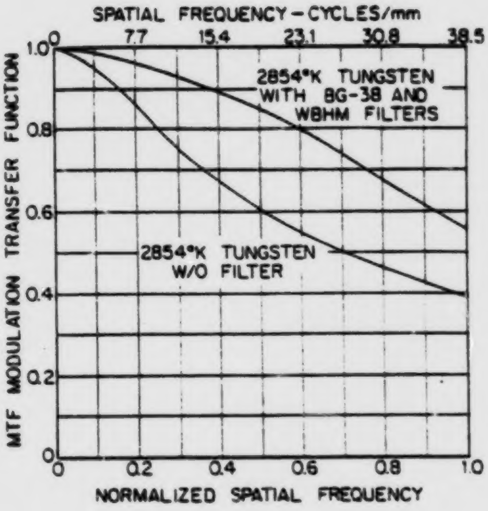

Figure 8. MTF measurement.

Conclusion

The design and performance of the CCD 133 and CCD 143 have been discussed in this paper. The devices contain 1024 or 2048 photo-sensing elements on 13 um centers. Only one DC power supply and two external clocks are required for their operation. Excellent results have been obtained up to 20 MHz output data rate.

The 1024 sensing elements of the CCD 133 provide 120-line-per-inch resolution across an 8-1/2 inch page, the 2048 sensing elements of the CCD 143 provide an 8-line-per-millimeter resolution across a 256 millimeter page for standard Japanese facsimile use. The devices should find applications in facsimile, optical character recognition and other imaging systems where high resolution, high sensitivity and high speed are desired.

Acknowledgments

The author wishes to thank Will Steffe for many helpful discussions, Sampath Ranganathan for on-chip MOS circuit design, and Richard Youden and Denice Denton for device characterization.

References

1. Kim, C. K., "Two-Phase Charge Coupled Linear Imaging Devices With Self-Aligned Barrier", IEDM, Tech. Digest, pp.55-58, 1974.
2. Steffe, W. C. and Wen, D. D., "Second Generation CCD Line Imaging Devices", ISSCC Tech. Digest, 1979.
3. Krambeck, R. H., Strain, R. J., Smith, G. W., and Pickar, K. A., "Conductively Connected Charge Coupled Device", IEEE Trans. on Electron Devices, ED 21, pp.70-72. 1974.
4. Wen, D. D., "A CCD Video Delay Line", ISSCC Tech. Digest, 1976.

B-41

CCD111

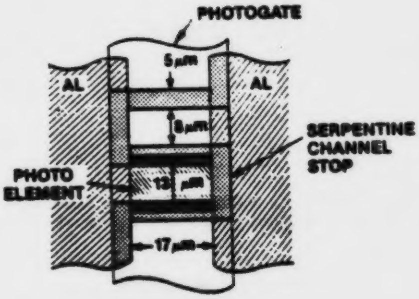

ALL DIMENSIONS ARE TYPICAL VALUES.

DC Characteristics: T_a = 25°C (Note 1)

Symbol	Characteristic	Limits Min	Typ	Max	Unit	Condition
V_{OD}	Output Transistor Drain Voltage	14.5	15.0	15.5	V	
V_{RD}	Reset Transistor Drain Voltage	11.5	12.0	12.5	V	
V_{OG}	Output Gate Voltage		5.0		V	
V_{PG}	Photogate Voltage	9.5	10.0	12.5	V	
TP1, TP3	Test Points		0.0		V	
TP2, TP4	Test Points	14.5	15.0	15.5	V	

Clock Characteristics: T_a = 25°C (Note 1)

Symbol	Characteristic	Limits Min	Typ	Max	Unit	Condition
$V_{\phi 1AL}$, $V_{\phi 1BL}$ $V_{\phi 2AL}$, $V_{\phi 2BL}$	Transport Clocks LOW	0.0	0.5	0.8	V	Note 2
$V_{\phi 1AH}$, $V_{\phi 1BH}$ $V_{\phi 2AH}$, $V_{\phi 2BH}$	Transport Clocks HIGH	7.5	8.0	8.5	V	Note 5
$V_{\phi XAL}$, $V_{\phi XBL}$	Transfer Clock LOW	0.0	0.5	0.8	V	Notes 2, 5
$V_{\phi XAH}$, $V_{\phi XBH}$	Transfer Clock HIGH	7.5	8.0	8.5	V	Note 5
$V_{\phi RL}$	Reset Clock LOW	0.0	0.5	0.8	V	Notes 2, 5
$V_{\phi RH}$	Reset Clock HIGH	7.5	8.0	8.5	V	Notes 3, 5
$f_{\phi 1A}$, $f_{\phi 1B}$ $f_{\phi 2A}$, $f_{\phi 2B}$	Maximum Transport Clock Frequency		5.0		MHz	Note 5
$f_{\phi R}$	Maximum Reset Clock Frequency (Output Data Rate)		10.0		MHz	Note 6

AC Characteristics: T_a = 25°C, $f_{\phi R}$ = 1.0 MHz, t_{int} = 320 µs, $t_{transport}$ = 289 µs, Light Source = 2854°K + filters as specified. All operating voltages nominal specified values. (Note 1)

Symbol	Parameter	Range Min	Typ	Max	Unit	Condition
DR	Dynamic Range (relative to rms noise) (relative to peak-to-peak noise)	1250:1 250:1	2500:1 500:1			Note 7
NEE	RMS Noise Equivalent Exposure		2×10^{-4}		µJ/cm²	
SE	Saturation Exposure		0.5		µJ/cm²	
CTE	Charge Transfer Efficiency		99.995		%	Note 8
SR	Spectral Response Range Limits		0.45 – 1.05		µm	
P	Power Dissipation		100		mW	V_{OD} = 15V
Z	Output Impedance		1000		Ω	
N	RMS Noise Peak-to-Peak Noise		80 400		µV	

Performance Characteristics: T_c = 25°C, $f_{\phi R}$ = 1.0 MHz, t_{int} = 320μs, $t_{[illegible]}$ = 250μs, Light Source = 2854°K + filters as specified. All operating voltages nominal specified values. (Note 1)

Symbol	Characteristic	Range CCD111A Min	 CCD111A Typ	 CCD111A Max	 CCD111B Min	 CCD111B Typ	 CCD111B Max	Unit	Condition
PRNU	Photoresponse Non-uniformity Peak-to-Peak								
	2854°K + 700 nm cutoff filter		35	70		25	70	mV	14, 15, 16
	2854°K + 900 nm cutoff filter		45	110		45	110	mV	14, 15, 16
	2854°K unfiltered		70			60		mV	14, 15, 16
	Single-pixel Positive Pulses		<10			<10		mV	15, 16
	Single-pixel Negative Pulses		20	60		20	60	mV	15, 16
RI	Register Imbalance ("Odd"/"Even")		<5			<5		mV	15, 16
DS	Dark Signal DC Component	0	<1	3	0	2	15	mV	2, 9, 10
	Low Frequency Component	0	<1	2	0	2	10	mV	2, 9, 11
SPDSNU	Single-pixel DS Non-uniformity	0	<1	2	0	1	2	mV	9, 11, 12
PR	Peripheral Response								
	2854°K + 700 nm cutoff filter		10	17		<2	5	% of V_{OUT}	14
	2854°K + 900 nm cutoff filter		12	20		3	7	% of V_{OUT}	14
	2854°K unfiltered		25			4		% of V_{OUT}	14
R	Responsivity								
	2854°K + 700 nm cutoff filter	0.7	1.3	2.1	0.5	1.1	2.0	V/μJ/cm^2	13, 14
	2854°K + 900 nm cutoff filter	1.3	2.4	3.9	0.8	1.6	2.4	V/μJ/cm^2	13, 14
	2854°K unfiltered		2.0			0.9		V/μJ/cm^2	13, 14
V_{SAT}	Saturation Output Voltage	500	900		500	900		mV	17

Notes

1. T_C is defined as the package temperature, measured on the back surface of the ceramic body.
2. Negative transients on any clock pin going below 0.0V may cause charge injection that results in an increase in the apparent Dark Signal.
3. $V_{\phi RH}$ should track V_{RD}.
4. The data output frequency $f_{\phi R}$ is twice that of each transport clock ($f_{\phi 1A}$, $f_{\phi 1B}$, $f_{\phi 2A}$, $f_{\phi 2B}$).
5. $C_{\phi XA} = C_{\phi XB}$ = 20pF, $C_{\phi 1A} = C_{\phi 2A} = C_{\phi 1B} = C_{\phi 2B}$ = 32pF, $C_{\phi R}$ = 5pF.
6. Minimum reset clock frequency is limited by the increase in Dark Signal.
7. Dynamic Range is defined as "V_{SAT}/rms (temporal) Noise" or "V_{SAT}/Peak-to-Peak (temporal) Noise."
8. CTE is measured for a one-stage transfer.
9. See photographs for Dark Signal definitions.
10. DC and low-frequency Dark Signal components approximately double for every 5°C increase in T_C. The shift register component is also inversely proportional to $f_{\phi R}$.
11. Single-pixel Dark Signal non-uniformity (SPDSNU) approximately doubles for every 6°C increase in T_C. They are also directly proportional to the integration time t_{int}.
12. Each SPDSNU is measured from the DS level adjacent to the base of the SPDSNU.
13. RESPONSIVITY is defined as the "volts of video output" per "Incident Radiant Energy measured over the 350 nm–1200 nm band." The device will not respond to infrared wavelengths longer than ≈ 1200 nm. However, 2/3 of the radiant energy from a 2854°K source is at $\lambda > 1200$ nm. For the unfiltered 2854°K source, the responsivity values for light measured over $0 < \lambda < \infty$ will be ~0.3X of the responsivity values for light measured over 350 nm $< \lambda <$ 1200 nm.
14. OPTICAL FILTERS: a "700 nm cutoff" filter is realized by using one "Wide Band Hot Mirror" (Optical Coating Labs, Inc., Santa Rosa, California) and one 2.0 mm thick "BG-38" blue glass (Schott Optical Glass, Duryea, Pennsylvania) filter in series. The "900 nm cutoff" filter is available on special order; consult Fairchild CCD Applications Engineering for details. Transmittance curves for the two cutoff filters and Spectral Energy Distribution curves for these filters with a 2854°K light source are given in the "Typical Performance Curves" section of this data sheet. It should be noted that the "2854°K + 700 nm cutoff" source is a good approximation to a Daylight Fluorescent bulb.
15. All PRNU measurements taken at a 300mV output level using a f/5.6 lens; all PRNU measurements exclude the outputs from the first and last photoelements of the array. The "f" number is defined as the distance from the lens to the array divided by the diameter of the lens aperture. As f number increases, the resulting more highly collimated light causes package window aberrations to dominate and increase the PRNU. A lower f number (f≤8) results in less collimated light, causing photosite blemishes to dominate PRNU.
16. See photographs for PRNU definitions.
17. See test load configuration.

B-36

PHOTOELEMENT DIMENSIONS

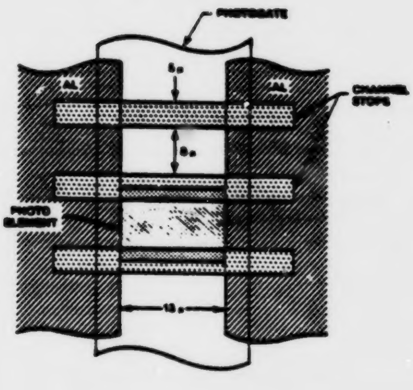

All dimensions are typical values

DC CHARACTERISTICS: $T_P = 25°C$ (Note 1)

SYMBOL	CHARACTERISTIC	RANGE			UNITS	CONDITIONS
		MIN	TYP	MAX		
V_{CD}	Clock Driver Drain Supply Voltage	12.0	13.0	14.0	V	
I_{CD}	Clock Driver Drain Supply Current		6.9	12.5	mA	
V_{OD}	Output Amplifier Drain Supply Voltage	12.0	13.0	14.0	V	
I_{OD}	Output Amplifier Drain Supply Current		6.9	12.5	mA	
V_{PG}	Photogate Bias Voltage	6.5	7.0	7.5	V	
V_T	DC Electrode Bias Boltage	4.5	5.0	5.5	V	Note 2
V_{IB}	Electrical Input Bias Voltage		11.4		V	Note 3
V_{SS}	Substrate (Ground)		0.0		V	

AC CHARACTERISTICS: (Note 1)
$T_P = 25°C$, $f_{CR} = 0.5$ MHz, $t_{int} = 10$ ms, light source = 2854°K + 3.0 mm thick Corning 1-75 IR-absorbing filter. All operating voltages nominal specified values.

SYMBOL	CHARACTERISTIC	RANGE			UNITS	CONDITIONS
		MIN	TYP	MAX		
DR	Dynamic Range					
	(relative to peak-to-peak noise)	250:1	500:1			Note 9
	(relative to rms noise)	1250:1	2500:1			
NEE	RMS Noise Equivalent Exposure		0.0002		$\mu J/cm^2$	Note 10
SE	Saturation Exposure		0.4		$\mu J/cm^2$	Note 11
CTE	Charge Transfer Efficiency		0.999995			Note 12
V_O	Output DC Level	3.0	5.5	10.0	V	
Z	Output Impedance		1.4	3.0	kΩ	
P	On-Chip Power Dissipation					
	Clock Drivers		90	150	mW	
	Amplifiers		90	150	mW	
N	Peak-to-Peak Noise		2.0		mV	

8-37

CLOCK CHARACTERISTICS: T_P = 25°C (Note 1)

SYMBOL	CHARACTERISTIC	RANGE			UNITS	CONDITIONS
		MIN	TYP	MAX		
$V_{\phi TL}$	Transport Clock LOW	0.0	0.3	0.5	V	Notes 4, 5
$V_{\phi TH}$	Transport Clock HIGH	9.75	10.0	10.5	V	Note 5
$V_{\phi XL}$	Transfer Clock LOW	0.0	0.5	0.5	V	Notes 4, 6
$V_{\phi XH}$	Transfer Clock HIGH	9.75	10.0	10.5	V	Note 6
$V_{\phi RL}$	Reset Clock LOW	0.0	0.3	0.5	V	Note 7
$V_{\phi RH}$	Reset Clock HIGH	9.75	10.0	10.5	V	Note 7
$f_{\phi R}$	Maximum Reset Clock Frequency (Output Data Rate)	1.0	2.0		MHz	Note 8

PERFORMANCE CHARACTERISTICS: (Note 1)

T_P = 25°C, $f_{\phi R}$ = 0.5 MHz, t_{int} = 10 ms, light source = 2854°K + 3.0 mm thick Corning 1-75 IR-absorbing filter. All operating voltages nominal specified values.

SYMBOL	CHARACTERISTIC	RANGE			UNITS	CONDITIONS
		MIN	TYP	MAX		
PRNU*	Photoresponse Non-uniformity					
	Peak-to-Peak		160	210	mV	Note 16
	Peak-to-Peak without Single-Pixel Positive and Negative Pulses		100		mV	Note 16
	Single-pixel Positive Pulses		85		mV	Note 16
	Single-pixel Negative Pulses		130		mV	Note 16
	Register Imbalance ("Odd"/"Even")		20		mV	Note 16
DS	Dark Signal					
	DC Component		5	15	mV	Notes 13, 14
	Low Frequency Component		5	10	mV	Notes 13, 14
SPDSNU	Single-pixel DS Non-uniformity		20	40	mV	Notes 13, 15
R	Responsivity	2.0	3.5	5.0	Volts per μJ/cm²	Note 17
V_{SAT}	Saturation Output Voltage	800	1400	1600	mV	Note 18

*All PRNU Measurements taken at a 700 mV output level using an f/2.8 lens and excluded the outputs from the first and last elements of the array. The "f" number is defined as the distance from the lens to the array divided by the diameter of the lens aperture. As the f number increases, the resulting more highly collimated light causes the package window aberrations to dominate and increase PRNU. A lower f number results in less collimated light causing device photosite [illegible] to dominate the PRNU.

NOTES:

1. T_P is defined as the package temperature.
2. V_T should be equal to (1/2) $V_{\phi TH}$.
3. V_B is used to generate the end-of-scan output and the white reference output. These two signals can be eliminated by connecting V_B to a voltage level equal to $V_{\phi RH}$ + 5 V.
4. Negative transients on any clock pin going below 0.0 V may cause charge-injection which results in an increase of apparent DS.
5. $C_{\phi T}$ = 700 pF
6. $C_{\phi X}$ = 200 pF
7. $C_{\phi R}$ = 5 pF
8. Minimum clock frequency is limited by increase in dark signal.
9. Dynamic range is defined as V_{SAT}/peak-to-peak (temporal) or V_{SAT}/rms noise.
10. 1 μJ/cm² = 0.05 fcs at 2854°K, 1 fcs = 20 μJ/cm² at 2854°K.
11. SE for 2854°K for light without 3.0 mm thick Corning 1-75 IR-absorbing filter is typically 0.8 μJ/cm².
12. CTE is the measurement for a one-stage transfer.
13. See photographs for DS definitions.
14. Dark signal component approximately doubles for every 8°C increase in T_P.
15. Each SPDSNU is measured from the DS level adjacent to the base of the SPDSNU. The SPDSNU approximately doubles for every 8°C increase in T_P.
16. See photographs for PRNU definitions.
17. Responsivity for 2854°K light source without 3.0 mm thick Corning 1-75 IR-absorbing filter is typically 2 V per μJ/cm².
18. See test load configurations.

PHOTOELEMENT DIMENSIONS

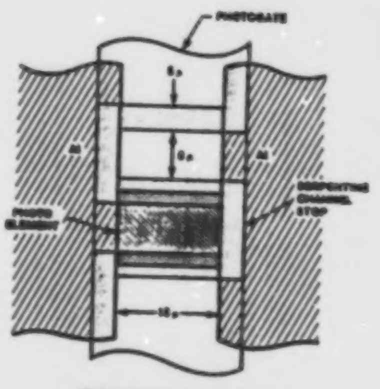

All dimensions are typical values.

AC CHARACTERISTICS: (Note 1)
T_P = 25°C, f_{DATA} = 5.0 MHz, t_{int} = 1.0 ms, Light Source* = 2854°K + 2.0 mm thick
Schott BG-38 and OCLI WBHM filters
All operating voltages nominal specified values

SYMBOL	CHARACTERISTIC	RANGE			UNITS	CONDITIONS
		MIN	TYP	MAX		
DR	Dynamic Range (relative to peak-to-peak noise) (relative to rms noise)	500:1 2500:1	1000:1 5000:1			Note 10
NEE	RMS Noise Equivalent Exposure		0.00013		μJ/cm²	Note 11
SE	Saturation Exposure		0.67		μJ/cm²	Note 12
CTE	Charge Transfer Efficiency		0.99999			Note 13
V_O	Output DC Level	4.0	8.0	11.0	V	
Z	Output Impedance		0.75	1.5	kΩ	
P	On-Chip Power Dissipation Clock Drivers Amplifiers		 100 170	 215 325	 mW mW	
N	Peak-to-Peak Temporal Noise		2.0		mV	

PERFORMANCE CHARACTERISTICS: (Note 1)
T_P = 25°C, f_{DATA} = 5.0 MHz, t_{int} = 1.0 ms, Light Source* = 2854°K + 2.0 mm thick
Schott BG-38 and OCLI WBHM filters
All operating voltages nominal specified values

SYMBOL	CHARACTERISTIC	RANGE			UNITS	CONDITIONS
		MIN	TYP	MAX		
PRNU**	Photoresponse Non-Uniformity:					Note 14
	Peak-to-Peak		180	340	mV	
	Peak-to-Peak Without Single-Pixel Positive & Negative Pulses		120		mV	
	Single-Pixel Positive Pulses		100		mV	
	Single-Pixel Negative Pulses		150		mV	
M_{VIDEO}	Video Mismatch		40	180	mV	Note 15
M_{DC}	DC Mismatch		0.5	2.0	V	Note 16
DS	Dark Signal:					Notes 17, 18
	DC Component		2.0	5.0	mV	
	Low Frequency Component		2.0	5.0	mV	
SPDSNU	Single-Pixel DS Non-Uniformity		5.0	20	mV	Notes 17, 19
R	Responsivity	1.8	3.0	4.5	Volts per μJ/cm²	Note 20
V_{SAT}	Saturation Output Voltage	1.0	2.0	2.5	V	Note 21

* OCLI WBHM = Optical Coating Laboratory, Inc. Wide Band Hot Mirror

** PRNU measurements include both register outputs but exclude the outputs from the first and last elements of the array. Also excluded from the measurement are video and dc mismatch.
All PRNU measurements are taken at a 800 mV output level using an f/5.6 lens.
The "f" number is defined as the distance from the lens to the array divided by the diameter of the lens aperture. As the "f" number increases, the resulting more highly columnated light causes the package window aberrations to dominate and increase PRNU. A lower "f" number results in less columnated light causing device photosite blemishes to dominate the PRNU.

B-3'

FAIRCHILD • CCD133/143

ABSOLUTE MAXIMUM RATINGS (Above which useful life may be impaired)

Storage Temperature		-25°C to +125°C
Operating Temperature (See curves)		-25°C to +70°C
CCD133:	Pins 2, 3, 4, 8, 11, 12, 14, 15, 16, 17, 18, 21, 22, 24	-0.3 V to 18 V
	Pin 13	0 V
	Pins 1, 5, 6, 7, 9, 10, 19, 20, 23	NC
CCD143:	Pins 3, 4, 5, 9, 12, 13, 17, 18, 19, 20, 21, 24, 25, 27	-0.3 V to 18 V
	Pins 14, 15, 16, 28	0 V
	Pins 1, 2, 6, 7, 8, 10, 11, 22, 23, 26	NC

CAUTION NOTE: These devices have [illegible] built-in gate protection. It is recommended that static discharge be controlled and minimized. Care must be taken to avoid shorting pins VIDEO$_{OUT}$ A&B and EOS$_{OUT}$ to V_{DD} or V_{SS} during operation of the devices. Shorting these pins temporarily to V_{SS} or V_{DD} may destroy the output amplifiers.

DC CHARACTERISTICS: T_P = 25°C (Notes 1, 2)

SYMBOL	CHARACTERISTIC	RANGE			UNITS	CONDITIONS
		MIN	TYP	MAX		
V_{CD}	Clock Driver Drain Supply Voltage	13.5	14	14.5	V	Note 3
I_{CD}	Clock Driver Drain Supply Current		7.0	15	mA	
V_{OD}	Output Amplifier Drain Supply Voltage	13.5	14	14.5	V	Note 3
I_{OD}	Output Amplifier Drain Supply Current		15	25	mA	
V_{PG}	Photogate Bias Voltage	4.5	5.0	5.5	V	
V_T	DC Electrode Bias Voltage	5.5	6.0	6.5	V	Note 4
V_{IP}	Electrical Input Bias Voltage		10.5		V	Note 5
V_{SS}	Substrate (Ground)		0.0		V	

CLOCK CHARACTERISTICS: T_P = 25°C (Note 1)

SYMBOL	CHARACTERISTIC	RANGE			UNITS	CONDITIONS
		MIN	TYP	MAX		
$V_{\phi XL}$, $V_{\phi TL}$	Transfer & Transport Clock LOW	0.0	0.3	0.5	V	Notes 6, 7
$V_{\phi XH}$, $V_{\phi TH}$	Transfer & Transport Clock HIGH	11	11.5	12	V	Note 7
$f_{DATA\ MAX}$	Maximum Output Data Rate	12	20		MHz	Notes 8, 9

NOTES

1. T_P is defined as the package temperature.
2. All V_{SS} pins must be grounded. All [illegible] pins must be connected and tied to [illegible]. All NC pins must be left unconnected.
3. V_{OD} = V_{CD}.
4. V_T = [illegible] $V_{\phi XH}$ = [illegible] $V_{\phi TH}$.
5. V_{IP} is used to generate the end-of-scan output and the white reference output. These two signals can be eliminated by connecting V_{IP} to a voltage level equal to V_{OD} + 5 V.
6. Negative transients on any clock pin going below 0.0 V may cause charge-injection which results in an increase in apparent DS.
7. $C_{\phi T}$ = [illegible] pF for CCD133, $C_{\phi T}$ = [illegible] pF for CCD143, $C_{\phi X}$ = [illegible] pF for CCD133, $C_{\phi X}$ = [illegible] pF for CCD143.
8. Minimum clock frequency is limited by increase in dark signal.
9. f_{DATA} = 2 X $f_{\phi T}$.
10. Dynamic range is defined as [illegible] temporal noise or [illegible] temporal noise.
11. 1 μJ/cm² = [illegible] fc-s at 2854°K, 1 fc-s = [illegible] μJ/cm² at 2854°K.
12. [illegible] for 2854°K broadband light without 2.0 mm Schott BG-38 and OCLI [illegible] filters is typically [illegible] μJ/cm².
13. CTE is the measurement for a one-stage transfer.
14. See photographs for PRNU definitions.
15. Video mismatch is the difference in [illegible] amplitude between VIDEO$_{OUT}$ and VIDEO$_{OUT}$ under uniform illumination. It can be eliminated by attenuation/amplification of one of the video outputs.
16. DC mismatch is the difference in dc output level [illegible] between VIDEO$_{OUT}$ and VIDEO$_{OUT}$.
17. See photographs for DS definitions.
18. Dark signal component approximately doubles for every [illegible]°C increase in T_P.
19. [illegible] is measured from the DS level adjacent to the base of the [illegible]. The [illegible] approximately doubles for every [illegible]°C increase in T_P.
20. Responsivity for 2854°K broadband light source without 2.0 mm Schott BG-38 and OCLI [illegible] filters is typically [illegible] V per μJ/cm².
21. See test load configurations.

FAIRCHILD
A Schlumberger Company

CCD IMAGING PRODUCTS
JUNE 1983
PRICE SCHEDULE

LINE SCAN SENSORS

Order Code	Number of Elements	Element Size	Max. Data Rate	1-9 Price
CCD111ADC	256x1	13x17 Microns	10MHz	$ 80
CCD111BDC	256x1	13x17 Microns	10MHz	150
CCD112DC	256x1	13x13 Microns	5MHz	150
CCD133DC	1024x1	13x13 Microns	20MHz	633
CCD134DC	1024x1	13x13 Microns	20MHz	750
CCD122DC	1728x1	13x13 Microns	2MHz	950
CCD123DC	1728x1	10x13 Microns	2MHz	730
CCD143DC	2048x1	13x13 Microns	20MHz	1300
CCD145DC	2048x1	13x13 Microns	8MHz	1500
CCD151DC	3456x1	7x7 Microns	5MHz	1500

LINE SCAN DESIGN AIDS (DO NOT INCLUDE SENSORS)

Order Code	Sensor Supported	1-9 Price
I-SCAN*	CCD111	$ 99
CCD133DB	CCD133DC	500
CCD122DB	CCD122DC	350
CCD143DB	CCD143DC	500
CCD151DB	CCD151DC	500

*I-SCAN includes CCD111 device.

AREA SENSORS

Order Code	Number of Elements	Grade	Max. Frame Rate	1-9 Price
CD222ADC	488x380	A	60Hz	$ 5,000
CD222BDC	488x380	B	60Hz	3,000
CD222CDC	488x380	C	60Hz	1,000

SIGNAL PROCESSING PRODUCTS

Order Code	Description	1-9 Price
CCD321A1	Broadcast Quality Video Delay Line	$ 150
CCD321A2	Industrial Quality Video Delay Line	60
CCD321A3	Time Base Correction Video Delay Line	90
CCD323AC	PAL Compatible Video Delay Line (Sample Quantities Only)	100
CCD321VM	Video Delay Module (Includes the CCD321A3)	500

APPENDIX C

TEXAS INSTRUMENTS

1. Virtual Phase CCD Technology
2. Type TC102 Linear Image Sensor
3. Type TC101
4. Type TC103
5. Type TC 104

VIRTUAL PHASE CCD TECHNOLOGY

J. Hynecek

Texas Instruments Incorporated
P.O. Box 225536
Dallas, Texas 75265

ABSTRACT

In this article a new concept of a single phase CCD, called "virtual phase", is described. Virtual phase technology employs only a single level gate electrode structure. This technology represents a new approach to fabrication of large area CCD devices which have both high performance and high yield.

An example of the application of virtual phase technology to the fabrication of a 490 x 328 CCD imager is presented, and several important design and performance parameters are discussed.

DESCRIPTION OF OPERATION OF THE VP CCD

In the following sections the discussion will be limited to N-channel devices, with the understanding that the P-channel equivalent can be obtained simply by reversing the signs of potentials and the type of dopants. Both P-channel and N-channel virtual phase devices have been built and operated successfully.

Virtual phase technology is an extension of two phase buried channel technology in which one phase is built into the silicon surface. The basic operating principles of VP devices are described below.

In Figure 1 a typical potential profile for a buried channel CCD is shown. The gate potential is indicated by V_g; the surface and maximum potentials are indicated by the symbols ϕ_s and ϕ_m respectively.

One important feature of the buried channel structure is that electrons are stored away from the surface in the vicinity of X_m and are therefore free from the undesirable influence of surface scattering and traps. Another important feature of the buried channel structure, noted also by others (1), is called the potential pinning phenomena. As the gate potential V_g is lowered toward more negative bias, the surface potential ϕ_s is also lowered until it reaches the point where $\phi_s = 0$. When this occurs, the holes from the channel stops will flow across the surface and prevent further lowering of ϕ_s. Therefore, ϕ_s is pinned to zero. Since the holes can occupy only a very thin region of space near the surface of the silicon, the potential profile within the silicon will not be affected by the amount of holes needed to compensate any additional field induced by the gate. As a result, the value of ϕ_m will also be pinned to some positive minimum, $\phi_{m\,min}$, regardless of further lowering of the gate potential. Since the pinned $\phi_{m\,min}$ remains positive, signal charge (electrons) can be effectively stored or transferred under the accumulated layer of holes, independent of further changes of the voltage on the overlying gate. In this case the holes accumulated at the surface act as a "virtual" gate for the underlying buried channel region. This basic principle is the cornerstone of the virtual phase technology. The use of this principle for the construction of charge transfer devices will now be explained.

One fundamental element, pixel, or bit of a virtual phase CCD is divided into four sections as indicated in Figure 2. The first two sections will be called the clocked phase, with the barrier being Section 1, and the well, Section 2. The second two sections are called the virtual phase. This phase is also composed of a barrier, Section 3, and a well, Section 4. All four sections are assumed to have a uniform buried channel doping (this is not shown in Figure 2). The potential well under the clocked phase is created by placing a shallow N-type implant within Section 2, and it is indicated there by the series of plus signs. The virtual phase is formed by a deep N-type doping in Section 3, with an even heavier dose in Section 4 to form a potential well there. Since this N-type doping is relatively large, it would be necessary to bias the gate to a large negative potential in order to obtain the desired surface potential pinning. However, this is not necessary if a shallow P-type implant of a sufficient dose is placed close to the surface of the silicon in Sections 3 and 4. This is indicated by a series of minus signs in Figure 2. If the dose of this doping is large enough, the surface potential will stay pinned to zero for positive as well as for negative potentials on the gate. In this case the gate electrode over the virtual phase is superfluous and can actually be eliminated, since it does not have any effect on the potential profile in the silicon. We can, therefore, have two types of virtual phase devices, one with a continuous gate electrode over the clocked phase area and the virtual phase area (as indicated in Figure 2) and one with a patterned gate electrode where only the clocked phase has an overlying gate structure, as will be described later.

The charge transfer process is illustrated in Figure 3, where only the maximum potentials were plotted for a section of the CCD channel in the direction of charge transfer.

From Figure 3 it is apparent that the operation of the virtual phase CCD is equivalent to the operation of the two phase CCD with one phase biased at some DC potential and the other clocked below and above this potential, as described elsewhere (2). The advantage of the virtual phase structure is that the DC biased electrode is not built over the gate dielectric but is actually built into the surface of the silicon and is biased at the substrate potential. This feature has significant advantages not only for ease of fabrication, but also in performance, as will be discussed in the following sections.

APPLICATION OF THE VP CONCEPT TO LARGE AREA IMAGERS

A large area CCD imager was selected as a test vehicle for demonstration of the virtual phase CCD concept. This imager has 490 x 328 elements and is designed to operate in a TV compatible, frame-store mode. The parallel section is divided into a separate image integration area and image storage area, each having 245 x 328 elements, as illustrated in Figure 4. On the bottom of the storage area is a serial register which allows one video line at a time to be clocked to the output amplifier. The output amplifier is a standard floating gate structure with gate reset capability (3). The topology of a single cell is also shown in Figure 4. Regions one and three are barriers, while regions two and four are wells. A cross-section of the device in various stages of fabrication is shown in Figure 5.

A typical image obtained from this device is shown in Figure 6. The modulation transfer function was measured at $\lambda = 6000Å$, it is 58% at the Nyquist limit. The charge transfer efficiency measured by optical signal injection is CTE = 0.99997. The maximum usable well population is N_V = 400,000 e^-. The resulting device is an N-channel virtual phase CCD with a patterned single polysilicon gate. This type of device is easily manufactured and yields excellent results in the front side illuminated mode of operation. The uncovered regions of the channel (virtual phase) do not block the light, hence the device has high quantum efficiency, particularly in the blue region of the spectrum compared to other polysilicon gate structure CCDs.

The last and most important performance parameter of the VP CCD to be discussed is the dark current. The absolute value of the dark current as well as the spatial distribution of the local dark current sources (blemishes) is crucial for the successful operation of the CCD as an imager. There are three major components of the total dark current in a CCD. These are the surface component, due to the SiO_2-Si interface states; depletion region component, where the bulk G-R centers supply the current; and the diffusion component, due to the minority carrier diffusion from the neutral undepleted bulk of the silicon. Of these three, the surface component is dominant in most buried channel CCD structures. For the virtual phase CCD, however, the surface component is significantly smaller than it is in other technologies. The reason for the reduction of the surface component of the dark current in virtual phase devices is that in the virtual phase region, the SiO_2-Si interface states are filled by holes. For standard buried channel device we have (4):

$$U_s = -S_o \cdot (n_i/2) \qquad (1)$$

But for the virtual phase region it can be easily derived, following the same analysis given in (4), that

$$U_s \cong -S_o \cdot (n_i/2) \cdot (2\,n_i/N_A) \qquad (2)$$

where N_A is the doping concentration at the surface of the virtual phase region. The factor $2n_i/N_A$ makes the surface contribution to the dark current in this region negligible. In addition, it is also possible to bias the clocked phase during the integrate period at a negative gate potential and thereby force holes to the surface over the entire imager area. The dark current measured under these conditions for the 490 x 328 virtual phase imager is 0.4 na/cm^2, which is approximately an order of magnitude lower than for two phase devices of the same geometry and fabricated on the same material.

A few photographs of the dark current signature at room temperature for 490 x 328 virtual phase CCD at various integrate conditions are shown in Figure 7 a and 7 b. Spectral response data is shown in Figure 8.

CONCLUSIONS

The performance data obtained from 490 x 328 pixel imager demonstrate that the virtual phase technology is a viable alternative for fabrication of large area imagers.

The absence of interlevel shorts, low dark current, simplicity of fabrication, high quantum efficiency in the front side illumination mode, as well as simplicity of clocking, make this technology particularly attractive for high volume and low cost production.

ACKNOWLEDGEMENTS

The author would like to thank Dr. H. H. Hosack for helpful comments on the manuscript, Dr. W. Dean Mercer for the device layout and mask design, Mr. H. Ray Shields for help with device characterization and testing, and the management of the Central Research Laboratories for providing

support for the development of virtual phase technology.

REFERENCES

1. Tetsuo Yamada, Haruo Okano, and Nobuo Suzuki, "The Evaluation of Buried-Channel Layer in BCCD's", IEEE Transactions on E.D., May 1978, Vol. ED-25, No. 5, p. 544.
2. Carlo H. Sequin and Michael F. Tompsett, Charge Transfer Devices, Academic Press, Inc., N.Y., 1975, p. 39.
3. J. E. Hall, J. F. Breitzmann, M. M. Blouke, and J. T. Carlo, "A Multiple Output CCD Imager for Imaging Processing Applications", Proceedings of the IEDM, Washington, D.C., December 1978.
4. A. S. Grove, Physics and Technology of Semiconductor Devices, John Wiley and Sons, Inc., N.Y. 1967, pp. 136, 145.

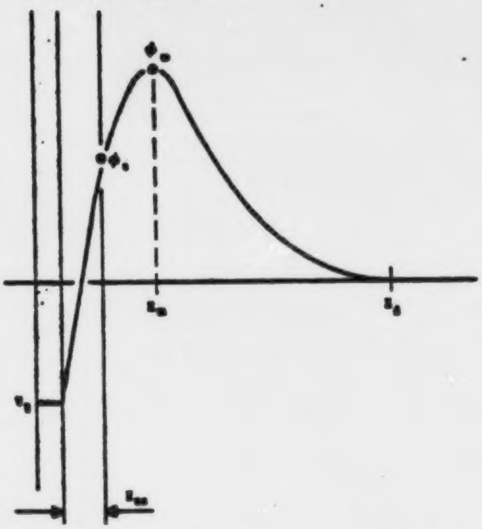

Figure 1. Potential profile in a typical N-type buried channel CCD device as function of the distance into the silicon

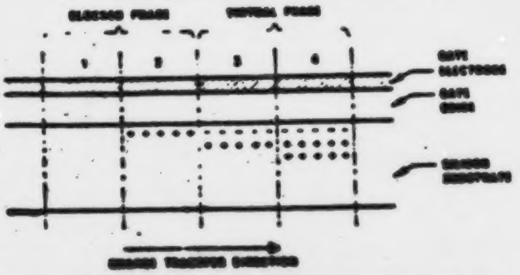

Figure 2. Division of a single pixel of the virtual phase CCD into the clocked phase and the virtual phase regions. It is assumed that uniform buried channel implant is provided.

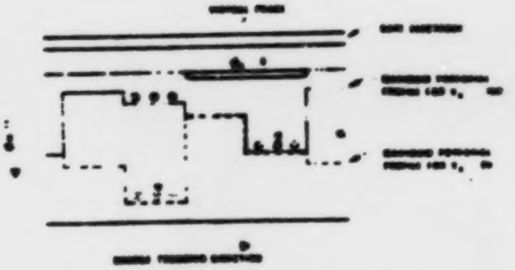

Figure 3. Maximum potential profile for two different gate bias conditions is plotted in the direction of charge transfer.

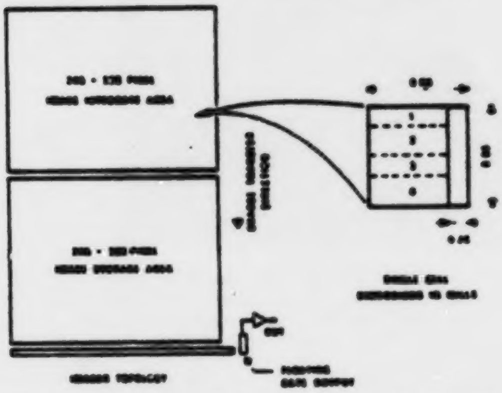

Figure 4. Topology and the single pixel dimensions of the 490 x 328 frame store imager

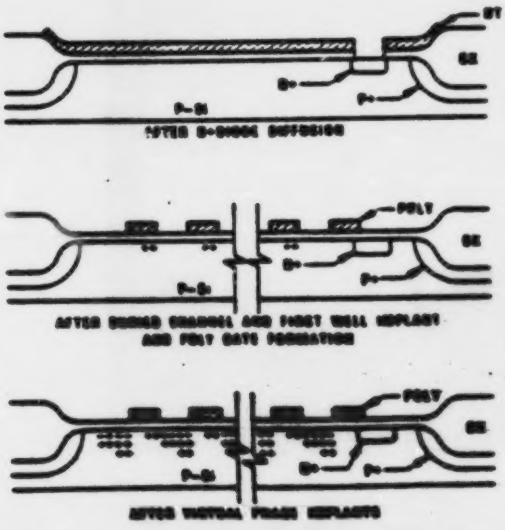

Figure 5. Cross section of the device at various stages of fabrication

.61

C-4

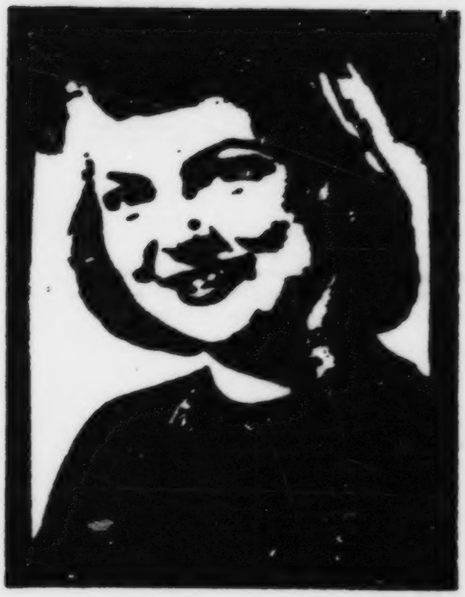

Figure 6. Image of the part of the IEEE standard facsimile test chart obtained by the virtual phase imager operated in the full frame mode at 5MHz

Figure 7b. Dark current signature of the 490 x 328 virtual phase CCD imager after 7 seconds of integration at 25°C

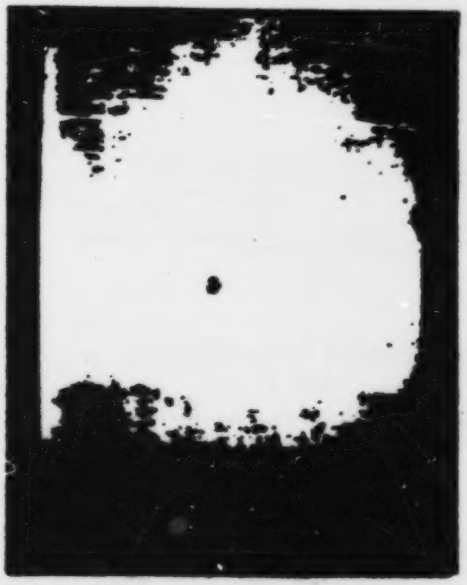

Figure 7a. Dark current signature of the 490 x 328 virtual phase CCD imager after 300 msec. of integration at 25°C.

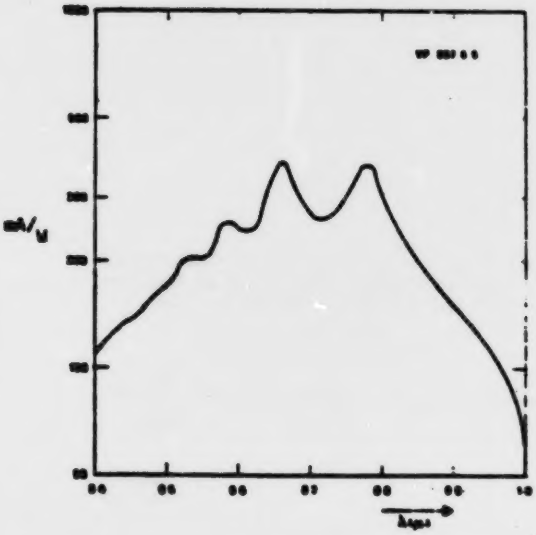

Figure 8. Spectral response of the 490 x 328 virtual phase CCD imager with the patterned polysilicon gate structure.

TYPE TC102
128 × 1 CCD LINEAR IMAGE SENSOR

D2664, APRIL 1982

- **128 x 1 Sensor Element Organization**
- **Virtual-Phase N-Channel Silicon MOS Technology**
- **High Quantum Efficiency**
- **Enhanced Blue Response**
- **Output Signal Approximately 1 Volt Peak-to-Peak**
- **Dynamic Range Relative to Peak-to-Peak Noise Typically 1000:1**
- **End-of-Scan Signal**
- **Internal Black and White References**
- **Simple and Stable Operation**

CERAMIC DUAL-IN-LINE PACKAGE

(TOP VIEW)

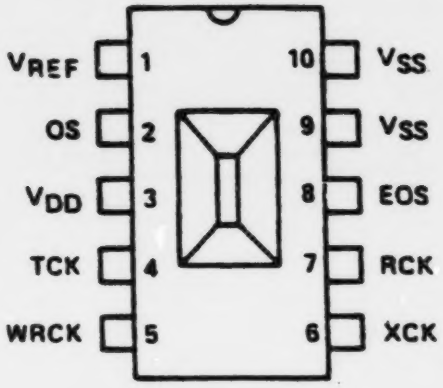

Caution. These devices have limited built-in gate protection. The leads should be shorted together or the device placed in conductive foam during storage or handling to prevent electrostatic damage to the MOS gates. Avoid shorting either OS or EOS to V_{SS} during operation to prevent damage to the output amplifiers.

description

The TC102, a 128-element CCD line image sensor, functions in high-resolution image scanning applications such as document reading and optical character recognition. The TC102 incorporates virtual-phase MOS technology, which provides simplified operation and high reliability.

This device is supplied in a 10-pin dual-in-line ceramic side-braze package designed for insertion in mounting-hole rows on 7.6-mm (0.300-inch) centers. The glass window may be cleaned by wiping with a cotton swab soaked in alcohol.

virtual-phase technology

This patented design results in simplified clocking circuits, reduced noise, and greater light sensitivity. Virtual-phase technology utilizes a junction-gate region at the substrate dc potential. This accomplishes the same gating and transport function as a separate gate electrode requiring multiple layers and multiple process steps common in other device designs. The resulting simplicity of process and ease of operation will increase performance and reliability for the user.

Copyright © 1982 by Texas Instruments Incorporated

functional block diagram

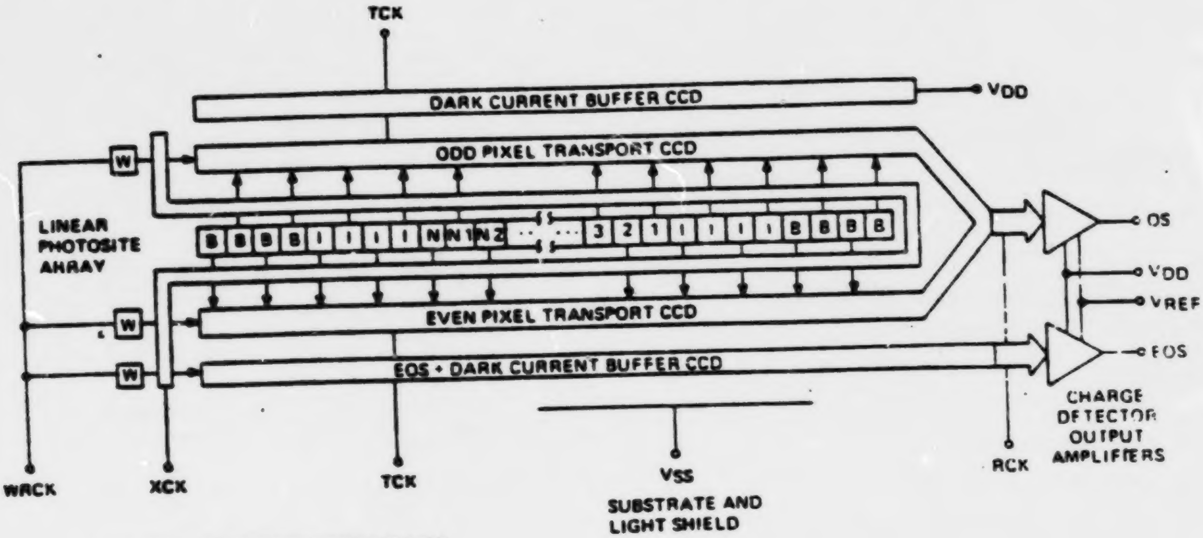
TCK
DARK CURRENT BUFFER CCD
VDD
W
ODD PIXEL TRANSPORT CCD
LINEAR PHOTOSITE ARRAY
B B B B I I I I N N-1 N-2 ... 3 2 1 I I I I B B B B
EVEN PIXEL TRANSPORT CCD
W
EOS + DARK CURRENT BUFFER CCD
W
OS
VDD
VREF
EOS
CHARGE DETECTOR OUTPUT AMPLIFIERS
WRCK
XCK
TCK
VSS
SUBSTRATE AND LIGHT SHIELD
RCK

W = WHITE REFERENCE INPUT DIODE
B = BLACK REFERENCE ELEMENT
I = ISOLATION ELEMENT
N = 128 SENSOR ELEMENTS

PIN FUNCTIONAL DESCRIPTION

PIN NUMBER	SIGNATURE	NAME	DESCRIPTION
1	V_{REF}	Reference Voltage	Bias input for the output amplifiers
2	OS	Output Signal	Video output from a cascaded source-follower MOS amplifier
3	V_{DD}	Supply Voltage	Output amplifier supply voltage
4	TCK	Transport Clock	Drives the CCD transport registers.
5	WRCK	White Reference Clock	Injects a controlled charge into the white reference CCD shift register elements to become white-reference and end-of-scan pulses.
6	XCK	Transfer Clock	Controls the transfer of charge packets from sensor elements to shift registers. The interval between pulses of the transfer clock determines the exposure time.
7	RCK	Reset Clock	Controls recharging of the charge-detection diodes in the output amplifiers, and clocks the output shift registers where the odd and even signals have been merged.
8	EOS	End-of-Scan Pulse	Indicates that all charge packets have been shifted out of the transport registers.
9, 10	V_{SS}	Substrate	All voltages are referenced to the substrate

functional description

image sensor elements

The line of sensor elements (also called photosites or pixels) consists of 128 photo-sensitive areas, 12.7 micrometers (0.5 milliinches) square and approximately 12.7 micrometers from center to center. Image photons create electron-hole pairs in the single-crystal silicon. The electrons are collected in the sensor elements and the holes are swept into the substrate. The amount of charge accumulated in each element is a linear function of the incident light and the exposure time. The output signal charge will vary in an analog manner from a thermally generated noise background at zero illumination to a maximum at saturation under bright illumination.

transfer gate

This structure is adjacent to the line of image sensor elements. The charge packets accumulated in the image sensor elements are transferred into the transfer gate storage well when the transfer gate voltage goes high. When the transfer gate voltage goes low, the charge is transferred into the CCD transport shift registers. The transfer gate also controls the exposure time for the sensor elements and permits charges to enter the end-of-scan (EOS) shift registers to create the end-of-scan waveform. In addition, the transfer gate permits entry of charge packets to the transport CCD shift register to create the white reference signals.

shift registers

There are two CCD transport registers, one on each side of the line of image sensor elements and outside of the transfer gate. Alternate charge packets are transferred to the CCD transport shift registers and moved serially to the output amplifier. The phase relationship of the reset clock and the transport clock and the geometric layout of the paths provide for alternate delivery of charge packets to re-establish the original sequence of the linear image data. The two outer buffer CCD shift registers protect the signal charges in the inner transport CCD shift registers from peripherally generated dark current noise.

black and white reference elements

Four additional sensor elements at each end of the sensor element array (labelled "B" in the block diagram) are covered by opaque metallization. They provide a black (no illumination) signal reference that is delivered at each end of the linear image output signal. Also included on the transport CCD shift register, at the opposite end from the amplifier, is an input diode that provides two white reference pulses in the output signal. The reference pulses are useful as inputs to external dc restoration and/or automatic exposure control circuitry. The white reference pulse amplitude is approximately 70% of the maximum output signal amplitude.

output signal amplifier

The charge packets are transported to a precharge diode whose potential changes linearly in response to the amount of the signal charge delivered. This potential is applied to the input gate of an N-channel MOS double-source-follower amplifier to produce an output signal (OS). A reset transistor, driven by the reset clock (RCK), recharges the charge-detector-diode capacitance before the arrival of each new signal charge packet from the CCD shift registers. A reference voltage (V_{REF}) is applied to the drain of the reset transistor and acts to bias the OS and EOS amplifiers. A current sink is used as an on-chip load for the amplifier output. No external current sink is needed. The output signal is a series of negative-going pulses on a dc level.

c-5

resolution

The modulation transfer function decreases at longer wavelengths (see Figures 7 and 8). If optimum resolution is required with a light source that has a significant infrared component, then the designer must use appropriate filters to restrict the optical pass band to shorter wavelengths.

end-of-scan amplifier

The EOS amplifier is similar to the OS amplifier. XCK transfers charge from the input diode into the EOS register where it is transported at the TCK clock frequency to the EOS amplifier. This EOS pulse is coincident with the first of the two white reference pulses that pass through the odd and even transport CCDs, respectively. The EOS output can be used to alert the external circuitry that the linear image data readout has been completed.

clocks

The transfer clock (XCK) pulse controls the exposure time of the sensor elements. The minimum exposure time is the time required to shift the entire contents of the transport registers to the output signal amplifier and equals 161 multiplied by the RCK period. The maximum exposure time is determined by the tolerable level of dark signal.

The transport clock (TCK) transports the linear image signal charge from the sensor element region to the output amplifier.

The reset clock (RCK) operates at twice the transport clock frequency so as to recombine the signal charge in the original sequence and present the charge to the output amplifier. The data rate is equal to the reset clock frequency.

The white reference clock (WRCK) runs at the transfer clock frequency and generates the white reference and the end-of-scan pulses. These pulses can be eliminated by connecting WRCK to V_{DD}. Transients on WRCK going below zero volts will cause charge injection resulting in an increase in apparent dark signal.

Figure 3 presents a suggested circuit for generating the clock waveforms. The RCK clock generator runs continuously. A binary divider halves the frequency to create TCK. After all signal charges have been transported to the output amplifier, TCK continues to run to keep thermally generated charges from accumulating in the transport registers.

The XCK and WRCK clock frequencies are submultiples of the TCK frequency. Figure 2 details the timing relationships among the different clock pulses.

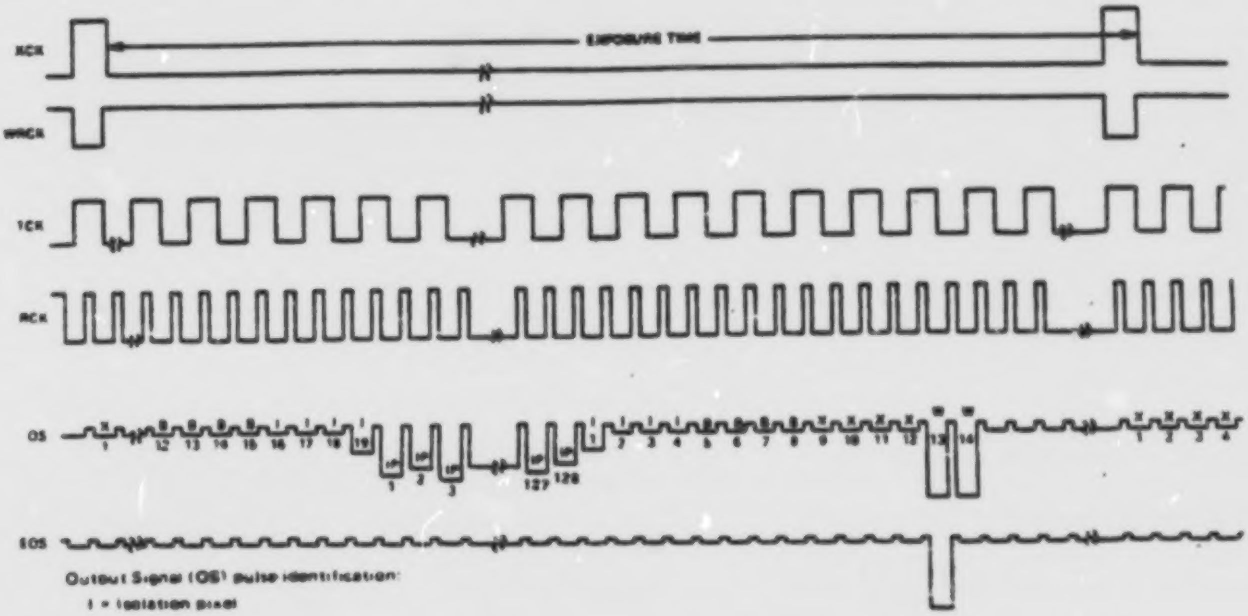

Output Signal (OS) pulse identification:

I = Isolation pixel
IP = Image pixel
B - Black reference pixel
W = White reference pixel
X = Empty pixel

FIGURE 1 – OPERATING INPUT AND OUTPUT VOLTAGE WAVEFORMS

absolute maximum ratings over operating free-air temperature range (unless otherwise noted) (see Note 1)

Amplifier drain voltage (V_{DD})	−0.3 V to 30 V
Amplifier reference voltage (V_{REF})	−0.3 V to 30 V
Transfer clock (XCK) voltage	−25 V to 5 V
Transport clock (TCK) voltage	−25 V to 5 V
Reset clock (RCK) voltage	−25 V to 5 V
White reference clock (WRCK) voltage	−0.3 V to 30 V
Storage temperature	−25 °C to 125 °C
Operating free-air temperature	−25 °C to 70 °C

NOTE 1: Voltage values are with respect to V_{SS}.

TYPE TC102
128 × 1 CCD LINEAR IMAGE SENSOR

recommended operating conditions at $T_A = 25°C$

		MIN	NOM	MAX	UNIT
V_{DD}	Supply voltage	15	16	20	V
V_{REF}	Amplifier reference voltage	6	7	8	V
$V_{IH(X)}$	Transfer clock high level input voltage	1	2	3	V
$V_{IL(X)}$	Transfer clock low-level input voltage	-17[¶]	-16	-15	V
$V_{IH(T)}$	Transport clock high-level input voltage	1	2	3	V
$V_{IL(T)}$	Transport clock low-level input voltage	-17[¶]	-16	-15	V
$V_{IH(R)}$	Reset clock high-level input voltage	1	2	3	V
$V_{IL(R)}$	Reset clock low-level input voltage	17[¶]	-16	15	V
$V_{IH(WR)}$	White reference clock high-level input voltage	15	16	20	V
$V_{IL(WR)}$	White reference clock low-level input voltage	6	7	8	V
f_{RCK}	Reset clock frequency (output data rate)		2	10	MHz

[¶] The algebraic convention, where the most negative limit is designated as minimum, is used in this data sheet for clock voltage levels only

electrical characteristics at 25°C free-air temperature, f_{RCK} = 0.5 MHz, t_{exp} = 10 ms, tungsten light source operating at color temperature of 2854 K with 2.0-mm-thick Fish-Schurman HA-11 IR-absorbing filter, and all operating voltages at nominal recommended values.

PARAMETER		MIN	TYP	MAX	UNIT
Dark-signal amplitude	Average		0.5	10	mV
	Low frequency component		0.5	5	
	Nonuniformity relative to average of adjacent pixels		1	20	
Sensitivity		2	3.5	5	$V/(\mu J\ cm^2)$
Output amplitude variation (PRNU)[‡]	Peak-to-peak		50	100	mV
	Adjacent pixels from alternate registers (imbalance)		10		
Peak-to-peak noise			1		mV
Equivalent exposure[§] of peak-to-peak noise			0.35		nJ/cm^2
Saturation exposure[§]			350		nJ/cm^2
Saturation output amplitude		700	1000	1400	mV
Dynamic range relative to peak-to-peak noise		500:1	1000:1		
Charge transfer efficiency			0.99999		
White reference amplitude		500	700		mV
End-of-scan amplitude		300	500		mV
Output offset (dc) voltage			10		V
Output impedance			1		kΩ
Resistance to V_{SS}	Transfer gate		45		kΩ
	Transport gate		45		
	Reset gate		45		
Capacitance to V_{SS}	Transfer gate		26		pF
	Transport gate		57		
	Reset gate		7		
I_{REF}	Amplifier reference current		3		nA
I_{DD}	Supply current		6.3	9.4	mA
Power dissipation			100		mW

[‡] Measured at 700 mV output amplitude with an f/2.8 lens.

[§] Exposure = intensity x time

timing requirements

		MIN	NOM	MAX	UNIT
t_{THXH}	Time delay from the transport clock rising edge to the transfer clock rising edge	0		100	ns
t_{THWL}	Time delay from the transport clock rising edge to the white reference clock falling edge	0		100	ns
t_{THRH}	Time delay from the transport clock rising edge to the reset clock rising edge	0			ns
$t_{w(RH)}$	Pulse duration of the high state for the reset clock	40			ns
t_{TLXL}	Time delay from the transport clock falling edge to the transfer clock falling edge	50			ns
t_{TLWH}	Time delay from the transport clock falling edge to the white reference clock rising edge	0		100	ns
t_{XLTH}	Time delay from the transfer clock falling edge to the rising edge of the next transport clock pulse	50			ns
t_r	rise time (all clocks)	15			ns
t_f	fall time (all clocks)	5			ns

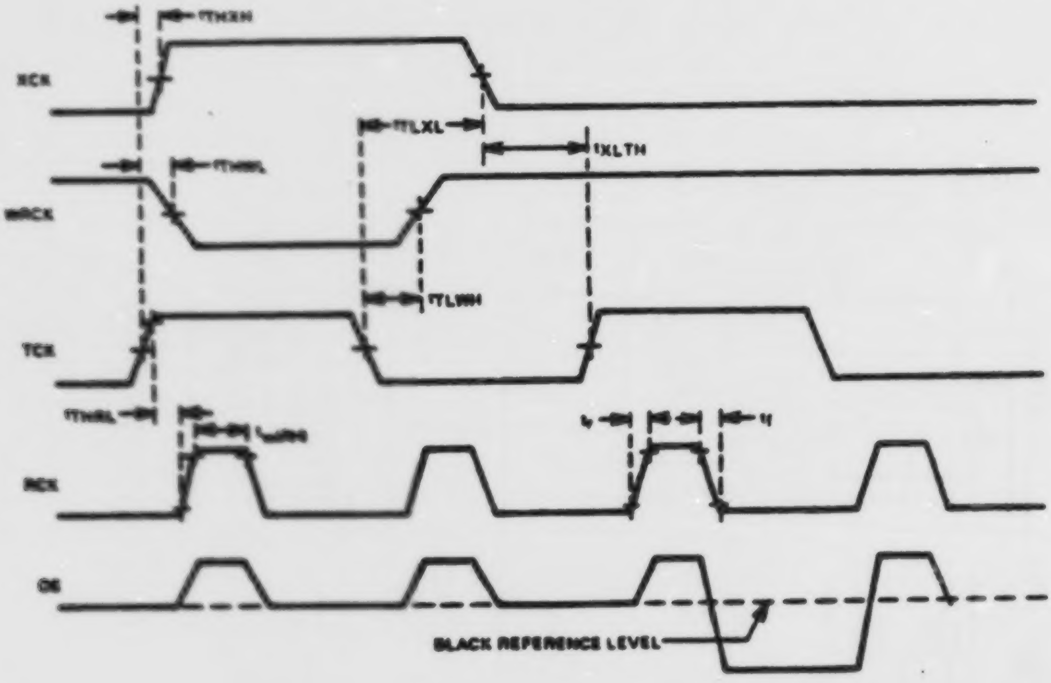

FIGURE 2 – DEVICE TIMING REQUIREMENTS

C-12

PARAMETER MEASUREMENT INFORMATION

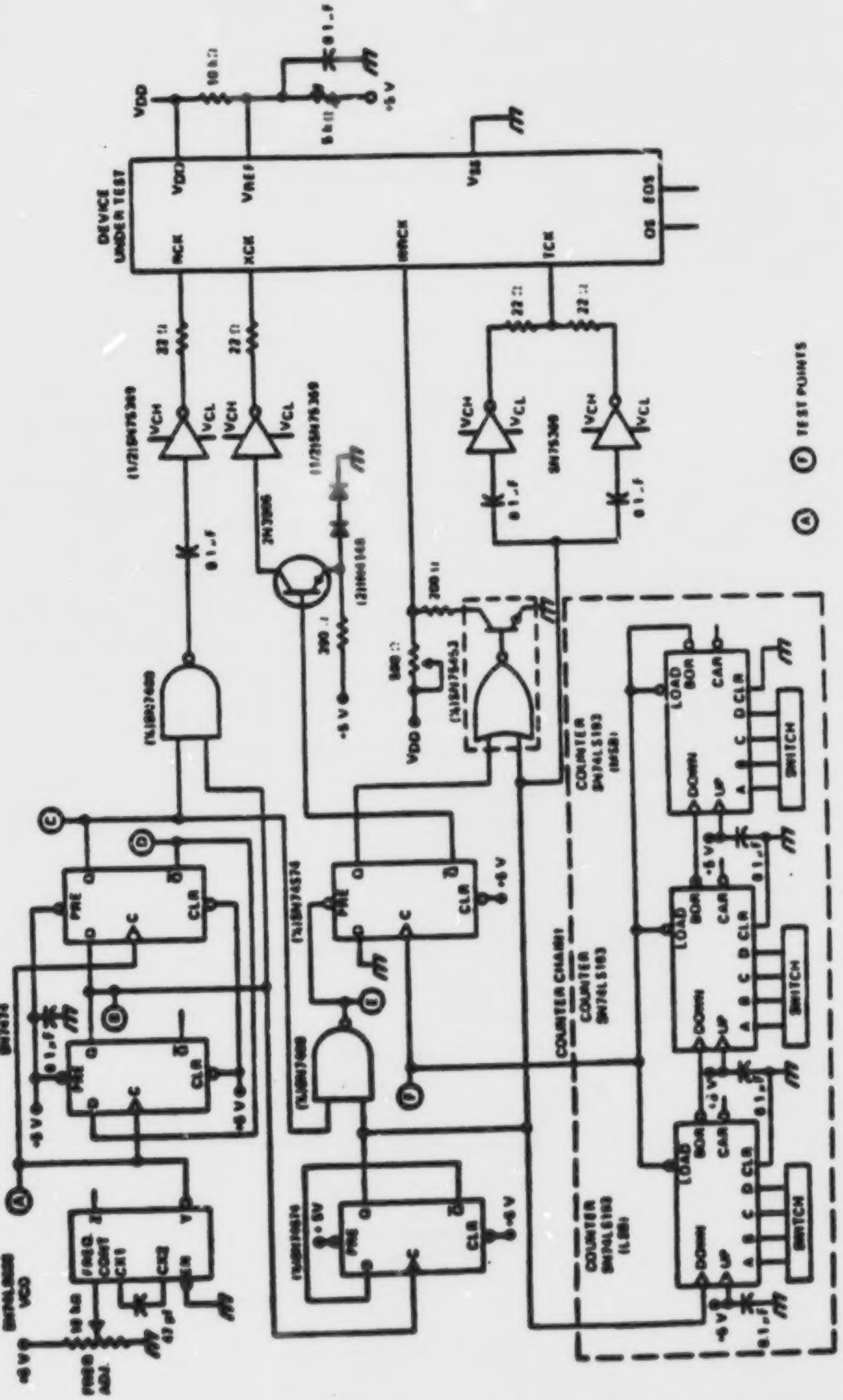
DEVICE UNDER TEST
VDD
VREF
VSS
RCK
XCK
MRCK
TCK
OS
EOS
VDD
10 Ω
5 kΩ
0.1 μF
+5 V
22 Ω
VCH
VCL
(1/2)SN75369
SN75369
0.1 μF
2N3906
(2)1N914
200 Ω
300 Ω
(1/4)SN7400
(1/2)SN75452
+5 V
VDD
SN7474
(1/2)SN7474
(1/4)SN7400
PRE
CLR
Q
C
FREQ CONT
CX1
CX2
EN
V
50 kΩ
47 pF
FREQ ADJ
SN74LS629
COUNTER CHAIN†
COUNTER SN74LS193
LOAD
BOR
CAR
DOWN
UP
A B C D CLR
SWITCH
A
B
C
D
E
F
Ⓐ – Ⓕ TEST POINTS

†The counter chain counts transport clock periods to generate the exposure time interval. The data rate is twice the count rate.

FIGURE 3 – DRIVER CIRCUIT FOR TESTING LINE IMAGE SENSOR

C-1-

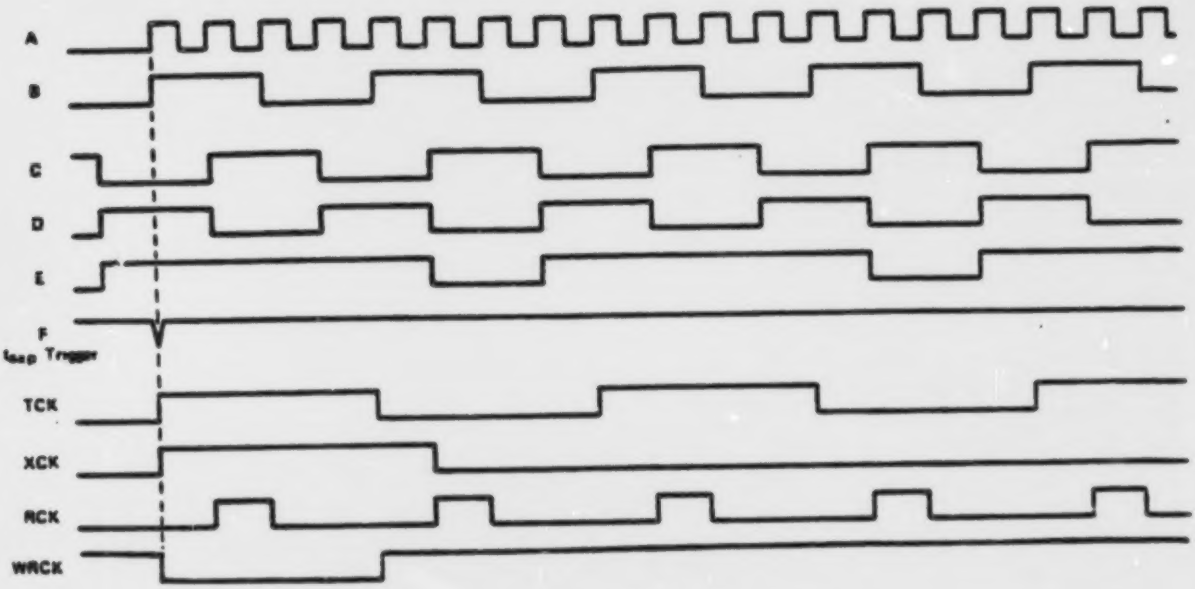

FIGURE 4 – WAVEFORMS IN DRIVER CIRCUIT

TYPICAL CHARACTERISTICS

(In the circuit of Figure 3 with T_A = 25°C, f_{RCK} = 0.5 MHz, t_{exp} = 10 ms, and all operating voltages at nominal recommended values, unless otherwise noted)

SENSITIVITY
vs
WAVELENGTH OF INCIDENT LIGHT

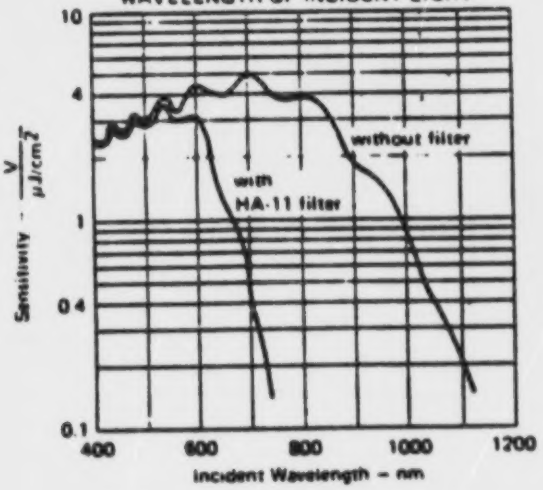

FIGURE 5

RESPONSIVITY
vs
WAVELENGTH OF INCIDENT LIGHT

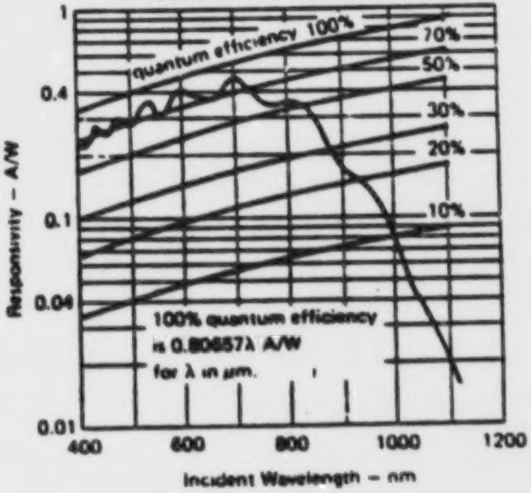

FIGURE 6

TYPICAL CHARACTERISTICS

(In the circuit of Figure 3 with $T_A = 25°C$, $f_{RCK} = 0.5$ MHz, $t_{exp} = 10$ ms, and all operating voltages at nominal recommended values, unless otherwise noted)

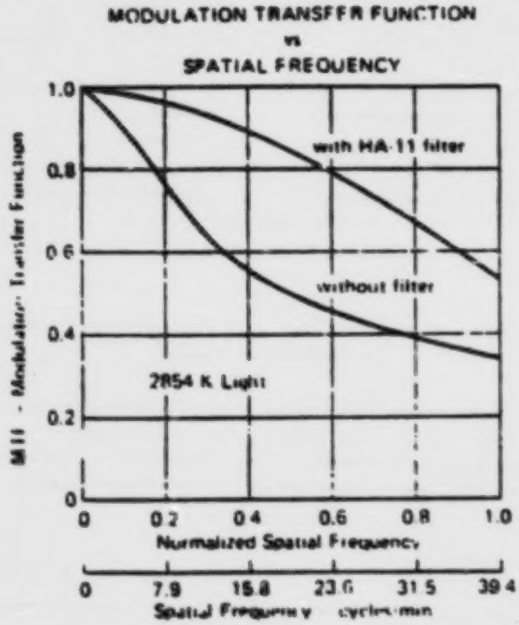

FIGURE 7

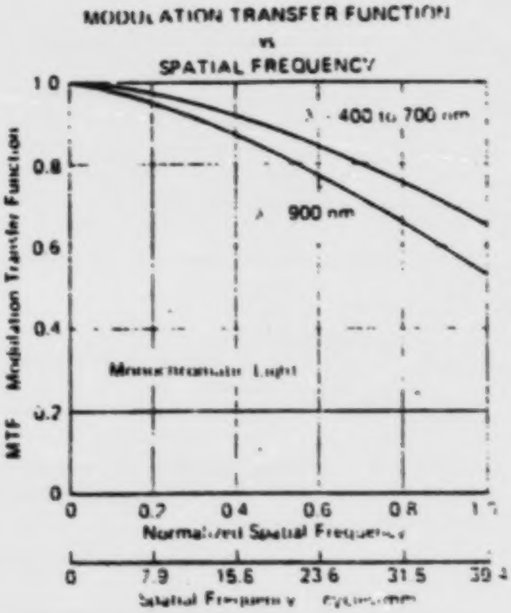

FIGURE 8

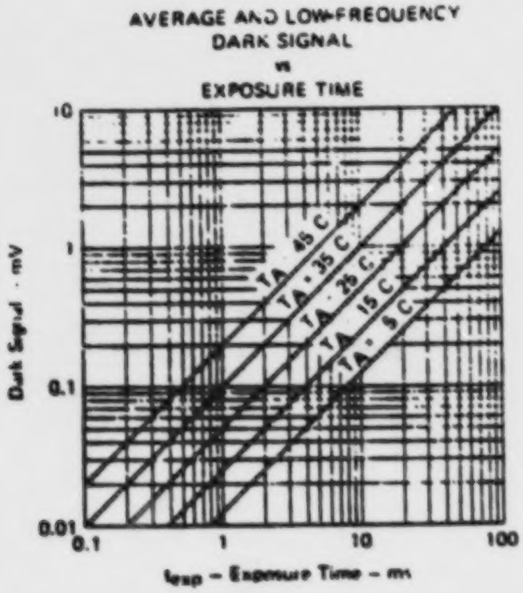

FIGURE 9

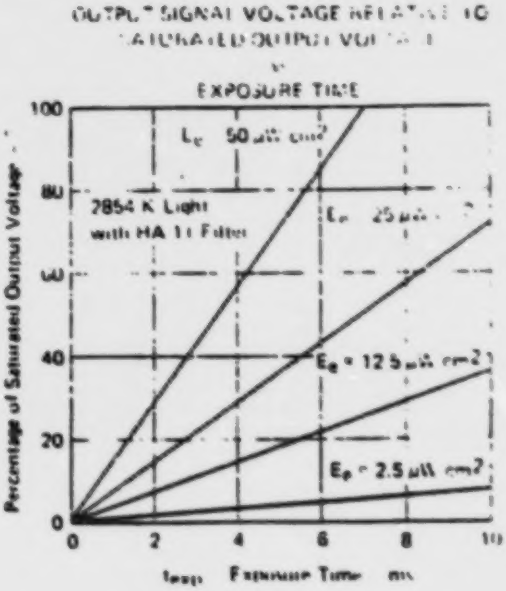

FIGURE 10

C-1

MECHANICAL DATA

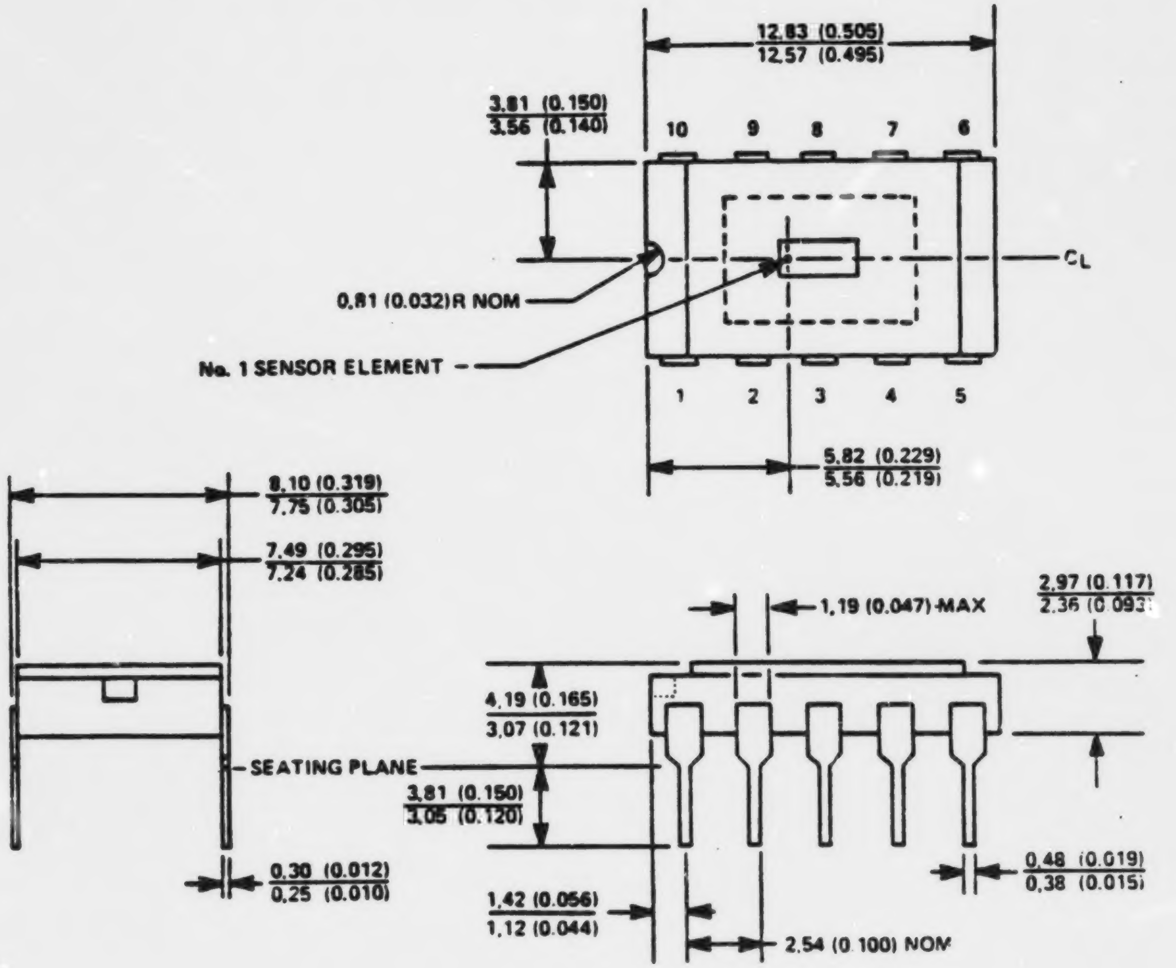
12,83 (0.505)
12,57 (0.495)
3,81 (0.150)
3,56 (0.140)
10
9
8
7
6
CL
0,81 (0.032)R NOM
No. 1 SENSOR ELEMENT
1
2
3
4
5
5,82 (0.229)
5,56 (0.219)
8,10 (0.319)
7,75 (0.305)
7,49 (0.295)
7,24 (0.285)
1,19 (0.047) MAX
2,97 (0.117)
2,36 (0.093)
4,19 (0.165)
3,07 (0.121)
SEATING PLANE
3,81 (0.150)
3,05 (0.120)
0,30 (0.012)
0,25 (0.010)
0,48 (0.019)
0,38 (0.015)
1,42 (0.056)
1,12 (0.044)
2,54 (0.100) NOM

NOTES 1. All dimensions are in millimeters and parenthetically in inches.

2. The distance between the top surface of the window and the surface of the sensor is nominally 0,89 (0.035). This is determined by observing the vertical motion of a microscope focused first at one plane, then at the other.

PRINTED IN U S A
TI cannot assume any responsibility for any [illegible] shown
or represent that they are free from patent [illegible]

TYPE TC101

- 1728 x 1 Sensor Element Organization
- Virtual-Phase N-Channel Silicon MOS Technology
- High Quantum Efficiency
- Enhanced Blue Response
- Output Signal Approximately 1 Volt Peak-to-Peak
- Dynamic Range Relative to Peak-to-Peak Noise Typically 1000:1
- End-of-Scan Signal
- Internal Black and White References
- Simple and Stable Operation

TOP VIEW

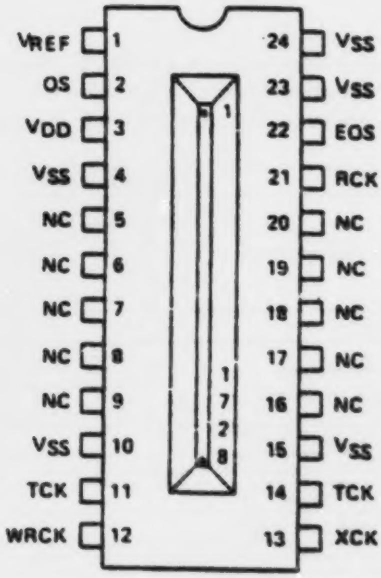

V_{REF} 1
OS 2
V_{DD} 3
V_{SS} 4
NC 5
NC 6
NC 7
NC 8
NC 9
V_{SS} 10
TCK 11
WRCK 12
24 V_{SS}
23 V_{SS}
22 EOS
21 RCK
20 NC
19 NC
18 NC
17 NC
16 NC
15 V_{SS}
14 TCK
13 XCK
1
1728

NC – No internal connection

C 11

recommended operating conditions at T_A - 25°C

		MIN	NOM	MAX	UNIT
V_{DD}	Supply voltage	15	16	20	V
V_{REF}	Amplifier reference voltage	6	7	8	V
$V_{IH(X)}$	Transfer clock high level input voltage	1	2	3	V
$V_{IL(X)}$	Transfer clock low level input voltage	179	16	15	V
$V_{IH(T)}$	Transport clock high level input voltage	1	2	3	V
$V_{IL(T)}$	Transport clock low level input voltage	179	16	15	V
$V_{IH(R)}$	Reset clock high level input voltage	1	2	3	V
$V_{IL(R)}$	Reset clock low level input voltage	179	16	15	V
$V_{IH(WR)}$	White reference clock high level input voltage	15	16	20	V
$V_{IL(WR)}$	White reference clock low level input voltage	6	7	8	V
f_{RCK}	Reset clock frequency (output data rate)		2	10	MHz

¶The algebraic convention, where the most negative limit is designated as minimum, is used in this data sheet for clock voltage levels only.

electrical characteristics at 25°C free-air temperature. f_{RCK} = 0.5 MHz, t_{exp} = 10 ms, tungsten light source operating at color temperature of 2854 K with 2.0-mm-thick Fish-Schurman HA-11 IR-absorbing filter, and all operating voltages at nominal recommended values

PARAMETER		MIN	TYP	MAX	UNIT
Dark-signal amplitude	Average		0.5	10	mV
	Low frequency component		0.5	5	
	Nonuniformity relative to average of adjacent pixels		1	20	
Sensitivity		2	3.5	5	V/(μJ.cm^2)
Output amplitude variation (PRNU)‡	Peak-to-peak		50	100	mV
	Adjacent pixels from alternate registers (imbalance)		10		
Peak-to-peak noise			1		mV
Equivalent exposure§ of peak-to-peak noise			0.35		nJ/cm^2
Saturation exposure§			350		nJ/cm^2
Saturation output amplitude		700	1000	1400	mV
Dynamic range relative to peak-to-peak noise		500 1	1000 1		
Charge transfer efficiency			0.99999		
White reference amplitude		500	700		mV
End-of-scan amplitude		300	500		mV
Output offset (dc) voltage			10		V
Output impedance			1		kΩ
Resistance to V_{SS}	Transfer gate		170		kΩ
	Transport gate		120		
	Reset gate		260		
Capacitance to V_{SS}	Transfer gate		260		pF
	Transport gate		590		
	Reset gate		16		
I_{REF}	Amplifier reference current		100		nA
I_{DD}	Supply current		6.3	9.4	mA
Power dissipation			100		mW

‡Measured at 700 mV output amplitude with an f/2.8 lens

§Exposure = intensity × time

TYPE TC103

- 2048 x 1 Sensor Element Organization
- Virtual-Phase N-Channel Silicon MOS Technology
- High Quantum Efficiency
- Enhanced Blue Response
- Output Signal Approximately 1.0 Volt Peak-to-Peak
- Dynamic Range Relative to Peak-to-Peak Noise Typically 1000:1
- End-of-Scan Signal
- Internal Black and White References
- Simple and Stable Operation
- OPTIONAL FEATURE:
  Internal Reference Voltage

TC103 . . . DUAL-IN-LINE PACKAGE
(TOP VIEW)

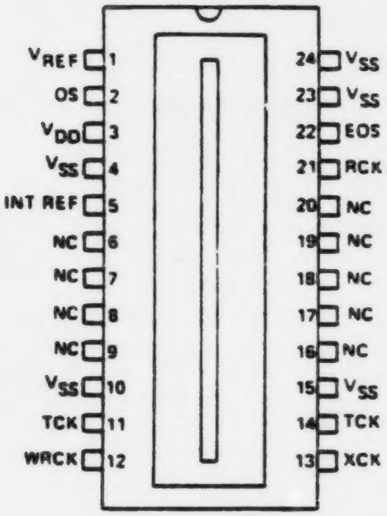
V_{REF} 1
OS 2
V_{DD} 3
V_{SS} 4
INT REF 5
NC 6
NC 7
NC 8
NC 9
V_{SS} 10
TCK 11
WRCK 12
24 V_{SS}
23 V_{SS}
22 EOS
21 RCK
20 NC
19 NC
18 NC
17 NC
16 NC
15 V_{SS}
14 TCK
13 XCK

NC – No internal connection

recommended operating conditions at T_A = 25°C (see Note 1)

		MIN	NOM	MAX	UNIT
V_{DD}	Amplifier supply voltage	13	14	15	V
$V_{IH(X)}$	Transfer clock high-level input voltage	3	4	5	V
$V_{IL(X)}$	Transfer clock low-level input voltage	−15†	−14	−13	V
$V_{IH(T)}$	Transport clock high-level input voltage	3	4	5	V
$V_{IL(T)}$	Transport clock low-level input voltage	−15†	−14	−13	V
$V_{IH(R)}$	Reset clock high-level input voltage	3	4	5	V
$V_{IL(R)}$	Reset clock low-level input voltage	−15†	−14	−13	V
$V_{IH(WR)}$	White reference clock high-level input voltage	13	14	15	V
$V_{IL(WR)}$	White reference clock low-level input voltage	6	7	8	V
f_{RCK}	Reset clock frequency (output data rate)			10	MHz

† The algebraic convention, where the most negative limit is designated as minimum, is used in this data sheet for clock voltage levels only.

NOTE 1: Voltage values are with respect to V_{SS}.

electrical characteristics at 25°C free-air temperature¶

PARAMETER		MIN	TYP	MAX	UNIT
Dark-signal amplitude	Average		0.5	10	mV
	Low frequency component		0.5	5	mV
	Nonuniformity relative to average of adjacent pixels		1.0	20	
Sensitivity		2	3.5	5	V/(μJ/cm²)
Output amplitude variation (PRNU)‡	Peak-to-peak		50	100	mV
	Adjacent pixels from alternate registers (imbalance)		10		
Peak-to-peak noise			1		mV
Equivalent exposure§ of peak-to-peak noise			0.35		nJ/cm²
Saturation exposure§			350		nJ/cm²
Saturation output amplitude		700	1000	1400	mV
Dynamic range relative to peak-to-peak noise		500:1	1000:1		
Charge transfer efficiency			0.99999		
White reference amplitude		500	700		mV
End-of-scan amplitude		300	500		mV
Output offset (dc) voltage			10		V
Output impedance			1		kΩ
Resistance to V_{SS}	Transfer gate		150		kΩ
	Transport gate		500		
	Reset gate		500		
Amplifier reference voltage, V_{REF}			7		V
Capacitance to V_{SS}	Transfer gate		250		pF
	Transport gate		600		
	Reset gate		16		
Amplifier supply current			8	12	mA
Total power dissipation			110		mW

‡ Measured at 700 mV output amplitude with an f/2.8 lens.

§ Exposure = intensity × time

¶ Test conditions are f_{RCK} = 0.5 MHz, t_{exp} = 10 ms, tungsten light source operating at color temperature of 2854 K with 2.0-mm-thick Fish-Schurman HA-11 IR-absorbing filter, and all operating voltages at nominal recommended values. The internal reference voltage is used.

TYPE TC104

- 3456 x 1 Sensor Element Organization
- Virtual-Phase N-Channel Silicon MOS Technology
- High Quantum Efficiency
- Enhanced Blue Response
- Output Signal Approximately 0.6 Volt Peak-to-Peak
- Dynamic Range Relative to Peak-to-Peak Noise Typically 1000:1
- End-of-Scan Signal
- Internal Black and White References
- Simple and Stable Operation
- OPTIONAL FEATURE: Internal Reference Voltage

TC104 . . . DUAL-IN-LINE PACKAGE

(TOP VIEW)

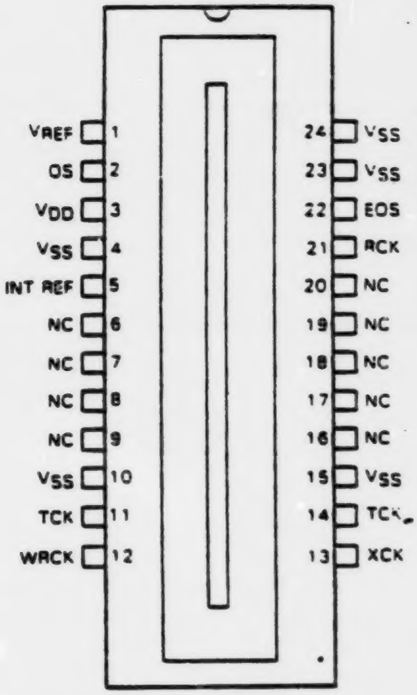

VREF 1
OS 2
VDD 3
VSS 4
INT REF 5
NC 6
NC 7
NC 8
NC 9
VSS 10
TCK 11
WRCK 12
24 VSS
23 VSS
22 EOS
21 RCK
20 NC
19 NC
18 NC
17 NC
16 NC
15 VSS
14 TCK
13 XCK

NC — No internal connection

C-21

TYPE TC104
3456 x 1 CCD LINEAR IMAGE SENSOR

recommended operating conditions at $T_A = 25\,°C$ (see Note 1)

		MIN	NOM	MAX	UNIT
V_{DD}	Amplifier supply voltage	13	14	15	V
$V_{IH(X)}$	Transfer clock high-level input voltage	3	4	5	V
$V_{IL(X)}$	Transfer clock low-level input voltage	−15†	−14	−13	V
$V_{IH(T)}$	Transport clock high-level input voltage	3	4	5	V
$V_{IL(T)}$	Transport clock low-level input voltage	−15†	−14	−13	V
$V_{IH(R)}$	Reset clock high-level input voltage	3	4	5	V
$V_{IL(R)}$	Reset clock low-level input voltage	−15†	−14	−13	V
$V_{IH(WR)}$	White reference clock high-level input voltage	13	14	15	V
$V_{IL(WR)}$	White reference clock low-level input voltage	6	7	8	V
f_{RCK}	Reset clock frequency (output data rate)			8	MHz

† The algebraic convention, where the most negative limit is designated as minimum, is used in this data sheet for clock voltage levels only.

NOTE 1: Voltage values are with respect to V_{SS}

electrical characteristics at 25 °C free-air temperature ¶

PARAMETER		MIN	TYP	MAX	UNIT
Dark-signal amplitude	Average		0.5	10	mV
	Low frequency component		0.5	5	mV
	Nonuniformity relative to average of adjacent pixels		4	20	
Sensitivity		1.4	2	3.5	V/(μJ cm^2)
Output amplitude variation (PRNU)‡	Peak-to-peak		30	60	mV
	Adjacent pixels from alternate registers (imbalance)		10		
Peak-to-peak noise			0.6		mV
Equivalent exposure§ of peak-to-peak noise			0.3		nJ/cm^2
Saturation exposure§			300		nJ/cm^2
Saturation output amplitude		400	600	800	mV
Dynamic range relative to peak-to-peak noise		500:1	1000:1		
Charge transfer efficiency			0.99999		
White reference amplitude		400	600		mV
End-of-scan amplitude		200	350		mV
Output offset (dc) voltage			6		V
Output impedance			1		kΩ
Resistance to V_{SS}	Transfer gate		150		kΩ
	Transport gate		700		
	Reset gate		700		
Amplifier reference voltage, V_{REF}			7		V
Capacitance to V_{SS}	Transfer gate		400		pF
	Transport gate		900		
	Reset gate		16		
Amplifier supply current			8	12	mA
Total power dissipation			112		mW

‡ Measured at 400 mV output amplitude with an f 2.8 lens.

§ Exposure = intensity × time

¶ Test conditions are $f_{RCK} = 0.5$ MHz, $t_{exp} = 10$ ms, tungsten light source operating at color temperature of 2854 K with 2.0-mm thick Fish Schurman HA-11 IR-absorbing filter, and all operating voltages at nominal recommended values using the internal reference voltage

APPENDIX D

OTHER AVAILABLE PRODUCTS

1. Threshold Detection of Visible and Infrared Radiation with PIN Photodiodes
2. Xarray Linear Position Sensitive X-ray Detector

D-1

HEWLETT PACKARD

APPLICATION NOTE 915

Threshold Detection of Visible and Infrared Radiation with PIN Photodiodes

Traditionally, the detection and demodulation of extremely low level optical signals has been performed with multiplier phototubes. Because of this tradition, solid-state photodetectors are often overlooked even though they have a number of clear functional advantages and in some applications provide superior performance as well. Some of these advantages are summarized below and become even more apparent in the following discussion.

ADVANTAGES OF PIN PHOTODIODES VERSUS MULTIPLIER PHOTOTUBES

1. Size and weight:
   PIN photodiodes are approximately three orders of magnitude smaller and lighter. This greatly simplifies and reduces the cost of mounting.
2. Power Supply:
   Multiplier phototubes require more than 1000 volts, which must be precisely regulated and divided among the dynodes. By comparison, PIN photodiodes and associated amplifiers operate stably on less than 20 volts, which does not require precise regulation.
3. Cost:
   The cost, including that of the necessary amplifier, is lower for the PIN photodiode because of lower power supply requirements.
4. Spectral Response:
   Broad skirts of the PIN photodiode make it useful from the ultra-violet, through the visible, and well into the infrared region. This exceeds the range of any other device of comparable sensitivity.
5. Sensitivity:
   Noise equivalent power of the PIN photodiode is lower than that of any other type of photodetector. The signal levels are extremely low, however, and to achieve low level performance they require a high gain, high input resistance amplifier. Multiplier phototubes have built-in gain and do not require additional low-noise amplification. Moreover, the high input resistance needed for sensitive performance precludes fast response, whereas the response time of multiplier phototubes may be in the nanosecond region even in the sensitive mode.
6. Stability:
   The characteristics of noise, responsivity, and spectral response of the PIN photodiode are not dependent on time, temperature, or other environmental considerations. The same conditions may be hazardous to multiplier phototubes.
7. Overloading:
   In the presence of excessive signal, multiplier phototubes of comparable sensitivity are capable of destroying themselves as a result of excessive output current. The PIN photodiode is unaffected by exposure to room light or even direct sunlight.
8. Ruggedness:
   PIN photodiodes can tolerate exposure to extreme levels of shock and vibration. Typical shock capability is 1500 G's for 0.5 millisecond.
9. Magnetic Fields:
   Multiplier phototube gain is affected by fields as small as one gauss. If the interfering field is fluctuating, the output will be modulated by it. The PIN photodiode is insensitive to magnetic fields.
10. Precision:
    The responsivity of the PIN photodiode is inherently precise and repeatable. Within a given type, the characteristics agree (from unit to unit) within plus or minus 0.1 decade. Responsivity of multiplier phototubes may vary over more than a decade from one unit to another.
11. Sensitive Area:
    The small sensitive area of the PIN photodiode makes it unnecessary to establish an aperture which may be required for some applications. However, in some applications good optical alignment is imposed by the small area.

PIN PHOTODIODE DETECTORS

At the present time a variety of different types of solid-state photodetectors are available. Of these, the Silicon PIN Photodiode has the broadest applicability and is the subject of this note. The PIN photodiode's main advantages are: broad spectral response, a wide dynamic range, high speed, and extremely low noise. With appropriate terminal circuits it is well suited for many applications that require converting an optical signal to an electrical signal. The

A-2

present discussion, however, will be limited to the description of the PIN photodiode's threshold detection sensitivity and the design of suitable terminal circuits that will realize this capability.

PHOTODIODE DESCRIPTION

Construction

A brief description of the PIN photodiode will be helpful in understanding its performance and the principles for designing appropriate circuits to be used with it. Figure 1 shows a typical construction of the PIN photodiode. This figure is for the purpose of explanation only and is not to scale. The relative proportions have been deliberately distorted for the sake of clarity.

The PIN structure is produced by diffusion through an oxide (S_iO_2) mask which also serves to protect the surface. Since most metals are very opaque to optical radiation, especially at infrared wavelengths, the gold contact is deposited only around the perimeter of the P-layer, and the gold contact pattern provides for lead attachment a short distance away from the junction region, so the lead is not in the light path.

Mode of Operation

When a photon is absorbed by the silicon it produces a hole and an electron. If the absorption of the photon occurs in the I-layer, as shown in Figure 1, the hole and the electron are separated by the electric field in the I-layer. For the highest quantum conversion efficiency (electrons per photon) it is desirable to have the P-layer as thin as possible and the I-layer as thick as possible. The thickness of the P-layer also determines the value of the parasitic series resistance (R_s in Figure 2). The thinner the P-layer the higher the R_s. Since R_s affects high frequency performance there is therefore a design trade-off between quantum efficiency and bandwidth. Once the trade-off is settled, the desired thickness is then controlled during the diffusion process. The effective thickness of the I-layer is controlled partly by the manufacturing diffusion process and partly by the magnitude of the electric field applied to the diode—the higher the field, the thicker will be the effective I-layer. It is therefore desirable to operate the diode with an external reverse bias, as shown in Figure 2. As the reverse bias voltage is increased from zero, there are three beneficial effects: hole and electron transit time decreases; conversion efficiency increases slightly; and most importantly, the capacitance decreases sharply with bias up to about ten volts and continues to decrease slightly up to about twenty volts reverse bias.

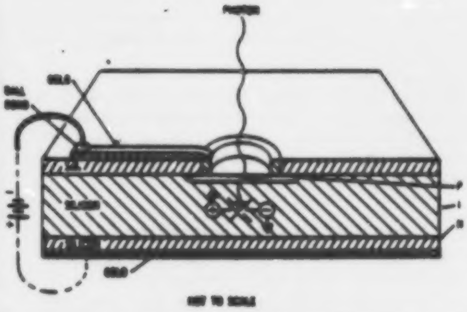

Figure 1. PIN Photodiode Cutaway View

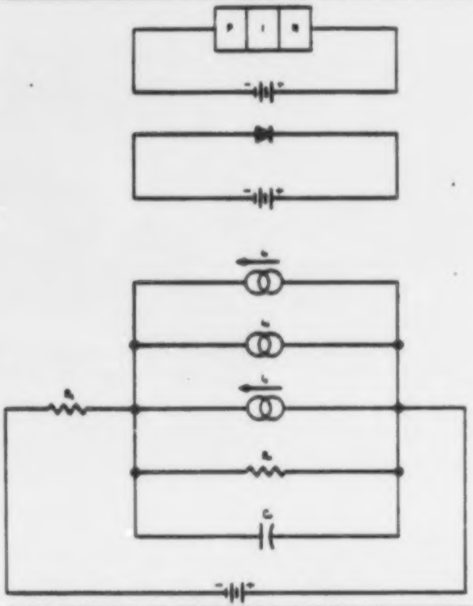

Figure 2. PIN Photodiode Schematic Symbol, and Equivalent Circuit

In the presence of optical signals there is a slight modulation of the shunt conductance as the presence of photon-produced holes and electrons in the I-layer modulate its conductivity. This effect can be quite significant at very high levels of illumination since the I-layer may become saturated, resulting in a decrease in quantum efficiency and an increase in rise time. Saturation can be prevented by applying a very high reverse bias voltage (up to 200 volts). However, such a high voltage, applied over a long period of time, may cause a degradation of the diode's leakage properties. Since our present concern is with threshold performance, reverse bias voltages greater than twenty volts need not be considered.

Equivalent Circuit

When properly biased, the PIN photodiode can be accurately represented by the equivalent circuit shown in Figure 2. Here i_s is the external current resulting when the diode is illuminated. It has a time constant of 10 picoseconds and a value of approximately 0.5 amp per watt of input at a wavelength of 8000 angstroms (800 nanometers). This corresponds to a quantum efficiency of 75%, that is, 0.75 electrons per photon. The quantum efficiency is constant from 500 nanometers to 800 nanometers (5,000 Å to 8,000 Å).

i_N is the noise current of the PIN photodiode. Since the diode is reverse biased, the shot noise formula is applicable, so that the noise current can be computed from:

$$\frac{i_N^2}{B} = 2qI_{dc} \qquad (1)$$

where B = system output bandwidth, Hz
q = electron charge, 1.6×10^{-19} coulombs
I_{dc} = dc current, Amp.

D-3

In the case of the photodiode, I_c is simply the dark current, I_R, which has a value determined by the construction and dimensions of the particular diode type. Maximum values are: 100 picoamps for 5082-4204, 150 picoamps for 5082-4205 and 2 nanoamps for 5082-4203.

Shunt resistance, R_p, is very large, being usually greater than 10 gigaohms (10,000 megohms), and its noise current may therefore be neglected. Shunt capacitance, C_p, has a value from two to five picofarads, depending upon the diode type and reverse bias. For high frequency operation it is important to minimize C_p because the cutoff frequency is determined by:

$$f_c = \frac{1}{2\pi R_s C_p} \qquad (2)$$

Although our present concern is with low frequency threshold operation, there is another reason for minimizing C_p. This will be discussed later, when circuit design principles are presented.

Performance

Threshold performance can and has been specified in a number of different ways. The most commonly understood and usable expression takes the form of a noise equivalent input signal. This is the input signal which produces an output signal level that is equal in value to the noise level that is present when no input signal is applied. The noise equivalent input in watts is called Noise Equivalent Power (NEP) and is defined by:

$$\text{NEP} = \frac{\text{NOISE CURRENT (amps per root hertz)}}{\text{CURRENT RESPONSIVITY (amps per watt)}} \qquad (3)$$

which has the units of watts per root hertz. Devices for photo-detection could then be compared on the basis of NEP. The lower the NEP the more sensitive is the device.

Another method of defining threshold sensitivity is on the basis of signal-to-noise ratio for given input signal power levels. Taking a power level of one picowatt, for example, the signal-to-noise ratio at the output can be obtained from:

$$\text{SNR} = \frac{\text{RESPONSIVITY} \left(\frac{\text{amps}}{\text{watts}}\right) \times \text{INPUT (watts)}}{\text{NOISE CURRENT (amps)}} \qquad (4)$$

This is a ratio of currents. To express it in dB we would take twenty times its log to base ten, even though the expression converts linearly to a power ratio. This is because the devices respond *linearly* to input *power*.

Figure 3 shows spectral sensitivity characteristics of several PIN photodiodes and multiplier phototubes. Sensitivity is given in terms of SNR and NEP. The latter is in terms of dBm. Several interesting features are evident in Figure 3. Although the quantum efficiency for PIN photodiodes is constant from 500 to 800 nanometers, the sensitivity curve is not. This is due to the fact that the energy per quantum (photon) of radiant energy varies with wavelength.

The curves for the three different PIN photodiodes also show the dependence of sensitivity on leakage current. Here the highest sensitivity is obtained with the 5082-4204 which has a maximum leakage current of 100 picoamps. Next is the 5082-4205 with 150 picoamps and finally the 5082-4203 with maximum leakage of 2 nanoamps. The three curves are in effect displaced by the magnitude of the noise current difference because quantum efficiency is equal for all. These curves also show the inherent broad response of PIN photodiodes with respect to multiplier phototubes. Therefore, the power responsivity of the PIN photodiode has a corresponding slope. Notice how the inherently broad response of silicon, enhanced by the thick I-layer construction, extends the range of useful performance over the response ranges of two types of photocathodes.

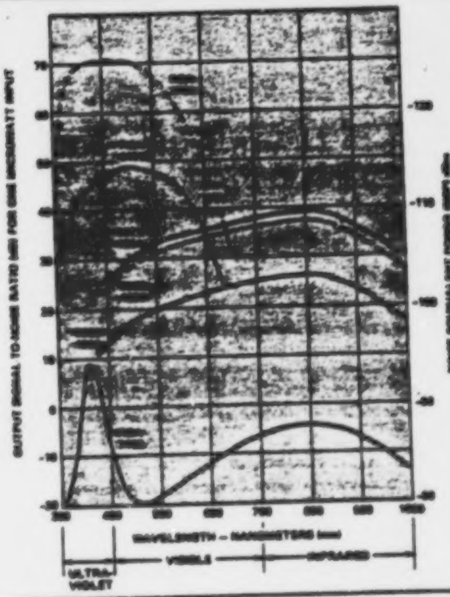

Figure 3. Spectral Sensitivity Comparisons of Photodetectors

Although the threshold sensitivity of multiplier phototubes is superior in the visible region, nevertheless for many applications the advantage is not significant enough to outweigh the disadvantages of generally unstable and temperature-sensitive gain, large size and weight, and the need of very high and stable power supply voltages. On the other hand, the superior red and infrared threshold performance of the PIN photodiode does not necessarily mean it is better in any application, because one must take into account its small sensitive area and low signal levels. Realization of the performance capability described in Figure 3 also requires fairly careful attention to the design of the terminal circuits into which the PIN photodiode operates.

TERMINAL CIRCUIT DESIGN PRINCIPLES

The design of the terminal amplifier must consider the usual design objectives of low noise, broad band, wide dynamic range, etc. In addition, there are two fundamental considerations which are dictated by the PIN photodiode:

1. High Reverse Voltage:
   The diode must be operated at ten to twenty volts of reverse bias to reduce shunt capacitance.
2. High Input Resistance:
   This is a fundamental consideration in the sensitivity/rise time trade-off.

The effects of reverse voltage on capacitance have been discussed earlier. However, the effect is sufficiently important to deserve a re-emphasis here.

A high input resistance is necessary in order to maintain a high signal-to-noise ratio. Since the output signal from the photodiode is a current, and its own internal noise is repre-

D-4

sented by a current, it is appropriate to represent the noise of the terminal amplifier as an equivalent noise current at the input. The smallest value of resistor which may be connected to the input is then limited by its noise current according to the formula for thermal noise:

$$\frac{i_N^2\,(\text{thermal})}{B} = \frac{4kT}{R} \qquad (5)$$

By comparing eq(1), relating diode noise current to leakage current, with eq(5), relating resistor noise current to its resistance value, it is clear that there is some value of resistance below which the NEP of the system, i.e., threshold sensitivity, would be degraded at the rate of 5 dB per decade of decreasing resistance. For example, in the case of the 5082-4203, assuming a maximum leakage current of 2 nanoamps, the value of resistance should be greater than 25 megohms, to avoid degrading the threshold sensitivity.

TRANSISTOR AMPLIFIER

In addition to keeping the input noise current low by using large values of input resistance, it is also important to keep other sources of noise in the amplifier at a minimum. Using ordinary transistors (PNP or NPN) it is not possible to approach the ultimate sensitivity of which the PIN photodiode alone is capable, even when low-noise transistors, such as the 2N2484, are used. However, in those applications where it is possible to sacrifice sensitivity for simplicity, transistors may be used. A typical transistor circuit is shown in Figure 4. With this circuit, a sensitivity corresponding to an NEP of − 95 dBm was obtained. In this case, Q1 was operated at the lowest possible collector current which would still give adequate gain. A high loop gain was desired in order to compensate, with negative feedback, for the long open-loop rise time produced by the high input resistance. A resistance higher than 10 megohms was not necessary here, since the transistor itself sets the fundamental noise limitation. A PNP transistor was selected for Q2 in order to balance out most of the base-to-emitter voltage of Q1, so that the output would tend to be near zero without any zero adjustment. A slight zero adjustment, provided by R2 and R3, gives the necessary range without appreciably attenuating the feedback current. As the photocurrent, I_p, increases, the amplifier causes the voltage at the emitter of Q3 to decrease, which causes a current in R1 to flow out of the node (base of Q1) into which I_p flows.

Basic Amplifier Arrangements

For linear operation, the photodiode should be operated with as small a load resistance as possible. Figure 5 shows the recommended amplifier arrangement. The negative-going input is at virtual ground; the dynamic resistance seen there by the photodiode is R_1 divided by loop gain. If the op-amp has extremely high input resistance, loop gain is very nearly the forward gain of the op-amp. R_2 can be omitted if the photocurrent is reasonably high — its purpose is only to balance off the effect of offset current. As shown, the output voltage will rise in response to the optical signal. If it is preferable to have the output drop in response to optical input, then *both* the photodiode *and* E_C should be reversed. E_C may, of course, be zero. Speed of response is usually limited by the time constant of R_1 with its own capacitance, so it is improved by using a string of two or more resistors in place of a single R_1.

Logarithmic operation requires the highest possible load resistance — at least 10GΩ. With an FET-input op-amp, this is

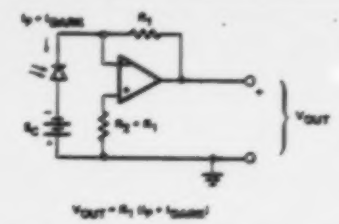

Figure 5. Linear Response; Photodiode and Amplifier Circuit Arrangement

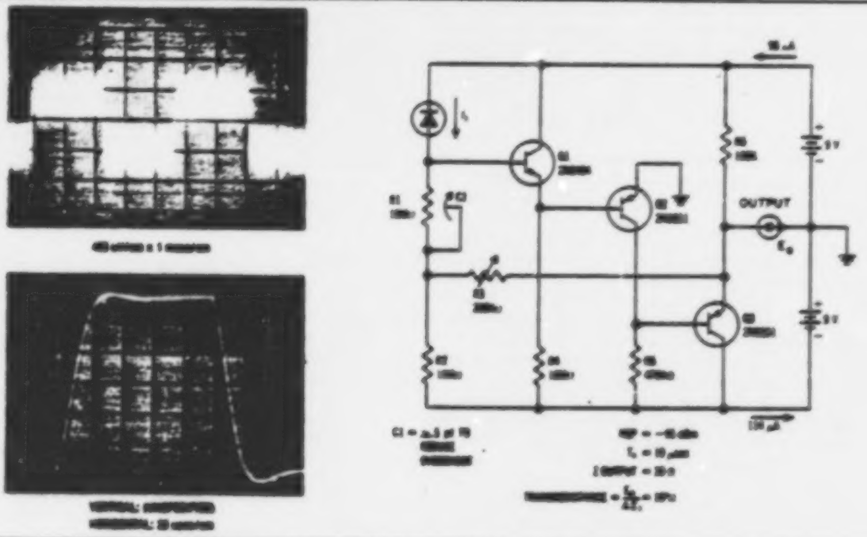

Figure 4. Transistor Photodiode Amplifier Schematic

D-5

easily achieved as in Figure 6. If the offset current of the amplifier poses a problem, a resistor can be added between the positive- and negative-going inputs. Its value should not be less than 10GΩ divided by loop gain. If the amplifier has a very high input resistance, loop gain is equal to the forward gain of the amplifier divided by (1 + R /R1) so making $R_2 = 0$ allows the smallest possible resistance between the inputs. The speed of response of this amplifier will be very low, with a time constant $\tau \approx 0.1$s. If high speed logarithmic operation is required, it is best to use the linear amplifier of Figure 5 followed by a logarithmic converter.

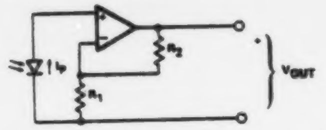

$$V_{OUT} = (1 + \frac{R_2}{R_1}) \frac{kT}{q} \log_e (1 + \frac{I_p}{I_S})$$

$$\frac{kT}{q} = 25\text{ mV}$$

$$I_S = \frac{I_p}{e^{\frac{qV}{kT}} - 1} \quad \text{AT} \quad 0 < I_p < 0.1\text{ mA}$$

Figure 6. Logarithmic Response; Photodiode and Amplifier Circuit Arrangement

High Speed Photodiode Amplifier

Applications that call for high speed data signaling, such as CRT light pens, require amplifiers that have a wider bandwidth than the circuit shown in Figure 5.

Using a five transistor array (RCA CA3127E) it is possible to construct a high speed, high gain photodiode amplifier. This circuit is shown in Figure 8. It is configured as a two stage amplifier. The first stage is composed of transistors Q1-Q3, where Q1 is an input emitter follower with feedback obtained from the emitter of Q3. Q2 functions as an inverting amplifier interconnecting Q1 to Q3. The second stage consists of Q4 and Q5 which provide additional gain and output buffering, of the first stage. These two stages provide an equivalent transresistance of 420K ohms. This means that the output voltage Vo is equal to the photocurrent, Ip, times 420K ohms.

When high speed circuit layout techniques are used it is possible to obtain the rise and fall time performance shown in Figure 7. This speed is equivalent to a bandwidth of 9.5MHz with an input flux of 1.9μW. This flux level can be obtained from a HEMT-6000 700nm High Intensity Subminiature Emitter when it is operated at 10mA, at a distance of 1cm from the 5082-4207 PIN photodiode.

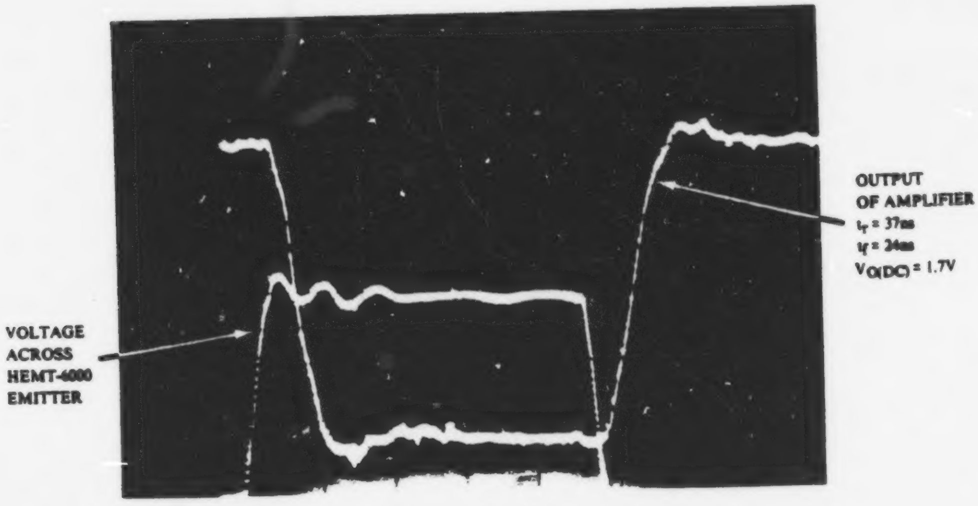

200mV/cm x 50ns/cm

Figure 7. Pulse Response of Photodiode Amplifier

D-6

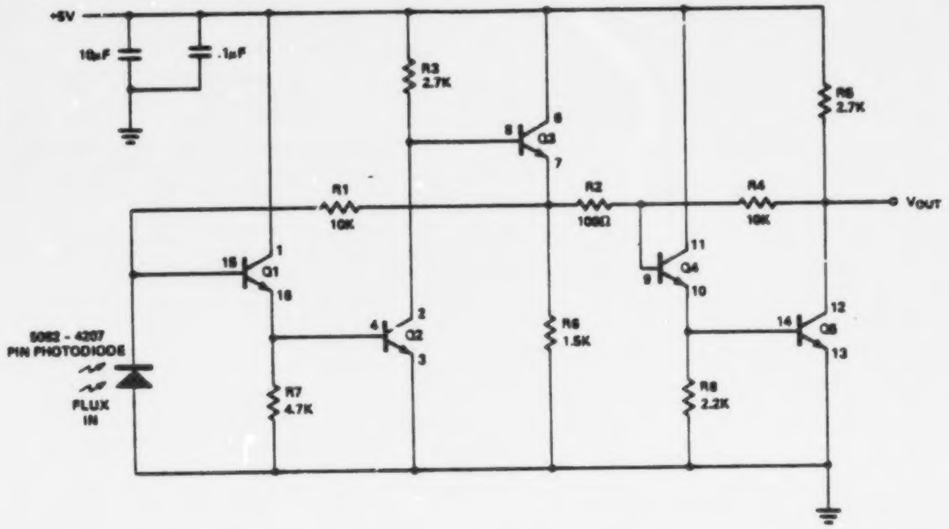
+5V
10µF
.1µF
R3
2.7K
R5
2.7K
8
Q3
6
7
R1
10K
R2
100Ω
R4
10K
VOUT
15
Q1
1
16
4
Q2
2
3
R6
1.5K
9
Q4
11
10
14
Q5
12
13
5082 - 4207
PIN PHOTODIODE
FLUX
IN
R7
4.7K
R8
2.2K

NOTES: TRANSISTORS ARE SINGLE PACKAGE, CA3127E. PINS LABELED FOR EACH. PIN 5 IS SUBSTRATE.

Figure 8. High Speed, High Gain Photodiode Amplifier

D 1

SDT

SCIENTIFIC DEVELOPMENT TECHNOLOGIES, INC.

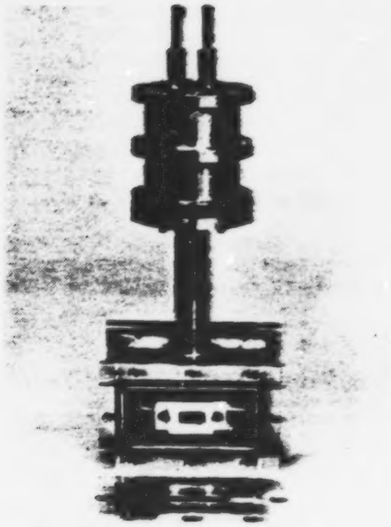

XARRAY LINEAR POSTION SENSITIVE X-RAY DETECTOR

The XARRAY linear position sensitive X-ray detector utilizes a Reticon S-series self-scanning photodiode array as the primary sensor controlled by digital electronics generating the required clocking waveforms appropriate for diffraction and scattering applications. The XARRAY detector is an integrating detector system. Incident photons are absorbed by each sensor element (pixel) and produce primary electrons which subsequently generate electron-hole pairs collected at diode junctions. The total integrated charge is then depleted when the appropriate scanning signals are applied and the analog signal is converted to a digital value and temporarily stored in a buffer memory. The digital intensity information can then be retrieved by an external data acquisition system in a sequential manner. The XARRAY system is designed to be compatible with any 8 or 16 bit computer system that might be used for data acquisition without the need for additional peripheral electronics.

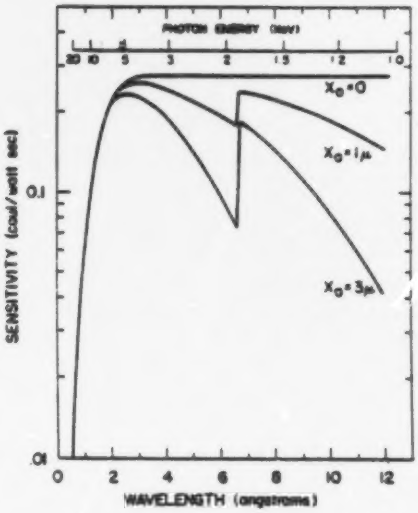

Plot of the sensitivity of the photodiode array versus the wavelength (energy) of the incident photon over the useful region of the X-ray spectrum with either a 0.1, or 3 micron thick protective oxide layer over the active surface of the device.

D8

As the timing signals controlling the XARRAY integration interval are under external control, the detector can be used to collect weak diffuse scattering over periods of many hours or to collect intensive Bragg reflections on a millisecond time scale. Of course, the integration interval is strongly dependent upon the temperature of the array. At room temperature the dark current of each photodiode saturates its output within 2-3 seconds. Cooling decreases this dark current roughly a factor of two for every 7 degrees C and is required to increase the dynamic range of the device.

Hence the XARRAY unit includes a liquid nitrogen (LN) cooling mechanism which can extend the useful integration interval by a factor of more than ten million. This mechanism consists of a direct flow cold finger mounted in a vacuum housing. The photodiode array is mounted on a block at the end of the finger within 1 cm of the entrance aperture of the housing. The housing is constructed with re-entrant liquid nitrogen tubing connections oriented vertically at the top of the housing . With adequate thermal insulation the system can be maintained near liquid nitrogen temperature with less than 2 liters per hour consumption of LN.

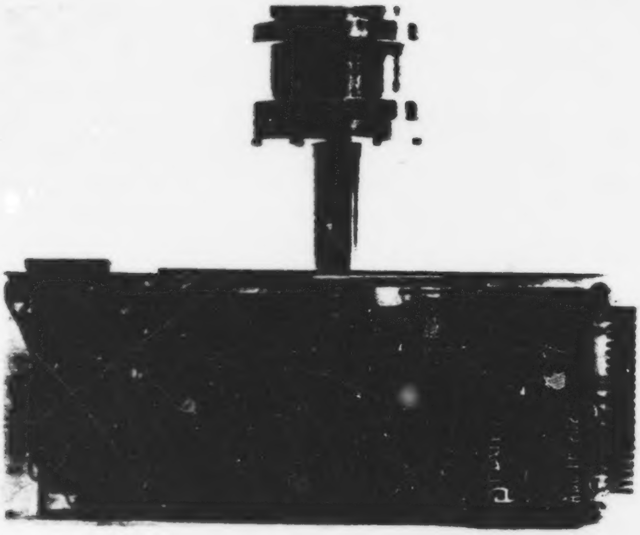

IR-100
1982 COMPETITION WINNER

Cited by Industrial Research & Development magazine for developing one of the 100 most significant technical products of the year

A Complete Detector System At An Affordable Price

Consider these unique characteristics

- low voltage operation
- low total system cost
- large pixel aspect ratio
- stable operation
- 25 micron linear resolution
- better than 10^6 photons/cm^2/sec count rate capability

SDT SCIENTIFIC DEVELOPMENT TECHNOLOGIES, INC. • 801 E. Ogden Ave., Suite 1083 Naperville, IL 60566 • [312] 369

TECHNICAL SPECIFICATIONS

Active Area: 2.5 mm X 25.6 mm

Pixel Aspect Ratio: 100:1

Spatial Resolution: 25 μm

Geometric Linearity: 25 μm

Linearity of Response: <3% full scale

Saturation Charge: $7X10^7$ 8kev photons/pixel

Readout rms moise: 25 photons/pixel

10 sec counting time → 400 photons/pixel signal

Dynamic Range: 3000:1

ADC resolution: 12 or 16 bits bipolar

ADC linearity: 0.02% or 0.001%

ADC conversion time: 2 μsec.

Integration Interval: variable from 2 sec (4 sec) for 512 (1024) element array.

Digiatal Interface: 8 or 16 bit parallel TTL

Voltage Requirements: +5V, +15V, & -15V

10^8 photons per sec

SDT XARRAY DETECTOR SYSTEM

PRICE LIST

March, 1983

DESCRIPTION	COST
Photodiode array with min oxide layer RETICON RL512S (RETICON RL1024S	 $2200 $4400)
XARRAY Interface electronics	$2500
Power supply	$ 500
Detector Vacuum Housing	$1500
Z80 based microcomputer, 64K RAM, dual floppy disk drives, monitor, and complete data acquisition and application software	$2500
Total system cost	$9200 ($11400)

Request quote for custom interface to your existing computer system. Components sold separately or as complete system.

Prices subject to change without notice. Prices fob, Naperville, IL.

Why is readout noise so high?

APPENDIX E

SILONEX INC.

1. PIN Photodiode
2. Blue Sensitive Photodiodes
3. Silcon Planar Photodetectors

NSL-530 PIN PHOTODIODE

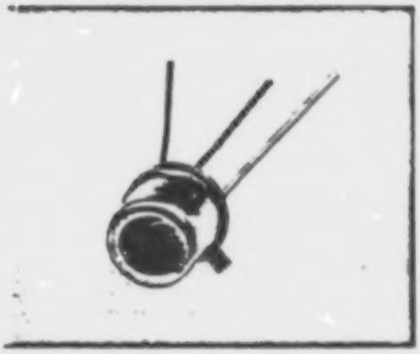

GENERAL DESCRIPTION

The NSL-530 series is a family of silicon PIN photodiodes with response time of the order of 5 nanoseconds, well suiting them for high speed switching applications like optical data transmission, laser and low light level detection, light demodulation, etc. This high speed photodiode is available in a number of TO-18 window variants; the NSL-530 with flat glass window, the NSL-531 with an open TO-18 can for optimal optical coupling, the low lensed NSL-532, and the high lensed NSL-533. Further details or information on customized pig-tail configurations are available from Silonex.

FEATURES

- **Low Operating Voltage, V_R = 45V**
- **Anti-Reflection Coated to Enhance Responsivity at 900 nm**
- **Spectral Response Range, 400 to 1100 nm (10% Points)**
- **Fast Response, 5 nS**
- **Optional Package Configurations**

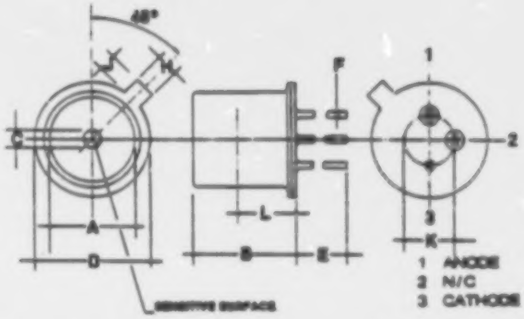

Ref	Inches		Millimeters	
	Min.	Max.	Min.	Max.
A	.178	.188	4.52	4.78
B	.196	.205	4.98	5.21
C	.039 dia.		1.0 dia.	
D	.202	.213	5.12	5.41
E	.5 Nominal		12.8 Nominal	
F	.016	.019	.41	.48
H	.035	.045	.89	1.16
J	.033	.048	.84	1.22
K	.096	.104	2.43	2.66
L	.105	.115	2.68	2.92

ABSOLUTE MAXIMUM RATINGS (25°C unless otherwise noted)
DC Reverse Operating Voltage, V_R
100V
Photocurrent, Ip
Average value, continuous operation 1.0 mA
Peak Value 10 mA
Forward Current, I_F
Average value, continous operation 10 mA
Peak Value 100 mA
Ambient Temperature
Storage - 60 to + 100° C
Operating - 40 to + 80° C

ELECTRICAL CHARACTERISTICS (at 25° C, unless otherwise noted)	At a DC Reverse bias of 45 Volts unless otherwise specified			Units
	Min.	Typ.	Max.	
Area		0.8		mm^2
Dark Current At V_R = 10 V AT V_R = 45 V		2×10^{-9} 1×10^{-8}	1×10^{-8} 5×10^{-8}	A A
Luminous Responsivity (2854° K)		8.5		mA/lm
Responsivity At 900 nm At 1060 nm	0.5 0.1	0.65 0.15		A/W A/W
Quantum Efficiency At 900 nm At 1060 nm	70 12	90 17		% %
Breakdown Voltage, V_{BR}	100			V
Capacitance At V_R = 10 V At V_R = 45 V		5 2.5	6 3	pF pF
Rise Time 10% to 90% R_L = 50 Ω, λ = 900 nm		3	5	ns
Fall Time 90% to 10% R_L = 50 Ω, λ = 900 nm		6	10	ns
Noise Current f = 1000 Hz, Δf = 1.0 Hz		6×10^{-14}	4.2×10^{-13}	A/$\sqrt{Hz}$
Noise Equivalent Power (NEP) f = 1000 Hz, Δf = 1.0 Hz At 900 nm At 1060 nm		1×10^{-13} 4×10^{-13}	8×10^{-13} 3.2×10^{-12}	W/$\sqrt{Hz}$ W/$\sqrt{Hz}$

NSL-580 PIN PHOTODIODE

GENERAL DESCRIPTION

The NSL-580 PIN silicon photodiode with response times of the order of 8 nanoseconds is well suited for OCR, laser and low light level detection, and light demodulation applications

PHOTOCELL BULLETIN No. 15028 A

FEATURES

- Fast Response, 8 nS
- Low Operating Voltage, V_R = 45V
- Low Noise and Capacitance
- Anti-Reflection Coated to Enhance Responsivity at 900 nm
- Spectral Response Range, 400 to 1100 nm (10% Points)

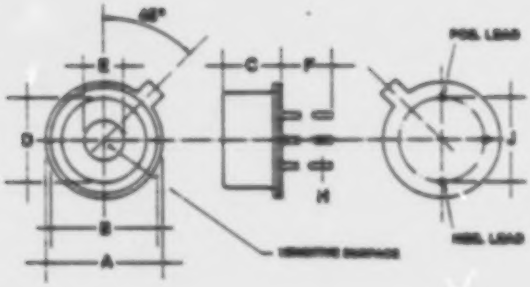

Ref	Inches Min.	Inches Max.	Millimeters Min.	Millimeters Max.
A	.362	.365	9.20	9.28
B	.320	.330	8.13	8.38
C	.180	.190	4.58	4.82
D	.236	.245	5.99	6.22
E	.099 dia.		2.52 dia.	
F	1.50	1.60	38.	40.6
H	.016	.019	.41	.48
J	.236	.245	5.99	6.22

ABSOLUTE MAXIMUM RATINGS (25°C unless otherwise noted)
DC Reverse Operating Voltage, V_R
100V
Photocurrent, I_P
Average value, continuous operation 1.0 mA
Peak Value 10 mA
Forward Current, I_F
Average value, continous operation 10 mA
Peak Value 100 mA
Ambient Temperature
Storage - 60 to + 100° C
Operating - 40 to + 80° C

ELECTRICAL CHARACTERISTICS (at 25° C, unless otherwise noted)	At a DC Reverse bias of 45 Volts unless otherwise specified			Units
	Min.	Typ.	Max.	
Area		5.0		mm²
Dark Current At V_R = 10 V AT V_R = 45 V		 5×10^{-9} 3×10^{8}	 2.5×10^{-8} 1.5×10^{-7}	 A A
Luminous Responsivity (2854° K)		8.5		mA/lm
Responsivity At 900 nm At 1060 nm	 0.5 0.1	 0.65 0.15		 A/W A/W
Quantum Efficiency At 900 nm At 1060 nm	 70 12	 90 17		 % %
Breakdown Voltage, V_{BR}	100			V
Capacitance At V_R = 10 V At V_R = 45 V		 12 8	 20 10	 pF pF
Rise Time 10% to 90% R_L = 50 Ω, λ = 900 nm		 5	 8	 ns
Fall Time 90% to 10% R_L = 50 Ω, λ = 900 nm		 8	 13	 ns
Noise Current f = 1000 Hz, Δf = 1.0 Hz		 1×10^{-13}	 7×10^{-13}	 $A/\sqrt{Hz}$
Noise Equivalent Power (NEP) f = 1000 Hz, Δf = 1.0 Hz At 900 nm At 1060 nm		 1.5×10^{-13} 6.5×10^{-13}	 1.2×10^{-12} 5.2×10^{-12}	 $W/\sqrt{Hz}$ $W/\sqrt{Hz}$

BLUE SENSITIVE PHOTODIODES

GENERAL DESCRIPTION

The NSL-780BG/880BG/883BG are TO-5 packaged, blue sensitive silicon photodiodes. With near-human eye response they are ideal for photographic and photometer applications such as illumination and exposure meters, colorimeters, etc. These photodiodes are well suited for operation with reverse bias, where the short circuit current output is linear over several decades of illumination.

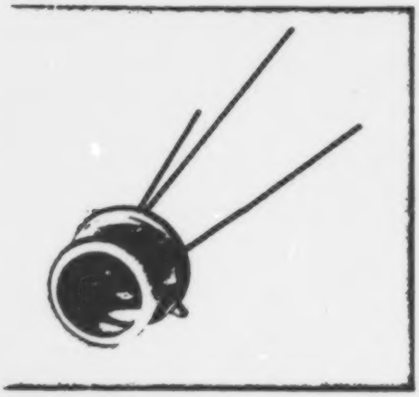

PHOTOCELL BULLETIN No. 15030 A REV. 1

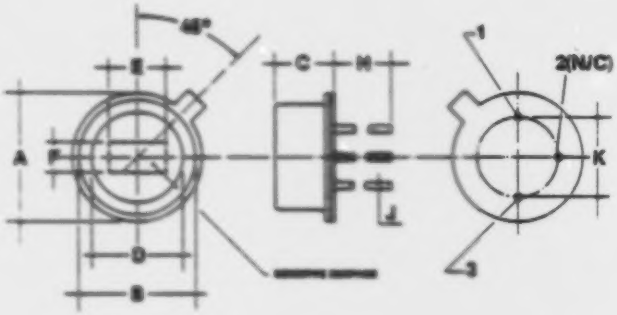

	Inches		Millimeters	
Ref	Min.	Max.	Min.	Max.
A	.325	.335	8.20	8.46
B	.320	.330	8.13	8.38
C	.270	.280	6.87	7.10
D	.245	.255	6.25	6.46
E	.145	.155	3.69	3.92
F	.085	.095	2.15	2.41
H	1.50	1.60	38.	40.6
J	.016	.019	.41	.48
K	.235	.245	5.96	6.22
E*	.120	.130	3.04	3.30

*DIMENSION OF NSL-883BG SQUARE CHIP

TYPICAL ELECTRO-OPTICAL CHARACTERISTICS (25°C Free Air unless otherwise noted)				
TYPE		NSL-780BG	NSL-880BG	NSL-883BG
Sensitivity (A/W)	@ 500 nm	.170	.170	.200
	@ 1000 nm	.005	.005	.005
Peak Sensitivity Wavelength (nm)		530	530	530
Short Circuit Current (µA) @ 500 Ftc. Tungsten 2870°K		35	35	40
Open Circuit Voltage (V) @ 500 Ftc. Tungsten 2870°K		.350	.300	.330
Dark Current (µA) @ V_R = 1V	@ 25°C	5.0	2.5	.010
	@ 55°C	10.0	5.0	.080
Maximum Reverse Bias (V)		5	10	20
Capacitance (pF) (zero bias, dark)		3000	375	400
Active Area (cm²)		.095	.095	.101
Pin Connection		Cathode-1 Anode-3	Cathode-1 Anode-3	Cathode-3 Anode-1

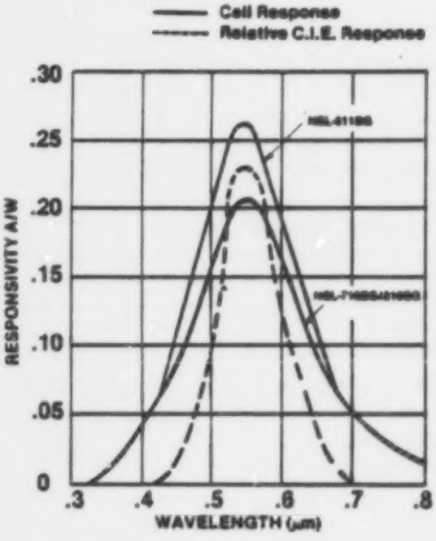

SPECTRAL RESPONSE

SILONEX INC

TWX 610-421-3382
2150 WARD STREET, MONTREAL, QUE. H4M 1T7 TEL. (514) 744-5507
331 CORNELIA ST., PLATTSBURGH, N.Y. 12901 TEL. (518) 561-3160
ALTRINCHAM, CHESHIRE, WA14 4NX. TELEX 51 669 663 TEL. (061) 928-3417

NSL-710BG/810BG/811BG

HOTOCELL BULLETIN No. 15030 REV. 1

BLUE SENSITIVE PHOTODIODES

GENERAL DESCRIPTION

The NSL-710BG/810BG/811BG are TO-18 packaged, blue sensitive silicon photodiodes. With near-human eye response they are ideal for photographic and photometer applications such as illumination and exposure meters, colorimeters, etc. These photodiodes are well suited for operation with reverse bias, where the short circuit current output is linear over several decades of illumination.

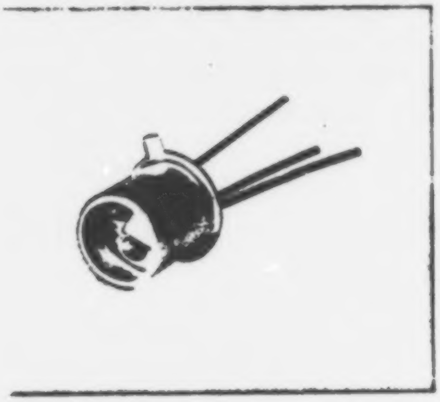

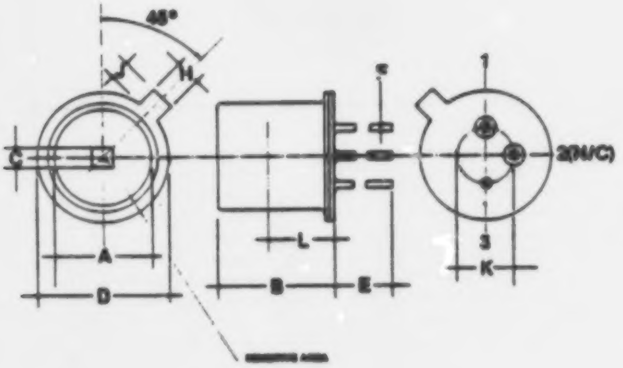

Ref	Inches Min.	Inches Max.	Millimeters Min.	Millimeters Max.
A	.178	.188	4.52	4.78
B	.196	.205	4.98	5.21
C	.070	.080	1.78	2.03
D	.202	.213	5.12	5.41
E	.5 Nominal		12.8 Nominal	
F	.016	.019	.41	.48
H	.035	.045	.89	1.15
J	.033	.048	.84	1.22
K	.096	.104	2.43	2.66
L	.105	.115	2.68	2.92

TYPICAL ELECTRO-OPTICAL CHARACTERISTICS
(25°C Free Air unless otherwise noted)

TYPE		NSL-710BG	NSL-810BG	NSL-811BG
Sensitivity (A/W)	@ 500 nm	.170	.170	.200
	@ 1000 nm	.005	.005	.005
Peak Sensitivity Wavelength (nm)		530	530	530
Short Circuit Current (μA) @ 500 Ftc. Tungsten 2870°K		18	18	18
Open Circuit Voltage (V) @ 500 Ftc. Tungsten 2870°K		.350	.300	.330
Dark Current (μA) @ $V_R = 1V$	@ 25°C	1.0	0.5	.005
	@ 55°C	2.0	1.0	.040
Maximum Reverse Bias (V)		5	10	40
Capacitance (pF) (zero bias, dark)		1000	135	100
Active Area (cm²)		.036	.036	.031
Pin Connection		Cathode-1 Anode-3	Cathode-1 Anode-3	Cathode-3 Anode-1

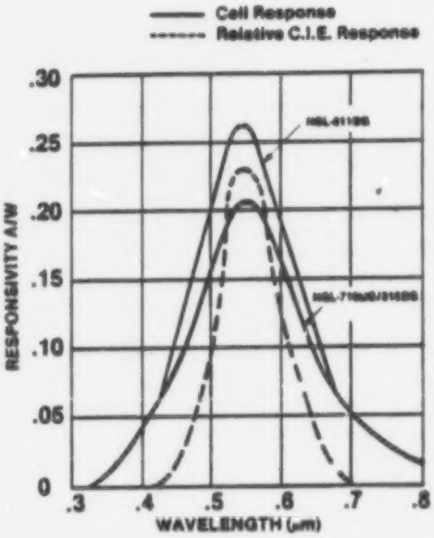

SPECTRAL RESPONSE

SILONEX INC

TWX 610-421-3362
2150 WARD STREET, MONTREAL, QUE. H4M 1T7 TEL. (514) 744-5507
331 CORNELIA ST., PLATTSBURGH, N.Y. 12901 TEL. (518) 561-3160
ALTRINCHAM, CHESHIRE, WA14 4NX. TELEX 51 669 663 TEL. (061) 928-3417

PHOTOCELL BULLETIN No. 15031

800 SERIES
SILICON PLANAR PHOTODETECTORS

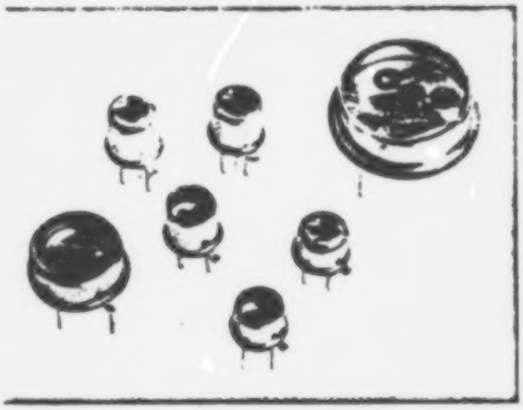

GENERAL DESCRIPTION

This is a family of planar, passivated photodetectors designed for photovoltaic and photoconductive applications. The high sensitivity and low dark currents make these devices ideal for low light detection. As well, their low capacitance and high speed make them useful for fast rise time applications. These detectors are available in a number of packaging variants, including TO-18, TO-5 and TO-8 hermetically sealed packages. NSL-811 and NSL-883 are also available as duals and quads in TO-5 and TO-8 packages.

For further information on customized devices, arrays and packaging configurations contact Silonex Inc.

FEATURES

- **Very low dark leakage current**
- **High sensitivity**
- **Low capacitance**
- **Hermetic packaging**
- **Linear response**
- **High reliability**

Silonex Part No.	Short Circuit Current (µA) @H=500 Ftc*		Open Circuit Voltage (V) @H= 500 Ftc*	Dark Current (nA) V_R = 5V T = 25°C		V_R=5V T=85°C	Breakdown Voltage (V)	Capacitance (Zero Bias) Typ. (pF)	Active Area (cm²)	Description
	Min.	Typ.		Max.	Typ.	Typ.				
NSL-811	100	120	0.41	5.0	0.3	300	40	50	.031	TO-18, Fig. 3
NSL-812	310	370	0.41	5.0	0.3	300	40	50	.031	TO-18, Fig. 3
NSL-813	220	280	0.41	5.0	0.3	300	40	50	.031	TO-18, Fig. 3
NSL-814	90	110	0.41	5.0	0.3	300	40	50	.031	TO-52, Fig. 4
NSL-815	240	280	0.41	5.0	0.3	300	40	50	.031	TO-52, Fig. 4
NSL-883	360	420	0.41	10.0	1.0	500	20	180	.101	TO-5, Fig. 5
NSL-893	800	980	0.41	20.0	5.0	800	10	380	.221	TO-8, Fig. 6

*The light source is Tungsten Lamp at a color temperature of 2870°K

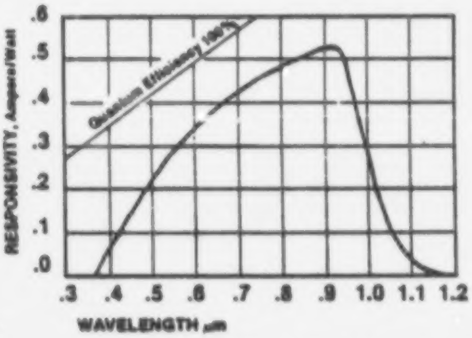

FIG 1 SPECTRAL RESPONSE

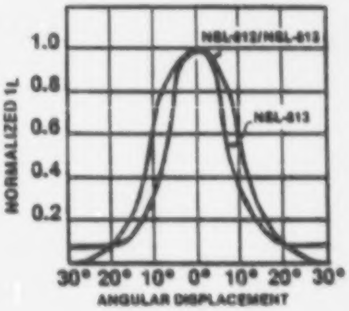

FIG 2
NORMALIZED ANGULAR RESPONSE

E-6

PHOTOCELL BULLETIN No. 15031

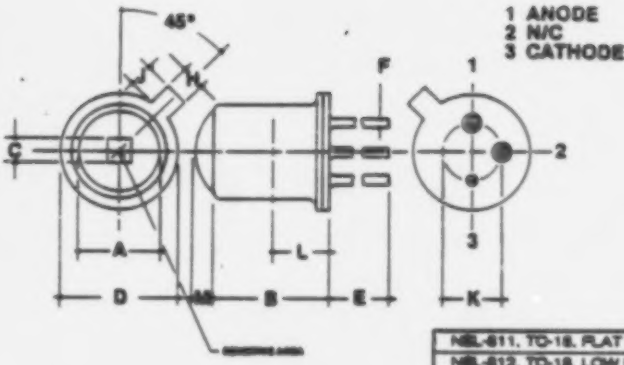

45°
J
H
C
F
1
2
3
A
L
K
D
B
E
SENSITIVE AREA
1 ANODE
2 N/C
3 CATHODE

	Ref	Inches Min.	Inches Max.	Millimeters Min.	Millimeters Max.
	A	.178	.188	4.52	4.78
	B	.196	.205	4.98	5.21
	C	.065	.075	1.65	1.91
	D	.202	.213	5.12	5.41
	E	.5 Nominal		12.8 Nominal	
	F	.016	.019	.41	.48
	H	.035	.045	.89	1.15
	J	.033	.048	.84	1.22
	K	.096	.104	2.43	2.65
	L	.105	.115	2.66	2.92
NSL-611, TO-18, FLAT WINDOW	M	-	.010	-	.25
NSL-612, TO-18, LOW LENS	M	.027	.033	.68	.84
NSL-613, TO-18, HIGH LENS	M	.052	.058	1.29	1.47

FIG 3: PACKAGE OUTLINE FOR NSL-611, NSL-612 AND NSL-613

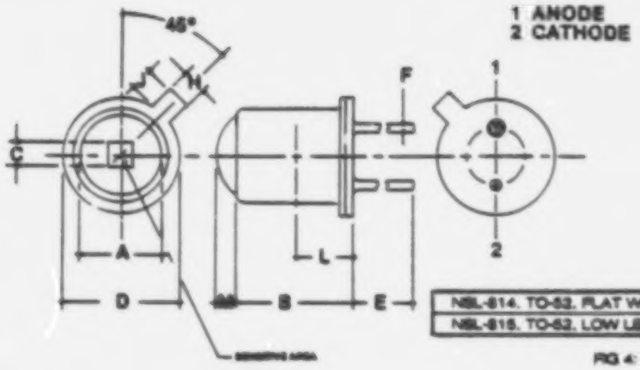

45°
J
H
C
F
1
2
A
L
D
B
E
SENSITIVE AREA
1 ANODE
2 CATHODE

	Ref	Inches Min.	Inches Max.	Millimeters Min.	Millimeters Max.
	A	.178	.188	4.52	4.78
	B	.142	.152	3.60	3.86
	C	.065	.075	1.65	1.91
	D	.202	.213	5.12	5.41
	E	.5 Nominal		12.8 Nominal	
	F	.016	.019	.41	.48
	H	.035	.045	.89	1.15
	J	.033	.048	.84	1.22
	L	.038	.048	.96	1.22
NSL-614, TO-52, FLAT WINDOW	M	-	.010	-	.25
NSL-615, TO-52, LOW LENS	M	.027	.033	.68	.84

FIG 4: PACKAGE OUTLINE FOR NSL-614, AND NSL-615

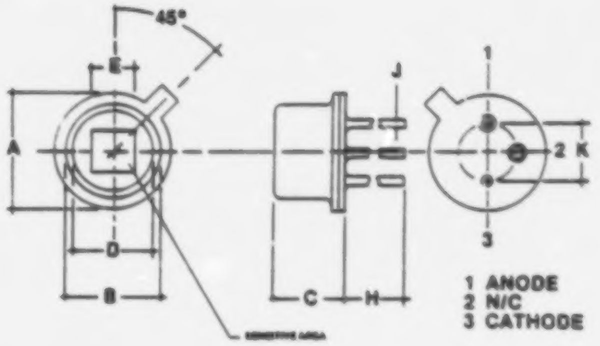

45°
E
A
J
1
2
3
K
D
B
C
H
SENSITIVE AREA
1 ANODE
2 N/C
3 CATHODE

Ref	Inches Min.	Inches Max.	Millimeters Min.	Millimeters Max.
A	.325	.335	8.20	8.48
B	.320	.330	8.13	8.38
C	.270	.280	6.87	7.10
D	.248	.258	6.28	6.45
E	.120	.130	3.04	3.30
H	1.50	1.60	38.0	40.8
J	.016	.019	.41	.48
K	.235	.245	5.96	6.22

FIG 5: NSL-883, TO-5, FLAT WINDOW

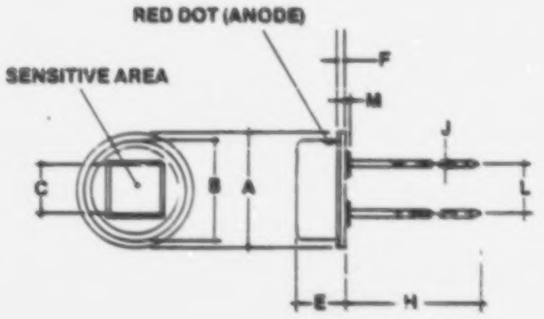

RED DOT (ANODE)
SENSITIVE AREA
F
M
J
C
B
A
L
E
H

Ref	Inches Min.	Inches Max.	Millimeters Min.	Millimeters Max.
A	.545	.555	13.84	14.10
B	.481	.491	12.21	12.46
C	.180	.190	4.57	4.83
E	.200	.226	5.08	5.73
F	.091	.101	2.31	2.56
H	1.50	1.60	38.10	40.64
J	.016	.019	.40	.48
L	.290	.300	7.36	7.62
M		.025		.63

FIG 6: NSL-893, TO-8, FLAT WINDOW

APPENDIX F

NORTHERN TELECOM

1. Charge-Coupled Device (CCD): Imaging Systems at the University of British Columbia

Charge-coupled device (CCD): imaging systems at the University of British Columbia (UBC)

Paul Hickson, Gregory G. Fahlman, Gordon A. H. Walker
Department of Geophysics and Astronomy, University of British Columbia, Vancouver, B.C., Canada V6T 1W5

Abstract

An imaging photometer employing a Bell-Northern Research (BNR) CCD has been developed at UBC and used on the Canada-France-Hawaii telescope (CFHT) in both a direct and an intensified mode. The intensified system is photon noise limited and linear from a 15th magnitude stellar source to the night sky limit. Intensified skylight provides a "bias" illumination that improves the low light level performance of the CCD.

Introduction

During the last few years CCD's have emerged as promising detectors for optical astronomy, and despite drawbacks of present devices they may be the best detectors for observing programs requiring a wide, linear, dynamic range, and high quantum efficiency. Because of these attractive characteristics we have developed a CCD imaging photometer at UBC, and have used it for several observing programs. The detector is a 100 x 100 element device manufactured by BNR and loaned to UBC. It was first employed in a directly illuminated mode for photometry of galactic nucleii. It could not be used directly to observe faint sources, however, because of systematic problems at low light levels (to be discussed) and so it was then optically coupled to a VARO three-stage image intensifier and used successfully for observations of faint quasars and BL Lacertae objects. The intensifier gain is sufficient to overcome CCD noise so that images are always photon noise limited. Unlike photon counting systems, however, the CCD provides storage so that coincidence effects do not limit the dynamic range.

The camera and data system

The organization of the camera, data, and control systems is shown in figure 1. The CCD housing and telescope interface is located at the telescope focus, with the camera electronics nearby. It is linked by a 100 meter cable to the control and data processing systems located in the telescope control room. PDP 11 software provides exposure sequencing and timing, data acquisition, image compensation, display, and storage. Simple operations such as flat fielding, sky subtraction, profile and luminosity measurements may be performed on line. The final storage medium is flexible diskettes (floppies) each of which has a capacity of 48 16 bit images.

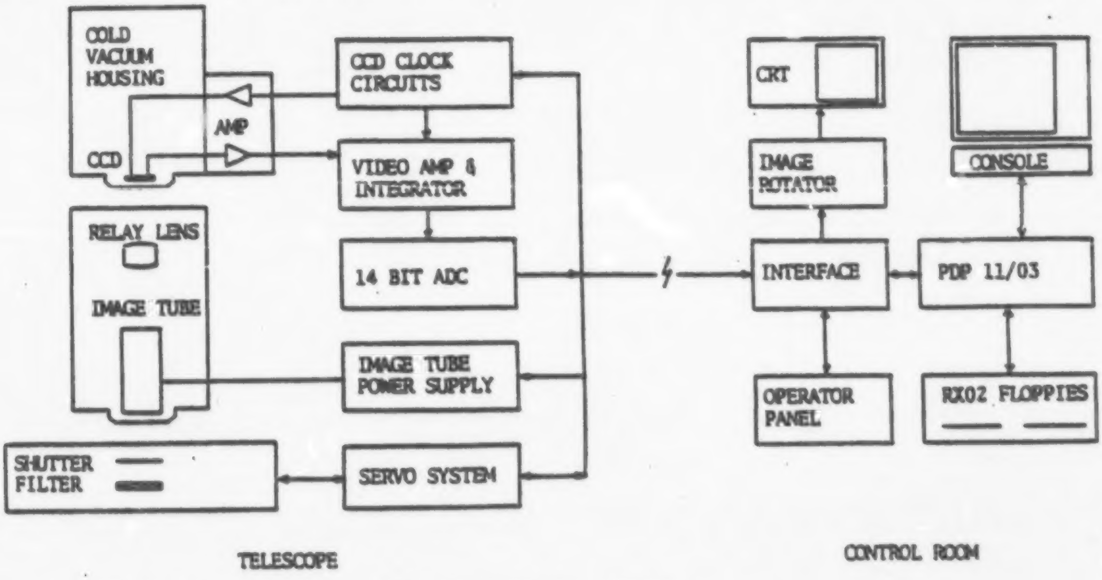

Figure 1. Block diagram of the UBC CCD imaging system.

a'

F-2

Hardware

The CCD is clamped to a copper block in a UBC vacuum-cryogenic housing designed by T. Lester and described elsewhere in this volume. Heat is transferred by conduction to a liquid nitrogen reservoir. The insulating vacuum is maintained by zeolite a substance that absorbs gas when cooled. This arrangement has proven very satisfactory; only rough pumping is required at the start of an observing run, and at the normal operating temperature of -120°C refilling is required only at 24 hour intervals.

For intensified operation a column containing the VARO image tube and a Nikon f/1.2 relay lens is installed between the telescope interface and the CCD housing. A regulated 2.65 volt supply powers the image tube which is mounted in a nylon retainer to avoid electrostatic discharge effects. The relay lens provides a 1:1 projection from the image tube fibre optic output to the CCD.

The CCD is coupled to drive circuits and a video amplifier located on the side of the housing by means of a thinned circuit board and vacuum feedthroughs. A short cable connects to a nearby box containing timing circuits, an integrator and 14 bit analog-to-digital converter, servo circuits for the shutter and filter wheel, and a cable interface. A "bias" voltage applied to the CCD inserts about 60,000 electrons into each storage site to prevent loss of photoelectrons in surface states. Power to the on-chip amplifier is switched off during integration to prevent heating and contamination of the image by optical emission from the amplifier.

Digital data is transmitted serially to the control room where it is demultiplexed by a special interface. It then goes directly into a PDP 11 random access memory (RAM) for bias compensation and display. The interface also transmits control signals to the instrument, and provides analog voltages to drive the oscilloscope display. This display consists of counters for the x and y positioning of the oscilloscope beam, 8 bit digital to analog converters and an image rotator module. The rotator introduces a linear transformation between the x, y and z analog lines. It performs rotate, tilt, pan and zoom operations at the turn of a dial which provides considerable flexibility of display. Because of speed limitations a long persistence oscilloscope phospher is used.

Software

The exposure sequence begins with three readout scans to reset the CCD. Integration is timed by a shutter, then data is readout sequentially at a rate of 10,000 pixels per second into a RAM "image". Three more readouts are performed to eliminate any remaining charge then a final "reference" readout occurs. This is subtracted pixel by pixel from the memory image in order to compensate for bias charge and any systematic readout noise.

When the CCD is used directly, exposure control is done in a "foreground mode" to allow other operations such as analysis and display of previous images to proceed simultaneously. In the intensified mode the CCD must be readout frequently and a different approach is used. An image is readout as above every 30 seconds and added to a 100 x 100 x 32 bit RAM buffer, updating the continuous display. This is very convenient as one can monitor the image as it is acquired. After the desired integration time the image is normalized to 16 bits and stored on a floppy disk. Focussing is done with readouts at 10 second intervals.

The display routine transmits 8 bits per pixel to the interface. A scale factor entered from the keyboard determines which bits are displayed. A cursor is also available for delineating pixels or areas of the image for analysis or numerical listing. A single scan can be performed for obtaining Polaroid hardcopy.

Processing operations that may be done at the telescope include division by a uniform reference exposure (flat field) of say the night sky, sky subtraction, cosmetic repairs, scaling, intensity profiles and aperture magnitudes, and a range of file handling operations.

Observations

In April of 1980 we obtained direct images of a number of objects, at the prime focus of the 3.6 meter CFH telescope on Mauna Kea an example of which is shown in figures 2 and 3. This is a 5 minute exposure of the BL Lacertae object Markarian 421 and a small companion galaxy. The prominent starlike central source is readily apparent, as is the large intensity ratio between it and the faint companion.

Intensified observations were made in January, 1981 of several faint quasars and BL Lac. objects. In figures 4 and 5 we see a raw and processed images respectively of a star field. The brightest star has a visual magnitude of 16 and the faintest 20.7. The surface brightness at the center of the faintest star is about one tenth the brightness of the night sky.

F-3

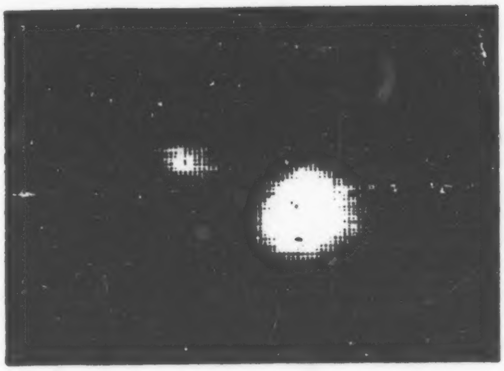

Figure 2. Direct CCD image of Mkn 421 and companion. 5 min. red light exposure at CFHT.

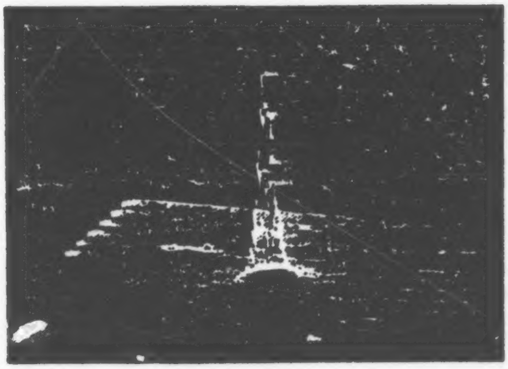

Figure 3. Perspective view of Mkn 421 illustrating the large intensity range in the data.

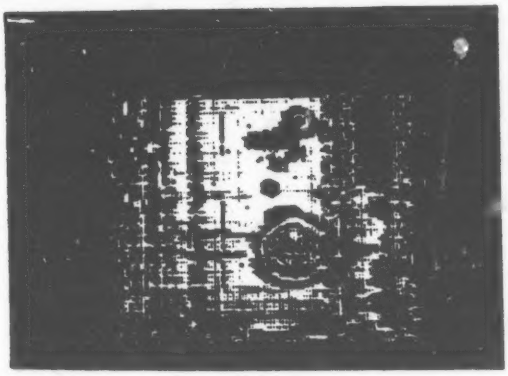

Figure 4. Unprocessed image of a star field with the intensified CCD camera. 10 min. exposure at CFHT.

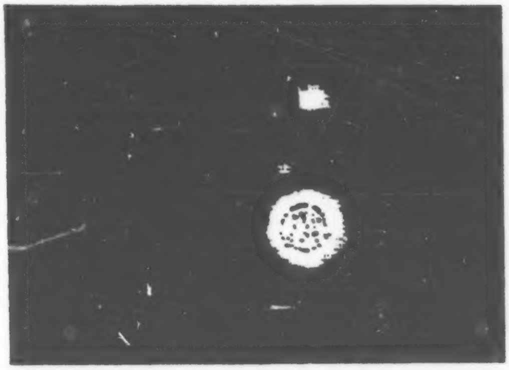

Figure 5. The same image after standard reduction and cosmetic repairs. Stars range from 16 to 20.7 visual magnitudes.

CCD performance

From data obtained at CFHT it is possible to evaluate the performance of this BNR CCD. The results are summarized in table 1 and discussed below.

Linearity

There appears to be a threshold of about 10^3 electrons below which no charge is readout. This can be overcome by a low level illumination or "pre flash" for each exposure. In the intensified mode, light from the sky was generally sufficient for this purpose. Above this threshold the device is linear to better than 5% up to the saturation charge of 2×10^5 electrons. Above this blooming occurs and charge spreads along the columns.

Charge transfer efficiency

At low light levels (about 10^3 electrons) charge transfer effects become severe. They are nonlinear in that the transfer efficiency is an increasing function of the transferred charge. A small amount of inefficiency can in principle be corrected by image processing. However, readout noise and truncation errors make this impractical. The best solution was to increase the light bias as the effect becomes negligible above a few thousand electrons.

Cosmetic defects

This array contains numerous defective or "hot" pixels and columns. Most are isolated and could be corrected by interpolation. However, a few large defects apparently affected the readout of the following pixels by creating a "trough" in the image. It was usually not possible to completely remove this effect by flat field division. Finally, there was a noticeable drop in sensitivity on the following side of each bad column, apparently due to charge loss at horizontal shift register defects. This could generally be corrected by.

F-4

flat field division.

Quantum efficiency

In order to determine this it is necessary to know the electron equivalent of a numerical unit in the image. This was estimated by measuring the variance in an image of uniform exposure that is photon noise limited. The result was 15 electrons per unit and a peak quantum efficiency of about 3% including 50% dead space near 6500Å. The device was useful from about 5000Å to 8500Å.

Readout noise

Using the above calibration the pixel to pixel standard deviation on a single readout was about 30 electrons.

Dynamic range

The saturation charge/light bias charge is a range of 100:1. In practice when the bias was provided by sky light observations could be made of any stellar object fainter than 15th magnitude.

Table 1. Characteristics of the BNR CCD

Format:	100 x 100 elements
Pitch:	32 x 28 microns per pixel
Architecture:	Front-illuminated surface channel
Quantum Efficiency:	5% peak at 6500Å
Spectral Range:	4000 to 9000Å (to 10% of peak QE)
Readout Noise:	30 electrons
Residual Noise:	5% of illumination at low levels
Threshold:	10^3 electrons

Conclusion

This CCD has been used successfully for direct observations of galactic nucleii and in a intensified mode for observations of fainter objects. Because of low light level limitations, best results were obtained in the intensified mode. The gain was sufficient to permit detection of individual photons, and the device could be used on stellar objects up to 15th magnitude and still be sky noise limited. The updating display facilitated acquisition and centering of objects.

The experience gained from this instrument has been valuable. We are presently upgrading to a newer and larger CCD and microchannel intensifier, and incorporating a holographic grating into the instrument to provide both an imaging and spectrophotometric capability.

APPENDIX G

OPTO-ELECTRONICS

1. High Speed Component Photodetectors
2. Germanium Photodiodes
3. High Speed Amplified Photodetectors

SERIES CD10
SERIES CD20

HIGH-SPEED COMPONENT PHOTODETECTORS

DESCRIPTION

Series CD10 and CD20 High-Speed Component Photodetectors are large area, non-avalanche photodiodes carefully mounted in TO-3 packages. They are used to detect high frequency CW optical signals, or short optical pulses. Each series consists of two models; the -01 model has a simple double convex lens directly in front of the photosensitive surface and the -02 model has a high quality, 50/125 micron core/cladding, graded index optical fiber permanently pigtailed to the package.

Series CD10 employs a silicon photodiode sensitive from 300-1100 nm and Series CD20, a germanium photodiode which may be used at longer wavelengths, up to 1800 nm.

These devices are especially useful in OEM applications where other common commercial photodiodes, having risetimes well above 0.5 nsec, are not fast enough. Their low cost permits systems comprising many picosecond photodetectors to be constructed economically. The TO-3 packages are designed to be easily soldered and unsoldered to a printed circuit board during design and prototype work. A miniature circuit board with integral BNC bias voltage and signal output connectors is available as an option. This board facilitates connections to the package and converts the basic device to an easy-to-use high speed photodetector.

SPECIFICATIONS

Bandwidth (-3 dB)[1.]		DC to > 1.2 GHz
Risetime[1.]		< 250 psec
FWHM Pulse Response[1.]		< 400 psec
Peak Flux Responsivity	Series CD10 @ 800 nm	0.15 A/W
	Series CD20 @ 1500 nm	0.20 A/W
Spectral Response Range	Series CD10	300-1100 nm
	Series CD20	500-1800 nm
Photodiode Active Area	Series CD10	500x500 microns
	Series CD20	100x130 microns
Noise Equivalent Power[2.]		$1\text{x}10^{-10}$ $\text{W}/\sqrt{\text{Hz}}$
Bias Voltage	Series CD10	15 Volts
	Series CD20	10 Volts
Maximum Average Optical Input before damage		100 mW
Output Impedance		50 ohms

Notes

1. Temporal response specifications are applicable for operation at the specified bias voltages only.
2. The N.E.P. is limited by the thermal noise of the load impedance.

Figure 1

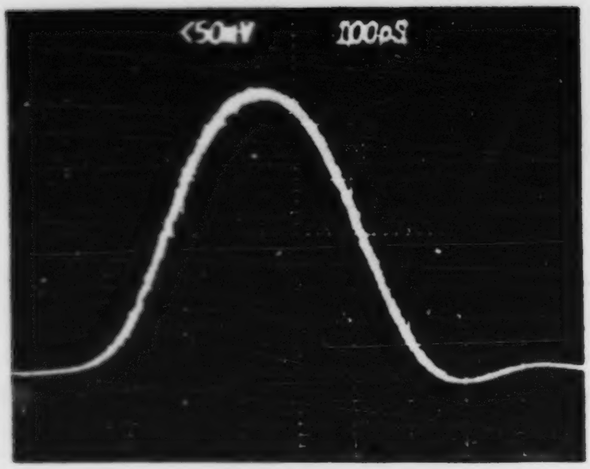

Typical response of a Series CD10 photodetector to a 70 psec wide, 900 nm wavelength, light pulse as monitored by a Tektronix 7904 oscilloscope with an S-4 sampling head.

SPECTRAL RESPONSE

Figure 2

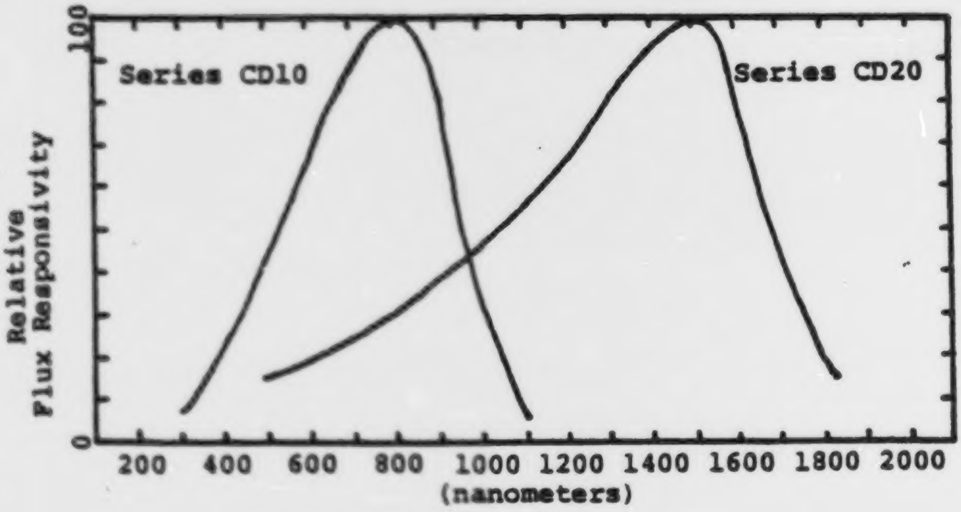

ORDERING INFORMATION

All prices and specifications are subject to change without prior notice. For further information and technical assistance, contact

Opto-Electronics Inc.
Unit 9, 2538 Speers Road
Oakville, Ontario, Canada, L6L 5K9
Telephone: (416) 827-6214 . Telex: 06-982392

PRICE LIST

Series CD10 and CD20

Component Photodetectors

October 1983

Unit Prices

Series Designation Model	CD10	CD20
-01 (lens type)	$330	$670
-02 (optical fiber type)	380	720

Quantity Purchase Unit Prices

Quantity	CD10	CD20
1-4	Unit Price	Unit Price
5-19	less $90	less $175
20-99	less $115	less $230
100-499	less $130	less $280

Orders for both models of a series may be combined to qualify for a quantity discount.

SERIES GD

GERMANIUM PHOTODIODES

DESCRIPTION

Series GD are high quality germanium photodiodes housed in TO-18 packages. The photosensitive area are square and range in size from 70 µm x 90 µm to 1000 µm x 1000 µm. Series GD photodiodes have the lowest dark current and highest sensitivity available with current germanium diode fabrication technology.

Each size is available with a lens, optical fiber pigtail, or flat window, designated by -01, -02, and -03.

Among the applications for germanium photodiodes are fiber optic power measurements, optical communications, IR/thermal instruments, and semiconductor laser monitors. The spectral response of germanium is especially suited for such applications at 1.3 µm and 1.5 µm.

Series GD are attractively priced and generous quantity discounts are available.

SPECIFICATIONS

	SERIES	GD25	GD20	GD10	GD8	Uni
	Photoactive Area	70x90	100x130	500x500	1000x1000	mic
	Flux Responsivity[1.] (at 1.5 μm)	0.7	0.7	0.7	0.7	A/W
	Reverse Bias	18	18	15	10	Vol
	Dark Current[1.]	0.3	0.5	5	10	μA
	Breakdown Voltage	25	25	20	15	Vo
	Noise Equivalent Power (at 1.5 μm)	4.5×10^{-13}	5.7×10^{-13}	1.8×10^{-12}	2.5×10^{-12}	W/√
	Bandwidth (-3 dB)[2.]	5000	5000	800	300	MHz
	Risetime[2.]	75	100	180	250	pse
	FWHM Impulse Response[2.]	200	300	600	1000	pse
	Capacitance[1.]	0.5	0.5	2	5	pf
	Capacitance[3.]	1	2	20	40	pf
	Impedance	160	100	10	5	kΩ
	MODEL					
PRICES	-01 (lens)	$175	$150	$130	$120	
	-02 (optical fibre)	375	350	330	-	
	-03 (flat window)	175	150	130	120	

Notes

1. At specified reverse bias voltage and 300 K.
2. At specified reverse bias voltage into 50 ohms at 300 K.
3. At 0 Volts and 300 K.

OPTO-ELECTRONICS INC.
RESEARCH IN ELECTRO-OPTICS

SERIES AD100

HIGH-SPEED AMPLIFIED PHOTODETECTORS

DESCRIPTION

Series AD100 High-Speed Amplified Photodetectors are large area, non-avalanche photodiodes coupled to a system of specially designed high frequency microwave amplifiers. They are used to detect weak high frequency optical CW signals, or short pulses, on any standard high-speed oscilloscope. Optical input may be made via an optical fiber, or directly from a light source, either in the field or in the laboratory.

There are two models: Model AD110 (Si photodiode) and Model AD120 (Ge photodiode). Model AD110 may be used at wavelengths up to approximately 1000 nm, and Model AD120 is used at longer wavelengths, up to 1800 nm.

Among the features of the Series AD100 are easy optical fiber or beam positioning, low loss optical coupling, wide dynamic range, and low voltage and temperature sensitivity.

Each Series AD100 unit consists of the photodetector head plus a separate power supply. There are two power supply models: Model PS100A is line-operated and Model PS100B is portable for possible field work. Model PS100B may be operated from the line or from its internal rechargable NiCd battery pack.

SPECIFICATIONS

Models AD110 and AD120 Amplified Photodetectors

Bandwidth (-3dB)	0.001 - >500	MHz
Risetime	<0.6	nsec
FWHM Pulse Response	<1	nsec
Peak Flux Responsivity (typical)	18	A/W[a.]
Minimum Detectable Input Signal (S/N=1)	5	μW[a.]
Spectral Response Range Model AD110	300 - 1100	nm[b.]
Model AD120	500 - 1800	nm[b.]
Photodiode Active Area	0.5 x 0.5	mm
Dynamic Range	340:1	
Peak Output for 1 dB Compression	1700	mV
Output Impedance	50	ohms

Notes

a. For Model AD110 at 800 nm, for Model AD120 at 1500 nm.

b. See Figure 2.

Models PS100A and PS100B Power Supplies

Line Voltage	110/220	VAC
Line Frequency	50/60	Hz
Power Consumption	10	Watts
Overall Dimensions Model PS100A	11W x 9H x 20D	cm
Model PS100B	21W x 10H x 33D	cm
Weight Model PS100A	1.5	kg
Model PS100B	4.0	kg[a.]
Continuous Operating Time Model PS100B	>8	hr[b.]

Notes

a. With battery pack.

b. From fully charged battery pack.

TEMPORAL RESPONSE

Figure 1

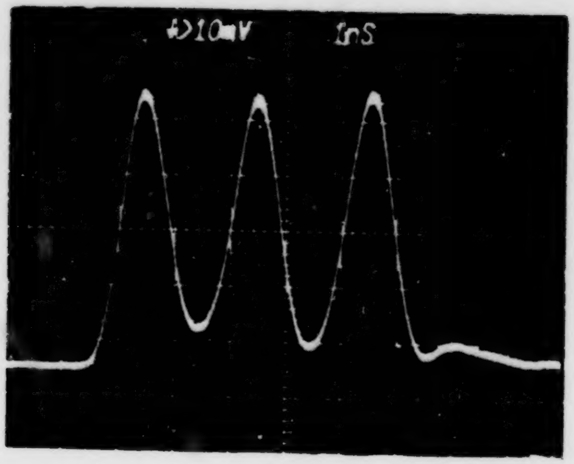

Output of a GaAs laser diode as monitored by a Model AD110 High-Speed Amplified Photodetector. The pulse train was obtained by optically delaying a single light pulse twice to generate the equivalent of 500 MHz modulation.

SPECTRAL RESPONSE

Figure 2

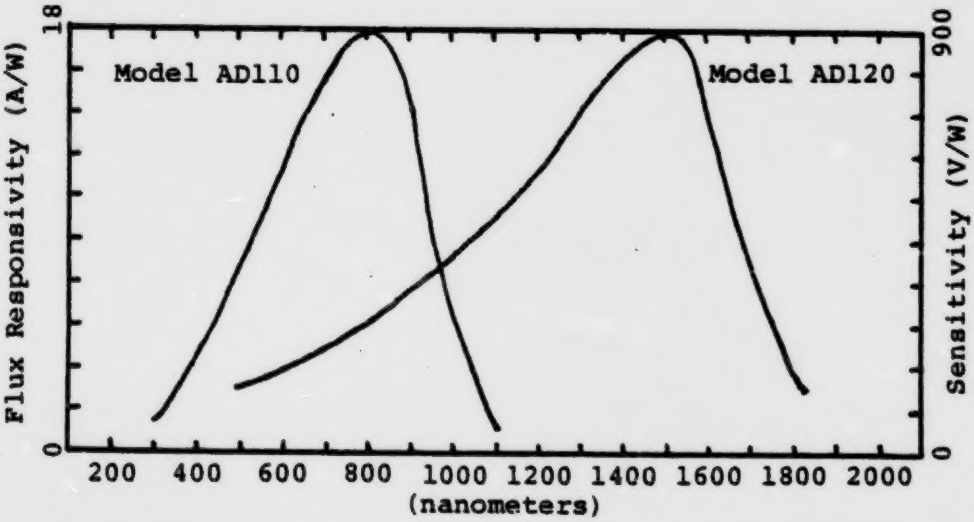

ORDERING INFORMATION

All prices and specifications are subject to change without prior notice. For further information and technical assistance, contact

Opto-Electronics Inc.
Unit 9, 2538 Speers Road
Oakville, Ontario, Canada L6L 5K9
Telephone: (416) 827-6214 Telex: 06-982392

APPENDIX H

CANADIAN PATENTS

1. Photodiode Detector with Selective Frequency Response
2. Buried-Channel Charge-Coupled Linear Device
3. Document Scanning Head
4. Photoconductor Device for Imaging a Linear Object

⑪ Ⓒ **No. 1003938**

㊺ **ISSUED** 770118

(52) **CLASS** 345-18
C.R. CL.

⑲⑫ CANADIAN PATENT

(54) **PHOTODIODE DETECTOR WITH SELECTIVE FREQUENCY RESPONSE**

(72) Dyment, John C.,
Canada

Granted to Bell Canada and Northern Electric Company, Limited, Canada

㉑ **APPLICATION No.** 209,401
㉒ **FILED** 740917

㉚ **PRIORITY DATE**

No. OF CLAIMS 7

DISTRIBUTED BY THE PATENT OFFICE, OTTAWA
CCA-274 (2-74)

H-7

This invention relates to photodiode detectors with selective frequency response.

In most photodiode detectors, a beam of light impinges on the diode in a direction perpendicular to the junction plane. Those photon energies greater than the bandgap energy of the detector are absorbed within a short distance below the surface of the detector, thereby creating electron-hole pairs. Those carriers which are collected by the junction are registered as a current in the external electrical circuit. The efficient collection of carriers is optimized by placing the junction at a depth approximately equal to the penetration depth of the photons, and by operating the diode in reverse bias. A conventional diode detector responds to a broad spectrum of photon energies provided these are greater than the detector bandgap energy.

The present invention provides a photodiode detector which has certain advantages over conventional photodiode detectors. A detector, in accordance with the present invention, has separate sections, each section generally absorbing photons in a certain, predetermined energy range. The output signal from a particular section will correspond to photons within this energy range. The width of the range can be varied, and can be controlled. The light is coupled to the detector along the junction plane so that the absorbed photons will always be close to the junction and the collection efficiency is improved.

The invention will be readily understood by the following description of the embodiment, by way of example, in conjunction with the accompanying drawings, in which:-

Figure 1 is a schematic diagram illustrating shifting of band edge with application of reverse bias;

Figure 2 is a diagrammatic cross-section through a detector in accordance with the present invention;

Figure 3 is a series of curves illustrating the energy bands of the device of Figure 2;

Figure 4 illustrates diagrammatically the reverse biasing of two sections of a device as in Figure 2;

Figure 5 illustrates an application of a device as in Figure 2.

Considering a double heterostructure device, in the waveguide region the absorption edge will normally be of the form indicated by curve 10 in Figure 1. The energy E_A will be determined by the basic structure of the material but will be about 1.4eV for GaAs at room temperature. Applying a reverse bias shifts the absorption edge as shown by curve 11. The amount of shift will depend upon the magnitude of the reverse bias V_R.

If the absorption edges were vertical, for example as indicated by the chain dotted lines 10a and 11a, then the structure would absorb all photons with energies above E_A and E'_A with the absorption efficiency being α max. However, as is well known the absorption edge is not vertical but is inclined as in curves 10 and 11. Thus there is some increase in absorption above zero ($\Delta\alpha''$) at energies below E_A, and E'_A, and some decrease in the absorption from α max ($\Delta\alpha'$) at energies above E_A, and E'_A. These changes in absorption (i.e. $\Delta\alpha''$ and $\Delta\alpha'$) are small effects compared to α max. For the purposes of subsequent discussion it is assumed that the absorption edges are vertical - as indicated by lines 10a and 11a - although the true situation, as indicated by lines 10 and 11, is appreciated.

Figure 2 illustrates a photodetector device which takes advantage of the ability to shift, or position, the absorption edge by reverse bias, to provide a detector which can give signals indicative generally of different levels of energy and which can also vary the bandwidth for the different levels of energy.

The structure of the device of Figure 2 is a double heterostructure comprising a substrate 20 on one surface of which are grown epitaxial layers 21, 22, 23 and 24. The layer 21 is a confining layer and is of the same doping type as substrate 20, for example n type. The layer 21 is of GaAlAs. Layer 22 is the active, or waveguide layer, is of doping type n, and is of GaAs, to which a small amount of aluminum - typically less than 10% can be added. Layer 23 is a further confining layer, of a doping type opposite to that of layer 22, and is of GaAlAs. Layer 24 is a capping layer, of the same doping type as layer 23 and is of GaAs. On layer 24 is formed a metal contact layer 25 and a metal contact layer 26 is also formed on the other surface of the substrate 20.

Following growing of layers 21, 22, 23 and 24, formation of layers 25 and 26, the structure is etched to define a number of electrically isolated sections, indicated at 30, 31, 32, 33 and 34. A reverse voltage bias is applied to each section with the high numbered sections being biased successively more negative. Light enters the waveguide, or active layer 22 in the direction of the arrow X.

Each section will generally detect photons which are absorbed in that particular section. Figure 3 illustrates the energy bands for the device of Figure 2, the curves 38 to 42 illustrating the upper energy edges for sections 34 to 30 respectively. As described in conjunction with Figure 1, as the absorption edges are inclined, there is some absorption of energies below a particular value and some non-absorption of energies above a particular value.

The output from a detector will depend upon the magnitude of α - the absorption coefficient. If α is high - which means a large amount of absorbed light - the photocurrent will be high also. Relating to Figure 1 the output voltage generated by this photocurrent across a resistor in the circuit will be a maximum when $\alpha = \alpha$ max. The photocurrent, or output voltage will have a curve which effectively has the same qualitative behaviour as Figure 1. Thus the output voltages can be indicated on Figure 1. Thus, at an energy of E_A there is an output voltage of V_A. If it is desired to have the detector respond only to $E > E_A$ for example, then it is necessary to provide a circuit which will only respond to an output voltage $V > V_A$, and reject those values of $V < V_A$.

This is illustrated diagrammatically in Figure 4 which shows two sections of the structure of Figure 2, sections 30 and 31. The sections 30 and 31 are shown as separate sections, but in practice would usually be on a common substrate, as in Figure 2. The back of each section is connected to a common source - normally ground. This would be obtained by the contact layer 26 of Figure 2. Each section is reverse biased by a circuit including a bias voltage supply indicated at 35. This can be made variable, as shown. The bias voltage may be applied in parallel with a condenser 36. The bias voltage supply 35, and condenser 36, are connected to the common source - ground - in series with a resistor 37 across which is an amplifier 43 connected in parallel with resistor 37. The amplifier 43 is arranged, in a known manner, to pass an output signal or pulse only when the potential across the resistor 37 exceeds a predetermined voltage. The reverse bias is increased for each section, in equal steps, or non-equal steps as will be described.

Referring to Figures 2 and 3, consider a light pulse of energy $E < E_{30}$ but $E > E_{31}$ as indicated on Figure 3 at 45. Curve 42 is the absorption edge for section 30 and curve 41 is the absorption edge for section 31. For section 30 the absorption coefficient is only α_A, which will produce only a small output voltage in section 30.

For section 31, the absorption coefficient is α_B and is very high. Therefore the corresponding output voltage V is high. By arranging that the amplifier 38 will be triggered only when a voltage exceeds the value corresponding to the absorption efficiency indicated by dotted line 46, section 31 will indicate detection of the energy pulse and section 30 will not. The line 46 can be set at any desired level. The line 45 is presented only as an indication of a particular value of E for purposes of description and can vary.

By providing means for varying the bias applied to any section it is possible to vary the absorption band width of that section. It is possible to provide control of the bias applied to each section so that it would be possible to select a particular limited range of energy and use two, three or four sections to operate within this range - giving a more detailed detection, for example, the remainder of the light input being detected by the remaining section or sections. Thus instead of the curves in Figure 3 being evenly spaced they can be given variable effective spacing.

A further variation which needs taking into consideration is that the slopes of the curves indicating the absorption edges become less steep as the reverse bias increases. As illustrated in Figure 3, the curves 38, 39, 40, 41 and 42 are shown as having the same slope. In practice the slopes will vary, somewhat as illustrated by the dotted curves 38a, 39a, 40a and 41a. To maintain an effective equal bandwidth it would be necessary to increment the reverse bias by increasing amounts for the higher numbered sections. If a variable effective spacing is required, as described above, then additional variation of the reverse bias will be necessary. As an alternative to increasing the reverse bias to offset the effect of variation in slope the section can be increased in length, i.e. section 34 longer than section 33 which is longer than section 32, and so on.

The structure of Figure 2 is useful as a demultiplexing device, and enables the sorting out of complex digital optical pulses. Figure 5 illustrates the application, with a series of multiplexed optical signals being indicated at 50a - 50f. The energy of the various pulses will differ and indicated below each of the optical signals is the related energy value with reference to a particular section of the structure. Thus pulse 50a is of an energy value which will be absorbed by section 30, pulse 50b by section 34, 50c by section 32, 50d by section 33, 50e by section 31 and 50f by section 34. The outputs from the sections are indicated at 51 to 55 for sections 30 to 34 respectively.

While the pulses are shown as separated in time this is not essential. Pulses of differing energy values can be coincident in time and the various sections will absorb the pulses and produce output signals.

The layers 21, 22, 23 and 24 are sequentially grown by liquid phase epitaxy, by well known techniques. Typical examples of processes and apparatus for growing layers sequentially are described in "Preparation of GaAs p-n Junctions" by B.I. Miller and H.C. Casey Jr., paper 24, 1972 Symposium on GaAs; and in Canadian Patent No. 902,803 issued June 13th, 1972.

In one form of apparatus substrate wafers are positioned in a carbon slider which moves sequentially beneath reservoirs containing epitaxy solution. At each reservoir, substrate and solution are cooled to cause epitaxial growth. At the end of the growing process, the substrates are finally cooled and cleaned.

The following table illustrates the characteristics of the various layers and the dopant concentrations in milligrams per 4 gm melt.

Layer	Type	Al	Te	Ge	Thickness(μm)	Carrier Concentration
21	n-$Ga_{0.65}Al_{0.35}As$	6	2	-	≈ 3	$\geq 5 \times 10^{17} cm^{-3}$
22	n-$Ga_{0.95}Al_{0.05}As$	1	Sn 20 mg	-	≤ 1	$\leq 2 \times 10^{16} cm^{-3}$
23	p-$Ga_{0.65}Al_{0.35}As$	7	-	120	≥ 1	$\geq 5 \times 10^{17} cm^{-3}$
24	p-GaAs	-	-	40	≈ 1.5	$\approx 10^{18} cm^{-3}$

In some cases, an amount of GaP is added to layers 21 and 23. The amount in the melt is 100μg/4gm and results in a general layer of the form $Ga_{0.65}Al_{0.35}As_{1-y}P_y$ where y is estimated to be less than 0.02. The incorporation of P causes a reduction in strain at the interfaces between layers 21 and 22 and between layers 22 and 23.

The thicknesses of the layers 21 and 23 are not critical but are preferably ≥ 1.0 μm in order that good waveguiding properties exist. Layer 22 should be about 1.0μm but can be thinner. The doping levels in the various layers are reasonably critical. In general, layers 21 and 23 should have more than an order of magnitude higher doping than layer 22. This ensures that most of the applied electric field will appear across layer 22 where it is required to affect the light in the waveguide. At carrier concentrations of 2×10^{16} cm^{-3}, the 1.0 μm thickness for layer 22 will be entirely depleted of free carriers even at zero bias (that is, the depletion width is approximately 1μm for carrier concentrations $\approx 2 \times 10^{16}$ cm^{-3}). Thus the doping level and thickness of layer 22 are reasonably critical to obtain the optimum device performance. Larger layer 22 thickness will result in less efficient coupling of the light to the electric field whereas values smaller than 1 μm will present some increased complexity in coupling light into the narrower waveguide.

Layer 24 is an optional layer and devices will operate satisfactorily without this layer.

Normally a plurality of devices will be fabricated simultaneously on a substrate. The fabrication steps for making devices as described above are as follows, after growing the four layers 21, 22, 23 and 24 as described, layer 22 of n type to provide adequate electrical isolation.

(a) diffuse Zn into layer 24, using $AnAs_2$ source in a nitrogen atmosphere for 15 minutes at 600°C;

(b) evaporate 2000Å of Au on layer 24, holding substrate at 200°C during evaporation;

(c) lap n-GaAs substrate to thickness of about 100 μm;

(d) clean and evaporate Au (12% Ge) to thickness of 4000Å on lapped surface with substrate at 200°C;

(e) alloy at 450°C for 3 minutes in nitrogen atmosphere - to form n contact 26;

(f) photoengrave a pattern on heterostructure side of structure to define stripes - to form isolation grooves 48 - Figure 2 - typically the stripes 50 μm wide on 500 μm centres and aligned with cleavage edge of substrate;

(g) remove Au layer 25 at stripes using etch $KI:I_2:H_2O$ (275g:15g:250g:) for 30 seconds to 60 seconds at room temperature; (shorter etch times are requested at 750°C);

(h) etch layer 24 away at stripes using $H_2O_2:NH_4OH$ (approximately 700:1 to provide pH=7.0) with agitation until layer 24 is removed. Typical etch rates are 0.1 µm/min. This preferentially removes layer 24 but not layer 23 which has a much higher Al content;

(i) etch layer 23 using concentrated HF. Typical etch times are 10 minutes to remove 1 µm. This preferentially removes layer 23 but not layer 22 which has a low Al content;

(j) cleave out devices which have the required number of sections - typically 4 or 5 sections. Overall device length for 5 sections is approximately 2.5mm and width is typically 0.25mm.

An alternative for step (i) is to use a $KI:I_2:H_2O$ (275g:15g:250g) etch at 75°C - as is used in step (g). Typical etch times of 15 to 30 seconds will remove 1 to 2 µ of p-GaAlAs.

To reduce the device capacitance by approximately a factor of 10X, which would decrease the response time, a stripe contact could be formed. Such stripe contacts could be formed by proton bombardment. This can be accomplished after step (i). An array of parallel wires, typically 25µm diameter at 250 µm centres, is positioned over the structure, the wires perpendicular to the cleavage edge and the etched grooves. The structure is bombarded with protons of energy 300-400 keV at desage of $3 \times 10^{15} cm^{-2}$. The protons create high resistivity material from the surface to a depth exceeding the junction, but only in the areas between wires. Low resistivity material occurs under the wires. The result of bombardment will be a lowering of the device capacitance by approximately a factor of 10X and this will decrease response time of the detector. A typical proton bombardment process is described in "Proton Bombardment Formation of Stripe-Geometry Heterostructure Lasers for 300K CW Operation", by J.D. Dyment, L.A. D'Asaro, J.C. North, B.I. Miller and J.E. Ripper, Proceedings of the IEEE., Vol. 60, No. 6, June 1972 pp 726-728.

A further modification is to evaporate an antireflection coating on the input end of each device to improve coupling efficiency.

As described the active or waveguide layer 22 is of the same doping type as the substrate 20 and confining layer 21 and opposite to layers 23 and 24. As an example, substrate 20 and layers 21 and 22 have been described as n-type and layers 23 and 24 of p-type. This can be reversed, substrate 20 and layers 21 and 22 of p-type and layers 23 and 24 of n-type.

Also instead of obtaining electrical isolation by etching grooves or slots, it is possible to obtain isolation by other methods, including doping on proton bombardment.

THE EMBODIMENTS OF THE INVENTION IN WHICH AN EXCLUSIVE PROPERTY OR PRIVILEGE IS CLAIMED ARE DEFINED AS FOLLOWS:-

1. A photodiode detector, comprising:

a substrate;

a multilayer structure on a surface of said substrate, said structure comprising a plurality of aligned detector sections;

said structure comprising a confining layer on said surface of said substrate and an active layer on said confining layer, said confining layer and said active layer of the same conductivity type and extending homogeneously across said substrate for all the detector sections;

said active layer providing a waveguide layer having a portion for each detector with said portions in optical alignment, the active layer having an input end;

a further confining layer on said active layer, said further confining layer of a conductivity type opposite to that of said active layer and separated into portions, a portion for each detector section, the portions of said further confining layer electrically isolated from each other;

means for applying a reverse bias to each detector section, the bias successively more negative for each successive section from said input end;

output means for each section for producing an output signal indicative of photon absorption in said section.

2. A detector as claimed in claim 1, including means for varying the reverse bias applied to each section.

H-12

3. A detector as claimed in claim 1, said output means for each section comprising circuit means for producing an output signal when an input signal to said circuit means exceeds a predetermined value.

4. A detector as claimed in claim 1, compris[illegible] doped gallium arsenide substrate, a doped gallium aluminum arsenide confining layer on said substrate and of the same conductivity type as said substrate;

a doped gallium aluminum arsenide active layer on said confining layer of the same conductivity type as said confining layer and of a lower doping level than said confining layer;

a further confining layer of gallium arsenide on said active layer of the opposite conductivity type to said active layer and of a higher doping level than said active layer.

5. A detector as claimed in claim 4, including a capping layer of gallium arsenide on said further confining layer of the same conductivity type as said further confining layer and of a higher doping level than said further confining layer.

6. A process for producing a photodiode photodetector having a plurality of detector sections in series, comprising:

sequentially epitaxially growing a confining layer, an active layer and a further confining layer on a substrate;

dividing said further confining layer into a plurality of electrically insulated sections arranged in series to form said plurality of detector sections, and forming a contact area on said substrate and a contact area for each detector section.

7. A process as claimed in claim 6, including forming a capping layer on said further confining layer.

1003938

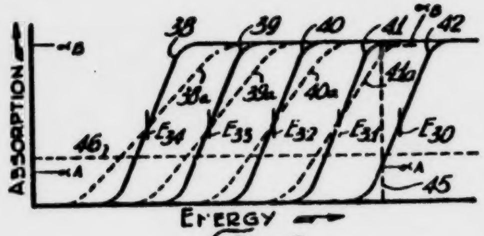

-Fig-3-

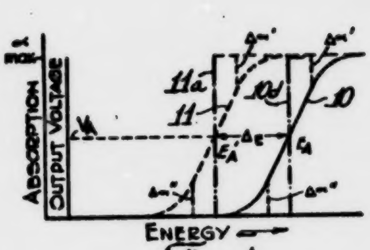

-Fig-1-

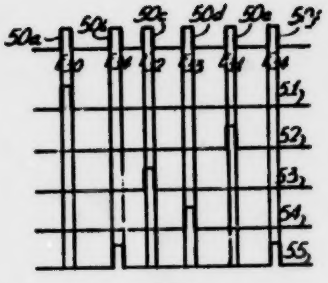
50a
50b
50c
50d
50e
57
E30
E31
E32
E33
E34
51
52
53
54
55

-Fig-5-

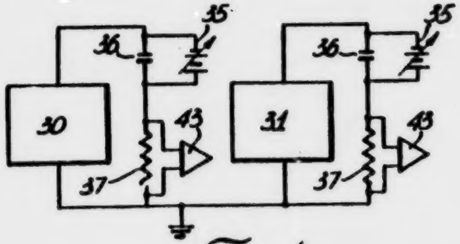
30
31
36
35
43
37

-Fig-4-

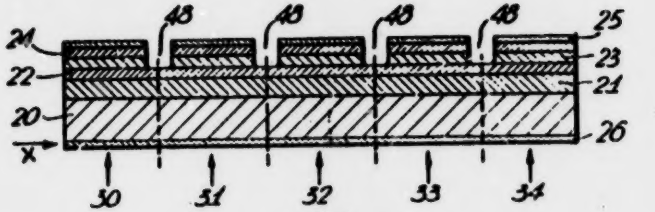
48
24
22
20
X
25
23
21
26
30
31
32
33
34

-Fig-2-

H-1[illegible]

⑪ Ⓒ No. 1020656

㊺ ISSUED 771108

(52) CLASS 345-1
C.R. CL. 352 82.2

CANADIAN PATENT

(54) BURIED-CHANNEL CHARGE-COUPLED LINEAR IMAGING DEVICE

(72) Kim, Choong-Ki and Dyck, Rudolph H.,
U.S.A.

Granted to Fairchild Camera and Instrument Corporation,
U.S.A.

㉑ APPLICATION No. 190,114
㉒ FILED 740115

㉚ PRIORITY DATE U.S.A. (343,759) 730322

No. OF CLAIMS 16

DISTRIBUTED BY THE PATENT OFFICE, OTTAWA
CCA-274 (2-74)

H-11

Background of the Invention

Field of the Invention

This invention relates to imaging devices and in particular to a linear imaging device using charge coupled device technology.

Prior Art

W. S. Boyle and G. E. Smith describe the basic concept of charge coupled semiconductor devices in an article published in the April 1970 Bell System Technical Journal, page 587, entitled "Charge Coupled Semiconductor Devices".

As described by Boyle and Smith, a charge coupled device (hereinafter called a "CCD") consists of a metal-insulator-semiconductor (MIS) structure in which minority carriers are stored in a "spatially defined depletion region" also called a "potential well", at the surface of the semiconductor material. This charge is moved along the surface by moving the potential energy minimum. This potential energy minimum will be a maximum voltage (where the word voltage is used in its conventional sense) when the charge carriers are electrons and a minimum voltage when the charge carriers are holes. A paper on page 593 of the same Bell System Technical Journal by Amelio et al entitled "Experimental Verification of the Charge Coupled Device Concept" describes experiments carried out to demonstrate the feasibility of the charge coupled device concept.

As discussed by Boyle and Smith, charge coupled devices are potentially useful as shift registers, delay lines, and in two dimensions, as imaging or display devices.

A CCD linear imaging array of the prior art detected a linear image by generating charge beneath each electrode in the CCD array proportional to the intensity of the impinging light. To read out the detected image, the generated charge representing the detected image is shifted along the detecting array by selectively varying the potentials on the electrodes. One problem with this type of linear imaging array is that the detected image is degraded by the continuous impinging of light on the array while the image is being read out. One way of improving the quality of the detected image is to increase the speed of reading out the charge. The speed of read out, however, is limited by the frequency response of the circuit.

Summary of the Invention

This invention overcomes some of the difficulties of the prior art CCD linear imaging arrays. In particular, this invention overcomes the degradation of the detected image by the continuous impingement of light on the detecting array while the charge representing the image is being read out of the array.

According to this invention, a charge coupled device linear imaging array comprises an array of light-sensing elements for generating charges proportional to the impinging light and at least two separate transport arrays for reading out the generated charges without degrading the image during readout. The transport arrays are shielded with an opaque material to prevent impinging light from affecting the quantity of charge being transferred along the transport arrays.

In one embodiment of this invention, the light sensing array and the transport arrays are all CCD linear arrays. The CCD linear array usually include a buried channel to give to the arrays a much better dynamic range than is obtained without such a channel. In another embodiment of this invention, only the transport arrays are CCD linear arrays. In still another embodiment only the light sensing array is a CCD linear array.

If desired, a preamplifier is incorporated on the same semiconductor chip with the light sensing and transport arrays to give a better signal-to-noise ratio than heretofore obtained.

When the light sensing elements comprise charge coupled devices, the electrodes (often called "gates") of the charge coupled devices are transparent to give a greater average quantum efficiency than obtainable with opaque gates.

In accordance with this invention, there is provided a linear imaging array comprising: a line of light sensitive elements including a plurality of transparent electrodes formed on the top surface of a layer of insulation formed over a semiconductor material; a first CCD shift register located on one side of said light-sensitive elements; a second CCD shift register located on the other side of said light-sensitive elements, said shift registers being covered with an opaque material; means for transferring charge packets generated in said line of light-sensitive elements to appropriate positions in said first shift register and said second shift register; first means for shifting said charge packets along said first and second shift registers including means for driving said charge packets along said first shift register and said second shift register at a first selected frequency; means for receiving charge packets at the ends of said first and second shift registers including a third CCD shift register located at the ends of said first and second shift registers for receiving said charge packets from said first and second shift registers, and further including means for sensing the magnitudes of said charge packets; second means for shifting said charge packets along said third shift register at a second frequency, said second frequency being twice said first frequency; and, output circuitry means at the output end of said third shift register for receiving said charge packets from said third shift register and for generating output signals in proportion thereto.

Figure 1 shows a cross-sectional view of a buried channel charge coupled device;

Figures 2a and 2b show top and cross-sectional views of a linear imaging array constructed according to this invention;

Figure 3 shows schematically a plan view of the functional arrangement of the linear imaging array shown in Figure 2a;

Figure 4 shows an alternative output circuit for processing the

the signals transmitted by the transport arrays 34a and 34b in Figure 3;

Figure 5 shows in block diagram form, one output circuit for processing the signals generated by the detected charge; and

Figures 6a through 6j show waveforms of use in explaining the operation of the structure of this invention.

Figure 1 shows a charge coupled device comprising a semiconductor substrate 11 in which is formed buried channel 14. As shown in Figure 1, substrate 11 is of P type conductivity. It should be understood, however, that the conductivity types of the various regions to be described in device 10 can be reversed and thus the following description is not to be interpreted as limiting the disclosed invention to the conductivity types described. Also, while the CCD devices employed in the embodiments of this invention described in this specification have a buried channel such as channel 14, if desired, this buried channel can be omitted.

While substrate 11 will be described as consisting of silicon semiconductor material, it should be noted that this invention can be used with any semiconductor material in which a charge coupled device can be formed.

The structure shown in Figure 1 has insulation 15 formed over the top surface of substrate 11. Typically, insulation 15 is an oxide of semiconductor material 11 and when material 11 is silicon, comprises a silicon oxide. Overlying the top surface of silicon oxide layer 15 in a repetitive, serially-spaced manner are electrodes 16a, 16b, 16c, 16d, 16e and 16f. In addition, an output electrode (often called a "gate") is shown just to the right of electrode 16f. While only six electrodes are shown on the structure of Figure 1, it should be understood that different numbers of electrodes, as desired, can be used in a charge coupled device. Electrodes 16a through 16f are contacted by output leads 17a through 17f. Depending upon the type of operation desired, output leads 17a through 17f can be connected so that the CCD device operates as a three or more phase system. P+ type regions 12a and 12b represent in cross section a closed channel stop region. This channel stop region, typically formed by diffusion, decreases the sentitivity of the device to leakage currents and forms a closed path around that portion of the surface of device 10 beneath which the charge generated by incident light is stored and transferred. Region 13, of N+ type conductivity, forms with substrate 11 an output diode for receiving charge transmitted along the charge coupled device and for producing an output signal in response thereto. Lead 19 contacts region 13.

A layer 14 of opposite conductivity type to the predominant conductivity of substrate 11 is formed in the top surface of substrate 11 beneath oxide layer 15. Preferably, layer 14 is formed using ion implantation techniques. The thickness of this layer at the completion of all high-temperature processing steps is, in one embodiment, 4,000 angstroms. Layer 14 provides a buried potential well which allows minority carriers (minority with respect to the predominant carrier in P type substrate 11) to be stored and transferred in the buried layer in the bulk semiconductor material near the interface of semiconductor substrate 11 and insulation 15 rather than at this interface. The structure shown in Figure 1 will not be described in further detail, but is described here to illustrate the cross section of a portion of one type of CCD linear array used in one embodiment of this invention.

Figure 2a shows a top view of a linear imaging array constructed using charge coupled device technology in accordance with the principles of this invention. Neither Figure 2a nor the other figures are drawn to scale; rather, many of the features shown in the figures are distorted for illustrative convenience.

A linear array of light-sensitive elements 32-1 through 32-14 extends along the middle of the structure shown in Figure 2a. These light-sensitive elements, shown in plan view in Figure 2a, are arranged in two groups; a first group comprising the odd-numbered light-sensitive elements 32-1, 32-3, 32-5, etc. all read out to the left of Figure 2a and an even-numbered group of light-sensitive elements 32-2, 32-4, 32-6, etc. all read out to the right of Figure 2a. In the embodiment shown in Figures 2a and 3, light-sensitive elements 32 comprise a linear array of charge-coupled devices, with the light-sensitive regions of semiconductor material covered by a single electrode rather than a corresponding plurality of electrodes as in a typical CCD shift register. As will be seen shortly, the charge generated in such a linear imaging array is first shifted out of the imaging array in at least one direction substantially perpendicular to the array before being further processed. A plurality of electrodes, properly connected to yield this result, could be used in place of the single electrode, if desired.

For the purpose of this specification the word "light" means any electromagnetic radiation which produces free charge in the depletion region of semiconductor material. Typically "light" includes infared, visible and ultraviolet radiations.

While the light-sensitive elements 32-1, 32-2, 32-3, etc.in general compromise depletion regions formed in underlying semiconductor material as part of a charge coupled device, these elements can be photodiodes.

A channel stop 31 (Figures 2a, 2b) is formed around three sides of each light-sensitive element 32-i (where *i* is an integer with a value given by $1 \leq i \leq K$ and *K* is the maximum number of light-sensitive elements 32) in such a manner that the channel stop forms a continuous region from one end of the light-sensitive elements 32 to the other, twisting in a serpentine fashion so as to be on three sides of each light-sensitive element. Thus, the channel stop forms a "U-shape" around each light-sensitive element, with the U being located on its side, and the legs of the U pointing either to the right or the left of Figure 2a (when the drawing is properly oriented to be read) depending upon whether the light-sensitive element is an even-numbered element or an odd-numbered element, respectively. The channel stop region 31, of like conductivity type to the predominant conductivity type of the semiconductor material in which the light-sensitive elements 32 are formed, effectively isolates each light-sensitive element 32-i from adjacent light-sensitive elements 32-(i-1) and 32-(i+1) and thus substantially defines the area of each light-sensitive element 32-i. While in Figure 2a *K* equals 14, *K* can, in general, equal any appropriate number, depending on design requirements.

A pair of transfer gates 33a and 33b control the transfer of charge from the odd-numbered light-sensitive elements 32-1, 32-3, 32-5...and the even-numbered light-sensitive elements 32-2, 32-4, 32-6..respectively. To the left and right of transfer gates 33-1 and 33-2 respectively are located electrodes (shown schematically as areas 34a and 34b, respectively) such as electrodes 16a through 16f (Figure 1) to form transport arrays 34a and 34b which in one embodiment of this invention comprise two charge coupled device analog shift registers. These transport arrays covered with an opaque material such as aluminum are parallel to, and on either side of, light-sensitive elements 32.

To provide proper direction to the charge packets being transferred from elements 32 to transport arrays 34a and 34b, the channel stop region can include the "L"-shaped extensions 31-1, 31-2, etc. shown in Figure 2a. These extensions give to the charge packets the directions shown by the arrows in Figure 3.

FIG 3 shows the layout of the elements shown in FIG 2a and described above. Light-sensitive elements 32 contain charge generated by incident radiation. The charge generated in light-sensitive area 32-1 is transferred by appropriate adjustment of the potentials on the leads labeled ϕ_p (connected to gate 36), ϕ_x (connected to transfer gates 33-1, 33-2 etc.) and ϕ_{v1} (connected to gates 34-1, 34-7, 34-13 etc., which are part of electrode string 34a and also to electrodes 34-2, 34-8, 34-14 etc. which are part of electrode string 34b) to the appropriate location in transport array 34a. To transfer charge from the odd-numbered light sensing elements 32-1, 32-3 ... , (hereinafter called the "odd elements") the potential on the ϕ_p lead is raised, the potential on the ϕ_x lead is held at a neutral level and the potential of the ϕ_{v1} lead 35-1 is raised to a maximum level thereby causing charge generated and stored in light sensitive element 32-1 to transfer to a region underlying gate 34-1. Simultaneously, the charge generated and stored in light sensitive element 32-3 is transferred from this element to the region beneath electrode 34-7. Similar transfers of charge occur simultaneously from all the odd elements.

In a similar fashion, and at the same time, charge stored in light sensitive element 32-2 is transferred to the region beneath gate 34-2 in response to the same arrangement of potentials. Simultaneously, the charges stored in all the other even-numbered, light-sensitive elements 32-4, 32-6 etc. in line 32 (hereinafter called the "even elements") are transferred to the regions of semiconductor material beneath gates 34-8, 34-14 etc. in the right CCD analog shift register 34b.

CCD analog shift registers 34a and 34b are each identical in operation to the other. Therefore, the operation of CCD analog shift register 34a will be briefly described and it should be understood that CCD analog shift register 34b operates in an identical fashion.

FIGS 6a through 6h show the potentials as a function of time on leads 35-1, 35-2, 35-3 and 38-1, 38-2 and 38-3. The abscissa of the curves shown in FIGS 6a through 6j is time, with the units of time (one such unit of time will hereinafter be called the "base period") being equal to one third the periods of the clock signals ϕ_{H1}, ϕ_{H2} and ϕ_{H3} on leads 38-1 through 38-3. Note that the periods of these clock signals are half those of the clock signals $_{v1}$, $_{v2}$ and $_{v3}$ on leads 35-1 through 35-3.

For convenience, the zero time in FIG 6a through 6j is placed 15 base periods after the beginning of the abscissas of these curves. To transfer charge packets from the light-sensitive elements 32 (FIG 3) into the areas beneath electrodes 34-1, 34-7, 34-(n-1), in CCD shift register 34a, and beneath electrodes 34-2, 34-8, 34-n in CCD shift register 34b, the voltage labeled ϕ_p (FIG 3) is lowered to a minimum value (FIG 6a) during the base periods -14 to -5 (i.e. the electron energy potential is raised to a maximum level). During the base periods -15 to about -9, the ϕ_x signal on leads 33a and 33b (FIG 6b) is raised to its maximum voltage or minimum electron energy potential. From about -9 base period to -3 base period the voltage level of the ϕ_x signal drops back to its low value. From -14 base period to -4 base period the ϕ_{v1} signal on lead 35-1 goes to a maximum voltage (i.e. to an electron energy minimum) (FIG 6c). Therefore charge is transferred from the light-sensitive elements 32 through the semiconductor material beneath the gates 33-1, 33-2, 33-3, 34-4 etc. to regions of semiconductor material beneath electrodes 34-1, 34-7 etc. and 34-2, 34-8 etc. The $_{v2}$ and $_{v3}$ clock signals on leads 35-2 and 35-3 respectively are held as a miniumum voltage (maximum electron energy) (FIGS 6d, 6e) during the transfer of charges from the light sensitive areas 32 to the selected locations in the transport arrays 34a and 34b. At -4 base period, the $_{v2}$ signal voltage rises abruptly to a maximum level. At the same time the $_{v1}$ voltage begins to drop.

Therefore, the charge stored beneath, for example electrode 34-1 (FIG 3) is transferred to beneath electrode 34-3. The charge stored beneath electrode 34-7 is prevented from being transferred to beneath electrode 34-3 by the low voltage (i.e. high electron energy) of the ϕ_{v3} signal on lead 35-3. Simultaneously, therefore, the charge beneath electrode 34-7 is transferred to beneath electrode 34-9. At -2 base period, the voltage of the ϕ_{v3} signal rises abruptly to its maximum value and simultaneously the voltage of ϕ_{v2} begins to drop gradually to its minimum value. The voltage of the ϕ_{v1} signal is now at a minimum and remains at this minimum for two base periods. Thus charge is now transferred from, for example, beneath electrode 34-3 to beneath electrode 34-5. The charge continues to be transferred once every two base periods from beneath a given electrode 34-i to a region beneath the next following electrode 34-(i+2). Thus the charges transferred from light-sensitive elements 32 to beneath selected ones of electrodes 34 are now transferred along transport arrays 34a and 34b.

During the transfer of this charge along shift registers 34a and 34b, the voltage on transfer gates 33a and 33b is held at a low level (i.e. electron energy is held at a high level) to prevent charge being accumulated in elements 32 from being transferred into these analog shift registers. Thus, degradation of the signal due to additional radiation incident on the light-sensitive elements 32 is prevented.

It should be noted that transport arrays 34a and 34b are covered with an opaque material to prevent light incident on light-sensitive elements 32 from likewise falling on the depletion regions associated with transport arrays 34a and 34b and thereby generating additional charge which degrades the image detected by light-sensitive elements 32.

Note that while the charge is being transferred along registers 34a and 34b, charge is also being transferred along shift register 37. This charge, however, is transferred at twice the frequency as is the charge transferred along registers 34a and 34b with the result that a given charge packet is moved six electrodes along register 37 in the time necessary to move a charge packet three electrodes in registers 34a and 34b. In one embodiment register 37 is also a CCD shift register of the same type as shift registers 34a and 34b.

CCD shift register 37 is driven in such a manner that when packets of charge are located beneath electrodes 34-(n+9) and 34-(n+10) these charge packets will be transferred to beneath electrodes 37-1 and 37-4 in shift register 37. Thus as shown in FIG 6c, the voltage on electrodes 34-(n+9) and 34-(n+10), which are connected to lead 35-3 carrying the ϕ_{V3} signal is at a high level for the first two base periods and then drops to a low level for the third and fourth base periods. This voltage remains at a low level for the fifth and sixth base periods after which it rises abruptly to a high voltage level. During the third base period, the ϕ_{H3} signal is at a high voltage (i.e. minimum electron energy). It is during this third period that the voltage of the ϕ_{V1} signal on lead 35-1 begins to drop. Thus the charge stored beneath electrode 34-(n+9) transfers from beneath this electrode to beneath electrode 37-1. Simultaneously, and for the same reason, the charge beneath electrode 34-(n+10) is transferred to beneath electrode 37-4.

An analysis of FIGS 6f, 6g and 6h shows that the charge stored beneath electrode 37-1 and 37-4 is then transferred along shift register 37 in the same manner as are the charge packets transferred along shift registers 34a and 34b but at twice the frequency. By the time the next packets of charge are beneath electrodes 34-(n+9) and 34-(n+1 the charge packets formerly transferred from beneath these electrodes to beneath electrodes 37-1 and 37-4 have been transferred to diode 38 and have been or are being used to generate an output signal by devices 39 and 40.

Devices 39 and 40 comprise MOS transistors wherein the gate of MOS transistor 40 is connected to the cathode of diode 38 and the source of MOS transistor 39. The drain of transistor 39 is connected to a voltage source V_{DR}. Voltage sources V_{DR} is typically between 10 and 15 volts. MOS transistors 39 and 40 are n-channel devices with the n-channel, in one embodiment, being formed by ion implantation simultaneously with the formation of the n-type layer 14 (FIGS 1 and 2b). Transistor 39 is such that when its gate voltage, denoted ϕ_R, (FIG 6i) is high, transistor 19 is turned on, thereby charging reversed-biased diode 38 to approximately the voltage of V_{DR}. Upon dropping the gate voltage ϕ_R to approximately ground, transistor 39 turns off, thereby disconnecting voltage source V_{DR} from diode 38. Diode 38, however, acts as a capacitor and thus retains the charge placed on it by source V_{DR}. Upon transfer of a packet of charge from beneath electrode 37-7 to the N type region of diode 38, the voltage across this diode drops. The cathode of diode 38 is connected to the gate of n-channel MOS transistor 40. The drop in voltage on the cathode of diode 38 lowers the gate voltage on MOS transistor 40 thereby changing the conductivity of the n-channel between the source and drain of this transistor. Accordingly, the current flowing from voltage source V_D (particularly about 10 to 15 volts) to voltage source V_S is modulated by the amount of voltage drop across diode 38. Once each three base periods, diode 38 is recharged. Therefore, each charge packet transferred from beneath electrode 37-7 to the N type region (region 13, FIG 1) changes the voltage across diode 38 from its recharged value to some new value reflecting the magnitude of this charge. Accordingly, the change in current flowing through the channel of MOS transistor 40 (FIG 6j) is a measure of the detected signal.

The analog CCD shift registers 34a, 34b and 37 each can be constructed as shown in cross section in FIG 1. The channel stop region 31 (FIG 2) winds along the array of linear light-sensitive elements 32 separating each element 32-i in essence from the adjacent elements 32-(i-1) and 32-(i+1) and forcing the charge generated in a given element to travel in such a manner that it ends up beneath the proper electrode in shift registers 34a and 34b when the proper potentials are applied to electrode 36 (FIG 2a) and to the transfer gates 33a and 33b and the electrodes in shift registers 34a and 34b.

The charge packets can be transferred from the light-sensitive elements 32-1 through 32-K, where K is a selected positive integer representing the maximum number of light sensitive elements, 32 once each readout period of CCD analog shift registers 34a and 34b. By "readout period" is meant at least the time necessary for charge packets beneath electrodes 34-1 and 34-2 to reach the area beneath, for example, electrodes 34-(n+9) and 34-(n+10). Thus, transfer of additional charge into the CCD analog shift registers 34a and 34b from light sensitive elements 32 will not degrade or interfere with the charge packets previously detected and transferred.

FIGS 4 and 5 show other techniques for processing the charge packets ger[illegible]ed in light sensitive elements 32-1 through 32-K. In FIG 5 the CCD se[illegible] and registers 100 produce output charges which are detected by preamp 101. CCD sensors and registers 100 could be structures described above in conjunction with FIG 2 for example. The output signal from sensors and registers 100 is sent to preamp 101 which in one embodiment comprises diode 38 and transistors 39 and 40 shown in FIG 3. Preamp 101 is driven by a signal from reset clock 106. In addition, dummy preamp 102 is also driven by reset clock 106. Differential amplifier 103 then compares the output signals from preamp 101 and preamp 102 sensing the difference. Accordingly, the output signal from differential amplifier 103 has had the coherent noise resulting from clock 106 removed from this signal.

A sample and hold circuit 104 produces an output signal which is transmitted to a driver and dc level control circuit 105. The output signal from driver and dc level control 105 can be sent to monitor 107 if desired where the output signal can be used or evaluated.

FIG 4 shows an additional technique for reading out the charge signals transmitted along transfer arrays 34a and 34b. Rather than use an additional CCD shift register 37 as shown in FIG 3, the signals used to drive one transport array are delayed by a selected amount relative to the signals used to drive the other transport array. The ou[illegible] signals from the transport arrays are then transmitted directly to diodes 110 and 111 such as diode 13 (FIG 1) or diode 38 (FIG 3) and there used to change the voltage across these diodes. The diodes 110 and 111 are periodically recharged by current from source V_{DR} attached to the drain of MOS transistor 112. MOS transistor 112 is periodically gated by a signal R such as shown in FIG 6i. The cathodes of diodes 110 and 111 are connected to the gate of MOS transistor 113. Changes in the voltage across diodes 110 and 111 as a result of the receipt of a charge packet from either transport array changes the voltage of the gate on MOS transistor 113 and thus changes the current passed from the source to drain of this transistor. This change in current represents the magnitude of the particular charge packet changing the voltage on the particular one of diodes 110 and 111 and is used to generate an output signal.

This invention has the advantage that all the components and elements shown in FIG 3 can be formed on one monolithic chip of semiconductor material.

While this invention has been described as using three phase CCD analog shift registers for registers 34a, 34b and 37, two phase and even one phase register can also be used for these shift registers, if desired, CCD analog shift registers operating in the two phase mode are described in an article by R. H. Krambeck, R. H. Walden and K. A. Pickar, entitled "Implanted-Barrier Two-Phase Charge-Coupled Device", published in Applied Physics Letters, Vol. 19, No. 12, pp. 520-522, 1971.

While the structure of FIGS 2a and 3 shows one linear imaging array together with two transport arrays for receiving charge packets generated by light incident on said linear imaging array prior to the transfer of these charge packets to a processor, it should be understood that, if desired, only one such transport array need be used in conjunction with light sensing elements 32. Thus, for example, in FIG 2a, the structure shown there would be modified by removing, for example, transport array 34b. The serpentine channel stop region 31 would then be reformed such that the channel stop surrounds three sides of each light-sensing element 32-i but leaves open the left side of each element 32-i. The channel stop regions would extend beneath transfer gate 33a as required to ensure that the charge from each light sensing element 32-i was properly placed in the correct region of transport array 33a. One disadvantage of using only a single transport array in conjunction with one linear imaging array is that the density of light sensing elements 32-i per unit length is cut in half over that which is obtainable using two transport arrays as shown in FIGS 2a and 3.

One feature of this invention which yields an added flexibility in the design of linear imaging arrays is that the regions of the transport arrays 34a and 34b extend beyond the last element 32-K (FIG 3) of the linear imaging array. These extensions of transport arrays 34a and 34b can thus be bent in such a manner that they properly intersect with the utilization structure designed to receive the charge from arrays 34a and 34b. This utilization structure corresponds, for example, to shift register 37 shown in FIG 3.

THE EMBODIMENTS OF THE INVENTION IN WHICH AN EXCLUSIVE PROPERTY OR PRIVILEGE IS CLAIMED ARE DEFINED AS FOLLOWS:

1. A linear imaging array comprising: a line of light sensitive elements including a plurality of transparent electrodes formed on the top surface of a layer of insulation formed over a semiconductor material; a first CCD shift register located on one side of said light-sensitive elements; a second CCD shift register located on the other side of said light-sensitive elements, said shift registers being covered with an opaque material; means for transferring charge packets generated in said line of light-sensitive elements to appropriate positions in said first shift register and said second shift register; first means for shifting said charge packets along said first and second shift registers including means for driving said charge packets along said first shift register and said second shift register at a first selected frequency; means for receiving charge packets at the ends of said first and second shift registers including a third CCD shift register located at the ends of said first and second shift registers for receiving said charge packets from said first and second shift registers, and further including means for sensing the magnitudes of said charge packets; second means for shifting said charge packets along said third shift register at a second frequency, said second frequency being twice said first frequency and, output circuitry means at the output end of said third shift register for receiving said charge packets from said third shift register and for generating output signals in proportion thereto.

2. Structure as in claim 1 wherein said plurality of electrodes are interconnected to form one electrode overlying a plurality of light-sensitive regions in said semiconductor material.

3. Structure as in claim 1 wherein said semiconductor material is of one conductivity type and has formed in the top surface thereof a region of opposite conductivity type.

4. Structure as in claim 3 wherein said regions of opposite conductivity type extend through the regions of said first and second shift registers,

said means for transferring, and said line of light-sensitive elements.

5. Structure as in claim 3 wherein said one conductivity type is P type and said opposite conductivity type is N type.

6. Structure as in claim 5 wherein said semiconductor material is silicon.

7. Structure as in claim 6 wherein said insulation is an oxide of silicon.

8. Structure as in claim 6 wherein said electrodes comprise polycrystalline silicon doped with a selected impurity.

9. Structure as in claim 8 wherein said polycrystalline silicon electrodes are separated from adjacent electrodes by regions of resistive undoped polycrystalline silicon.

10. Structure as in claim 1 wherein said first, second and third shift registers comprise a plurality of electrodes formed on an insulating layer overlying semiconductor material of one conductivity type.

11. Structure as in claim 10 wherein said semiconductor material is of one conductivity type and has formed in one surface adjacent and underlying said insulation, regions of opposite conductivity type.

12. Structure as in claim 11 wherein said region of one conductivity type is of P type conductivity and said region of opposite conductivity type is of N type conductivity.

13. Structure as in claim 10 wherein said electrodes in said first, second and third shift registers are selectively doped regions of polycrystalline silicon.

14. Structure as in claim 13 wherein said electrodes in each of said first, second and third shift registers are separated by regions of undoped polycrystalline silicon.

15. Structure as in claim 1 wherein said light-sensitive elements are separated from adjacent light-sensitive elements by a heavily doped channel stop region formed in the top surface of semiconductor material, said heavily doped channel stop regions surrounding each light-sensitive element on three sides such that the every other light-sensitive element has open to one of said first and second shift registers a side on which there is no channel stop region.

16. Structure as in claim 15 wherein said channel stop region includes a plurality of selectively shaped extensions thereof for ensuring that said charge packets are transferred from said line of light-sensitive elements to the appropriate locations in said first and second shift registers.

H-50

1020656
4-1

FIG.1

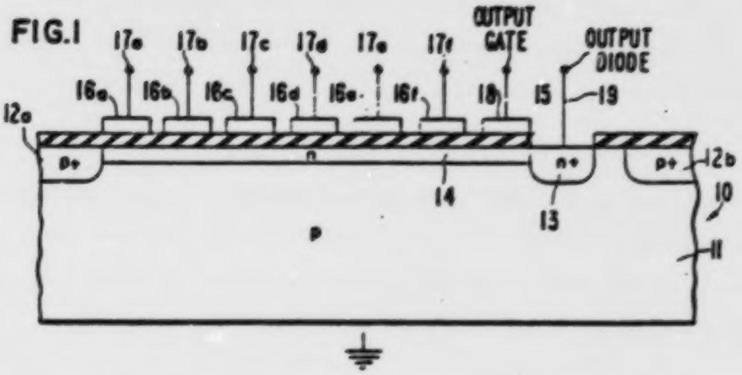
17a
17b
17c
17d
17e
17f
OUTPUT GATE
OUTPUT DIODE
16a
16b
16c
16d
16e
16f
18
15
19
12a
p+
n
n+
p+
12b
14
13
10
p
11

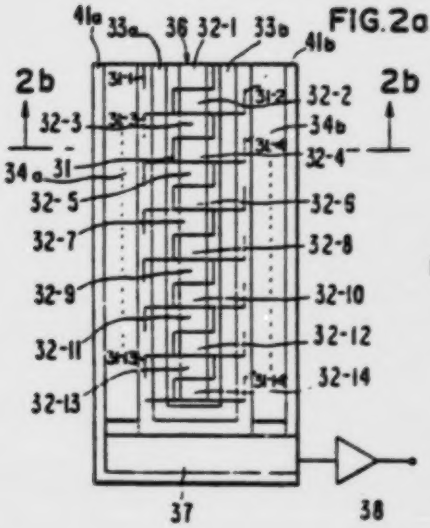
41a
33a
36
32-1
33b
41b
2b
2b
31-1
31-2
32-2
32-3
31-3
34b
31-4
32-4
31
34a
32-5
32-6
32-7
32-8
32-9
32-10
32-11
32-12
31-13
32-13
31-14
32-14
37
38

FIG.2a

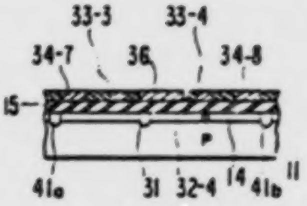
33-3
33-4
34-7
36
34-8
15
p
41a
31
32-4
14
41b
11

FIG.2b

H·5

1020056

4-2

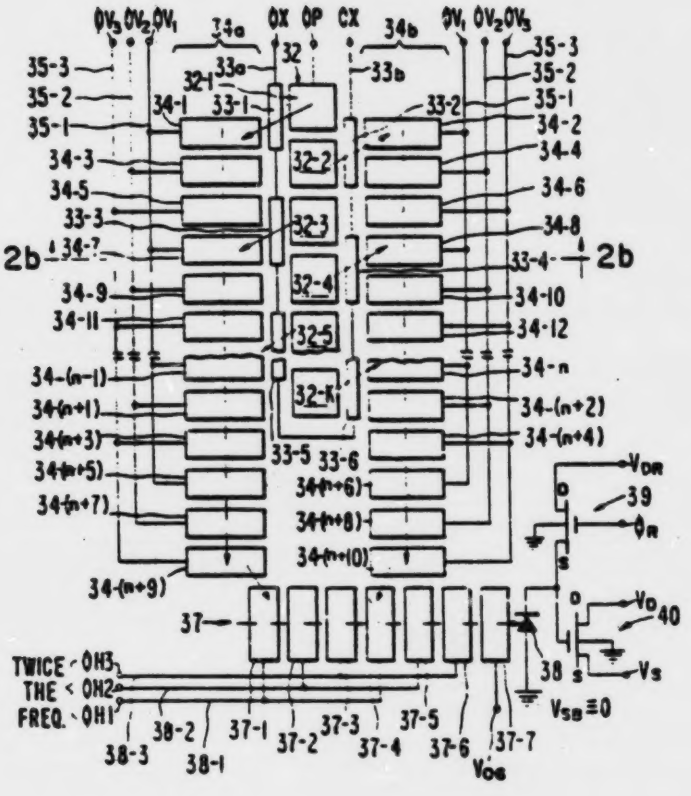

ØV3 ØV2 ØV1
34a
ØX ØP CX
34b
ØV1 ØV2 ØV3
35-3
35-2
35-1
32-1
33a
32
33b
33-1
33-2
34-1
34-2
34-3
34-4
32-2
34-5
34-6
33-3
32-3
34-8
2b
34-7
33-4
2b
32-4
34-9
34-10
34-11
32-5
34-12
34-(n-1)
34-n
32-K
34-(n+1)
34-(n+2)
34-(n+3)
34-(n+4)
33-5
33-6
34-(n+5)
34-(n+6)
VDR
39
D
ØR
34-(n+7)
34-(n+8)
34-(n+10)
S
34-(n+9)
D
VD
40
37
38
S
VS
TWICE
THE
FREQ.
ØH3
ØH2
ØH1
VSB=0
38-3
38-2
38-1
37-1
37-2
37-3
37-4
37-5
37-6
37-7
VOG

FIG. 3

1020656

4-3

H-21

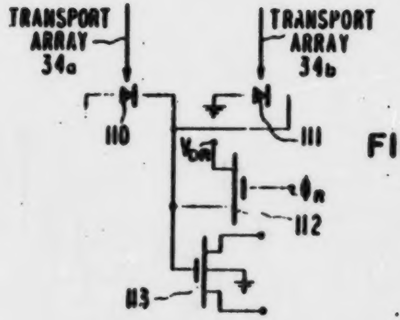
TRANSPORT ARRAY 34a
TRANSPORT ARRAY 34b
110
111
V_{DR}
ϕ_R
112
113

FIG. 4

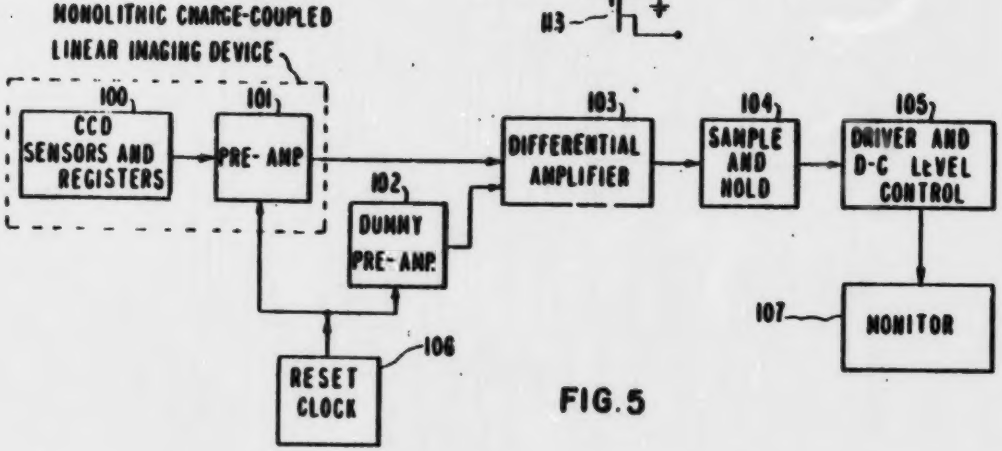
MONOLITHIC CHARGE-COUPLED LINEAR IMAGING DEVICE
100
CCD SENSORS AND REGISTERS
101
PRE-AMP
102
DUMMY PRE-AMP.
103
DIFFERENTIAL AMPLIFIER
104
SAMPLE AND HOLD
105
DRIVER AND D-C LEVEL CONTROL
106
RESET CLOCK
107
MONITOR

FIG. 5

H-2

1C20656

4-4

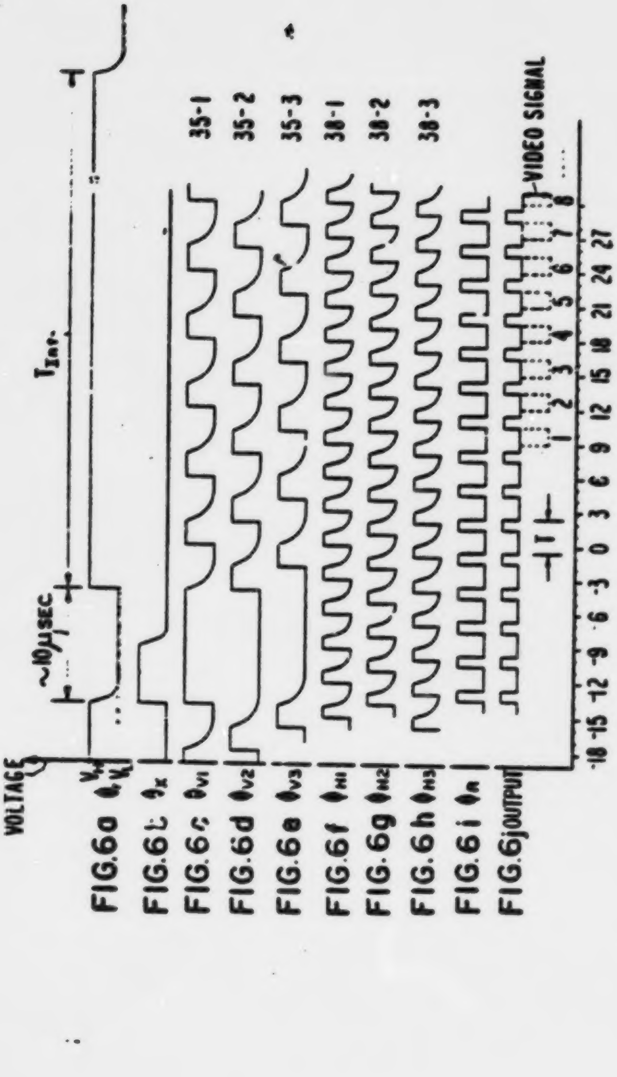
VOLTAGE
V_H
V_L
ϕ
ϕ_x
ϕ_{V1}
ϕ_{V2}
ϕ_{V3}
ϕ_{H1}
ϕ_{H2}
ϕ_{H3}
ϕ_R
OUTPUT
~10μSEC
$T_{INT.}$
35-1
35-2
35-3
38-1
38-2
38-3
VIDEO SIGNAL
1 2 3 4 5 6 7 8
T
-18 -15 -12 -9 -6 -3 0 3 6 9 12 15 18 21 24 27

FIG.6a

FIG.6b

FIG.6c

FIG.6d

FIG.6e

FIG.6f

FIG.6g

FIG.6h

FIG.6i

FIG.6j

H-51

(11) (A) No. 1101113

(45) ISSUED 810512

(52) CLASS 345-15
C.R. CL. 350-15

(51) INT. CL.^{2} H04N 1/12

(19) (CA) CANADIAN PATENT (12)

(54) DOCUMENT SCANNING HEAD

(72) Parsons, Robert R.;
Wei, John S.S.,
Canada

(73) Granted to Northern Telecom Limited
Canada

(21) APPLICATION No. 304,934

(22) FILED 780607

No. OF CLAIMS 14

DISTRIBUTED BY THE PATENT OFFICE, OTTAWA
CCA-274 [illegible]

H-4c

This invention relates to a scanning device for scanning documents and extends to a method of using such a scanning device, for example, in connection with facsimile systems.

In scanning documents, it is often necessary to use a lens system to produce a small image of a page being scanned. The reason is that photodetectors usually are only obtainable in small sizes. To make many photodetector elements, device characteristics are more controllable if the detector array has restricted dimensions. However, as finer optical resolution becomes necessary, a larger number of detector elements must be accommodated on a single chip. For example, a charge coupled device (CCD) imager may have 1728 elements on a 1" chip. Small defects in the material or in the photomasks can easily incapacitate the entire CCD array.

The scanning device of the present invention obviates the lens system and produces a structure in which spacing between photodetector elements is relatively large thereby enabling reduced tolerances in fabrication.

According to one aspect of the invention there is provided a scanning device suitable for use in scanning documents, said device comprising a substrate of semiconductor material having a plurality of apertures therethrough, photodetector means formed in the semiconductor material and presenting active surfaces at the boundaries of the apertures, said semiconductor material being so contoured at the boundaries that the photodetector means are substantially shielded from direct incidence of light directed into the apertures from one side of the semiconductor material and intercept a substantial portion of light directed into the apertures from the other side of the semiconductor material.

The photodetector means can comprise photosensitive junctions between n and p type layers of the semiconductor material, and the semiconductor material can be stepped over at least a part of the boundaries of the apertures so that one of the n and p type layers overhangs the other layer.

The apertures are preferably rectangular, the photodetector means at the boundary of each aperture comprising an element, the elements being arrayed in a regular rectangular matrix.

In typical embodiments of the invention the spatial density of the elements ranges from 50/sq.in., to 200/sq.in.

The preferred semiconductor materials are silicon or gallium arsenide especially such materials having crystallographic orientations permitting V-sectioned apertures to be readily etched in the material, since, in a preferred structure, at least a part of the boundaries of the apertures taper inwardly from an outer face of the semiconductor material to the junction between the n and p type layers.

The tapered parts bounding the overhanging layer should be covered with an opaque, non-reflecting coating so that light directed into the apertures is not reflected therefrom. The surface at the other side of the substrate should have a protected layer of, for example, oxide. In use a document to be scanned by the scanning device is held against the surface at the other side of the substrate and the document and the scanning device are slid relative to one another so the protected layer prevents deterioration of the p or n type layer at said other side of the substrate.

The scanning device can include electrical conducting regions formed in the semiconductor material for connecting the photosensitive junctions to sensing circuits. Preferably an addressing circuit is provided for cyclically addressing the sensing circuits.

An embodiment of the invention will now be described by way of example with references to the accompanying drawings, in which:-

Figure 1 is a cross-sectional view of an element of a scanning device according to the invention;

Figure 2 is a perspective view showing a plurality of such elements;

Figure 3 is a circuit diagram showing sensing circuitry and part of addressing circuitry for cyclically sensing elements of the scanning device; and

Figures 4 and 5 show bottom and top surfaces of a part of the scanning device.

Referring to the drawings in detail, figure 1 shows a semiconductor substrate 1 for example silicon, which is doped to have n-type conductivity throughout. Afterwards, one surface of the substrate is doped to have p-type conductivity, shown as layers 3 and 5 in figure 1. With the appropriate electrical voltages applied to the n and p sides of the substrate, a photodiode or a photosensitive junction exists between the two layers at locations exemplified by 11 and 12. With light incident on 11, current flows between regions 4 and 5. This current is detected by a sensing circuit connected to the regions 4 and 5.

In use, the photosensitive junctions 11 and 12 function as sensors of a document reader. A document 13, is placed in intimate contact with a protected layer of, for example, silicon oxide thermally grown on the layer 5. The document is illuminated through an aperture 7 etched in the substrate 1.

H-20

By choosing a substrate with the proper crystallographic orientation, V-shaped apertures can be etched with excellent definition. In figure 1, V-shaped apertures are fashioned on both sides of the junctions 11 and 12. The shape and slope of the apertures are arbitrary although the V-section is preferred. It is important, however, that the aperture in the region of layers 3 and 5 be wider than that in the region of layers 2 and 4. Thus the photosensitive junctions 11 and 12 are shielded from the direct incidence of light coming from a source 8. Also, sides 9 and 10 of the aperture are coated with an opaque film to avoid generating reflections from the sides which may be incident directly on the photosensitive junctions. Because of the narrow aperture 7, only a small region of the document 13 is illuminated. Light reflected from the document falls on junctions 11 and 12. The size of the detected signal depends directly on the amount of light reflected. A dark printed spot on a white document, for instance, would reflect little light compared to that from the white background. By moving either the document 13 or the scanning device, it is possible to reconstruct a pattern on the document from detected signals.

Referring to the perspective view of figure 2, the apertures 7 which are in the form of windows isolate strips 14 and 15 of the p-type layer from one another. The array of apertures 7 and the p-type regions such as 14 and 15 are fabricated on a single substrate of semiconductor material. A window 17 is also etched through the protective layer 6. A strip of conducting material 18 makes electrical contact with the p-type region 14. The conducting strip 18 is used to electrically connect together photosensors on either side of the aperture 7 as described with reference to figure 5. Conducting strips similar to 18 are used

H 4

also on the substrate for connection to the sensing and addressing circuitry.

In order to detect the light induced signals, a column and a row electrical addressing circuit is used as shown in figure 3. A p-type region, such as 14 in figure 2, together with the associated photosensitive junction 11, is symbolized as 20 in the figure 3. Region 19 and its photosensitive junction are shown as 20a in figure 3. In an electrical addressing scheme used, 20 and 20a are labelled (1,1) and (1,2) respectively. The column label is the first number in the bracket and the row label the second. When a column 1 terminal, 25, is pulsed to a positive voltage, for example 5 volts, devices 20 and 20a are properly biased to collect current generated by incident light. The current from (1,1) is AC coupled through a capacitor 27 to an amplifier 29 and resistor 28, resulting in an output signal at a terminal 30. The light induced signal from (1,2), on the other hand, appears at terminal 34, after similar amplification. When terminal 25 is pulsed positive, terminals 26, 35, 36, etc. are held at zero voltage by a timing circuit (not shown). Thus only the photosensitivities of elements (1,1) and (1,2) are enhanced. Thus signals from a particular column are identified by pulsing only that column positive while holding all the rest at zero voltage. Interconnecting lines such as 23 and 24 are fabricated on the substrate. Therefore, instead of lines addressing the elements individually, a considerably small number of external connections suffices. In practice, each column has more than two elements shown in figure 3. For example, 1600 photosensitive elements can be connected in a 40 column by 40 row matrix. Only 80 external connections need be made, 40 for column terminals such as 25 in figure 3, and 40 for outputs such as 33 in figure 3. In the circuit of figure 3,

H-45

lines 23 and 24 are held at AC ground by action of the amplifier 29. Because of the photosensor characteristics of elements such as 20, little current can flow when the column terminal, for example, 25 is held at ground. Capacitor 27 is used to block leakage current through the photosensitive junctions in the absence of light; with low leakage, the capacitor can be dispensed with.

An exemplary pattern of electrical connections to the photosensitive sides 11 and 12 is shown in detail in figures 4 and 5. The substrate 1 is heavily doped n type so that regions such as 2 and 4 shown in figure 1 as the bottom of the substrate are sufficiently conducting. Detectors 14 and 19 shown in the top elevation of figure 5 can be connected in parallel by a block contact 37 at the bottom of the substrate as shown in figure 4. The contact 37 corresponds to the column terminal 25 in figure 3. If the substrate is thick compared to the spacing between photosensors, a voltage applied to 37 may affect other photosensors in parallel with 14 and 19. A zig-zag type of detector arrangement can be used to solve this problem. Thus as shown in figure 4, the second column connection 38 is made on the side opposite to 37, across the line of apertures 39. The connection 38 would correspond to column terminal 26 in figure 3. In effect, only half the available photosensors are in use. The two sensors between (1,2) and (3,1), for example, are not used. This redundancy alleviates problems in manufacturing yield; only half the photosensors have to function. The row connections are shown in figure 5. Element (1,1) is connected to element (2,1) by a conducting strip 18 shown in part in figure 1. A similar strip connects (1,2), (2,2) and (3,2).

In a typical embodiment of the invention the spatial density of apertures is of the order of 200/sq.in., the area of the apertures is of the order of 25 sq.mm. and the area of the photosensitive junctions at each aperture is also of the order of 25 sq.mm.

H40

THE EMBODIMENTS OF THE INVENTION IN WHICH AN EXCLUSIVE PROPERTY OR PRIVILEGE IS CLAIMED ARE DEFINED AS FOLLOWS:-

1. A scanning device suitable for use in scanning documents, said device comprising a substrate of semiconductor material having a plurality of apertures therethrough, photodetector means formed in the semiconductor material and presenting active surfaces at the boundaries of the apertures, said semiconductor material being so contoured at the boundaries of the apertures that the photodetector means are substantially shielded from direct incidence of light directed into the apertures from one side of the semiconductor material and intercept a substantial portion of light directed into the apertures from the other side of the semiconductor material.

2. A scanning device as claimed in claim 1, wherein the photodetector means comprises photosensitive junctions formed between n and p type layers of the semiconductor material, and the semiconductor material is stepped over at least a part of the boundaries of the apertures so that one of the n and p type layers overhangs the other layer.

3. A scanning device as claimed in claim 1, wherein the apertures are rectangular, the photodetector means at the boundary of each aperture comprising an element, the elements being arrayed in a regular rectangular matrix.

4. A scanning device as claimed in claim 3, wherein the spatial density of elements ranges from 50/sq.in. to 200/sq. in.

5. A scanning device as claimed in claim 1, wherein the semiconductor material is either silicon or gallium arsenide.

6. A scanning device as claimed in claim 2, wherein at least a part of the boundaries of the apertures taper inwardly from outer faces of the semiconductor material to the junction between the p and n type layers.

7. A scanning device as claimed in claim 6, wherein at least part of the tapered boundaries follow natural crystallographic planes of the semiconductor material.

8. A scanning device as claimed in claim 6, wherein the tapered parts bounding the overhanging layer have an opaque coating.

9. A scanning device as claimed in claim 6, wherein an outer face of the semiconductor material at said other side thereof has a ~~protected~~ protective oxide layer.

10. A scanning device as claimed in claim 2, wherein electrically conducting regions on said semiconductor material connect said photosensitive junctions to respective sensing circuits.

11. A scanning device as claimed in claim 10, wherein electrically conducting regions also extend between adjacent pairs of photosensitive junctions so that the conducting state of a plurality of photosensitive junctions can be sensed together.

12. A scanning device as claimed in claim ~~12~~ 10, and also including an addressing circuit to cyclically operate the sensing circuits.

16

H-4c

13. A scanning device as claimed in claim 1, further including means for locating a document against the outer face of the semiconductor material at said other side thereof and means for moving the document and the scanning device relative to one another.

14. A method of using a scanning device having a substrate of semiconductor material, a plurality of apertures therethrough, photodetector means formed in the semiconductor material and presenting active surfaces at the boundaries of the apertures, the semiconductor material being so contoured at the boundaries of the apertures that the photodetector means are substantially shielded from direct incidence of light directed into the apertures from one side of the semiconductor material and intercept a substantial portion of light directed into the apertures from the other side of the semiconductor material, electrically conducting regions on said semiconductor material connecting said photosensitive junctions to respective sensing circuits to sense the condition of said photosensitive junctions, and an addressing circuit to cyclically address the sensing circuits, said method comprising:

locating a document to be scanned against an outer surface of the semiconductor material at said other side thereof;

directing light through the apertures in the semiconductor material to illuminate areas of the document; and

simultaneously with operating the addressing circuit to cyclically address the sensing circuits, sliding the document and the scanning device relative to one another at a velocity commensurate with the cyclic operation of the addressing circuit.

*

P.

H-217

1101113
2-1

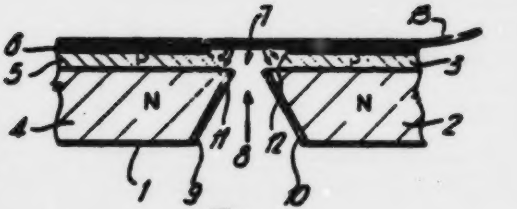
7
13
6
5
3
N
N
4
2
11
12
8
1
9
10

-Fig-1-

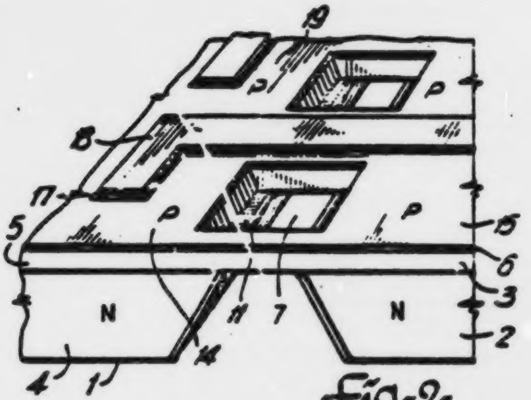
19
P
P
18
17
P
P
5
15
6
3
N
N
11
7
2
4
1
14

-Fig-2-

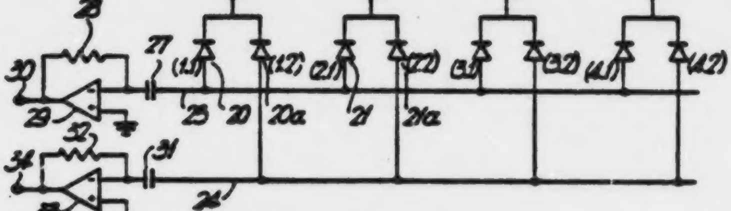
25
26
35
36
28
27
(11)
(12)
(21)
(22)
(31)
(32)
(41)
(42)
30
29
23
20
20a
21
21a
32
31
34
33
24

-Fig-3-

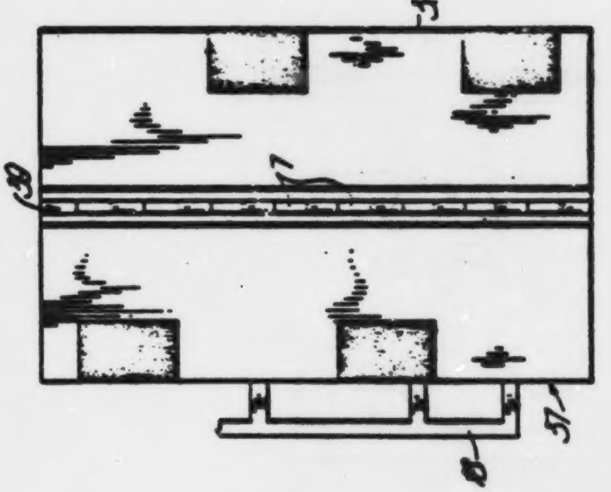

Fig-4-

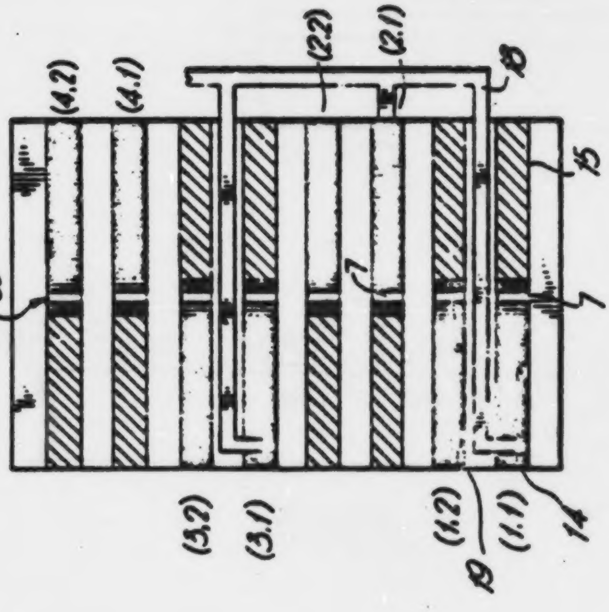
(4.2)
(4.1)
(2.2)
(2.1)
18
30
7
7
15
(3.2)
(3.1)
(1.2)
(1.1)
19
14

Fig-5-

(11) (A) No. 1101973

(45) ISSUED 810526

(52) CLASS 345-1

(51) INT. CL. ^{2} H01L 31/14

(19) (CA) CANADIAN PATENT (12)

(54) PHOTOCONDUCTOR DEVICE FOR IMAGING A LINEAR OBJECT

(72) Koo, Steven;
Baraff, David R.,
Canada

(73) Granted to Northern Telecom Limited
Canada

(21) APPLICATION No. 312,090

(22) FILED 780926

No. OF CLAIMS 4

DISTRIBUTED BY THE PATENT OFFICE OTTAWA
CCA-274 (3-80)

H-5

1101973

This invention relates to a photoconductor device for imaging a linear object and is particularly applicable to line imaging in such applications as facsimile read and print systems.

Conventionally, in a reading, or imaging device, the object is imaged onto a detector array such as a charge-coupled device (CCD) array. Such systems are expensive.

The present invention provides a device which is much cheaper to produce. The device comprises a linear photo-conductive member and associated conductors and connectors arranged as a matrix, in rows and columns. The photoconductive member can be a continuous bar of photoconductive material, or a plurality of closely spaced separate elements of photoconductive elements. A detector circuit is associated with the device.

The invention will be readily understood by the following description of certain embodiments, by way of example, in conjunction with the accompanying drawings, in which:-

Figure 1 is a diagrammatic plan view of part of an array;

Figure 2 is a plan view of one form of photoconductive member and associated conductor patterns;

Figure 3 is a typical cross-section to a greatly enlarged scale, on the line III-III of Figure 2·

Figure 1 illustrates, very diagrammatically, a section of a device or array. A plurality of photoconductive elements 10a to 10n extend in a line. To one side are made connections via connectors 11, which are arranged in columns, in the present example three connectors 11 forming a column. To each column is connected a conductor 12a, 12b and 12c. On the other side of the line of elements 10 are connectors 13. In the example illustrated the connectors 13 are connected to conductors 14a, 14b and 14c in rows, three elements 10 to each row.

As stated, Figure 1 is a section of a device and normally many more elements 10 would be provided. For example, for reading of a line of print on a page there would be 1600 elements assuming a line 8" long and a resolution of 200 lines per inch. These would be connected, via connectors 11 and 13 and conductors 12 and 14 as a 40x40 matrix, that is 40 rows and 40 columns. Each row would connect to 40 elements and each column would connect to 40 elements.

While the elements 10 are shown as separate from each other in Figure 1, the elements are preferably formed as a continuous bar, as indicated by the dotted lines 15. The continuous bar may be scribed, as by a laser, to reduce the thickness of the bar between elements.

A device can operate as follows. Column 12a would be taken to voltage V, typically 20V. columns 12b, 12c--------12n would be grounded. A detector circuit would look at the currents flowing through the elements 10a, 10b and 10c. Typical currents would be 2.0ma (10K) in the on state to 0.2ma (100K) in the off state, the on and off states depending upon whether or not light impinged on the elements. Thus by sequentially "looking" at the elements it would be possible to produce signals, indicative of the on or off state of an element, thus indicative of a light or dark spot on the line being read or scanned and these signals can then be transmitted to a printer.

Some indication of the sensitivity and accuracy of the system is as follows. Typical print reflectivities exhibit contrast ratios of 10:1, although in the case of poor print it may be as low as 5:1. The resistivity is approximately inversely proportional to light power and will also be in the ratio of 5:1 in the poor print example. Thus on white prints the resistance will be near 10,000 ohms and on dark prints the resistivity will be near 50,000 ohms. As a worst case analysis, with column 12a raised to 20V and the remaining columns grounded, a detector on elements 10a, 10b and 10c must sense the difference between 2.0 ma for a white area flowing to virtual ground and 0.4 ma for a black area flowing to vertical ground.

Possible parallel paths place as little as 250 ohms (10,000/40) or as high as 1250 ohms in parallel with the detection impedance which therefore should be below 25 ohms to reduce signal shift to below 10%. The voltage signal generated across 25 ohms by 2.0ma is 50mV and the signal generated by 0.4ma across 25 ohms is 10 mV. This gives an effective on signal to off signal of 5:1. The 50mV to 10mV swing is in the range where good signal to noise ratio is possible.

Figure 2 illustrates one form of arrangement for the linear photoconductive member and conductor patterns associated therewith. The photoconductive member or bar is indicated at 20. At one side of the bar 20 extends a pattern of closely spaced electrical connectors 21, the connectors 21 being parallel and extending from beneath the bar 20 and being connected in columns or blocks to contact pads 22a to 22n. The connectors 21 correspond to connectors 11 of Figure 1 while the contact pads 22a-22n correspond to the conductors 12a-12c and so on of Figure 1.

On the other side of the bar 21 is a pattern comprising a plurality of parallel transverse electrical conductors 23a to 23n extending as rows across the substrate 24. From the conductors 23 extend electrical connectors 25. A connector 25 connects between each conductor 23 to the bar 20, the connector connecting to the bar in opposition to a connector 21. The connectors from a particular conductor 23 are spaced apart so that each connector 25 is connected to the bar opposite a connector 21 from a different contact pad 22. Thus, for example, assuming that twenty connectors 21 extend from each contact pad 22, the first conductor 23a is connected to the bar 20 by connectors 25 which are opposed to the first connector 21, then the twenty-first, forty-first and so. The next conductor 23b is connected to the second connector 21, the twenty-second, the forty-second and so on. This continues for each conductor 23. By this arrangement, by selection of a particular contact pad 22 and a particular conductor 23, an unique position on the bar 20 can be connected to a circuit. Contact pads 26 are provided at alternate ends of the conductors 23. In one method of forming the conductor patterns, the conductors 23 are formed on the substrate 24, a layer of electrically insulating material formed over the conductors and then the connectors 25 formed. Electrical connection is provided between connectors 25 and conductors 23 through vias formed in the insulating layer, the vias indicated at 27.

Figure 3 illustrates to a larger scale a typical cross-section through the bar 20, connectors 21 and 25, conductors 23 and contact pads 22. Also shown in Figure 3 is insulating layer 28, between connectors 25 and conductors 23.

In use as a detector or reading head, the device is connected via leads from the contact pads 22 and 26 to drive circuitry. The drive circuitry can be of conventional form and effectively connects each pad 22 to a particular potential and then sequencially connects each pad 26 to, for example, a unity gain switch, the switches connected to a level detection circuit. Light falling on the bar makes it conductive. Thus if a line of print is imaged on the bar 20, each picture element will be either photoconductive or non-conductive, depending upon whether the related portion of the image is white or black. By stepping connections to pads 22a-22n, and to pads 26, the whole bar can be scanned to produce a pattern of output pulses from the detector circuit indicative of white (or light) picture elements.

A particular process for producing a device as in Figures 2 and 3 is as follows. The electrical connectors 21 and 25 are formed by thin film techniques, either by first forming a patterned mask on the substrate 24 and then forming the conductors. Alternatively the substrate can be covered with the connector material and then the material photolithographically etched to produce the connectors. The layer of insulating material 28 is applied and then the through connection vias prepared. Conductors 23 are then formed by deposition through a mask, or by a layer which is photolithographically etched to produce the desired pattern. Conductors 23 can be thin film form. Again, as an alternative, the conductors 23 can be deposited by thick film techniques. Finally the photoconductive material forming the bar 20 is deposited. This can again be thin film techniques.

Instead of forming the insulating layer over the entire pattern of connectors 23, the layer can be in sections, the edge of a section inclined from the bar 20, to define the particular position on each connector 25 at which the conductor

H-51

make contact with the particular connector. The conductors 23 could be formed first on the substrate 24, then the areas of insulating layer formed and then the connectors 25 formed.

One example of material for the bar 20 is cadmium selenide, and a further example is cadmium sulphide. The conductors and connectors can conveniently be of a three part layer; a first layer of titanium for good adhesion to the substrate, a second layer of palladium which gives good adhesion to the titanium and provides good adhesion for the third layer of gold. The three layers can be formed by evaporation.

The contact between the connectors and bar would normally be ohmic contacts with the materials described, but by appropriate choice of metal to semiconductor (bar) contacts, rectifying junctions can be provided. Such junctions would minimize any loop current problem in the detection circuitry. An example of a rectifying junction contact is a sandwich structure, with the photoconductor, for example, of cadmium sulphide contained between an Indium (metal) contact and tin oxide (semiconductor).

THE EMBODIMENTS OF THE INVENTION IN WHICH AN EXCLUSIVE PROPERTY OR PRIVILEGE IS CLAIMED ARE DEFINED AS FOLLOWS:-

1. A photoconductor device for imaging a linear object, said photoconductor device comprising:-

an insulating substrate;

an elongate bar of photoconductive material;

a first plurality of parallel closely-packed equispaced thin film conductors extending from the bar in a first direction and having end contact regions overlain by one side edge of the bar;

a second plurality of parallel, closely-packed, equispaced thin film conductors extending from the bar in a direction opposite to said first direction and having end contact regions overlain by the opposite side edge of the bar, the end contact regions of said first plurality of conductors being opposed to respective end contact regions of said second plurality of conductors whereby to produce a series of spaced pairs of contact regions extending, equispaced, along the photoconductive bar and wherein the junction between the bar and one contact region of each pair is an ohmic contact and the junction between the bar and the other contact region of each pair is a rectifying junction.

2. A photoconductive device as claimed in claim 1, in which said second plurality of conductors is overlain with an insulating layer and the common terminals to which said second plurality of conductors are connected extend along at least said one side of the substrate, each such terminal being connected to

APPENDIX I

INTERVIEW GUIDELINE

INTERVIEW GUIDE

X-RAY DIFFRACTOMETER

1. DO YOU CURRENTLY CONDUCT RESIDUAL STRESS MEASUREMENTS?

YES ____ NO ____ DO YOU SEE ANY FUTURE NEEDS? IF NOT, WHY NOT? ____

2. ARE THE MEASUREMENTS PERFORMED:

__ IN-HOUSE __ OUTSIDE

WHICH DEPT ____ WHAT FIRM ____

3. HOW ARE THE RESULTS USED? ____

4. DESCRIBE THE APPLICATION:

Type of component or structure ____
Materials tested ____
Location (lab, field, plant, etc) ____
Environment: Dust ____
Corrosive ____
Contaminants ____
Temperature ____
Other ____
Frequency of measurements ____
Size of area to be scanned ____

Other comments ____

5. DISCUSS DESIRED FEATURES OF THE DIFFRACTOMETER. INDICATE IF IT IS A NECESSITY OR JUST DESIRED.

Physical Size: smallest opening ____________________
weight ____________________
____
degree of portability: none ____________________
minimum ____________________
wheeled on shop floor ____________________
transported by vehicle ____________________
maximum ____________________

Method of mounting: directly on specimen ____________________
head mounted on boom ____________________

Resolution (mm) ____________________

Accuracy (Kpsi) ____________________
____

Power source (if used in field): Battery pack ____________________
Other ____________________

Length of control cable ____________________

Ease of use: Who operates unit ____________________
definition ____________________
____
____

Degree of operator control: High (complete with keyboard) ____________________
Partial ____________________
Function specific panel ____________________
Minimum (specific controls) ____________________

Output: immediate ____________ stored ____________
on video ____________ floppy disk ____________
graphic ____________ internal ____________
numeric ____________

After sales: training ____________________
____
service ____________________
____
warranty ____________________
____

Other Comments ____________________
____
____
____
____

- 6. WILL YOU BE PURCHASING AN X-RAY DIFFRACTOMETER?
  WHEN ______
  HOW MANY ______

7. WHAT ARE YOUR MOST IMPORTANT PURCHASING CRITERIA?
(features, specifications, price, etc)

8. DESCRIBE THE PURCHASING NETWORK FOR A DIFFRACTOMETER.

OTHER COMMENTS ______

APPENDIX J

CANMET PORTABLE STRESS DIFFRACTOMETER

J-1

CANMET

PORTABLE STRESS DIFFRACTOMETER

REAL TIME DATA ACQUISITION & ANALYSIS OF STRESSES IN METALS THROUGH X-RAY DIFFRACTION

- Non Destructive Direct Reading Of Stress
- Computer Automated System
- Permanent Data Record
- Simple Calibration
- Error Compensating Accuracy ± 2 KPSI

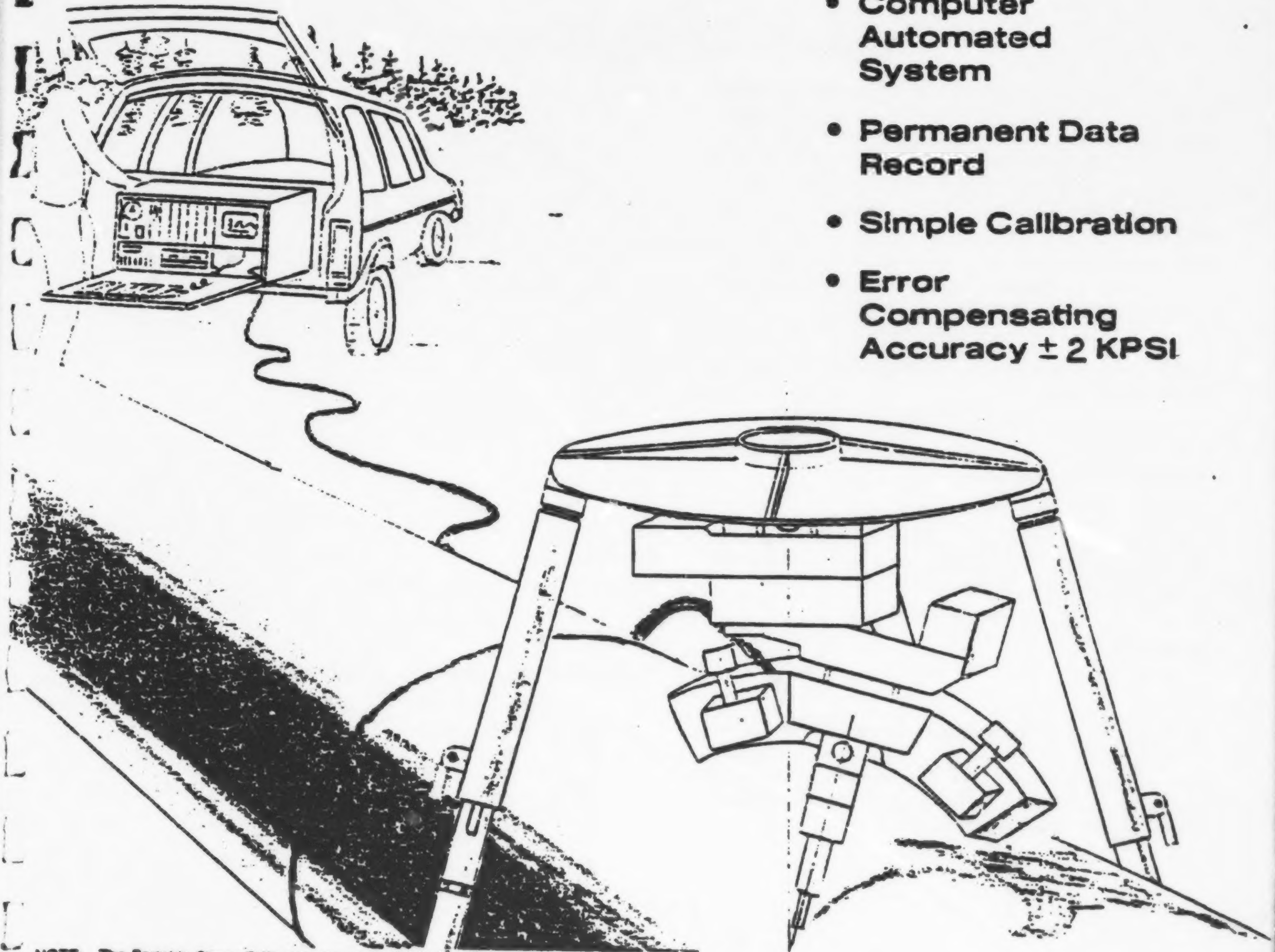

NOTE: The Portable Stress Diffractometer described within is presently under development and exists only as a working prototype.

FUNCTIONAL SPECIFICATIONS

The CANMET portable X-ray diffractometer is designed to measure stresses in engineering structures of all kinds on site and in the field. The instrument uses dual position sensitive detectors for determining surface stresses in real time from the relative displacement of two X-ray diffraction lines.

The X-ray tube scans, rotating about the irradiated point on the specimen surface, to ensure uniform sampling and to measure line displacement precisely even in specimens having a large grain size.

The diffractometer can rotate through 360° on an axis normal to the specimen surface, permitting the surface stress to be measured for any orientation, and enabling the principal stresses to be determined.

An omega rotation of the diffractometer head is provided giving a range of the specimen direction angle from −45° to +45°.

Two translation axes at right angles, parallel to the specimen surface enable the instrument to follow a stress gradient in any direction in the specimen surface. For rapidly changing stress the beam width can be reduced to 1 mm.

X-ray diffraction line broadening occurs with lattice deformation and with fine sub grain size. In addition to the stress, the scattering distribution width of the X-ray reflection can also be output. This parameter is a measure of the deformation in the strained atomic lattice.

The diffractometer is connected by a 20′ umbilical cord to a high tension supply and to the dual detector electronic circuits. A microcomputer, remotely located, controls and operates the diffractometer, collects and analyses the X-ray diffraction data, providing stress measurement in real time.

THEORY OF OPERATION

In an isotropic material the surface stress in a given direction can be determined from lattice strain measurements in two directions in the material. In the dual detector diffractometer the two directions lie in the plane of scanning. The diffractometer is oriented so that the normal to the stress direction lies at an angle χ, to the incident X-ray beam.

The lattice spacing, d, for crystal planes can be determined from the X-ray wavelength, and the back reflection diffraction angle, $\varnothing$, using Bragg's relation,

$$d = \lambda/(2 \cdot \cos(\varnothing/2)$$

The lattice strain ϵ is given by the displacement δ ($\varnothing/2$) of the diffraction line:

$$\epsilon = \tan(\varnothing/2 \cdot \delta\,(\varnothing/2)$$

The surface stress τ is determined from strain in two directions in the material as,

$$\tau = E \cdot (\epsilon_1 - \epsilon_2) / (K_1 - K_2)$$

where E is Young's Modulus and ν is Poisson's ratio. The term K_i is determined from the tilt α_i of the diffracting plane to the surface normal as:

$$K_i = \sin^2(\alpha_i) - \nu \cdot (\cos^2(\alpha_i))$$

where i = 1,2

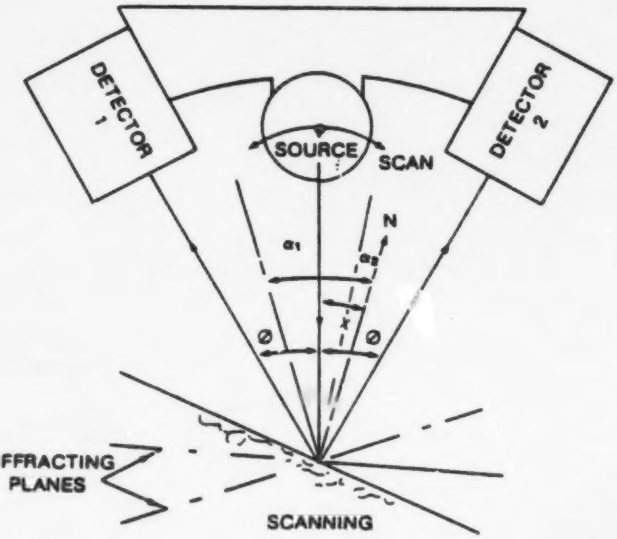

ACCURACY OF STRESS MEASUREMENT

An uncertainty of +− 0.01 degrees in measuring the displacement of a diffraction line leads to an estimated standard deviation which depends on the back reflection angle $\varnothing$ in the following way.

DIFFRACTION ANGLE	STANDARD DEVIATION		
	Strain	Stress	
20	27×10^{-6}	1.1 kpsi	8 MPa
25	55	1.5	11
30	79	2.4	17
35	118	3.5	24
40	171	5.2	35

respective ones of said second plurality of conductors by a series of parallel intermediate conductors overlying said insulating layer, extending transversely over said second plurality of conductors, and electrically connected to said respective conductors by vias through the insulating layer.

3. A photoconductive device according to claim 1 in which each of the ohmic contacts comprises a first layer of titanium adjacent the substrate, a second layer of palladium and a third layer of gold.

4. A photoconductive device as claimed in claim 1 in which each of the rectifying junctions is a sandwich structure with the photoconductive material contained between an indium contact layer and a tin oxide semiconductor layer.

*

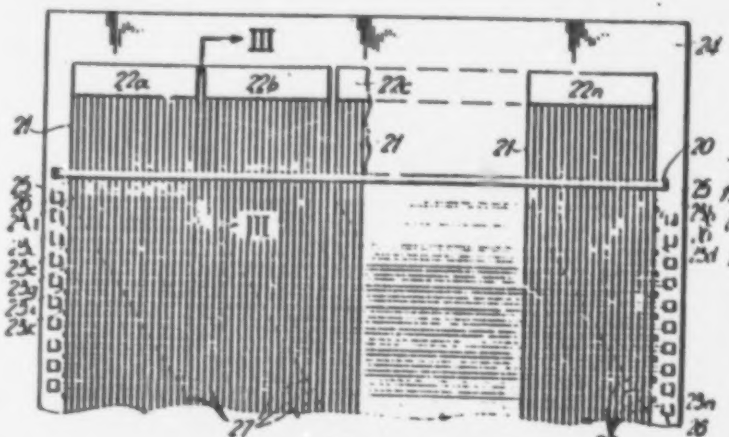
24
22a
III
22b
22c
22n
21
21
21
20
25
25
24b
23d
23a
23b
23c
23n
26
27
27
III

-Fig-2-

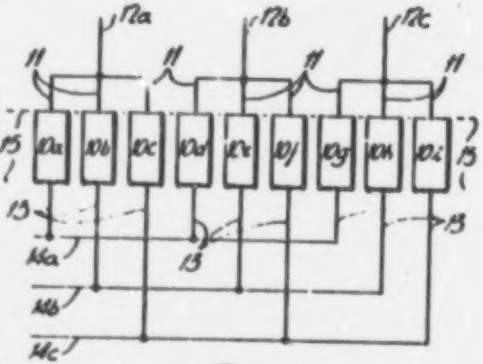
12a
12b
12c
11
11
11
11
15
15
10a
10b
10c
10d
10e
10f
10g
10h
10i
13
13
13
14a
14b
14c

-Fig-1-

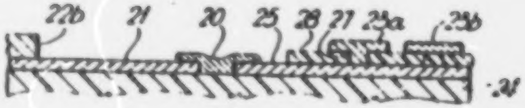
22b
21
20
25
28
27
23a
23b
24

-Fig-3-

1101973

SET UP AND PREPARATION

ALIGNMENT

The head is brought to the structure in the region where stress is to be measured, aligned with the rotation axis along the specimen normal, and the mount secured. The instrument can then be located exactly by driven translations parallel and normal to the specimen surface, using a controller connected to the computer.

A sequence of stress measurements can be carried out with a single set up. The diffractometer head can be rotated to change the direction of stress measurement in the surface and tranversed to measure stress gradients over a + – 5 cm. length without resetting.

CALIBRATION

The instrument is calibrated using a stress free standard of the corresponding pure metal, i.e. iron for specimens of ferritic steel, copper for specimens of bronze alloys, and aluminum for aluminum rich alloys.

SURFACE PREPAPATION

X-ray penetration of the surface is small, on the order of 10 micrometers. Scale and corrosion products must be removed. However mechanical abrasion will cause plastic flow and induced stresses in the surface. The surface can be prepared by either chemical or by electrolytic polishing.

SPECIFICATIONS

X-RAY DIFFRACTOMETER HEAD AND DRIVE

Overall Dimensions	18 in. D 10 in. H 18 in. W 45 cm. D 25 cm. H 45 cm. W
Overall Weight	44 lbs./20 kg.
Translations	X – 5 cm. Y – 5 cm. Z - 2 cm.
Head Rotation	360°
X-Ray Tube Targets	50 watts @ 40 KV Cr, Mn, Co, Cu, Fe
Position Sensitive Detectors	Sealed, Xenon-Methane gas filled Carbon coated quartz anode, 100 micron resolution = 1mm.

MOUNT AND STAND

Design of the mount and stand is dependent upon the application. Various standard mounts are under development.

DETECTOR ELECTRONICS AND POWER SUPPLY

NIM modular and rack mounted with umbilical connection to the diffractometer

Size	20"W × 15"H × 24"D 50 cm. W × 38 cm. H × 60 cm. D
Weight	25 lbs./12 kg.

COMPUTER/VIDEO TERMINAL/DISK

Microcomputer with 128K byte memory.

Dual floppy or hard disk storage.

Video Terminal with graphic display.

Single exposure stress and microstrain evaluation program for diffractometer control, data acquisition and real time stress an deformation determination.

Size	20"W × 15"H × 24"D 50 cm. W × 38 cm. H × 60 cm. D
Weight	25 lbs./12 kg.

ENVIRONMENT & POWER

Operating Temperature	-15° F to 150° F -10° C to 65° C
Humidity Range	5% to 95% non condensing
Power Requirements	110 volts 10 amps (includes draw from Computer/ Video Term/Disk and Head Drive System)

Cabling Provided

30 ft./10meters interconnecting umbilical cord to X-ray head contains data channels and power cord.

FEATURES

NON-DESTRUCTIVE TESTING

The CANMET diffractometer is designed to measure elastic stress non-destructively in structures in the field.

DIRECT READING OF STRESS

Dual position sensitive detectors measure lattice strains simultaneously in two directions in a specimen, providing a measure of the relative strain difference and giving the stress directly.

REAL TIME EVALUATION

Position sensitive detectors collect diffracted X-rays simultaneously over an active length of 5 cm., accumulating the diffraction line with a speed up to 50 times that of conventional detectors.

Thus the instrument measures surface stresses by X-ray diffraction in 1 to 3 minutes giving on line stress evaluation in real time.

ACCURACY (± 2 kpsi)

The X-ray tube scans to ensure that a set of irradiated grains pass through the full diffraction range. Thus a smooth and accurate diffraction line is obtained, even with coarse grained specimens.

ERROR COMPENSATING

The dual detector arrangement inherently compensates for systematic errors, particularly the centering error, which can occur with single detector diffractometers.

RANGE OF ψ AND φ

An omega rotation of the head, coaxial with the scan rotation gives a range of specimen directions $0 \leq \psi \leq 45°$ for each rotation angle φ. The rotation angle φ. The rotation about specimen normal gives a range of φ from 0° to 360°. This is the full range of ψ and φ required for triaxial stress determination.

SIMPLE CALIBRATION

The instrument is calibrated by a strain free specimen having a diffraction line close to that of the specimen.

AUTOMATED OPERATION

The diffractometer mount is automated so that once the instrument is set up stresses can be measured at different orientations in the surface and a sequence of measurements can be made in any desired direction in the specimen surface to determine the stress gradient.

DATA ACQUISITION & DISPLAY

The computer software package provided controls the diffractometer, collects data in a multichannel mode, graphically displays the diffraction line and calculates stresses in real time. Deformation broadening, which is a measure of the combined effect of microstrain and fine sub grain size, is an additional output that is optional. All data can be stored on disk to provide a permanent record.

MODULAR DESIGN

The system has been designed in five basic modules

1. Diffractometer Head with dual position sensitive detectors, X-ray tube and rotation mount.
2. Translation drives, X and Y parallel, and Z normal to the specimen surface, controlled by stepping motor.
3. Detector Electronics/Power Supply with 20 ft. (6.1 m.) unbilical cord connector to the diffractometer
4. Computer/Video Terminal/Disk Storage

5. Mount: according to application.

APPLICATIONS

Aircraft manufacturers and companies engaged in aircraft maintenance.

Steel mills, particularly those producing line pipe, and line pipe construction firms.

Construction firms manufacturing large steel structures.

Hydro electric companies.

Nuclear power manufacturing and operating companies.

Petroleum refining, and coal gasification plants using large reactors.

Railways, particularly in the production of welded rail.

Off shore structures.

Industries where stress corrosion is encountered, i.e. in the chemical industry, and the paper industry.

Regulatory Agencies.

FOR MORE INFORMATION CALL OR WRITE

Market Development Manager CANMET DIFFRACTOMETER

Telephone (519) 737-6330
(313) 965-2900

PSM

PROTO
MANUFACTURING LTD.

Michael Brauss

APPENDIX K

RIGAKU STRAINFLEX

Rigaku

RIGAKU/STRAINFLEX SERIES
X-ray Stress Analyzers

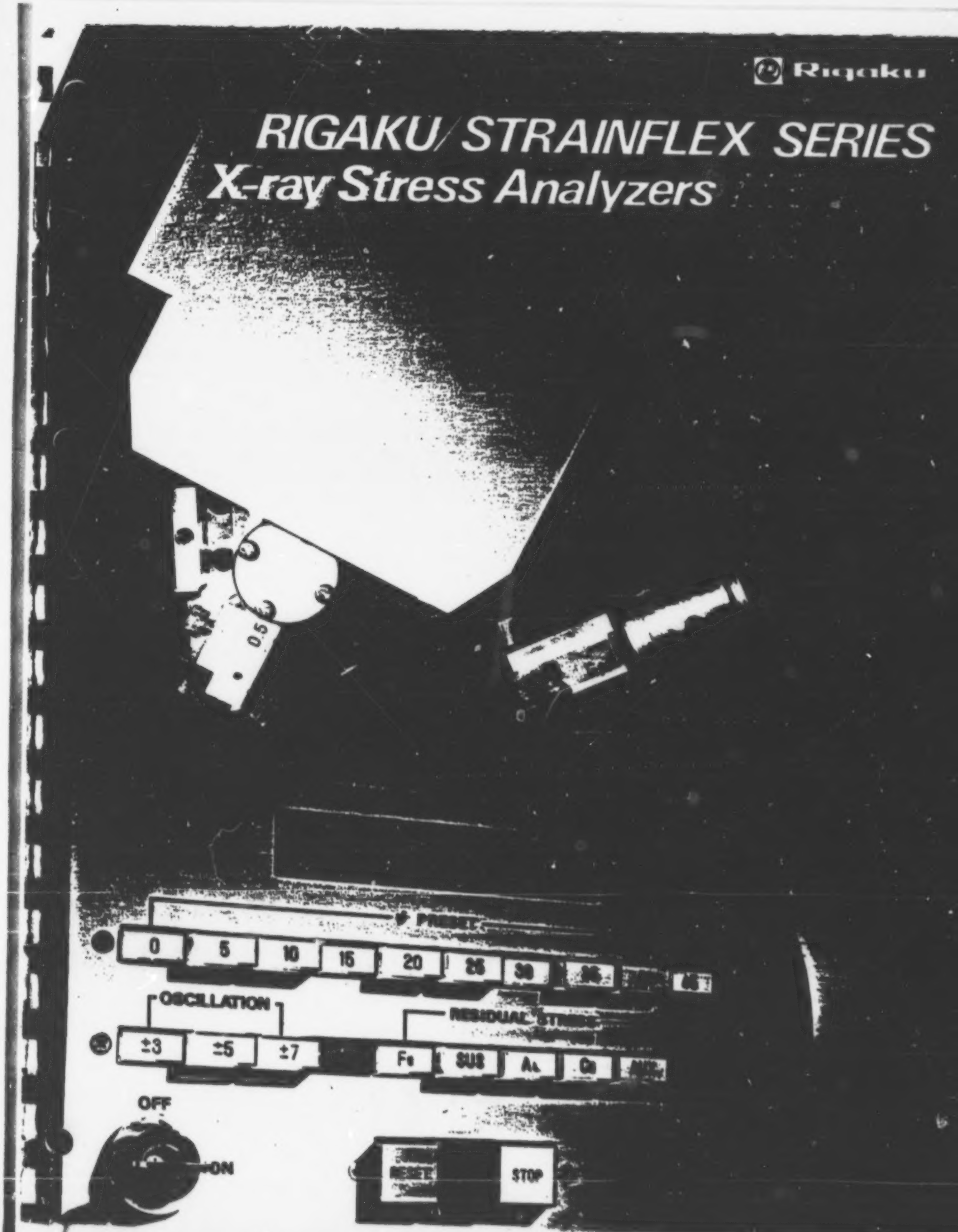
0.5
PRESET
0
5
10
15
20
25
30
35
45
OSCILLATION
±3
±5
±7
RESIDUAL STRESS
Fe
SUS
AL
Cu
OFF
ON
RESET
STOP

The final data comes out by your

1 The fixed ψ_0 method and the fixed ψ method ($\theta - 2\theta$ or $\psi - 2\theta$ linking) are available (Utility Model No.1016485, U.S.Pat.No.3634686).

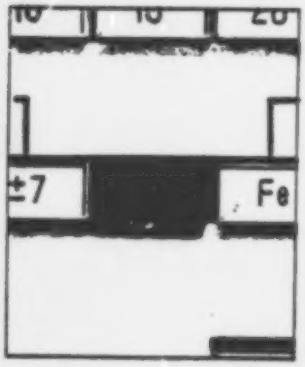

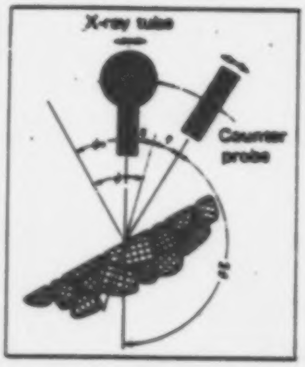

When anisotropy exists in the crystal plane orientation, more accurate measurement results can be obtained by the fixed ψ method, compared with the fixed ψ_0 method (θ fixed). The former method is especially indispensable in cases of worked plastic goods, castings having a coarse grain size, and welded parts.

2 The stress value can be learned in no time. A microprocessor performs goniometer control and data-processing of the measurement result so that the stress value comes out immediately without the trouble of setting the measuring conditions, plotting the measurement result, and so on.

3 The newly developed step oscillation method permits measurement according to the crystal grain size of the object material (patent pending).

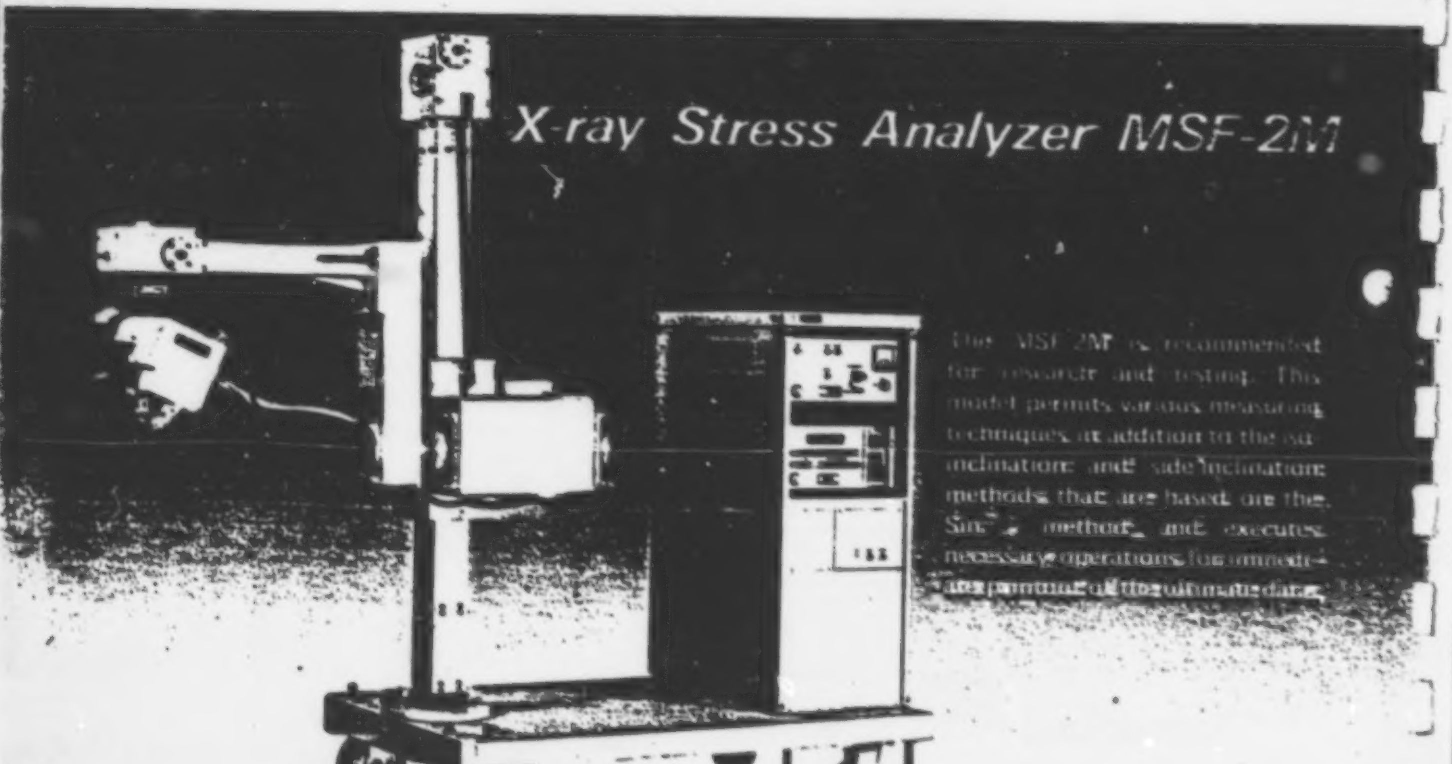

X-ray Stress Analyzer MSF-2M

The MSF-2M is recommended for research and testing. This model permits various measuring techniques in addition to the iso-inclination and side-inclination methods that are based on the $\sin^2\psi$ method, and executes necessary operations for immediate printout of the ultimate data.

K-2

●single finger push.

4 The MSF stand incorporates a variety of adjusting mechanisms (U.S.Pat.No.3868506, U.K.Pat. No.1390710).
[Standard for MSF-2M]

Once the setting of a sample is made, stress distributions can be measured in all directions (two-dimensional distribution). Also, the goniometer can be set accurately by X, Y, and Z axial rotations along with the longitudinal (X) and vertical (Z) fine moving mechanisms in a manner of no contact with the measurement plane. Both the iso-inclination method and side-inclination method are available.

5 Limitations due to the shape of the object for measurement have been reduced (Pat.No. 991292).

A dedicated small-size X-ray tube is employed to enable measurement of such shapes and locations as are unmeasurable with the conventional unit.

6 Safe operation.

A multi-stage fail-safe function prevents accidental exposure of operator to X-rays during the sample setting.

7 Operations and data processing are also possible with a personal computer owned by the user (option).

Any personal computer provided with the RS232C serial port allows the measurement condition setting and data processing with software optionally created by the user (interpreter system).

X-ray Stress Analyzer PSF-2M

PSF system in storage

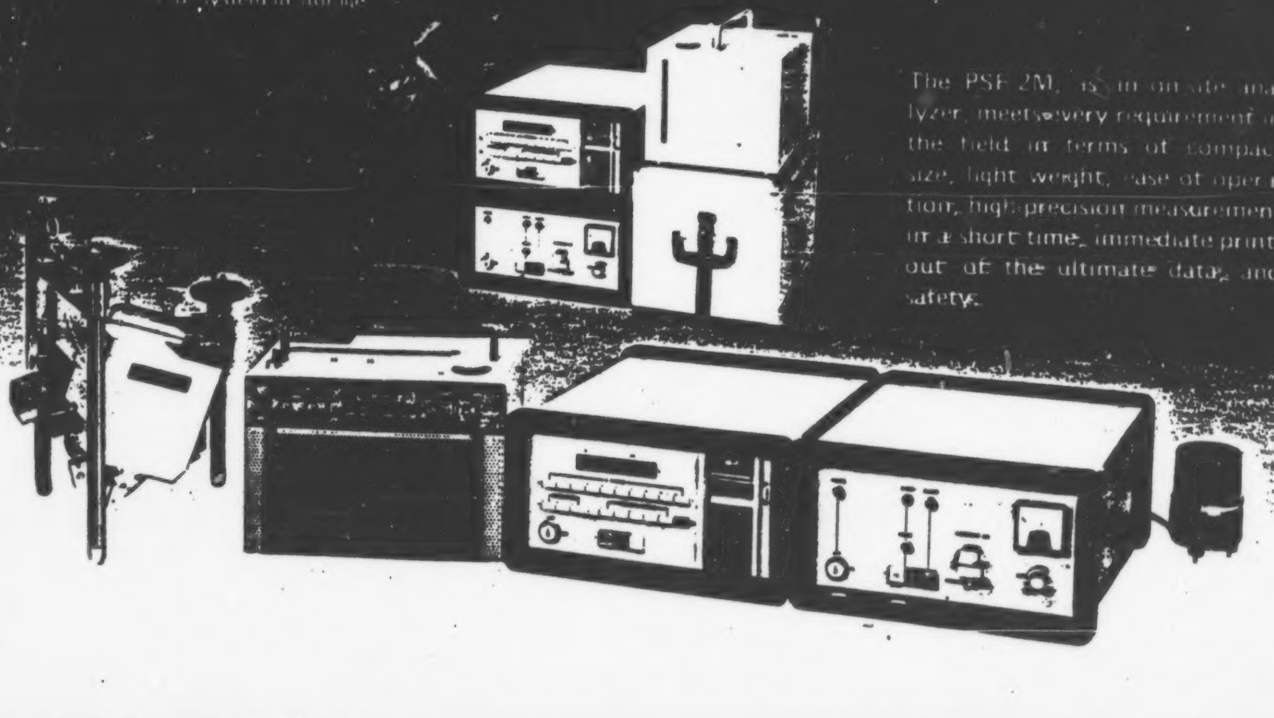

The PSF-2M, as an on-site analyzer, meets every requirement in the field in terms of compact size, light weight, ease of operation, high-precision measurement in a short time, immediate print-out of the ultimate data, and safety.

A versatile analyzer which can be a laboratory system and in the

Strainflex MSF-2M

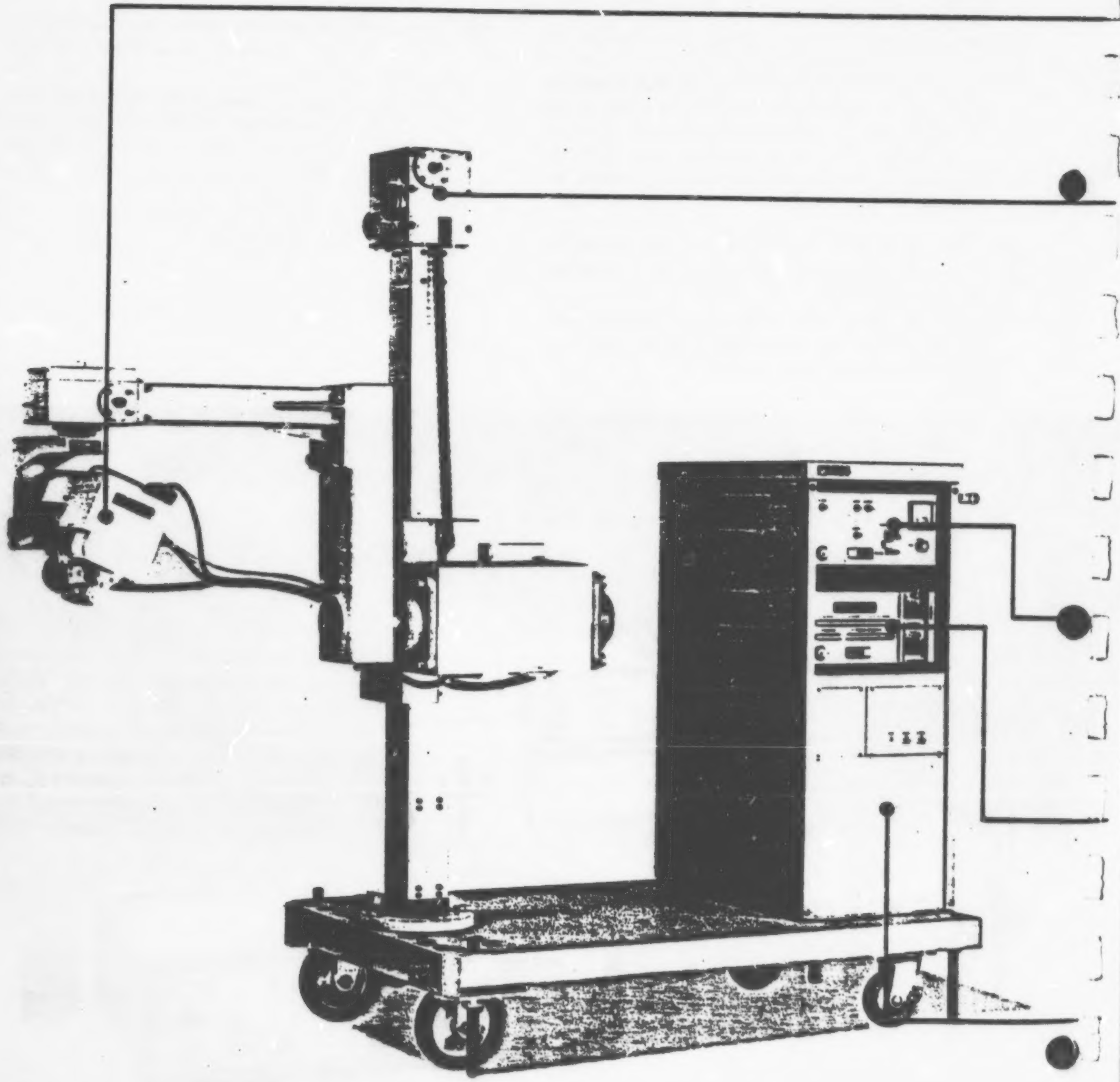

K-5

used as
field as well.

Strainflex PSF-2M

Goniometer 2905G1
Common.
A high-precision goniometer by stepping motor driving, yet compact and lightweight (14 kg). Provided with incident angle oscillation mechanism. The measuring range is expandable to $2\theta = 120^\circ \sim 150^\circ$ by use of an attachment as option.

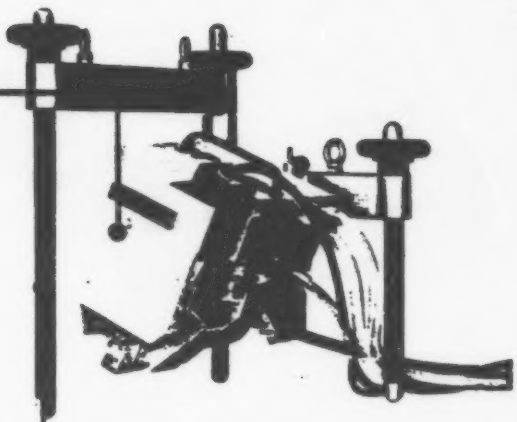

MSF Stand for Medium Structure 2905S1
Permits measurement in X-Y directions, the iso-inclination and side-inclination methods, and two-dimensional stress distribution measurement.

PSF Stand for Field Operation 2912S2
Compact and lightweight. Also usable as a desktop stand. Recommended for measurement of large structures, e.g. spherical tank. A stand tailored to the specific purpose may be also fabricated.

X-ray Generator 4005A1
Common.
30 kV fixed, 2 ~ 10 mA variable.
Compact and lightweight (25 kg).
Stability: 0.1% or better.

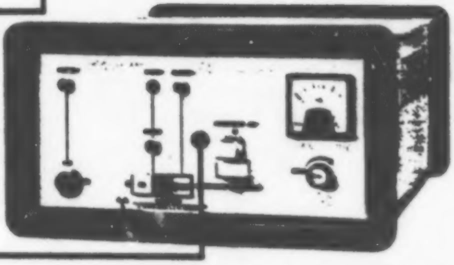

Control/Data Processing Unit 5072S2
Common.
Performs sequence control of the goniometer and other parts as well as counting and data processing. After correction of all data, printout is made about the stress value, integrated intensity of peak, FWHM, integral breadth, reliability, slope of $\sin^2\psi$ curve, measuring conditions, and volume fraction of retained austenite.

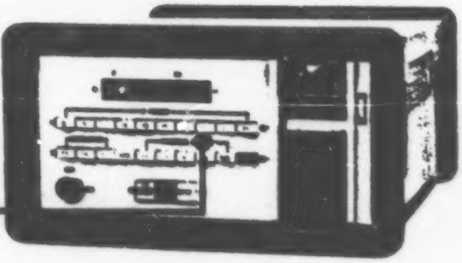

Heat Exchanger 4810A1
Common.
Features excellent portability to ensure perfect cooling in the field.

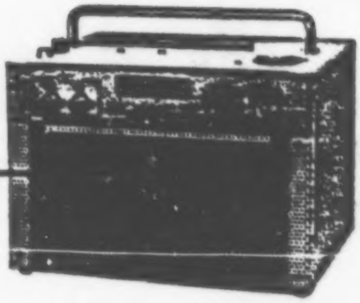

Build-up Functions(Option)

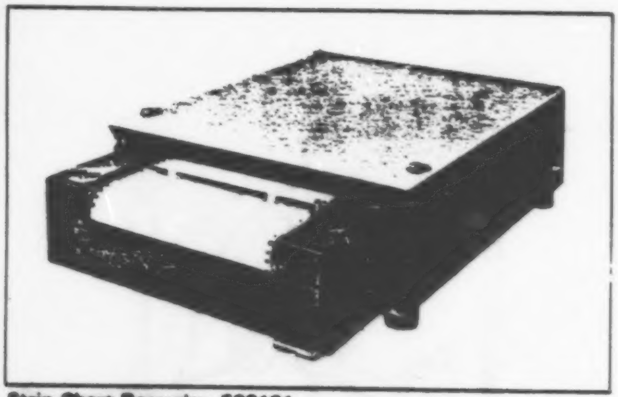

Strip Chart Recorder 5321S1
Used for chart recording of peak profiles when necessary.
(With ratemeter)

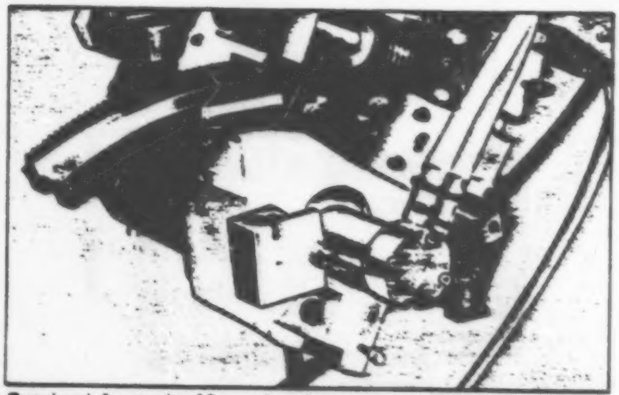

Retained Austenite Measuring Attachment 2905R1
Permits quantitative measurement of retained austenite simply in the field. The angle measuring range is expandable to $2\theta = 120^\circ \sim 150^\circ$ (option).

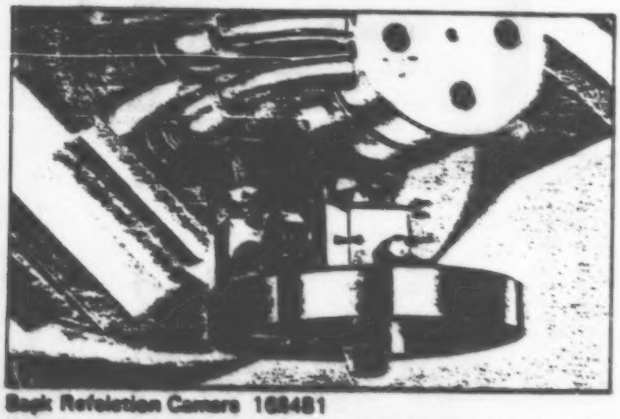

Back Reflection Camera 168481
Used for examining the state of grains, in conjunction with the X-ray stress analyzer.

Electrolytic Polisher 2904D1
A compact, lightweight portable type. It can carry out electrolytic polishing in a minute or so.

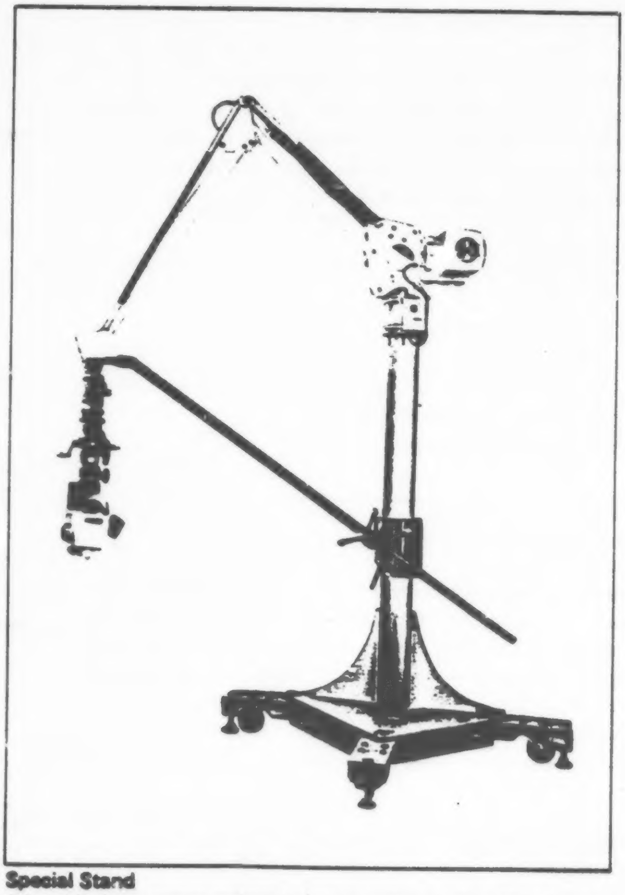

Special Stand
Selectable from among various types according to diversified requirements. A stand tailored to the specific purpose may be newly fabricated.

K-1

Specifications

	MSF-2M	PSF-2M
Goniometer 2906G1	The iso-inclination method, side-inclination method, oscillation method, and $\theta-2\theta$ method are available. (Utility Model No.1016485, U.S.Pat.No.3634686) 2θ = 140° ~ 170° (120° ~ 150° : option)	
X-ray generator 4006A1	30 kV (constant potential), 2 ~ 10 mA continuously variable, solid-state negative feedback control	
Control/data processing unit 907282	Once the goniometer is set up, the microprocessor will select optimum measuring conditions and execute measurement for printout of the final data. Incident angle selection: 0°, 5°, 10°, ... 40°, 45°; 10 steps Sample selection: Fe, SUS, Aℓ, Cu, other Oscillation: OFF, ± 3°, ± 5°, ± 7° Operation: Peak search, output of the stress value, quantitation of retained austenite	
Detector 5721S1	Scintillation counter probe	
X-ray tube 9432	One out of Cr, Co, and Cu. Cr unless specified. Max. load: 30 kV, 10 mA	
High voltage cable 4262S1	10 m, 1 pc	
MSF Stand for Medium Structure 2906S1 PSF Stand for Field Operation 2912S2	Patent pending (U.S.Pat.No. 3868506, U.K. Pat.No.1390710) Allows measurement in X-Y directions, and the iso-inclination method and side-inclination method. A measuring device for two-dimensional stress distribution is newly added.	Suitable for field operation as well as for use as a desktop stand. (Pat.No.981292)
Heat exchanger 4810A1	Compact type self-containing a radiator equipped with forced air cooling fan.	

Installation Requirements

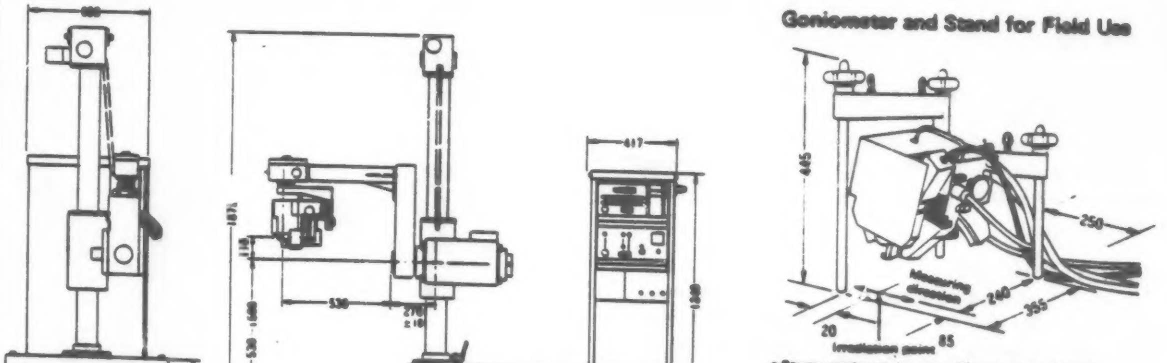

- Power supply requirement: Single phase 100 V AC within ± 10%, 15 A as standard. Other voltages are available as option. Please specify voltage when inquiring.
- Grounding: Grounding resistance . . . 100 Ω or less. The 3P [illegible] receptacle is standard for grounding as well as for power supply.
- Cooling water and drain facility: Unnecessary except that 5 liters of distilled water for circulation used in the heat exchanger should be replaced at 3-month intervals.

X-ray Stress Measuring Method

The X-ray stress measuring method as one of the stress measuring techniques has become prevalent among industrial and academic sectors, thus producing brilliant achievements, as the result of strenuous efforts made for the spread up to now, with Japan and the U.S.A. playing the key role. (The Committee on Mechanical Behavior of Materials, The Society of Materials Science, Japan; The Fatigue Design and Evaluation Committee, S.A.E.)

Features

This X-ray stress measuring method is said to be one and only means of non-destructive measurement of residual stress. The stress in the material can be directly measured in a non-contact manner.

The method allows also measurement under the condition that a load is applied, in which case the sum of the residual stress and the added stress are measured.

It exhibits an excellent correspondence to the strain gauge method, as seen in the figure at right, thus offering high reliability and leading to wider applications for field measurements.

The employment of the parallel X-ray geometry greatly facilitates the setting, and consequently, the measurement of fairly complicated shapes is now made possible.

The stress measured by X-rays is that located up to about ten microns deep from the surface. By utilizing this characteristic, it is also possible to measure the stress distribution in the direction of depth with the aid of an electrolytic polisher.

The application of the X-ray stress measuring method ranges from the measurement of a local residual stress by use of a mask for limiting the irradiated area to macroscopic measurements. Furthermore, in the case of such a material where different phases are present, the stress of each phase can be measured as well.

Measuring Principle

When a stress is applied to a material, the interatomic distance in the crystal will be extended or compressed within the elastic limit in proportion to its force. Based on this fact, the X-ray diffraction technique is employed to measure the variations of the interplaner d spacing in the crystal so that the stress will be calculated. From the Bragg's condition for diffraction, the correspondence to the stress can be figured out.

$n \cdot \lambda = 2d \sin\theta$ Bragg equation

where λ is the X-ray wavelength, θ is the diffraction angle, and d is the interplaner spacing in the crystal.

$$\varepsilon = \frac{\Delta d}{d} = -\cot\theta_0 \cdot \Delta\theta$$

where ϵ is the quantity of strains, and $\Delta\theta$ is the quantity of variations of the diffraction angle.

That is, from the quantity of variations of the X-ray diffraction angle $\Delta\theta$, the quantity of strains will be calculated, and further, the stress σx in the X-direction on the surface will be obtained by the following equation.

$$\sigma x = \frac{E}{1+\nu} \cdot \frac{\Delta\varepsilon(\psi)}{\Delta\sin^2\psi} = \frac{-E\cot\theta_0}{2(1+\nu)} \cdot \frac{\Delta 2\theta}{\Delta\sin^2\psi} = K \cdot \frac{\Delta 2\theta}{\Delta\sin^2\psi}$$

where E is the Young's modulus, ν is the Poisson's ratio, ψ is the angle between the normal of the sample surface and the normal of the crystal plane, and K is the stress coefficient to be determined by an object for measurement.

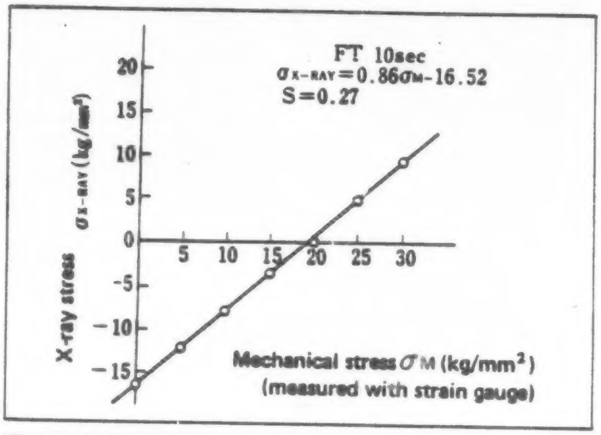

Principle

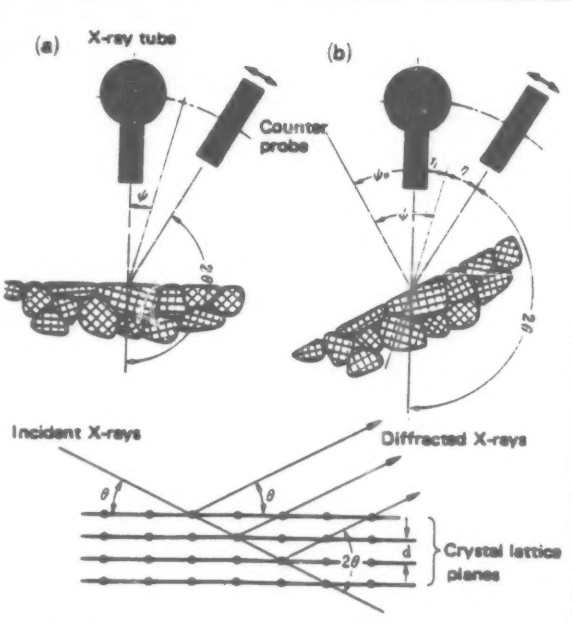

K-5

Measurement Examples

Coiled Spring (11 mm dia.)

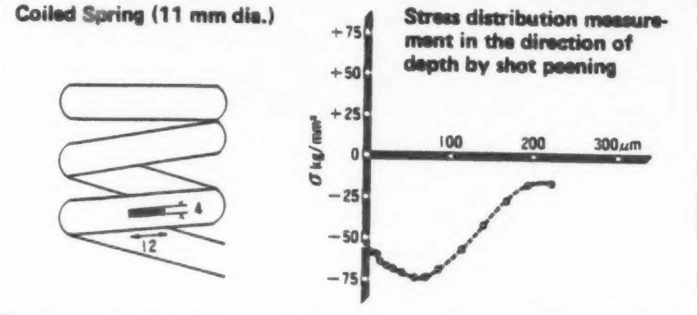

High Chromium Steel

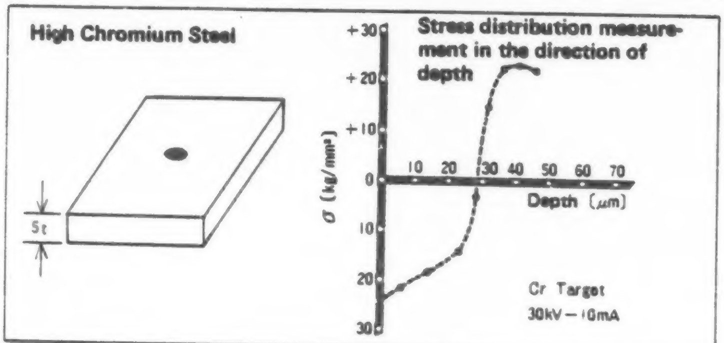

Fillet Weld
High Tensile Steel
(60 kg class)

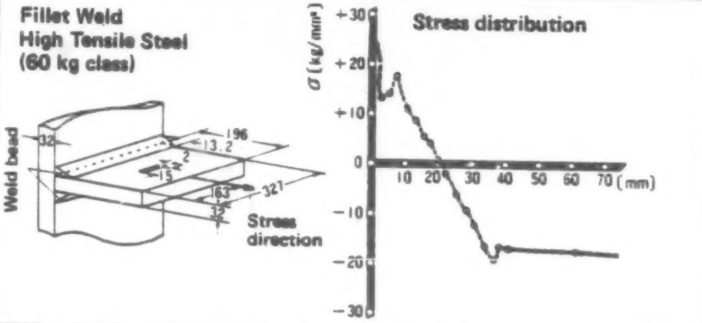

Al Rolled Plate

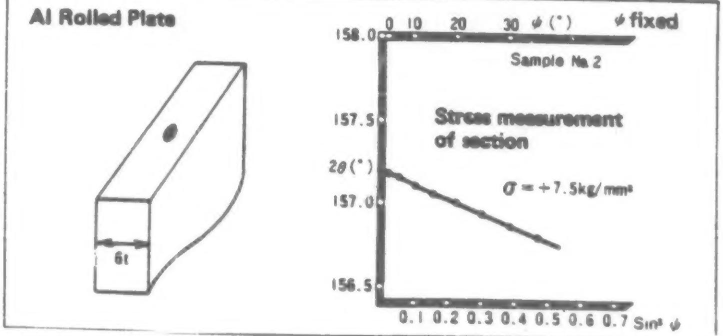

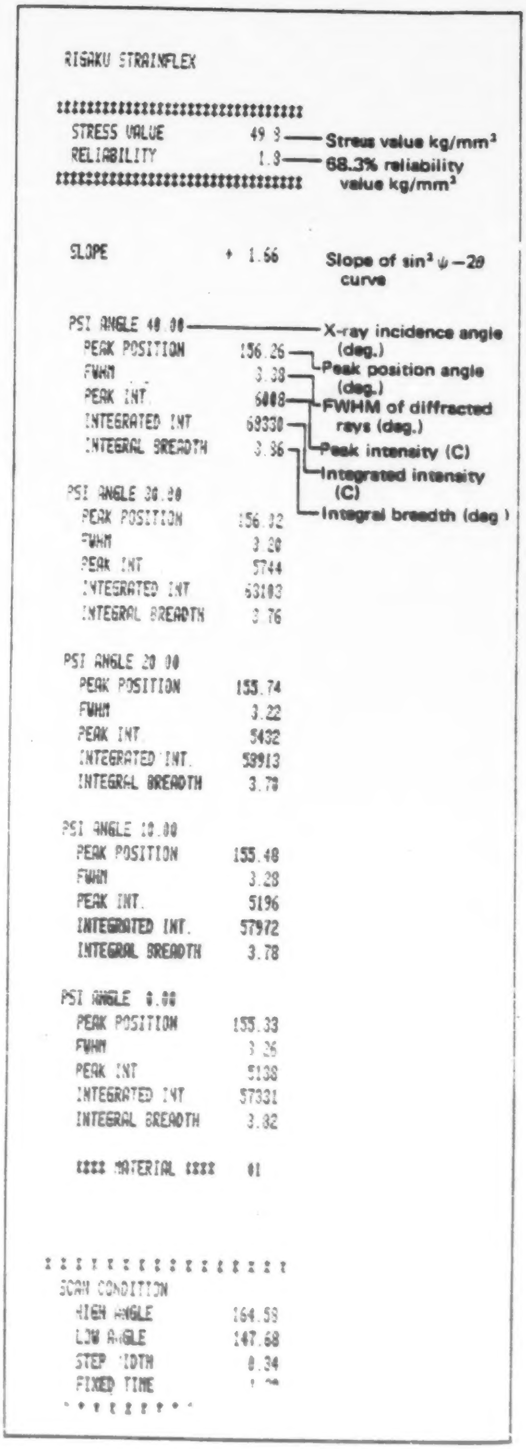

```
RIGAKU STRAINFLEX

################################
 STRESS VALUE          49.3 —— Stress value kg/mm²
 RELIABILITY            1.8 —— 68.3% reliability
################################      value kg/mm²


 SLOPE              + 1.66    Slope of sin² ψ − 2θ
                                curve

 PSI ANGLE 40.00 ————————————— X-ray incidence angle
   PEAK POSITION       156.26    (deg.)
   FWHM                  3.38    Peak position angle
   PEAK INT.             6008     (deg.)
   INTEGRATED INT       68330    FWHM of diffracted
   INTEGRAL BREADTH      3.36     rays (deg.)
                                 Peak intensity (C)
 PSI ANGLE 30.00                 Integrated intensity
   PEAK POSITION       156.02     (C)
   FWHM                  3.20    Integral breadth (deg.)
   PEAK INT              5744
   INTEGRATED INT       63103
   INTEGRAL BREADTH      3.76

 PSI ANGLE 20.00
   PEAK POSITION       155.74
   FWHM                  3.22
   PEAK INT.             5432
   INTEGRATED INT.      58913
   INTEGRAL BREADTH      3.78

 PSI ANGLE 10.00
   PEAK POSITION       155.48
   FWHM                  3.28
   PEAK INT.             5196
   INTEGRATED INT.      57972
   INTEGRAL BREADTH      3.78

 PSI ANGLE  0.00
   PEAK POSITION       155.33
   FWHM                  3.26
   PEAK INT              5138
   INTEGRATED INT       57331
   INTEGRAL BREADTH      3.82

   #### MATERIAL ####    01



################
 SCAN CONDITION
   HIGH ANGLE          164.58
   LOW ANGLE           147.68
   STEP WIDTH            0.34
   FIXED TIME
   *********
```

19

LINE OF BUSINESS

X-ray Equipment for Science and Industry

X-ray Diffractometer and Attachments
X-ray Generators
X-ray Diffraction Cameras
X-ray Spectrometers
Piezo Goniometers
X-ray Stress Analyzers
Industrial X-ray Radiographic Equipment

Thermal Analysis Equipment

Differential Thermal Analyzers
Thermobalance Equipment
Thermomechanical Analyzers
Differential Scanning Calorimeters

radionics scientific inc.
EXCLUSIVE CANADIAN REPRESENTATIVE
REPRESENTANT CANADIEN EXCLUSIF

595 Canarctic Drive
Downsview, Ontario M3J 2P9
Tel: (416) 736-1600

Montreal —514-335-0105
Ottawa —613-521-8251
Vancouver —604-732-7661

Rigaku
WE CARE ABOUT TECHNOLOGY... THAT MAKES THE DIFFERENCE.

Rigaku Corporation
SEGAWA BLDG. 2-8, Kandasurugadai, Chiyoda-ku, Tokyo, JAPAN
Cable: RIGAKUDENKI TOKYO, Telex: J24931 RDXRAY Phone: Tokyo (03) 295-3311

Rigaku Industrial Corporation
SEGAWA BLDG. 2-8, Kandasurugadai, Chiyoda-ku, Tokyo, JAPAN
Cable: RIGAKUDENKI TOKYO, Telex: J24931 RDXRAY Phone: Tokyo (03) 295-3062
Telex (Osaka): 5336509 RDKOSA Phone (Osaka): (0726)-93-1131

Rigaku USA Inc.
3 Electronics Avenue, Danvers, Massachusetts 01923, U.S.A.
Telex: 7103476511 RIGAKU US DARS. Phone: (617)-777-2446

Printed in Japan CED88A/811130KAI

APPENDIX L

TEC 1600 STRESS ANALYSIS SYSTEMS

TEC 1600 X-ray Stress Analysis Systems

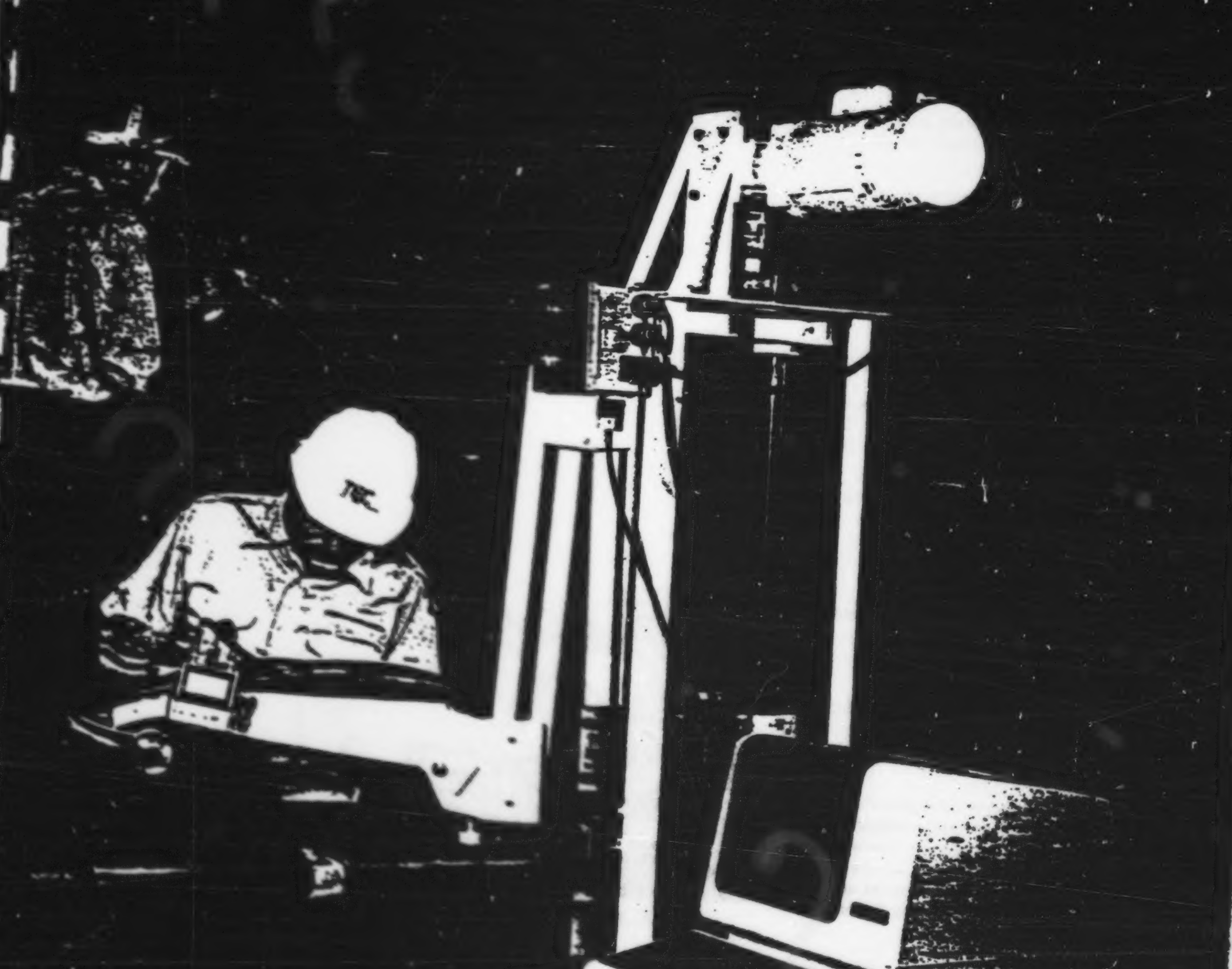

CAPABILITIES AND APPLICATIONS

The 1600 series X-Ray Stress Analysis Systems developed by Technology for Energy Corporation (TEC) incorporate a number of recent technological advances, including position-sensitive proportional counters, lightweight x-ray tubes, microcomputers, and robotics. These innovations allow us to offer systems that are:

FAST:
position-sensitive proportional counters permit complete stress measurements to be made in less than two minutes, thus significantly increasing sample throughput.

ACCURATE:
complete diffraction pattern analysis means more accurate stress results.

ON LINE:
the self-contained computing system provides immediate stress analysis and graphical presentation of results.

EASY TO USE:
the TEC x-ray stress analysis systems are non-destructive, non-contact, and often require little or no sample preparation.

USER FRIENDLY:
the Stress Analysis Monitor is a powerful system designed for easy use in the field.

RUGGED:
robust, air-conditioned environmental enclosures and diffractometers with few moving parts mean systems that can be used in the factory or field.

EASY TO MAINTAIN:
modular hardware and software result in systems that are easy to maintain and expand.

SAFE:
meticulous attention to radiation safety maximizes both personnel safety and machine integrity.

SUPPORTED:
TEC is committed to total post-sales customer support through solid programs of system installation, training, warranty service, extended service contracts, software enhancement and upgrade service, and a Stress Analyzer User's Group.

Residual stresses and loading stresses are of great significance to design, metallurgical, and quality control engineers because of their effect on such parameters as safe design load limits, fatigue, stress corrosion cracking, and component warping. Residual stresses arise from a wide range of metal treating and joining procedures including carburizing, nitriding, heat treatment (phase transformations), welding, rolling, drawing, forging, grinding, machining, shot peening, and from the thermal expansion/contraction of constrained parts. TEC's modular systems permit accurate, rapid stress measurements to be made in a wide range of configurations and environments.

Applications for the direct measurement of both loading and residual stresses are found in a number of industries including:

- **Aircraft:** air frames, landing gears, tail hooks, bearings, turbine blades
- **Automotive:** auto and truck chassis, steering columns, bearings, crank shafts
- **Heavy Equipment:** chassis, scraper blades, engine bearings, crank shafts
- **Ordnance:** penetrator warpage, cannon barrels
- **Petroleum:** pipeline welds, off-shore towers, drill pipes, well casings
- **Power Plants:** welds in steam and cooling pipes, pressure vessels
- **Research:** studies of the theories of residual stresses, loading stresses, fatigue, and creep
- **Shipbuilding:** hull welds, bearings, crankshafts

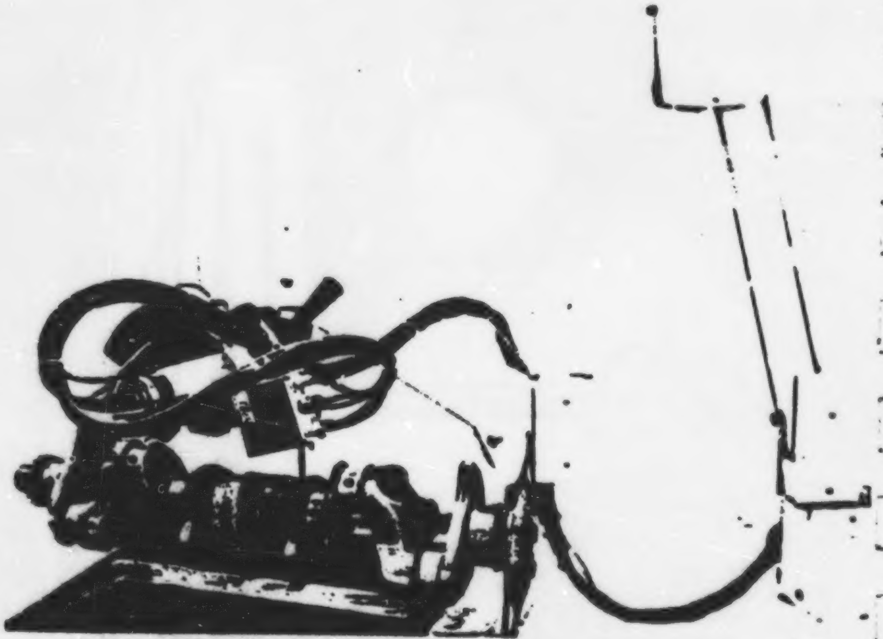

Model 651 Articulated Arm with Model 670 Diffractometer

PRINCIPLES OF OPERATION

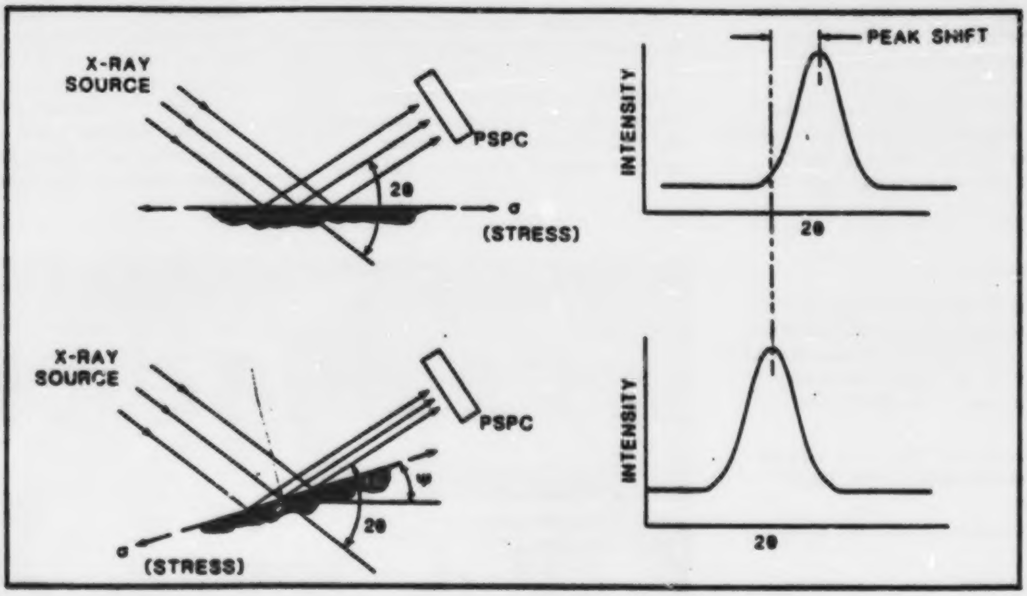

Measurement of Stress by X-Ray Diffraction

Of the various techniques for measuring residual stresses, the x-ray diffraction method is the most developed and widely used. It is the only technique that is applicable to all crystalline materials, that can measure the absolute stress in the component without the need for a measurement of the sample in the unstressed state, and that is capable of making measurements in a localized region as small as 1 mm in diameter. Because the penetration of the long wavelength X-rays is only a few tens of microns, the Model 1600 Stress Analysis Systems are used to measure surface stresses.

Stresses are determined by measuring the strain in the atomic lattice and by relating the strains to stresses through the elasticity theory. An incident beam of essentially monochromatic radiation of wavelength λ is diffracted at an angle 2θ which obeys Bragg's Law

$$n\lambda = 2d \sin\theta, \qquad (1)$$

where n is the order of the reflection and d is the atomic spacing of the selected crystalline lattice planes. The sample surface is at an angle θ to the incident beam, and only grains with atomic planes parallel to the surface diffract. From the 2θ position of the peak, the atomic spacing of the diffracting planes may be determined.

When the sample is tilted an angle ψ, the atomic planes that make an angle ψ with respect to the surface now diffract. If there is no stress in the sample, the two diffraction curves superimpose. However, in the presence of surface stresses, the atomic planes in different orientations are compressed or dilated and a peak shift results. The stress, σ, can be determined from the shift through the relationship

$$\sigma = \frac{E}{1+\nu}\;\frac{1}{\sin^2\psi}\;\frac{(d_\psi - d_o)}{d_o} \qquad (2)$$

where d_ψ is the lattice spacing at a tilt angle ψ and E and ν are Young's modulus and Poisson's ratio appropriate to the selected crystallographic planes. The values of d_ψ are obtained from Bragg's Law (Equation 1) by careful analysis of the diffraction peak. Note that it is not necessary to know the d-spacing of the unstressed material. Thus, an accurate and rapid measurement of the location of the diffraction peaks can be used to determine the presence of loading or residual stresses.

With the advanced computer technology and the TEC Stress Analysis Monitor used in the TEC Model 1600-series X-ray Stress Analysis Systems, more complex data analyses are possible to account for such effects as stress components normal to the sample surface, and complicating metallurgical variables such as preferred orientation, large grain size, and stress and composition gradients.

Position-Sensitive Proportional Counters

In traditional x-ray diffractometry, a proportional or scintillation counter, preceded by a narrow slit, is scanned through a range of 2θ angles, and the resultant scattered intensity is recorded in analog form on a strip chart or in digital form with a scaler/printer or perhaps a computer. This procedure requires a precision diffractometer to control the detector/slit motion and is time consuming because data at each 2θ angle are recorded serially. Furthermore, such devices are bulky and suitable for use only in the laboratory.

TEC is a world-leader in the development of a new detector known as a position-sensitive proportional counter (PSPC). These detectors have the capability of recording not only the presence of a photon, but also its location along a line. The TEC Model 205 PSPC, developed specifically for the 1600 Stress Analysis System, has a spatial resolution of 50 μm, and can record data at 1000 locations (scattering angles) simultaneously.

Two significant improvements in stress measurements result from these devices: a simple diffractometer with no 2θ motion can be built because the PSPC subtends a sufficiently large 2θ angular range to record the entire Bragg peak for a particular class of samples; and all the data are recorded simultaneously with a decrease in data acquisition time of up to 100 times. Measurement times as short as a few seconds are now possible, even with low-power x-ray sources.

SYSTEM COMPONENTS

Three stress analysis systems are offered to meet the wide range of applications and environments in which x-ray stress analyses must be made: (1) the Model 1600 Stationary System, (2) the Model 1610 Mobile System, and (3) the Model 1620 Portable System. Each system consists of an identical set of common components that are packaged appropriate to the end use.

The common components comprising the minimum configuration that provides a complete residual stress apparatus include: a manual diffractometer; a collimator and shutter; an x-ray source, power supply, and recirculating heat exchanger; a position-sensitive proportional counter plus electronics system; an on-line Digital Equipment Corporation (DEC) PDP 11/03 microcomputer with dual floppy disks, printer-plotter, and graphics display screen; and an x-ray safety system. A complete software system, the TEC Stress Analysis Monitor, which controls data acquisition, calibration, file storage, and stress analysis is also provided.

Diffractometer

The Model 670 Diffractometer incorporates the motions necessary to implement the $\sin^2\psi$ or multiple tilt technique of stress measurement in an elegant, but simple manner. Features of the diffractometer include:

- modular design to permit mounting on a wide variety of positioning devices
- easily mounted, prealigned x-ray tubes
- easily interchanged, inexpensive, position-sensitive detector mounts which allow rapid change of the mean 2θ angle subtended by the center of the PSPC
- easily aligned feeler gauge which rapidly and accurately directs the user to place the desired location on the sample surface at the axis of rotation of the diffractometer
- optional alignment telescope and alignment jigs
- optional retained austenite accessory
- optional computer-controlled ψ-angle motion and shaft encoder

The ψ angle is changed by moving a spring-loaded handle. This handle has a locking device that holds the diffractometer at the desired location. A ψ-angle scale is machined on the diffractometer, and the ψ-angle vernier is mounted on the PSPC mount. This technique assures that, regardless of the nominal center Bragg angle of the PSPC mount, the ψ angle scale always reads correctly. The ψ angle can be rotated from −45° to +60°

The diffractometer is accurately held on one of several positioning devices by two screws and two alignment pins. The prealigned x-ray tube assembly is held on the diffractometer by two thumb screws, as is the detector mounting block. Thus, it is simple to move the unit between positioning devices, to change from one x-ray wavelength to another, and to change the mean 2θ angle of the detector. Typically, the system can be completely interchanged and aligned in less than five minutes.

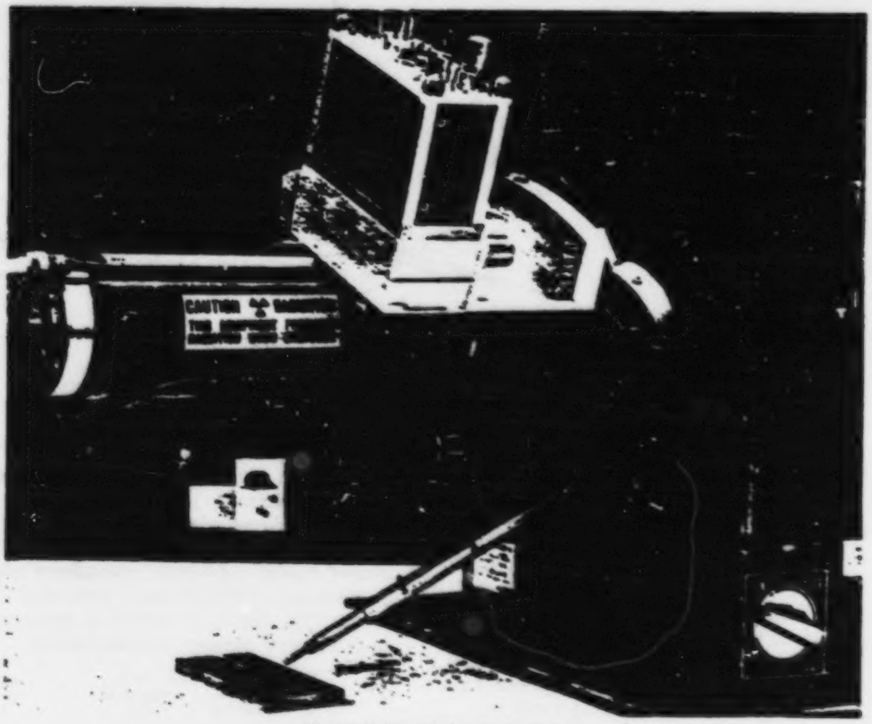

Model 670 Diffractometer

The diffractometer is positioned accurately over the sample by means of a feeler gauge that locates the exact axis of rotation of the diffractometer. This device has a dial gauge that indicates displacement of the sample surface from the axis of rotation with a resolution of 3 μm. The feeler gauge is retracted out of the x-ray beam while measurements are being made.

X-Ray Tube Assembly

The Model 661 X-ray Tube Assemblies are built around various 50-kV, 2-mA wound filament x-ray tubes. A variety of target materials is available, including Cr, Cu, Co, Fe, and Mo. A mounting assembly, which is prealigned at the factory, has been developed so that the x-ray tube is aligned with respect to the collimator. The entire assembly is held in place on the diffractometer by two mounting screws and locating pins. Thus, an x-ray tube and collimator system can be changed in the field, and no tedious alignment procedure is necessary.

HV Supply

The Model 660 X-ray Tube HV Supply features include:

- 50-kV, 2-mA dc operation
- independent kV, mA, and filament current display meters
- system key lock
- external independent computer control of both kV and mA
- safety system shutdown interlock

L-5

SYSTEM COMPONENTS

Recirculating Cooling System

The recirculating x-ray tube cooling system is provided to maintain the x-ray tube at constant temperature, thus helping to maintain the stability of the diffractometer during ambient temperature excursions. It is a completely sealed system that includes a circulating pump and a heat exchanger, and provides a "low coolant" signal as well as a "no-coolant flow" signal to the safety system.

Position-Sensitive Detector and Signal Processing Electronics

The Model 205 Linear Position-Sensitive X-ray Detector is the smallest, lightest, highest resolution position-sensitive proportional counter manufactured. It was designed specifically for use with the Model 670 Diffractometer and has the shortest possible distance between the first resolution element and the end of the detector. This design feature increases the maximum 2θ angle that can be reached to 163°.

The position-sensitive detector analog signal processing electronics system includes: a nuclear instrument module (NIM) bin and power supply; a PSPC position decoder; a detector HV bias; a biased time-to-amplitude converter; a 100-MHz, analog-to-digital converter; a computer interface module; and a pulse generator.

For each photon detected in the PSPC, a digitized address plus appropriate control signals are generated by these electronics modules, the address being the representation of the position along the detector anode wire where the photon arrived.

Computer and Data Acquisition System

The data acquisition, control, and analysis system for the 1600-series stress analysis systems is built around a standard, unmodified computer system from Digital Equipment Corporation and other computer peripheral device vendors. TEC has carefully selected each component for its ability to perform the necessary functions reliably, while being cost effective.

The system includes: a PDP® 11/03 computer with floating point processor and 64 kbytes of memory; an EPSON MX-82 printer/plotter; a Digital Engineering Model VT-640 graphics terminal; and a Data System Design Model 470-2A dual floppy disk drive (2 Mbytes).

The data acquisition function consists of recording the address corresponding to the arrival location of each photon at the detector and building a histogram of the diffraction pattern. Addresses are moved from the detector interface in direct memory access (DMA) block transfers to a double buffer in the computer memory where a software routine uses these data to build the histogram.

Control of the various operating functions of the each stress analysis system is accomplished through a 64-channel I/O interface. The x-ray source high-voltage and milliampere control, x-ray safety system, and optional ψ-angle motor drive and shaft encoder are interfaced through this single board. The hardware and software systems have been designed such that on system initialization the software can determine which of the optional hardware features have been installed.

X-Ray Safety System

The Model 641 X-ray Safety System provides for both maximum operator safety as well as integrity of the stress analysis system. It features:

- radiation shield interlock
- fail-safe "X-RAY ON" red light on diffractometer
- shutter position monitor
- sample in place monitor
- x-ray high-voltage safety interlock
- cooling water flow and temperature monitors
- open beam/closed beam key override
- microcomputer and host computer failure indicators

The system is controlled by an on-board microcomputer that monitors all safety conditions. All safety violations are handled in a fail-safe mode that prevents X-rays from emanating from the collimator either by closing the shutter or turning off the x-ray high voltage. The state of the safety system is displayed on a front panel by a sequence of light-emitting diodes (LEDs).

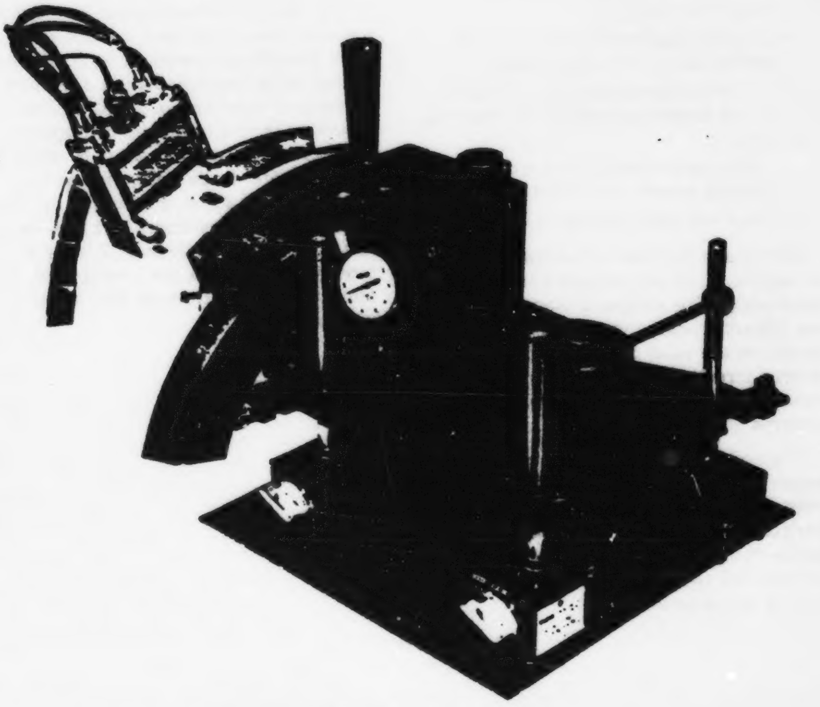

Model 650 Diffractometer Mount

®PDP is the registered trademark of Digital Equipment Corporation.

SYSTEM CONFIGURATIONS

MODEL 1600 STATIONARY SYSTEM

The Model 1600 Stationary Stress Analysis System is designed for use in a fixed location. Typical applications are in research laboratories, or in manufacturing facilities where small parts can be brought to the system. The Model 1600 consists of all of the common components plus the following:

Instrument Enclosure and Power Distribution System

The instrument is housed in a Model 681 42-in. high by 30-in. deep standard rack mounting cabinet. The power distribution system includes a master power off/on circuit breaker switch and power indicator lamp and a 115-V 60-cycle isolation transformer.

Diffractometer Mount

The Model 650 Diffractometer Mount is a semi-portable device that carries the Model 670 Diffractometer and can be used on a table top, on large flat parts, or on large diameter pipes.

Features of the mount include:

- Wide range of vertical motion through use of posts mounted in magnetic blocks
- ± 2.5-cm accurate vertical motion controlled by rack and pinion
- ± 1.6-cm horizontal twisting motion at the sample controlled by eccentric cam
- ± 2.5-cm horizontal forward/reverse motion with lever arm
- Wear-resistant Tufram finish

With these degrees of freedom, samples of varying sizes and shapes can be measured easily. The sample is placed under the diffractometer, the unit coarsely positioned on the steel columns, and then steered directly over the exact spot to be measured with the fine-positioning controls.

The unit is ideally suited for use with simple customer-designed sample placement jigs such as V-blocks. With such devices, many samples of the same geometry can be routinely measured without any tedious alignment of each sample in the beam.

MODEL 1610 MOBILE SYSTEM

The Model 1610 Mobile Stress Analysis System is designed for use on a shop or factory floor where it is necessary to move the stress analyser to large, bulky, or immoveable components. The Model 1610 consists of all of the common components plus the following:

Transport Cart

All components of the complete stress analysis system are mounted in the Model 689 Mobile Transport Cart. The same power distribution system is used as in the Model 1600 system.

Special features of the cart include:

- pneumatic tires to provide a cushioned ride during movement from one site to another
- leveling jacks to provide a level, rigid platform for the system even on rough surfaces
- push bar for manual movement
- mounting for manual or robotic diffractometer positioning arms
- optional air conditioning for environmental control

Articulated Arm

The Model 651 Articulated Arm diffractometer mount has been developed to allow the diffractometer to be positioned against large immoveable parts. A horizontal 2 m extension is possible. The mounting gimbal has three orthogonal degrees of rotational freedom to allow the diffractometer to be positioned in any orientation. The arm is mounted on two rigid, vertical, steel shafts and may be raised and lowered through 2 m by a motor-driven lead screw mechanism. The entire arm pivots through 200° about a vertical axis.

MODEL 1620 PORTABLE SYSTEM

The Model 1620 Portable X-Ray Stress Analysis System is designed for uses in which measurements must be made in locations with difficult access. Typical applications are measurements in the field such as on oil pipelines, ship hulls, reactor pressure vessels, or power plant steam or cooling pipes. The Model 1620 consists of all of the common components plus the following:

Instrument Enclosures

All electronic components are mounted in two Rack-Pack® shock-mounted instrumentation cases, while the x-ray diffractometer and Model 650 diffractometer mount are contained in a Shok-Stop® foam-filled shipping case. The CRT and printer/plotter are contained in a second Shok-Stop® shipping case. The entire system is self-contained in these four cases, and may be easily moved into the field by truck and/or air freight. The same power distribution system is used as in the Model 1600 system.

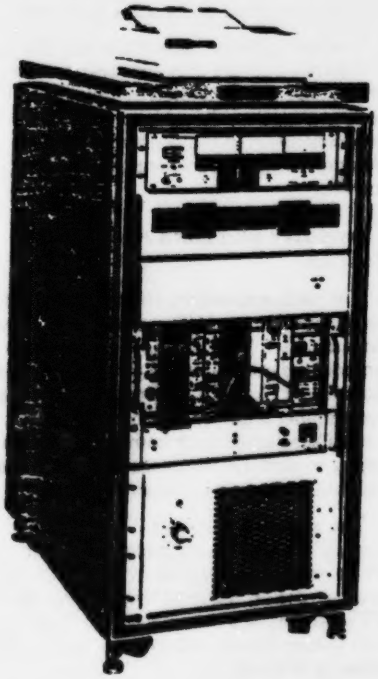

Model 1600 Stationary System

®Rack-Pack and Shok-Stop are the registered trademarks of Thermodyne International, Ltd.

OPTIONS AND ACCESSORIES

Each stress analysis system can be enhanced by adding optional hardware features. These include: a diffractometer ψ-angle motor drive; a diffractometer ψ-angle shaft encoder; a NEMA-12 air-conditioned instrument enclosure and alternative isolated system power supplies; a computer-controlled robotic diffractometer mount; additional pre-aligned x-ray tube assemblies with various targets; a variety of position-sensitive detector mounting brackets; alternative computer peripheral devices; an extended on-site service contract; and detailed customer training courses.

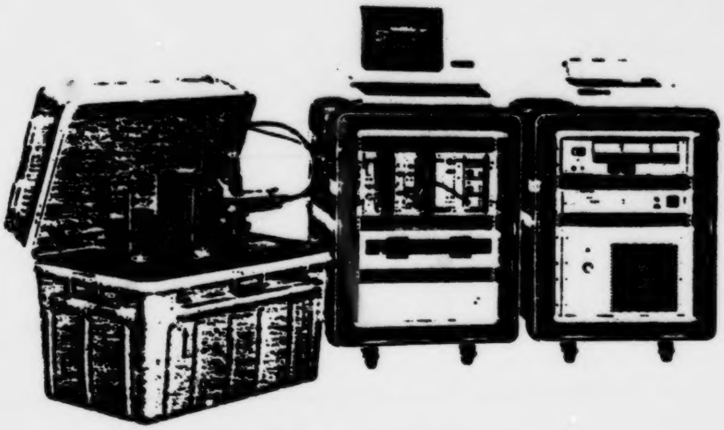

Model 1620 Portable System

Diffractometer Motor Drive

The Model 672 Diffractometer Motor Drive Kit allows complete computer control of the ψ angle via a dc motor, a ψ-angle coupling mechanism, a computer interface module, and an associated software package. The motor mounts on the Model 670 Diffractometer and couples to the ψ-angle motion through a rack and gear mechanism. It is interfaced to the computer via a module which plugs into the Model 673 Encoder Module. All parts, interface logic modules, interconnecting cables, and software are provided.

This option increases the speed with which the experiments can be performed, reduces the human interaction with the system, and results in data with fewer operational errors. It also permits the ψ angle oscillations that may be required when large grain sizes are encountered.

The Model 672 Diffractometer Motor Drive requires the Model 673 Shaft Encoder as a prerequisite.

ψ-Angle Encoder

The Model 673 ψ-Angle Encoder Kit consists of a 12-bit absolute shaft encoder, a coupling mechanism, a computer interface module, and an associated software package. Each time the system requires the present value of the ψ angle, the data are obtained automatically from the encoder rather than by computer-operator interactive dialog. The shaft encoder is mounted on the Model 670 Diffractometer and is coupled to the ψ-angle motion with a precision timing gear and chain mechanism that is driven by a rack and gear mounted in slots already provided on the diffractometer. The encoder is interfaced to the computer via a module that plugs into the Model 641 Safety System. All parts, interface logic modules, interconnecting cables, and software are provided.

Computer-Controlled Robot Arm

The Model 652 Computer-Controlled Robot Arm is offered for those applications in which the Model 651 manually operated articulated arm is inappropriate, such as in automated production line testing of parts. The robot arm has five degrees of freedom, allows all of the motions possible with the Model 651, and is completely computer-controlled. The robot arm may be mounted in a fixed place on a production line, with the electronics mounted in a Model 681 or 682 Enclosure, or on the Model 689 Mobile Transport Cart in place of the Model 651 Articulated Arm.

Power Distribution Systems

The standard isolation transformer provided in the Model 667-1 Power Distribution System operates on 115-V 60-cycle ac power. A 230-V 60-cycle single-phase transformer can be provided in its place (Model 667-2).

The Model 667-3 operates from either 115-V or 230-V power sources without the need for complex wiring and/or isolation transformer interchanges. Conversion from one voltage to the other simply requires interchanging the power input cable.

Instrument Enclosure

The Model 682 Instrument Enclosure is a sealed, watertight, air-conditioned NEMA-12 cabinet and may be used to replace the Model 681 enclosure in the stationary stress analysis system. It has 60 in. of vertical space for standard 19-in. rack mounting modules up to 30-in. deep. A plexiglass front door provides a view of all components mounted in the rack. An air-conditioning system is mounted on the side of the cabinet.

This cabinet will keep the computing system and associated electronic modules free from dust, dirt, and other environmental particles as well as provide controlled temperature and humidity for more trouble-free operation.

DATA ACQUISITION AND ANALYSIS

Each 1600-series X-Ray Stress Analysis System includes a powerful FORTRAN-based real-time data acquisition, control, display, and analysis system — the TEC Stress Analysis Monitor (SAM). SAM is a highly structured software system of proven architecture which produces clear, high-quality documentation, simplifies system validation and verification, and permits fast modifications to incorporate recent research results or to meet special customer requirements.

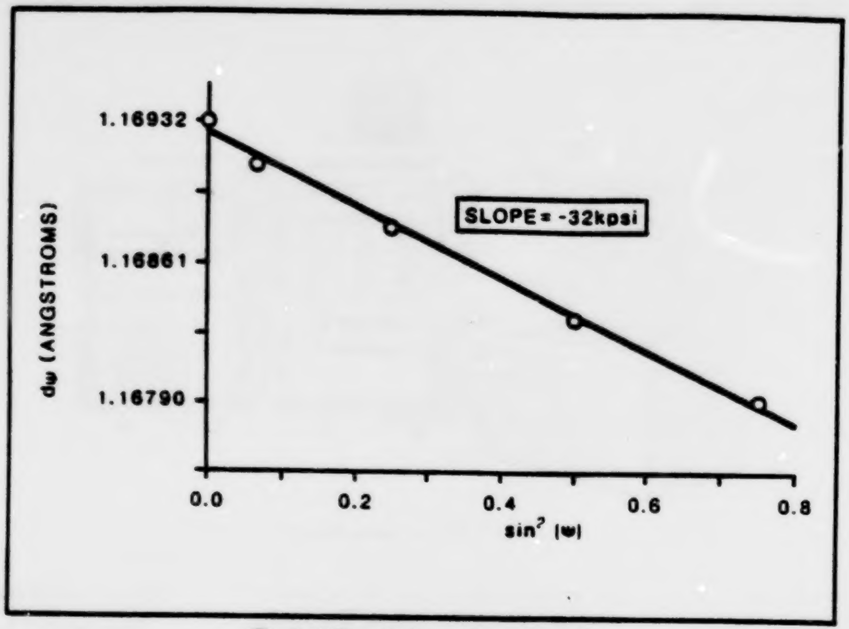

Typical Result from Steel Sample

Data Acquisition and Control

The software system's primary function is the calculation of the stress in the part under test. The x-ray data acquisition processor provides control of the analog/digital detector interface, the detector HV bias supply, and the optional ψ-angle motor drive and shaft encoder. It also controls the graphic display process and is responsible for the acquisition and storage of diffraction, background, and calibration spectra.

Display Processor/Display Formatter

The display processor/formatter software duplicates the graphical display functions found in powerful computer-based multichannel analyzers. Commands to the display processor enter through the command dispatcher. All operator interaction with the system is through simple, prompted dialog via the keyboard and graphics display screen. Ease of operator use has been emphasized.

The point plotter generates the spectra part of the display. Any two spectra may be displayed simultaneously. An exact copy of the current display on the CRT may be reproduced on the printer/plotter via the plotter formatter.

Material Constant Librarian

The Material Constant Librarian (MCL) is a software package that maintains a library of x-ray stress constants for a wide range of metals and alloys. To date, constants for over 50 materials have been entered, and the list is being continually updated. Provision has been made for user modifications and updates.

Data Analysis

The SAM data analysis processor corrects all diffraction curves for both background and detector sensitivity prior to any analysis for peak shape. Furthermore, since the position-sensitive detector records the entire diffraction curve, x-ray powder diffraction corrections for such effects as Lorentz polarization, sample absorption, and $K_{\alpha 1}$ — $K_{\alpha 2}$ peak splitting have also been included.

The d-spacing of the lattice planes is computed for each ψ angle using Bragg's Law, and these values plotted against $\sin^2\psi$. The stress and its standard deviation are computed from the slope of a least squares straight line fitted to the data.

A statistical analysis of the data is performed to provide the confidence limits within which the linear fit is found to be valid. Statistically significant variations from linearity are flagged with an operator warning of inappropriate data analysis.

SERVICE AND SUPPORT

TEC offers six levels of service in support of its Model 1600 family of x-ray stress analysis instruments. These include: (1) system installation and acceptance, (2) customer use and maintenance training courses, (3) warranty service and repair, (4) extended service contracts, (5) software upgrade and enhancement packages for incorporating the most recent software developments into existing instruments, and (6) the Stress Analysis Users' Group.

System Installation

TEC has developed a rigorous set of hardware and software test and demonstration procedures which, insofar as is possible, verify the correct operation of each stress analysis system. Each modular subassembly is tested prior to integration into the system, and each system is thoroughly tested at the TEC factory as described in a written Test and Acceptance Plan. On delivery of the system, representatives of TEC will perform the same Test and Acceptance Plan at the customer's site.

Training Courses

TEC offers a three-day, in-depth training course in the theory, use, and maintenance of its stress analysis systems. The documentation used for the course consists of: the operator's and service manuals provided with the instrument, texts which cover the theory of stress measurements by x-ray diffraction, and review papers which present the theory of position-sensitive detectors. The course is offered at TEC or at the customer's site in conjunction with the performance of the Test and Acceptance Plan.

Warranty Service and Repair

TEC warrants each 1600-series X-Ray Stress Analysis System to be free of defects in workmanship or materials for a period of 12 months after system installation. All warranty repairs and service are based on return of the system or failed component to the factory. TEC will, at its option, repair or replace the component.*

Extended Service Contract

The annual Extended Service Contract (ESC), which is offered to enhance TEC's standard one-year, return-to-factory hardware warranty, includes:

- all parts, materials, and labor
- on-site repair service within 48 hours of verification that a fault exists
- software update and enhancement service
- one annual preventive maintenance servicing of the instrument
- one annual hardware and software refresher course for the customer's operators and service personnel

The Extended Service Contract may be renewed annually. On purchase of the ESC, TEC's standard one-year warranty is explicitly extended for the duration of the new contract.

Software Update and Enhancement Service

The Model 1600-series X-Ray Stress Analysis Systems are dynamic products. TEC will offer new hardware options, and will improve, update, and enhance the computer software on a regular basis. Many of these software enhancements will be a result of direct customer feedback and suggestions made through the User's Group and some will result from TEC's direct involvement with customers to develop customized features for specific applications.

Users' Group

The measurement of loading or residual stresses in the field with portable or mobile instruments such as the 1600-series is dependent on each customer's specific application. TEC is committed to serving its customers with instruments that meet those needs. We have designed the system in a modular fashion such that each unit may be customized to the application. To assist in designing new modules which meet the various application needs of our customers, TEC has founded and supports the X-Ray Stress Analysis Users' Group. This group meets at least annually, at which time the users and representatives from TEC's Product Design, Manufacturing, and Product Management organizations have an opportunity for interchange of information and ideas on any aspect of the system.

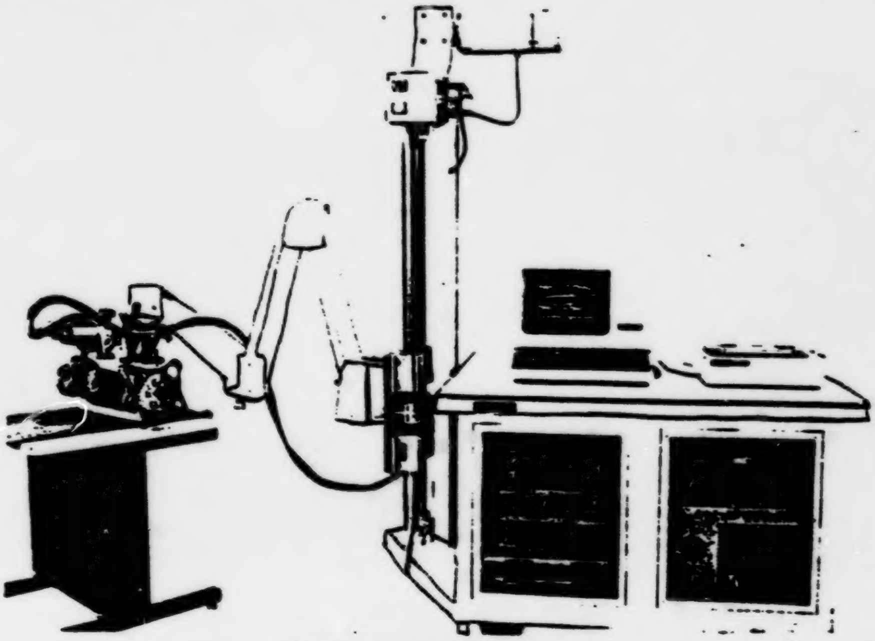

Model 1610 Mobile System

---

*See formal Warranty statement for terms and conditions.

APPENDIX M

AMERICAN ANALYTICAL CORPORATION

1. "Fastress" Automatic Stress Analyzer
2. "Fastress" User List
3. Retained Austenite in Steels

FEB 21 1984

American Analytical Corporation

PHONE: 926-2821
AREA CODE 216

569 NORTH MAIN
GRAFTON, OHIO 44044

Febuary 15, 1984

Mr. Andrew Lowry
ROBERTSON NICKERSON LTD.
75 Albert Street
Suite 610
Ottawa, Ontario K1P 5E7
Canada

Re: Your inquiry about our Fastress* Systems.

Dear Mr. Lowry:

Enclosed you will find our brochure, at the current time we have two models. Model 1200 is a Fastress* Residual Stress Measurement Analyzer this model sells for $63,500.00. Model 1300 is a Fastress* Residual Stress Measurement and Retained Austenite Analyzer this model sells for $84,040.00.

Should you have any questions regarding the above systems or would like more information, please contact us.

Sincerely,
AMERICAN ANALYTICAL CORPORATION

Charles J. Lambright

Charles J. Lambright
President

CJL/ss
Enclosure

The company we keep . . N.A.S.A.
PONTIAC MOTOR DIV.
CHEVROLET MOTOR DIV.
NORTHROP CORPORATION
DETROIT DIESEL ALLISON DIV.
WRIGHT PATTERSON A.F.B.
WESTINGHOUSE ELECTRIC CORP.
U.S. ARMY TANK AUTOMOTIVE
CLARK EQUIPMENT CO.
MOTOR WHEEL CORP.
FORD MOTOR COMPANY
CATERPILLAR TRACTOR CO.
CHRYSLER CORPORATION
J. I. CASE COMPANY
EMS LABORATORIES
GENERAL MOTORS CORP. OF CANADA
W. HEGENSCHEIDT GMBH
GENERAL MOTORS CORP. (MICH.)
OLDSMOBILE DIV.

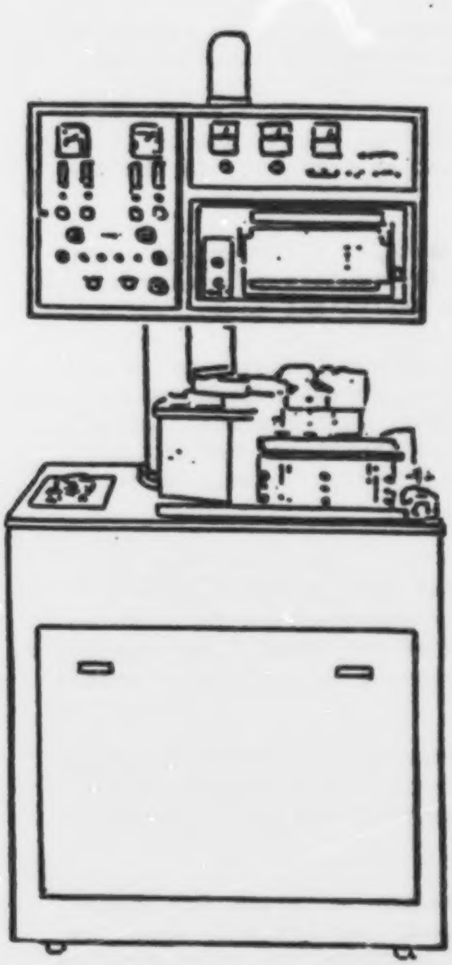

AUTOMATIC
STRESS
ANALYZER
FASTRESS*
*T.M. of GENERAL MOTORS CORP
RESIDUAL STRESS MEASURMENTS
IN LESS THAN ONE MINUTE

GENERAL ELECTRIC CO.
ROCKWELL INTERNATIONAL
BORG & BECK DIV.
FIRESTONE STEEL PRODUCTS
MASSEY-FERGUSON, INC.
WESTERN GEAR CORPORATION
HYDRA-MATIC DIVISION
ATLAS CRANKSHAFT CORP.
MORSE CHAIN DIVISION

AMERICAN ANALYTICAL CORPORATION
589 N. MAIN STREET • GRAFTON, OHIO 44044 • (216) 926-2821

NEW PRODUCTION TOOL MEASURES RESIDUAL STRESSES on the LINE

Built for in-plant use, this compact X-ray instrument can measure stresses in about 30 sec. Even faster operation in a "go-no-go" mode can cull out substandard parts, fitting the machine for routine 100% nondestructive testing.

The Fastress system was developed by General Motors for routine laboratory and production use; a modern system for rapid X-ray diffraction measurement of residual stresses. Fastress* has been licensed by General Motors to the American Analytical Corporation for commercial production. This instrument has been used to determine stresses, tensile or compressive, in steering knuckles, shot-peened coil springs, and many other automotive components. Rugged enough to be employed for routine stress determinations on the production line, Fastress has one console for all the equipment, and is light enough to be rolled on casters or carried by crane or fork-lift to the desired site.

The use of X-ray equipment to measure stress in metals, although not a new technique, has gained in importance in many non-destructive laboratories due to its proven capability as a rapid and accurate analytical tool.

Fastress has been developed to meet the needs of modern industry by providing the means to obtain a faster more accurate measurement automatically; in about thirty seconds. In addition, the Fastress, with the addition of the new Retained Austenite Development by American Analytical Corporation, provides endless possibilities to present Fastress users, as well as to new users.

The Fastress is now in use in major industries. This instrument has two X-ray sources, 60° apart, which irradiate the same area of the sample at the same time. The detected output drives two servomechanisms to find two points of equal corrected intensity on each peak of reflected X-ray energy. Differences between peaks indicate the stress which is automatically recorded in psi directly on strip chart.

One of the many applications of the Fastress system is employed to monitor heat treated bearings, check carburized parts for tensile stresses (which indicate decarburization), and determine the extent of residual stresses generated during surface finishing operations.

The projected applications of the Fastress system are unlimited for checking stress-bearing components for residual stresses, particularly when the part has an important safety function. Already, bearings and other critical components such as gears and shafts, etc. are undergoing this Fastress technique. Reliability and quality are becoming very fashionable functions of the auto and other industries — to remain competitive in the world and domestic markets.

As one quality control engineer stated, the Fastress is a test instrument that keeps up with your imagination!

*T.M. of GENERAL MOTORS CORP.

AMERICAN ANALYTICAL CORPORATION
[illegible] N. [illegible] STREET • GRAFTON, OHIO 44044 • [illegible]

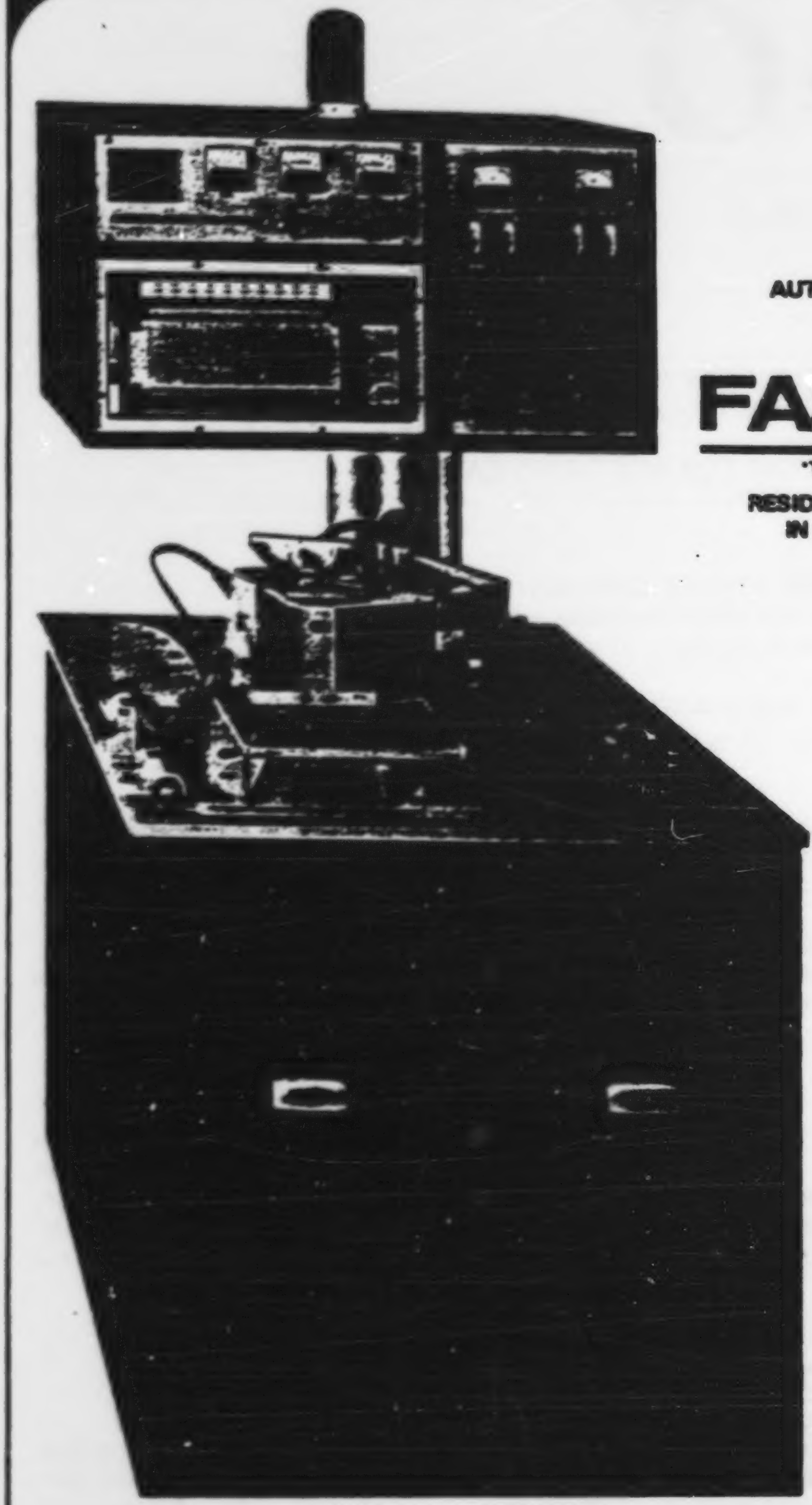

AUTOMATIC
STRESS
ANALYZER

FASTRESS*

*T.M. of GENERAL MOTORS CORP.

RESIDUAL STRESS MEASURMENTS
IN LESS THAN ONE MINUTE

- ● Automatic X-Ray Residual Stress Analyzer.
- ● Non-Destructive for Most Applications.
- ● Provides Rapid Stress Gradient Profiles.
- ● Aids Study of Wear and Failure Analysis.
- ● Provides Close Quality Control and Reduces Cost.
- ● Aids Material Selection and Plant Process Development

AMERICAN ANALYTICAL CORPORATION

[illegible] N. MAIN STREET • GRAFTON, OHIO 44044 • (216) 926-2821

FASTRESS* σ

RESIDUAL STRESS MEASUREMENTS IN LESS THAN ONE MINUTE…

FASTRESS* is the two X-Ray tube dual beam peakseeking diffractometer system that can perform residual stress determinations of soft steel in 10 seconds, hardened steel in 30 seconds and also aluminum alloys in less than 30 seconds.

1. **FASTRESS* IS AN AUTOMATIC X-RAY RESIDUAL STRESS ANALYZER.**
   Presents data directly on calibrated strip chart recorder in psi.
2. **FASTRESS* IS NONDESTRUCTIVE FOR MOST APPLICATIONS.**
   Positioning flexibility permits stress measurements on surfaces of large cumbersome components without dissection or destruction of residual stress fields or levels.
3. **FASTRESS* RADILY PROVIDES STRESS GRADIENT PROFILES.**
   Rapidity of measurments permits either step-wise or continuous slow scan of surface area in in order to locate surface stress gradients or show the nonexistance of such conditions.
4. **FASTRESS* AIDS STUDY OF WEAR AND FAILURE ANALYSIS.**
   Take guess-work out of determining direction of level of stresses at near potential areas of failure.
5. **FASTRESS* PROVIDES CLOSE QUALITY CONTROL CAPABILITIES AND REDUCES COST.**
   Ease of specimen fixturing and speed of measurment provides critical data within minutes of production or continued processing.
6. **FASTRESS* AIDS MATERIALS SELECTION AND PLANT PROCESS DEVELOPMENT.**
   Confirms best selection of alloy, production parameters and confirms plant procedures for greatest cost savings and reliability.

INTRODUCTION TO PROGRESS…

The FASTRESS* concept, a modern system for extremly rapid X-Ray diffraction surface stress studies, was developed for production and laboratory use.

For many years the X-Ray technique has provided the greater mass of residual stress data and with the advent of the FASTRESS*, the improved technique will reduce measurement cost, manpower cost and provide the best data possible in the shortest time.

COMMON APPLICATIONS…

The effects of heat treating, shot or stress peening, of nonthermal treating such as cold rolling, roller finishing or deep rolling can be measured, as well as stress gradients in cross section of welded materials or other components and materials.

Stresses are measured in fabricated components, in-process materials, and finished components. FASTRESS* can evaluate plant processes, control processes, monitor supplies, and develop, accept or reject criteria.

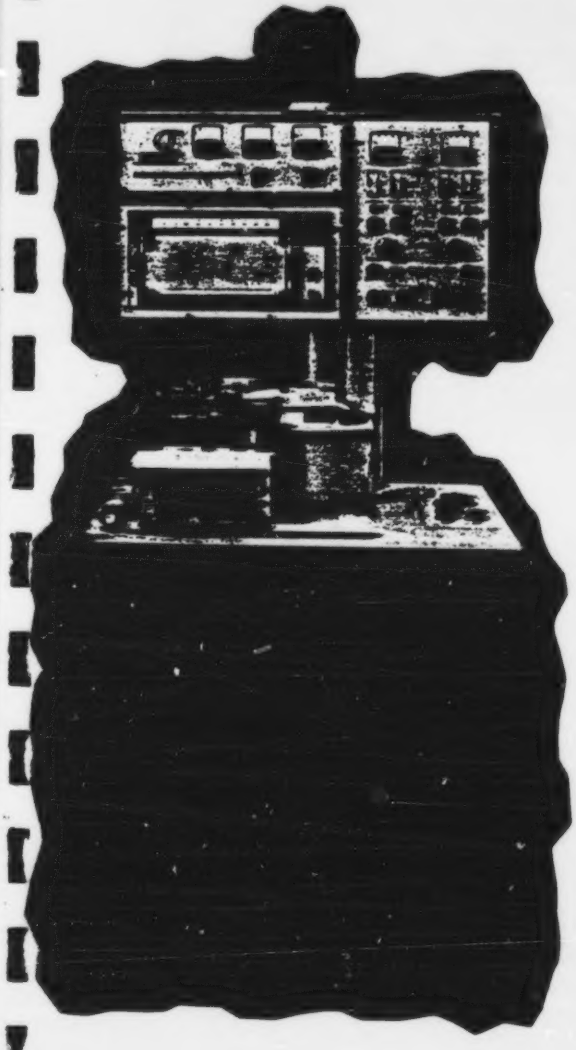

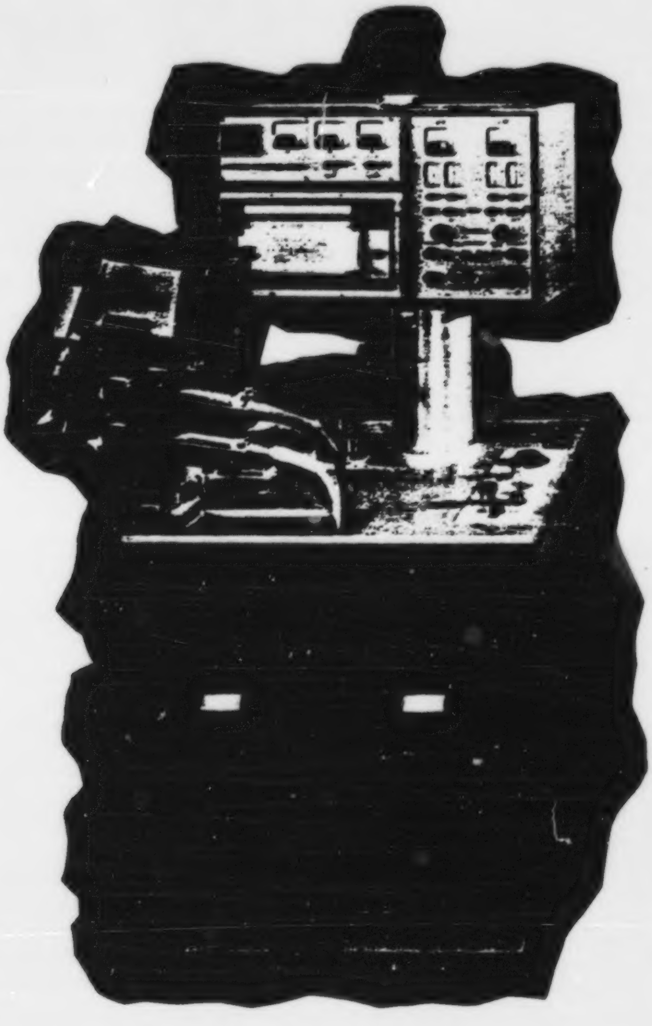

IMPORTANT FEATURES OF FASTRESS...

By moving the sample past the X-Ray beams or by transversing the goniometer, the recorder will indicate level changes in stress as to compressive or tensile stress and magnitudes. Researchers have shown that very steep gradients over small physical dimension can and do lead to premature failure. FASTRESS* is convenient and safe, requires no more alignment, or radial slide adjustment, and eliminates long cumbersome calculations and/or mistakes.

Photographs courtesy of Stress Measurements Incorporated Hawthorne, Calif.

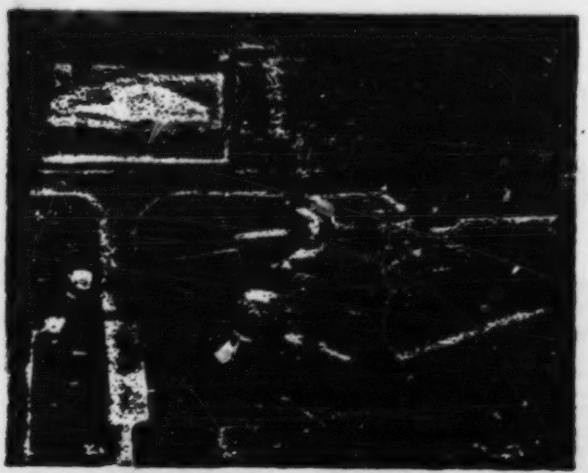

Close-up of goniometer head of FASTRESS*, showing a weldment positioned before the dual X-Ray beams. One of the two dual geiger counters is in foreground.

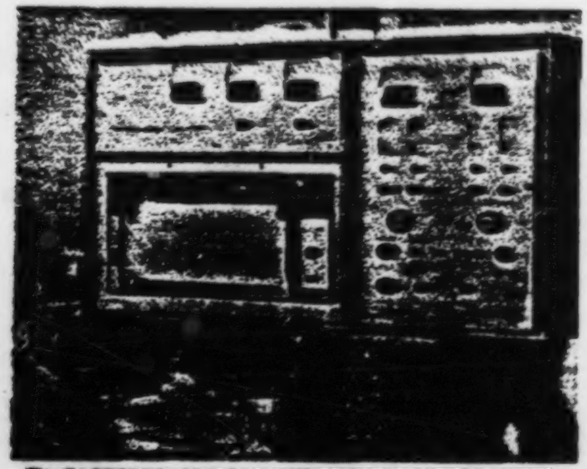

The FASTRESS* RESIDUAL STRESS ANALYZER in use to measure residual stresses on a complex steel weldment.

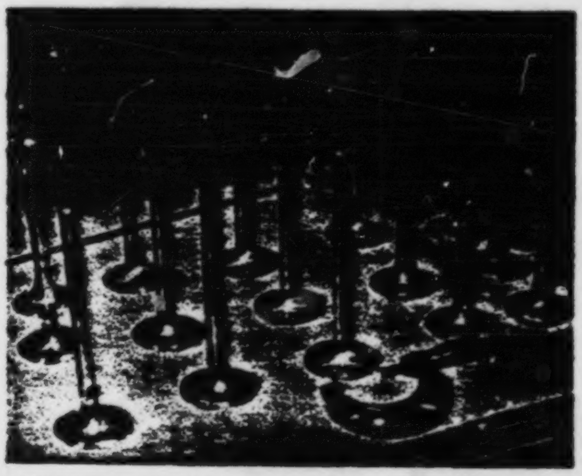

Valve stems used in a large diesel engine. Residual stresses were measured at the surface, and at depths below surface by electrolytic polishing layer removal.

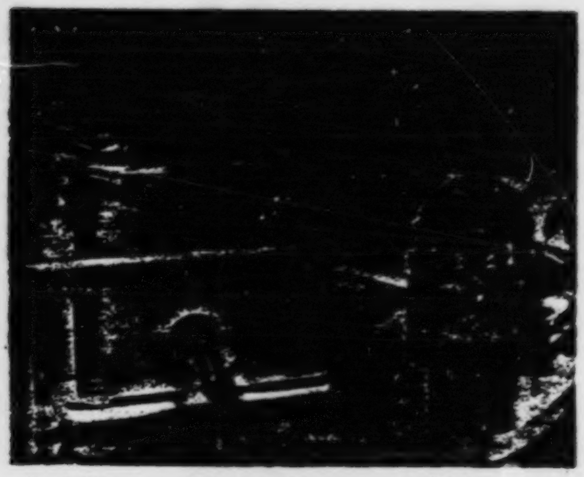

A spiral-bevel gear is inspected to measure residual stress at critical points.

FASTRESS* SYSTEM
ARRANGEMENT OF X-RAY TUBES (T)
AND COUNTERS (C)

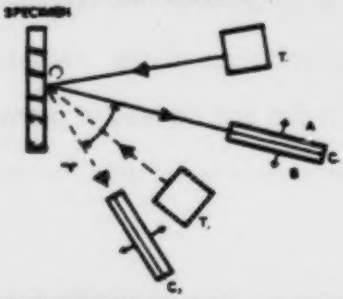

FASTRESS* is:

1. Designed for measurements on ferritic and martensitic steels.

2. Able to investigate materials that produce a diffraction line in the 152°-159° 2 Theta range.

3. Mobile and may be used in either plant or laboratory.

4. Well suited to making a rapid exploration of possible stress variations from point to point on a surface.

5. A device that incorporates the most modern sample alignment, mechanical and/or optical.

AMERICAN ANALYTICAL CORPORATION

589 N. MAIN STREET • GRAFTON, OHIO 44044 • (216) 926-2821

FASTRESS USER LIST

Serial No. Installation	Company
1001-72 3/14/72	N.A.S.A. George C. Marshall Space Flight Center, Alabama 35812 Mr. Ed Risch (205) 453-2492
1002-72 11/ /72	Pontiac Motor Divsion General Motors Corporation Plant #1 Pontiac, Michigan 48053 Peter Novasell (313) 857-2485 Mrs. Cesarz
1003-72 10/26/72	Chevrolet Motor Division General Motors Corporation Livonia Plant, Spring & Bumper Livonia, Michigan 48151 John Cary (313) 464-2200 Vic Deogravas
1004-72 12/5/72	Northrop Corporation Aircraft Division 3901 W. Broadway Hawthorne, CA 90250 George Blake (213) 970-4963
1005-72 3/21/73	Detroit Diesel Allison Division General Motors Corporation 13400 W. Outer Drive Detroit, Michigan 48228 Jim Feehan (313) 592-5749 Crag Allen
1006-73 6/20/73	Wright Patterson A.F.B. Flight Dynamics Laboratory Area B Wright Patterson AFB, Ohio 45433 John Potter, AFFDL/FBR (513) 255-6104
1007-73	Wright Paterson State University

FASTRESS USER LIST
PAGE 2

Serial No. Installation	Company
1008-73 12/19/73	Westinghouse Electric Corporation Power Generation Division Steam Turbine Group Essington, PA. 19029 Terry Laughain (215) 237-2964
1009-74 3/8/74	U.S. Army Tank Automotive Command Warren, MI. 48090 Sam Catalano (313) 574-8837 System Placed at Firestone Dick Hayworth (317) 773-0650 X 373
1010-74 6/6/74	Clark Equipment Company Manufacturing Research Dept. 324 E. Dewey Ave. Buchanan, MI. 49107 Ken Spray (616) 697-8593
1011-74 10/16/74	Motor Wheel Corporation 1600 North Larch Lansing, MI. 48914 Garth Lawrence (517) 458-9131 x 243 Roger Jenks
1012-74 2/22/75	Ford Motor Company Manufacturing Development Center Sterling Heights Axil Plant Detroit, MI. 48914 ~~Wallace Lesnick~~ (313) 533-1035, x 2841 Bart Osiewicz 592-2268
1013-75 4/23/75	Caterpillar Tractor Company 600 West Washington Street East Peoria, IL 61611 Robert Buenneke (309) 675-2011

M-10

Serial No. Installation	Company
1014-75 11/6/75	Chrystler Corporation Engineering Laboratory 12800 Oakland Blvd. Highland Park, MI. 40203 Gary Robertson (313) 956-4621
1015-76 6/29/76	J. I. Case Company Corporation Test Center Tractor Plant Racine, Wisconsin 53403 Theodore Weins (414) 636-7480
1016-76 8/13/76	EMS Laboratories Hawthorne/Airport Business Park 12517 Crenshaw Boulevard Hawthorne, CA. 90250 Mrs. Bernidene Tooper (213)973-6694
1017-76 7/17/76	General Motors Corporation of Canada Ltd. Ontario Street St. Catharines, Ontario Tony Frankcavilla (416)685-2218 ~~Linda Mens~~ ~~Howie Abraham~~
1018-76 9/12-77	W. Hegenscheidt GMBH Neusser Str. 3 5140 Erkelenz West Germany
1019-76 10/4/77	General Motors Corporation Manufacturing Development Reserach Center 12 Mile and Mound Roads Warren, Michigan 48090 Henry Patterson (313) 575-0850

Serial No. Installation	Company
1120-77 12/18/78	Oldsmobile Division General Motors Corporation Lansing, Michigan 48921 Jay Harrison (517) 373-5722
1121-77 1/5/78	General Electric Company Large Steam Turbine-Generator Operation 273 North Avenue Schenctady, New York 12345 Harry Beattie (518) 385-7369
1122-77 1/10/78	Central Foundry Division General Motors Corporation 77 West Center Street Saginaw, Michigan 48605 Gene Wistehuff (517) 776-3459
1123-78 4/27/78	Rockwell International Automotive Operation 2135 West Maple Road Troy, Michigan 48084 Mike Johnson (313) 435-1715
1124-78 9/15/78	Borg & Beck Division Borg-Warner Corporation 6700 18½ Mile Road Sterling Hts, Michigan 48078 Daniel Olah (313) 739-6000
1125-78 10/30/78	Firestone Steel Products 1600 Firestone Parkway Akron, Ohio 44301 Charles Scarton (216) 379-6426

M-16

FASTRESS USER LIST
PAGE 5

Serial No. Installation	Company
1126-78	Auburn Gear Aburn, Indiana 46706 Ervin Richert (219) 925-3200 x 242
1127-79	Burton Spring 2441 West 48th Street Chicago, IL 60632-1493 Chester Gniadecki (312) 376-1200
1328-79 11/5/79	Western Gear Corporation 14724 East Proctor Avenue City of Industry, CA 91744 Perry Glen (213) 968-6535
1329-79 4/7/80	Hydra-Matic Division General Motors Corporation Willow Run, MI. Marilyn Smith (313) 485-5038
1230-79 5/1/80	Atlas Crankshaft Corporation P.O. Box 846 Fostoria, Ohio 44830 Larry Midla (419) 435-8531
1231-80	General Electric Company System placed at TRW Bearings Jamestown, New York
1232-80	Borg Warner Corporation 770 Warren Ithaca, NY. 14850 Paul Beeman
1333	American Analytical Corporation 569 North Main Street Grafton, Ohio 44044 Charles J. Lambright (216) 926-2821

Serial No. Installation	Company
1234-81	Cummins Engine Company Jamestown Engine Plant 4720 Baker Street Lakewood, NY. 14750 Bruce Pfeffer (716) 456-2459
1335-81	Detroit Diesel Allison Division of General Motors Corporation P.O. Box 894 Indianapolis, IN 46206 Ray Anderson (317) 242-2895
1236-81	Split Ballbearing Division of MPB Corporation Highway Four Lebanon, New Hampshire 03766 Bill Ogden (603) 448-3000 x 211 John Bressond
1337-81	Eaton Corporation Engineering & Research Center 26201 Northwestern Highway Southfield, Michigan 48037 Aquil Ahmad (313) 354-2789 Roy Doby
1238-81	The Embassy of Pakistan in Germany
1339-82	U.S. Army Tank Automotive Command 6501 E. Eleven Mile Road Bldg. 203 Warren, MI 48090 Sam Catalano (313) 574-8837
1340-83 6-7-83	Warner Gear Division of Borg-Warner Corporation 5401 Kilgore Ave. Muncie, Indiana 47302 William P. Ashman (317) 286-6347

Serial No. Installation	Company
1341-83	Clark Equipamentos Clark Ltda Bia Anhanguera, KM84 Valinhos SP P.O. Box 304 Campinas SP Brazil Phones 712444, 713444 (PABX)

[illegible]

American Analytical Corporation

PHONE: 926-2821
AREA CODE 216

569 NORTH MAIN
GRAFTON, OHIO 44044

RETAINED AUSTENITE IN STEELS

For the past 12 years American Analytical Corporation has been the major supplier of instrumentation for the measurement of residual stresses by X-Ray Diffraction and in particular by the Fastress* concept as developed by General Motors Corporation in 1967, however, almost from the very beginning American Analytical Corporation has been asked to also incorporate a retained austenite device with the Fastress* for rapid stress measurement and simultaneous retained austenite. In November 1979 we supplied the first such system and since than we have supplied 5 more dual systems.

Since not all potential users require residual stress values we can also supply the Retained Austenite as a separate free standing unit. The American Analytical Corporation, Retained Austenite system is based on a muliple stationary counter tube array and stationary X-Ray tube concept. After conferring with several engineers whom routinely use X-Ray Diffraction for Retained Austenite measurement and reviewing the SEA manual SP-453 "Retained Austenite and Its Measurement by X-Ray Diffraction", we have developed the current system.

With the use of a chromium x-ray diffraction tube $K\alpha$ 2.29°A and selecting the most common two peak method, the volume percentage of Retained Austenite is determined from the measured integrated intensities of the (200) martensite and (220) austenite peaks using the following equation.

$$\text{Volume \% A} = \frac{100\ Vc}{1 + \frac{I(200)_M}{I(220)_A} \times 2.55}$$

Where Vc is the percentage of carbide by volume, 2.55 is the ratio of measured intensities of $\frac{220A}{200M}$ calculated for as quenched (untempered) 1.0% carbon steel which shows random orientation and no significant texture or preferred orientation. The Vc value, intensity ratio value and counting time are input via thumbwheel switches.

The novel portion of the American Analytical Corporation, Retained Austenite system is primarily based on the rapid accumulation of integrated intensities of the 200M and 220A diffraction peaks. Instead of a single scanned or step-scanned diffracted beam slit to accumulate the peak data, the American Analytical Corporation system uses a multiple counter tube array to collect data. A step like series of 2° wide opening in a radused body intersecting the 200 Martenite at approximately 107° 2 θ and the 220 Austenite peak at approximately 128° 2 θ, is fundamentally a counter tube at every 2 degrees wide diffracted beam slit, which covers the total diffracted peak. In order to determine net intensity above background, the two outer most 2° slits for each peak are used for backgound averaging and by subtracting same from the total integrated intensity, net accumulated intensities can be supplied to a microprocessor as well as the other previously input parameters such as intensity ratio, volume carbides and counting time.

American Analytical Corporation has developed a novel concept for ratioing the varified X-Ray efficiencies from 11 to 24 individual GM counter tubes by using a scattering media which has not diffraction peaks in the angular ranges utilized. In this fashion is not necessary to select matched counter tubes or matched vanadium beta filters.

Normal daily start-up requires about 100 seconds to collect data for the counter tube rationing procedure. Should the operator desire a standardization, a routine has been made avaible for calibration to known standards.

Samples with from 2% to 5% Retained Austenite can be determind in from 100 to 200 seconds and samples with from 5% to 10% require routinely 100 seconds and samples of 10% to 50% require about 50 seconds of analysis time. Since 2% is usually the lower limit of deiectablity for most labs, we believe from experience that our reproducablity is well within ± 1% Retained Austenite.

The American Analytical Corporation Retained Austenite System is not designed as a basic research tool or to replace standard diffractometer systems, but a concept to accumulate Retained Austenite values in well documented material types in less than 2 to 3 minutes, we have successfully determined Retained Austenite in M50 and 52100 type steels as well as other steels.

Should a customer desire additional diffraction peaks, American Analytical Corporation can design detector arrays to meet such requirements.

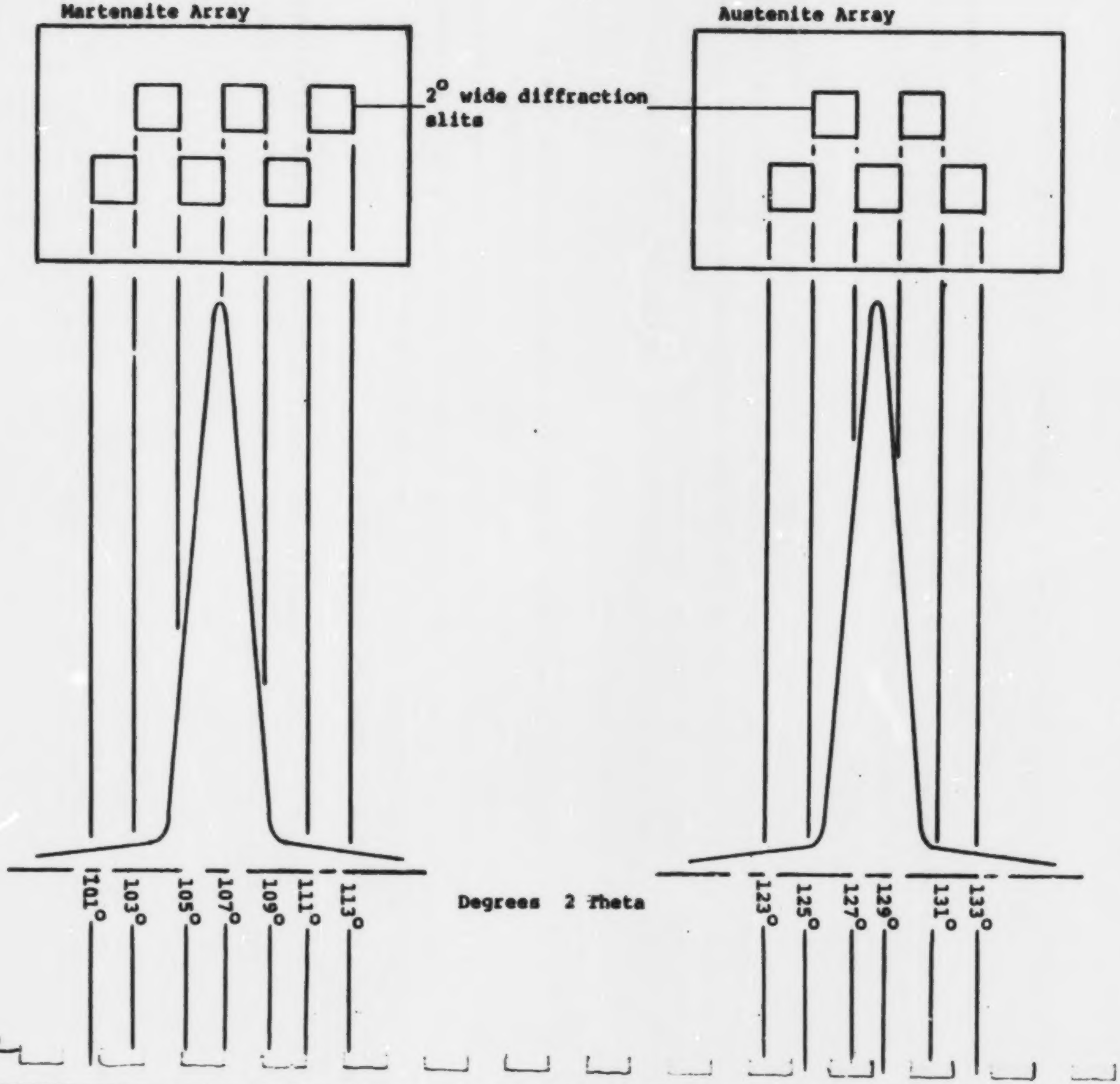
Martensite Array
Austenite Array
2° wide diffraction slits
101°
103°
105°
107°
109°
111°
113°
Degrees 2 Theta
123°
125°
127°
129°
131°
133°

Not to scale

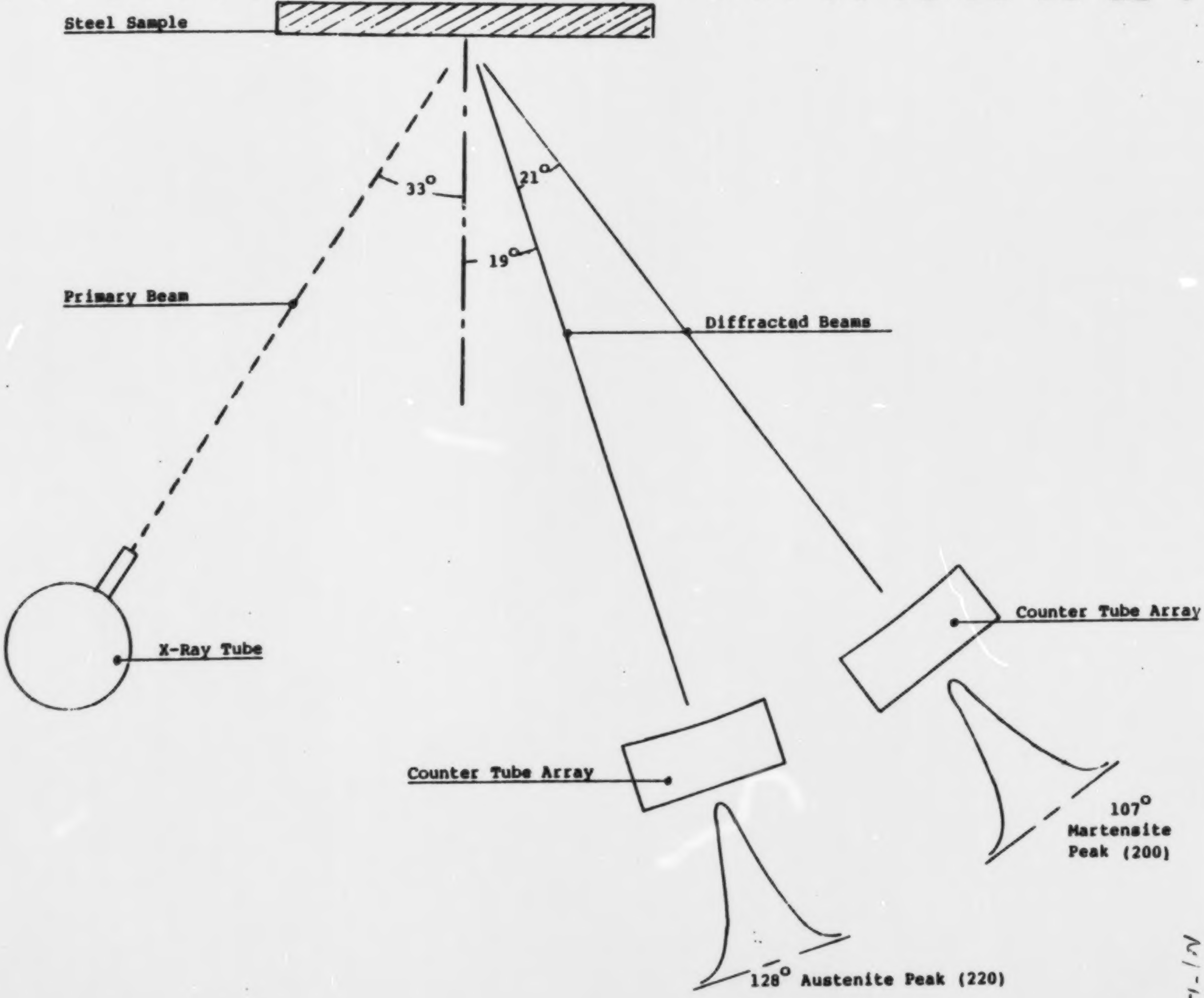
Steel Sample
33°
21°
19°
Primary Beam
Diffracted Beams
X-Ray Tube
Counter Tube Array
Counter Tube Array
107° Martensite Peak (200)
128° Austenite Peak (220)

NT-12

APPENDIX N

SIEMENS-ALLIS

1. X-ray Measurement of Residual Stress on a Welded Stainless Steel Pipe Joint Connection
2. X-ray Analysis of a Pipeline

SIEMENS

RECEIVED
AUG 16 1982
T.F. GRODEN

Applications note No. 68

X-Ray Measurement of Residual Stress on a Welded Stainless Steel Pipe Joint Connection

by R. Prümmer and H.W. Pfeiffer-Vollmer
Fraunhofer-Institut für Werkstoffmechanik

Introduction

Non-corroding austenitic steels may be sensitive to cold working or welding. The change in the structural and mechanical properties due to these processes may adversely affect the ductility and corrosion resistance and therefore the structural behavior. Residual stress is an indicator of this behavior and is therefore of great importance. Also, exact details of the heat treatment used after welding are often missing. References are found in the AD pamphlets AD-W2, AD-W10 and AD HP 7-3 of the Deutsches Regelwerk [German Control Installation] of the AD-Federations.

In this study, a welded T-joint of austenitic steel was subjected to an X-ray residual stress analysis near the welding seam.

Principles of X-ray Stress Measurement

If an X-ray beam of wavelength λ is diffracted through the lattice planes of the crystallites near the surface of a multi-crystalline material, diffraction occurs at an angle which satisfies the Bragg equation.

$$2\,d \sin \Theta = \lambda \tag{1}$$

where d represents the lattice spacing of the analysed crystal planes.

Stress changes the lattice spacing and thereby also changes the Bragg angle Θ; the following relationship exists between these changes

$$d\,\Theta = -\tan \Theta \,\frac{d\,(d)}{d} \tag{2}$$

If one now equates the relative change in the lattice spacing $\frac{d\,(d)}{d}$ with the strain term in the fundamental equation of elasticity theory for the double axial stress condition (for angular relationship see Fig. 1)

$$\varepsilon_{\phi,\psi} = \frac{\nu + 1}{E}(\sigma_1 \cos^2 \phi + \sigma_2 \sin^2 \phi) \sin^2 \psi - \frac{\nu}{E}(\sigma_1 + \sigma_2) \tag{3}$$

$\xi_{\phi,\psi}$ = strain in any random direction
λ = Poisson's ratio
E = elasticity modulus [Young's modulus]
σ = principal stresses

and so the basic equation for X-ray stress measurements by the "$\sin^2\psi$–procedure" is derived.

$$-\cot \Theta\, d\,\Theta = \cot \Theta_0\,(\Theta_0 - \Theta_{\phi,\psi}) = \frac{\nu + 1}{E}\sigma_\phi \sin^2\psi - \frac{\nu}{E}(\sigma_1 + \sigma_2) \tag{4}$$

with Θ_0 = Bragg angle of the non-stressed phase
σ_1, σ_2 = Principal stresses

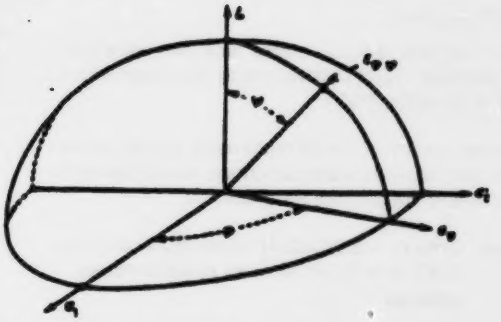

Fig. 1 Determination of the direction ϕ, ψ, for X-ray stress measurements. ϕ = azimuth angle relative to the principal stress σ_1; ψ = angle relative to the surface normal L of a sample with the principal stresses σ_1 and σ_2 perpendicular to each other.

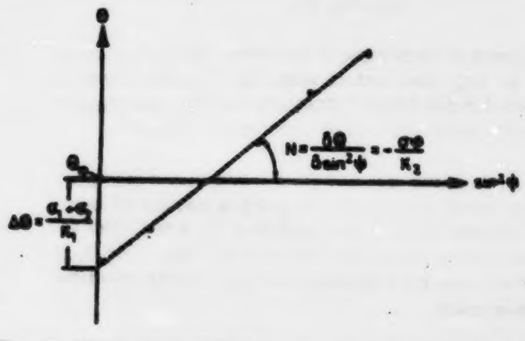

Fig. 2 X-ray determination of elastic stresses from the change in the Bragg angle.

A plot of the Bragg angles measured at various angles ψ versus $\sin^2\psi$, for each angle ϕ, results in a constant which is a function of the Bragg angles shift versus $\sin^2\psi$.

Substitution of the following into equation (4)

$$K_1 = \frac{E}{\nu} \cot \Theta_0$$

$$K_2 = \frac{E}{\nu + 1} \cot \Theta_0$$

$$N = \delta\Theta_{\phi,\psi} / \delta \sin^2\psi$$

$$\Delta\Theta = \Theta_{\phi,\psi=0} - \Theta_0$$

it follows that for the stress component $\sigma\ \phi$

$$\sigma_\phi = -K_2 \cdot N \qquad (5)$$

meaning, $\sigma\phi$ is proportional to the slope N of the measured $\Theta - \sin^2\psi$ line in Fig. 2.

The sum of the principal stresses which appears in equation (4) is given as

$$(\sigma_1 + \sigma_2) = K_1 \cdot \Delta\Theta$$

and is therefore proportional to the y-intercept in Fig. 2.

For further details the appropriate literature is referenced[1) 2)].

Experimental Procedure

The X-ray structural and residual stress analyses were performed with a Siemens D500 Diffractometer equipped with a position sensitive detector (PSD).

The fully automatic control of the diffractometer as well as the data acquisition and analysis were performed with a Siemens computer PR 310 and the System Program 310.

Radiation used: CrKα (λ = 2.28962 Å) for structural analysis
CrKβ (λ = 2.08479 Å) for residual stress analysis

Beam Divergence: 1°
PSD Opening: 6°

Tube Current/Voltage: 30mA/40kV
Measuring Point (1, 2): spot size 2 x 2mm², 7mm distant from the center of each welding seam (see Fig. 11).

For the alignment of the sample in the diffractometer a special holder with an alignment fixture was built. Figures 3 and 4 show the T-joint in the D500 Diffractometer. The micrometer permits sample alignment with an accuracy of ± 5μm.

Since the surface of the test sample showed traces of impact and pressure marks, a portion of the sample was cut off, electrolytically polished (20μm) and centured on a pin. This allowed the insertion of the portion into a swivel mount (Fig. 5) in order to rotate it around the pipe axis and thereby examine the entire circumference.

Before the residual stress analysis, in order to determine the crystallinity of the sample, a photographic diffraction pattern was recorded with a flat camera which was mounted on the tube stand of the D500. Fig. 6 shows the arrangement used and Fig. 7 the pattern. From this pattern, the suspicion of a coarse crystal formation near the weld of the T-joint could be ruled out. Using an aperture of 0.5mm diameter (approx. identical to the irradiated spot on the sample), single diffraction spots would have to show up if a coarse crystalline sample were present.

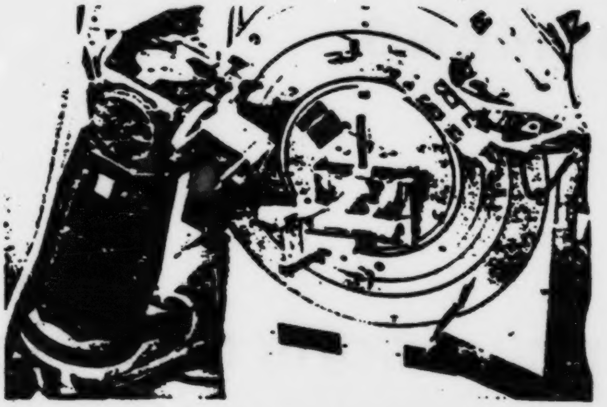

Fig. 3 Sample holder for T-joint in the Siemens D500 diffractometer equipped with position sensitive detector.

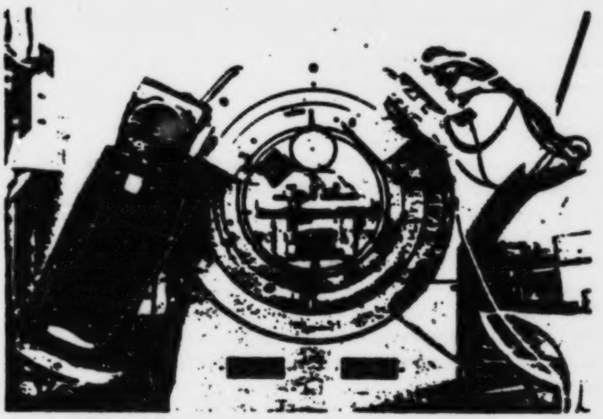

Fig. 4 Alignment fixture for accurate positioning of the sample in the D500 diffractometer.

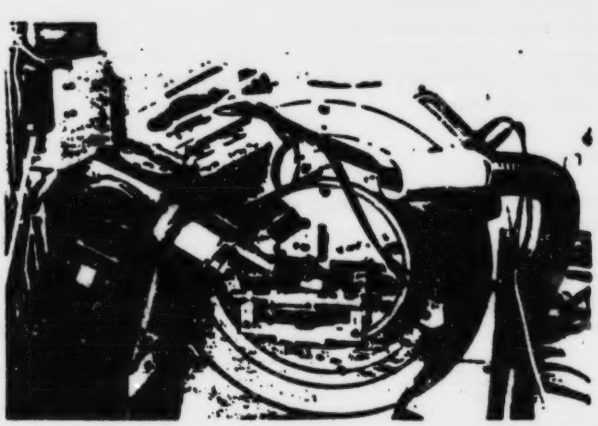

Fig. 5 Sample in holder for residual stress measurement during sample rotation.

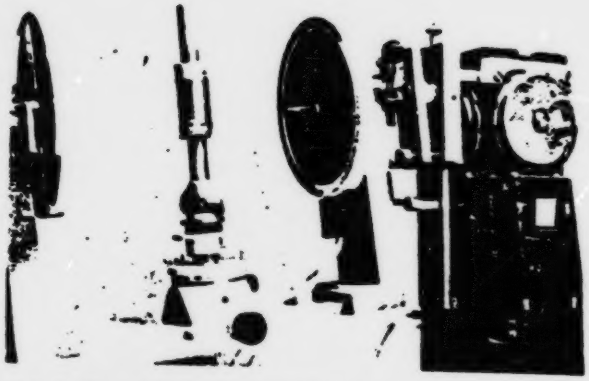

Fig. 6 Positioning of the back-reflection Debye-Scherrer camera on the D500.

For the actual residual stress analysis, the peak positions of the {311}–Kβ–diffraction line were measured with various positive and negative ψ off set angles. For this, only the portion of the diffraction line profile which exceeded 50% of the maximum intensity after subtraction of the background (Fig. 8) was used. The line positions of the corresponding positive and negative ψ–angles were averaged arithmetically.

The elongation values calculated by the 2Θ–sin²ψ procedure were converted to stress values using mechanically determined values of E = 210,000 N/mm² and ν = 0.28.

Results

Since no specifications for the material to be tested were available, the pipe piece was initially subjected to a structural analysis (as described under 3, Experimental Procedure). The diffraction pattern (Fig. 9) shows the typical reflections of a pure austenitic phase and is identified as such. In view of this result the following theoretical reflections are available for residual stress analysis:

1. { 420}, 2 Θ = 148° with CuKα radiation
2. .{ 222}, 2 Θ = 137° with FeKα radiation
3. { 311}, 2 Θ = 148° with CrKβ radiation

Because the CuKα radiation causes strong fluorescence radiation in the sample (recognized by the high background), preference must be given, in this case, to the CrKβ and reflection 3. A determination of the diffraction angle from raw material filings resulted in $2\,\Theta_o = 148.090°$ and therefore a lattice constant of a = 3.589 Å for the austenitic steel.

First residual stress analyses were performed on the original surface of the specimen. Fig. 10 shows the {311} –Kβ reflection, as it was used for those stress measurements. This refers to the measuring point 1 in Fig. 11. A strong broadening of the peak is present, which complicates the exact determination of the line position. Therefore, wide scatter appears in the data points of the 2 Θ – sin² ψ plots. Fig. 12 shows the plot which results from the determination of the stress component $\sigma_{u,1}$ at point 1.

This results in a compression residual stress of

$\sigma_{u,1} = -170 \pm 68$ N/mm².

The observed scatter in the points is most likely due to the faulty surface of the material as a result of the manufacturing process. Mill scale and edgelike compression marks are present. The influence of surface irregularities, possibly present in the pipe can be largely excluded, since the intensity of the diffraction lines determined under various ψ–directions, does not show a ψ–dependence. This is shown in Fig. 13.

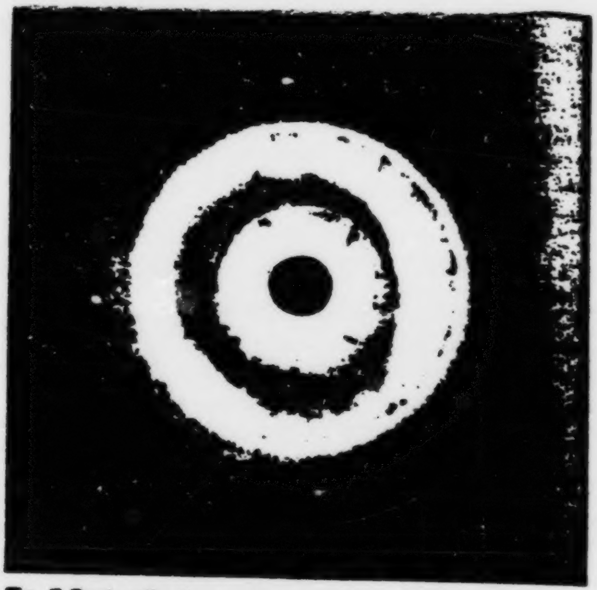

Fig. 7 Back reflection pattern produced by the austenitic T-joint CrKα, {220}–plane (outer ring) and {200}–plane (inner ring).

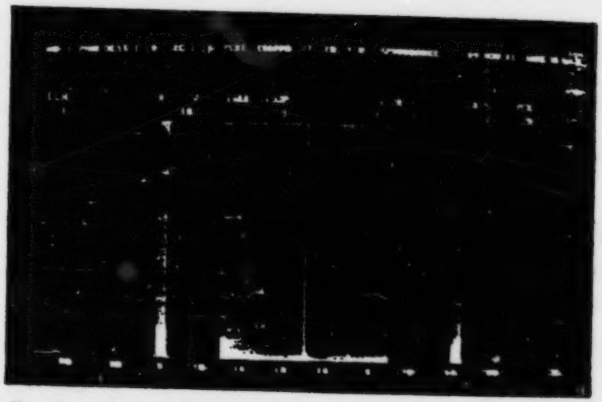

Fig. 8 { 311} –Diffraction peak used for stress analysis with measuring windows for background and peak position.

In order to obtain unambiguous measuring results, the impure surface layer was electrolytically removed and the cleaned portion was measured under rotation, as is seen in Fig. 5.

The diffraction pattern as seen in Fig. 14 shows significantly sharper diffraction peaks as compared to Fig. 10. Accordingly, the 2 Θ –sin² ψ plots show significantly less scattering of the data points around the line (Fig. 15) and residual stress values have a significantly smaller standard deviation, namely

$\sigma_{u,2} = 94 \pm 11$ N/mm²

in tangential direction and

$\sigma_{ax,2} = -58 \pm 2$ N/mm²

in axial direction at measuring point 2 of the pipe piece.

The distribution of the intensities of the diffraction lines above the inclination angle again confirm the lack of surface defects on the analysed material (Fig. 16 and 17).

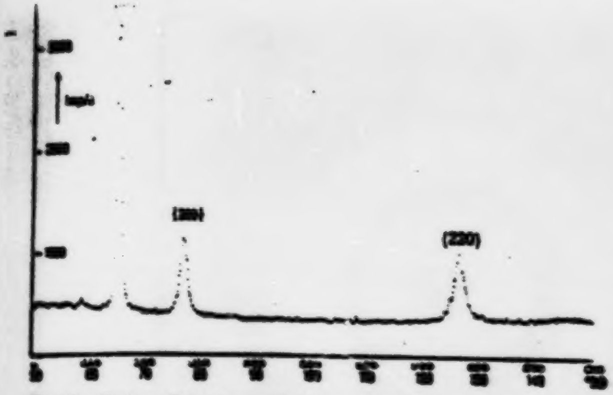

Fig. 9 Debye-Scherrer reflections with CrKα–radiation from the T-joint background suppression, 400 counts/s, smoothed x2.

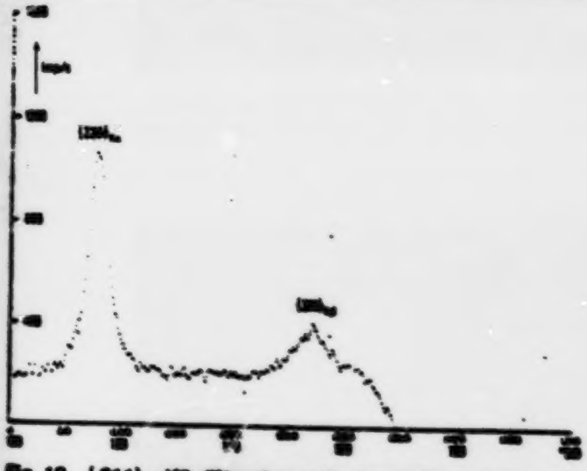

Fig. 10 {311} – Kβ diffraction at the immediate sample surface, background suppression 1500 counts/s, smoothed 1x.

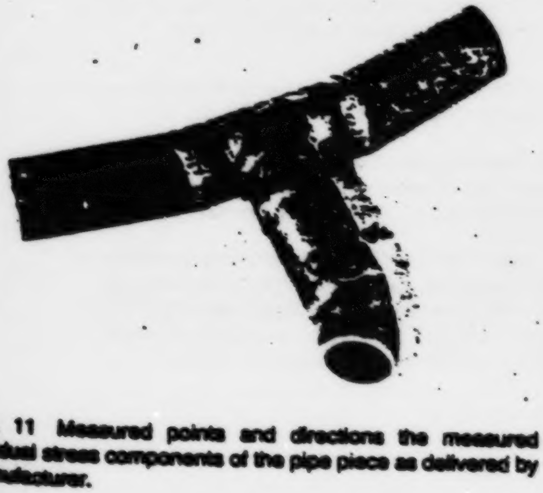

Fig. 11 Measured points and directions the measured residual stress components of the pipe piece as delivered by manufacturer.

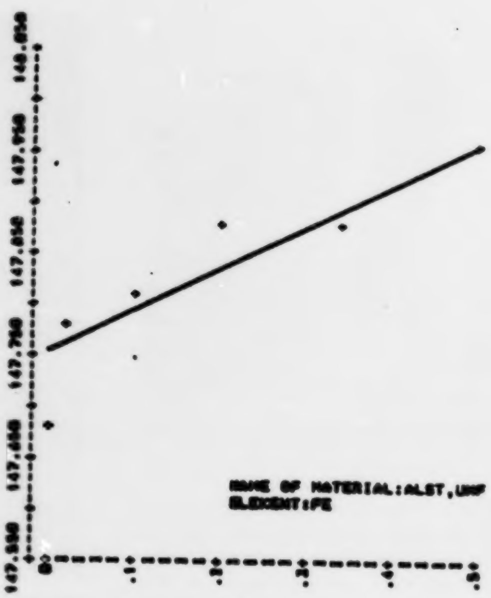

Fig. 12 2Θ – sin²ψ plot for the analysis of the stress components in the pipe piece (as received from the manufacturer).

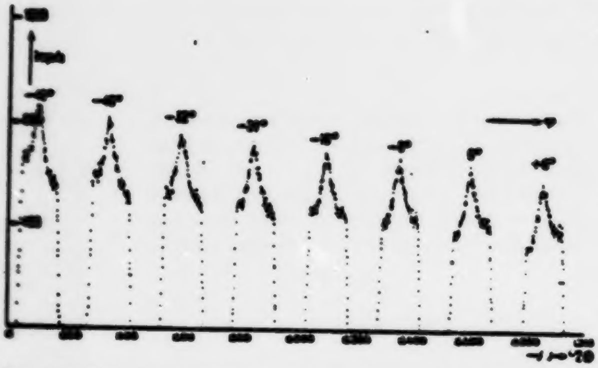

Fig. 13 {311} –Kβ peak positions, determined at different ψ-angles for the pipe, background suppression: 2000 counts/s.

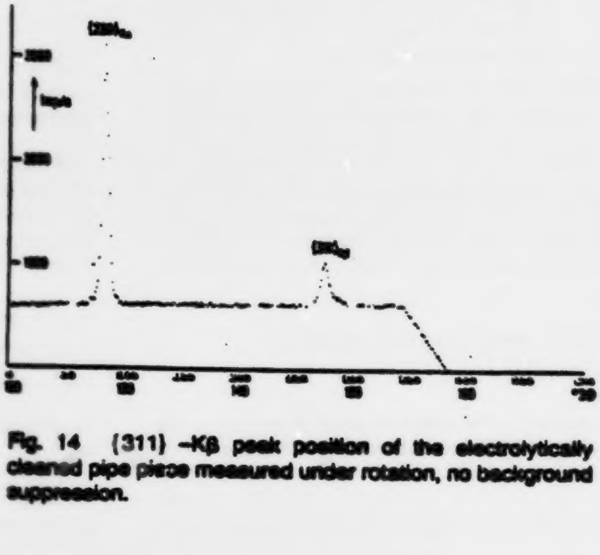

Fig. 14 {311} –Kβ peak position of the electrolytically cleaned pipe piece measured under rotation, no background suppression.

N-7

mechanical values for the elastic modulus [Young's modulus] and the lateral contraction value. The possible influence of the consequence of the elastic anisotropy of the austenite crystal in combination with the analysed material should be ascertained in the simplest case by experiments. Such measurements can be easily determined with the help of a strain gauge installed in the diffractometer instead of the sample holder. The compression stresses measured in the vicinity of the weld bead correspond to reported welding residual stresses[7].

The tension residual stresses which are present in the welding seam are compensated for by compression residual stresses outside the welding seam. Proceeding on the assumption that tension residual stresses are of about the same magnitude as the measured compression residual stresses, then an unfavorable condition for corrosion resistance and strength is present. A clarification of these interrelations should be investigated.

References

1) P. Müller u. E. Macherauch: Das $\sin^2\psi$–Verfahren der röntgenographischen Spannungsmessung, Z. ang. Phys. 13 (1961), 305-312

2) R. Prümmer: Grundlagen und Anwendung der rötgenographischen Eigenspannungsanalyse, Kerntechnik, Isotopentechnik und Chemie, 13 (1971), 69-77

3) G. Lucas u. L. Weigel: Röntgenographische Messung der Eigenspannung im Martensit und Austenit gehärteter Stähle, Mat. Prüf. 6 (1964) Nr. 5, 149-56

4) C. Kim: Determination of Residual Stresses in Austenite and Martensite in Case-Hardened Steels by the $\sin^2\psi$–Method, Report L-193-131, 1981, Climax Molybdenum Company of Michigan

5) I. Kraus u. R. Kralova: Eine rötgenographische Methode zur Bestimmung von Eigenspannungen in austenitischen Werkstoffen, Korove Materialy 14 (1976) No. 2, 165-168

6) R. Prümmer: Röntgenographische Eigenspannungsbestimmungen an dem austenitischen Stahl AM 53, Bericht, Kiel, 1986

7) R. Prümmer: Röntgenographische Eigenspannungsmessungen an elektronenstrahlgeschweißten Proben, Mitteil. der SLV Mannheim Nr. 74, DVS-Ber. Bd. 5, "Strahltechnik III", 1989.

Issued by Measurement Systems Division
1 Computer Drive, Cherry Hill, New Jersey 08034 (609) 424-2524

FRAUNHOFER-INSTITUT FÜR WERKSTOFFMECHANIK
Rosastr. 9, 7800 Freiburg

V 31/82

X-Ray stress analysis of a pipeline

R. Prümmer and H.W. Pfeiffer-Vollmar

durchgeführt im Auftrag der Fa. Siemens AG, Brüssel

Oktober 1982

5 Seiten page
3 Literaturstellen reference
1 Tabelle table
7 Abbildungen figure

Vervielfältigung und Weiterverbreitung
sind nur mit Zustimmung der Fraunhofer-
Gesellschaft gestattet.

INTRODUCTION

The ARAMCO-Refinerie at Ras Tanura, Saudi Arabia, is connected to the nearby, world's greatest oil-harbour by a voluminous system of pipelines.

Continuous improving and routine repair work sometimes requires the cutting of pipes.

The cutting of pipes without problems can be done, if there exist only small values of mechanical stresses in the material, normally accomplished by expansion loops.

In cases, however, where branching of pipelines occurs or where pipelines change from open air to subground installation residual strains caused by temperature variations and/or small movements of ground supports are inevitable. If such pipes have to be cut, great amounts of elastic energies can be released at high rates, sometimes leading to accidents, when part of a pipeline is suddenly accelerated to velocities at great amplitudes.

So, before cutting such a pipeline, it has to be sure, that the elastic stresses in the pipeline are below a critial value.

A recognized and approved method for a nondestructive measurement of load- and residual stresses is represented by the X-Ray Stress Analysis [1,2,3]. Therefore this method was used to determine the residual stresses of the 30 inch pipeline QRTS (.375 inch thick) at "zero-ancor", Ras Tanura, in order to be sure that a safe cutting of the pipe can be undertaken.

The portable Siemens X-Ray stress analyzer SMD 2000 (Fig. 1) was used. It is normaly operated by a computer, enabling a rapid measurement. But because of the extreme climatic conditions the computer equipment had not been used.

BASIC PRINCIPLES OF THE METHOD

The principle of the X-ray stress analysis method is based on the Bragg equation .

$$2D \sin \theta = \lambda. \qquad (1)$$

N-8

An X-ray beam with a wavelength λ is diffracted at the lattice planes of the crystallites of a poly-crystalline material with a lattice plane spacing D at the Bragg angle θ (Fig. 2). If the crystallites are distorted by elastic stresses, i.e., if the lattice plane spacing D is altered by an increment or decrement dD, the angle θ is also altered by an increment or decrement $d\theta$ according to the equation

$$d\theta = - \tan\theta \ \frac{dD}{D} . \qquad (2)$$

The task of X-ray stress analysis is to determine this angle variation, from which it is then possible to calculate the lattice strain dD/D. In contrast to mechanical and other methods, the lattice strain can be determined at any angle ψ (Fig. 3) with respect to the perpendicular to the surface of the specimen, up to 70°.

In a biaxial state of stress with the principal stresses σ_1 and σ_2 (Fig. 3), the lattice strain in the direction φ, ψ is given by the equation of the linear theory of elasticity

$$\left(\frac{dD}{D}\right)_{\varphi,\psi} = \varepsilon_{\varphi,\psi} = \frac{1}{2} s_2 (\sigma_1 \sin^2\varphi + \sigma_2 \sin^2\varphi) \sin^2\psi + \frac{1}{2} s_2 \sigma_\varphi \qquad (3)$$

where $1/2\ s_2 = (\nu + 1)/E$ and $s_1 = -\nu/E$ are the Voigt conelasticity. The direction of measurement (see Fig. 3) is defined by the azimuthal angle with respect to the principal stress σ_1 and by the angle with respect to the perpendicular to the surface of the specimen. The stress component acting in the direction $\varphi, \psi = 90^\circ$ is given by

$$\sigma_\varphi = \sigma_1 \cos^2\varphi + \sigma_2 \sin^2\varphi . \qquad (4)$$

The $\sin^2\psi$ method of X-ray stress analysis is based on the fact that, when the azimuthal angle φ is kept constant, the lattice strain $\varepsilon_{\varphi,\psi}$ is linearly proportional to $\sin^2\psi$. The lattice strains are measured for various values of ψ at a constant azimuth φ, and are plotted against $\sin^2\psi$. The plot for any given azimuth φ is a straight line with a slope

$$\frac{\partial \varepsilon_{\varphi,\psi}}{\partial \sin^2\psi} = \frac{1}{2} s_2 (\sigma_1 \cos^2\varphi + \sigma_2 \sin^2\varphi) = \frac{1}{2} s_2 \ \sigma_\varphi \qquad (5)$$

Making use of the Voigt constant $1/2\ s_2 = \frac{\nu+1}{E}$, this equation makes it possible to determine the stress component σ_φ. If the measurement is carried out at an azimuth $\varphi = 0$, then σ_φ is the principal stress σ_1; if $\varphi = 90^0$, then σ_φ is the principal stress σ_2. Finally, making use of the Voigt constant s_1, the intercept of the strain plot on the axis of ordinates, which is the same for all azimuths, gives the sum of the principal stresses according to the equation:

$$\varepsilon_{\varphi, 0} = s_1(\sigma_1 + \sigma_2). \qquad (6)$$

Thus, the determination of stresses requires only the strain distribution and the two basic constants of the theory of elasticity, i.e., Poisson's ratio and Young's modulus, from which the two Voigt constants are built up. The stresses can then be calculated with the aid of Eqs. (5) and (6).

MEASUREMENT PROCEDURE

Before starting the X-Ray measurement the rust at the pipeline's surface had to be removed by polishing with sandpaper. Then stresses caused by this procedure and perhaps other fortuitous mechancial treatments (for example during pipe transport) were deleted by electrolytical removal of 0.1 mm (0.004 in) thick surface layers.

At 8 spots, prepared this way at different locations at a circumference of the pipe, X-Ray measurements had been performed (each two spots at 12, 9, 6 and 3 o'clock position, Fig. 4).

The interferences of the {211} planes of iron, using Cr K_α -Radiation (λ= 2.28962Å, penetration depth ≈ 4 μm), where registrated by an X-T recorder at 6 different ψ-angels.

The simultaneous recording of {211} interferences of chromium calibration powder insured a good alignment of the diffractometer.

Fig. 5 shows one of these recordings. The exact location of the Bragg's angle θ of the recorded interferences was determined using the width of the interference at half weight of maximum counting rate (with subtracted background radiation).

RESULTS AND DISCUSSION

The measured 2θ vs. $\sin^2\psi$ -relationships are given in Fig. 6,7. Tab. 1 summarizes the results of the X-ray residual stresses, measured in axial direction of the pipe. At 12 o'clock position (top of the pipe) a tensile stress of 137 N/mm^2 (19574 psi) and at 6 o'clock position (bottom of pipe) a stress of 183 N/mm^2 (26098 psi) is obtained.

The result, that the amount of tensile stresses at the bottom of the pipe are greater than at the top of the pipe are either an indication of the bending of the tube in between two supports and/or could be due to thermal stresses, arising from temperature differences between the top and bottom side of the tube during the measurement with 120°F and 105°F, respectively. This assumption is also prooved by the equivalent stresses obtained at 3 o'clock position, with 116 N/mm^2 (16747 psi) being nearly identical with the ones measured at 12 o'clock position. Two measurements of loop stresses at 9 o'clock position showed average tensile stresses of 245 N/mm^2 (35523 psi).

For a detailed investigation data about the pressure inside the tube and possible fluctuations of it should be known. Also the maximum possible temperature variations and their frequencies should be known. The accuracy of X-ray measurement could be improved if the circumstances of measurement (tent or mobile equipment at the place with water and cooling equipment included) could be improved. It is recommended to investigate the whole stress state also including the third principal stress component.

The amount of stresses measured give evidence to this proposal. With approximately a value of 2/3 of the yield strength of the pipe material at about 115°F the reserve strength still is pretty good unless corrosion and other embrittling effects on the pipe's material can be neglected.

However, it is recommended, if a cutting of the pipe is necessary, it should be done at certain intervals. The cutting operation should be started at one side of the tube, interupted in order to start at the opposite side of the tube and so on. This way the sudden release of the stored elastic energy with its detremental effects can be avoided. It is also recommended, that the pipe material should be investigated in certain intervals of time, that is perhaps after every 10 years. The investigations should include fracture behavior (fatigue crack propagation probability, toughness) and residual stress state, especially at welds.

REFERENCES

[1] R. Prümmer: Basic principles and applications of X-Ray analysis of residual stresses, Kerntechnik, Isotopentechnik und Chemie 13 (1971), Heft 2, 68-77

[2] U. Wolfstieg: Stand und Möglichkeiten der röntgenographischen Spannungsanalyse, VDI-Bericht Nr. 313, 1978

[3] G. Maeder, J.L. Lebrun and J.M. Sprauel: Present possibilities for the X-Ray diffraction method of stress measurement, NDT International, Okt. 1981, S. 235-247

point of measurement	direction of stress	stress value	temperature
12 o'clock/1	axial	130 ± 16 N/mm^2 (18849 ± 2320 psi)	120^{0}F
12 o'clock/2	axial	141 ± 30 N/mm^2 (20444 ± 4350 psi)	118^{0}F
3 o'clock/1	axial	76 ± 16 N/mm^2 (11020 ± 2320 psi)	122^{0}F
3 o'clock/2	axial	155 ± 24 N/mm^2 (22474 ± 3480 psi)	122^{0}F
6 o'clock/1	axial	126 ± 52 N/mm^2 (23488 ± 7540 psi)	107^{0}F
6 o'clock/2	axial	198 ± 42 N/mm^2 (28708 ± 6090 psi)	108^{0}F
9 o'clock/1	loop	240 ± 16 N/mm^2 (34798 ± 7540 psi)	122^{0}F
9 o'clock/2	loop	249 ± 46 N/mm^2 (36103 ± 6670 psi)	122^{0}F

Tab. 1: Measurement spots, directions and values of residual stresses measured by X-Ray, pipe-temperature during measurement.

N-12

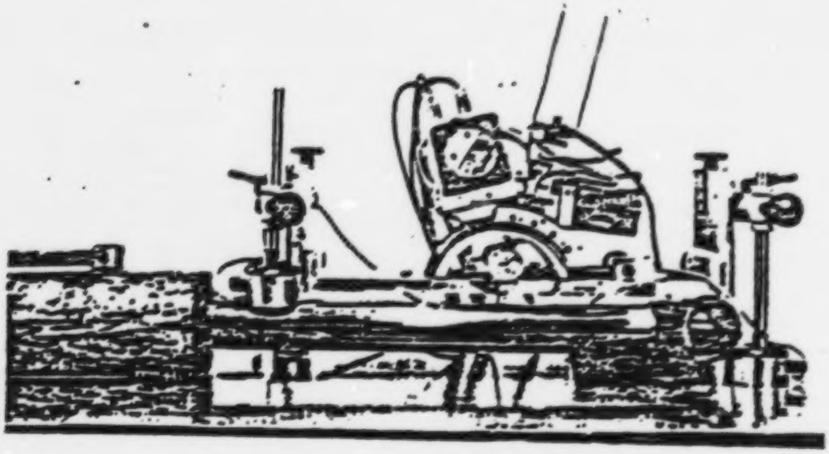

Fig. 1: Portable Siemens X-Ray goniometer

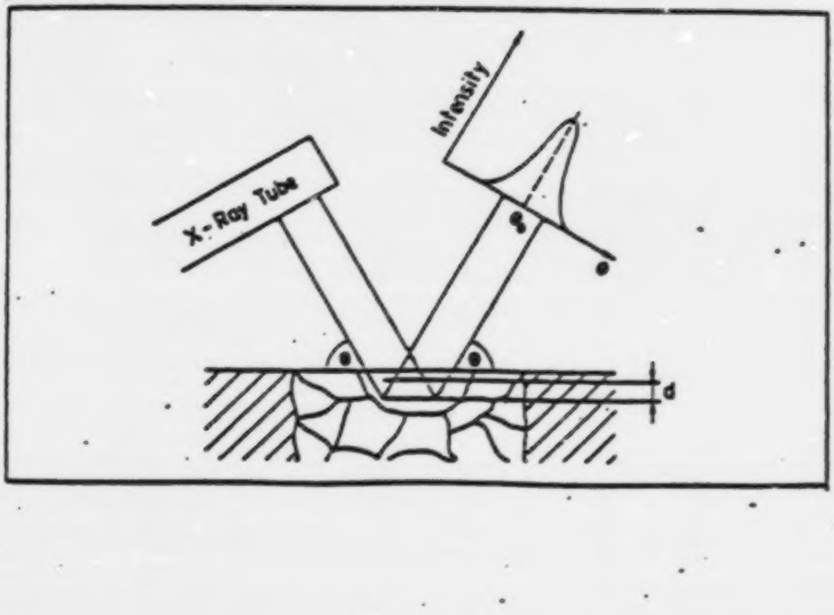
X-Ray Tube
Intensity
θ_0
θ
θ
θ
d

Fig. 2: Schematic sketch of the diffraction of an X-ray beam at a lattice plane with a lattice plane spacing d

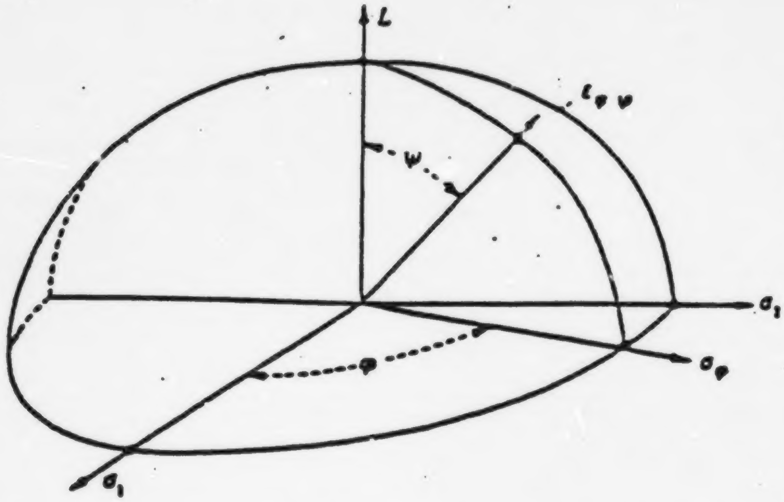
L
$\varepsilon_{\varphi\psi}$
ψ
σ_1
σ_φ
φ
σ_1

Fig. 3: Definition of the direction φ,ψ in which an X-ray lattice strain measurement is carried out. The specimen is in a biaxial state of stress with the principal stresses σ_1 and σ_2, φ is the azimuthal angle with respect to the principal stress σ_1; ψ is the angle with respect to the perpendicular L to the surface of the specimen

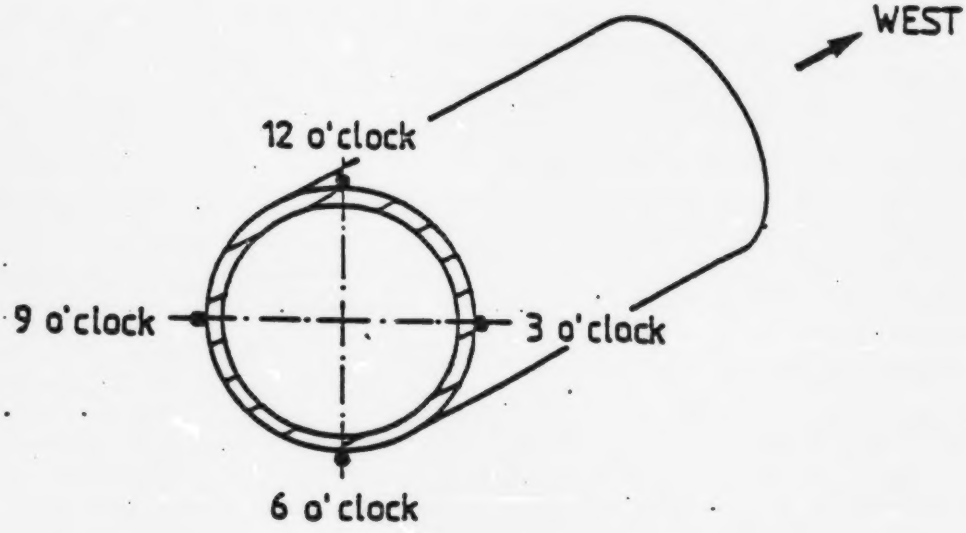
WEST
12 o'clock
9 o'clock
3 o'clock
6 o'clock

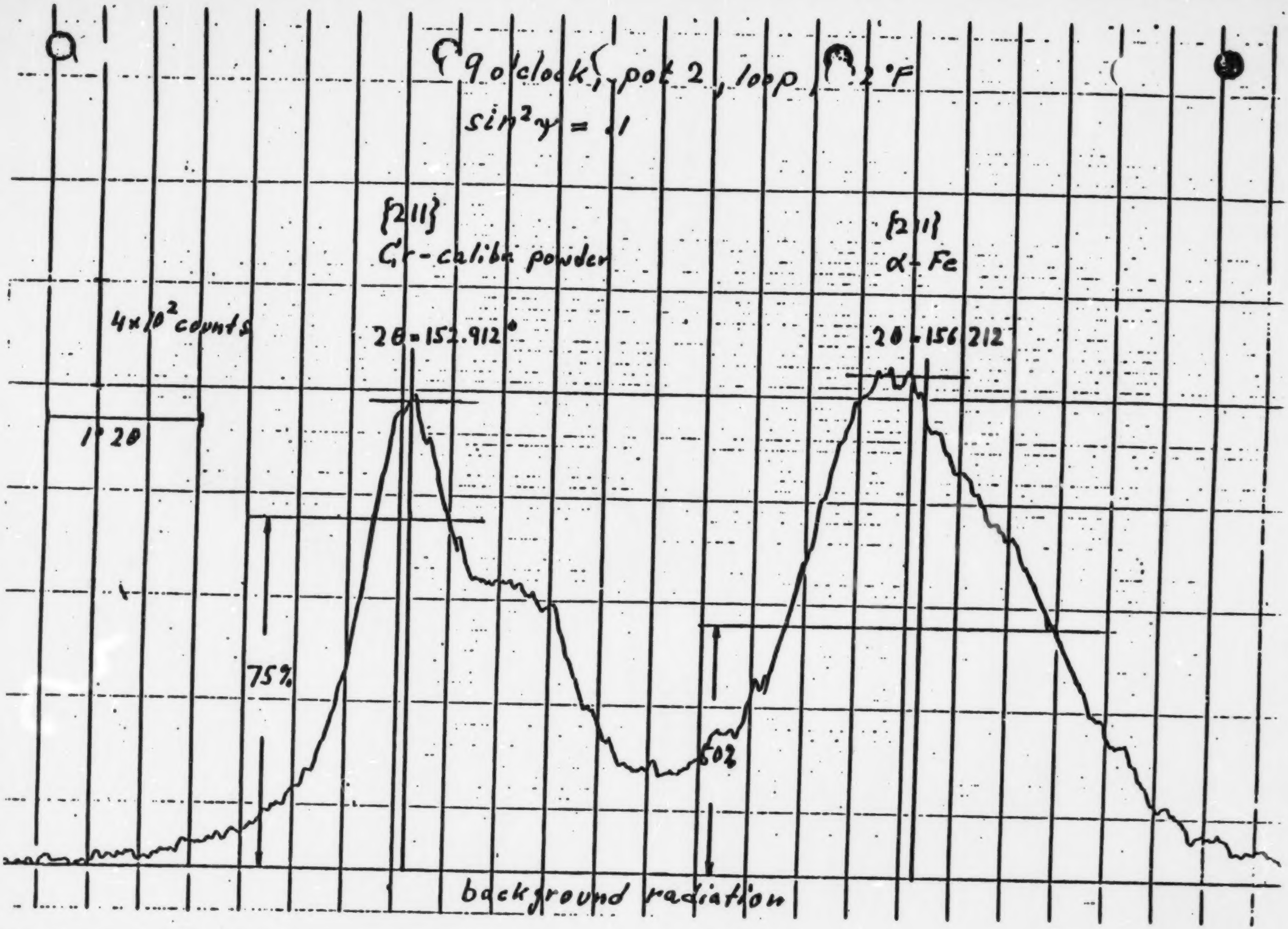

ig. 5: Recorded {211} interferences of Cr-calibration powder and pipeline's steel. Fixing of the Bragg's angle 2θ

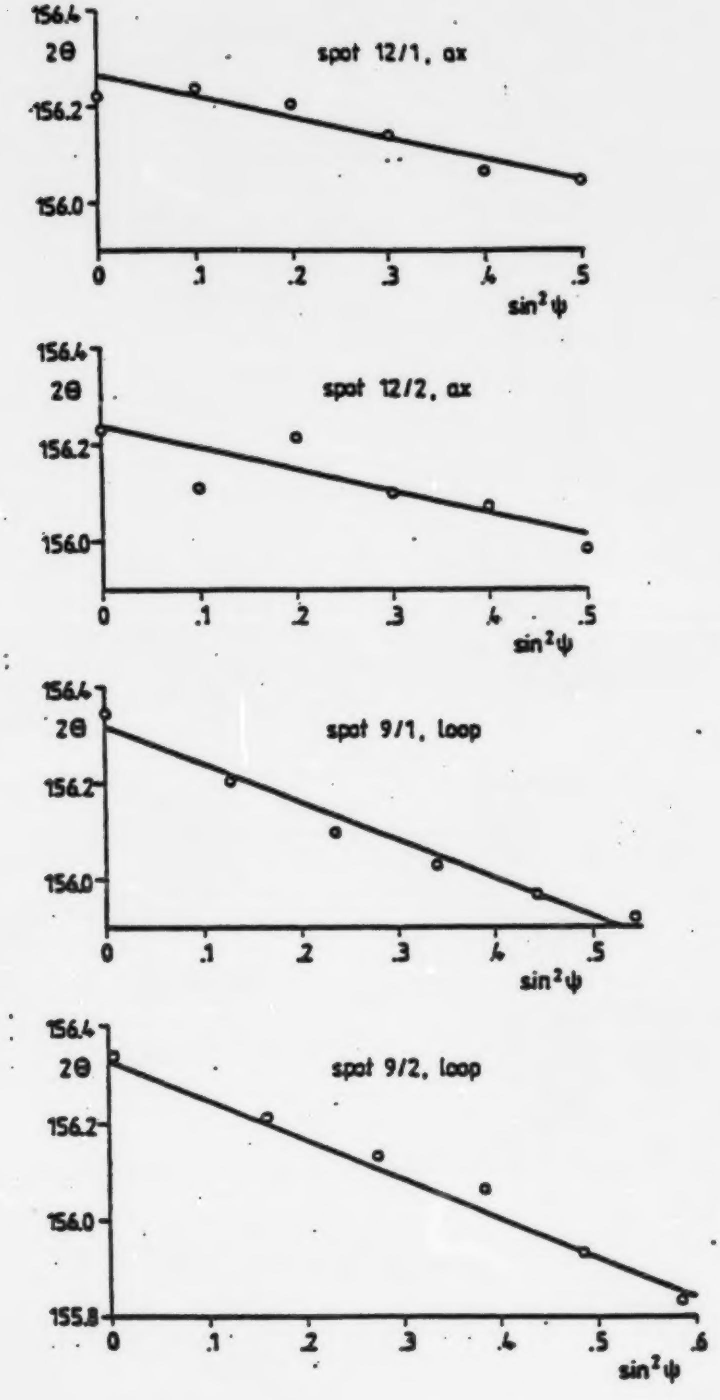

Fig. 6: Measured 2θ vs. $\sin^2\psi$ relationships, measuring spots 12 o'clock and 9 o'clock (Braggs' angle 2θ ~ strain $\varepsilon_{\varphi,\psi}$)

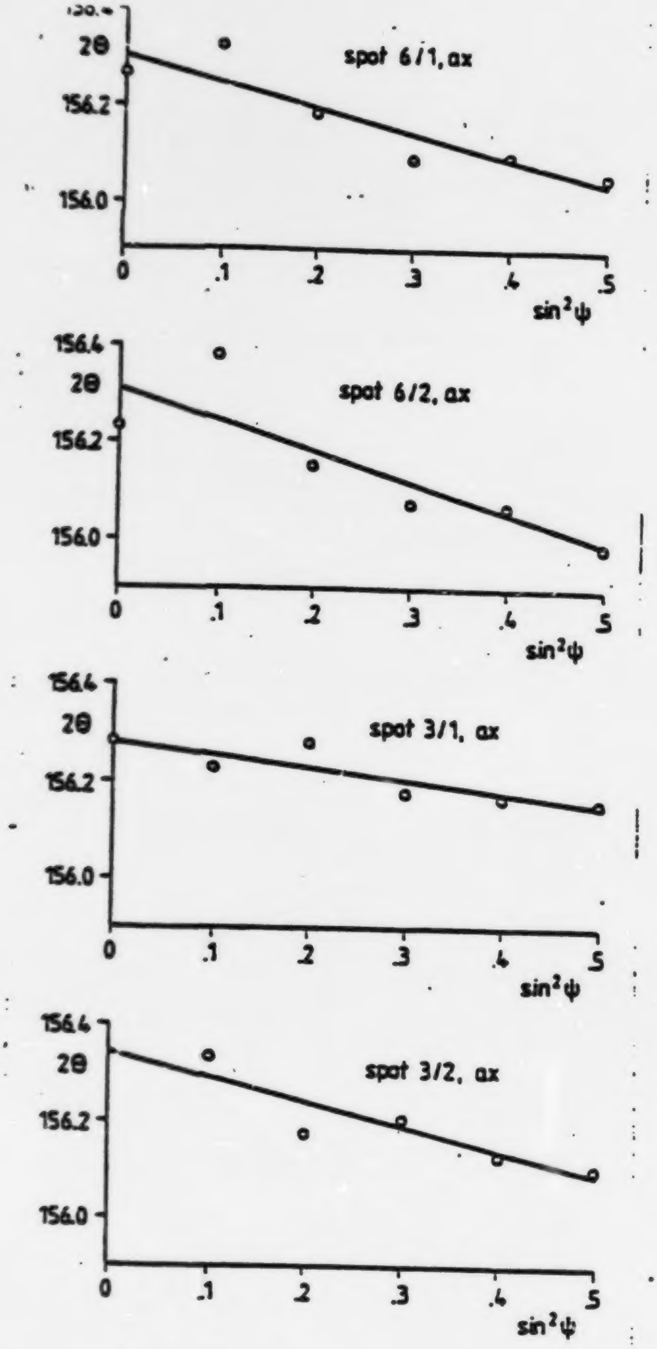

Fig. 7: Measured 2θ vs. $\sin^2\psi$ relationships, measuring spots 6 o'clock and 3 o'clock (Braggs' angle 2θ ~ strain $c_{\psi,\psi}$)

APPENDIX O

SELECTED ARTICLES

1. "PARS" - A Portable X-ray Analyzer for Residual Stresses
2. X-ray Analysis and Advances in Portable Field Instrumentation
3. Position-sensitive Detector Improves X-ray Powder Diffraction
4. X-ray Residual Stress Measurement Systems for Army Material Problems
5. Problems with Residual Stress in the Railroad Industry

24: O-1

M. James[1] *and J. B. Cohen*[2]

"PARS"—A Portable X-Ray Analyzer for Residual Stresses

REFERENCE: James, M. and Cohen, J. B., " 'PARS'—A Portable X-Ray Analyzer for Residual Stresses," *Journal of Testing and Evaluation*, JTEVA, Vol. 6, No. 2, March 1978, pp. 91–97.

ABSTRACT: The design, operation, and testing of a 7 to 11-kg hand-held X-ray device for measuring residual stresses are described. The instrument is based on a miniature X-ray tube and generator and a position-sensitive detector. No motion of the detector is needed to record a peak, eliminating the expensive and heavy gearing characteristic of a conventional diffractometer: the only mechanical motion during a measurement is one change of the orientation of the device to the object. An entirely portable instrument is therefore available for use in the plant or in the field. Tests are reported in which the stress is measured to ±40 MPa (±6 ksi) or better in 4 to 20 s, depending on the specimen.

KEY WORDS: residual stress, portable equipment, X ray stress analysis, position sensitive detector

X-ray methods of measuring residual stresses in crystalline materials have been tested and compared to other methods [*1*] and are in wide use throughout the world. Indeed, manuals [*2,3*] have been written for their use. For the most part, measurements are still made manually on a conventional powder X-ray diffractometer or with a film unit, but there are more rapid units [*4*] that can make measurements in 3 to 15 min with reasonable precision and other devices that can be moved about to some degree.[3] In this paper a unit that can be carried like a large camera and can make measurements in the field in 4 to 20 s will be described in detail and its design principles will be examined.

Consider the method of X-ray powder diffraction with a single wavelength λ and a flat specimen in a conventional diffractometer. Assume the detector is moved over a range of angles 2θ to find the maximum of the diffraction from grains that satisfy Bragg's law, that is, grains that have planes of atoms with interplanar spacing d such that $\lambda = 2d \sin \theta$. Grains that have planes with this d spacing which are parallel to the surface will diffract; this is shown in Fig. 1*a*. This diffraction takes place from a thin surface layer (≈ 20 μm). If the surface of the specimen is in compression, because of Poisson's ratio the d spacing of these planes is larger than in the unstressed state. If the specimen is now tilted with respect to the incoming X-ray beam (Fig. 1*b*) new grains diffract and the orientation of the diffraction planes is more nearly perpendicular to the stress direction. The result is that with the tilt, the d spacing decreases. The interplanar spacing is effectively acting as an internal strain gage. From isotropic elastic theory the change in d spacing with tilt can be employed to give the stress in any direction φ on the surface [*2*]:

$$\frac{d_{\varphi,\psi} - d_0}{d_0} = \epsilon_{\varphi,\psi} = \left(\frac{1+\nu}{E}\right)\sigma_\varphi \sin^2\psi + \frac{d_{\varphi,\psi=0} - d_0}{d_0}$$

or

$$\frac{d_{\varphi,\psi} - d_{\varphi,\psi=0}}{d_0} = \left(\frac{1+\nu}{E}\right)\sigma_\varphi \sin^2\psi \cong \frac{d_{\varphi,\psi} - d_{\varphi,\psi=0}}{d_{\varphi,\psi=0}} \tag{1}$$

where

ψ = specimen tilt,
$d_{\varphi,\psi}$ = d spacing after specimen tilt ψ,
d_0 = stress-free spacing,
E = Young's modulus,
ν = Poisson's ratio,
ϵ = strain, and
σ = stress.

The axial system is shown in Figs. 1*c* and 2. From Eq 1 it is clear that the stress can be obtained simply from the slope of d versus $\sin^2\psi$, if the elastic constants are known. If accurate stress values are desired it is best to prepare a calibration curve for a given material by deforming it on a diffractometer under known stresses, because the required constants vary for different specific diffracting planes (see Ref *5* for a recent review of this problem). This is not necessary if only relative values or only the sign of the stress is important.

Because of the linearity of d versus $\sin^2\psi$, many investigators use only the so-called two-exposure method to increase the speed of measurement,[4] generally ψ = 0 deg and 45 or 60 deg. Then

---

[1] Department of Materials Science and Engineering, The Technological Institute, Northwestern University, Evanston, Ill. 60201; currently, research associate, Laboratorium voor Fysische Metaalkunde, Nijenborgh 18, Universiteitscomplex Paddepoel, University of Groningen, The Netherlands.

[2] Frank C. Engelhart professor of materials science and chairman of the Department of Materials Science and Engineering, The Technological Institute, Northwestern University, Evanston, Ill. 60201

[3] CGR, 48.50 Boulevard Gallienii 92133 Issy-les-Moulineaux, BP66, France; Rigaku-Denki Co. Ltd., Bldg. 208 Kanadasurugadai, Chiyoda-ku, Tokyo, Japan; Shimadzu Seisakusho, Ltd., 14-5, Uchikanda 1-chome, Chiyoda-ku, Tokyo 101, Japan.

[4] If the stress is produced by a method that concurrently produces a texture (as in rolling) and the material is a single phase (for example, brasses or stainless steels) or has only a low volume fraction of a second phase (low carbon steels), d may not be linear with $\sin^2\psi$. For details on how to measure stresses in such cases see Refs *6* and *7*. The instrument described in this paper can be employed in this case as well as for the normal two-exposure method.

© 1978 by the American Society for Testing and Materials

0090-3973/78/0003-0091$00.40

44

C-2

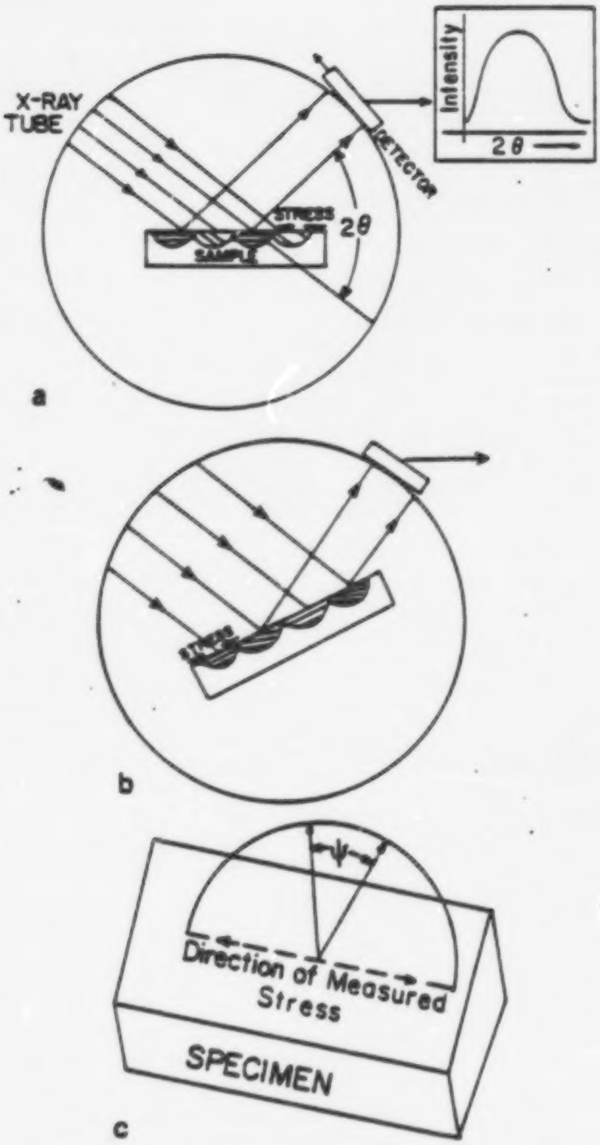

FIG. 1—(a) *Schematic of a diffractometer. The incident beam diffracts from planes that satisfy Bragg's law in crystals with these planes parallel to the sample's surface. If the surface is in compression, because of Poisson's ratio these planes are further apart than in the stress-free state. The* d *spacing is obtained from the peak in intensity versus scattering angle 2θ and Bragg's law.* (b) *After the specimen is tilted, diffraction occurs from other grains, but from the same planes, and these are more nearly perpendicular to the stress. These planes are less separated than in* (a). (c) *After the specimen is tilted, the stress is measured in a direction which is the intersection of the circle of tilt and the surface of the specimen.*

with Eq 1, $\sigma_\phi = K\,(\Delta d/d)$, where $K = E/[(1+\nu)\sin^2\psi]$. If the stresses are moderate, then from Bragg's law this equation can also be written as $\sigma = K'\,\Delta 2\theta$, where $K' = -(K/2)\cot\theta_{avg}$. A high-angle diffraction peak (from planes of low d spacing) is chosen to give the maximum change in angle for a given stress

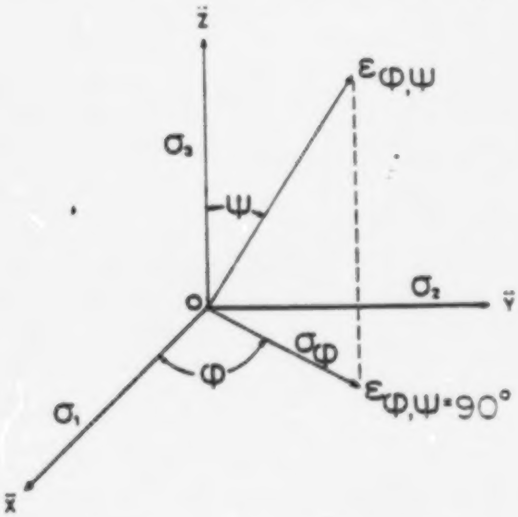

FIG. 2—*Axial system and symbols employed in the equations for stress measurement by X-rays.*

(the smallest possible "stress constant" K'). For example, for steel, a 211 diffraction peak, with chromium K_α, and a ψ tilt of 6 deg the peak moves ≈0.1 deg 2θ for every 39 MPa (5.5 ksi) an it is generally relatively easy to measure a shift to ±0.02 deg 2θ (The scattering angle between incident and scattered beams is 2θ.)

The method is based on recording a diffraction peak by movin a detector around the specimen to record the peak shape, tiltin it one or more ψ angles, and repeating the process. This is usuall done in a conventional diffractometer and requires expensive, heavy gearing.

PARS

But is it really necessary to move the counter to the vario points over a peak? A new X-ray detector called a position-sens tive detector (PSD) has recently been developed. It is capable of yielding information on both the quantity and relative position incoming X-ray photons. The unit we used, manufactured Tennelec, Inc., Oak Ridge, Tenn., employs an argon-3% carbon dioxide mixture flowing around a high-resistance graphite-coated wire [8]. When an X-ray photon ionizes the gas in the detecto a pulse runs along the wire. By comparing the pulse shape at bo ends of the wire, the ionization event can be located to a precision of ≈180 μm. With suitable electronics the entire peak can then be "observed" over several degrees (20 deg 2θ, if necessar by means of a multichannel analyzer (MCA). The pulses at eith end are summed to allow for energy discrimination. If the energy is not within prescribed values, storage in the MCA does not occu This reduces background. The horizontal axis on the MCA converted to degrees 2θ by calibration with known peaks. Wh the detector is flat and not curved to fit a circle around the specimen (as a diffractometer is) the error is small [9, 10]. For examp for a peak shift of 2 deg, indicating a stress of 1400 MPa (200 k in steel, the error is only 5 MPa. With such a device no motion of the counter is needed, eliminating the heavy and expensive gearing of a conventional diffractometer. Because the entire peak is o

240

0-3

lected simultaneously, the time to measure a stress is reduced by large factors, 8 to 100 [*9, 10*], the larger value being for sharper peaks. A least-squares parabolic fit is made to all the data points in the top 15% of the peak (generally 15 to 200 points in that region, the number depending on the peak breadth). All these points are obtained simultaneously in the multichannel analyzer. Replicate measurements indicate that the error in this case is only that resulting from counting statistics, whereas with fewer points the error is larger [*9, 10*]. Peaks can be located with a PSD from ±0.01 to ±0.02 deg 2θ by fitting a parabola. No background subtraction is necessary with so many points. All data processing can be carried out by an on-line minicomputer in a second or less. The detector employed occupied a volume of 0.2 by 0.13 by 0.045 m, with an active length of 0.1 m.

The gas-flow-type PSD used in this study can be pressurized for a day so that it is not necessary to consider gas supply as part of the design. Sealed units are also available commercially. Another important technological advance, the miniature X-ray tube, was adopted to make the instrument truly portable. We chose one manufactured by Watkins-Johnson Co., Scotts Valley, Calif. The tube is only ≈0.06 m long and with its shielding weighs 2.3 kg. It is air-cooled. The chromium target tube obtained for this study was designed for fluorescence but proved to be adequate. The target is rotated 24 deg around an axis in the plane of diffraction, which is a much larger take-off angle than usually employed in diffraction (2 to 6 deg). Partly because of this difference and partly because of the special grid system employed in the tube's construction, it was found that for the same beam size, at the tube's maximum rating (50 kV, 2 mA), the intensity was 20% greater than that from a standard water-cooled X-ray tube operated at 50 kV and 11 mA. These miniature tubes are available at ratings up to 5 mA.

In general the data in this study were taken at 40 kV, 1.7 mA. The beam size at the specimen was usually ≈0.003 by 0.004 m.

The basic configuration of PARS is shown in Fig. 3*a*. For the diffraction angle for steel, ≈156 deg 2θ, the PSD had to be located behind the tube. In Fig. 3*b* the basic design of the instrument is sketched. The detector and tube move on a dovetailed track to a stop for a ψ tilt of 45 deg. For these developmental studies, flat specimens were used and three position rods (A_1, A_2, A_3) that were not co-planar were employed to locate the tube to specimen distance properly and simply by manual pressure. Other positioning devices are possible for other sample geometries, and the instrument could be readily designed to allow a simple interchange between these. Furthermore, electromagnets or suction pads could be used to hold the position more easily. Only a single calibration experiment is necessary to transform positional data from the PSD into scattering angles.

The prototype instrument is shown in Fig. 4. Figure 4*a* is a view facing the X-ray tube; Fig. 4*b* is a view from the rear. In both cases the device is mounted on a stand for photographing. This stand, which is on wheels, could also be used to move the instrument from place to place within a plant. There are two grips for PARS that can be seen in the figures—a handle and a rubber-covered rod for tilting. A trigger could be incorporated in the handle to start the X-ray tube only if all positioning devices were in place on a specimen. Note the plastic backscatter safety shield.

In Fig. 5 the device is shown in use hanging from a strap around the neck of one of the authors (M. J.). Figure 6 shows the peaks on the oscilloscope of the MCA at the two tilts from a 1045 steel specimen with −397 MPa (−58 ksi) stress. The peak shift is clear. One of the interesting additional features of the device is the fact that the entire peak shape is recorded and therefore the breadth is obtained, which is often useful in view of the known empirical relationships between this quantity and hardness. Because of the wide angular range covered by the detector (≈20 deg 2θ), peaks from two phases can be examined. With different stops for the detector and X-ray tube, either stresses in different materials can be measured or the quantity of retained austenite can be determined.

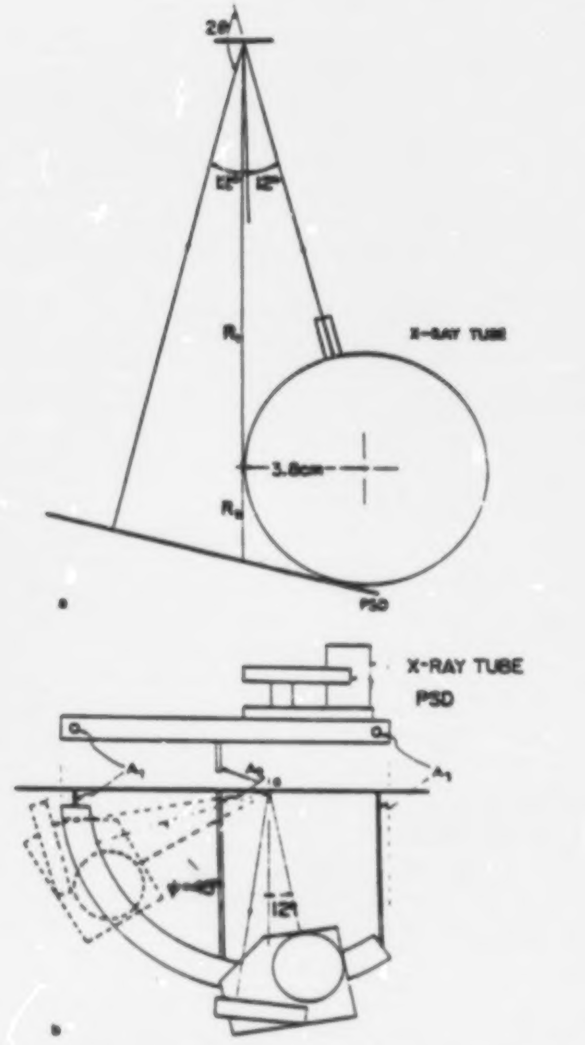

FIG. 3—(a) *Schematic of the X-ray tube and PSD for the portable unit PARS.* (b) *Schematic of movement of detector and X-ray tube for* ψ = *0-deg and* ψ = *45-deg measurements. The* A_i *symbols represent positioning rods:* A_1 *and* A_3 *lie on a horizontal plane with* A_2 *below this plane.*

Not shown in these figures are the associated electronics, which were not packaged for this prototype. The entire X-ray generator is only 0.5 by 0.5 by 0.15m (about the size of a large digital voltmeter) and weighs 23 kg. The entire electronics for the PSD, the

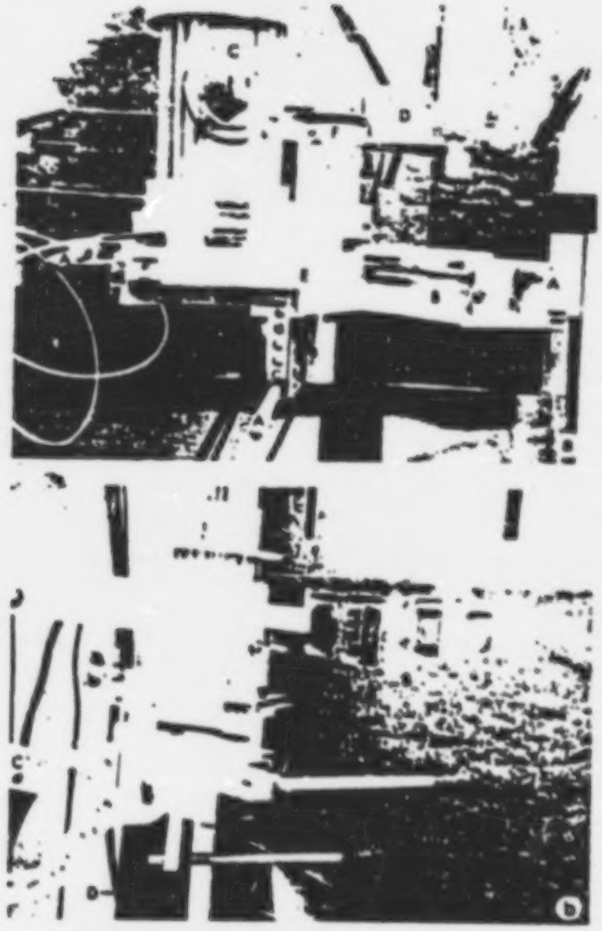

FIG. 4—(a) *Front view of the portable residual stress analyzer. The positioning bumpers* (A) *are located on the stationary or female member of the circular dovetail bracket* (B). *The X-ray tube* (C) *and detector* (D) *are mounted on the movable dovetail bracket* (E). *A distance indicator* (F) *is used to set the correct sample to detector distance when small samples are used.* (b) *Portable residual stress analyzer located at ψ = 45 deg. The three bumpers* (A_1, A_2, A_3) *position the apparatus on the flat plane* (B). *The device can be manually held by using the two handle* (C) *for support or mounted on the stand* (D) *and rolled into position.*

MCA, and a hard-wired microcomputer could be designed into a box 0.5 by 0.5 by 0.2 m. The only controls needed daily are two switches—on-off and high voltage. The peak stress (and perhaps hardness) would appear on an oscilloscope screen. Cabling to the portable head as long as 7 m is possible.

Table 1 compares data on a variety of specimens with results from our (automated) conventional diffractometer. Note that with PARS, measurements at both tilts can be performed in a total time of 4 to 20 s. The observed variation in five tests on each material is nearly the same as the error resulting from counting statistics, indicating that this error is the only principal one with PARS. For the sample with the lowest stress (Sample 1090-1) there appears to be a difference in both sign and magnitude of the stress measured by the portable unit and the conventional diffractometer. But the stress is so small that the sum of the erro with both methods includes this difference.

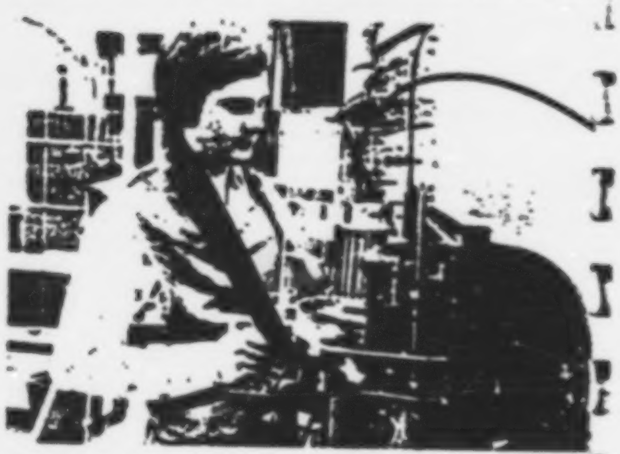

FIG. 5—*Unit in use. Note that it is carried with a strap around th neck.*

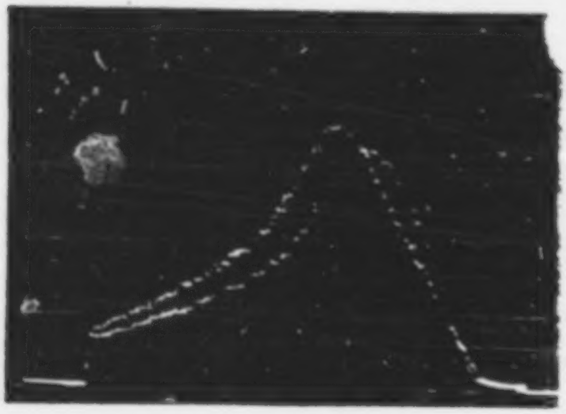

FIG. 6—*Peaks from SAE 1045-2 sample (see Table 1) at ψ = 0 de 45 deg, 211 peak, filtered CrK$_\alpha$ radiation. The peak shift caused by the stress of* −*397.1 MPa (*−*57.6 ksi) is clearly shown.*

The prototype of the portable head weighs ≈11 kg, but th tracks are much bulkier than actually needed and the slide f the tube and detector is not necessary. A second model wou weigh only 7 kg.

Design of the Instrument

Many preliminary studies were carried out before final decisions were made on the instrument just described. There are thr basic geometries for stress measurements with X-rays in use toda and these are illustrated in Fig. 7. The parallel beam method i essentially completely free of errors caused by sample position, while the stationary slit method has an error of about 14 MPa ksi) for a 0.5-mm displacement.[5] The parafocusing method most sensitive to positioning errors, giving an error of ≈70 MPa (≈10 ksi) for a 0.5-mm displacement [9, 10]. The former two do

---

[5] For iron-based specimens, 211 peak, CrK$_\alpha$ radiation, ψ = 60 deg.

2-1 0-5

TABLE 1—*Replicate measurements with PARS (five measurements; ψ tilt: 45 deg; CrK$_\alpha$ radiation).*

Sample[a]	Description	Stress with Normal Diffractometer		Average Stress, 5 tests with PARS		PARS Time, s	Observed Error, 5 tests—PARS		Calculated Statistical Counting Error	
		MPa	ksi	MPa	ksi		MPa	ksi	MPa	ksi
1090-1; w = 0.45 deg	disk, austenitized at 800°C, air-cooled, ground, stress-relieved in grey iron chips 2 h, 679°C, slow cooled	+32	+4.6	−12	−1.7	10[b]	±25	±3.7	±20	±2.8
1045-3; w = 3.45 deg	disk, austenitized at 815°C, oil-quenched, tempered at 370°C, 1 h, HRC = 44.5, shot peened	−699	−101	−703	−102	20	±28	±4.1	±29	±4.3
1045-2; w = 5.1 deg	plate, austenitized at 820°C, oil-quenched, tempered at 370°C, 1 h, shot peened (0.84-mm shot), HRC = 61	−397	−58	−396	−57	20	±43	±6.2	±37	±5.3

[a] w = width at half maximum in deg 2θ.
[b] Measurements to ±34 MPa statistical counting error in 4 s.

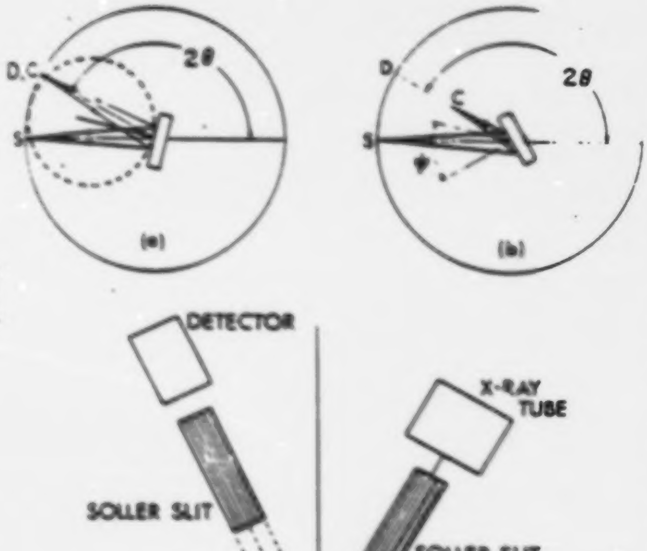

FIG. 7—*(a) The divergent beam usually employed on a diffractometer to expose a wide area on the specimen and still have a sharply focused beam at (C). The source (S), sample, and detector (D) are on a circle (shown dotted) to obtain this focusing. (b) When the specimen is tilted ψ deg during a stress measurement the focal point shifts. In the parafocusing method the counter is moved to this new position. In the stationary slit method the detector remains at D. (c) Parallel beam geometry. The angle 2θ is defined by the angle between two "Soller" slits and is independent of sample position. (The dashed lines indicate sample positions that would not affect the scattering angle.)*

not produce a sharply focused beam, so if the peak is sharp, as it often is, there is some broadening (and hence a lowering of intensity at any point near the peak) with these techniques. It is less for the stationary slit method than for the parallel beam geometry. This means that in a given time the error in locating a peak is largest for the parallel beam geometry (sometimes as much as twice as large [9]).

There is still another method to be considered, the so-called single-exposure method illustrated in Fig. 8. In effect, two tilts are achieved by examining a peak in a powder X-ray pattern from two different sets of grains. This is often done with film, but the error in stress caused by a given uncertainty in peak position is considerably greater (as much as twice), leading to an uncertainty in typical cases greater than that resulting from 0.5 mm-displacement. For all these reasons we chose the stationary slit-multiple exposure technique.

Two other major factors controlled the design of PARS. The intensity of a diffracted beam decreases as the detector moves away from the sample as a result of both air absorption and the increasing size of the diffraction cone. Thus the error arising from counting statistics increases. On the other hand, as the detector is moved close to the specimen, angular errors in a peak as a result of uncertainties in the sample position and errors in the calibration of the detector (position to scattering angle) increase. An analysis of these errors [*9, 10*] led to curves like those in Fig. 9. These illustrate the counting time to achieve the indicated error in stress versus detector position for various uncertainties in specimen position. These curves clearly show that, provided the specimen to detector distance is large enough, there is little variation in time with a still larger distance. A distance of 0.21 m was chosen based on these calculations and the necessity of combining off-the-shelf components—the detector and the tube.

Many tests have been carried out with PARS on specimens of steel and cast iron of various geometries. These tests have also shown that the error analysis illustrated by Fig. 9 is correct; compare the times of analysis in Table 1 for a 0.21-m sample to target distance with the curves. Because this prototype incorporated a slide for the detector and tube the sample detector distance

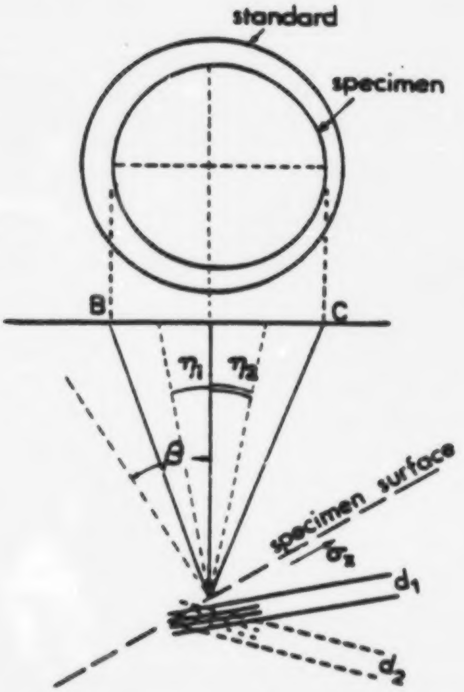

FIG. 8—*The single exposure method. The angles η_1, η_2 are different as they come from different grains with different spacings d_1, d_2. A standard powder is often placed on the specimen so that angles can be measured with respect to its diffraction peak. The angle β is between the surface normal and the primary beam.*

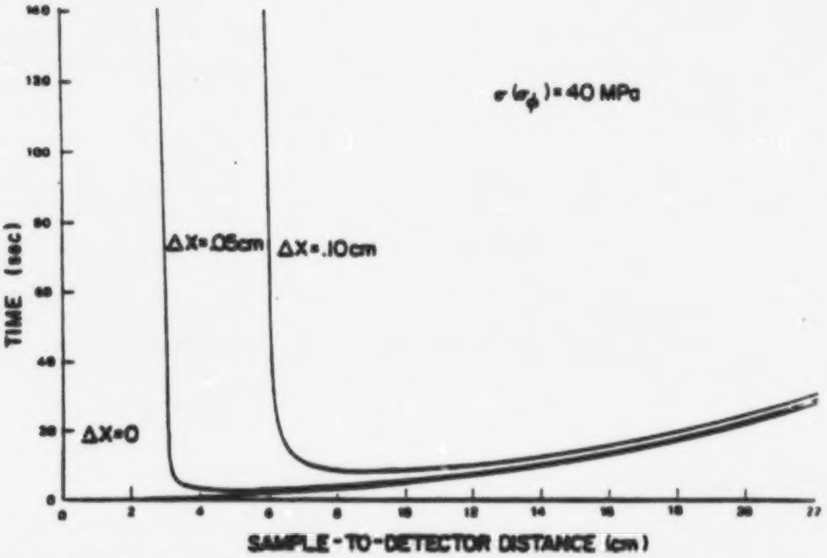

FIG. 9—*Counting time for an error in stress measurement of 40 MPa (5.7 ksi) versus sample-to-detector distance for SAE 1045-2 steel specimen (see Table 1); ΔX is uncertainty in sample position. (The error includes counting statistics and geometric errors, principally this displacement.)*

241 0-7

could be varied by ±0.025 m. For a preset error of ±40 MPa in the measured stress, the measurement time varied from 16 to 30 s for the shortest and longest sample to detector distances. Displacing a specimen forward 1 and 2 mm gave changes in the stress of 10 and 23 MPa. The calculated values for this displacement were 10 MPa for each 1 mm. This result also shows that the errors are small for quite appreciable uncertainties in positioning.

Acknowledgments

This research was sponsored by the Office of Naval Research (ONR). We would like to thank ONR personnel, especially Dr. B. MacDonald, for their continued support throughout the several years required to bring this project to fruition. This paper is a portion of a thesis submitted in partial fulfillment of the requirements for the Ph.D. degree at Northwestern University by one of the authors (M. J.). Support for him during one year by a Ford Motor Co. Fellowship is also gratefully acknowledged. We thank Mr. J. Hahn for constructing the head and graciously making the numerous changes required to obtain the final design. Professor B. D. Cullity of the University of Notre Dame provided helpful comments on a draft of this paper. Mr. W. Evans, Caterpillar Tractor Co., kindly supplied the specimens.

References

[1] Christenson, A. L., Ed., "The Measurement of Stress by X-Rays," SAE Technical Report 182, Society of Automotive Engineers, New York, 1960.

[2] Hilley, M. E., Ed., "Residual Stress Measurement by X-Ray Diffraction," SAE Information Report J784a, Society of Automotive Engineers, New York, Aug. 1971.

[3] Committee on Mechanical Behavior of Materials, "Standard Method for X-Ray Stress Measurement," The Society of Materials Science, Japan, 1973.

[4] Weinman, E. W., Hunter, J. E., and McCormack, D. D., "Determining Residual Stresses Rapidly," *Metals Progress*, July 1969, pp. 88–90.

[5] Marion, R. H. and Cohen, J. B., "The Need for Experimentally Determined X-Ray Elastic Constants," *Advances in X-Ray Analysis*, Vol. 20, 1976, pp. 355–368.

[6] Bollenrath, F., Hauk, V., and Weidemann, W., "Zur Deutung der Gittereigenverformungen in plastisch verformtem α-Eisen," *Archiv für das Eisenhüttenwesen*, Vol. 38, Oct. 1967, pp. 793–800.

[7] Marion, R. H. and Cohen, J. B., "Anomalies in Measurement of Residual Stresses," *Advances in X-Ray Analysis*, Vol. 18, 1975, pp. 466–501.

[8] Borkowski, C. J. and Kopp, M. K., "New Type of Position-Sensitive Detectors of Ionizing Radiation Using Risetime Measurement," *Review of Scientific Instruments* (New York), Vol. 39, Oct. 1968, pp. 1515–1522.

[9] James, M., "An Examination of Experimental Techniques in X-Ray Residual Stress Analysis," Ph.D. thesis, Northwestern University, Evanston, Ill., Jan. 1977.

[10] James, M. and Cohen, J. B., "Study of the Precision of X-Ray Stress Analysis," *Advances in X-Ray Analysis*, Vol. 20, 1976, pp. 291–308

250 O-8

X-Ray Analysis and Advances in Portable Field Instrumentation

Clayton O. Ruud
Denver Research Institute
University of Denver
Denver, Colo.

Portable x-ray stress analysis takes a great step forward in accuracy and speed, thanks to application of fiber optics.

The x-ray diffraction method is the only time-proven, truly non-destructive method for the measurement of residual stresses. Proof of its reliability lies in documentation of its use by thousands of engineers and scientists over the past two decades.[1-5] These applications have spanned from stress analysis of uranium/zirconium fuel rods to aluminum-alloy landing-gear components, and have included measurement of stresses in metal-powder-doped polymeric materials and tempering evaluation of carburized steels. The Society of Automotive Engineers considers the method of sufficient practical importance to have printed a Handbook Supplement on the subject three times.[6]

Even so, this non-destructive technology has been largely restricted to the laboratory due to peculiarities in the state-of-the-art components involved and the design and construction of available equipment. Instrumentation for bringing this technology into the manufacturing area has advanced rapidly in the last few years toward increasing the portability, compactness, and speed of operation of the equipment without serious reduction in its accuracy. Despite the marked improvements that have been made in this direction, there have been many demands for equipment that is still more portable, compact, and rapid than any of the presently available devices. Two metallurgists at the University of Denver Research Institute realized this a few years ago and therefore set out to devise more suitable instrumentation. The result was the invention of a very compact, highly versatile position-sensitive x-ray detector based upon x-ray principles and recent developments in electro-optics.

This paper will discuss the concept of the x-ray diffraction techniques, and describe the principles involved in the instruments used to apply these to stress analysis. The evolution of advanced instrumentation will be summarized and a new portable x-ray stress analyzer will be described, together with the implications of its use in industry and the laboratory.

PRINCIPLE

When a metal or ceramic polycrystalline material is placed under stress, the elastic strains in the material are manifest in the crystal lattice of the individual grains. The stress applied externally or residual within the material, when below its yield strength, is taken up by interatomic strain. The x-ray diffraction techniques are capable of actually measuring the interatomic spacings, which are indicative of the macro strain undergone by the specimen. Stress values are obtained from these elastic strains in the crystals by knowing the elastic constants of the material and assuming that stress is proportional to strain, a reasonable assumption for homogeneous, nearly isotropic materials as are most metals and alloys of practical concern.

The important parameters involved in the mechanics of x-ray diffraction are described by the Bragg relation,

$$n\lambda = 2d \sin\theta$$

where

n = 1,2, . . . i.e., any integer; it is the order of reflection, and for stress work is usually unity.
λ = wavelength of the diffracted radiation
d = spacing of the reflecting planes of atoms
θ = Bragg angle.

This relationship is illustrated in Figure 1.

In all applications where the determination of d is required, either λ or θ is known. In most practical applications, including stress analysis, λ is a constant and is known, and 2θ is measured. In a powder where particles show no preferred orientation, an x-ray beam only a few square millimeters in crossection is diffracted as a cone of x-ray beams by a large number of randomly oriented crystallites (see Figure 2). The cone's semi-apex angle (180°-2θ) is not infinitely sharp, in that a plane perpendicular to the cone's axis would show that the diffracted energy is distributed over a few tenths to several degrees of 2θ (see Figure 3). Therefore the angular distribution of the diffracted beam intensity must be ascertained as a function of 2θ. In other words, the diffracted x-ray intensity must be measured at several angular positions or a continuum of positions, in order to determine the mean diffraction angle 2θ.

The basic equation relating x-ray diffraction principles to stress-strain relations can be written as

$$\epsilon_{\phi\psi} = \left(\frac{1+\nu}{E}\right) \sigma_{\phi} \sin^2\psi - \frac{\nu}{E}(\sigma_1 + \sigma_2) \tag{1}$$

where ν and E = elastic constants
σ_{ϕ} = stress in the plane of the surface of the specimen at an angle of ϕ with a principal stress direction in the specimen surface
ψ = angle between the surface normal and the normal to the crystallographic planes from which an x-ray peak is diffracted
$\epsilon_{\phi\psi}$ = strain in the direction defined by the angles ϕ and ψ
σ_1 and σ_2 = principal stresses in the surface plane of the specimen.

This may be rewritten as

$$\sigma_{\phi} = \frac{d_{\phi\psi} - d_1}{d_1}\left(\frac{E}{1+\nu}\right)\frac{1}{\sin^2\psi} \tag{2}$$

where $d_{\phi\psi}$ = interatomic planer spacing for those crystal planes for which the normal is defined by the angles ϕ and ψ
d_1 = interatomic planer spacing for crystal planes parallel to the specimen surface.

It should be noted that only those planes within a selected *d*-space range will be measured due to the narrow selection of Bragg angle imposed by the stress measurement arrangement.

A modification of Equation 2 for a rapid and rather simple stress-measurement technique will be discussed subsequently.

Now since the difference between $d_{\phi\psi}$ and $d_\perp$ is small, then from Bragg's Law $\Delta d/d = -\cot\theta(\frac{\Delta 2\theta}{2})$ and Equation 2 may be rewritten as

$$\sigma_\phi = (2\theta_\perp - 2\theta_\psi)\frac{\cot\theta_\perp}{2}\left(\frac{E}{1+\nu}\right)\frac{1}{\sin^2\psi}\left(\frac{\pi}{180}\right) \tag{3}$$

Instrumentation

X-ray peaks in the far back-reflection range, *i.e.*, peaks with 2θ angles near 180°, are much preferred for stress analysis because they show the greatest change in diffraction angle with a given amount of applied or residual stress. Table I shows typical interatomic planes, radiation, and 2θ angles used for common metal alloys. Equation 3 shows that the greater the ψ angle ($90 \geq \psi \geq 0$), the greater the difference ($2\theta_\perp - 2\theta_\psi$) for a given stress; also, the smaller the Young's modulus, the greater the effective 2θ differential. If the engineer is interested in applying a stress which is a given fraction of the yield strength, a high yield strength is an advantage, *i.e.*, the higher the yield strength the greater the value of $2\theta_\perp - 2\theta_\psi$. Thus, heat-treated aluminum alloys demonstrate much larger x-ray shift when subjected to a stress that is a given percent of yield strength than does annealed austenitic stainless steel. Finally, the spatial resolution with which a shift in the x-ray peak can be measured is important not only because at a given distance from sample to detector or film the accuracy in stress measurement depends upon this spatial resolution, but also because higher resolution permits operation at smaller distances and consequently at higher speeds or with weaker diffracted beams.[7]

The state of the art offers three main methods for measuring intensity versus the angle 2θ. These are:

1. Scanning goniometer (diffractometer)
2. Film camera
3. Position-sensitive proportional counters

The scanning goniometer is by far the most commonly used of these. It is essentially a mechanical turntable capable of positioning a sample at a given θ position with respect to an incident x-ray beam, and a detector (*e.g.*, proportional or scintillation type) at an angle 2θ with respect to the incident beam. In this way, the detector is in position to intercept the diffracted x-ray beam, Figure 4. There are several excellent descriptions of this device including Barrett,[8] Cullity,[9] and Klug and Alexander.[10] In research work, it is usually possible to work with a stressed specimen small enough to be mounted on the diffractometer, and this is necessary for standard laboratory instruments. However, a few x-ray instrument manufacturers have developed diffractometers which do not require that the sample be mounted upon the instrument. This has enabled stress (strain) measurement on large "real-world" parts of practical importance to industry.

Table I: Commonly Used Parameters for X-Ray Stress Analysis

System	Radiation	Indices of Reflection	Interatomic Spacing, *d*	2θ Angle, degrees
Al	$CuK\alpha_{1,2}$	(333,511)	0.779	162.5
BCC-Steel	$CrK\alpha_{1,2}$	(211)	1.170	156.1
FCC-Steel	$CrK\beta$	(311)	1.085	147.8
FCC-Steel	$CrK\alpha_{1,2}$	(220)	1.273	128.2
Ni	$CuK\alpha_{1,2}$	(420)	0.788	155.7

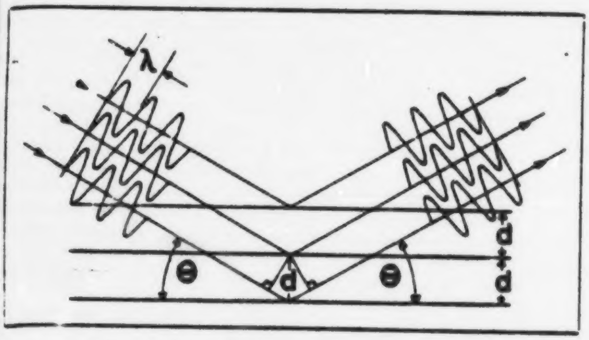

Figure 1. Illustration of the Bragg relation.

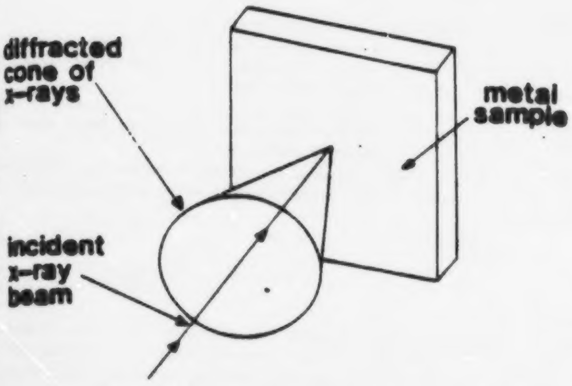

Figure 2. Diffracted cone of x-rays from a polycrystalline metal.

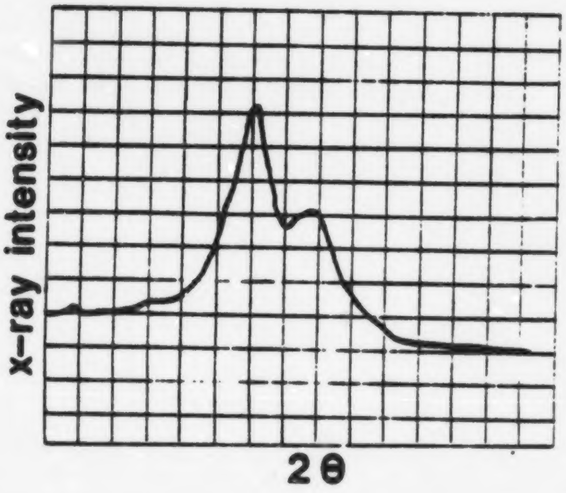

Figure 3. Diffracted x-ray intensity distribution plotted against 2θ for a $K\alpha_{1,2}$ doublet.

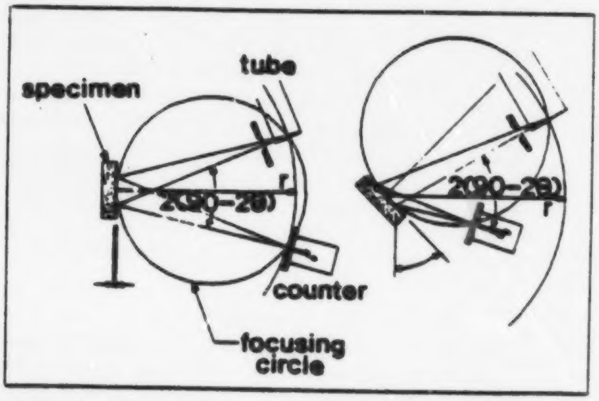

Figure 4. Schematic of x-ray diffractometer with detector in back-reflection position (i.e. $2\theta > 90°$).

However, these devices, especially the measuring heads (which must be manipulated into position to make the stress measurement), are bulky and not easily portable. Therefore these devices are applicable in only a very limited number of industrial applications.

Film cameras for stress measurement have been marketed by at least two manufacturers over the last two decades. The principle of application is to place film on each side of or surrounding the incident beam so as to intercept the diffracted x-ray cone (see Figure 2) at a high 2θ angle, Figure 5. The x-ray source and film holder comprise the stress-measuring head. These stress heads are about 1½ times the size of a quart thermos bottle and about the same shape. Because of the good portability and compactness of the stress head, the film instruments have found application in a number of manufacturing applications. Bolstad and Quist[3] and Norton[3] describe the methodology and illustrate some applications. The disadvantages of the film technique include the exposure time of several minutes, the subsequent development time, the time required for reading the film, and the relatively low accuracy. Polaroid techniques have been attempted, but the time saved in film development has not been worth the loss in accuracy due to the poorer spatial resolution.

The third method, involving position-sensitive proportional detectors (PSPD), has been applied to x-ray stress analysis in Europe, Japan, and the U.S.A., and James and Cohen of Northwestern University are responsible for the first application in this country.[11] The PSPDs have permitted the construction of portable stress heads smaller than goniometer types and yield good accuracy and high speed. The most severe limitation of this technique involves the size and shape of the x-ray detector that must be placed adjacent to the x-ray tube. Spatial resolution of available detectors is also a limitation and affects the minimum stress detectable from a stressed metal. Also, as discussed previously,[7] the better the spatial resolution of a detector or minimum detectable x-ray peak shift, the closer the stress head can be brought to the stressed sample and, thus, the higher the observed x-ray intensity and the higher the operational speeds. This concern also bears upon the applicability of an x-ray device for stress measurement in confined spaces.

X-Ray Stress Measurement Techniques

There are three basic techniques for obtaining stress (strain) readings from a polycrystalline material by the x-ray method. These are called sin-square-psi technique, double-exposure technique (DET), and single-exposure technique (SET). In order for the x-ray method to be used as an absolute measure of the residual or applied stress, the d spacing of planes of the same Miller indices must be measured at two different orientations with the metal surface. What is meant by absolute measurement is that no previous or subsequent measurement of that metal piece need have been obtained in a zero-stress condition for comparison.

The sin-square-psi ($\sin^2\psi$) technique is recommended where high confidence is required on specimens likely to display marked texture.[12] Furthermore, the several x-ray readings at a series of different ψ values contribute to its statistically superior accuracy. The technique is based upon Equation 1. Application requires that several readings be made to obtain interatomic spacings d_1, d_2, d_3, etc., with a wide range of ψ values. The plane containing the incident and diffracted beam is kept the same for all psi angles and the line of coincidence of this plane and the plane of the specimen surface is the direction of the measured stress. The x-ray-measured interatomic spacing d is plotted against $\sin^2\psi$. If the set of crystallographic planes selected for measurement show no texture, the plot will fall on a straight line. The intercept with the axis at $\sin^2\psi = 0$ is equal to $\frac{\nu}{E}(\sigma_1 + \sigma_2)$, and the slope m is given by

$$\sigma_\psi = m\frac{E}{1+\nu}$$

where m is the slope of the line in the $(d-d_o)/d$ vs. $\sin^2\psi$ plot, where d_o is the spacing for unstressed material. If the plot is not a straight line, the cause may be texture in the metal, *i.e.*, preferred orientation. Marion and Cohen[13] have proposed an approach to obtain stress (strain) readings in such conditions. The sin-squared-psi method is time-consuming and requires precise repositioning of the specimen or stress head for each reading. Errors in repositioning could contribute so severely to poor readings that the inherent accuracy of the technique is compromised. This technique is not recommended for any but laboratory applications except in rare cases where the psi angle and distance from the detector to the specimen can be accurately controlled or conveniently measured.

The double-exposure technique (DET) requires that the interplanar spacing of planes with two orientations with the specimen surface are obtained. Usually, one at $\psi = 0$ and one at $\psi = 45$ or 60 degrees is selected. Figures 4 and 5 illustrate the two arrangements for film and diffractometer. The relation of the stress in a given direction in the surface to the x-ray reading is based upon Equation 2. This technique is really no different from the sin-squared-psi method except that interplanar spacing of planes with only two orientations with the surface is obtained, one at $\psi = 0$ (*i.e.*, ψ_1).

The single-exposure technique (SET) is based on the fact that a single incident x-ray beam is diffracted in an entire cone of reflections, Figure 2. A plane perpendicular to the cone axis intercepts the cone in a circle when the specimen is unstressed, but if the specimen is stressed, the circle becomes an ellipse and the deviation of its shape from a circle is indicative of the stress (strain) in the sample.[7] To read this deviation, detectors are placed 180° apart, as shown in Figure 6. The following equation mathematically describes the SET:

$$\sigma_\phi = \left(\frac{E}{1+\nu}\right)\frac{1}{4R_o \sin^2\theta, \sin 2\theta}(S_2 - S_1) \qquad (4)$$

where R_o is the detector-to-specimen distance, β the angle between the specimen surface normal and the incident x-ray beam, and (S_2-S_1) as shown in Figure 6. Until now, the SET has been largely re-

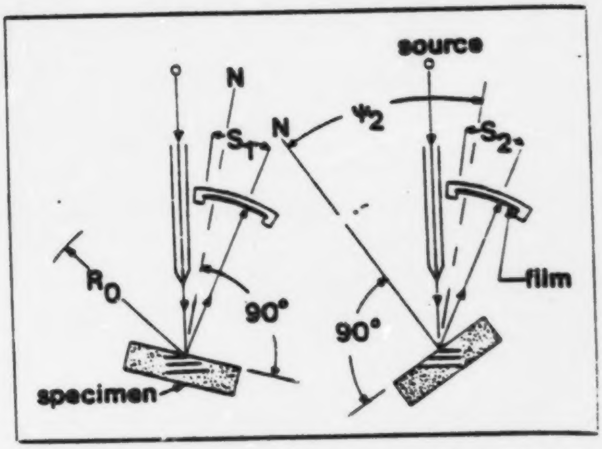

Figure 5. Schematic of the double-exposure technique arrangement.

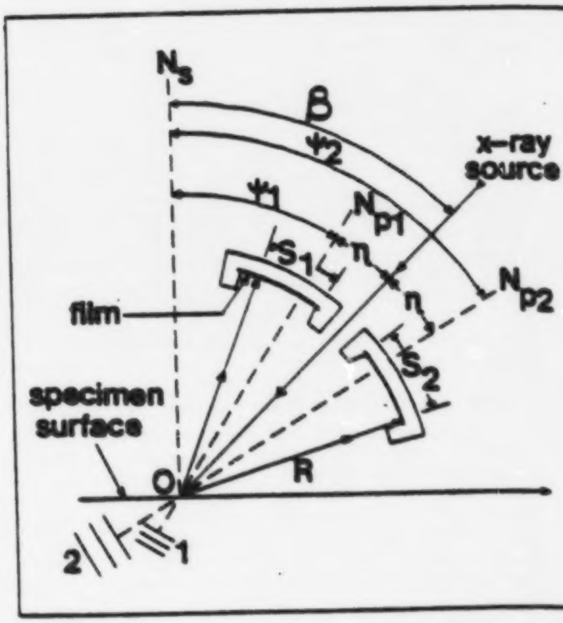

Figure 6. Schematic of the single-exposure technique arrangement.

single detector. The major advantages in the SET is speed and the fact that only a single adjustment of the stress-measuring head with respect to the specimen need be made. This avoids errors caused by rearrangement for subsequent ψ readings. The major disadvantage is that the difference between the high- and low-angle ψ is restricted to $180°-2\theta$, where θ is the Bragg angle for the unstressed planes selected for the analysis.

The portable rapid stress-measuring (Porta/Rapid/Stress) instrument about to be described is designed for SET; however, it may be applied in the DET or sin-squared-psi technique as well as most other instruments. Furthermore, it provides two ψ readings for each incident beam angle used in these two techniques.

In spite of the appearance of the elastic constants E and ν in the preceding equation, it is recommended that the proportionality of stress, σ_ϕ, versus the x-ray-peak shift $(S_r\text{-}S_l)$ or change in calculated interplanar spacing, Δd, be determined experimentally. This is done for the thermo-mechanical condition of the alloy in which stresses are to be determined and with the experimental arrangement to be used. This can be done through use of specially constructed mechanical calibration devices, four-point beam-bending devices, or tensile machines where a given specimen deflection can be related to stress in the surface of the specimen.[13,14] It also is often accomplished through electrical-resistance strain gages attached to a bend specimen at a point near where the x-ray strikes. The x-ray data are then plotted against applied stress to produce a calibration curve, the slope of which is the constant K_{-ST} for the SET method of Figure 6 in the corresponding equation:

$$\sigma_\phi = K_{-ST}(S_r\text{-}S_l)$$

This calibration procedure is recommended because the commonly recognized E and ν values are determined mechanically from bulk materials and represent elastic constants for the average of all the crystallographic directions of the metal lattice. However, in the x-ray techniques, strain measurements in a single selected crystallographic direction, dependent upon the Miller indices of the diffracting planes, are used. The difference between the x-ray and bulk elastic constants are often of the order of 10% and sometimes as high as 50%.

BACKGROUND

Recognizing the potential applicability of the x-ray diffraction technique and the limitations to its use in industry, Dr. C. S. Barrett and the author set out to design more viable instrumentation for the XRD method. The goal was to develop a device with a stress head no larger than that of the film camera devices previously described, and with the capability of application of the SET. Also, the instrument should give stress readings in less than one minute with accuracies heretofore impossible except under laboratory conditions. The size and shape of the film-camera devices were selected as a configuration goal because it was recognized that these devices could be applied in confined spaces, *e.g.*, inside of pipe. The device would also have to be rugged enough to survive and operate under field and shop conditions. The necessary auxiliary hardware, including power supplies, would also have to be packagable into a carriage easily moveable by one man across a typical manufacturing-area floor. Moreover, the only external connection should be a 220-volt power cable. The stress head would have to be remote, on the end of at least a ten-foot cable, and weigh less than 10 lbs. Operation of the device should be relatively insensitive to its environment, including power-source fluctuation. The stress reading produced should be in the form of a hard copy and should read in stress units, *e.g.*, psi, kg/mm² or MPa. Finally, the components should be readily available and of domestic manufacture, especially those with finite lifetimes, *e.g.*, the x-ray tube.

Development of the New Stress-Measuring Instrument

Early in our investigation, we determined that the most promising direction for development of a compact stress head was to use a position-sensitive x-ray detector. Available instrumentation was surveyed and a position-sensitive proportional detector procured for testing. However, it was quickly concluded that this device did not offer the flexibility of design that was needed for general application, especially to the single-exposure technique. Moreover, the particular detector obtained proved to be unreliable, and was therefore returned to the manufacturer; the character of its failure left some question as to the inherent ruggedness of its design.

Simultaneously, a concept for a position-sensitive scintillation detector (PSSD) was evolving, and an electronics engineer, Ronald E. Sturm, joined the two metallurgists in the eventual invention of a unique x-ray detector. The detector's design was possible due to rather recent developments in electro-optical devices. The principle of its operation is based upon the conversion of x-rays to light by a scintillation material coated upon the input faces of two fiber-optic bundles. The bundles are rectangular in cross section, about 3 mm by 13 mm. Each bundle is placed so that it intercepts the cone of diffracted rays on each side of the incident beam, *i.e.*, at points 180° apart as in the film camera devices previously described. The coherent fiber optics then transmit the light from the scintillators to the detector electronics package where the light signal is amplified and converted into an electronic signal that gives the intensity and position of the diffracted x-ray beams. Figure 7 shows a drawing of the front view of the stress head, including the detector, that has been developed at the University of Denver Research Institute using these principles. This package is a cube approximately two inches on an edge which is hermetically sealed, and its sensitive components are mounted so that they are isolated from mechanical shock. A more detailed description is given by Staffen and Ruud.[7]

The PSSD is designed for maximum sensitivity to 5-10 keV x-rays. X-ray filters to reduce background are attached. The filter type depends upon the analyzing radiation, *e.g.*, nickel foil for CuKα, and chromium foil for CrKβ. The spatial resolution of the detector has been shown to be approximately 50 μm for CuKα x-rays. The power supplies, controls, and data-retrieval electronics can be packaged into less than 22,000 cm³ (0.75 ft³). Water cooling of the detector is required; however, this is obtained from the same closed circuit coolant supply used by the x-ray tube.

The great advantage of this PSSD lies in its inherent versatility. The active x-ray-sensitive surface covers 95% of the detector surface, and the spatial resolution is uniform across its length. Since the x-ray-sensitive surfaces are at one end of flexible fiber optics, they can be easily placed in the optimum position for intercepting the diffracted x-rays. The good spatial resolution allows for a precision of ±0.03 degrees in peak locations with a specimen-to-stress-head distance of 40 mm. This radius is shorter than that used with goniometers or other position sensitive devices; despite the fact that the conversion efficiency of x-ray photons to electronic signal is only 10 to 20% with this detector, the more-compact x-ray optics contribute to greater x-ray intensities. Furthermore, the compactness of the x-ray-sensing surface allows the use of high 2θ angles, and the flexible fiber-optic bundles allow for easy conversion from one set of 2θ angles to another. The fiber-optic holder, which is attached to the incident-beam collimator, can be changed to give various 2θ receiving angles at a constant radius of approximately 40 mm. This is necessary for application to both BCC and FCC iron and steel with CrKα and CrKβ radiation.

Availability and ease of change of the x-ray source tube in the stress head shown in Figure 7 allow for rapid conversion to other x-radiations, *e.g.*, CuKα, needed for aluminum alloys. The versatility of the stress head permits use of the instrument for stress work on other materials as well, such as Ti and Ni alloys, ceramics, and filled polymerics. The figure illustrates only one configuration of the

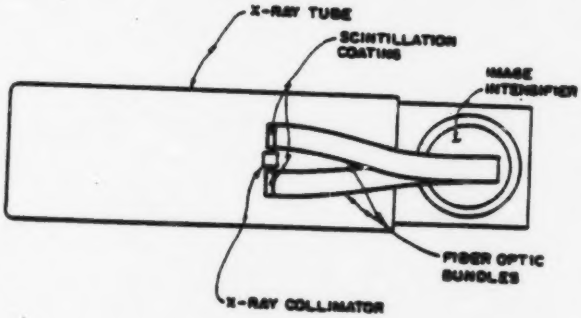

Figure 7. Front view of x-ray stress head showing x-ray tube housing and detector package from image-intensifier side.

---

*American Analytical's "Fast Stress" is capable of the SET, however.

stress head. Other configurations tailored to specific applications are possible; for instance, fiber-optic bundles up to nearly one meter long are being designed into a smaller x-ray stress head, to be attached to very small x-ray tube to measure stresses *in situ* at the inside wall of 4-inch pipe. The stress head is rugged, weighs less than 10 lbs, and is about the same size as the film-camera devices. Its combined power, water, and signal cable weigh less than 0.5 lbs/ft, and its signal output is easily interfaced to a mini-computer for data storage and processing.

Experience with this stress head has been gained on aluminum, stainless steel, and martensitic steel alloys; stress readings in all of these cases require less than one minute and in the last requires only about 15 seconds. These times are for x-ray data accumulation. The calibration curve shown in Figure 8 for 304 stainless steel demonstrates a standard deviation of ±1.5 ksi, which to the author's knowledge is the best precision published on austenitic stainless steel.

Equation 3 for the SET shows that with a given experimental arrangement all parameters are constant or read by the detector except R_o and β. In the past, these parameters were controlled carefully in using the diffractometer, or carefully measured and adjusted. When the x-ray-data accumulation is obtained in several minutes to an hour, these techniques are satisfactory. However, in the case of the Porta/Rapid/Stress, the setup could require 10 to 100 times more time than the actual stress reading. As a result, a technique of using a stressed/unstressed standard was conceived.[11] This is a combination of an unstressed powder of one composition overlaid on a stressed coupon of a second composition. With this coupon, the stress head could be roughly placed into position with the approximate R_o and β desired. Then, with the stressed-unstressed coupon placed upon the specimen area in which stresses are to be measured, an exposure of that coupon can be made. The information from the two peaks can be stored in the mini-computer of the stress device for calculation of R_o and β by the following relation:

$$R_o = \frac{(X_1)_{unstressed}}{\text{Tan}\,(180 - 2\theta_u)} = \frac{(X_2)_{unstressed}}{\text{Tan}\,(180 - 2\theta_u)}$$

where θ_u = Bragg angle of unstressed powder, $X_1 = S_1 +$ Constant, and $X_2 = S_2 +$ Constant (See Figure 6) and

$$\sin 2\beta = \left(\frac{E}{1+\nu}\right)\frac{(S_2-S_1)_{stressed}}{4R_o \sin^2\theta\, \sigma_{stressed}}$$

With this technique, the R_o and β parameters can be determined in a few seconds. This would make it possible to accomplish 10-20 accurate stress readings in an hour, including the setup time.

RESULTS

The calibration curve shown in Figure 8 for a 304 stainless steel four-point-bend specimen is indicative of the inherent precision of the described instrument. The statistical advantage of using twenty or more data points to establish the location of a peak is shown in this figure by the precision in locating peaks to less than ±10µm on the detector scanner; this amounts to ±0.01° 2θ with an R_o = 43 mm. Figures 9 and 10 compare results from a standard laboratory diffractometer and the PSSD with annealed aluminum powder. The diffractometer data were acquired using a ¼° detector slit and a continuous scanning speed of 1°/min. X-ray measurements from the two ψ angles necessary for stress measurements would have required 24 minutes on the diffractometer but only one minute with the PSSD. Comparison of the $K\alpha_1/K\alpha_2$ doublet resolution in the two figures illustrates that resolution consistent with speed is possible with the PSSD. As an illustration of the x-ray peaks from aluminum, Figure 11 shows a CRT photo of CuKα peaks from the (333,511) planes of 6061-T6 aluminum alloy. Figure 12 shows CRT photos for CrKα radiation diffracted from the (211) planes of a cold-rolled steel sheet. These required less than 15 sec to accumulate.

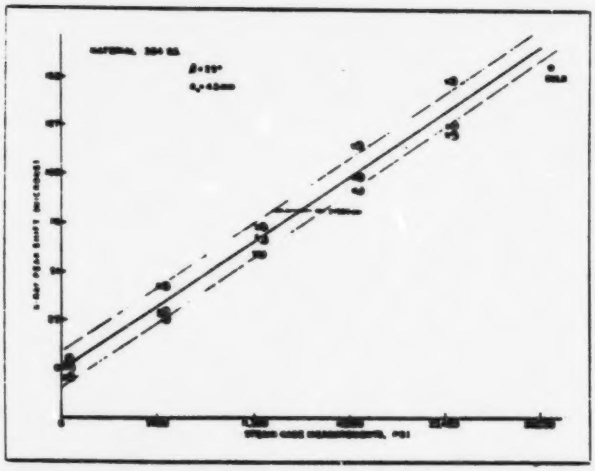

Figure 8. Stress calibration curve from 304 stainless steel showing strain-gage measurement (induced stress) versus x-ray measurements (peak stress).

Figure 13 shows x-ray CRT data representing the kind of peaks obtained in a residual stress study of the inside wall of 10-inch Schedule 80 304 stainless-steel pipe. These data show highly compressive surface stresses and were obtained several inches from the end, inside the pipe.

X-ray stress techniques use beams that have very shallow penetration of most metals; this is a limitation, but can sometimes be a useful characteristic. A characteristic of the instrument described herein is the small size of the irradiated area on the specimen. This can be a problem when the sample is large-grained, but there are techniques to overcome this difficulty. When stress gradients are steep, a small irradiated area may in fact be advantageous.

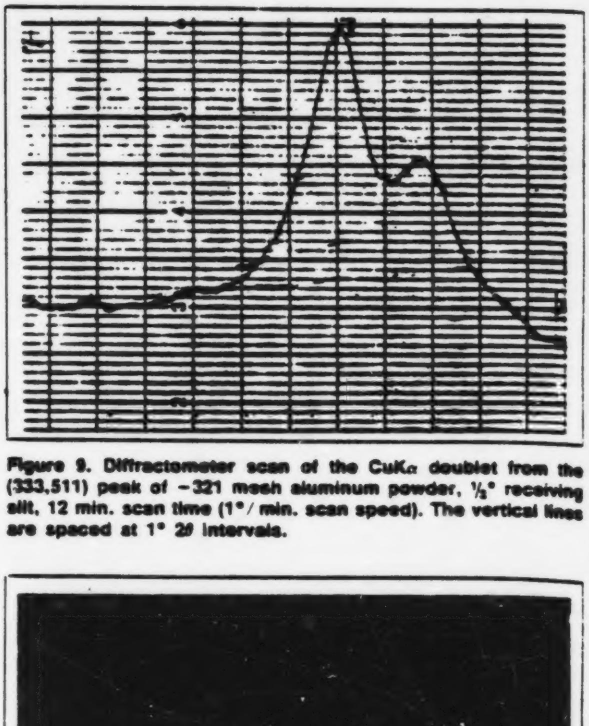

Figure 9. Diffractometer scan of the CuKα doublet from the (333,511) peak of −321 mesh aluminum powder, ½° receiving slit, 12 min. scan time (1°/min. scan speed). The vertical lines are spaced at 1° 2θ intervals.

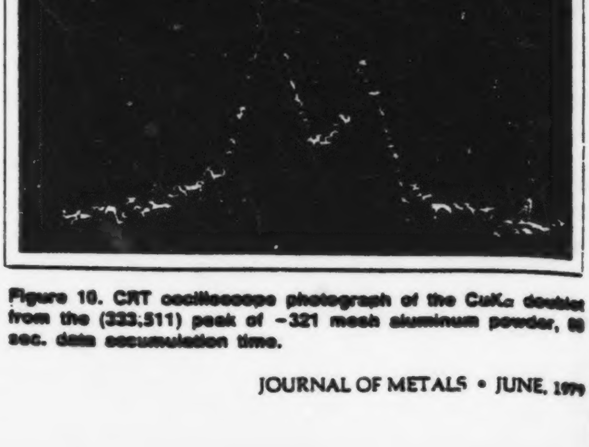

Figure 10. CRT oscilloscope photograph of the CuKα doublet from the (333,511) peak of −321 mesh aluminum powder, 60 sec. data accumulation time.

Q-12

CONCLUSIONS

The x-ray diffraction method of stress (strain) analysis in materials has been shown to be valid by dozens of engineers and scientists in application to a variety of metal alloys and parts of practical concern. In order to expand the application to the field and shop and to more practical types of parts, a highly compact, portable, rapid, and accurate x-ray instrument for stress measurement has been developed. This has been the result of the invention of a unique position-sensitive scintillation x-ray detector.

The prototype stress head is capable of stress measurements in confined areas (such as inside pipe), dynamic applications, use at elevated temperatures, and in a variety of manufacturing applications. The inherent versatility of the PSSD opens the possibility for tailoring x-ray-diffraction measurements to on-line manufacturing inspection. The detector's adaptability to the single-exposure technique provides an advantage in many practical stress measurements over the single-beam detector devices. The stress-head developments described herein seem ideally suited to field and shop stress measurements and possibly commercialization for wide distribution.

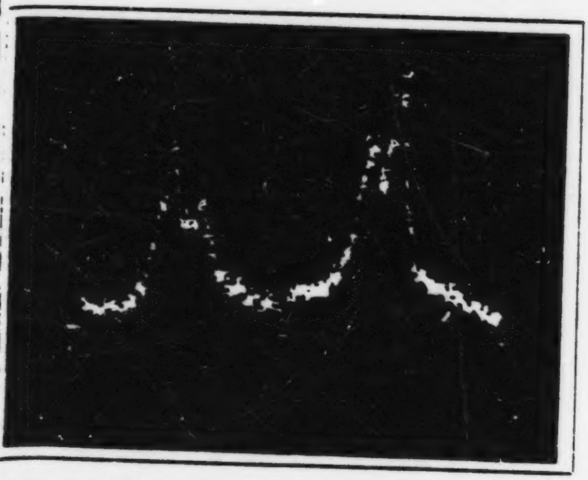

Figure 11. CRT oscilloscope photograph from the position-sensitive scintillation detector. The specimen was 6061-T6 aluminum sheet, and the x-ray peaks are the $CuK_{\alpha_{1,2}}$ doublet diffracted from the (333,511) set of crystallographic planes; data accumulation required less than one minute for both sets of peaks.

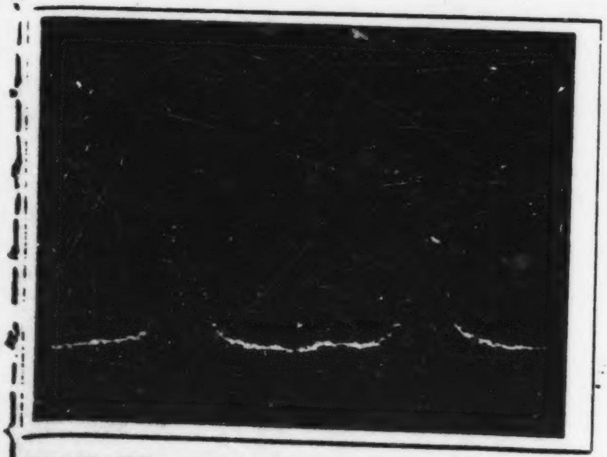

Figure 12. CRT oscilloscope photograph from the position-sensitive scintillation detector. The four-point-bend specimen was cold-rolled sheet steel; the x-ray peaks are the $CrK_{\alpha_{1,2}}$ doublet diffracted from the (211) set of crystallographic planes; data accumulation required 15 sec. (Note that the data outputs are reversed, making the peaks a mirror image of the actual data).

ACKNOWLEDGMENTS

The author thanks Drs. Charles S. Barrett and Paul K. Predecki for their constructive criticisms and helpful suggestions, and James F. Smith for his effort on the graphics.

References

1. R. J. Weedon, E. C. House, and R. E. Ogilvie, "Precision X-Ray Stress Analysis of Uranium and Zirconium," in *Advances in X-Ray Analysis*, Vol. 3, pp. 331-338; Plenum Press, N.Y., 1960.
2. D. A. Bolstad and W. E. Quist, "The Use of a Portable X-Ray Unit for Measuring Residual Stresses in Aluminum, Titanium, and Steel Alloys," *Advances in X-Ray Analysis*, Vol. 8, pp. 26-37, Plenum Press, N.Y., 1965.
3. J. T. Norton, "X-Ray Stress Measurement by the Single-Exposure Technique," *Advances in X-Ray Analysis*, Vol. 11, pp. 401-410; Plenum Press, N.Y., 1968.
4. J. M. Potter and R. A. Millard, "The Effect of Temperature and Load Cycling on the Relaxation of Residual Stresses," *Advances in X-Ray Analysis*, Vol. 20, pp. 309-319; Plenum Press, N.Y., 1977.
5. C. S. Barrett, "Diffraction Technique for Stress Measurement in Polymeric Material," *Advances in X-Ray Analysis*, Vol. 20, pp. 329-336; Plenum Press, N.Y., 1977. Also see Paul Predecki and Charles S. Barrett, "Stress Measurement in Graphite/Epoxy Composites by X-Ray Diffraction from Fillers," to be published in J. Composite Materials.
6. SAE, "Residual Stress Measurement by X-Ray Diffraction - SAE J784a," Society of Automotive Engineers, Inc., Warrendale, Pa 1971.
7. D. A. Steffen and C. O. Ruud, "A Versatile Position Sensitive X-Ray Detector," *Advances in X-Ray Analysis*, Vol. 21, pp. 00; Plenum Press, N.Y. 1978.
8. C. S. Barrett and T. B. Massalski, *Structure of Metals*, 3rd ed., McGraw-Hill Book Co., N.Y., 1966.
9. B. D. Cullity, *Elements of X-Ray Diffraction*, 2nd ed., Addison-Wesley, Reading, Mass., 1978.
10. H. P. Klug and L. E. Alexander, *X-Ray Diffraction Procedures*, 2nd ed., John Wiley and Sons, New York, 1974.
11. M. R. James and J. B. Cohen, "The Application of a Position-Sensitive X-Ray Detector to the Measurement of Residual Stresses," *Advances in X-Ray Analysis*, Vol. 19, pp. 695-708; Kendall Hunt, Dubuque, Iowa, 1976.
12. R. H. Marion and J. B. Cohen, "Anomalies in Measurement of Residual Stress by X-Ray Diffraction," *Advances in X-Ray Analysis*, Vol. 18, pp. 466-501; Plenum Press, N.Y., 1975.
13. B. A. MacDonald, "Application of the X-Ray Two-Exposure Stress Measuring Technique to a Carburized Steel," *Advances in X-Ray Analysis*, Vol. 13, pp. 487-500; Plenum Press, N.Y., 1970.
14. P. S. Prevey, "A Comparison of X-Ray Diffraction Residual Stress Measurement Methods on Machined Surfaces," *Advances in X-Ray Analysis*, Vol. 19, pp. 709-724; Kendall/Hunt, Dubuque, Iowa, 1976.
15. C. O. Ruud, "Stress-Unstressed Standard for X-Ray Stress Analysis and Method of Making Same," U.S. Patent No. 4,042,825.

ABOUT THE AUTHOR

Clayton O. Ruud is Manager of the Materials Analysis Laboratory at the University of Denver's Denver Research Institute, working primarily in the areas of x-ray diffraction application to metals characterization and powder diffraction instrumentation development. He received a BS in Physical Metallurgy from Washington State University, an MA in Materials Science from San Jose State College, and a PhD in Materials Science from the University of Denver.

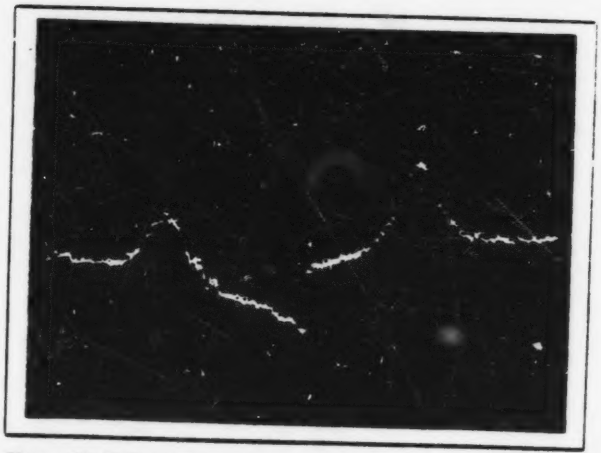

Figure 13. CRT oscilloscope photograph showing the $CrK\beta$ x-ray peak diffracted from the (311) crystallographic planes of 304 austenitic stainless steel. The data were obtained *in situ* 12 inches inside a 24-inch-long section of 10-inch diameter Schedule 80 pipe.

256 0-14

Clayton O. Ruud
Pennsylvania State Univ.

Position-sensitive detector improves x-ray powder diffraction

Performing x-ray powder diffraction analysis on crystalline materials has long been a slow, sometimes inaccurate process involving instruments that offer little flexibility. A recently developed position-sensitive scintillation detector promises to alleviate these and other analysis problems.

A NEW APPROACH to x-ray powder diffraction, position-sensitive scintillation detection, promises improved speed and accuracy and expanded versatility over existing techniques. It is based on coherent conversion of the diffracted x-ray pattern into an optical signal, *i.e.*, light; the conduction of this light signal over several linear centimeters of two coherent, flexible, fiber-optic bundles; the amplification of this signal by electro-optical image intensification; the electronic conversion of the signal; and transfer of the electronic signal to a computer for refinement and interpretation.

The present version of the position-sensitive scintillation detector (PSSD) has a linear (x-ray peak position) resolution of approximately 50 μm over its entire length along with a photon conversion efficiency of about 15%. This compares well with a very best resolution of about 60 μm at the center of the detector for a few position-sensitive proportional detectors (PSPD) and 100 to 200 μm for most of the PSPDs used in x-ray diffraction. Furthermore, PSPDs usually show poorer resolution away from the center of their x-ray-sensitive area.

Linear resolution is defined as the detector's ability to accurately identify the point along its x-ray detection length at which an x-ray photon is incident. The resolution value given is essentially the degree of uncertainty associated with the reported position of an x-ray peak.

The scintillation-coated glass bundle that makes up the x-ray-sensitive surface of the PSSD does not limit the surface shape to a long, thin plane. It can be ground and polished to other configurations; *e.g.*, a circle to conform to the radius of the focusing circle in a special x-ray diffraction application. Also, since the x-ray-sensitive surface is a simple fiber end, it is possible to adapt the PSSD to any number of x-ray focusing geometries.

Proportional detectors, whether they are position sensitive or not, are inherently capable of processing only one x-ray photon at a time with a time delay, or dead time, during which no other photon can be processed. The dead time usually is a few microseconds, and the maximum x-ray flux in which a detector is functional is a few ten-thousand counts. This means that under application conditions where rapid data accu-

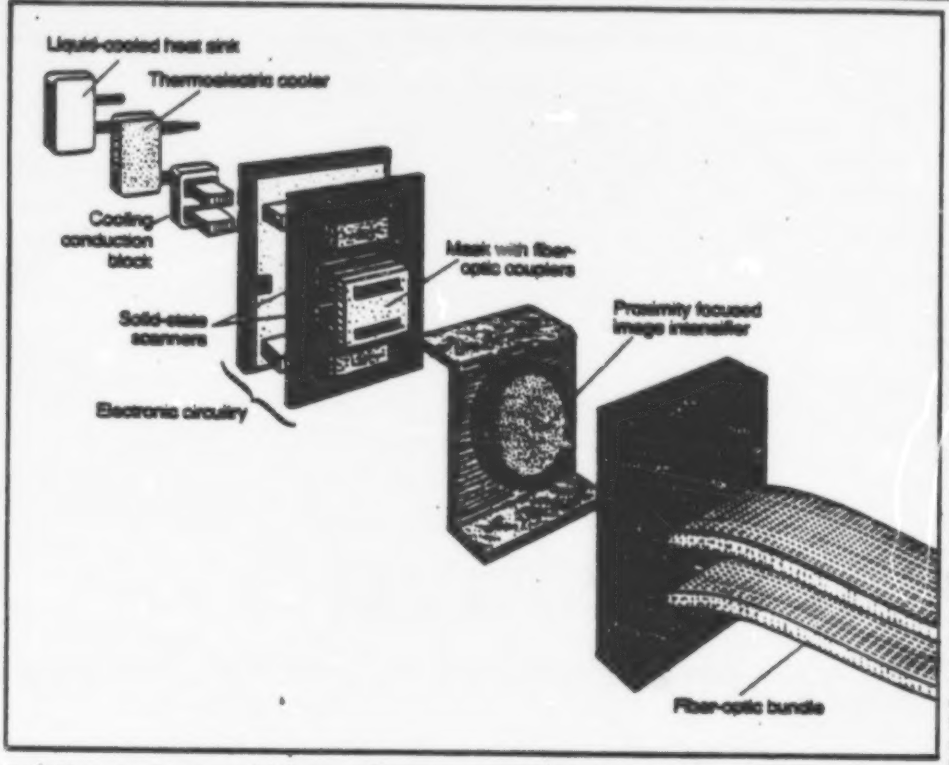
Liquid-cooled heat sink
Thermoelectric cooler
Cooling conduction block
Mask with fiber-optic couplers
Solid-state scanners
Proximity focused image intensifier
Electronic circuitry
Fiber-optic bundle

Left: Illustration shows exploded view of the position-sensitive scintillation detector (PSSD). The two fiber-optic bundles are connected to an image intensifier in the PSSD electronics cube where the light signal of the x-ray pattern is amplified. Two fiber-optic couplers then transfer the light signal to solid-state scanners which convert the light to an electronic signal. The cooler keeps the cube at −20 C to reduce electronic noise.

Below: Illustration shows fiber-optic bundles from the PSSD cube in a holder with the x-ray unit. In the single-exposure technique, the incident x-ray beam is diffracted by crystallographic planes immediately below the specimen surface back to the fiber-optic bundles.

mulation requires very high x-ray fluxes, a PSPD would be ineffective.

The PSSD has no dead-time period and therefore is effective over a very broad range of x-ray flux intensities. For example, it has been shown to be applicable to faintly diffracted x-ray peaks as might be provided with a 100 to 200 W x-ray tube source; on the other hand, it has been shown to be operable in the direct x-ray beam of an x-ray source operating with more than a kilowatt of power.

The PSSD is inherently rugged. Since the electronics detection cube is her-

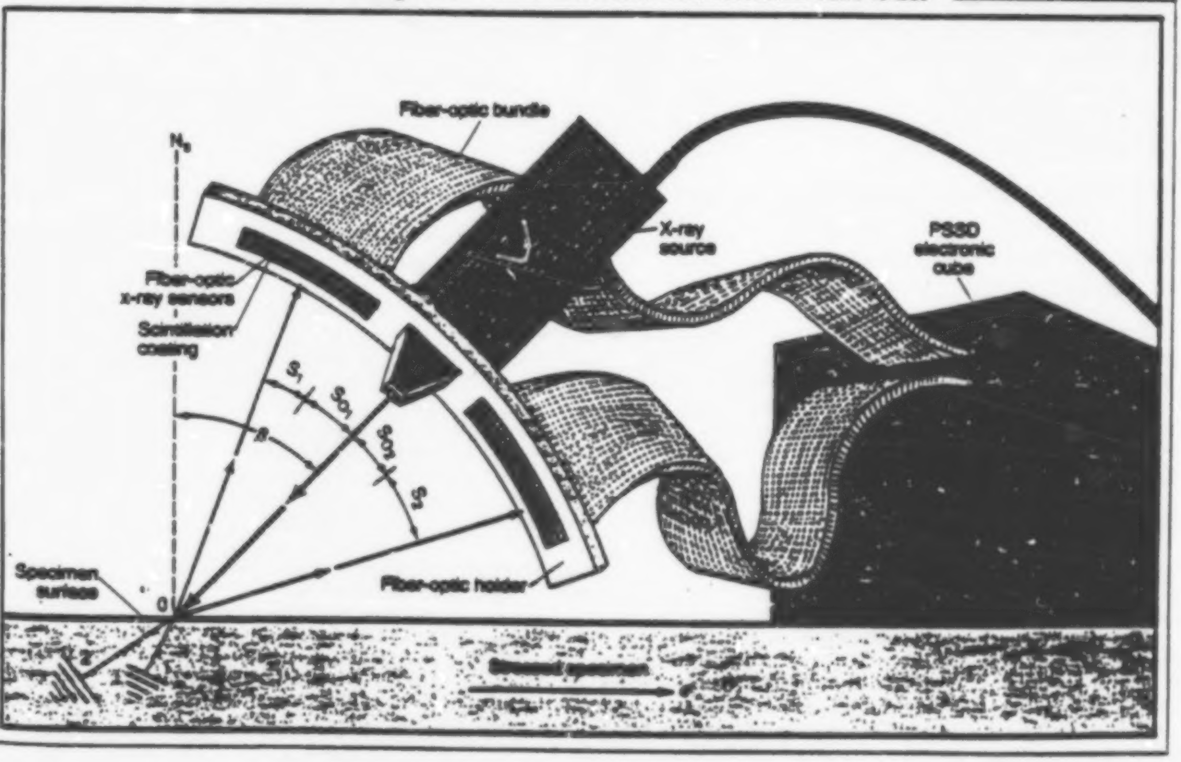
Fiber-optic bundle
N_s
X-ray source
PSSD electronic cube
Fiber-optic x-ray sensors
Scintillation coating
S_1
S_{O_1}
S_{O_2}
S_2
β
Specimen surface
0
Fiber-optic holder
Stressed specimen

X-ray powder diffraction

Over the past few decades, x-ray powder diffraction (XRPD) has become a basic materials-analysis tool. It is applicable to virtually all crystalline materials and provides not only phase identification but quantitative analyses and information as to crystallographic character such as atomic ordering, mechanical strain, and particle size.

With regard to phase identification, the International Center for Diffraction Data has established a data base in the form of a powder diffraction file to aid in crystalline material identification through XRPD.

In its most elementary form, XRPD is based on the phenomenon expressed in the Bragg equation, $n\lambda = 2d \sin\theta$, where n is unity in most cases, λ is the wavelength of analytical x-ray radiation, d is the distance between certain crystallographic planes in the material being analyzed, and θ is the Bragg angle and the quantity measured in XRPD analysis.

There are several basic types of instrumentation used for material analyses and characterization by XRPD, but the most popular is the Bragg-Brentano parafocusing goniometer. Several manufacturers in the free world are marketing diffractometers based on the Bragg-Brentano design, which has remained fundamentally the same for several decades.

Essentially this XRPD diffractometer consists of a mechanical turntable capable of positioning a powder specimen at various known θ angles with respect to an incident x-ray beam, and a detector that can be scanned at twice the angle through which the specimen is rotated. The scanning is accomplished in such a way that the detector is in a position to intercept the diffracted x-ray beam whenever the Bragg condition is met.

This scanning detector device has been the workhorse of XRPD analysis since the late 1940s. Most modern versions are computer automated.

In the early 1970s, however, the technology for x-ray detectors which did not have to be moved (i.e., mechanically scanned) to detect Bragg angle x-ray diffraction evolved to produce reliable devices with sufficient spatial resolution to be suitable for application to XRPD.

These so-called position-sensitive detectors had many applications when they were substituted for the x-ray detector normally used on the scanning diffractometers. By and large these detectors were based on the same principle as proportional x-ray detectors and thus are named position-sensitive proportional detectors (PSPD).

Attempts also were made to use these detectors in XRPD geometries other than the Bragg-Brentano diffractometer. Although the attempted designs were innovative and scientifically sound, many practical shortcomings prevented their general acceptance, and the PSPD has essentially remained an accessory to the Bragg-Brentano goniometer.

data collection through stress calculation and hard copy printout) is about 90 sec. This indicates that approximately 30 readings can be made in one hour.

Application of the PSSD to heavy plate weldments, 450 to 500 kg (1,000 to 2,000 lb), has demonstrated its use on large specimens; its use on nickel-based tubing has demonstrated its ability to resolve stress gradients over very small areas with previously unattainable data collection speed and accuracy.

A second PSSD was incorporated in a residual stress analyzer designed to be inserted into pipe with inside diameters as small as 230 mm (9 in.). This instrument has been applied to nondestructive residual stress measurement on the inside of girth-welded austenitic stainless steel piping.

No other XRPD stress measurement instrumentation approach can provide an instrument capable of being inserted into the piping, and the accuracy and precision which have been demonstrated are unprecedented for XRPD stress measurement on stainless steel. For example, calibration curves comparing applied stress and XRPD measured stress show standard deviations of less than 20 MPa.

A number of other applications of the two PSSD-based instruments are being investigated. One is to measure the amount of cold work induced in metallic components by shot peening. Cold work in metals is indicated by x-ray peak broadening as well as residual stress inducement. These two quantities can be measured simultaneously with the PSSD instrument. Most important, however, is that the measurements can be done rapidly enough to be used to inspect parts for quality control.

A research application of interest involves XRPD studies of high temperature crystalline phase transformations in ceramic materials. Currently used scanning goniometers require heating the specimen to a specific temperature and holding that temperature for several minutes to an hour while the scanning instrument makes measurements.

Close temperature control is complicated by the fact that thermal expansion tends to disrupt the precise x-ray optical condition necessary for accurate measurements. With the PSSD, the two sensing surfaces allow for inherent measurement and correction for dimensional changes. Long periods of constant temperature are not necessary due to the high data collection speed.

The PSSD design is inherently adaptable to performance improvements by retrofitting. For example, the scintillation coating is presently the limiting component in providing linear resolution. Ongoing investigations aimed at development of more-efficient conversion coatings could decrease resolution by a factor of two. Further, new, more-advanced electro-optical components are on the horizon which will improve the performance of the PSSD and can be retrofitted to existing units. ☐

THE AUTHOR

Clayton O. Ruud is a senior research associate in the materials research laboratory at Pennsylvania State Univ. where he is principal investigator for research projects in nondestructive testing and evaluation methods for materials measurement. Ruud also conducts research in residual stress measurement and measurement methodology development and manages the automated x-ray analytical instrumentation laboratory.

Sine-square-psi, DET, and SET

The sine-square-psi technique for obtaining stress readings usually is recommended where certain characteristics (e.g., texture, severe stress gradients) are likely to degrade the x-ray stress measurement accuracy. Furthermore, the various readings taken at a series of different attitudes of the x-ray beam to the specimen surface contribute to the statistically superior accuracy of the technique. However, the technique increases the time for each stress measurement manyfold and therefore is seldom used.

The double-exposure technique (DET) measures the interplanar atomic (d) spacing of planes with two orientations directed at the specimen surface. To accomplish this, the incident x-ray beam must be directed at two different angles to the specimen surface. The necessary reorientation is done either by rotating the specimen about the center of the analysis area or by moving the x-ray source and detector through an arc with the area of analysis at the center of rotation.

This technique was developed for the application of instruments with a single detector (e.g., a scanning diffractometer) or those with a single position-sensitive detector surface. The major criticism of the DET is that it requires considerably more time than the SET and that its accuracy is severely compromised by the necessary reorientation of either the specimen or the x-ray source and detector.

The single-exposure technique (SET) is the preferred technique for rapid XRPD stress measurements because it is convenient and provides accurate results. The SET is based on the fact that a single x-ray beam, incident on at least a few ten-thousand powder grains, is diffracted at a constant θ angle such that a cone of diffracted radiation is formed with the incident beam as the axis. The intersection of the specimen surface and the incident x-ray beam is the cone apex.

The cone half-angle, 2η, is equal to twice the Bragg angle subtracted from 180 deg. A plane perpendicular to the cone axis intercepts the cone in a circle when the specimen is unstressed. If the specimen is stressed, the circle becomes an ellipse, and the deviation of its shape from a circle is indicative of the stress (elastic strain) in the sample.

Until now, the SET has largely been restricted to x-ray film apparatuses, since conventional scanning diffractometers have only a single detector. In addition, the size of the position-sensitive proportional detectors prevents conveniently placing more than one of them near the x-ray source.

metically sealed and the flexible fiber optics are enclosed in a heavy plastic envelope, the PSSD can be used in dusty, humid industrial environments. Furthermore, temperature ranges between 4 and 43 C (40 and 110 F) have little effect on the detector's operation. The instrument shows no loss of linear resolution or stability under moderate mechanical vibration.

However, the computer to which the detector is connected is subject to normal computer environmental limits but it can be operated remotely from the detector cube. It should be noted that the detection cube can be placed remotely from the x-ray source since the flexible fiber optics can be 2-m long. This allows application of the PSSD in high electrical and/or magnetic fields.

The PSSD has been applied mainly to x-ray residual stress measurement. This is not because its application to other x-ray powder diffraction (XRPD) uses is more difficult, but because x-ray residual stress measurement is the first application that was attempted and there has been a great demand for this type of stress data from various sources.

There are three basic techniques for obtaining stress (strain) readings from a polycrystalline solid by the XRPD method. (Polycrystalline metals and ceramics are essentially powders with the grains fused together; thus, their study by x-ray falls into the definition of XRPD.) The three are called the sine-square-psi technique (sine$^2\psi$), the double-exposure technique (DET), and the single-exposure technique (SET).

It must be noted that in order for the x-ray method to be used to measure absolute residual or applied stress, the "d" spacing (see Bragg relation) of planes of the same crystallographic character (*i.e.*, Miller indices) must be measured at two different orientations with the polycrystalline solid's surface. What is meant by absolute measurement is that no previous or subsequent measurement of that metal piece, in a zero-stress condition or some other known stress condition, is needed for calibration.

The PSSD is well suited to SET application, the major reason being that it can have at least two detection surfaces that are spatially efficient since the active detection surfaces cover more than 95% of the fiber optics cross section. The ability of the PSSD to perform the SET provides a great advantage for its use in x-ray stress measurement over other detectors and diffractometers. The PSSD also can perform the sine-square-psi and double-exposure techniques, usually with more proficient and rapid data collections and equal accuracy when compared to other XRPD instrumentation.

Two x-ray stress measurement instruments have been built utilizing the PSSD. One has been mounted on a horizontal rack with a carriage capable of translating the stress measuring head in two orthogonal directions. This instrument is used for mapping surface stresses in large specimens. It has been used to investigate stress corrosion cracking problems in "Inconel" tubing and bronze naval ship propellors, and for mapping residual stress fields in heavy steel plate weldments.

Calibration results indicate that the detector is accurate to less than 7 MPa with a standard deviation of 7 MPa for ferritic steels. Data collection times for ferritic steels range from 1 to 10 sec, and the time required for one complete reading (*i.e.*, from

. Mindlin, "Stress Distribution Around a Hole Near the of a Plate Under Tension", Proc. Soc. Exptl. Stress Anal. 5, (1948), pp 56-68.

X-RAY RESIDUAL STRESS MEASUREMENT SYSTEMS FOR ARMY MATERIAL PROBLEMS

Charles P. Gazzara

Army Materials and Mechanics Research Center
Watertown, Massachusetts 02172

ABSTRACT

A summary of the work in X-ray diffraction stress analysis performed at the U.S. Army Materials and Mechanics Research Center (AMMRC, Formerly Watertown Arsenal), beginning in 1925, up to the present time, is presented.

The technical problems affecting X-ray stress measurements, such as texture, grain size, and surface preparations, along with progress made in fabricating residual stress standards, is discussed.

The development of X-ray stress equipment to meet the Army's needs, in particular, the subject of a Materials Testing Technology (MTT) Program entitled "A General Purpose Residual Stress Analyzer", is described, along with applications on various Army systems.

INTRODUCTION

It is fitting that the subject of this report began in the U.S. Army and specifically on the same military grounds. In 1925, H. H. Lester and R. H. Aborn introduced the concept of measuring residual stresses by measuring the displacement of X-ray diffraction lines using a simple camera, and calculating the change in the d spacing and hence the "unit cell" strain[1]. Subsequently, an improved X-ray diffraction system was constructed at Watertown Arsenal (see Figure 1). This stimulated some interest at the Arsenal since the manufacturing process of producing cannon was found to introduce residual stresses. The residual stress work

f the 30's is reviewed in part by W. S. Baird[2]. A camera, designed
/ G. Sachs and J. Weerts in 1930, was built, but the strain ellip-
oid could not be determined until R. K. Haskell[3] developed the
lastic equations in a form that could be applied to the X-ray dif-
raction case. C. Barrett and M. Gensamer[4] could solve the ellip-
oidal problem under a special case where $\phi = 45^\circ$ and $2\theta = 135^\circ$,
it it was shortly after that the R. Glocker and E. Osswald were
le to measure residual stresses in any chosen direction in the
lane of the material by measuring X-ray diffracted spectral line
ifts at two inclination angles: $\phi = 0$, $\phi = 45^\circ$[5]. Hence, this
thod has been used almost exclusively since the middle 70's (and
yet used with caution), and has come to be known as the "Glocker
thod".

Advances in the state of the art of X-ray residual stress
alysis, RSA, have been slow and beset with problems and short-
mings, most of which have been addressed. In spite of this,
rthwhile applications have been made. A summary of the X-ray
thods is treated in an SAE X-ray Manual[6].

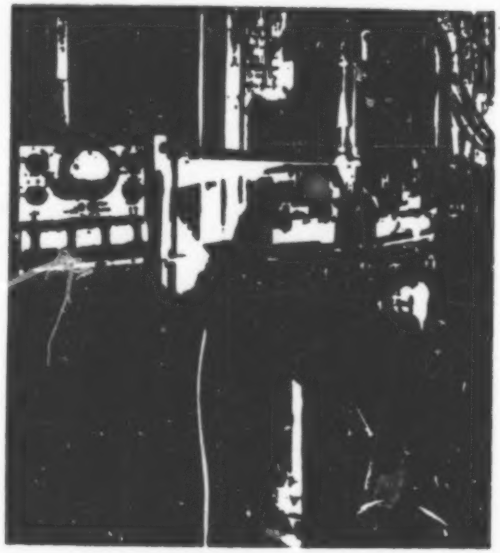

Figure 1. "Where it Began". First X-Ray System at Watertown Arsenal (H.H. Lester). Shown with G. Sachs and J. Weerts. Residual Stress Camera, Circa 1933.

The problems in RSA, presently of greatest concern at AMM
are broken down into two areas, equipment and technical.

The equipment problems involve development of an X-ray sy
that is fast, portable, safe, reliable, easy to use, accurate,
standard.

The U.S. Army has sponsored the development of a high spe
system at the Denver Research Institute (DRI), utilizing a sol
state position sensitive detector[7]. This effort was funded as
of the Materials Testing Technology Program (MTT) of which AMM
the program administrator and MERADCOM, Fort Belvoir, the cont
administrator. This system was designed for application on al
alloy (and aluminum composite) assault bridges (see Figure 2),
is yet in the state of development.

The final form of the high speed X-ray unit is now suppor
by the Electric Power Research Institute (EPRI) at SAI Inc.,
La Jolla, California.

A system currently in use at AMMRC, is a Rigaku strainfle
X-ray system utilizing an X-ray head that can be employed in t

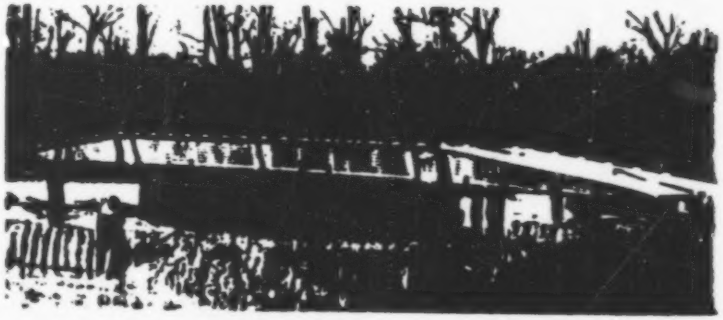

Figure 2. Photograph of a 31 Meter Aluminum Alloy Assault Bri
at Fort Belvoir.

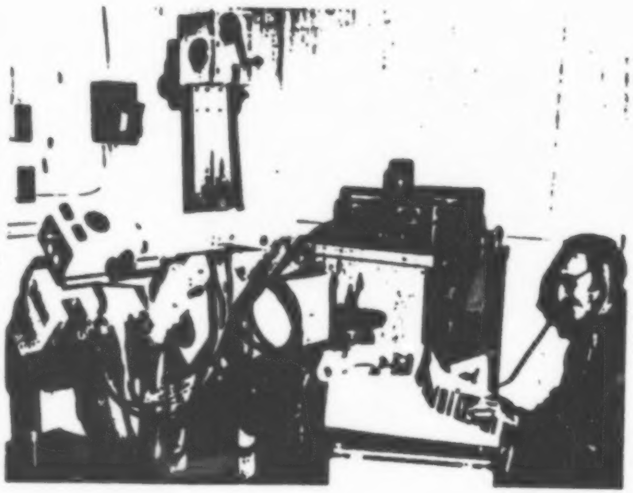

3a.

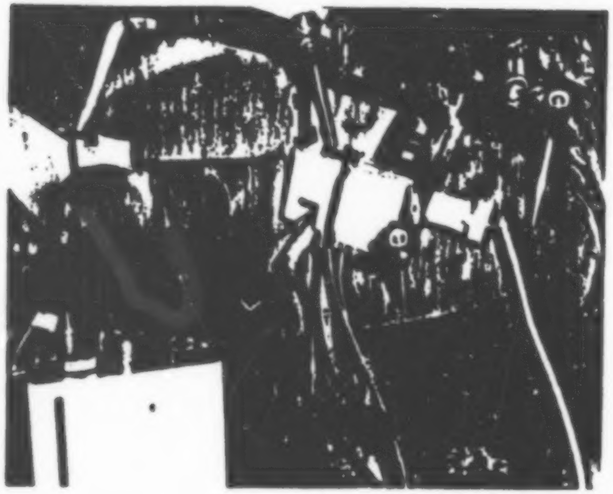

3b.

Figure 3. (a) The Parallel Beam Residual Stress X-Ray System (RIGAKU MSF) and (b) The X-Ray Head Mounted on Tripod in the Portable Arrangement (PSF). (See Figure 11 for Larger View).

computer controlled laboratory mode or mounted on a tripod and use in a portable mode (see Figure 3). This system is primarily being used to set up procedures for various Army systems, help solve special technical problems, and serve as a backup system for othe residual stress apparatus in the U.S. Army.

The technical problems of greatest concern in RSA at AMMRC, a essentially in three areas; the effects of texture, grain size, an surface preparation.

Texture Effect in RSA. In 1934, H. Möller and J. Barbers[8] co cluded "the grains are not taking up strain homogeneously" and tha

a. there are different physical properties in different directions.
b. anisotropy exists in the grain boundaries.
c. grain size can give erroneous residual stresses.

The problem of texture and anisotropy ellicited much activity and a review is given by R. Marion and J. Cohen[9] along with an approach to correcting the X-ray stress for texture, based on the work of W. Wiedeman[10].

B. D. Cullity[11] gave a further explanation as to the degree o complexity of characterizing microstresses in differentiating between directionality in the grain boundaries, introducing the concept of a pseudomacrostress, PMS, associated with swaging, rolling, etc. as opposed to a nondirectional grain boundary stress caused by grinding, machining, etc. Recently, H. Dölle[12] and J. Cohen[13] have presented an analytical approach to solving the texture problem in RSA. Although their approach is technically feasible, the practicality is questionable. However, the authors suggest efficient solutions to this problem which must be tested before applications can be made in systems such as those in the U.S. Army.

Grain Size. Although grain size effects in RSA were suspecte early[8], F. Gisen, R. Glocker, and E. Osswald[14] attempted the first experimental means to minimize errors due to this condition by oscillating the film in an X-ray camera.

This problem has not been effectively solved, as will be discussed later, particularly in measuring stresses in aluminum alloys.

Surface Preparation. The first work at Watertown Arsenal in surface preparation for RSA was performed by W. S. Baird[2], and a summary of the bulk of the work in this area is given in the Residual Stress Manual[6]. Some of the results of work performed in this area at AMMRC are presented herein.

APPLICATIONS

Systems

The primary purpose of this work is to establish procedures, with associated equipment, and to accurately and efficiently measure residual stresses in specific material for:

a. inspection, and to maintain quality control.
b. use as a tool in failure analyses.
c. developing and improving experimental systems.

Following is a list of materials systems under investigation illustrating the range of applications of RSA at AMMRC.

Steels

a. M735 penetrator-material maraging steel[15] (see Figure 4).
b. Tube-launched, optically tracked, wire-guided missile (TOW) case.
c. M329A2, 4.2" and M437A2-HE 175-mm projectiles.
d. M392 (tungsten carbide penetrator).
e. Copperhead (4340 steel).
f. Cannon tube plates.

Figure 4. The X-Ray Diffraction MSF System with an M735 Penetrator Maraging Steel Case.

Uranium Penetrators

a. GAU 8A.
b. XM774.
c. XM833.

Tungsten

a. M735 penetrator.

Aluminum

a. Assault bridges (Figure 2).
b. LAW missile case.

X-Ray Apparatus

Unless noted otherwise, the X-ray diffraction apparatus emplo throughout this study is a Rigaku Strainflex MSF (MSF denotes manu strainflex but consists of a console that allows one to select ψ_0 values of 0-45° in 5° increments and can be operated in a manual or computer controlled mode). The computer, a Wang 60G, is programme to perform a linear least squares analysis of σ versus $\sin^2\psi$ (with up to four values of ψ. The other version of the Rigaku Strainfle which operates in a strictly manual mode, is the PSF (PSF - portabl strainflex means that the head containing the X-ray tube and ψ - 2 goniometer can be removed and mounted on a portable tripod. The el tronics control is manual and the only recording of the diffraction peak is effected with a portable recorder). This system has paral-lel beam optics which is achieved with beam and receiving slit col-limation. The Rigaku MSF/PSF is fully described in an AMMRC TR[16], and a schematic of the optics is shown in Figure 5.

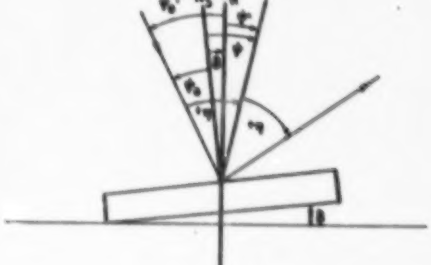

Figure 5. A Schematic Drawing of the Rigaku Strainflex X-Ray Diffrac-tion Geometry.

Prior to the acquisition of the Rigaku X-ray system, a divergent beam DIANO (GE XRD-5) X-ray system was employed at AMMRC. This system incorporated a specimen holder that could be variably set to select a value of ψ from 0^{0} to 60^{0} with a corresponding setting of the receiving slit on the ψ related focussing circle.

The DRI X-ray diffraction apparatus discussed is a developmental high speed X-ray apparatus that is capable of providing two ψ settings with each exposure (approximately 15 seconds) and with a recording of the entire diffraction peak by means of solid state detectors (see Figure 6 for a schematic of the DRI system)[7].

STANDARDS

It was determined that the need existed for obtaining and maintaining a set of standards which could be used for:

1. calibrating equipment.
2. testing for residual stress equipment malfunctioning, including faulty operation of specific components.
3. correlation of X-ray stress with mechanical stresses.

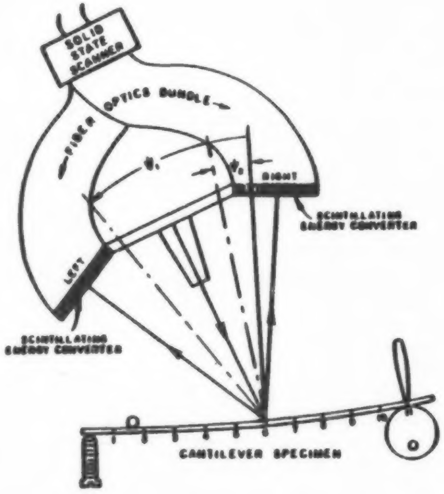

Figure 6. A Schematic Drawing of the DRI X-Ray Residual Stress Single Exposure Geometry with Aluminum Standard Specimen.

The necessary qualities of the standards are: to maintain con stant stress levels with time (minimum creep), optimum grain size, the selection of required stress levels, removal of distorted surface layers, protection of surface from oxidation or corrosion, and reproducibility of measuring area (or to minimize stress gradients).

In the case of the steel standard, a piece of cold rolled stc was cut and polished in a manner to be discussed below, in order t remove surface damage. The residual stresses were measured with t DIANO system by plotting $\Delta 2\theta$ versus $\sin^2\psi$ for values of ψ=0, 15, 3 45, and 52^{0} and with the Rigaku MSF system in both the automatic a recorded mode. This standard was also tested with a Fastress X-ra system at TARADCOM and at two laboratories employing Rigaku strain flex X-ray units (G.E. Schenectady and at Bethlehem Steel, Homer Research Lab). Finally, this standard was employed in order to tc the DRI X-ray device[7]. Schematic drawing of the steel standard di playing the X-ray residual stress values is shown in Figure 7.

In order to obtain an accurate, reproducible aluminum standaı it was necessary to mechanically introduce the stresses when required, due to the occurrence of creep. A commercial cantilevei

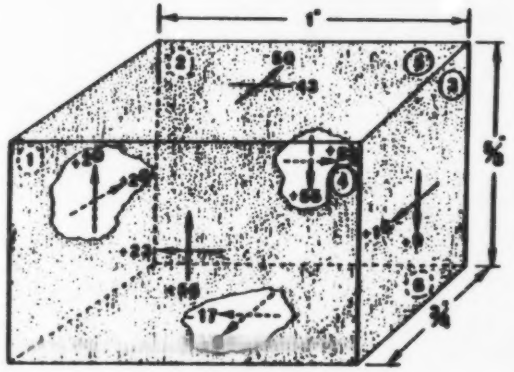

Figure 7. Drawing of a Steel Residual Stress Standard Specimen Illustratin the Stress Values on Each Face.

C-22

fixture was modified in order to provide a surface, of the X-ray standard, that would be accessible to any X-ray system (see Figure 8). Aluminum standard bars 1" x 12" in various thicknesses, up to 1/4", were machined, etched, and marked in 1" increments and deflected a fixed amount, at the end of the bar, in order to afford stress levels of 1-12 ksi along the bar. The strain levels were measured with strain gauges and also calculated[17]. These aluminum standards were used to test the DRI instrument in a manner similar to that using the steel standard. The results of the readings obtained with the Rigaku and DRI instrument are shown in Table 1. The Rigaku strainflex has a feature that enables the X-ray head to oscillate, to minimize the effects of grain size, while the DRI instrument does not. This is the reason for being unable to obtain residual stress readings with the DRI instrument at all positions on the standard bar at this time. Creep tests reveal that the bars can be kept flexed for 24 hour periods without affecting the residual stress readings.

PROBLEM AREAS

Grain Size

The problem of grain size in X-ray measurements yet persists. Increasing the area radiated by X-rays can only be achieved at the sacrifice of resolution of the stress positions. Oscillation of specimens is usually impractical in that most test specimens are not amenable to oscillation. In addition, a large error is introduced when the position of the specimen surface (normal to the surface) is changed. This error is ten times greater in divergent beam X-ray systems than those utilizing parallel beam optics. The Rigaku strainflex allows for an oscillation of the entire goniometer and X-ray tube assembly $\pm 3^0$, $\pm 5^0$, $\pm 7^0$ ϕ. This, of course, results in an uncertainty in ϕ_0 as well as a demand for "slowing down" the scan rates while increasing the time constant, and hence the measuring times. Increase in measuring times by a factor of four are common with the presence of large grains and in the case of grains 300μM long, with the 6061 bar not shown in Table 1, stress readings were unobtainable even with oscillation of ±7°.

It appears that with the presence of large grains, as in aluminum, that extreme caution is necessary in X-ray RSA. As with the DRI instrument, further development includes increasing radiation area, employment of high energy radiation, and oscillation of the X-ray source (possibly laterally as well as in an angular fashion, as with the Rigaku strainflex).

Future areas of investigation may include single crystal diffractometry, when grain sizes are determined to be too large to be subjected to powder diffraction techniques.

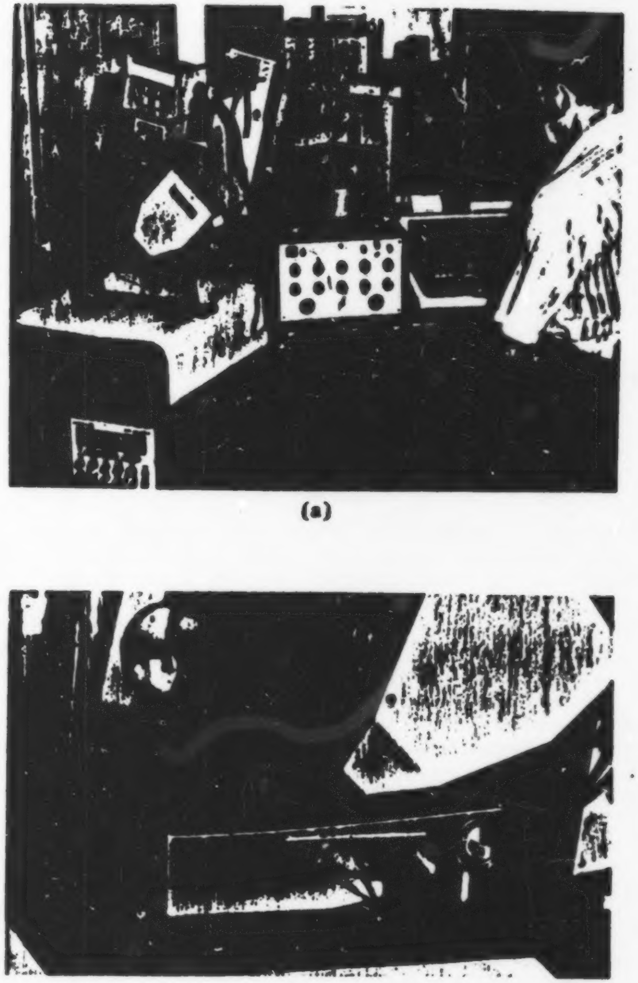
(a)

(b)

Figure 8. (a) X-Ray Residual Stress Measurement (MSF), of an Ela tically Bent Aluminum Alloy (7005) Standard Bar. Noti the Strain Gauge Test Arrangement for Simultaneous X-R and Mechanicla Stress Measurements. (b) Close-up of Aluminum Bars (With Attached Strain Gauges) in Cantile Bending Fixture.

Table 1. Residual Stress Values (KSI) of Aluminum Alloy Bars

Alloy 2024 T3 - 0.090" Thickness

Bar Position	Theoretical Stress	Stress (Strain Gauge)	X-Ray Rigaku(222)CrKα ±5° Oscill. TC=1 Sec. (Auto Mode)	±7° Oscill. TC=10 Sec. (Graph)	DRI 333/511 CuKα
4	7.0	5.6	6.0 (11) σ=±1.7*	9.0	10.0
7	4.0	3.4	7.1 (7) σ=±1.4	6.0	(Scatter Too Large)
10	1.0	1.1	3.0 σ=±1.2	3.0	3.0

Alloy 7005 (750°F, 3 Hours, Furnace Cool) 0.250" Thickness

Bar Position	Theoretical Stress		(Graph)	(Graph)
4	15.7		13±2†	14±2
7	9.6		10±2	9±2
10	3.5		5±2	5±1.5

*σ = Standard Deviation. Based on Number of Measurements (11) of Residual Stress.

†Error in Residual Stress Based on Uncertainty of Diffraction Peak Position Only.

Surface Preparation

The distortion of the surface of the material can affect the stress profile to a degree that is significant for meaningful stress analysis. It is well known that an electropolishing or chemical polishing treatment should be applied before X-ray residual stress measurements are made. As with most applications, particularly in the case where NDT is performed for quality control, the chemical or electropolish is too destructive and when examining steel, sometimes dangerous (a perchloric solution is the electrolyte of choice, but is explosive).

The procedure that has been followed at AMMRC is to make X-ray measurements before and after chemical/electropolishing to determine if the measurements before specimen removal can be correlated with those after surface removal (assuming that the surface preparation conditions, i.e. machining, grinding, etc., are not changed). Examples of such a cost effective analysis have been performed on a TOW maraging steel case and the results shown in Figure 9[18]. Here, a longitudinal stress profile shows a tensile stress at a potential trouble spot both before and after electropolishing*. It was found that subsequent measurements need only be performed in the as-received condition on TOW missile cases. Another example is that of a RSA performed on an MBTA steel axle (see Figure 10). The ax is given a thermal quench to create a surface layer in compressiv stress. Residual stresses (longitudinal), at the center of the axle before and after removal of 0.005", with etching, show an apparent change in stress from a compressive to a tensile mode. Subsequent residual stress measurements of this axle, using the hole-boring technique substantiated the X-ray RSA before etching with little change measured at a 0.005" deeper level. This illus trates the importance of the surface preparation, in that the etc employed, in this case, relieved the surface of the axle of resid stress. But, in the X-ray case, a decrease in compressive stress at one point does reveal a potential trouble spot in both the as-received and etched condition. This indicates a potential qualit control application in the as-received condition even with the us of CrKα radiation.

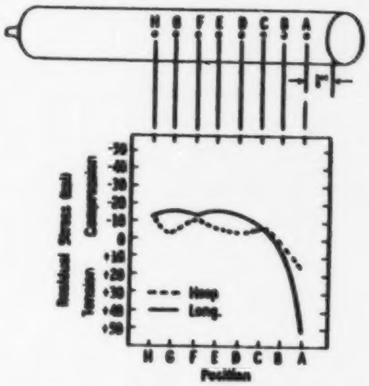

Figure 9. Residual Stress from Computerized MSF of TOW M-114 Maraging Steel Motor Case (As-Received).

A less successful situation occurs, particularly on painted surfaces and in field applications (see Figures 11 and 12). In these cases, the surface revealed disturbed conditions with the need of surface removal, a rather difficult and destructive prospect. This points out the need for improved X-ray techniques, su as the use of harder (deeper) penetrating radiation.

One alternative to chemical or electropolishing is mechanica polishing. A technique developed at AMMRC[19] makes use of a vibra tory polishing sequence that leaves the surface free from cold wo This was shown to be true for the cases of titanium alloys that a highly sensitive to cold work, in that phase transformations are

---

*Barkhausen measurements performed by H. Hatch indicated that residual stress levels were symmetrical around the TOW missile and that only one set of X-ray readings along the cylinder was necessary.

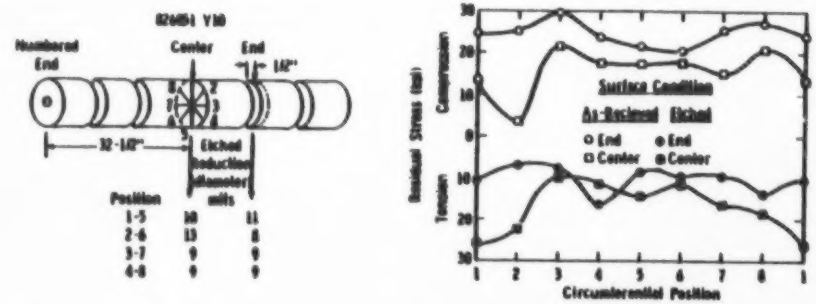

Figure 10. Residual Stress (Longitudinal) from Computerized MSF of MBTA Steel Axle Before and After Surface Etch.

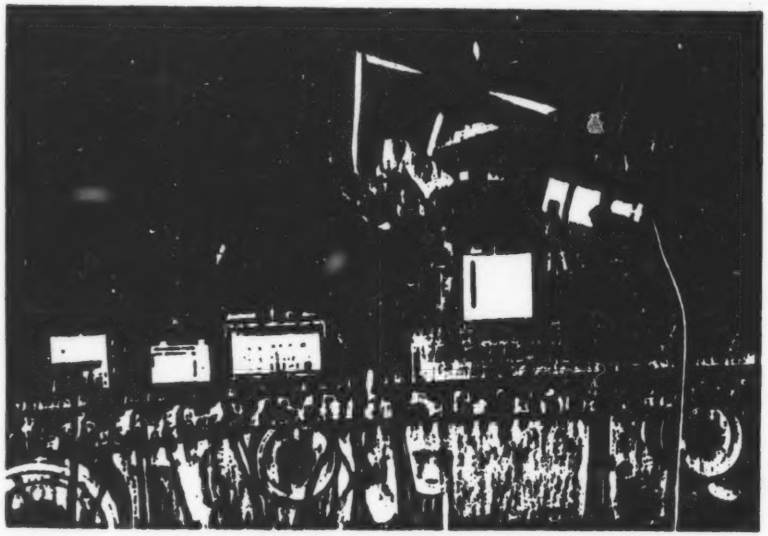

Figure 11. Residual Stress Field Measurements of Welds in Steel on M-88 Tank Retriever with Portable X-Ray System (PSF).

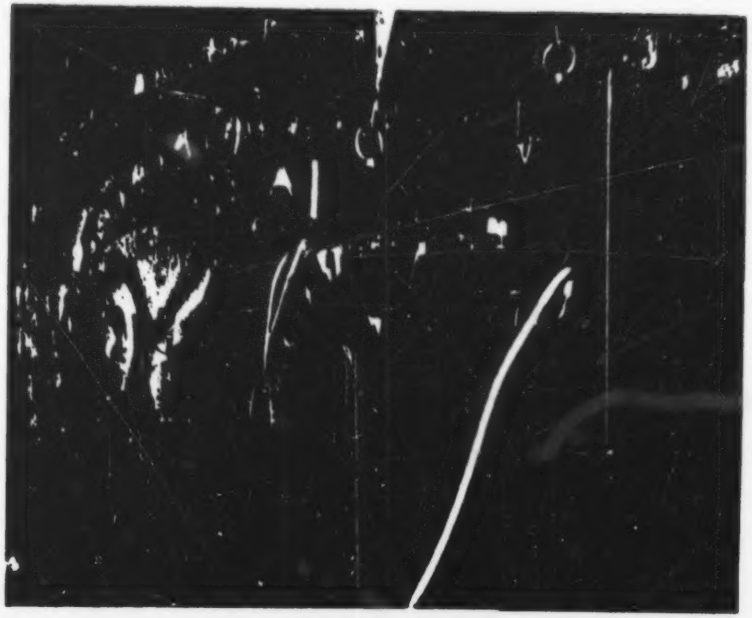

Figure 12. Residual Stress Field Measurements on a Steel Knuckle of a D-7S Dozer with Portable X-Ray System (PSF).

easily produced. Indeed, a metastable titanium alloy (transage Ti 129) that undergoes strain induced martonsitic transformation (α'') at very low strains (at approximately a 5% reduction, the transformation has been observed to occur) has been prevented usin the above mentioned polishing procedure[20].

This technique has been applied to the steel standard on all six faces and on all specimens that can be accomodated in the meta lographic polishing equipment. The application of this method has become extremely valuable for RSA, but unfortunately can only be employed in limited cases due to the geometry of the specimens. Perhaps a portable vibratory polisher can be developed in cases where chemical or electropolishing equipment cannot be effectively employed.

TEXTURE

The method of R. Marion and J. Cohen to correct the X-ray residual stress for texture[9] was applied in the case of a highly textured 4340 steel armor plate. An X-ray intensity, I, versus ψ_o plot reveals a standard iron texture along the rolling direction (see Figure 13). The corresponding 2θ (211) diffraction peak position versus ψ_o plot should be in phase with the I versus ψ_o curve for the correction procedure[9] to be effective. However, as may be seen, such is not the case with large errors in the calculated σ resulting[21] (see Figure 14).(Alignment of the I and 2θ versus ψ_o curves results in a meaningful correction.) This error may be due to a heretofore unknown systematic error peculiar to the parallel beam optics (absorption), or an error in the alignment procedure, or to a PMS effect[11]. H. Dölle and J. Cohen[13] have suggested employing the CrKα (310) reflection in the case of textured iron or steel and the (h00) or (hhh) reflections for textured cubic materials. Further experimental work will be performed to evaluate the effectiveness of such proposals.

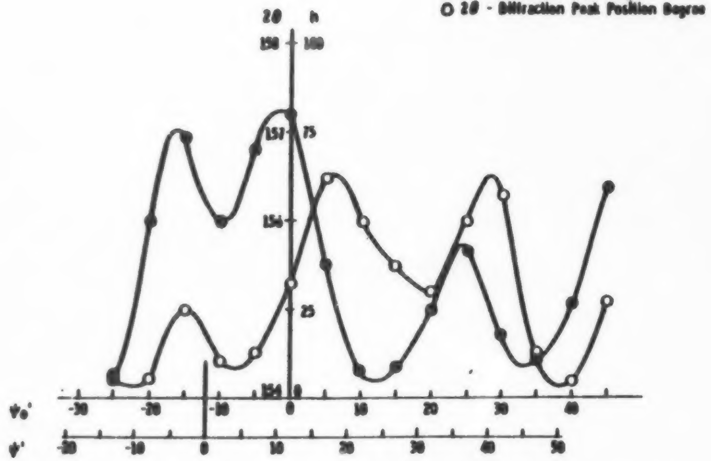

Figure 13. Bragg Angle (2θ) and Height (h) of the CrKα (211) Diffraction Peak Versus ψ' for a Textured Steel Specimen (4340).

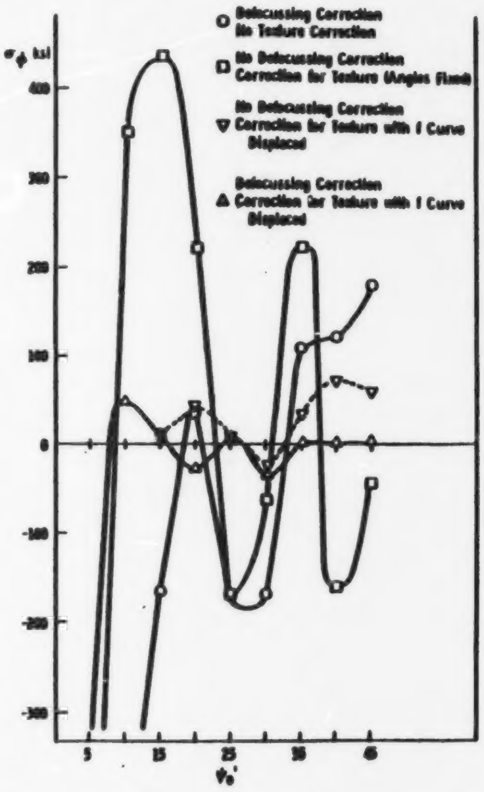

Figure 14. Measured Residual Stress, Versus σ_0^1 for Textured Steel Specimen (4340) Showing the Effect of Defocussing Correction and Making the I and 2θ peak Curves of Figure 13 Coincident.

PORTABILITY

A portable system, PSF, has been tested (see Figures 11 and 1 and although of acceptable accuracy, found to be slow and cumberso Portable systems are presently available that are fast. A system called "PARS"[22] employs a position wire detector and measurement times comparable to the DRI/SAI apparatus are possible. But a system that can also correct for grain size, surface distortion effects, not disturb protected surfaces, (i.e. paint), is lightweight, radiation proof, and safe, has yet to be found to satisfy U.S. Army needs.

CKNOWLEDGEMENTS

The author would like to extend his thanks to technicians
. Rudy and T. Sheridan for taking measurements, to A. Zarkades
or the use of the steel texture specimen, to N. Hornung and
. Alex, to Photographers J. Correggio and Sgt. Billy Cox, to
. Parker and D. Oplinger for their help with the strain fixture,
o R. Middleton, A. Zani, and J. Downing for their help in surface
reparation, MTT Managers P. Rolston and N. Fahey; P. Fopiano,
. Lenoe, and to MERADCOM, ARRADCOM, Fort Devens, and to the MBTA/
OT. In addition, thanks are extended to G. Brewer for affording
he hole boring RSA results on the MBTA axle, and to H. Hatch for
erforming the Barkhausen measurements on the TOW missile.

EFERENCES

1. H. H. Lester, and R. H. Aborn, Behavior Under Stress of the Iron Crystals, Army Ordnance, 6:120, 200, 283, 364 (1925,1926).

2. W. S. Baird, Critical Review of Recent Literature on Stress Measurements Utilizing X-Ray Diffraction Methods, Watertown Arsenal Report #160/7, 1, Watertown, MA (1936).

3. R. K. Haskel, X-Ray Diffraction as Applied to the Determination of Stress Conditions in Gun Steel, Watertown Arsenal Report #160/2, Watertown, MA (1934).

4. C. S. Barrett, and M. Gensamer, Stress Analysis by X-Ray Diffraction, Phys. Rev. (Abstract), 45:563 (1934); Physics, 7:1 (1936).

5. R. Glocker, and E. Osswald, Unique Determination of the Principal Stresses with X-Rays, Z. Tech. Physik, 16:237 (1935).

6. Residual Stress Measurement by X-Ray Diffraction, SAEJ784a, Soc. of Aut. Engrs. Inc., Warrendale, PA (1971).

7. C. O. Ruud, R. E. Sturm, and C. S. Barrett, A Nondestructive X-Ray Instrument to Instantly Measure Residual Stresses, Type II Interim Technical Report Phase I, Denver Res. Inst., U.S. Army MERADCOM, Fort Belvoir; F. P. Venditti, R. E. Sturm, E. D. Wardzala, and S. Tegtmeyer, Prototype Instrument for Instantaneous Measurement of Residual Stresses, Interim Technical Report #2698, Denver Res. Inst., Denver, CO (1979).

8. H. Möller, and J. Barbers, X-Ray Investigation of the Stress Distribution and Overstraining in Ingot Steel, Mitt. Kaiser-Wilhelm-Inst., EisenForsch, Düsseldorf, 16:21 (1934).

9. R. H. Marion, and J. B. Cohen, Anomalies in Measurement of Residual Stress by X-Ray Diffraction, in Adv. X-Ray Anal., 18:466, Plenum Press, NY (1975).

10. W. Weidemann, PHd. Thesis, Technische Hochschule, Aschen, Germany (1966), Synopsis in 9. also published with V. F. Bollenroth, and V. Hauk, Zur Dentung der Gittereigenverformungen in Plastich Verformtem-Eisen, Arch. Eisen, 10:793 (1967).

11. B. D. Cullity, Some Problems in X-Ray Stress Measurements, in Adv. X-Ray Anal., 20:259, Plenum Press, NY (1977).

12. H. Dölle, The Influence of Multiaxial Stress States, Stress Gradients, and Elastic Anisotropy on the Evaluation of Resid
Stresses by X-Rays, J. Appl. Cryst., 12:489 (1979).

13. H. Dölle, and J. B. Cohen, Evaluation of Residual Stresses i
Textured Cubic Metals, Met. Trans. A., 11A: 831 (1980).

14. F. Gisen, R. Glocker, and E. Osswald, Individual Determinat
of Elastic Stresses by X-Rays, (Communication from X-Ray La
of the Technischen Hochschule, Stuttgart to Watertown Arsen
Watertown Arsenal Report #160/9, Watertown, MA (1936).

15. A. J. Delai, and T. DeSisto, Evaluation and Characterizatio
the M735 Projectile, AMMRC Technical Report, in print (1981

16. C. P. Gazzara, A General Purpose Residual Stress Analyzer, AMMRC Technical Report (Final), in print (1981).

17. N. L. Hornung, X-Ray Stress Analysis Development of Aluminu
Standards, Special AMMRC Technical Report, in print (1981).

18. C. F. Hickey, H. Hatch, and C. P. Gazzara, Residual Stress Analysis Relative to TOW Rocket Motor Case Failures, AMMRC Technical Report, in print (1981).

19. P. J. Fopiano, and A. J. Zani, Metallographic Preparation o
Two-Phase Titanium Alloys for Replica Electron Microscopy, Metallography, 3,2:209 (1970).

20. R. M. Middleton, and C. F. Hickey, Transformation Character
tics of Transage Ti 129, in Titanium and Titanium Alloys - Scientific and Technological Aspects, J. C. Williams and A. F. Belov, eds., Plenum Press, NY (1981).

21. C. P. Gazzara, The Measurement of X-Ray Residual Stress in Textured Cubic Materials, AMMRC Technical Report, in print (1981).

22. M. James, and J. B. Cohen, "PARS" - A Portable X-Ray Analyzer for Residual Stresses, JTEVA, 6,2:91 (1978).

RESIDUAL STRESSES AND STRESS RELIEVING IN URANIUM ALLOYS

Kenneth H. Eckelmeyer

Sandia National Laboratories
Albuquerque, New Mexico 87185

ABSTRACT

The kinetics of thermal stress relieving of uranium - 2.3 w
% niobium, uranium - 2.0 wt. % molybdenum, and uranium - 0.75 wt
titanium are reported and discussed. Two temperature regimes of
stress relieving are observed. In the low temperature regime (T
300°C) the process appears to be controlled by an athermal micr
plasticity mechanism which can be completely suppressed by prio
age hardening. In the high temperature regime (300°C < T < 550
the process appears to be controlled by a classical diffusional
creep mechanism which is strongly dependent on temperature and
time. Stress relieving is accelerated in cases where it occurs
simultaneously with age hardening.

The potential danger of residual stress induced stress cor
rosion cracking of uranium alloys is discussed. It is shown th
the residual stress relief which accompanies age hardening of
uranium - 0.75% titanium more than compensates for the reductio
in K_{ISCC} caused by aging. As a result, age hardening actually
creases the susceptibility of this alloy to residual stress ind
stress corrosion cracking.

INTRODUCTION

Dilute uranium alloys are used in a variety of application
because of their high densities (> 18 g/cm^3) and/or their spec

---

*This work was supported by the U. S. Department of Energy (DOE
under contract DE-AC04-76-DP00789.

**A U. S. Doe facility.

PROBLEMS WITH RESIDUAL STRESS IN THE RAILROAD INDUSTRY

D. H. Stone

Association of American Railroads
3140 S. Federal Street
Chicago, Illinois 60616

INTRODUCTION

Residual stresses are of principal concern to the railroad industry with respect to two components, wheels and rails.

While railway wheels are manufactured with an aim to producing residual compressive hoop stresses, normal aspects of their usage tend to alter the stress pattern induced during manufacturing. The cold working of the wheel tread surface alters the residual stress pattern of the wheel, but it is probably beneficial as the work hardening decreases the rate of wear. For more important, is the fact that locomotive and freight car wheels also serve as a brake drum. During normal service braking conditions, wheel temperatures can increase to 455°C (850°F).[1-4] However, under severe or improper conditions thin layer of martensite[5,6] may be formed on the wheel surface indicating tread surface temperatures in excess of 732°C (1350°F). Such thermal imputs can lead to residual tensile hoop stresses which in term can lead to spontaneous wheel fracture.

Residual stress creates two sets of problems in rails. The first is the contribution to the formation and growth of defects, and the second is the problem of buckling of track employing continuous welded rail. Continuously welded rails are one of the most remarkable and most economical railroad developments of this century. Continuously welded rails represent a truly revolutionary technology, one in which the physical principle of the expansion of steel under the action of heat has apparently been overcome. As numerous inquiries indicate, even today it is still inexplicable

271 C-25

to many people how railroads can neutralize this natural law.

These conceptions naturally are based on the mistaken ideal that it is really possible to cancel a physical law. In reality, ill that is involved is preventing the phenomenon of the expansion of a material under the action of heat, by means of a track structure as rigid against distortions as possible and anchored in well-filled and compacted ballast bed. If the rail were mounted without friction it would expand like any other body according to he law $\Delta l = \alpha \cdot l \cdot \Delta t$. If the expansion is prevented, energy must e stored in the form of a compressive stress. In the case of inhibited contraction, under the action of cold, the rail xperiences a tensile stress of magnitude $\sigma_t = \alpha \cdot E \cdot \Delta t$.[7]

However, the track structure if subjected to sufficiently igh longitudinal compressive forces in the rail, can exhibit udden and rapid lateral or vertical movement over a relatively hort length. This lateral movement, or buckling of the track, esults in a severe misalignment condition that may not permit he safe negotiation of train traffic (Figure 1). If buckling ccurs under the train, a derailment is likely to occur. If it ccurs between trains, traffic must either be stopped or slowed own until the buckled track condition is corrected.

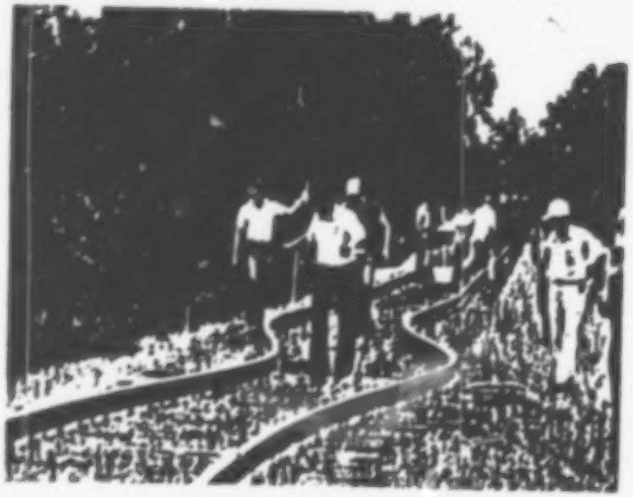

Figure 1. Buckled Track

The magnitude of this problem can be seen in the fact that, ring 1977, there were 109 train derailments attributed to ckling of the track. The reported damage for these derailments amounted to over $5.5 million. Furthermore, for every track buck that resulted in a derailment, there were three to four instance of buckled track where the railroad maintenance forces were able to correct the problem before a derailment occurred. Consequent countless hours of maintenance time are devoted to inspecting fo and correcting buckled track.

WHEELS

As stated in the introduction, wheels are manufactured so a to produce compressive stresses in the wheel rim which are balan by wheel plate tensile stresses.[8] The magnitude of these stress may be influenced by wheel design,[9] heat treatment[9,10] tempering practice,[11] or manufacturing method.[12]

Results of residual stress measurements made on new wheels by several investigators are summarized in Table 1. The radial and tangential stresses reported for various wheels act in the same direction at comparable measurement locations. However, th is considerable variation in the magnitude of the stresses, whic presumably results from variations in the design and/or processi of the wheels. Tangential compressive stresses in the rim are within the range of 15 to 45 ksi. It is important to note that rim stresses shown in table 1 were based on a few measurements made at the rim surface, and do not reflect the stress gradients in the rim.

The residual stresses which result from braking are primari a function of the thermal gradient developed. This is determine by the thermal loads experienced by the wheel and their rate of dissipation. Other factors which are believed to affect the magnitude of the residual stresses include the following:[8]

- elevated temperature strength of the wheel steel
- volumetric changes associated with microstructural transformation changes
- stress relaxation at elevated temperatures
- the Bauschinger effect
- the initial residual stresses
- wheel design

Residual stresses in a new wheel and a wheel removed from service in Europe[13] show that tensile stresses of about 30 ksi h developed in the rim during service and are balanced by compress stresses in the plate.

Figure 2 shows a wheel that failed from a back-rim thermal crack with a fatigue crack 0.69 inch (17.5 mm) deep.

C-30

Table 1. Residual Stresses in As-Manufactured, Rim-Quenched Wheels, From Ref. 8

Wheel		Radial Stress (ksi)				Tangential Stress (ksi)						Remarks
Design	Class	FFN1	FFN2	BFN1	BFN2	FR	BR	FFN1	FFN2	BFN1	BFN2	
833	NR	-2	+11	+4	-3	NR	NR	0	-1	0	-7	Average for six wheels
40, F36	NR	NR	+20 to +25	+20 to +35	NR	NR	NR	NR	NR	NR	NR	Reported as typical values
36-in. dia.	C	-10	+25	+1	-13	-30	-43	+6	+13	-3	-10	Reported as typical values
European 36-in. dia.	0.5% carbon (tempered above 932 F)	-14.2	+12.8	+11.4	-22.7	-40.7	-40.7	[illegible]	+1.4	0	-26	One wheel
		-15	+16.3	+15	-18.4	-23	-13	NR	NR	NR	NR	Average for five wheels
36-in. dia.	C (tempered at 900 F)	-6	+16	+6	-11	-30	-16	+6	+6	+3	-10	One wheel
36-in. dia.	C (tempered at 800 F)	-18	+20	+23	-36	-38	-46	+6	+17	+10	-17	One wheel

NR = Not reported

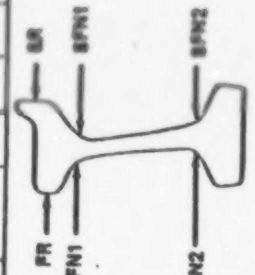

From Carter and Caton[8] the fracture toughness, K_{IC}, of grad wheels is 44,000 psi $\sqrt{in}$ at 40°F. Using these data the stress causing fracture can be calculated from the equation:

$$\sigma_f = \frac{K_{IC}}{0.9\sqrt{a}}$$

where σ_f is fracture stress
K_{IC} is fracture toughness
a is the crack depth
therefore,
σ_f = 51,700 psi (356.46 MPa)

The fracture stress is the combination of the applied stre and the residual stress. Thus,

$$\sigma_f = \sigma_a + \sigma_r$$

where σ_a is applied stress
σ_r is residual stress

It can be shown from Novak, Greenfield and Stone[3] that the tensi stress applied perpendicular to the crack is approximately 25,50 (175.82 MPa),

therefore σ_r = 51,700 psi - 25,500 psi
σ_r = 26,200 psi (180.64 MPa)

About one-half the stress necessary to cause the fractures is residual stress from brake overheating. It is interesting to no that the normal tangential residual stress in a BR wheel is a compressive 20,000 to 25,000 psi (137.90 to 172.37 MPa), approxi mately the amount needed to cancel the effect of applied stress.

RAILS

Longitudinal Rail Forces and Buckling

The track structure is subject to both mechanically and thermally induced longitudinal rail forces. When the magnitude these forces, either individually or in combination, exceeds the restraint capacity of the track structure, track buckling or rai pull-apart occurs. It is not the purpose of this paper to attem to explain the mechanisms of track buckling or rail pull-apart (extensive surveys and summary papers are already available.)[14,1] However, a brief description of the loading mechanisms and corre sponding rail behavior will help to define the measurement probl

27:

C-31

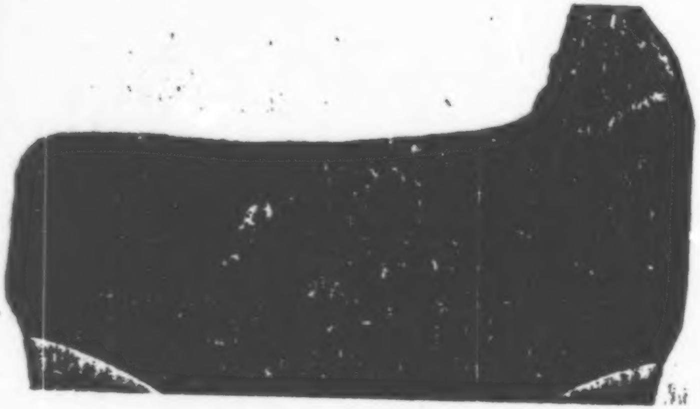

Figure 2. Wheel Failure from a Thermal Crack

Thermally induced longitudinal rail force occurs when the rail no longer free to expand; i.e., when the joints are either closed in a tight or frozen joint situation or altogether eliminated as the case with CWR track. When a constrained rail of length L is hject to a uniform temperature rise (or drop) ΔT, the longitudinal npressive (tensile) force experienced by the track is N_t = EA α ΔT; ·re E is the Young's modulus of the rail steel, A is the cross- ·tional area of the two rails, and α is the coefficient of linear ·rmal expansion.

It should be noted however, that, although the longitudinal ess in the rail changes with temperature, the constrained portion the rail does not move. Thus, the strain in the center portion the rail section, away from the end regions is zero, although the ess and force in the rail is not. It is this absence of strain ıt results in many of the difficulties encountered in the measure- t of thermally induced longitudinal rail forces.[17]

Since it is the change in rail temperature from its initial or ing temperature that determines the magnitude of the thermally ıced rail force, proper selection and control of the CWR tallation temperature is of great importance.[16] Consequently, y railroads have defined installation temperatures for different graphic locations. When the ambient temperature at the time of tallation is below the recommended installation temperature, the l is artificially brought to the proper "temperature" through her heating the rail or mechanically stretching it to the ropriate length. In the latter case, mechanical strains and

---

consequently stresses (tensile) are introduced. Furthermore, rail installed in and near curves often undergoes contraction and expansion cycles that result in a shifting of the track, usually noted by a change in the curvature. This behavior often changes t actual installation temperature so that it no longer is the same a the initial laying temperature. In fact, in many cases, this stre free temperature is no longer known.

Finally, it must be noted that, in addition to the stresses introduced into the rails by temperature change, installation, and train action, residual stresses in the rail section can be present These residual stresses are introduced by the rail manufacturing process, by various heat treatment techniques, by the work hardeni and softening of the rail head under wheel-rail interaction, and b the welding process (in the vicinity of the welds). However, thes residual stresses generally are distributed so that the net force across the rail section is zero. This stress distribution is simi to that encountered by the rail in bending, where at any given poi in the rail section a stress can be present. However, the net for in the rail section, obtained by summing all the stresses in the cross section, is zero. In that case, the effect of these residu stresses on track buckling is negligible, since it is the net longitudinal force in the rails that contributes to this track failure mode.[17]

Consequently, it is necessary to be able to distinguish betwe those stresses in the rail that produce net longitudinal force, su as those introduced by temperature change, installation, train acceleration or braking, and rail creep and those stresses that produce little or no net longitudinal force, such as rail bending stresses and residual stresses introduced by manufacturing, heat treatment, wheel-rail interaction, and welding. It is for this reason that the measurement of the resultant forces, rather than stresses, must be the objective of any track measurement device.[17]

Rail Residual Stresses and Defect Growth

The contact-induced shear stresses which develop within the railhead cause plastic deformation which, under the influence of many wheel passages, leads to work hardening of the upper portion the railhead such that eventually the stress reversals become essentially elastic, and further plastic flow becomes minimal.

The shelling-type flaw develops well below the region of max shear stress and maximum hardness as is illustrated in Figure 3.[1] This region has been shown to be characterized by stresses which been caused by the cold working of the railhead.[19] These residua stresses probably also contribute to the generation of other head defects such as horizontal and vertical split heads.

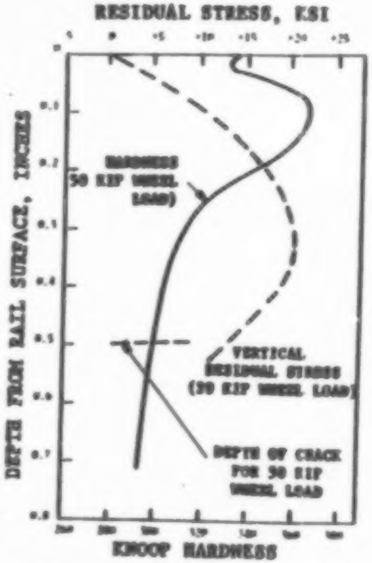

igure 3. Variation of Hardness[18] and Residual Stress[19] with Depth Below Running Surface of Rail in Rolling Load Type Tests

The rate of fatigue damage accumulation would be reduced in the gion of maximum shear stress ~0.1 to 0.2 inch (~2.5 to 5 mm) neath the running surface if work hardening is allowed to progress d concomitantly the region at that depth sees compressive residual ress at least in the longitudinal and transverse directions igure 3). Consider that the normal tensile fatigue endurance rength of rail steel is near 60 ksi (410 MPa),[20] implying a shear tigue endurance strength near 30 ksi (205 MPa). Presuming that e endurance strength increases due to cold work in about the same oportion as the increase in ultimate tensile,[21] the shear endurance rength at ~0.1 to 0.2 inch (~2.5 to 5 mm) depth of the rail shown Figure 3 would rise to 40 ksi (~275 MPa). By reference to gure 4 showing the octahedral shear stress as a function of wheel ad, wheel loads as low as 10 000 lb (45 kN) would cause some mage within the region of maximum shear stress. But if the sidual stresses, predominantly compressive at 0.1 to 0.2 inch .5 to 5 mm) depth, are factored into the calculation of octahedral ear stress the value of octahedral shear at ~20 000 lb (~90 kN) eel load would be found to drop to ~36 000 lb (~160 kN) under the durance limit; indeed, wheel loads as high as 25 tons (50 000 lb) 3-inch-diameter wheel) would be expected to cause little fatigue mage in the region of maximum shear.

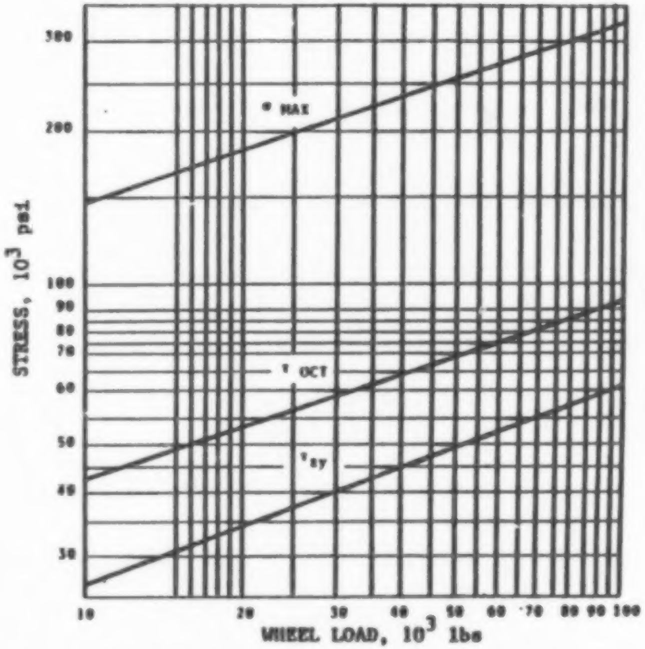

Figure 4. Maximum Compressive, Octahedral Shear, and Alternating Traverse Shear Stress in a Rail for New 33-Inch-Diamet Wheel and rail having 10 inch crown radius[21]

However, the region beneath the cold-worked layer can see a substantial vertical tensile stress of perhaps as high as 40 per of the tensile fatigue endurance strength.[19] Considering that endurance strength is actually a statistical distribution as sho in the modified Goodman diagram of Figure 5, the tensile residu stresses can increase the likelihood of fatigue crack initiation Indeed the benefit of using stronger rail can be seen by the upw and rightward displacement of the endurance life line. A second advantage of harder rail is that its use will reduce the cyclic plastic flow as reflected in the depths of the peak hardnesses (compare Figures 3 and 6), thereby delaying the occurrence of adverse residual stresses beneath the cold-worked region. Modes vertical wear of the rail will permit the residual stress patter to move downward gradually so that a volume of metal originally the residual tensile stress field will come under the influence compressive stresses, and the rate of accumulation of fatigue da will diminish.[22]

275

0-33

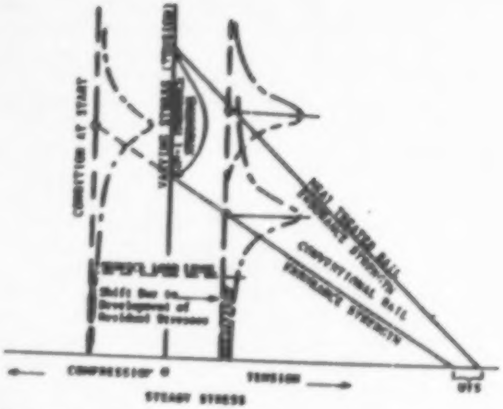
CONDITION AT START
VARYING STRESS (STRENGTH)
HEAT TREATED RAIL
FATIGUE STRENGTH
CONVENTIONAL RAIL
ENDURANCE STRENGTH
Shift Due to Development of Residual Stresses
COMPRESSION 0
TENSION
STEADY STRESS
UTS

ıre 5. Modified Goodman Diagram Showing Effect of Residual Stress and Distribution of Fatigue Strength on Rail Fatigue Behavior

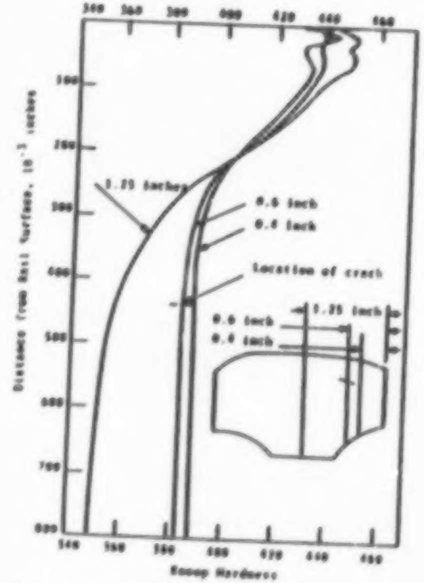

ıgure 6. Hardness Profile of Heat-Treated Standard Rail Under Rolling Load Test[18]

REQUIREMENTS FOR STRESS MEASURING DEVICES

Given the foregoing sets of problems with rails and wheels, many attempts have been made to develop nondestructive devices fo use in the railroad industry. Attempts have been and are being m to apply the following techniques to measuring residual stresses the railroad industry.[23]

- * Strain gage techniques
- * Rail force transducers
- * Rail vibration
- * X-ray diffraction
- * Ultrasonic birefringence
- * Magnetomechanical acoustic emission

All of the above techniques currently have some limitations when attempts are made to apply them to railway environments and conditions.

Zarembski[17] has listed the requirements such a system should have in order to be successfully used in the railway industry as follow:

1. It should be ruggedly constructed and capable of survivin in the field.
2. It should be easy to handle and require only limited inte pretation of data.
3. It should be nondestructive to the rail and track structu
4. It should not require the disturbance of the track struct either during application or during "zeroing," if the lat is at all necessary.
5. It should require minimum or no calibration. If calibrat is needed, it should not require heavy equipment or significant track time.
6. It should be independent of or readily compensated for:
   a. rail size
   b. rail metallurgy
   c. heat treatment
   d. rail head wear
   e. work hardening or softening of the rail head
7. It should require minimum or no surface preparation of the rail.

8. It should provide for direct measurement of net longitudinal force (absolute).

9. It should not have to be permanently affixed to the rail or track structure.

10. It should permit "continuous" or at a minimum very frequent measurement of rail force from a moving vehicle.

The above requirements are exactly the same requirements for ieels except that in the case of wheels one is interested in stress ither than force.

FERENCES

1. T. Hirooka, H. Teramura, T. Saito, T. Hirakawa, and K. Ishii, "On the Thermal Effect of Tread Braking upon Car Wheels", Quarterly Reports, Japan Soc of Railway Engineering, Vol. 11, No. 3, 1970, pp. 160-162.
2. G. E. Novak and B. J. Eck, "Asymmetrical Wheel Stresses Caused by Simulated Thermal and Mechanical Service Loads", ASME Paper 72-WA/RT-13, November, 1972.
3. G. E. Novak, L. P. Greenfield and D. H. Stone, "The Effects of Wheel Design and Service Environment on the State of Stress in 28-Inch Diameter Freight Car Wheels", Proceedings of the Fifth International Wheelset Congress, Tokyo, October, 1975.
4. H. R. Johnson, R. E. Welch and K. W. Yeung, "Analysis of Thermal Stresses and Residual Stress Changes in Railroad Wheels Caused by Severe Drag Braking", ASME Paper 75-WA/RT-3, November, 1975.
5. J. M. Wandrisco and F. J. Devez, Jr., "Study of the Defects that Originate and Develop in the Treads of Railroad Wheels During Service", ASME Paper 60-RR-1, February, 1960.
6. J. L. Van Swaaij, "The Mechanism of Thermal Cracking in Railway Wheels", Proceedings of the Third International Wheelset Congress, Sheffield, 1969.
7. H. Schultheiss, "Fabrication and Maintenance of Continuously Welded Rails", In Railroad Track, F. Fastenrath, Ed., Ungar, New York, 1981.
8. C. S. Carter and R. G. Caton, "Fracture Resistance of Railroad Wheels (Interim Report)", Department of Transportation Report DOT-TSC-617, April, 1974.
9. W. Brohl and N. Brinkman, "Quenching and Tempering Treads of Solid Wheels: Significance in Rail Traffic", Proceedings of the Third International Wheelset Congress, Sheffield, 1969.
10. A. S. Babb, B. Sweeney and G. Birkbeck, "Residual Stresses in Straight Webbed Monobloc Wheels", Proceedings of the

Fifth International Wheelset Congress, Tokyo, 1975.
11. J. LeClerc and C. Camut, "Tests on Rim Treated Wrought Wheel Residual Stresses and Microstructure of New Wheels", Proceedings of the Third International Wheelset Congress, Sheffield, 1969.
12. H. R. Wetenkamp, O. M. Sidebottom and H. R. Schrader, "The Effect of Brake Shoe Action on Thermal Cracking and on Failure of Wrought Steel Railway Car Axles", University of Illinois, Experimental Engineering Station Bulletin No. 387, 1950.
13. M. Castagna, et al., "Contribution of Fracture Mechanics to the Search for Optimal Quality in Monobloc Wheels", Proceedings of the Fourth International Wheelset Congress, Paris, 3, 1972.
14. A. D. Kerr, "Lateral Buckling of Railroad Tracks Due to Constrained Thermal Expansion--A Critical Survey", In Railroad Track Mechanics and Technology, Ed., A. D. Kerr, Proceedings of symposium held at Princeton University, April 21-23, 1975, Elmsford, New York, Pergamon Press, 1978.
15. A. D. Kerr, "A Bibliography on the Determination of Stresses in Rails and Ties and Thermal Track Buckling", Report prepared for Department of Transportation, Transportation Systems Center, February, 1976.
16. A. D. Kerr, "Thermal Buckling of Straight Tracks, Fundamentals, Analyses, and Preventive Measures", Bulletin of the American Railway Engineering Association, Bulletin 669, Vol. 80, September, 1978.
17. A. M. Zarembski, "On the Nondestructive In-Track Measurement of Longitudinal Rail Force", In Nondestructive Techniques for Measuring the Longitudinal Force in Rails, DOT Report FRA/ORD-80/50, December, 1980.
18. W. S. Hyler and H. J. Grover, AREA Proceedings, Vol. 55, 1954, pp. 840-854.
19. "Behavior of the Metal of Rails under the Repeated Action of Wheels", ORE Report C53/RP9/E, Int. Union of Railways, Utrecht, 1971.
20. G. J. Fowler, "Fatigue Crack Initiation and Propagation in Pearlitic Rail Steels", Ph.D. Thesis, UCLA, 1976.
21. T. G. Johns and K. B. Davis, BCL Interim Report 30, Department of Transportation Report DOT-TSC-1038, June, 1976.
22. D. H. Stone and R. K. Steele, "The Effect of Mechanical Properties Upon the Performance of Rail Steels", In Rail Steels-Developments, Processing and Use, ASTM STP 644, D. H. Stone and G. G. Knupp, Ed., ASTM, Philadelphia, 1978.
23. P. Elliot, Ed., "Nondestructive Techniques for Measuring the Longitudinal Force in Rails", Department of Transportation Report FRA/ORD-80/50, December, 1979.